UNIVERSITI TEKNOLOGI MARA

PERFORMANCE OF CEMENT STABILIZED COLD-IN-PLACE RECYCLING WITH GROUND COAL BOTTOM ASH AND CALCIUM CHLORIDE

MOHD IZZAT BIN JOOHARI

PhD

June 2026

UNIVERSITI TEKNOLOGI MARA

PERFORMANCE OF CEMENT STABILIZED COLD-IN-PLACE RECYCLING WITH GROUND COAL BOTTOM ASH AND CALCIUM CHLORIDE

MOHD IZZAT BIN JOOHARI

Thesis submitted in fulfilment
of the requirements for the degree of
Doctor of Philosophy
(Civil Engineering)

Faculty of Civil Engineering

June 2026

CONFIRMATION BY PANEL OF EXAMINERS

I certify that a Panel of Examiners has met on 29th January 2026 to conduct the final examination of Mohd Izzat Bin Joohari on his Doctor of Philosophy thesis entitled "Performance of Cement Stabilized Cold-In-Place Recycling with Ground Coal Bottom Ash and Calcium Chloride" in accordance with Universiti Teknologi MARA Act 1976 (Akta 173). The Panel of Examiners recommends that the student be awarded the relevant degree. The Panel of Examiners was as follows:

Ismacahyadi Bagus Mohamed Jais, PhD
Associate Professor
Faculty of Civil Engineering
Universiti Teknologi MARA
(Chairman)

Noor Azreena Kamaluddin, PhD
Senior Lecturer
Faculty of Civil Engineering
Universiti Teknologi MARA
(Internal Examiner)

Mohd Ezree Abdullah, PhD
Professor
Fakulti Kejuruteraan Awam dan Alam Bina
Universiti Tun Hussein Onn Malaysia
(External Examiner)

PROF DR HJH ZURAEDA BINTI IBRAHIM
Dean
Institute Postgraduate Studies
Universiti Teknologi MARA
Date: 30 June 2026

AUTHOR'S DECLARATION

I declare that the work in this thesis was carried out in accordance with the regulations of Universiti Teknologi MARA. It is original and is the results of my own work, unless otherwise indicated or acknowledged as referenced work. This thesis has not been submitted to any other academic institution or non-academic institution for any degree or qualification.

I, hereby, acknowledge that I have been supplied with the Academic Rules and Regulations for Postgraduate, Universiti Teknologi MARA, regulating the conduct of my study and research.

Name of Student	:	Mohd Izzat Bin Joohari
Student ID. No.	:	2022784435
Programme	:	Doctor of Philosophy (Civil Engineering) – CEEC950
Faculty	:	Civil Engineering
Thesis Title	:	Performance of Cement Stabilized Cold-In-Place Recycling with Ground Coal Bottom Ash and Calcium Chloride
Signature of Student	:	
Date	:	June 2026

ABSTRACT

Cold In-Place Recycling (CIPR) is a pavement rehabilitation technique where existing deteriorated asphalt pavement is pulverized, stabilized, and compacted in place to form a new base layer. In Malaysia, Ordinary Portland Cement (OPC) is the most commonly used stabilizing agent. However, cement-treated layers are highly dependent on proper curing to achieve adequate hydration and early strength development. Insufficient curing often leads to premature cracking and long-term performance issues. This research investigated the use of Ground Coal Bottom Ash (GCBA) and Calcium Chloride ($CaCl_2$) with OPC to accelerate early strength development and improve the mechanical performance of CIPR base layer. In addition, predictive models were developed using Response Surface Methodology (RSM) to analyze the interaction effects among the variables and to optimize the material design parameters. Three combinations of Crushed Aggregate (CA) and Reclaimed Asphalt Pavement (RAP) were examined: CA75RAP25, CA50RAP50, and CA25RAP75. Each mix was stabilized with varying contents of OPC (1-4%), GCBA (0-3%), and $CaCl_2$ (0-3%) by weight of material. The research was conducted in four phases, beginning with the characterization of material properties, followed by compaction testing to determine Optimum Moisture Content (OMC), Maximum Dry Density (MDD) and bulk density. Strength evaluation was then conducted using Unconfined Compressive Strength (UCS), Indirect Tensile Strength (ITS), and Resilient Modulus (M_R) tests at different curing periods (1, 3, 7, 14 and 28 days). In the final phase, RSM was employed to develop a predictive model describing the relationship between stabilizer content and strength performance, validate predictions, and identify optimal mix designs. The results revealed that the proposed mix design had a significant influence on the material characteristics and compaction properties. Higher CA content led to increased OMC, while bulk density showed only minor variation, indicating that the stabilizing agents improved bonding rather than particle packing. The CA50RAP50 mix achieved the highest UCS and ITS, especially during early curing, while CA75RAP25 demonstrated better M_R performance. Although strength performance decreased with 3% GCBA, a mix combination of 0-1% GCBA, 1% $CaCl_2$, and 3-4% OPC produced better performance compared to the control specimen containing 4% OPC alone. This indicated enhanced binder efficiency and early strength development while reducing OPC usage. The developed RSM models showed strong predictive accuracy, with high R^2 values confirming their reliability. Model validation revealed close agreement with laboratory results, and the optimization analysis identified CA50RAP50 with 4% OPC and 1-2% $CaCl_2$ as the best performer in UCS and ITS, whereas CA75RAP25 achieved the highest M_R with the same stabilizer composition. Overall, the findings highlight that the stabilizing agents mix comprising 0-1% GCBA, 1% $CaCl_2$, and 3-4% OPC offers a sustainable and practical alternative to conventional cement-only mixes for enhancing CIPR base performance in Malaysian road rehabilitation projects.

ACKNOWLEDGEMENT

Assalamualaikum W.B.T. Praise be to Almighty Allah, the Most Gracious and the Most Merciful, for His boundless blessings, guidance, and strength throughout this enriching journey of knowledge and discovery. This journey would not have been possible without His divine mercy and favour.

First and foremost, I would like to express my heartfelt gratitude to my main supervisor, Professor Madya Ir. Ts. Dr. Ekarizan Shaffie, for her exceptional guidance, insightful advice, and unwavering support throughout this research. Her dedication, expertise, and encouragement have been invaluable and deeply appreciated.

In addition, I would like to extend my heartfelt thanks to Dr. Anas Ibrahim, my co-supervisor, for his continuous support and valuable feedback throughout my research. His encouragement and advice have been a great source of strength and have significantly contributed to the refinement of this research.

I am also honoured to have worked with the dedicated laboratory assistant engineers, Mohd Hurman Abdul Ghani, Ahmad Afuan Ismail, Mohammad Suhairi Hj. Mohamad, Muhamad Hazli Shariei, Mohamad Azrul Aswad Mohd Nor, Md Faizal Zakaria, Salahuddin Abdullah and Suzana Hj. Ahmad. Their invaluable assistance, exceptional efforts, and dedication in supporting my experimental work have exceeded my expectations. Their valuable technical skills and unwavering patience played a crucial role in ensuring the successful completion of the laboratory testing stages in this research.

My appreciation also extends to Faculty of Civil Engineering UiTM Shah Alam and UiTM Cawangan Pulau Pinang for providing excellent facilities, a conducive working environment, and unwavering support that greatly facilitated the progress of my research. I would also like to extend my gratitude to TNB Jana Manjung, THB Maintenance Sdn. Bhd., and Kajang Quarry for generously supplying the materials essential for this research, enabling me to carry out the experimental work effectively.

I am deeply grateful to my beloved family, most especially my lovely wife and cherished daughter for their unwavering love, patience, and understanding. Their constant encouragement, support, and inspiration have been my greatest source of strength throughout this journey. I would also like to extend my heartfelt appreciation to my parents and in-laws, whose prayers, love, and selfless sacrifices have consistently inspired and guided me along the way.

Lastly, I wish to acknowledge and thank everyone who has contributed, whether directly or indirectly, to this work, including colleagues, friends, and those who have offered their assistance, but whose names may not have been mentioned here. Your support, in ways big and small, has not gone unnoticed, and I am deeply grateful for your kindness.

TABLE OF CONTENTS

		Page
CONFIRMATION BY PANELS OF EXAMINERS		**ii**
AUTHOR'S DECLARATION		**iii**
ABSTRACT		**iv**
ACKNOWLEGEMENT		**v**
TABLE OF CONTENTS		**vi**
LIST OF TABLES		**xii**
LIST OF FIGURES		**xv**
LIST OF PLATES		**xxiii**
LIST OF SYMBOLS		**xxiv**
LIST OF ABBREVIATIONS		**xxv**
CHAPTER 1 INTRODUCTION		**1**
1.1	Research Background	1
1.2	Problem Statement	4
1.3	Objectives	5
1.4	Scope and Limitation of Research	6
1.5	Significance of Research	6
1.6	Research Thesis Outline	7
CHAPTER 2 LITERATURE RIVIEW		**8**
2.1	Introduction	8
2.2	Asphalt Recycling	8
2.3	Cold-In Place Recycling	9
2.4	Advantages and Disadvantages of Cold-In Place Recycling	11
2.5	Materials of Cold-In Place Recycling Mix	12
2.6	Cold In-Place Recycling Process	12
2.7	Recycling with Stabilizing Agents	14

2.7.1 Cement Stabilizer 14
2.7.2 Bitumen Emulsion Stabilizer 15
2.7.3 Foamed Bitumen Stabilizer 17
2.8 Coal Waste 18
2.9 Properties of Coal Bottom Ash 21
2.9.1 Physical Properties 21
2.9.2 Chemical and Pozzolanic Properties 22
2.9.3 Morphological Characteristics 23
2.10 Ground Coal Bottom Ash 24
2.10.1 Physical Properties of Ground Coal Bottom Ash 25
2.10.2 Chemical Composition of Ground Coal Bottom Ash 25
2.11 Strength Performance of Ground Coal Bottom Ash with Cement 26
2.12 Coal Bottom Ash in Pavement Construction 28
2.13 Calcium Chloride in Cement Application 32
2.14 Calcium Chloride in Pavement Construction 34
2.15 Methods for Evaluating Stabilized Base Course Performance 35
2.16 Technical Standards for Cold In-Place Recycling 37
2.16.1 Material Requirements 38
2.16.2 Laboratory Evaluation Protocol 38
2.16.3 Preliminary Laboratory Testing and Gradation 38
2.16.4 Compliance Requirements for Cement Stabilization 39
2.17 Analytical Method Using Response Surface Method 40
2.18 Gap of Research 44

CHAPTER 3 RESEARCH METHODOLOGY 45
3.1 Introduction 45
3.2 Materials 48
3.2.1 Cold In-Place Recycling Sample 48
3.2.2 Reclaimed Asphalt Pavement Sample 49
3.2.3 Crushed Aggregate 50
3.2.4 Stabilizing Agent 51
3.3 Phase One: Mix Design and Material Characterization 52
3.3.1 Mix Design 54

3.3.2 Material Characterization 55
3.3.2.1 Particle Size Distribution 55
3.3.2.2 Specific Gravity 56
3.3.2.3 Particle Shape 57
3.3.2.4 Material Durability 59
3.3.2.5 pH Index 61
3.3.2.6 Scanning Electron Microscope and Energy Dispersive X-Ray 62
3.3.2.7 X-Ray Diffraction 64
3.4 Phase Two: Compaction Properties Test 64
3.4.1 Optimum Moisture Content and Maximum Dry Density 67
3.4.2 Bulk Density 68
3.5 Phase Three: Strength Performance Test 69
3.5.1 Unconfined Compressive Strength 70
3.5.2 Indirect Tensile Strength 72
3.5.3 Resilient Modulus 73
3.6 Phase Four: Model Development and Mix Design Optimization 75
3.6.1 Model Development 76
3.6.2 Model Verification 79
3.6.3 Mix Design Optimization 79
3.7 Concluding Remark 80

CHAPTER 4 RESULTS, ANALYSIS AND DISCUSSION 81
4.1 Introduction 81
4.2 Phase One: Characteristic Properties of Mix Design 81
4.2.1 Verification of Particle Size Distribution 82
4.2.1.1 Particle Size Distribution for Crushed Aggregate 82
4.2.1.2 Particle Size Distribution for CA-RAP 83
4.2.1.3 Particle Size Distribution for Site Samples 84
4.2.2 Specific Gravity 86
4.2.3 Particle Shape Analysis 88
4.2.4 Aggregate Durability 90
4.2.4.1 LA Abrasion 90

4.2.4.2 Aggregate Impact Value 91
4.2.5 pH Index Value 92
4.2.6 Scanning Electron Microscope and Energy Dispersive X-Ray 95
4.2.6.1 Scanning Electron Microscope 95
4.2.6.2 Energy Dispersive X-Ray 105
4.2.7 X-Ray Diffraction 113
4.3 Phase Two: Determination of Compaction Properties 115
4.3.1 Optimum Moisture Content and Maximum Dry Density 116
4.3.2 Bulk Density 118
4.4 Phase Three: Performance Analysis of Stabilized CIPR Base Course 122
4.4.1 Unconfined Compressive Strength Test 123
4.4.1.1 Effect of Varying Percentages of Stabilizing Agent on Compressive Strength 123
4.4.1.2 Influence of Stabilizing Agents on Compressive Strength 139
4.4.1.3 Effect of Varying CA-AP Ratio on Compressive Strength 140
4.4.1.4 Influence of Varying CA-RAP Ratio on Compressive Strength 145
4.4.1.5 The Proposed Mix Design Ranking 146
4.4.2 Indirect Tensile Strength Test 150
4.4.2.1 Effect of Varying Percentages of Stabilizing Agent on Indirect Tensile Strength 150
4.4.2.2 Influence of Stabilizing Agent on Indirect Tensile Strength 168
4.4.2.3 Effect of Varying CA-AP Ratio on Indirect Tensile Strength 169
4.4.2.4 Influence of Varying CA-RAP Ratio on Indirect Tensile Strength 173
4.4.3 Resilient Modulus Test 174
4.4.3.1 Effect of Varying Percentages of Stabilizing Agent on Resilient Modulus 174

4.4.3.2 *Influence of Stabilizing Agent on Resilient Modulus* 190
4.4.3.3 *Effect of Varying CA-AP Ratio on Resilient Modulus* 191
4.4.3.4 *Influence of Varying CA-RAP Ratio on Resilient Modulus* 195
4.4.4 Influence of Material Properties on Strength Performance 195
4.4.4.1 *Specific Gravity* 195
4.4.4.2 *Particle Shape* 196
4.4.4.3 *Aggregate Durability* 196
4.4.4.4 *pH Index* 197
4.4.4.5 *Mineralogy* 197
4.4.5 Summary of Strength Test Results 197
4.4.5.1 *Unconfined Compressive Strength Results* 198
4.4.5.2 *Indirect Tensile Strength Results* 199
4.4.5.3 *Resilient Modulus Results* 200
4.5 Phase Four: Model Development, Data Verification and Optimization 202
4.5.1 Unconfined Compressive Strength Model 202
4.5.1.1 *CA75RAP25 Mix Design* 203
4.5.1.2 *CA50RAP50 Mix Design* 204
4.5.1.3 *CA25RAP75 Mix Design* 205
4.5.1.4 *3-D Model of UCS Analysis* 206
4.5.1.5 *Predictive Versus Actual Analysis of UCS* 210
4.5.2 Indirect Tensile Strength Model 215
4.5.2.1 *CA75RAP25 Mix Design* 216
4.5.2.2 *CA50RAP50 Mix Design* 217
4.5.2.3 *CA25RAP75 Mix Design* 218
4.5.2.4 *3-D Model of ITS Analysis* 219
4.5.2.5 *Predictive Versus Actual Analysis of ITS* 223
4.5.3 Resilient Modulus Model 227
4.5.3.1 *CA75RAP25 Mix Design* 228
4.5.3.2 *CA50RAP50 Mix Design* 229

4.5.3.3 *CA25RAP75 Mix Design* 230
4.5.3.4 *3-D Model of M_R Analysis* 231
4.5.3.5 *Predictive Versus Actual Analysis of M_R* 235
4.5.4 Mix Design Optimization Using Regression Analysis 240
4.5.4.1 *Unconfined Compressive Strength* 241
4.5.4.2 *Indirect Tensile Strength* 243
4.5.4.3 *Resilient Modulus* 245

CHAPTER 5 CONCLUSIONS AND RECOMMENDATIONS 248
5.1 Conclusions 248
5.1.1 Material Characterization 248
5.1.2 Effect of Proposed Stabilizing Agent on The Compaction Properties 249
5.1.3 Effect of Proposed Stabilizing Agent on The Strength Performance 250
5.1.4 Model Development and Optimization 251
5.1.5 Overall Conclusion 251
5.2 Recommendations 253

REFERENCES 255

APPENDICES 278

AUTHOR'S PROFILE 351

LIST OF TABLES

Tables	Title	Page
Table 2.1	Coal Power Plant in Malaysia	19
Table 2.2	Physical Properties of CBA	21
Table 2.3	Chemical Characteristics of OPC and CBA	23
Table 2.4	Physical Properties of GCBA	25
Table 2.5	Chemical Compositions of GCBA	26
Table 2.6	Compressive Strength Test Results	30
Table 2.7	Gradation Limits for Recycled Layer Material	39
Table 2.8	Requirements for Cement Stabilized CIPR Layer Material	39
Table 2.9	CCD Arrangements	40
Table 3.1	Gradation of Base Type II Aggregate	50
Table 3.2	Percentage Gradation of CA and RAP Mix	54
Table 3.3	Percentage of Stabilizing Agent	54
Table 3.4	Gradation Limit for Recycled Layer Material	55
Table 3.5	Moisture Content and Stabilizing Agent Percentage	66
Table 3.6	Variables Used in for Model Development	77
Table 4.1	Particle Size Distribution Result For CA	82
Table 4.2	Particle Size Distribution Result for Proposed CA and RAP Ratio	83
Table 4.3	Particle Size Distribution Result for Site 1 and 2	85
Table 4.4	Specific Gravity of The Materials	86
Table 4.5	Particle Shape Analysis	89
Table 4.6	LA Abrasion for Proposed CA-RAP Ratio and Site Samples	90
Table 4.7	AIV For Proposed CA-RAP Ratio and Site Samples	91
Table 4.8	pH Index Value for Proposed Mix Design	93
Table 4.9	pH Index Value for Site Samples	94

Tables	Title	Page
Table 4.10	Chemical Composition of Stabilizing Agent Obtained By EDX	111
Table 4.11	XRD Analysis of Mix Design	113
Table 4.12	Optimum Moisture Content and Maximum Dry Density of Proposed Mix Design	116
Table 4.13	Result Of Bulk Density	119
Table 4.14	Ranking of the Overall Result for CA75RAP25 Mix Design	147
Table 4.15	Ranking of the Overall Result for CA50RAP50 Mix Design	148
Table 4.16	Ranking of the Overall Result for CA25RAP75 Mix Design	149
Table 4.17	Summary of UCS Results - CA75RAP25 Mix	198
Table 4.18	Summary of UCS Results - CA50RAP50 Mix	198
Table 4.19	Summary of UCS Results - CA25RAP75 Mix	199
Table 4.20	Summary of ITS Results - CA75RAP25 Mix	199
Table 4.21	Summary of ITS Results - CA50RAP50 Mix	200
Table 4.22	Summary of ITS Results - CA25RAP75 Mix	200
Table 4.23	Summary of M_R Results - CA75RAP25 Mix	200
Table 4.24	Summary of M_R Results - CA50RAP50 Mix	201
Table 4.25	Summary of M_R Results - CA25RAP75 Mix	201
Table 4.26	ANOVA Results for UCS - CA75RAP25 Mix	203
Table 4.27	ANOVA Results for UCS - CA50RAP50 Mix	204
Table 4.28	ANOVA Results for UCS - CA25RAP75 Mix	205
Table 4.29	ANOVA Results for ITS - CA75RAP25 Mix	216
Table 4.30	ANOVA Results for ITS - CA50RAP50 Mix	217
Table 4.31	ANOVA Results for ITS - CA25RAP75 Mix	218
Table 4.32	ANOVA Results for M_R - CA75RAP25 Mix	228
Table 4.33	ANOVA Results for M_R - CA50RAP50 Mix	229
Table 4.34	ANOVA Results for M_R - CA25RAP75 Mix	230
Table 4.35	Fit Statistic of CA75RAP25 Mix for UCS Test	241

Tables	Title	Page
Table 4.36	Fit Statistic of CA50RAP50 Mix for UCS Test	242
Table 4.37	Fit Statistic of CA25RAP75 Mix for UCS Test	242
Table 4.38	Fit Statistic of CA75RAP25 Mix for ITS Test	243
Table 4.39	Fit Statistic of CA50RAP50 Mix for ITS Test	244
Table 4.40	Fit Statistic of CA25RAP75 Mix for ITS Test	244
Table 4.41	Fit Statistic of CA75RAP25 Mix for M_R Test	246
Table 4.42	Fit Statistic of CA50RAP50 Mix for M_R Test	246
Table 4.43	Fit Statistic of CA25RAP75 Mix for M_R Test	247

LIST OF FIGURES

Figures	Title	Page
Figure 1.1	Comparison of Conventional and CIPR Methods	2
Figure 2.1	CIPR Process	10
Figure 2.2	Recycling Train for Cement	14
Figure 2.3	Recycling Train for Bitumen Emulsion	15
Figure 2.4	Recycling Train for Cement and Bitumen Emulsion	16
Figure 2.5	Recycling Train for Foamed Bitumen	17
Figure 2.6	Typical Steam Generating System That Generate Coal Combustion	19
Figure 2.7	Particle Image of CBA Under (a) 100× and (b) 300×	24
Figure 2.8	Compressive Strength of Mortar Containing Untreated CBA	31
Figure 2.9	The Effect of Coal Waste and Coal Waste Ash on Tensile Strength	31
Figure 2.10	3-D Surface Plot of TSR Versus Lime and Grading	41
Figure 2.11	Predicted Versus Actual Values of UCS	42
Figure 2.12	3-D Model of Each Parameter	43
Figure 3.1	Research Methodology Framework	47
Figure 3.2	Framework of Phase 1	53
Figure 3.3	Framework of Phase 2	66
Figure 3.4	Framework of Phase 3	70
Figure 3.5	Framework of Phase 4	76
Figure 4.1	Particle Size Distribution Curve of CA	83
Figure 4.2	Particle Size Distribution Curve of Proposed CIPR Mix	84
Figure 4.3	Particle Size Distribution Curve of Site 1 and 2	85
Figure 4.4	Microstructure of CBA at (a) 300× and (b) 1000× Magnifying Power	95
Figure 4.5	Microstructure of GCBA at (a) 300× and (b) 1000× Magnifying Power	96

Figures	Title	Page
Figure 4.6	Microstructure of OPC at (a) 300× and (b) 1000× Magnifying Power	96
Figure 4.7	Microstructure of 3% GCBA + 1% OPC at (a) 300× and (b) 1000× Magnifying Power	97
Figure 4.8	Microstructure of 3% GCBA + 1% OPC + 1% $CaCl_2$ at (a) 300× and (b) 1000× Magnifying Power	97
Figure 4.9	Microstructure of 3% GCBA + 1% OPC + 2% $CaCl_2$ at (a) 300× and (b) 1000× Magnifying Power	98
Figure 4.10	Microstructure of 3% GCBA + 1% OPC + 3% $CaCl_2$ at (a) 300× and (b) 1000× Magnifying Power	98
Figure 4.11	Microstructure of 2% GCBA + 2% OPC at (a) 300× and (b) 1000× Magnifying Power	99
Figure 4.12	Microstructure of 2% GCBA + 2% OPC + 1% $CaCl_2$ at (a) 300× and (b) 1000× Magnifying Power	99
Figure 4.13	Microstructure of 2% GCBA + 2% OPC + 2% $CaCl_2$ at (a) 300× and (b) 1000× Magnifying Power	100
Figure 4.14	Microstructure of 2% GCBA + 2% OPC + 3% $CaCl_2$ at (a) 300× and (b) 1000× Magnifying Power	100
Figure 4.15	Microstructure of 1% GCBA + 3% OPC at (a) 300× and (b) 1000× Magnifying Power	101
Figure 4.16	Microstructure of 1% GCBA + 3% OPC + 1% $CaCl_2$ at (a) 300× and (b) 1000× Magnifying Power	101
Figure 4.17	Microstructure of 1% GCBA + 3% OPC + 2% $CaCl_2$ at (a) 300× and (b) 1000× Magnifying Power	102
Figure 4.18	Microstructure of 1% GCBA + 3% OPC + 3% $CaCl_2$ at (a) 300× and (b) 1000× Magnifying Power	102
Figure 4.19	Microstructure of 4% OPC + 1% $CaCl_2$ at (a) 300× and (b) 1000× Magnifying Power	103
Figure 4.20	Microstructure of 4% OPC + 2% $CaCl_2$ at (a) 300X and (b) 1000× Magnifying Power	103

Figures	Title	Page
Figure 4.21	Microstructure of 4% OPC + 3% $CaCl_2$ at (a) 300× and (b) 1000× Magnifying Power	104
Figure 4.22	Spectroscopy of GCBA	105
Figure 4.23	Spectroscopy of OPC	105
Figure 4.24	Spectroscopy of 3% GCBA + 1%OPC	106
Figure 4.25	Spectroscopy of 3% GCBA + 1%OPC + 1% $CaCl_2$	106
Figure 4.26	Spectroscopy of 3% GCBA + 1%OPC + 2% $CaCl_2$	106
Figure 4.27	Spectroscopy of 3% GCBA + 1%OPC + 3% $CaCl_2$	107
Figure 4.28	Spectroscopy of 2% GCBA 2% OPC	107
Figure 4.29	Spectroscopy of 2% GCBA 2% OPC + 1% $CaCl_2$	107
Figure 4.30	Spectroscopy of 2% GCBA 2% OPC + 2% $CaCl_2$	108
Figure 4.31	Spectroscopy of 2% GCBA 2% OPC + 3% $CaCl_2$	108
Figure 4.32	Spectroscopy of 1% GCBA 3% OPC	108
Figure 4.33	Spectroscopy of 1% GCBA 3% OPC + 1% $CaCl_2$	109
Figure 4.34	Spectroscopy of 1% GCBA 3% OPC + 2% $CaCl_2$	109
Figure 4.35	Spectroscopy of 1% GCBA 3% OPC + 3% $CaCl_2$	109
Figure 4.36	Spectroscopy of 4% OPC + 1% $CaCl_2$	110
Figure 4.37	Spectroscopy of 4% OPC + 2% $CaCl_2$	110
Figure 4.38	Spectroscopy of 4% OPC + 3% $CaCl_2$	110
Figure 4.39	Moisture Content Versus. Dry Density Curve	117
Figure 4.40	Bulk Density for CA75RAP25 Mix	119
Figure 4.41	Bulk Density for CA50RAP50 Mix	120
Figure 4.42	Bulk Density for CA25RAP75 Mix	120
Figure 4.43	Bulk Density for 1% OPC + 1% GCBA + Various Percentages of $CaCl_2$	121
Figure 4.44	Bulk Density for 2% OPC + 2% GCBA + Various Percentages of $CaCl_2$	121
Figure 4.45	Bulk Density for 3% OPC + 1% GCBA + Various Percentages of $CaCl_2$	121
Figure 4.46	Bulk Density for 4% OPC + Various Percentages of $CaCl_2$	122

Figures	Title	Page
Figure 4.47	UCS for CA75RAP25 On Day 1	124
Figure 4.48	UCS for CA75RAP25 On Day 3	125
Figure 4.49	UCS for CA75RAP25 On Day 7	126
Figure 4.50	UCS for CA75RAP25 On Day 14	127
Figure 4.51	UCS for CA75RAP25 On Day 28	128
Figure 4.52	UCS for CA50RAP50 On Day 1	129
Figure 4.53	UCS for CA50RAP50 On Day 3	130
Figure 4.54	UCS for CA50RAP50 On Day 7	131
Figure 4.55	UCS for CA50RAP50 On Day 14	132
Figure 4.56	UCS for CA50RAP50 On Day 28	133
Figure 4.57	UCS for CA25RAP75 On Day 1	134
Figure 4.58	UCS for CA25RAP75 On Day 3	135
Figure 4.59	UCS for CA25RAP75 On Day 7	136
Figure 4.60	UCS for CA25RAP75 On Day 14	137
Figure 4.61	UCS for CA25RAP75 On Day 28	138
Figure 4.62	Impact of CA-RAP Ratio on Mix Design of 1% OPC + 3% GCBA with a) 0% $CaCl_2$, b) 1% $CaCl_2$, c) 2% $CaCl_2$ and d) 3% $CaCl_2$	141
Figure 4.63	Impact of CA-RAP Ratio on Mix Design of 2% OPC + 2% GCBA with a) 0% $CaCl_2$, b) 1% $CaCl_2$, C) 2% $CaCl_2$ and d) 3% $CaCl_2$	142
Figure 4.64	Impact of CA-RAP Ratio on Mix Design of 3% OPC + 1% GCBA with a) 0% $CaCl_2$, b) 1% $CaCl_2$, c) 2% $CaCl_2$ and d) 3% $CaCl_2$	143
Figure 4.65	Impact of CA-RAP Ratio on Mix Design of 4% OPC with a) 0% $CaCl_2$, b) 1% $CaCl_2$, c) 2% $CaCl_2$ and d) 3% $CaCl_2$	144
Figure 4.66	ITS for CA75RAP25 On Day 1	151
Figure 4.67	ITS for CA75RAP25 On Day 3	152
Figure 4.68	ITS for CA75RAP25 On Day 7	153
Figure 4.69	ITS for CA75RAP25 On Day 14	154

Figures	Title	Page
Figure 4.70	ITS for CA75RAP25 On Day 28	155
Figure 4.71	ITS for CA50RAP50 On Day 1	157
Figure 4.72	ITS for CA50RAP50 On Day 3	158
Figure 4.73	ITS for CA50RAP50 On Day 7	159
Figure 4.74	ITS for CA50RAP50 On Day 14	160
Figure 4.75	ITS for CA50RAP50 On Day 28	161
Figure 4.76	ITS for CA25RAP75 On Day 1	163
Figure 4.77	ITS for CA25RAP75 On Day 3	164
Figure 4.78	ITS for CA25RAP75 On Day 7	165
Figure 4.79	ITS for CA25RAP75 On Day 14	166
Figure 4.80	ITS for CA25RAP75 On Day 28	167
Figure 4.81	Impact of CA-RAP Ratio on Mix Design of 2% OPC + 2% GCBA with (a) 0% $CaCl_2$, (b) 1% $CaCl_2$ and (c) 2% $CaCl_2$	170
Figure 4.82	Impact of CA-RAP Ratio on Mix Design of 3% OPC + 1% GCBA with (a) 0% $CaCl_2$, (b) 1% $CaCl_2$ and (c) 2% $CaCl_2$	171
Figure 4.83	Impact of CA-RAP Ratio on Mix Design of 4% OPC with (a) 0% $CaCl_2$, (b) 1% $CaCl_2$ and (c) 2% $CaCl_2$	172
Figure 4.84	M_R for CA75RAP25 On Day 1	175
Figure 4.85	M_R for CA75RAP25 On Day 3	176
Figure 4.86	M_R for CA75RAP25 On Day 7	177
Figure 4.87	M_R for CA75RAP25 On Day 14	178
Figure 4.88	M_R for CA75RAP25 On Day 28	179
Figure 4.89	M_R for CA50RAP50 On Day 1	180
Figure 4.90	M_R for CA50RAP50 On Day 3	181
Figure 4.91	M_R for CA50RAP50 On Day 7	182
Figure 4.92	M_R for CA50RAP50 On Day 14	183
Figure 4.93	M_R for CA50RAP50 On Day 28	184
Figure 4.94	M_R for CA25RAP75 On Day 1	185
Figure 4.95	M_R for CA25RAP75 On Day 3	186

Figures	Title	Page
Figure 4.96	M_R for CA25RAP75 On Day 7	187
Figure 4.97	M_R for CA25RAP75 On Day 14	188
Figure 4.98	M_R for CA25RAP75 On Day 28	189
Figure 4.99	Impact of CA-RAP Ratio on Mix Design of 2% OPC + 2% GCBA with (a) 0% $CaCl_2$, (b) 1% $CaCl_2$ and (c) 2% $CaCl_2$	192
Figure 4.100	Impact of CA-RAP Ratio on Mix Design of 3% OPC + 1% GCBA with (a) 0% $CaCl_2$, (b) 1% $CaCl_2$ and (c) 2% $CaCl_2$	193
Figure 4.101	Impact of CA-RAP Ratio on Mix Design of 4% OPC with (a) 0% $CaCl_2$, (b) 1% $CaCl_2$ and (c) 2% $CaCl_2$	194
Figure 4.102	3-D Model of UCS Analysis for CA75RAP25 Mix Design Consist of (a) 2% OPC + 2% GCBA, (b) 3% OPC + 1% GCBA and (c) 4% OPC with Various Percentages of $CaCl_2$	207
Figure 4.103	3-D Model of UCS Analysis for CA50RAP50 Mix Design Consist of (a) 2% OPC + 2% GCBA, (b) 3% OPC + 1% GCBA and (c) 4% OPC with Various Percentages of $CaCl_2$	208
Figure 4.104	3-D Model of UCS Analysis for CA25RAP75 Mix Design Consist of (a) 2% OPC + 2% GCBA, (b) 3% OPC + 1% GCBA and (c) 4% OPC with Various Percentages of $CaCl_2$	209
Figure 4.105	Predictive Versus Actual Graph of UCS Analysis for CA75RAP25 Mix Design Consist of (a) 2% OPC + 2% GCBA, (b) 3% OPC + 1% GCBA and (c) 4% OPC with Various Percentages of $CaCl_2$	211
Figure 4.106	Predictive Versus Actual Graph of UCS Analysis for CA50RAP50 Mix Design Consist of (a) 2% OPC + 2% GCBA, (b) 3% OPC + 1% GCBA and (c) 4% OPC with Various Percentages of $CaCl_2$	212

Figures	Title	Page
Figure 4.107	Predictive Versus Actual Graph of UCS Analysis for CA25RAP75 Mix Design Consist of (a) 2% OPC + 2% GCBA, (b) 3% OPC + 1% GCBA and (c) 4% OPC with Various Percentages of $CaCl_2$	214
Figure 4.108	3-D Model of ITS Analysis for CA75RAP25 Mix Design Consist of (a) 2% OPC + 2% GCBA, (b) 3% OPC + 1% GCBA and (c) 4% OPC with Various Percentages of $CaCl_2$	220
Figure 4.109	3-D Model of ITS Analysis for CA50RAP50 Mix Design Consist of (a) 2% OPC + 2% GCBA, (b) 3% OPC +1% GCBA and (c) 4% OPC With Various Percentages of $CaCl_2$	221
Figure 4.110	3-D Model of ITS Analysis for CA25RAP75 Mix Design Consist of (a) 2% OPC + 2% GCBA, (b) 3% OPC +1% GCBA and (c) 4% OPC With Various Percentages of $CaCl_2$	222
Figure 4.111	Predictive Versus Actual Graph of ITS Analysis for CA75RAP25 Mix Design Consist of (a) 2% OPC + 2% GCBA, (b) 3% OPC +1% GCBA and (c) 4% OPC With Various Percentages of $CaCl_2$	224
Figure 4.112	Predictive Versus Actual Graph of ITS Analysis for CA50RAP50 Mix Design Consist of (a) 2% OPC + 2% GCBA, (b) 3% OPC +1% GCBA and (c) 4% OPC With Various Percentages of $CaCl_2$	225
Figure 4.113	Predictive Versus Actual Graph of ITS Analysis for CA25RAP75 Mix Design Consist of (a) 2% OPC + 2% GCBA, (b) 3% OPC +1% GCBA and (c) 4% OPC With Various Percentages of $CaCl_2$	226

Figures	Title	Page
Figure 4.114	3-D Model of M_R Analysis for CA75RAP25 Mix Design Consist of (a) 2% OPC + 2% GCBA, (b) 3% OPC +1% GCBA and (c) 4% OPC With Various Percentages of $CaCl_2$	232
Figure 4.115	3-D Model of M_R Analysis for CA50RAP50 Mix Design Consist of a(a) 2% OPC + 2% GCBA, (b) 3% OPC +1% GCBA and (c) 4% OPC With Various Percentages of $CaCl_2$	233
Figure 4.116	3-D Model of M_R Analysis for CA25RAP75 Mix Design Consist of (a) 2% OPC + 2% GCBA, (b) 3% OPC +1% GCBA and (c) 4% OPC With Various Percentages of $CaCl_2$	234
Figure 4.117	Predictive Versus Actual Graph of M_R Analysis for CA75RAP25 Mix Design Consist of (a) 2% OPC + 2% GCBA, (b) 3% OPC +1% GCBA and (c) 4% OPC With Various Percentages of $CaCl_2$	236
Figure 4.118	Predictive Versus Actual Graph of M_R Analysis for CA50RAP50 Mix Design Consist of (a) 2% OPC + 2% GCBA, (b) 3% OPC +1% GCBA and (c) 4% OPC With Various Percentages of $CaCl_2$	237
Figure 4.119	Predictive Versus Actual Graph of M_R Analysis for CA25RAP75 Mix Design Consist of (a) 2% OPC + 2% GCBA, (b) 3% OPC +1% GCBA and (c) 4% OPC With Various Percentages of $CaCl_2$	239

LIST OF PLATES

Plates	Title	Page
Plate 2.1	CIPR Process (a) Milling of Asphalt, (b) Distribution of Cement (c) Spreading of Cement, (d) Recycling Process (e) Compaction and (f) Placement of Premix as Finish Layer	13
Plate 3.1	Sampling Location (a) Jalan Bandar Baharu - Merbau Pulas, Kulim, Kedah and (b) Jalan Butterworth - Ipoh, Pulau Pinang	49
Plate 3.2	CIPR Sample	49
Plate 3.3	RAP Sample	50
Plate 3.4	Stabilizing Agent Consist of (a) OPC, (b) GCBA and (c) $CaCl_2$	51
Plate 3.5	Sample of GCBA	57
Plate 3.6	Elongation Gauge	58
Plate 3.7	Flakiness Thickness Gauge	58
Plate 3.8	LA Abrasion Drum	60
Plate 3.9	Aggregate Impact Test	61
Plate 3.10	pH Meter	62
Plate 3.11	SEM Analysis Machine	62
Plate 3.12	XRD Analysis Setup (a) XRD Specimen and (b) XRD Machine	64
Plate 3.13	Modified Proctor Test Specimen	67
Plate 3.14	Compaction Test of Bulk Density Determination	68
Plate 3.15	UCS Testing (a) UCS 100 mm Briquettes Specimen, (b) Specimen Before and (c) After Test	71
Plate 3.16	ITS Testing (a) Before and (b) After	73
Plate 3.17	Specimen Under Resilient Modulus Test	74

LIST OF SYMBOLS

Symbols

α	Alpha
Å	Ångström (Unit of Length, 1 Å = 0.1 Nanometers)
^{o}C	Degree Celsius
G	Gravity
d_{mean}	Mean Diameter
µm	Micrometer
±	Plus-Minus
R^2	Proportion of the Variance in the Dependent Variable
Gs	Specific Gravity
θ	Theta
ΔH_T	Total Recoverable Horizontal Deformation
V_{RT}	Total Resilient Poisson's Ratio
λ	Wavelength

LIST OF ABBREVIATIONS

Abbreviations

ARRA	Asphalt Recycling Association
ASTM	American Society for Testing and Materials
BS	British Standard
CA	Crushed Aggregate
$CaCl_2$	Calcium Chloride
CBA	Coal Bottom Ash
CBR	California Bearing Ratio
CCD	Central Composite Design
CCP	Coal Combustion Power Plants
CEM	Calcium-Enriched Mixture
CIPR	Cold In-Place Recycling
EDX	Energy Dispersive X-Ray
EN	European Standards
FA	Fly Ash
FS	Flexural Strength
GCBA	Ground Coal Bottom Ash
ITS	Indirect Tensile Strength
JKR	Jabatan Kerja Raya (Public Work Dept., PWD)
LA Abrasion	Los Angeles Abrasion
LVDT	Linear Variable Differential Transducer
MDD	Maximum Dry Density
MS	Malaysian Standard
OBC	Optimum Binder Content
OMC	Optimum Moisture Content
OPC	Ordinary Portland Cement
PWD	Public Work Department
RAP	Reclaimed Asphalt Pavement
RCCP	Roller-Compacted Concrete Pavement

RSM	Response Surface Methodology
SCM	Supplemental Cementitious Material
SDG	Sustainable Development Goals
SEM	Scanning Electron Microscope
SIRIM	Standard And Industrial Research Institute of Malaysia
TNB	Tenaga Nasional Berhad
TSR	Tensile Strength Ratio
UCS	Unconfine Compressive Strength
UTM	Universal Testing Machine

CHAPTER 1
INTRODUCTION

1.1 Research Background

Under the Twelfth Malaysia Plan (RMK-12) 2021-2025, infrastructure development strongly emphasizes sustainability, durability, and the efficient management of existing assets rather than extensive new construction (Economic Planning Unit, 2021). In line with this national agenda, the road network remains one of the most critical infrastructure systems, playing an important role in supporting economic growth, mobility, and social connectivity. According to *Statistik Jalan Malaysia Edisi 2023* (JKR, 2023), published by the Malaysian Public Works Department (JKR), the total road network in Malaysia covering federal, state, and other agency roads reached beyond 289,000 km as of December 2022. This requires substantial and continuous investment in maintenance and rehabilitation to ensure long-term serviceability, structural performance, and cost-effective asset management, consistent with the objectives outlined in RMK-12.

Despite these strategic efforts, achieving the intended service life of pavements under RMK-12 is increasingly challenging due to rising traffic demand and induced stresses, particularly from heavy vehicles operating under higher loads and frequencies. The loading magnitude, configuration, and frequency of heavy vehicles significantly affect the performance of the pavements (Alnadish et al, 2025; Sharad and Gupta, 2015). Increased traffic volume, larger and heavier trucks carrying loads above the intended weight limit, and higher tyre pressures have all contributed to pavement deterioration and a reduced service lifespan (Qadir et al., 2024; Nurhidayat and Kamarudin, 2024). To address these challenges, a well-designed pavement structure must not only meet functional requirements but also ensure structural durability. More importantly, it must be capable of distributing traffic loads effectively so that the stresses transmitted by wheel loads are minimized, thereby preventing damage to the bearing capacity of the subgrade and base layers (Lilian et al., 2025; Matthew, 2009). When the base layer is unable to support traffic loads, structural damage can occur, often requiring reconstruction through the removal and replacement of the affected section. This

conventional approach generates significant waste, mainly due to the disposal and long-distance transport of damaged asphalt and foundation materials.

As a sustainable alternative, the Cold In-Place Recycling (CIPR) method has gained attention for its ability to reuse existing pavement materials, known as Reclaimed Asphalt Pavement (RAP), to reconstruct the base layer. By milling the existing asphalt to a specified depth and mixing it with stabilizing agents, CIPR reduces material waste and lowers rehabilitation costs compared to conventional methods (Cao et al., 2024). Ensuring the structural integrity of the recycled base layer is essential, which is achieved using appropriate stabilizing agents. Common chemical stabilizers used in Malaysia include cement and lime, with the choice depending on the type of existing pavement, required strength, and cost. The first CIPR project in Malaysia was implemented in 1985, followed by larger projects in 1989, establishing CIPR as a widely accepted method for pavement repair (Sufian et al., 2009). Figure 1.1 illustrates a comparison between the conventional and CIPR methods.

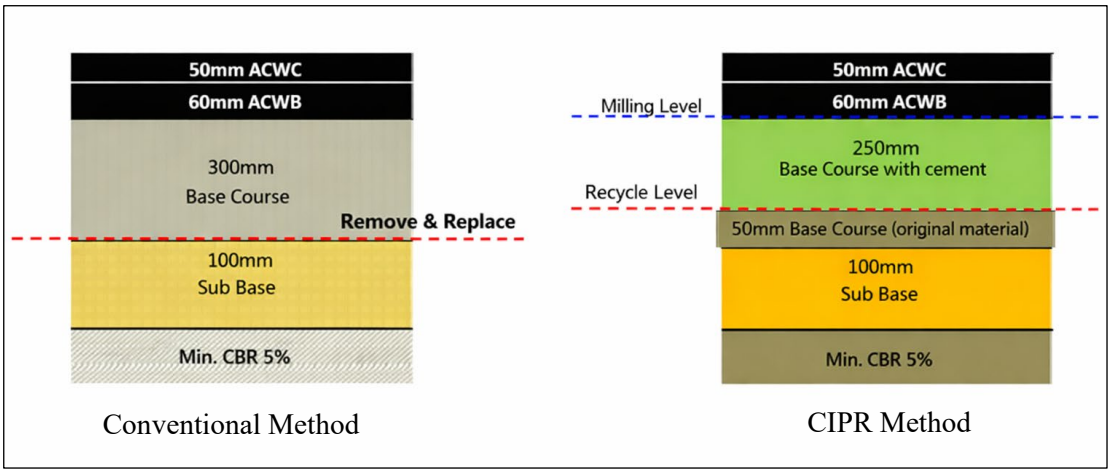


Figure 1.1 Comparison of Conventional and CIPR Methods (Selia Group, 2018)

Ordinary Portland Cement (OPC) has historically been the most commonly used chemical stabilizer for CIPR in Malaysia. Identifying alternative materials to partially replace OPC is essential for sustainable development and for reducing reliance on natural resources, preserving them for future generations. The increased consumption of these resources has contributed to environmental degradation and industrial waste accumulation (Khankhaje et al., 2015). Consequently, researchers are increasingly interested in using industrial waste materials to replace natural resources in the

construction sector, focusing on the sustainability of construction materials (Parera and Ranjit, 2025; Sabrin et al., 2024; Singh et al, 2023).

One such waste is Coal Bottom Ash (CBA), which is produced by coal-based thermal power plants and can be effectively utilized. CBA has long been recognized as a construction material, but its use as a cement alternative remains minimal due to its relatively large particle size and high porosity. Compared to Fly Ash (FA), CBA has a coarser texture with particle morphologies closer to natural sand (Ku Meh et al., 2022; Wongkeo, 2010). As such, raw CBA is generally regarded as an inert material unsuitable as a supplementary cementing ingredient, though it has been used as a fine aggregate replacement in various civil engineering applications. To overcome the limitations of raw CBA, researchers have explored grinding it into finer particles to increase surface area and enhance reactivity (Schackow et al, 2025; Guan et al, 2023; Awang, 2012). When finely ground, CBA exhibits pozzolanic properties similar to those of FA (Zainal, 2014). Given the proven success of FA as a cement replacement in pozzolanic Portland cement, mortar, and concrete, Ground Coal Bottom Ash (GCBA) shows strong potential as either a partial cement replacement (stabilizing agent) or a filler material in pavement recycling (Poudel et al., 2024: Kim et al., 2024; Chuang et al., 2023).

While GCBA improves the pozzolanic activity and filler effect in cementitious mixtures, the addition of chemical accelerators like Calcium Chloride ($CaCl_2$) can complement its role by accelerating cement hydration and enhancing early strength gain (Wang et al., 2022; Haro et al., 2018; Kishar et al., 2013). Beyond concrete applications, $CaCl_2$ has also been shown to improve the performance of expansive soils by reducing plasticity, swelling potential, and increasing strength when combined with cement (Almajed et al., 2023). Given its availability and relatively low cost (Sharma, 2024; Kishar et al., 2013), $CaCl_2$ is considered a practical and effective supplement to conventional cementitious stabilizers in pavement construction.

Despite growing interest in sustainable pavement technologies, comprehensive data on the engineering performance of CIPR mixes stabilized with OPC, GCBA, and $CaCl_2$ remain limited. Addressing this research gap is essential to optimize material use, reduce OPC consumption, and enhance the performance of recycled pavements. Moreover, this research aligns with the Malaysia Sustainable Development Goals (SDG), particularly SDG 9 (Industry, Innovation, and Infrastructure) and SDG 11 (Sustainable Cities and Communities), emphasizing the broader relevance of

sustainable pavement rehabilitation to government policy, industry practices, and societal benefits.

1.2 Problem Statement

Asphalt pavements generally have a service life of 10 to 15 years, requiring regular maintenance and timely repairs to extend their lifespan. According to ATJ 5/85 manual (Pindaan 2013) by JKR, a design period of 10 years is recommended for low-volume and rural roads, while a minimum of 20 years is suggested for roads with medium to high traffic volumes. JKR places a high priority on the maintenance and rehabilitation of local and federal roads to ensure safe and long-lasting infrastructure. Nevertheless, structural deterioration can still occur, often originating from weakening of the base layer due to traffic loads and moisture infiltration (Rokitowski et al., 2021). According to the JKR Standard Specifications for Road Works: Flexible Pavement (JKR/SPJ/2008-S4, 2008), the conventional approach to pavement rehabilitation recommended typically involves removal and replacement of severely damaged pavement sections, followed by overlaying with bituminous layers to restore structural capacity and serviceability. While effective, this approach can be costly and consumes significant raw materials (Joohari et al., 2024). CIPR offers a more sustainable alternative, particularly for damaged base layers, by reusing RAP along with a portion of the existing base material and stabilizing agent. In Malaysia, OPC is commonly incorporated into the CIPR process to act as a stabilizing agent, enhancing the strength and durability of the recycled base layer (Harun et al., 2010). During this process, the blended materials are mixed with water, compacted, and left to harden, forming a stronger, moisture-resistant layer that improves material efficiency compared to conventional repair methods (Mallick et al., 2002).

A key challenge in using cement-treated CIPR is the required curing period, as the material is prone to cracking and must be carefully managed. Arshad (2016) identified two main types of cracking in cement-treated materials: shrinkage cracks from cement hydration and traffic-induced cracks. Such cracks can reduce the strength of the base course, and if the base strength does not reach the optimum level, vehicles may impose significant loads during construction, forming microcracks that shorten the pavement lifespan (Zhang et al., 2015). During this stage of the CIPR process, only the completed pavement sections can safely support vehicle loads. JKR/SPJ/2008-S4

(2008) stated that cement-stabilized layers must be cured for a minimum of 72 hours or three days before being overlaid with hot mix asphalt. This requirement poses practical challenges, particularly on single-lane roads or heavily trafficked areas, as extended closures can cause significant traffic disruptions.

Therefore, this research examines the effect of incorporating GCBA and $CaCl_2$ alongside OPC as stabilizing agent to reduce the curing period while enhancing early strength development. Previous research has demonstrated that GCBA can improve the compressive strength of cementitious materials. However, such improvements typically become evident only after 28 days (Chuang and Chen, 2025; Menéndez et al., 2021; Bajare et al., 2013). To accelerate this process, $CaCl_2$ is introduced as a chemical accelerator. Adding 1-2% $CaCl_2$ may promote faster cement hydration, potentially reducing the curing period by up to two-thirds (Occidental Chemical Corporation, 2006). Despite its promising potential, this specific combination of stabilizing agent has not yet been implemented in CIPR base layer in Malaysia, primarily due to limited awareness and a lack of comprehensive performance data among pavement engineers. This research aims to address this gap by evaluating the mechanical performance of the proposed stabilizing agent, thereby supporting their practical application in sustainable pavement rehabilitation.

1.3 Objectives

The purpose of this research is to assess the performance of stabilized CIPR base course using GCBA, OPC and $CaCl_2$ as stabilizing agent. This is achieved through the following objectives, undertaken in number of phases:

1. To investigate the material characterization of the CIPR base course stabilized with GCBA, OPC, and $CaCl_2$.
2. To determine the compaction properties of the CIPR mix design using various compositions of Crushed Aggregate (CA), Reclaimed Asphalt Pavement (RAP), and stabilizing agent.
3. To evaluate the early and overall strength development of the stabilized CIPR mix design incorporating the proposed stabilizing agent.

4. To develop a statistical model using Response Surface Methodology (RSM) for strength verification, prediction and material optimization of the proposed mix design.

1.4 Scope and Limitation of Research

This research examined the mechanical performance of CIPR pavement base layers that were stabilized using a combination of GCBA, OPC and $CaCl_2$. The focus was limited to the base layer only, utilizing mixes primarily composed of RAP and CA, without extending the analysis to the subgrade layer or surface course.

CIPR samples were obtained from pavement rehabilitation works carried out by THB Maintenance in Kedah and Penang while CA obtain from quarry in Kajang. RAP was sourced from a construction site in Putrajaya. The CBA used in this research was obtained from TNB Jana Manjung, Perak. Testing took place at the Highway and Geotechnical Laboratories of Universiti Teknologi MARA, Cawangan Pulau Pinang and Shah Alam.

The experimental work included extensive laboratory testing to evaluate the material characterization, compaction properties and strength performance. A total of 1,530 specimens were prepared specifically for the strength performance tests, which included Unconfined Compressive Strength (UCS), Indirect Tensile Strength (ITS), and Resilient Modulus (M_R). Additionally, RSM was used to develop statistical models for optimizing the proportions of stabilizing agent.

Despite the comprehensive approach, the research had several limitations. Field validation was not conducted, and the research was restricted to laboratory-scale experiments under controlled conditions. The influence of environmental factors, long-term durability, and economic analysis were outside the scope of this research. Furthermore, only specific combinations and proportions of stabilizing agent was considered, while the broader range of material properties were not explored.

1.5 Significance of Research

Using recyclable materials to construct new foundation layers offers a cost-effective and sustainable solution for infrastructure projects. CIPR is known for its environmental and economic benefits. By reusing RAP and existing CA, it reduces the

need for new materials and lowers transportation costs. Additionally, recycling RAP also helps reduce construction waste and supports a circular economy.

This research aimed to improve pavement performance by developing a mix design that enhances the base layer, which in turn strengthens the overall pavement structure and ultimately results in smoother and more durable surfaces. A smoother pavement condition increases comfort, improves travel efficiency, and reduces vehicle wear and tear, leading to lower operating costs for road users.

From an industry perspective, the research provided new insights into the use of a combination of GCBA, OPC, and $CaCl_2$ as stabilizing agent in the CIPR method. The findings could assist practitioners, government agencies including JKR, in exploring alternative materials for pavement rehabilitation.

Environmentally, the research helps reduce the accumulation of CBA waste by repurposing it in pavement construction, promoting greener and more sustainable practices.

Overall, the outcomes of this research have practical relevance for government agencies, industry stakeholders, and society by supporting more efficient, durable, and environmentally responsible pavement construction.

1.6 Research Thesis Outline

This research thesis is organized into five chapters. Chapter 1 introduces the background of research, states the problem, outlines the objectives, discusses the scope and significance of research. Chapter 2 provides a literature review on CIPR, including the properties of various stabilizing agents, the applications of proposed materials in the construction industries, the method used to assess the mechanical performance and the model development. Chapter 3 outlines the experimental design, laboratory procedures, and data analysis methodologies used in this research. Chapter 4 presents the analysis of the results and discusses the findings. Finally, Chapter 5 offers the conclusion and recommendations based on the findings.

CHAPTER 2
LITERATURE REVIEW

2.1 Introduction

This chapter presents a comprehensive literature review related to CIPR. It begins with a brief overview of asphalt recycling, followed by a discussion of the CIPR process. Various stabilizing agents reported in the literature are reviewed, with a focus on the characteristic properties and performance of GCBA, OPC, and $CaCl_2$, which are the primary stabilizing materials used in this study. The review also considers the criteria and guidelines established by JKR in the Standard Specification for Road Works, Section 4: Flexible Pavement (JKR/SPJ/2008-S4), which provide benchmarks for the suitability and quality of stabilized base layer. Finally, previous research on methods for developing predictive models is presented at the end of the chapter.

2.2 Asphalt Recycling

Pavement waste management has become a growing global concern due to its contribution to landfill overcrowding and the reduction of habitable land. Taha et al. (2002) reported that approximately 50 million tons of asphalt were milled annually in the United States. In response, engineers developed recycling techniques to mitigate environmental impacts (Delancy, 1976). The rising costs of energy and asphalt binder further highlight the need for efficient recycling and reclamation methods to enhance life-cycle performance and support cost-effective pavement rehabilitation. Asphalt pavement recycling reduces the consumption of natural resources such as aggregates, asphalt binders, and fuels, thereby promoting a more sustainable transportation infrastructure.

New strategies involving the reuse of RAP have been continually developed and tested to address the increasing volumes of RAP generated during pavement rehabilitation and reconstruction works (Sukhija and Coleri, 2025; Zhang et al., 2022). Asphalt recycling is considered one of the most viable solutions for engineers seeking sustainable and efficient pavement practices. As defined by the Asphalt Recycling and

Reclaiming Association (ARRA), asphalt recycling can be broadly classified into five categories. These categories are:

a. Cold Planning (CP)
b. Hot Recycling
c. Hot In-Place Recycling (HIPR)
d. Cold In-Place Recycling (CIPR)
e. Full Depth Reclamation (FDR)

However, CIPR techniques have become increasingly popular in recent decades for reconstructing low-volume roadways. These techniques are generally categorized as either CIPR or FDR, depending on the milling depth. CIPR typically refers to the reclamation of most of the existing asphalt concrete layer(s), whereas FDR involves the recycling of the entire asphalt layer along with a significant portion of the underlying base materials. Although the distinction between the two methods has only become clear in recent years, some interchangeability in their terminology is still observed (Berthelot et al., 2000).

The CIPR method has been shown to be effective in extending the service life of rehabilitated pavements by up to 15 years through improvements in structural strength (Kim et al., 2011), which this research intends to further examine and build upon.

2.3 Cold-In Place Recycling

CIPR is a pavement rehabilitation technique that reuses existing pavement materials in their original location without the use of heat (ARRA, 1992). In this process, the asphalt components are pulverized in place, compacted to form a new base, and overlaid with a wearing course to restore the pavement surface (Arshad, 2006). As a cold recycling method, CIPR addresses various issues associated with ageing asphalt pavements. Arshad (2006) also reported that CIPR alleviates a range of pavement distresses, including rutting, cracking, surface irregularities, and minor foundation problems. It serves as an alternative to traditional structural overlays and full reconstruction methods. ARRA (1992) defines CIPR as a partial-depth recycling process targeting the existing surface layer.

CIPR involves the complete pulverization of the asphalt layer along with a portion of the unbound aggregate base. Partial-depth recycling typically utilizes 50-100 mm of the asphalt layer to create a new base course and is generally applied to thicker, more uniform asphalt pavements using specialized recycling equipment (Cox and Howard, 2013). Meanwhile, FDR is conducted to depths of up to 300 mm, although common applications range between 150 and 225 mm (Better Roads, 2001). The crushed material is blended with stabilizing agents and reused as a stabilized base course (Kandhal, 1997). Although termed "full-depth reclamation," this technique essentially extends the CIPR principle to the entire HMA layer and a designated portion of the subbase. As shown in Figure 2.1, the CIPR process involves in situ pulverization and blending of the asphalt with the underlying base material, allowing the pavement to be rehabilitated without altering existing elevations.

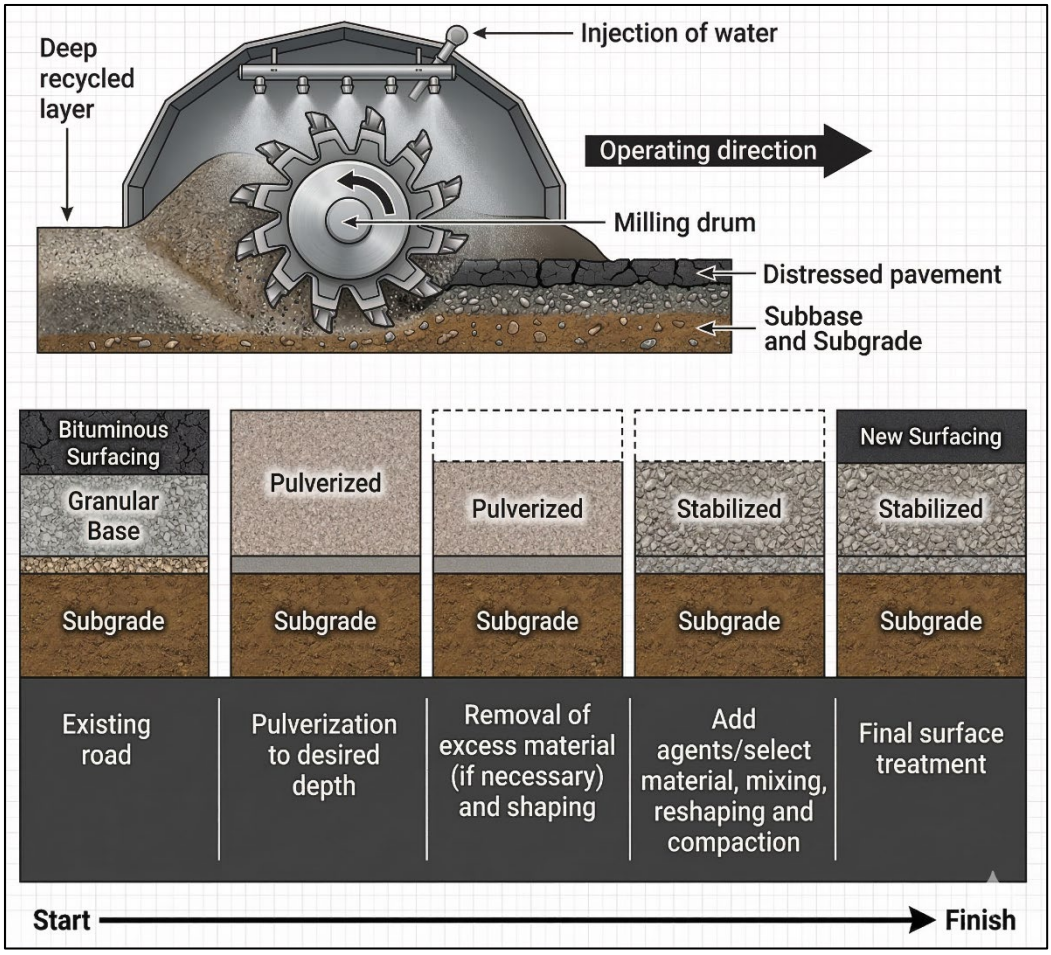


Figure 2.1 CIPR Process (Ruston Paving, 2023)

Accordingly, the advantages and limitations of CIPR can be evaluated to understand its effectiveness in pavement rehabilitation.

2.4 Advantages and Disadvantages of Cold-In Place Recycling

CIPR offers several advantages over conventional pavement restoration methods, particularly in terms of cost savings and sustainability. Liu et al. (2022) and Guthrie et al. (2007) provided a more detailed explanation of the advantages of CIPR as follows:

a. Ecological advantages: Most CIPR materials can be recycled directly on-site, which decreases the need for transporting materials and, consequently, reduces noise pollution from heavy vehicles. This reduction in transport also lowers greenhouse gas (GHG) emissions. Additionally, because CIPR utilizes cold asphalt, the mixing process typically occurs at ambient temperatures. Unlike hot recycling (HR), which requires heating asphalt to 120-160 °C, CIPR significantly reduces fuel consumption and associated GHG emissions by eliminating the need for additional heating.
b. Operational advantages: The use of integrated systems for milling, mixing, paving, and compacting during road recycling, which improve construction efficiency as well as transportation safety and convenience.
c. Sustainable advantages: The asphalt pavement recovered through recycling can be reused to produce fresh RAP aggregates, eliminating the need to test newly sourced RAP before construction.
d. Environmental advantages: CIPR significantly reduces the volume of debris destined for landfill.

Despite these advantages, CIPR is not without limitations. One key drawback is the necessary curing period required for strength development, especially when cement is used as the primary stabilizing agent. Moreover, factors such as ambient temperature, moisture content, and wind conditions play a critical role in affecting construction quality and the long-term performance of the recycled pavement layers (Zhao et al., 2023; Liu et al., 2022: FHWA, 2019a).

To address these limitations and ensure consistent performance, it is important to examine the materials used in CIPR construction.

2.5 Materials of Cold-In Place Recycling Mix

According to ARRA (2006), the CIPR mix can consist of a homogeneous blend of aggregate, RAP, stabilizing agent, and water. Additional additives may also be incorporated if necessary. The selection of materials and their application rates is determined based on the mix design and specific project requirements.

Only asphalt-coated materials are permitted for use as RAP and must be free from contamination such as silt, clay, or dirt (ARRA, 2012). The RAP must be reclaimed from the existing pavement and processed according to contract specifications. As stated by FHWA (1998), milled RAP generally exhibits a finer and denser gradation compared to virgin aggregates. Factors such as the type of milling machinery used, the composition of the original asphalt aggregate, and whether underlying base or subbase materials are unintentionally incorporated during removal can all influence the particle size distribution of the milled or crushed RAP. ARRA (2006) further specifies that 100% of the RAP must pass through a 1.25-inch (31.5 mm) sieve. To ensure structural integrity, the materials must be properly blended and proportioned so as not to compromise the base strength of the pavement.

Once the appropriate materials are identified, the subsequent stage involves the systematic execution of the CIPR construction process. Understanding how these materials are handled, blended, placed, and compacted is essential to ensure that the recycled base layer achieves the intended mechanical performance and long-term durability.

2.6 Cold In-Place Recycling Process

CIPR is carried out using specialized recycling machines equipped with a milling drum containing numerous hardened steel picks at its core (Lewis et al., 1999). The process begins with milling the existing asphalt layer, with the milling depth determined based on the desired final asphalt layer elevation. If the milled surface falls below the required level, an additional aggregate layer is placed to achieve the target elevation.

Next, the stabilizing agent, typically cement, is manually applied and evenly distributed across the recycling section. The recycling machine then scarifies the existing pavement layers, including the cement, to a depth ranging from 150 mm to 200

mm, depending on the structural design of the pavement. During the milling and mixing process, water is supplied from a tanker positioned ahead of the recycler. This water is delivered through a flexible hose and sprayed into the mixing chamber. A microprocessor-controlled pumping system ensures that the water is precisely metered and thoroughly mixed with the pulverized material to achieve the optimal moisture content for compaction (Lewis et al., 1999).

Following the recycling process, the material is initially compacted using a roller, and a motor grader profiles the surface. A vibratory roller is then used to achieve the required density. If the mix is stabilized with cement or bitumen emulsion, a curing period is necessary for strength development before the pavement can be opened to traffic. Finally, a surface course consisting of a binder and wearing layer is placed over the recycled base to ensure a smooth riding surface (Arshad, 2006). Plate 2.1 illustrates the full sequence of the CIPR process.



Plate 2.1 CIPR Process (a) Milling of Asphalt, (b) Distribution of Cement (c) Spreading of Cement, (d) Recycling Process



Plate 2.1(cont.) CIPR Process (e) Compaction and (f) Placement of Premix as Finish Layer (Selia Group, 2018)

The effectiveness of this process depends largely on the properties and selection of the materials, with particular emphasis on the type of stabilizing agents used in the CIPR mix. This factor directly influences the strength and durability of the stabilized base.

2.7 Recycling with Stabilizing Agents

Stabilizing agent plays a crucial role in the CIPR process by enhancing the performance of the recycled pavement, particularly in terms of strength, durability, and resistance to moisture damage. According to ARRA, stabilization can be achieved through mechanical means, chemical additives, or the use of asphalt-based binders.

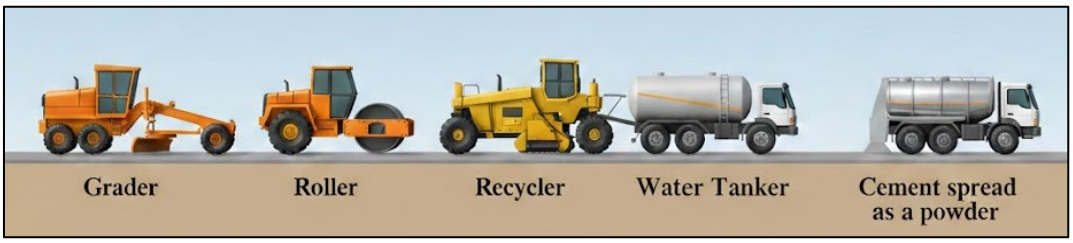
2.7.1 Cement Stabilizer

According to Lewis et al. (1999), when this stabilizing ingredient is utilized, typically between 2% and 4% (by mass) of cement is applied throughout the recycling process. Cement can be added in three different ways:

i. Spreading onto the surface of the pavement ahead of the recycler. The recycler goes over the spread cement in a single process, mixing it with the underlying material;
ii. Mixing with water to create a slurry in a specifically built design mixer which is then injected straight into the mixing chamber. This provides precise application rates and prevents cement waste; or

iii. Applying with the use of a specialized cement spreader built within the frame of the recycler.

The recycled layer is first profiled using a motor grader positioned behind the recycling machine, followed by compaction with a vibratory roller. To achieve a well-knitted and uniform surface finish, a rubber-tyred roller is typically employed as the final compaction stage. Once compaction is complete, a bituminous surfacing layer should be applied. Depending on the anticipated traffic load, this may range from a minimal surface treatment for lightly trafficked roads to one or more layers of hot-mix asphalt for heavily used pavements. The complete configuration of the recycling train is illustrated in Figure 2.2.



OR

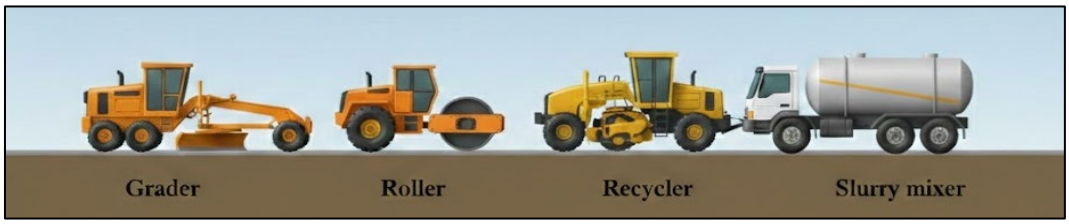


Figure 2.2 Recycling Train for Cement (Sufian et al., 2009)

2.7.2 Bitumen Emulsion Stabilizer

Emulsifying agents are used to combine bitumen and water to produce a bitumen emulsion, which typically consists of approximately 60% bitumen and 40% water. A key advantage of bitumen emulsion is its liquid state at room temperature, allowing it to be mixed with pavement-building materials without the need for heating, unlike in hot-mix asphalt production (Lewis et al., 1999).

In the CIPR process, bitumen emulsion is transported in a tanker positioned ahead of the recycling machine, as illustrated in Figure 2.3. A flexible hose transfers the emulsion to the recycling machine, where it is sprayed into the mixing chamber as the equipment moves forward. Inside the chamber, the milled pavement material is

thoroughly blended with the bitumen emulsion before being discharged from the rear of the recycler and shaped by a motor grader. The newly formed layer is then compacted using the same method applied to cement-treated layers (Lewis et al., 1999).

Bitumen emulsion is generally added to granular pavement materials at a rate of approximately 5% by mass. However, if the existing pavement contains a thick asphalt layer, the emulsion content can be reduced to between 3% and 4%, depending on the proportion of asphalt present in the mix (Lewis et al., 1999).

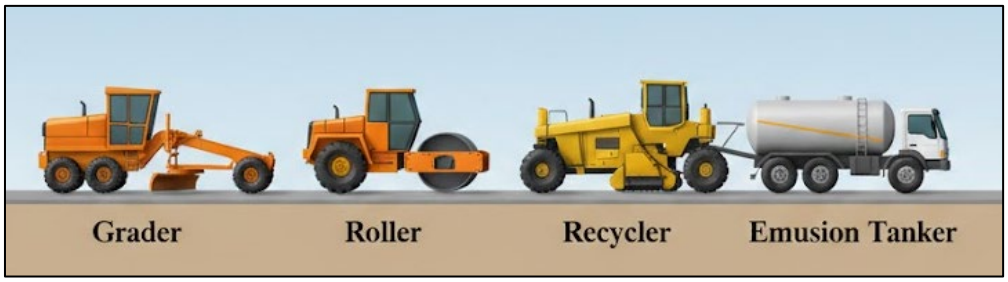


Figure 2.3 Recycling Train for Bitumen Emulsion (Lewis et al., 1999)

A combination of bitumen emulsion and cement has proven effective in many CIPR applications. The quantity of cement incorporated typically ranges from 1% to 3% by mass, depending on the selected mix design approach. It is blended with the bitumen emulsion and integrated into the recycled mix using the previously outlined procedures (Lewis et al., 1999). Figure 2.4 illustrates the configuration of the recycling train that incorporates both cement and bitumen emulsion in the stabilization process.

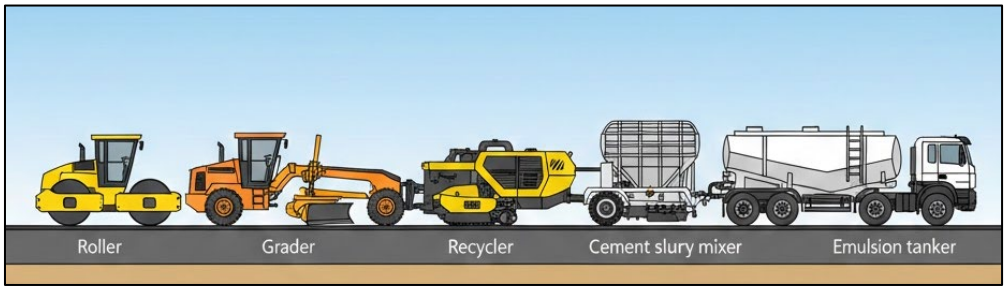


Figure 2.4 Recycling Train for Cement and Bitumen Emulsion (Lewis et al., 1999)

The following are some of the benefits of utilizing a mix of cement and bitumen emulsion:

i. Increased bitumen adhesion to the aggregate;
ii. Faster strength gain, allowing the road to be opened to traffic sooner; and
iii. Improved the final strength of the recycled layer.

2.7.3 Foamed Bitumen Stabilizer

Foamed bitumen is produced onboard the recycling machine through a process in which a small amount of water is injected into hot penetration-grade bitumen. Like bitumen emulsion, the foamed bitumen is sprayed directly into the mixing chamber of the recycling machine. The foaming process enables conventional grades of bitumen to be blended with cold, damp recycled materials without requiring prior emulsification.

For granular materials, foamed bitumen is typically applied at a rate of 3% to 5% by mass. When the recycled material contains a substantial proportion of existing asphalt, the foamed bitumen content is often reduced to between 2% and 3% (Lewis et al., 1999).

The addition of small quantities of cement, generally between 1% and 2%, has demonstrated performance enhancements in foamed bitumen mixes, similar to its role in bitumen emulsion stabilization. The cement may be introduced either in dry powder form or as a cement–water slurry, the latter prepared using a specialized slurry mixer (Lewis et al., 1999). Figure 2.5 illustrates a typical recycling train configuration that employs both foamed bitumen and cement.

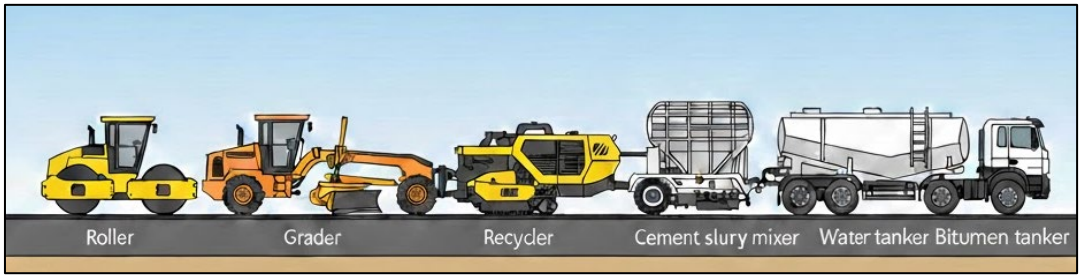


Figure 2.5 Recycling Train for Foamed Bitumen (Lewis et al., 1999)

In addition to conventional stabilizers, various alternative materials have been developed to improve the strength and durability of the base course, ultimately contributing to a longer-lasting asphalt layer. Pozzolanic materials such as lime, FA, and CBA have shown potential for use in combination with cement as effective base course stabilizers (Al Biajawi et al., 2022; Guan et al., 2023; Mousa, 2023).

The following section of the literature review focuses on the utilization of coal waste material which reflects the primary focus of this research.

2.8 Coal Waste

The use of novel cementitious stabilizing agents in the CIPR process offers a sustainable alternative to the conventional reliance on OPC, particularly in the Malaysian context. Among the potential materials, coal waste has emerged as a promising option due to its local availability and pozzolanic properties. Incorporating waste coal into OPC formulations contributes to sustainability by reducing energy consumption and the demand for raw materials.

Coal remains the most commonly used fuel in thermal power plants for electricity generation. In these facilities, raw coal is pulverized to a flour-like consistency before being force-fed into the furnace. During pulverization, clay particles and other non-combustible materials embedded in the coal are released. Upon combustion in the furnace, these residues form coal ash, which is categorized into FA and CBA. The finer and lighter particles are carried away by swirling flue gases and are subsequently captured by electrostatic precipitators before the exhaust enters the atmosphere.

In Malaysia, coal is found in Peninsular Malaysia, Sarawak, and Sabah. It remains a major fuel source for electricity generation in Malaysia, with an installed coal-fired capacity of around 12-13 GW, accounting for roughly 45 % of total generation capacity. Major coal plants include Manjung (~4,100 MW), Tanjung Bin (~3,100 MW), and Jimah East (~2,000 MW), while smaller units at Kapar, Mukah, Balingian, PPLS, and Sejingkat also contribute to the national grid. These facilities continue to support the electricity demand in Malaysia while the energy sector gradually transitions toward greater renewable integration (NS Energy, 2019; Sarawak Energy, 2024; Business Today, 2024; GEM Wiki, 2024; OpenInfraMap, 2025). Table 2.1 summarizes the coal-powered power plants currently operating in Malaysia.

Table 2.1
Coal Power Plant in Malaysia

Power Plant	Location	Capacity (MW)
Manjung (Sultan Azlan Shah)	Perak	~4,100
Tanjung Bin	Johor	~3,100
Jimah East	Negeri Sembilan	~2,000
Sultan Salahuddin Abdul Aziz (formerly Kapar)	Selangor	~1,600
Balingian	Sarawak	~600
PPLS	Sarawak	~440
Mukah	Sarawak	~270
Sejingkat	Sarawak	~210

Source: OpenInfraMap (2025)

Approximately 10% of coal used in power generation is converted into Coal Combustion Products (CCPs), including FA, CBA, boiler slag, and flue gas desulfurization gypsum. With the increasing shift from gas-fired to coal-fired power plants in Malaysia, the production of CCPs has risen significantly (Foo, 2015). Among these by-products, FA accounts for approximately 75-85%, which is carried through flue gas ducts and subsequently extracted using electrostatic precipitators. In contrast, around 15-25% of the CCPs comprise CBA, which is collected as coarser material at the bottom of the combustion chamber (Marto and Tan, 2016). The process of coal combustion and the generation of FA and CBA in a thermal power plant is illustrated in Figure 2.6.

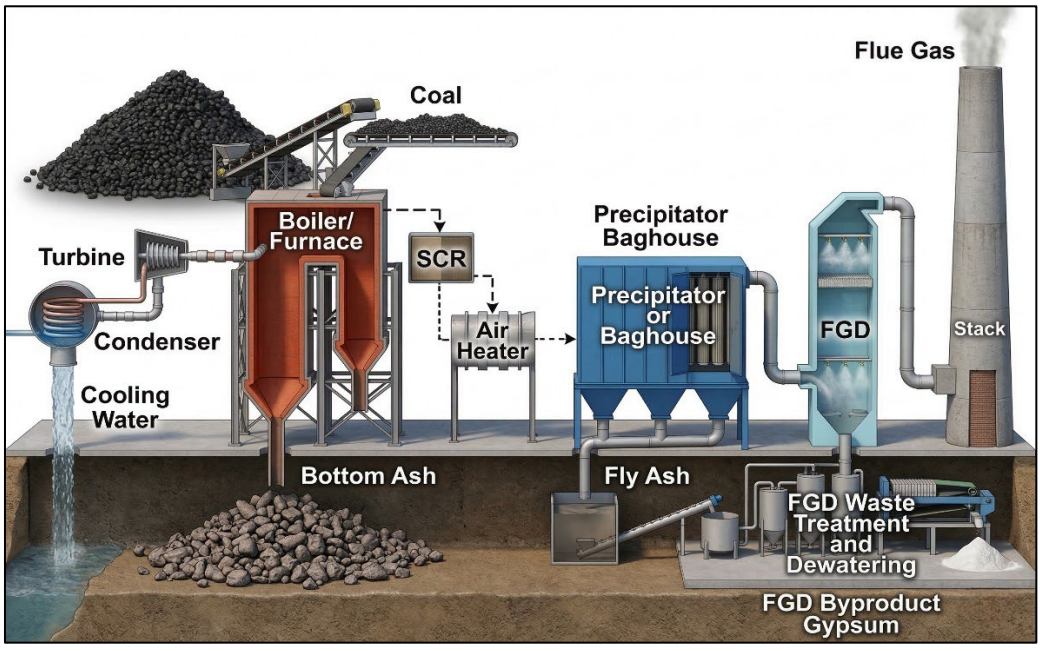


Figure 2.6 Typical Steam Generating System That Generate Coal Combustion (NETL, 2006)

CBA and FA are waste by-products generated from coal-fired power plants. FA is widely utilized as a Portland cement constituent, a Supplementary Cementitious Material (SCM) in concrete, a fine aggregate replacement, and as a material in highway subbase layers and various other construction applications (Argiz et al., 2015; Poulikakos et al., 2017). According to Lo et al. (2016), the European Standard EN 197-1 (EN 197-1, 2011) formally recognizes FA as a constituent of Portland cement. Globally, it is used in cement production to reduce the environmental impact of raw material extraction and to lower CO_2 emissions associated with cement manufacturing. Conversely, CBA is typically used as a sand substitute in concrete and in other limited applications or otherwise disposed of in landfills (Singh and Siddique, 2013).

In terms of waste classification, Colonna et al. (2012) note that coal ash is not classified as hazardous waste in the United States. Similarly, in certain European countries, coal ash is considered non-hazardous special waste under D.L.152/06 and is categorized within the European Waste Catalogue (EWC). However, the classification and regulatory frameworks for coal ash usage vary by country, and no universal standard has been established.

In research conducted by Vasudevan (2017), CBA tested by Standards and Industrial Research Institute of Malaysia (SIRIM) was found to have the following characteristics:

i. The components in the waste sample do not have inherent properties such as explosiveness, ignitability, or flammability.
ii. No hazardous compounds were found as major constituents in the compositions.
iii. The ash sample is safe for the environment and free of infectious bacteria.

The disposal of coal ash has reached an alarming level, making its utilization in construction not just beneficial but increasingly necessary. Large-scale application of coal ash in the construction industry has the potential to reduce both construction costs and the volume of ash waste (Mohamed et al., 2021).

While much of the existing research have focused on FA due to its finer texture and widespread use as a SCM (Permatasari et al., 2023), this research focused on CBA to explore its potential in optimizing the use of waste coal ash for sustainable construction applications. To understand its suitability as a SCM, it is essential to first review the properties of CBA.

2.9 Properties of Coal Bottom Ash

The properties of CBA are influenced by several factors, including the source and type of coal used. Coal is generally classified into four main types: anthracite, bituminous, sub-bituminous, and lignite (Kim et al., 2014). Among these, anthracite contains the highest carbon content, followed by bituminous, sub-bituminous, and lignite.

2.9.1 Physical Properties

Laboratory tests conducted by Muhammad (2010) revealed that CBA consists of angular particles with a porous surface texture. The particle sizes varied from gravel to fine sand, with minimal silt- and clay-sized fractions. CBA is generally sand-sized, with 50-90% passing the 4.75 mm (No. 4) sieve. It typically has a top size exceeding 19 mm, while 10-60% passes the 0.42 mm (No. 40) sieve, and 0-10% passes the 0.075 mm (No. 200) sieve.

According to BS 882:1992, fine sand is classified as material that passes the 600 μm sieve within a range of 55% to 100%. In BS 882:1973, the grading requirements for fine aggregates were divided into four zones based on the percentage passing the 600 μm (No. 30 ASTM) sieve. This classification is based on the observation that many natural sands fall within this particle size range, with relatively consistent gradation above and below that threshold (Neville, 1995). Table 2.2 presents other physical properties of CBA in addition to particle size distribution.

Table 2.2
Physical Properties of CBA

References	Specific Gravity (No Unit)	Water Absorption (%)	Moisture Content (%)	Fineness Modulus (No Unit)	Surface Area (cm^2/g)
Hannan et al., 2020	2.21	-	-	2.71	-
Mangi et al., 2019	2.41	32	-	-	3835.75
Hashemi et al., 2019	1.8	-	-	-	10500
Singh et al., 2019	2.08	6.8	-	1.5	-
Baite et al, 2016	2.22	20.15	-	2.71	-

Source: Mohammed et al., 2021

Table 2.2 (cont.)
Physical Properties of CBA

References	Specific Gravity (No Unit)	Water Absorption (%)	Moisture Content (%)	Fineness Modulus (No Unit)	Surface Area (cm^2/g)
Rafieizonooz et al. 2016	1.88	11.61	-	3.44	-
Singh and Siddique, 2016	1.39	31.58	-	1.37	-
Zhang and Poon, 2015	2.21	11.17	-	-	-
Onprom et al., 2015	2.10	6.18	0.43	2.10	-
Kim and Lee, 2011	1.87	5.4	-	2.36	-
Topcu and Bilir, 2010	1.39	12.10	-	-	-

Source: Mohammed et al., 2021

These physical characteristics influence not only the grading and compaction behaviour of CBA but also its chemical reactivity in cementitious systems.

2.9.2 Chemical and Pozzolanic Properties

Wongkeo and Chaipanich (2010) reported that CBA is primarily composed of silica, alumina, and iron, along with smaller quantities of calcium, magnesium, sulfate, and other minerals. This chemical composition enables CBA to function as a pozzolanic material and act as a SCM in cement-based applications.

To be effective as a cementitious ingredient, a material must exhibit pozzolanic activity, its ability to react with Calcium Hydroxide (portlandite, CH) and form Calcium Silicate Hydrate (C-S-H), the primary strength-giving compound in cementitious systems. Although several methods are available to assess pozzolanic reactivity, chemical composition analysis offers useful preliminary of the materials potential (Mangi et al., 2019).

According to ASTM C618, a pozzolanic material must contain a combined total of at least 70% Silicon Dioxide (SiO_2), Aluminum Oxide (Al_2O_3), and Iron Oxide (Fe_2O_3) to be classified as Class F pozzolans. As shown in Table 2.3, the chemical composition of CBA meets and exceeds this requirement, supporting its classification as a viable pozzolanic material (Mangi et al., 2018).

Table 2.3
Chemical Characteristics of OPC And CBA

Chemical Composition	Rafieizonooz et al. (2016)	Jaturapitakkul and Cheerarot (2003)	Muhardi et al. (2010)	Rafieizonooz et al. (2016)	ASTM C618
	OPC (%)	Coal Bottom Ash (%)			
SiO_2	20.40 - 0.62	48.12	42.7	45.3	
A_2lO_3	5.20 - 5.22	23.47	23.0	18.10	SiO2 + Al2O3 + Fe2O3 > 70% Class 'F'
Fe_2O_3	3.10 - 4.19	10.55	17.0	19.84	
$SiO_2 + Al_2O_3 + Fe_2O_3$		82.14	82.7	83.24	
CaO	62.39 - 4.99	11.65	9.8	8.70	-
MgO	0.91 - 1.55	3.45	1.54	0.969	Max 5.0
NaO_2	0.50	0.07	0.29	-	Max 15.0
SO_3	2.11 - 2.70	1.76	1.22	0.352	Max 5.0
LOI	1.13 - 2.36	4.02	-	-	Max 6.0

Source: Mangi et al., 2018

2.9.3 Morphological Properties

Scanning Electron Microscope (SEM) images are commonly used to analyze the surface textures and particle morphologies of bottom ash particles. This analysis aids in understanding the behaviour of ash materials during testing and provides insight into their hydration properties (Sanjeev et al., 2006).

Research by Ayob et al. (2014) examined the morphological properties of coal ash mixes from the Jana Manjung Power Plant using SEM. The findings revealed that CBA particles are angular and irregularly shaped, exhibiting a rough and uneven surface texture. This roughness is attributed to the presence of unburnt carbon, which distinguishes it from FA.

Additionally, Ramzi et al. (2016) investigated the physical properties of CBA from the Tanjung Bin Power Plant. Their research showed that CBA particles also possess a rough texture, angular in shape, and appear porous. Some particles displayed a popcorn-like texture, while others were spherical. The smallest observed bottom ash particle size was 10.05 micrometres. These observations were made using microscopes with magnifying powers of 100× and 300×, as illustrated in Figure 2.77.

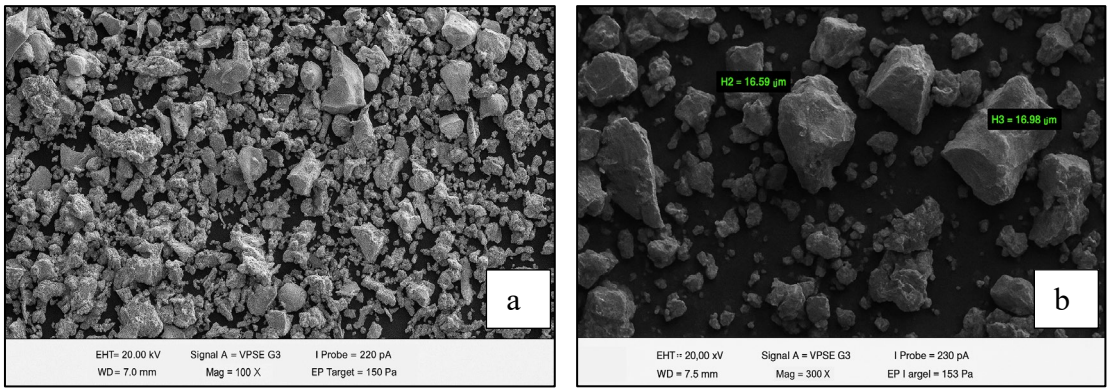


Figure 2.7 Particle Image of CBA Under (a) 100× and (b) 300× (Ramzi et al., 2016)

The rough, porous, and irregular morphology observed in Malaysian CBA explains their higher water absorption and reduced workability when compared to finer FA particles. To overcome the coarse, porous, and irregular nature of CBA, grinding it into ground coal bottom ash (GCBA) enhances its pozzolanic activity and suitability as a partial cement replacement.

2.10 Ground Coal Bottom Ash

GCBA is a fine pozzolanic material obtained by processing CBA. The production of GCBA involves grinding and sieving CBA to achieve a finer particle size, which enhances its reactivity and suitability as a partial cement replacement in construction applications. According to Jaturapitakkul and Cheerarot (2003), CBA should not be used as a pozzolanic material in its natural state. However, it demonstrates good pozzolanic properties after being ground until less than 5% of the particles are retained on the No. 325 sieve (44 µm), effectively converting CBA into GCBA. In addition, bottom ash requires a cementing agent such as quicklime, hydrated lime, or OPC that reacts with water to produce cementitious compounds.

GCBA has attracted attention in sustainable pavement and concrete technologies due to its potential to improve mechanical properties, reduce environmental waste, and promote the reuse of industrial byproducts (Poudel et al.,2024; Chuang and Chen, 2025). Its performance, however, is closely linked to the characteristics of the parent CBA, which vary depending on several factors, including the source and type of coal used.

Isaia et al. (2012) stated that the interaction between pozzolanic materials and cementitious paste varies depending on several factors, including particle fineness, the proportion used in the mixture, and the chemical and/or physical activity of the material.

2.10.1 Physical Properties of Ground Coal Bottom Ash

The physical properties of GCBA, including particle size, shape, density, and water absorption, are key factors that influence its performance in cementitious applications. The physical properties of GCBA presented in Table 2.4 indicate that it is composed of relatively fine, angular, and irregular particles, with particle sizes ranging from <45 μm up to 436 μm. The specific gravity values (2.41-2.56) and bulk density (~952 kg/m³), which may influence the volumetric proportioning and compaction behaviour in cementitious mixes. High water absorption (16.45 %) and low moisture content (1.5-1.97 %) indicate that GCBA can absorb a significant amount of mix water, which should be considered during mix design to ensure proper workability and hydration (Ahmed et al., 2025; Poudel et al., 2024; Chuang & Chen, 2025).

Table 2.4
Physical Properties of GCBA

Property	Typical value/range		
Particle size (μm)	436	<45	11.83
Particle shape	Angular, irregular	-	-
Specific gravity	2.41	2.56	-
Bulk density (kg/m³)	952	-	-
Water absorption (%)	16.45	-	-
Moisture content (%)	1.97	1.5	-
Color	Dark grey-Light black	-	-
pH	8.10	-	-
Reference	Ahmed et al., 2025	Poudel et al., 2024	Chuang and Chen, 2025

Source: Ahmed et al., 2025; Poudel et al., 2024; Chuang & Chen, 2025

2.10.2 Chemical Composition of Ground Coal Bottom Ash

The chemical composition of GCBA plays a crucial role in determining its pozzolanic reactivity and suitability as a SCM in cementitious applications. GCBA is inherently a pozzolanic material that primarily contains silica (SiO_2), alumina (Al_2O_3), and iron oxide (Fe_2O_3), which react with calcium hydroxide ($Ca(OH)_2$) released during cement hydration to form secondary C-S-H (Poudel et al., 2024). Although GCBA itself

does not contain hydration products such as C-S-H or CH, these phases are observed in the binder matrix when GCBA partially replaces cement, indicating ongoing cement hydration and pozzolanic reaction (Ahmed et al., 2025). The presence of calcium oxide (CaO) contributes to self-cementing potential, while minor oxides such as potassium oxide (K_2O) and titanium dioxide (TiO_2) reflect the mineralogical origin of the parent coal and combustion conditions (Chuang and Chen, 2025). Table 2.5 presents the chemical composition of GCBA.

Table 2.5
Chemical Compositions of GCBA

Chemical Composition (%)	Ahmed et al., 2025	Poudel et al., 2024	Chuang and Chen, 2025
Sulphur oxide (SO_3)	1.82	-	1.07
Sodium oxide (Na_2O)	1.12	-	
Aluminium Oxide (Al_2O_3)	26.32	13.34	4.57
Iron Oxide (Fe_2O_3)	13.51	14.54	26.90
Magnesium Oxide (MgO)	2.59	6.26	
Potassium Oxide (K_2O)	1.06	-	2.75
Silicon dioxide (SiO_2)	1.86	36.61	31.85
Calcium Oxide (CaO)	4.33	20.06	13.96
Titanium dioxide (TiO_2)	-	-	3.92
LOI	4.21	9.8	12.07

Source: Ahmed et al., 2025; Poudel et al., 2024; Chuang and Chen, 2025

The characterization of GCBA, including both its physical (Table 2.4) and chemical (Table 2.5) properties, provides critical insight into its behaviour as a SCM. The particle size, shape, density, and water absorption influence workability, compaction, and overall mix stability, while the chemical composition supports pozzolanic reactions and potential self-cementing behaviour. With reference to these material properties, the strength performance of GCBA-based mixes is reviewed to assess their contribution to mechanical properties.

2.11 Strength Performance of Ground Coal Bottom Ash with Cement

Previous research have shown that replacing cement with GCBA in concrete mixes can either reduce or enhance strength performance. Poudel et al. (2024) investigated the feasibility of using GCBA and ground coal boiler slag (GCBS) as partial OPC replacements to reduce environmental impacts associated with cement production and coal waste disposal. The research identified optimum replacement levels

of 10% for GCBA and 5% for GCBS. Concrete incorporating 10% GCBA exhibited improved tensile strength, modulus of elasticity, and durability compared to the control mix. Chloride penetration resistance was significantly enhanced, with 10% GCBA concrete recording substantially lower charge passed in the Rapid Chloride Penetration Test at 56 days, indicating improved durability. The incorporation of nanoclay further increased the effective GCBA replacement level and compressive strength, demonstrating potential for synergistic material combinations.

Chuang and Chen (2025) evaluated finely ground coal bottom ash (FGCBA) as a SCM in self-compacting concrete (SCC) at cement replacement levels of 20-60% under varying water-to-binder ratios. The research assessed fresh and hardened properties, including workability, setting time, strength, permeability, and water absorption. While fly ash improved workability and contributed to long-term strength development, FGCBA exhibited lower early-age strength but significantly enhanced durability, particularly by reducing chloride ion permeability and promoting microstructural densification. These findings highlight the potential of FGCBA as a low-carbon OPC substitute that supports resource efficiency and circular economy objectives.

Liew et al. (2024) investigated low-calcium GCBA as a SCM in binary and ternary mixed cements with OPC and ground granulated blast-furnace slag (GGBS). Cement replacement levels ranged from 5% to 25%, with sand-to-binder and water-to-binder ratios held constant. The research found that 5-15% GCBA improved mechanical strength, with ternary blended mortars (GCBA + GGBS) outperforming the binary mixtures. Flow diameter increased and setting times were slightly extended with higher GCBA content, while replacements above 20% reduced strength. Overall, 15% GCBA substitution provided the optimal balance of workability and compressive strength.

Ahmed et al. (2025) explored GCBA combined with coconut coir fiber (CF) as partial replacements for cement to produce high-performance, low-carbon concrete. Using optimal proportions of 33.6% GCBA and 4.3% CF with a superplasticizer, the concrete achieved improvements of 44.5% in compressive strength and 48.1% in tensile strength, along with enhanced flexural performance and durability. CF reduced cracking, while GCBA improved long-term performance through better particle packing and pozzolanic reactions. The GCBA-CF mixtures also reduced embodied carbon and energy consumption, demonstrating their potential for sustainable concrete production.

Menéndez et al. (2021) assessed the pozzolanic properties of GCBA compared to FA for blended cement. Various binary and multicomponent mixes were prepared with GCBA and FA at proportions ranging from 0% to 100% and total ash contents of 10%, 25%, and 35%. GCBA exhibited pozzolanic reactivity comparable to FA, with a slow early-age reaction that accelerated over time. The research concluded that mechanically GCBA is a promising SCM, offering both technical feasibility and environmental benefits by reducing landfill waste.

Earlier research by Mangi et al. (2019) and Khan and Ganesh (2016) also examined the effect of GCBA on compressive strength. Mangi et al. found that optimal strength was achieved with up to 10% OPC replacement, while higher levels reduced strength due to dilution of cementitious compounds. Similarly, Khan and Ganesh reported that GCBA concrete initially showed lower compressive strength at 28 days but surpassed the OPC control at 56 days, reflecting the delayed pozzolanic reaction of GCBA. Kurama and Kaya (2008) observed increased compressive and flexural strength up to 15% replacement, while replacements beyond 10-15% led to reduced performance. Jaturapitakkul and Cheerarot (2003) further demonstrated that grinding CBA significantly improved mortar strength, with fineness contributing to enhanced early and later-age compressive strength, achieving over 60% higher values than unground CBA.

Many research have examined the influence of GCBA on strength performance in concrete applications, and the results remain inconsistent due to variations in testing methodologies, curing conditions, and replacement levels (Mangi et al., 2019; Khan and Ganesh, 2016; Poudel et al., 2024). These inconsistencies indicate that the effectiveness of GCBA is highly dependent on mix design and material interactions, emphasizing the need for further investigation under different stabilization conditions. Although most research focused on concrete, limited studies have explored the use of coal-based pozzolanic materials in stabilized pavement base course.

2.12 Coal Bottom Ash in Pavement Construction

CBA has several engineering properties that make it suitable for use in pavement construction. It has been utilized in various types of pavements as an alternative to aggregates, a substitute for cement, an additive for bitumen, and a filler for asphalt pavement. In most cases, CBA is intended to serve as a partial or complete replacement

for sand or fine aggregate in pavement construction because of its similarities to natural sand (Abdullah, 2019).

Recent research by Mohamed et al. (2025) has explored the use of CBA as a sustainable replacement for fine aggregate in stone mastic asphalt (SMA) pavements. Performance evaluations indicated that replacing up to 30-50% of fine aggregate with CBA improves durability and resistance to permanent deformation, although higher replacement levels reduce these properties. Stiffness and tensile strength ratio (TSR) decrease with increasing CBA content, but TSR remains above the 80% threshold required by JKR for replacements of 50% or less, demonstrating the potential of CBA to enhance mechanical performance while supporting environmentally friendly pavement construction

Thanasisathit et al. (2025) investigated the use of CBA as a partial replacement for sand in cement-stabilized mixtures for pavement applications. Mixtures containing 0-50% BTA and 1-7% cement were evaluated for mechanical performance, durability, and microstructural characteristics. Results showed that 20% CBA with 7% cement achieved optimal unconfined compressive strength and load-bearing capacity, while maintaining environmental safety with respect to heavy metal leaching. The research highlighted the feasibility of incorporating CBA into subbase and base layers, demonstrating its potential as a sustainable and cost-effective material for pavement construction.

Lynn et al. (2017) outlined the applications of CBA in subbase layers, pavement base materials, and bituminous binder mixes. Their analysis indicated that CBA possessed adequate bearing capacity for low-strength applications such as subbase layers and embankment fills. However, its use in pavement base materials is influenced by the substitution percentage, as increasing the bottom ash content tends to reduce the compressive strength.

In research by Hesami et al. (2016), coal waste ash, coal waste powder, and limestone powder were used as partial cement replacements in Roller-Compacted Concrete Pavement (RCCP) at levels ranging from 5% to 20%. The researchers assessed various mechanical properties, including elastic modulus, splitting tensile strength, flexural strength, and compressive strength over curing periods from 7 to 90 days. The results showed that the water-to-cement ratio increased when coal waste ash and powder were added to the mix. Furthermore, the compressive strength of the RCCP mixes decreased with higher coal waste ash content, as illustrated in Table 2.6. However, when

coal waste ash was combined with limestone powder, the mechanical performance of the concrete improved. The research concluded that coal waste ash required combination with other pozzolanic materials to enhance its mechanical properties.

Table 2.6
Compressive Strength Test Results

RCCP Mixes	Compressive Strength (MPa)		
	7 days	28 days	90 days
OPC	22.3	34.7	38.9
CWP-5	23.2	36.1	43.4
CWP-10	16.7	31.4	35.3
CWP-20	14.8	25.5	31.5
CWA-5	24.8	36.8	42.3
CWA-10	24.0	33.9	38.0
CWA-20	21.0	32.3	34.4
CWA-5-LS	24.3	36.2	42.5
CWA-10-LS	24.6	35.3	40.5
CWA-20-LS	20.2	29.1	35.1

Source: Hesami et al., 2016

A similar outcome reported by El Moudni El Alami et al. (2019), who emphasized the need to treat coal waste products with other pozzolanic materials to enhance their mechanical properties. The research investigated the feasibility of using CBA in the foundation layer or subbase of pavements. The findings revealed that incorporating CBA into the subbase mix led to a reduction in certain mechanical properties, particularly compressive strength, as shown in Figure 2.8. This reduction was attributed to the inherent porosity of CBA, where the presence of pores within the mortar weakened its structural integrity. To mitigate this issue, the researcher treated the mix with lime and calcarenite sand. Lime content ranged from 1% to 5%, while calcarenite sand accounted for 5% to 25% of the total mixture by weight. The results demonstrated that mechanical properties such as compressive strength, CBR value, and dry density improved significantly, with optimal performance achieved at 4% lime content.

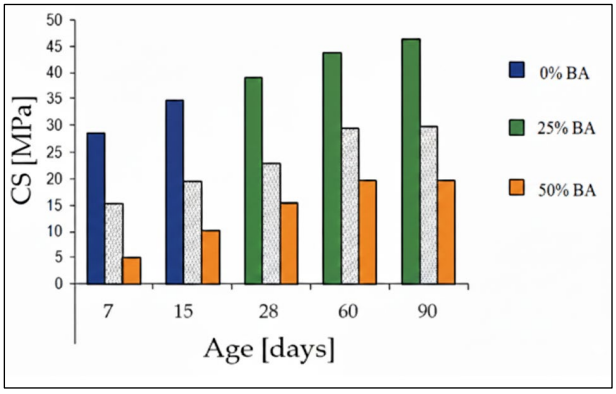


Figure 2.8 Compressive Strength of Mortar Containing Untreated CBA (El Moudni El Alami et al., 2019)

Modarres and Ayar (2014) investigated the incorporation of coal waste and coal waste ash as additives in cold recycled asphalt pavement mixes. These materials were mixed with bitumen emulsion using emulsified cold recycling technology to mix 100% RAP with additives passing through a 0.075 mm sieve. The research evaluated additive contents of 3%, 5%, and 7% within the emulsion. The results showed that the inclusion of coal waste and its ash enhanced the mechanical properties of the pavement, as illustrated in Figure 2.9. This improvement was attributed to the pozzolanic content of the coal waste materials, which contributed to strength development in the recycled mix (Modarres and Ayar, 2014).

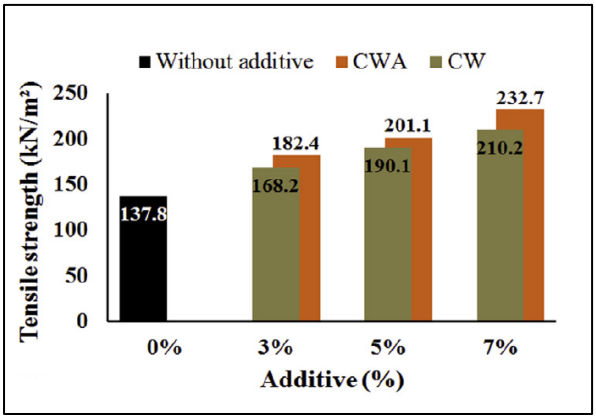


Figure 2.9 The Effect of Coal Waste and Coal Waste Ash on Tensile Strength (Modarres and Ayar, 2014)

Research on CBA in pavement applications mostly focused on its use as a partial replacement for sand or fine aggregate. Research showed that optimal replacement levels can improve durability, load-bearing capacity, and resistance to deformation, while higher or untreated CBA often reduced mechanical performance due to its porous nature. These limitations can be mitigated by combining CBA with other pozzolanic

materials or cementitious binders, demonstrating both the potential and the need for careful mix design in sustainable pavement construction (Abdullah, 2019; Mohamed et al., 2025; Thanasisathit et al., 2025; Hesami et al., 2016; El Moudni El Alami et al., 2019; Modarres and Ayar, 2014).

Despite these findings, the application of GCBA in stabilized pavement base, particularly in combination with OPC and chemical accelerators such as $CaCl_2$, remains underexplored. This gap highlights the need to investigate the synergistic effects of GCBA, OPC, and $CaCl_2$ on the mechanical and structural performance of pavement base materials, making it necessary to review the role of $CaCl_2$ in cementitious applications.

2.13 Calcium Chloride in Cement Applications

The curing process for cementitious materials typically requires a significant amount of time, potentially leading to increased project costs and delays in construction schedules. To mitigate this issue, accelerators are often incorporated into the mixture to enhance the rate of curing. Among the various types of chemical accelerators, $CaCl_2$ remains one of the most widely used due to its affordability and ready availability (Kishar et al., 2013). $CaCl_2$ is commercially available in two primary forms: regular flake and concentrated flake, pellet, or granular formulations (ACI Committee 212, 1963). According to Occidental Chemical Corporation (2006), the addition of 1-2% $CaCl_2$ can significantly accelerate cement hydration, reducing the setting time by up to two-thirds. Beyond its accelerating properties, $CaCl_2$ also provides additional benefits, including:

i. Enhances the workability of the cement mixture, and less water is required to generate a given slump, regardless of the mix design.
ii. Increases the strength of air-entrained concrete by adjusting for the loss of strength with a higher cement factor.
iii. Curing acceleration causes rapid stiffening, which reduces bleeding and allows for faster final finishing.

Rahmani et al. (2025) investigated the use of $CaCl_2$ as an accelerator in eco-friendly mortars incorporating ground granulated blast-furnace slag (GGBS) and glass

powder (GP) as partial cement replacements. The addition of 1 % $CaCl_2$ improved fresh-state workability by approximately 4 % and significantly enhanced early-age strength due to accelerated pozzolanic reactions. Mortars containing GGBS achieved compressive strengths of about 37 MPa at 7 days, representing an increase of roughly 60 % compared to mixes without $CaCl_2$, while maintaining comparable strength at 28 days. The incorporation of GP reduced total shrinkage, and $CaCl_2$-enriched mixes exhibited improved resistance to chemical attack, indicating enhanced durability.

Li et al. (2023) studied the effects of $CaCl_2$ and sodium chloride (NaCl) as accelerators on the compressive strength of carbide slag activated GGBFS, a low-carbon alkali-activated binder. Their results showed that 5 % $CaCl_2$ significantly boosted early strength by 127 % at 3 days, and also substantially increased 28-day and 90-day compressive strengths due to accelerated hydration and greater formation of hydration products like hydrocalumite, which refine microstructure and enhance long-term strength.

William et al. (2020) evaluated the effects of $CaCl_2$ as a partial replacement for cement on the mechanical properties of concrete, focusing on compressive and split tensile strength. $CaCl_2$, used in powder form, accelerates concrete hardening and reduces finishing time. Concrete cubes and cylinders were cast with cement partially replaced by $CaCl_2$ at 1%, 2%, 3%, and 4% by weight, following ACI mix design for C30 concrete, and cured for 28 days. Results showed that 3% replacement yielded the highest performance, with an average compressive strength of 39 N/mm^2 (17% higher than the control) and an average split tensile strength of 2.9 N/mm^2. Beyond 3% replacement, both compressive and tensile strengths decreased proportionally.

Salain (2019) used $CaCl_2$ as an accelerator on the compressive strength development of concrete made with Portland Pozzolan Cement (PPC). Concrete was mixed with natural sand, crushed stone, and a water-binder ratio of 0.57, with $CaCl_2$ added at 0%, 1%, 1.5%, and 2% by binder weight. Compressive strength was tested at 1, 3, 7, 28, and 90 days. Results showed that $CaCl_2$ accelerated early-age strength gain, with 36-48% improvement at 1 day and 29-33% at 3 days compared to control. Long-term strength also increased by 3-16% at 28 days and 7-19% at 90 days. The optimal $CaCl_2$ dosage was 1.5%, which provided the highest early-age and long-term compressive strength.

Rattanasak et al. (2011) assessed the effect of chemical admixtures on high-calcium fly ash geopolymer, which typically suffers from low workability and rapid

setting due to the high viscosity of the sodium silicate solution. $CaCl_2$ was found to significantly shorten both the initial and final setting times, while sucrose delayed the final set. All admixtures enhanced the degree of reaction and increased compressive strength, indicating their potential to improve the workability and early-age performance of fly ash geopolymer.

$CaCl_2$ has been widely studied as a chemical accelerator in cementitious materials, indicating its ability to shorten setting times and enhance early-age strength (Salain, 2019; William et al., 2020; Li et al., 2023). Its effectiveness has been demonstrated across various binders, including OPC, PPC, and alkali-activated slag, with optimal dosages ranging from 1-5 %. In addition to accelerating hydration, $CaCl_2$ has been shown to improve workability and promote pozzolanic reactions in systems incorporating supplementary cementitious materials such as GGBS and FA (Rahmani et al., 2025; Rattanasak et al., 2011). While these research consistently report early-age performance benefits, the long-term strength outcomes vary depending on the type of binder and mix design.

Although $CaCl_2$ has been widely studied in concrete, its application in pavement construction, particularly with recycled or coal-based pozzolanic materials, remains limited.

2.14 Calcium Chloride in Pavement Construction

In pavement construction, $CaCl_2$ has attracted considerable interest due to its ability to modify moisture distribution within unbound aggregates and its potential to accelerate cementitious and pozzolanic reactions when combined with SCM.

$CaCl_2$ is traditionally used for dust control on unpaved or low-volume roads. Al Bargi et al. (2023) investigated the use of $CaCl_2$ as a dust suppressant and base stabilizer for unpaved roads. Natural gravel was mixed with 2-4% $CaCl_2$ by volume of dry soil, and the mixtures were evaluated for Atterberg limits, grading, maximum dry density (MDD), optimum moisture content (OMC), and California Bearing Ratio (CBR). Results showed that OMC decreased with increasing $CaCl_2$, while MDD increased from 2.15 Mg/m^3 to 2.36 Mg/m^3. Correspondingly, CBR improved by 25-36%, indicating enhanced soil strength and flocculation due to better particle bonding. The research concluded that $CaCl_2$ is an effective stabilizer for unpaved roads, potentially reducing lifecycle costs, minimizing dust emissions, and improving environmental sustainability.

Shon et al. (2010) investigated the addition of $CaCl_2$ to fly ash-treated roadbeds and found that the soluble calcium species enhanced particle cohesion, accelerated setting, improved compaction efficiency, and increased both early-age and long-term strength. Laboratory tests supported these findings, and a predictive mathematical model was developed to estimate composite strength. Field performance data confirmed that fly ash can be effectively incorporated in road construction when supplemented with $CaCl_2$, yielding stronger and more durable pavement layers.

In another research, Saylak et al. (2008) compared trial sections of pavement base treated with FA and $CaCl_2$ to untreated control sections. Results show no improvement in structural quality with FA alone, as the CBR value drops to 43. In contrast, the combination of FA and $CaCl_2$ results in a CBR exceeding 100, highlighting the effectiveness of the dual stabilizer system in enhancing both strength and durability.

Although $CaCl_2$ is known to improve moisture distribution in aggregates and accelerate cementitious reactions, its use in pavement construction remains limited. Most research has focused on dust control for unpaved roads, where $CaCl_2$ enhances compaction, dry density, and CBR (Al Bargi et al., 2023). Research combining $CaCl_2$ with FA have shown that it overcomes the slow early strength development of FA, improving cohesion, setting, and long-term strength (Shon et al., 2010; Saylak et al., 2008).

Research on $CaCl_2$ in pavement construction has largely focused on dust control and improving compaction and CBR in unpaved roads (Al Bargi et al., 2023), or on enhancing early-age strength and long-term performance of fly ash-treated layers (Shon et al., 2010; Saylak et al., 2008). However, the synergistic effects of $CaCl_2$ in combination with GCBA and OPC for stabilizing pavement base layer remain unexplored. Investigating this combination in CIPR base layer through laboratory testing provides an opportunity to evaluate key mechanical properties, assess early-age strength development, forming the basis for the experimental methods used in this study for sustainable pavement construction.

2.15 Methods for Evaluating Stabilized Base Course Performance

UCS and ITS are the most commonly used tests to evaluate the performance of stabilized base courses. In addition to these, researchers also establish tests to evaluate material properties and performance under various types of loading.

According to Baghini et al. (2016), UCS, Flexural Strength (FS), and unsoaked CBR tests were used to evaluate the short-term performance of stabilized soil–aggregate specimens under different stress sequences. For long-term performance assessment, soaked CBR, dynamic creep, and wheel-tracking tests were conducted.

Sufian et al. (2009) evaluated the strength performance of a stabilized CIPR mix by conducting ITS, UCS, and resilient modulus (M_R) tests. They also analyzed several parameters, including Optimum Moisture Content (OMC), Maximum Dry Density (MDD), and Optimum Binder Content (OBC) for each RAP proportion. In another research, Sufian et al. (2009) investigated the effects of moisture content variation on the strength characteristics of treated specimens using cement and hydrated lime as stabilizing agents. This research involved UCS, ITS, and M_R testing as part of the FDR process.

Cai and Liu (2020) conducted a compaction test to determine the OMC and MDD of the stabilized mix. Their research focused on assessing the mechanical properties of pavement base or subbase materials. They also performed UCS and ITS tests to evaluate the ultimate strength and tensile performance of the stabilized base under loading. Additionally, they measured the compressive resilient modulus to assess the stiffness of the base or subbase course, applying a maximum pressure equal to 60% of the UCS.

Gonzalo-Orden et al. (2019) carried out the flexural strength test to analyze the behaviour of FDR using cement. The test characterized the recycled pavement over a 90-day curing period. A four-point flexural beam test was performed to induce failure at the weakest point of the specimen. After testing, the specimens broke roughly at midspan. The remaining halves were then reused for UCS and ITS testing without trimming, allowing for a correlation between UCS, ITS, and FS of the original specimen.

Mohd Kamal et al. (2017) evaluated the strength performance of CIPR mixes incorporating polymer-modified asphalt emulsion. The mechanical properties were assessed using UCS and ITS tests, which provide insight into both compressive and tensile behaviour of the recycled mixes. UCS testing measures the load-bearing capacity of the stabilized specimens, while ITS testing captures their tensile resistance under indirect loading. The combined evaluation allows for a comprehensive understanding of the structural integrity and durability of the CIPR base course.

Most recently, Chilufya et al. (2024) conducted a detailed evaluation of laterite

pavement bases stabilized with emulsions incorporating biochar using a suite of mechanical tests. The UCS test was first performed to determine compressive resistance, followed by ITS testing to provide insight into tensile behaviour and moisture sensitivity. The resilient modulus was determined through the indirect tensile method according to Australian standards, characterizing the elastic response under repeated loading. In addition, flexural performance was evaluated using four-point beam tests to assess modulus and fatigue behaviour, while rutting susceptibility was examined through wheel-tracking tests.

Overall, UCS and ITS are the most commonly adopted tests to evaluate the mechanical performance of stabilized base courses, while additional tests such M_R, CBR, and FS provide further insights into stiffness, durability, and long-term behaviour (Baghini et al., 2016; Cai & Liu, 2020; Gonzalo-Orden et al., 2019; Mohd Kamal et al., 2017; Chilufya et al., 2024; Sufian et al., 2009). Laboratory and field study consistently use these tests to evaluate a wide range of stabilizers, including cement, hydrated lime, polymer-modified asphalt emulsion, and emulsions incorporating biochar, demonstrating their effectiveness in capturing both compressive and tensile responses under various loading conditions.

Based on these established methods, this research employed UCS, ITS, and M_R testing to evaluate the performance of CIPR base layer stabilized with GCBA, $CaCl_2$, and OPC, allowing for a comprehensive evaluation of both early-age and long-term mechanical behaviour. In addition to laboratory evaluation, compliance with JKR technical specifications helps ensure the suitability of stabilized base layers for pavement construction.

2.16 Technical Standards for Cold In-Place Recycling

According to the Standard Specification for Road Works, Section 4: Flexible Pavement (JKR/SPJ/2008-S4, 2008), the CIPR process involves a systematic selection of materials and strict adherence to mix design parameters to ensure structural integrity. These requirements provide benchmarks for material properties, compaction, strength, and durability, which serve as a reference for evaluating the suitability of stabilizers in pavement rehabilitation projects.

2.16.1 Material Requirements

The specification allows for the introduction of imported pavement materials to the recycled mix. This is done to adjust the grading, supplement volume for shape correction, or improve the structural properties of the pavement. These materials typically include:

i. Natural materials: sand and gravel.
ii. Crushed stone products: graded products, crusher dust, etc.
iii. Salvaged RAP: reclaimed asphalt pavements from other sites.

For stabilization, OPC (MS 522) is the standard stabilizing agent, though alternatives may be approved if they offer cost benefits without technical detriment. Additionally, water used in the process must be potable, clean, and free from harmful matter.

2.16.2 Laboratory Evaluation Protocols

Before the addition of any stabilizing agent, laboratory tests are conducted on representative samples from the existing pavement or designated borrow areas to establish the base properties of the recycled material. These tests are essential for determining:

i. The specific volume of additional material required from borrow areas to supplement the existing pavement.
ii. The optimal type and application rate of the stabilizing agent to ensure structural requirements are met.
iii. The exact amount and classification of any additives necessary to enhance the mixture performance.

2.16.3 Preliminary Laboratory Testing and Gradation

To ensure the mechanical integrity of the recycled pavement, the material must exhibit high resistance to fragmentation. The particle shape is strictly regulated, requiring a flakiness index of 25% or less when evaluated under MS 30 standards.

The material must also conform to the gradation limits specified in the standard to ensure a stable matrix as shown in the Table 2.7 (Table 4.10.2 in JKR/SPJ/2008-S4).

Table 2.7
Gradation Limits for Recycled Layer Material

Sieve Size (mm)	Cumulative % Passing
50.0	100
37.5	85 - 100
20.0	60 - 100
10.0	40 - 90
5.0	30 - 75
2.36	20 - 60
0.425	10 - 45
0.075	2 - 20

Source: JKR/SPJ/2008-S4

2.16.4 Compliance Requirements for Cement Stabilization

The performance of the cement-stabilized recycled layer is governed by strength and density requirements. The mix design must achieve a balance between stiffness and flexibility to prevent premature cracking. The compliance requirements are given in Table 2.8 (Table 4.10.3 in JKR/SPJ/2008-S4).

Table 2.8
Requirements for Cement Stabilized CIPR Layer Material

Parameter			Requirements
Unconfined Compression Test (UCS)	Minimum 97% of Modified AASHTO density	Range (MPa) (minimum and maximum limit)	2 - 5
Indirect Tensile Test (ITS)	Minimum 97% of Modified AASHTO density	Minimum (MPa)	0.2
Maximum cement content by weight (%)			5

Source: JKR/SPJ/2008-S4

Although JKR/SPJ/2008-S4 provide performance criteria for stabilized base layers, they do not prescribe how different stabilizer combinations and proportions interact and should be optimized. To address this, the Response Surface Method (RSM) is employed as a systematic analytical tool to evaluate the interactive effects of GCBA, $CaCl_2$, and OPC on the mechanical performance of CIPR base layer.

2.17 Analytical Method Using Response Surface Method

RSM is a collection of continuous statistical techniques used to explore the relationships between variables and their responses (Uche et al., 2022). The main objective of RSM is to identify the correlations between dependent and independent variables, as well as their interactions, to achieve optimal results (Mohammed et al., 2019).

According to Badri et al. (2020), a specific type of Central Composite Design (CCD) is often employed to implement necessary adjustments in experimental methods rather than using traditional designs. This approach ensures that all specified maximum and minimum points are represented within the design space. CCD has proven effective in examining interactions between input parameters and response variables (Myres and Montgomery, 2002).

RSM is widely applied across various disciplines, including pavement engineering. Khodaii et al. (2012) utilized RSM to analyze how aggregate gradation and lime content influence the tensile strength ratio of both dry and saturated hot mix asphalt. The CCD arrangement and the corresponding responses from the mixtures are detailed in Table 2.9, which presents the response values for each of the ten factorial combinations generated based on RSM principles.

Table 2.9
CCD Arrangements

Run	Factor		Mixture Tensile Strength and Ratio		
	Lime (%)	Grading	TSR (%)	ITS_{dry} (kPa)	ITS_{sat} (kPa)
1	0	D1	64	786	500
2	0.5	D1	65	797	520
3	1	D1	68	824	552
4	0	D2	70	832	585
5	0.5	D2	73	840	612
6	1	D2	77	850	658
7	0	D3	75	858	647
8	0.5	D3	79	864	689
9	1	D3	86	866	742
10	0.5	D2	72	841	611

Source: Khodaii et al.,2012

The optimization of process responses can be achieved using second-order polynomial models that interpolate between the levels of two factors. The maximum

intended responses for TSR, ITS_{dry}, and ITS_{sat} can be determined by generating a surface plot. Figure 2.10 illustrates the Three-Dimensional (3D) surface plot depicting the relationship between the percentage of TSR, lime, and grading (Khodaii et al., 2012).

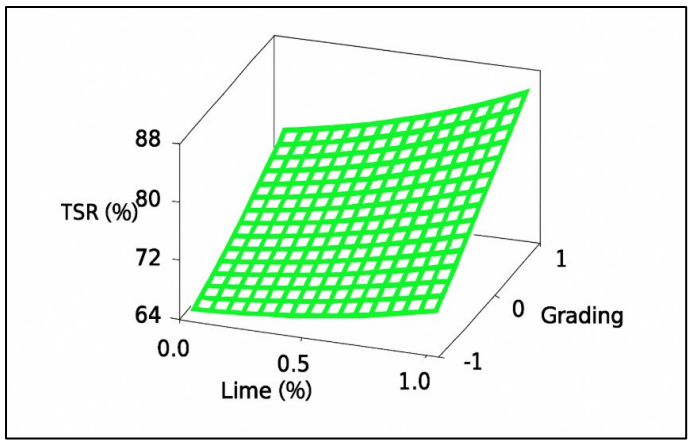


Figure 2.10 3-D Surface Plot of TSR Versus Lime and Grading (Khodaii et al., 2012)

Research conducted by Jamshidi et al. (2013) utilized RSM to examine how varying amounts of Sasobit influence the rheological properties of asphalt binder at high temperatures. In 2015, Hamzah et al. applied RSM to investigate the effects of extended short-term ageing on the rheological properties of binders at intermediate temperatures. Additionally, Hamzah and Omranian (2016) explored the impact of ageing on asphalt binder behaviour at high temperatures, using RSM for their evaluation.

Separate research by El Moudni El Alami et al. (2019) focused on the subbase layer of pavement and employed RSM to identify how parameters such as lime and sand affect the mechanical properties of the material. These studies effectively demonstrate the usefulness of the RSM technique in characterizing the complex behaviour of asphalt binders and related mixtures.

Almajed et al. (2021) analyzed chemically stabilized fibre-reinforced soil using RSM to optimize reinforcement parameters, including fibre length, fibre dosage, and curing time, to improve the geotechnical properties of the stabilized soil. Laboratory testing was performed on all samples to gather empirical data, which are then used in RSM to develop a complete quadratic model and design plots. Equation (2.1) represents the UCS using regression coefficients, while Figure 2.11 illustrates the predicted versus actual UCS values.

$$UCS = 2445.03 + 160.257A + 151.905C - 189.415AB - 80.28AC - 84.3816BC - 167.996C^2 \quad (2.1)$$

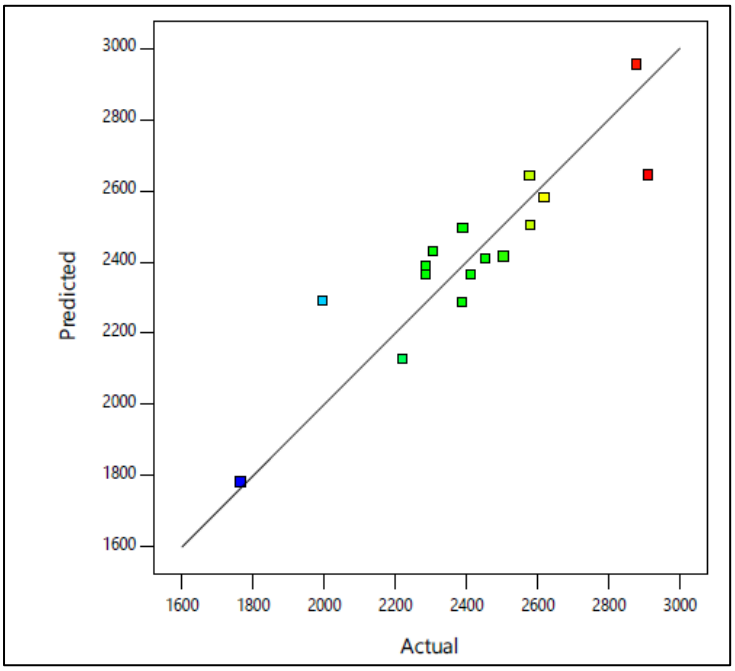


Figure 2.11 Predicted Versus Actual Values of UCS (Almajed et al., 2021)

In recent research, Shiong et al. (2023) investigated the volumetric properties of stone mastic asphalt reinforced with steel fibre using RSM. Statistical techniques were employed to develop mathematical models based on experimental data. Additionally, Analysis of Variance (ANOVA) was applied to evaluate the influence of experimental parameters, offering a comprehensive assessment of the results. Equations (2.2), (2.3), and (2.4) present the simplified forms of the linear, two-factor interaction (2FI), and quadratic models involving two independent variables as used in their research.

$$Y = C_0 + C_1X_1 + C_2X_2 \quad (2.2)$$

$$Y = C_0 + C_1X_1 + C_2X_2 + C_{12}X_1X_2 \quad (2.3)$$

$$Y = C_0 + C_1X_1 + C_2X_2 + C_{12}X_1X_2 + C_{11}X_1^2 + C_{22}X_2^2 \quad (2.4)$$

Shiong et al. (2023) also developed three-dimensional models for each parameter in their research, including specific gravity, stiffness compaction, Marshall stability, flow, and air voids. These models were generated using a statistical framework derived from their analysis, as illustrated in Figure 2.12.

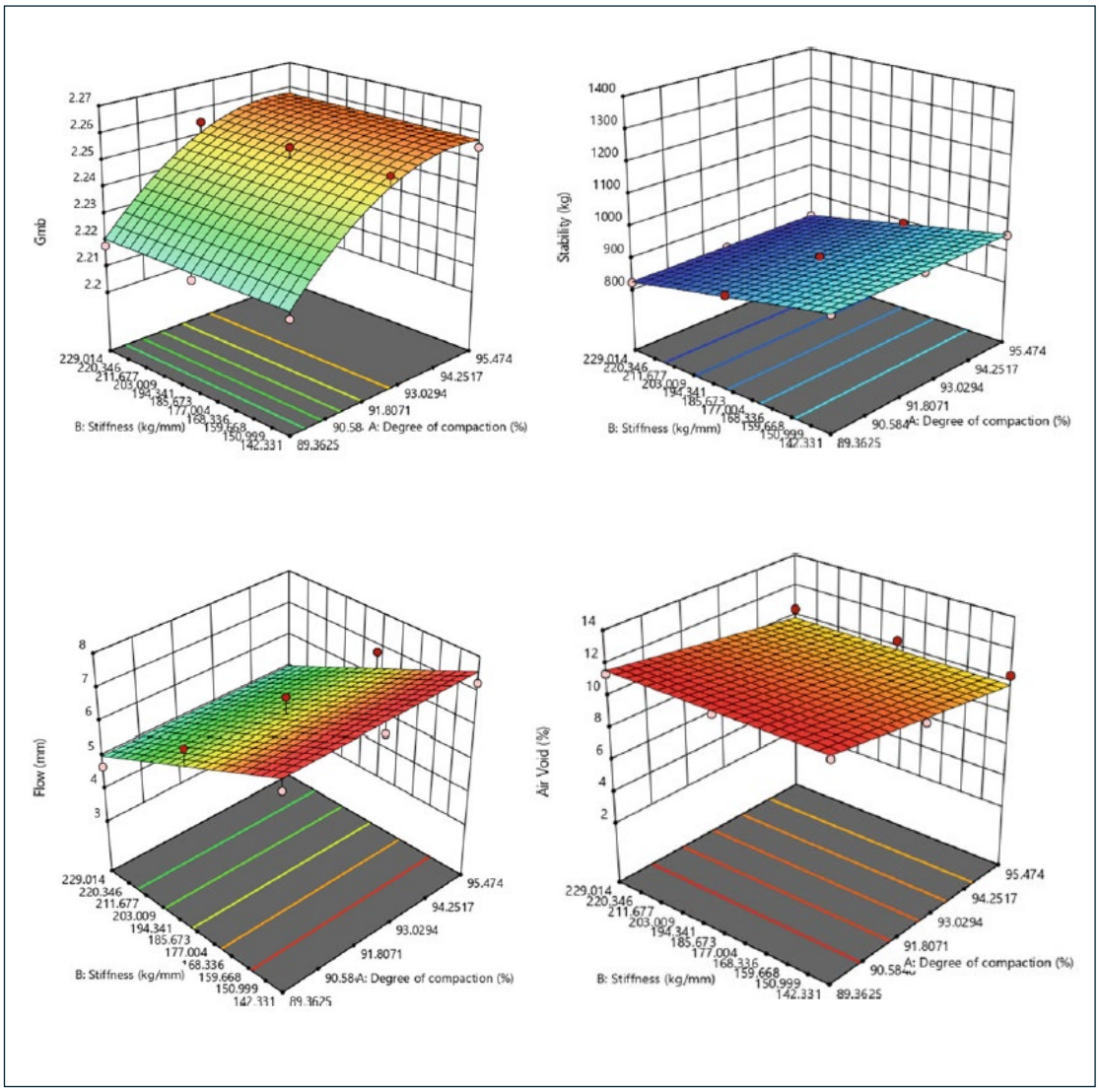


Figure 2.12 3-D Model of Each Parameter (Shiong et al., 2023)

In terms of material optimization, research by Ahmad et al. (2020) applied RSM and desirability analysis to optimise the mechanical properties of recycled aluminium–alumina metal matrix composites. The researchers identified the optimum process conditions at the upper levels of the experimental factors, where the highest responses for strength, elongation, and hardness were obtained. This finding demonstrated the effectiveness of using the maximum predicted values within the model domain as the optimization criterion, highlighting the capability of RSM to determine the most desirable combination of factors for achieving enhanced mechanical performance

Overall, previous studies have demonstrated that RSM is a powerful statistical tool for modelling, analyzing, and optimizing (Jamshidi et al., 2013); El Moudni El Alami et al., 2019; Almajed et al., 2021; Shiong et al., 2023; Ahmad et al., 2020). Its flexibility in handling multiple variables and interactions has enabled researchers to

develop reliable predictive models for strength, durability, and rheological properties across diverse applications. Building on these findings, this research applied RSM to evaluate the influence of stabilizing agents on the strength performance of treated CIPR base course. This approach allows the development of statistical models and the identification of optimal stabilizer proportions for the proposed mix design.

2.18 Gap of Research

CBA has long been utilized in the construction industry, primarily as a SCM in concrete and cement. Based on this, GCBA, produced by finely grinding CBA, offers a higher surface area and improved reactivity, which could enhance its performance in stabilization applications. However, most previous literatures have focused on GCBA in structural concrete, leaving its potential role as a stabilizing agent in pavement base courses and rehabilitation processes largely unexplored. Its performance in the CIPR has not yet been thoroughly investigated.

At the same time, $CaCl_2$ is widely recognized as an accelerator in concrete mixtures, yet its combined effects with GCBA in pavement base materials remain unexamined. Although GCBA shows promise as a sustainable alternative to OPC, its application in CIPR is constrained by slow hydration and delayed early-age strength development, which are incompatible with rapid “open-to-traffic” requirements. To date, no research has investigated how $CaCl_2$ influences the chemical activation of GCBA and OPC or determined the optimum dosage for the combined GCBA-OPC-$CaCl_2$ mix in recycled base course.

This highlights a clear research gap in defining the optimum chemical-mineral balance needed to achieve adequate early-age strength without compromising long-term durability. To address the gap, this research investigated the application of GCBA in CIPR base stabilization in combination with $CaCl_2$ and OPC, aiming to provide new insights into sustainable stabilizing agent alternatives and support the broader adoption of GCBA and $CaCl_2$ in pavement rehabilitation practice.

CHAPTER 3
RESEARCH METHODOLOGY

3.1 Introduction

This research involved laboratory work to evaluate the performance of GCBA mixed with OPC as stabilizing agent in the CIPR base course, along with the effect of $CaCl_2$ as a curing accelerator. The experimental results were subsequently used to develop a predictive model that established the relationship between the proposed stabilizing and the strength performance of the base layer.

This chapter begins by outlining the research framework, followed by a detailed explanation of the experimental design. It describes the proposed mix design, material characterization methods, testing procedures, and data analysis techniques. The research was organized into four main phases:

1. Phase One focused on proposing the appropriate proportions of CA and RAP as the primary base structure, followed by selecting the percentages of stabilizing agent, including OPC, GCBA, and $CaCl_2$. During this phase, the characterization of the CIPR materials, including their physical, chemical and mineralogical characterization were conducted on samples obtained from the sites and those prepared in the laboratory. Sieve analysis was first performed to determine the aggregate gradation of both the recycled samples collected from the site and the laboratory-produced samples. Additional tests, such as aggregate durability, particle shape, specific gravity, pH index, Scanning Electron Microscope (SEM), Energy-Dispersive X-Ray (EDX), and X-Ray Diffraction (XRD) analyses, were subsequently carried out.

2. Phase Two focused on determining the OMC, MDD and bulk density of the specimens based on the proportions of the mix design. An analysis was conducted to examine the relationship between OMC and MDD when varying compositions of CA and RAP were applied. The modified Proctor test was utilized for this purpose. The OMC and MDD values obtained were

subsequently used to calculate the bulk density of the modified specimens containing different percentages of stabilizing agent.

3. Phase Three focused on evaluating the strength performance of the proposed mix design through UCS and ITS tests based on the OMC and MDD obtained. Additionally, M_R test was also performed. Prior to strength testing, the specimens were subjected to different curing periods.

4. The final phase focused on developing a statistical model for the proposed stabilized CIPR base course using RSM. Statistical analysis was performed using Design-Expert software. Laboratory strength performance data were used to analyze the interaction effects of stabilizing agent content on the CIPR base course, validate the results, and optimize the proposed mix design.

The research methodology framework for this research is illustrated in Figure 3.1. The strength performance of the stabilized base course served as the primary focus.

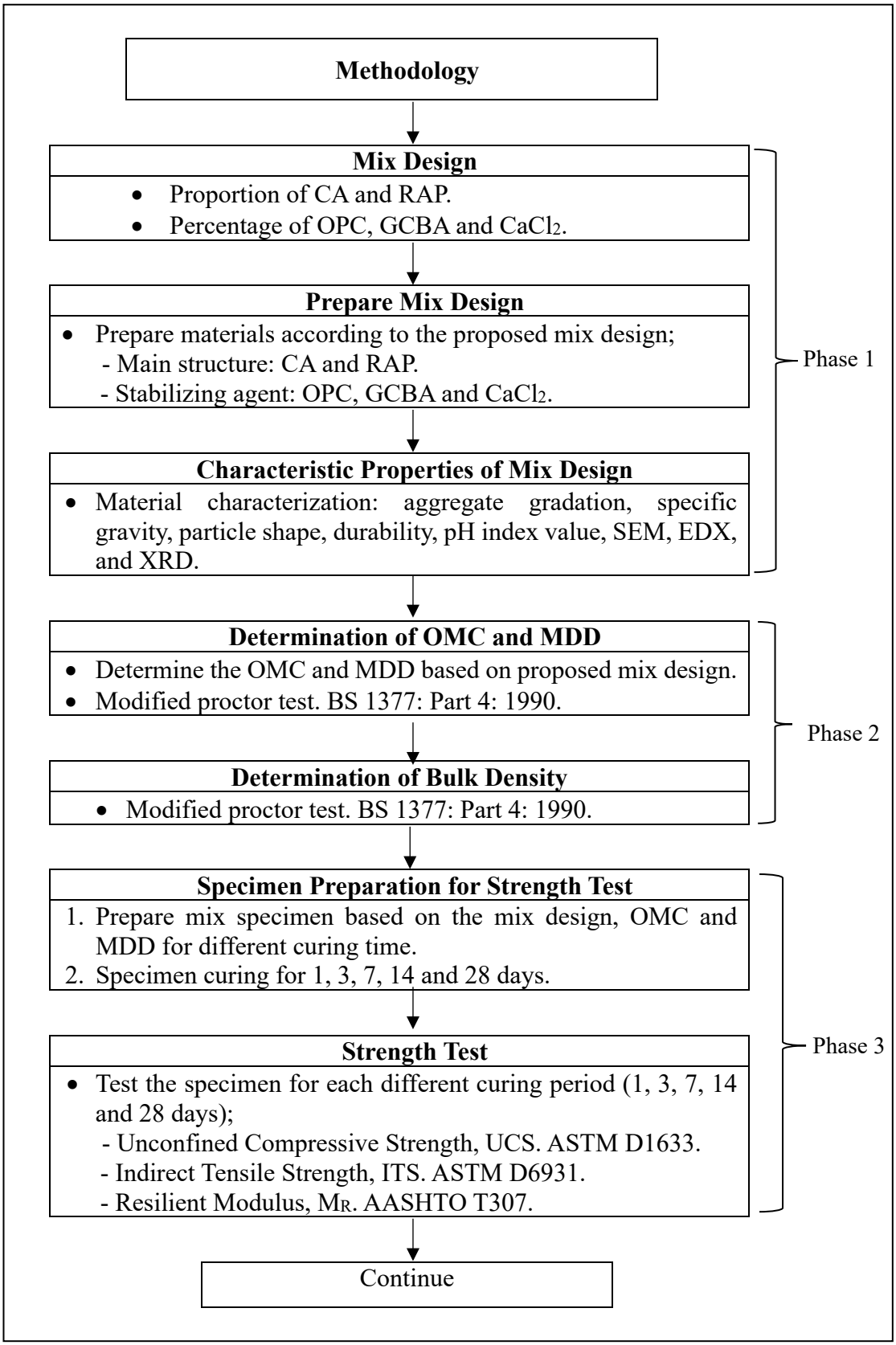


Figure 3.1 Research Methodology Framework

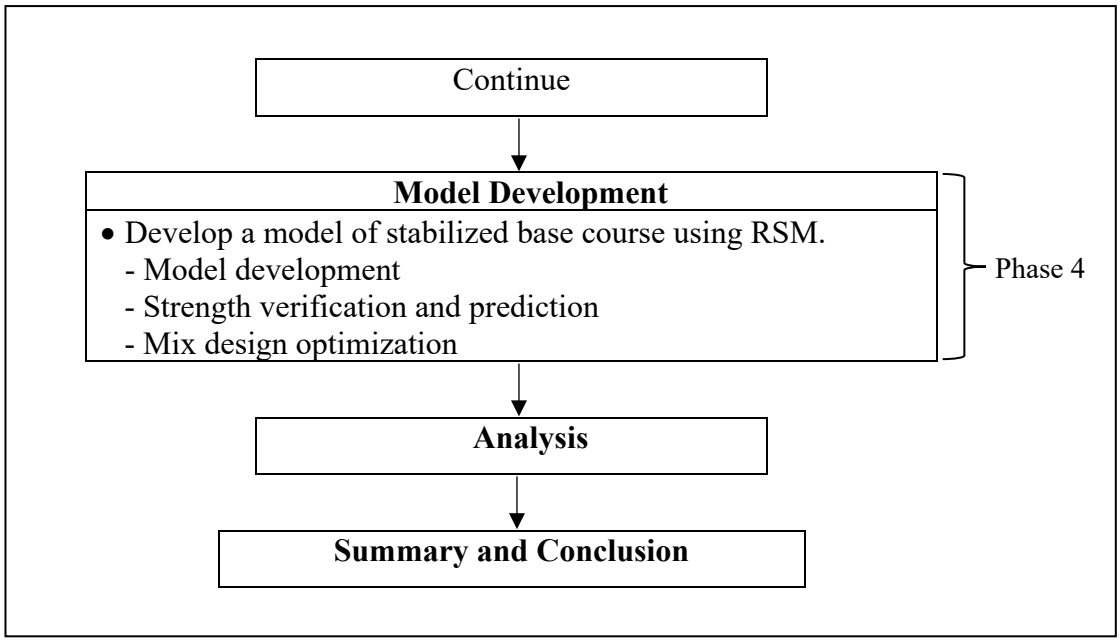


Figure 3.1 (cont.) Research Methodology Framework

3.2 Materials

The laboratory work began with the collection of materials from the sites, followed by an evaluation of their quality, durability, and sources. These assessments ensured that the selected materials could contribute effectively to the structural integrity of the pavement.

3.2.1 Cold In-Place Recycling Sample

The Cold In-Place Recycling (CIPR) samples were collected from the construction sites at Jalan Bandar Baharu - Merbau Pulas, Kulim, Kedah, and Jalan Butterworth - Ipoh, Pulau Pinang, as shown in Plate 3.1. The CIPR material of the existing pavement primarily consisted of an asphalt layer and a granular base layer. Most of the pavement was rehabilitated due to extensive cracking. The CIPR process involved stabilizing the base with OPC, meaning the collected samples were already mixed with OPC. These samples were taken to the laboratory to assess their physical properties, and the homogeneity of their material gradation was used as a reference for replicating the specimens prepared in the laboratory.



Plate 3.1 Sampling Location at (a) Jalan Bandar Baharu - Merbau Pulas, Kulim, Kedah and (b) Jalan Butterworth - Ipoh, Pulau Pinang

At the construction site, the material proportion was determined based on the trial pit report. Generally, the CIPR samples taken from the sites contained nearly 50% RAP, 50% CA, and 4% OPC. The characteristic properties of the CIPR samples were evaluated in terms of the gradation size, particle density, material durability, and pH index. Plate 3.2 shows the sample of CIPR material taken from the site.



Plate 3.2 CIPR Sample

3.2.2 Reclaimed Asphalt Pavement Sample

The Reclaimed Asphalt Pavement (RAP) sample was collected from a construction site in Putrajaya. This material was incorporated into a newly proposed mix design, where the RAP, as illustrated in Plate 3.3, was mixed with CA to form the main structure of the base layer. Additionally, the physical properties of the RAP were tested.



Plate 3.3 RAP Sample

3.2.3 Crushed Aggregate

Crushed Aggregate (CA) granite type was used in this research as a granular base layer material mixed with RAP. Most pavement construction in Malaysia used granite rather than limestone due to its more accessible sources. The CA was obtained from Kajang Rocks Quarry in Selangor. To replicate the aggregate size at the site, the CA in this research was sieved to the desired size distribution as required by JKR/SPJ/2008-S4 specifications. Table 3.1 shows the gradation for Type II aggregate pavement base material of the granular base layer.

Table 3.1
Gradation of Base Type II Aggregate

BS Sieve Size (mm)	% Passing by Weight
50.0	100
37.5	85-100
28.0	70-100
20.0	60-90
10.0	40-65
5.0	30-55
2.0	20-40
0.425	10-25
0.075	2-10

Source: JKR/SPJ/2008-S4

3.2.4 Stabilizing Agent

Stabilizing agent was added to achieve the primary objective of binding the particles together, thereby increasing strength and reducing the curing period. Two types of cementitious materials were utilized as stabilizing agent: OPC, which complies with the Malaysian Standard MS EN 197-1:2007 for CEM type I, and GCBA. A 74% minimum flake Industrial-grade $CaCl_2$ was employed as a curing accelerator. The OPC and $CaCl_2$ were sourced from the supplier, while raw CBA (before grinding) was obtained from TNB Jana Manjung.

Raw CBA is generally not suitable for use as a pozzolanic material due to its physical characteristics, which can adversely affect the mechanical properties of the mix. To address this, a physical treatment was conducted by grinding the CBA to a smaller size range, specifically targeting particles that pass through a 45μm sieve, nearly similar to the size range of OPC.

According to the JKR/SPJ/2008-S4, the maximum cement stabilization content is 5% by weight of the material. Field practice in Malaysia typically uses 4% of OPC as the optimal value. Therefore, for this research, a total content of 4% (OPC + GCBA) by weight of the material was used as the primary stabilizing agent, consistent with field practice. OPC and GCBA provided the main cementitious and pozzolanic reactions. According to Occidental Chemical Corporation (2006), 1-2% $CaCl_2$ can reduce the curing period by up to two-thirds. Hence, a range of 0-3% $CaCl_2$ (by weight of the material) was applied in this research in addition to the 4% primary stabilizing agent, serving as an accelerator to enhance early-age strength. Collectively, these components (OPC + GCBA + $CaCl_2$) constituted the stabilizing agent system for the CIPR base layer. Plate 3.4 illustrates the stabilizing agent utilized in this research.



Plate 3.4 Stabilizing Agent Consist of (a) OPC, (b) GCBA and (c) $CaCl_2$

3.3 Phase One: Mix Design and Material Characterization

Phase one of the research began with the process of proposing a mix design, followed by comprehensive material characterization. This initial phase was designed to focus primarily on the material properties inherent in the proposed mix design. These material properties were categorized into two distinct groups: the site samples and the laboratory-produced mix design samples. Each group underwent a series of tests and analyses to assess various aspects of their composition and behaviour.

The site samples, representative of the actual conditions encountered in the field, served as a crucial reference point for the subsequent laboratory investigations. Tests conducted on the site samples, such as sieve analysis, provided invaluable data that guided the formulation and replication of the mix design in the controlled environment of the laboratory. This approach ensured that the laboratory-produced sample closely mirrored the characteristics and properties observed in the site samples, providing the comparisons and interpretations throughout the research. Figure 3.2 shows the framework for phase one.

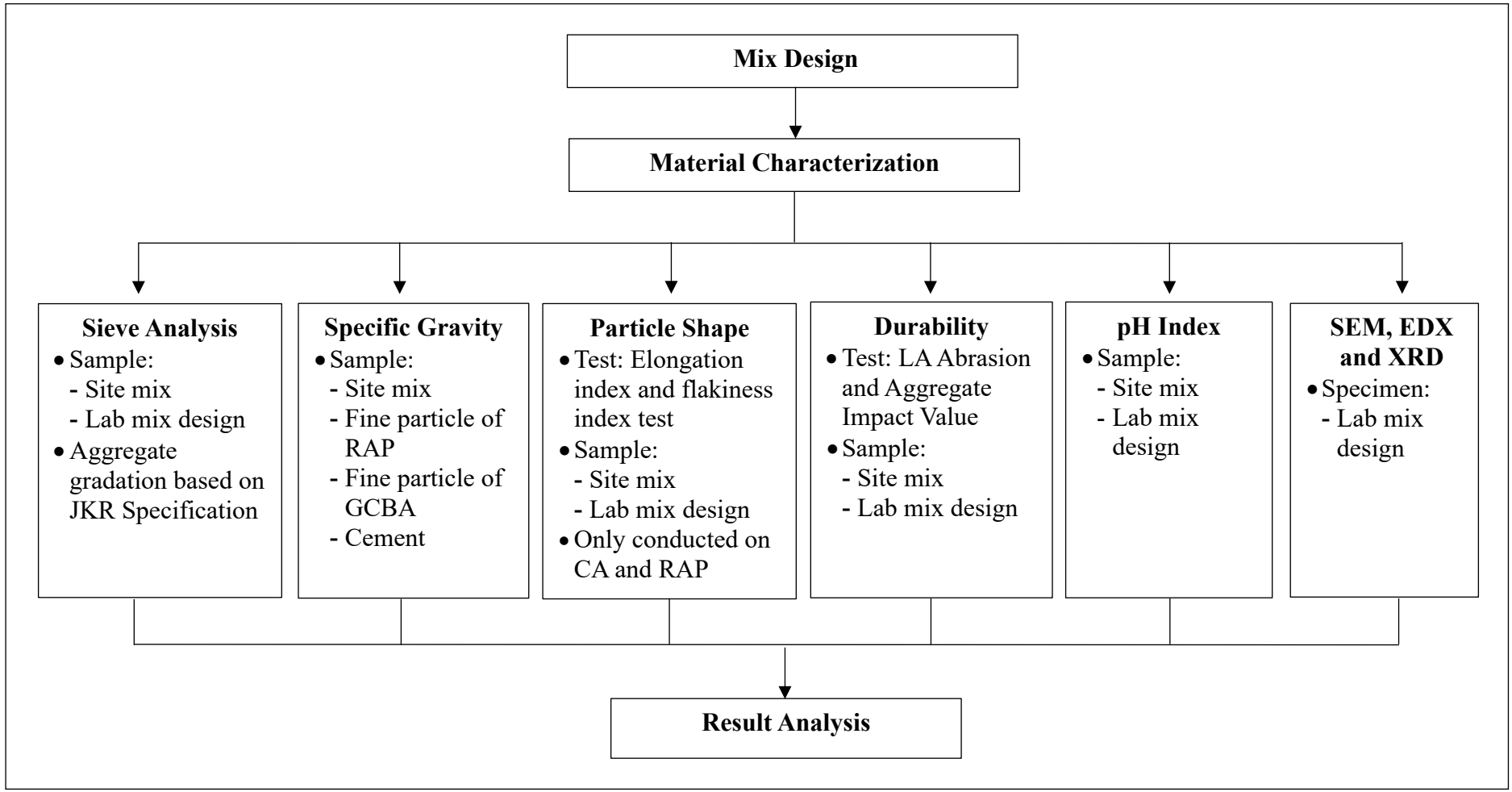


Figure 3.2 Framework of Phase 1

3.3.1 Mix Design

Specimens conducted in the laboratory were mixed with varying proportions of RAP and CA and stabilized with OPC, GCBA, and $CaCl_2$ to simulate the CIPR-treated base course at the construction site. The proposed mix designs consist of CA and RAP gradations ranged from 25% to 75%, involving three experimental proportions that could exist during construction, as shown in Table 3.2.

Table 3.2
Percentage Gradation of CA and RAP Mix

Specimen Reference	CA (%)	RAP (%)
CA75RAP25	75	25
CA50RAP50	50	50
CA25RAP75	25	75

The experimental matrix for the compositions of primary stabilizing agent in this research was designed based on the replacement of 4% OPC content, which is the optimum value used at the construction site. This means the combined percentage of OPC and GCBA was maintained at 4% as the primary stabilizing agent. The range of GCBA used was between 0% and 3%. GCBA cannot fully replace OPC, as it requires a cementing agent such as OPC to react with water and produce a cementitious mixture (Ramzi Hannan et al., 2017). Meanwhile, $CaCl_2$ was incorporated at contents ranging from 0% to 3%, where it acted as an accelerator in the stabilizing agent system. The control specimens were prepared with 4% OPC, serving as the reference mix. Table 3.3 shows the percentage of stabilizing agent used.

Table 3.3
Percentage of Stabilizing Agent

Percentage of Primary Stabilizing Agent (OPC + GCBA)	OPC (%)	GCBA (%)	$CaCl_2$ Accelerator (%)
4% (by weight)	1	3	0,1,2,3
	2	2	0,1,2,3
	3	1	0,1,2,3
	4	0	0,1,2,3
Control Specimen	4	-	-

3.3.2 Material Characterization

Material characterization is important for assessing and understanding a physical and chemical properties of the materials used in the research. This process provides valuable insights that are crucial for addressing significant issues, such as the failure of pavement structures or materials. It also allows researchers to make informed choices regarding material selection. Both recycled materials from the site and materials from the laboratory were subjected to a series of tests to evaluate their quality and index properties.

3.3.2.1 Particle Size Distribution

The most common test for aggregates used in pavement base construction is particle size distribution or the aggregate gradation. Conducting particle size distribution analysis on aggregate samples was essential to ensure their suitability for the intended application. The resulting data were used to verify whether the aggregates satisfied the design requirements. Sieve analysis was performed to classify the material based on particle size distribution.

A dry sieve analysis was conducted on each individual material in accordance with the BS812-113.1 standard. Prior to testing, each sample was oven-dried at 100°C for a minimum of four hours. The dried material was then placed in a stack of standard sieves arranged in descending order of aperture size. The stack was subjected to mechanical shaking for 10 minutes. After sieving, the mass of material retained on each sieve was recorded to determine the particle size distribution. Table 3.4 presents the gradation requirements for the recycled material as specified by JKR/SPJ/2008-S4.

Table 3.4
Gradation Limit for Recycled Layer Material

BS Sieve Size (mm)	Cumulative % Passing
50.0	100
37.5	85-100
20.0	60-100
10.0	40-90
5.0	30-75
2.36	20-60
0.425	10-45
0.075	2-20

Source: JKR/SPJ/2008-S4

3.3.2.2 Specific Gravity

Specific gravity is one of the critical parameters used to evaluate the density and quality of a material. It indirectly reflects the porosity of the material and its ability to retain moisture, both of which influence the performance of a stabilized base course. In mixes where the stabilizing agent exhibits high moisture absorption or retention, the overall strength development may be adversely affected.

To assess this, the specific gravity of the stabilizing agent (OPC and GCBA) along with CA and RAP was determined using the pycnometer method in accordance with ASTM D854 (2000), Method A. This method is typically used for fine powders and relies on accurately measuring the volume of displaced water. $CaCl_2$ was not included in this test, as it readily dissolves in water and therefore could not be measured using this method.

In the procedure, a known mass of the dry material was placed in a pycnometer bottle, followed by the addition of water to fill the bottle. The mass of the filled pycnometer was recorded and compared to the mass of the empty bottle and the bottle filled with water only. The specific gravity was then calculated based on the displacement principle, as illustrated in Plate 3.5. Three specimens were prepared for each material to obtain the average values. The specific gravity of the material can be calculated using Equation (3.1).

$$\textit{The specific gravity, } G_s \textit{ of the material} = \frac{M2 - M1}{(M2 - M1) - (M3 - M4)} \quad (3.1)$$

Where;

M1 = Mass of empty bottle

M2 = Mass of the bottle and dry particle

M3 = Mass of bottle, particle and water

M4 = Mass of bottle filled with water only



Plate 3.5 Sample of GCBA

3.3.2.3 Particle Shape

The shape of aggregate particles plays a significant role in influencing compaction behaviour, deformation resistance, and overall workability of pavement layers. Flaky and elongated particles are generally undesirable, as they tend to create weak zones within the mix, which can compromise the strength and durability of the base course.

In this research, particle shape analysis was conducted based on a combination of the elongation index and flakiness index to evaluate the overall shape characteristics of CA and RAP aggregates. The tests were conducted in accordance with BS 812-105.2:1990 and MS 30.

a) Elongation Index

In the Elongation Index (EI) test, an aggregate is considered elongated if its length exceeds 1.8 times the average sieve size of the size fraction to which it belongs. The sizes of the aggregates used ranged from 63 mm to 6.3 mm. Each aggregate was tested to determine whether it could pass through a specified gauge length, as illustrated in Plate 3.6, using its longest dimension. Any elongated particles that failed to pass through this gauge were separated. The maximum allowable elongation index according to MS 30 is 25% for the base course. The EI was calculated based on the total weight of the aggregates retained on various length gauges, as expressed in Equation (3.2).

$$EI = [W2 / W1] \times 100 \text{ (in percentage \%)} \quad (3.2)$$

Where;

W1 = Total mass of aggregates

W2 = Mass of aggregates passing through 1.8 x d_{mean} size



Plate 3.6 Elongation Gauge

b) Flakiness Index

The Flakiness Index (FI) test measures the thickness of aggregate pieces less than 0.6 times the average sieve size through which the aggregate passes and the largest sieve size on which the aggregate is retained. According to JKR/SPJ/2008-S4, the FI must not exceed 25% when tested in accordance with MS 30.

The test involved using aggregates with sizes ranging from 63 mm to 6.3 mm, following a procedure similar to that used for determining the elongation index. A measuring gauge with standard-sized slots was employed to assess the samples, allowing particles to either pass through or be retained. The FI was calculated by dividing the mass of aggregates that passed through the slots by the weight retained on the gauge, as described in Equation (3.3). Plate 3.7 shows the flakiness index thickness gauge used for this measurement.

$$FI = (W2 / W1) \times 100 \text{ (in percentage \%)} \quad (3.3)$$

Where;

W1 = Total mass of aggregates sample

W2 = Mass of aggregates passing through the flakiness gauge (flaky particles)



Plate 3.7 Flakiness Thickness Gauge

3.3.2.4 Material Durability

The durability of a material refers to its ability to resist degradation over time. Aggregates with poor durability can adversely affect the integrity and long-term performance of the pavement structure. In this research, durability tests were conducted on various CA and RAP mixes (CA75RAP25, CA50RAP50, and CA25RAP75) to evaluate their resistance to mechanical degradation under load impacts. The tests performed included the Los Angeles (LA) abrasion test and the Aggregate Impact Value (AIV) test.

a) Los Angeles Abrasion Test

The Los Angeles (LA) abrasion test was conducted to assess the resistance of aggregates to abrasion and mechanical degradation during handling, mixing, and service. The test was carried out in accordance with ASTM C131-96.

Initially, the aggregate sample was thoroughly washed, oven-dried at 110 ± 5 °C, and weighed to determine their initial dry mass. The dried aggregate sample of 5 kg was then placed into a rotating steel drum along with 12 steel balls, as illustrated in Plate 3.8. Inside the drum, a fixed shelf lifted and dropped the aggregate and steel balls during rotation to simulate impact and abrasion forces.

The drum was rotated for 500 revolutions at a speed of 30-33 rpm, causing the aggregate particles to break down under repeated impact. After completion of the test, the sample was sieved through a 1.70 mm (No. 12) sieve, and the material retained on the sieve was collected, washed, and oven dried.

The percentage loss was calculated by comparing the mass of the material before and after testing. The LA abrasion value should not exceed 45% in accordance with ASTM C131-96, as higher values indicate poor abrasion resistance, which may compromise long-term durability in base course applications. The aggregate abrasion value can be calculated using Equation (3.4).

$$Aggregate\ Abrasion\ Value = [(A-B)/A]\ X\ 100 \quad (3.4)$$

Where;

A = Mass in gm of oven-dried sample

B = Mass in gm of fraction retained on 1.70 mm IS Sieves after washing and oven-dried



Plate 3.8 LA Abrasion Drum

b) Aggregate Impact Value Test

The Aggregate Impact Value (AIV) test was conducted to determine the resistance of aggregates to impact in accordance with BS 812-112: 1990 and MS 30. Given the traffic loads, aggregates are typically subjected to impact and pounding, which can cause them to break into smaller pieces. Therefore, pavement aggregates must be durable enough to resist fracture under sudden impacts and moving loads.

The apparatus for the test consists of a steel mould and a falling hammer, as depicted in Plate 3.9. The aggregate sample, which passed through a 12.70 mm sieve and retained on a 9.52 mm sieve, was washed and oven-dried at 110°C. Ensuring that

the drying process did not exceed 4 hours was crucial, as prolonged exposure could damage the aggregate. Once dried, the sample was placed in a steel mould where a hammer delivered 15 blows, falling from a height of 381 mm onto the test specimen.

Following the impact test, the crushed aggregate was sieved through a 2.36 mm sieve, and the mass of material passing the sieve was weighed to determine the percentage of crushed material relative to the initial sample mass. According to MS 30, the AIV, when tested, should not exceed 25%. The AIV was calculated using Equation (3.5).

$$Aggregate\ Impact\ Value = [W2/ (W1+W2)] \times 100 \quad (3.5)$$

Where;
W1 = Mass of the fraction passing through a 2.36 mm IS sieve
W2 = Mass of sample retained on 2.36 mm IS sieves



Plate 3.9 Aggregate Impact Test

3.3.2.5 pH Index

The pH index test was carried out in accordance with ASTM D4972-19 to determine the acidity or alkalinity of the mix design. This measurement is essential in evaluating the chemical compatibility of the material with cementitious stabilizers. According to Baghini et al. (2016), a pH below 5.3 or an organic content exceeding 2%

may inhibit effective pozzolanic or cementitious reactions. Conversely, a pH value above 12.0 suggests that the presence of organic matter is unlikely to interfere with the cement hydration process.

Since the proposed CIPR mix design consisted of aggregate materials mixed with OPC, GCBA, and $CaCl_2$, this test was essential to ensure favourable conditions for the hardening process. The test aimed to determine whether the mix design samples exhibited a pH level suitable for cement-based stabilization.

To perform the test, 20 g of air-dried material (passing the 2.00 mm [No. 10] sieve) was placed in a clean glass container. 20 mL of distilled water was added, and the mix was stirred thoroughly and allowed to stand for one hour. The pH value was then measured using a calibrated pH meter, as illustrated in Plate 3.10. The chemical interaction among OPC, GCBA, and $CaCl_2$ was not analyzed in this research, as it was beyond the intended scope.

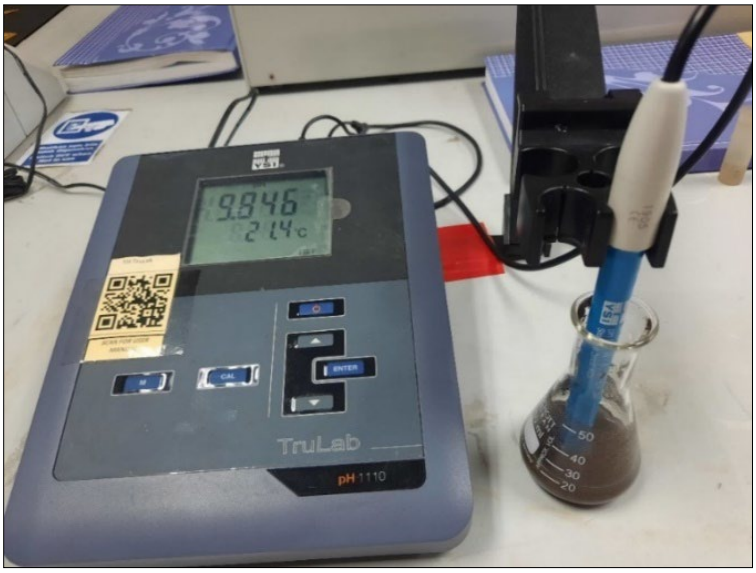


Plate 3.10 pH Meter

3.3.2.6 Scanning Electron Microscope and Energy Dispersive X-Ray

The Scanning Electron Microscope (SEM) (Model: SU3500) provides enlarged images that reveal a size, shape, composition, crystallography, and other physical characteristics of the specimens. The stabilizing agent, which consists of OPC, GCBA, and $CaCl_2$, was analyzed to observe the interactions between these components when mixed and to compare them with untreated CBA.

The GCBA was sieved through a 45 μm sieve for the analysis. The resulting specimen was then oven-dried at 45°C for approximately 24 hours before being coated with a thin conductive layer using a sputter coater to enhance conductivity and image resolution for SEM observation. During examining the microstructure of the specimen, magnifications ranging from 100 to 10,000 times were applied using the SEM, as illustrated in Plate 3.11. However, for data analysis, magnifications of 300× and 1000× were employed to obtain both general and detailed views of the specimen microstructure. The 300× magnification provided a broader perspective of the surface morphology, particle bonding, and distribution of hydration products. Meanwhile, the 1000× magnification allowed a closer examination of finer microstructural features such as pores and microcracks. Higher magnifications were not used, as they reduced the observable area and limited the ability to assess overall bonding uniformity within the mix. The SEM images obtained were primarily monochrome, representing the electron or X-Ray flux generated from the interactions between the electron beam and the specimen surface.

Additionally, Energy Dispersive X-Ray (EDX) analysis was conducted using the same microscope to determine the elemental composition of the specimen. This information provided valuable insights into the types and distribution of elements present, thereby supporting the interpretation of the microstructure of the material and chemical characteristics.

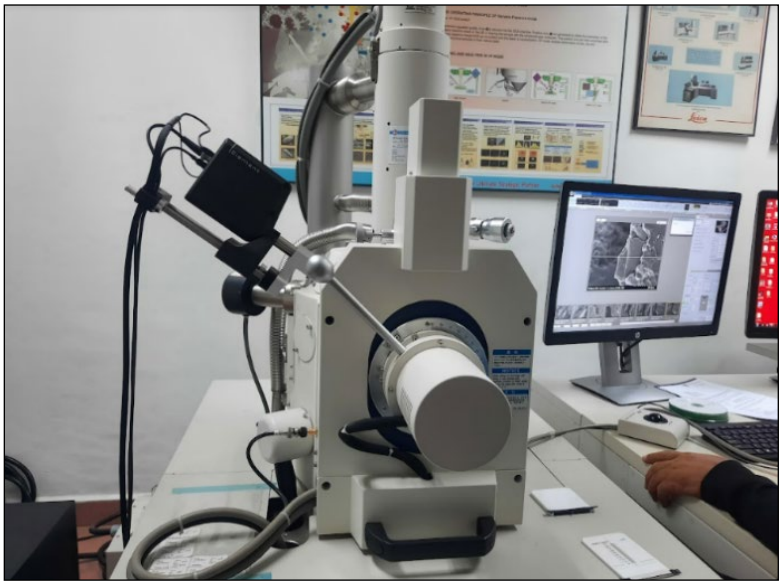


Plate 3.11 SEM Analysis Machine

3.3.2.7 X-Ray Diffraction

X-Ray Diffraction (XRD) technology was used to identify the mineralogy in the mix design specimen. Using a Rigaku Ultima IV diffractometer that was operated at 60 kV and mA with Cu Kα radiation (λ = 1.542 Å), the diffraction pattern of the specimen was determined. A detector was scanned with 0.05° steps and a dwell time of 2 seconds over a scattering angle (2θ) range of 10° to 80°. The entire process was carried out at room temperature. The crystalline phases were characterized by powder diffraction patterns that passed through a 45μm sieve. Plate 3.12 shows the specimen and the XRD machine used in the research.

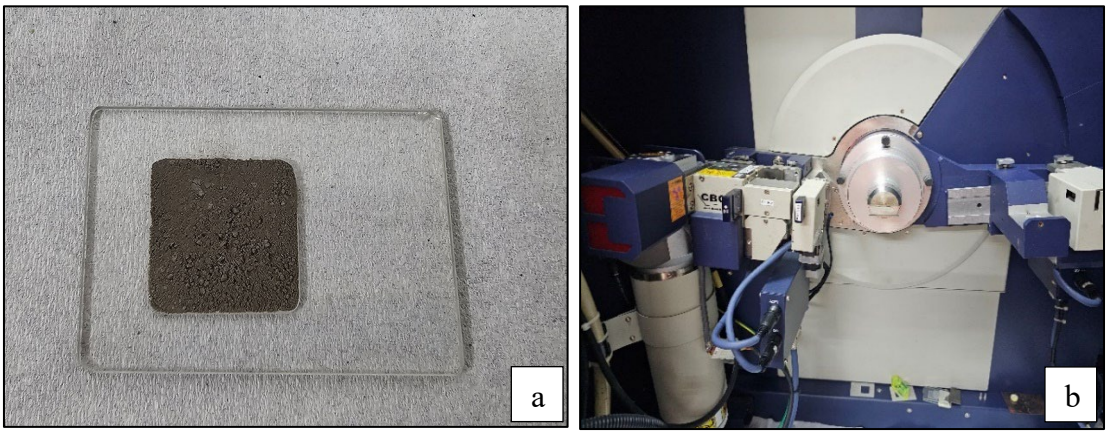


Plate 3.12 XRD Analysis Setup (a) XRD Specimen and (b) XRD Machine

3.4 Phase Two: Compaction Properties Test

In phase two, the specimens were carefully prepared to determine their Optimum Moisture Content (OMC) and Maximum Dry Density (MDD) using the Modified Proctor Test. This phase was fundamental in establishing the moisture-density relationship of the materials, which is crucial for achieving optimal compaction and long-term durability in pavement construction.

The specimens were prepared with varying percentages of moisture content, ranging from 4% to 8%. This range was selected based on the moisture content levels identified in the soil investigation report from the construction site, ensuring that the specimens accurately reflected the potential variability in moisture conditions encountered in real-world scenarios.

Before introducing the stabilizing agent, the OMC and MDD for each gradation were determined through systematic experimentation. This process involved

compacting the specimens at different moisture contents using the modified Proctor test apparatus and measuring their corresponding dry densities. By adjusting the moisture content and observing the dry densities, the moisture-density relationship for each gradation was established.

A key aspect of phase two included plotting a graph of OMC versus MDD, which provided valuable insights into the relationship between moisture content and density. This graphical representation helped visualize trends and patterns, allowing for the identification of the moisture content that yields the maximum dry density for each gradation. These results formed a crucial foundation for the subsequent phases of experimentation and analysis.

Additionally, the data obtained from the OMC-MDD graph were used to calculate the bulk density of the mix design. Bulk density is an important parameter in pavement design, as it provides important information about the compacted volume of the material per unit weight.

Figure 3.3 illustrates the structured framework for phase two, outlining the sequential steps involved in specimen preparation, testing, and analysis.

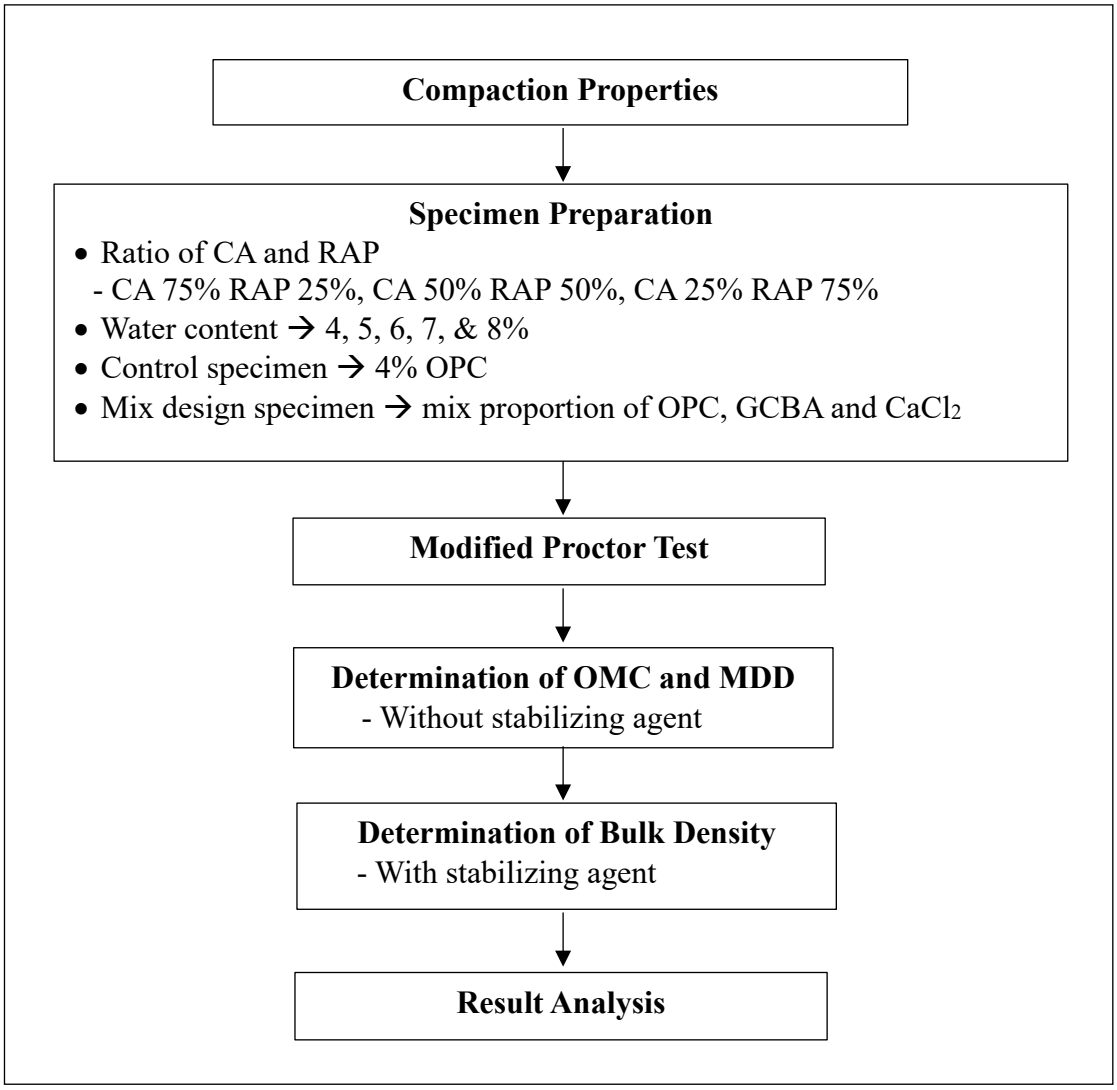


Figure 3.3 Framework of Phase 2

Table 3.5 illustrates the percentage of moisture content and stabilizing agent. The selected percentage of moisture content (4-8%) was based on the soil investigation report from the site located at Jalan Merbau Pulas, Kulim, Kedah.

Table 3.5
Moisture Content and Stabilizing Agent Percentage

Percentage of Primary Stabilizing Agent (OPC + GCBA)	OPC (%)	GCBA (%)	$CaCl_2$ Accelerator (%) by weight	Moisture Content (%) by weight
4% (by weight)	1	3	0,1,2,3	4,5,6,7,8
	2	2	0,1,2,3	4,5,6,7,8
	3	1	0,1,2,3	4,5,6,7,8
	4	0	0,1,2,3	4,5,6,7,8
Control Specimen	4	-	-	4,5,6,7,8

3.4.1 Optimum Moisture Content and Maximum Dry Density

The Modified Proctor test was conducted in accordance with BS 1377: Part 4: 1990 (Heavy compaction method). This testing method was used to determine the relationship between moisture content and dry density based on the specified degree of compaction for the mix design specimen.

At this stage, stabilizing agent was not incorporated, as the test was performed solely on the mixes of CA and RAP materials. A total of 15 specimens were prepared for OMC and MDD determination, calculated as follows;

i. Level of moisture content = 5 (4-8%, each percentage 1 specimen with 3 readings; top, middle, bottom, taken for average value)
ii. Ratios of CA-RAP = 3 (CA75RAP25, CA50RAP50, CA25RAP75)
iii. Total: 5 × 3 = 15 specimens

Prior to conducting the compaction test, the specimens were prepared from aggregates that passed through a 20 mm sieve. The specimens, consisting of the proposed ratios of CA and RAP, were prepared in cylindrical moulds with an internal diameter of 105 mm and a height of 115.4 mm, incorporating the appropriate amount of water. It was then compacted into five layers, with 27 blows applied to each layer using standard compaction techniques. A 4.5 kg rammer was dropped onto the surface of the specimen from a height of 45 cm.

Finally, the specimens were extruded for moisture content analysis. Small portions were collected from the top, middle, and bottom of each compacted specimen to obtain the average values, which were then used to determine the OMC and MDD of the mix. Plate 3.13 illustrates the specimen prepared for the modified Proctor test.



Plate 3.13 Modified Proctor Test Specimen

3.4.2 Bulk Density

The bulk density of pavement base material is a crucial parameter in pavement construction, as it influences the volume of material required and directly affects the stability and performance of the base layer. To evaluate bulk density, the test was conducted using the Modified Proctor method in accordance with BS 1377: Part 4: 1990, as illustrated in Plate 3.14.

At this point, the stabilizing agent were incorporated into the mixes to assess their effect on bulk density. A total of 96 specimens were prepared for bulk density determination, calculated as follows;

i. Numbers of mix design = 16 (different combination of OPC + GCBA + $CaCl_2$)
ii. Each mix design = 2 specimens for average value
iii. Ratios of CA-RAP = 3 (CA75RAP25, CA50RAP50, CA25RAP75)
iv. Total: 16 × 2 × 3 = 96 specimens

The specimens were prepared at their respective OMC obtained from the compaction test, using a cylindrical mould similar to that used for OMC and MDD determination. Each specimen was compacted in five layers, with each layer receiving 27 blows from a 4.5 kg rammer. After compaction, the specimens were weighed to calculate bulk density. Two specimens were prepared for each mix design, and the average values were recorded.



Plate 3.14 Compaction Test for Bulk Density Determination

3.5 Phase Three: Strength Performance Test

Phase three represented a critical stage of this research, emphasizing the evaluation of the strength performance of the proposed mix design. This phase provided insight into both the early strength development and the overall performance of the mix, which are essential aspects of pavement base course construction. Since pavement base materials form the foundation of transportation infrastructure, it is vital to assess their resistance to deformation under applied loads. Such evaluation offers valuable information about the strength and stiffness characteristics of the materials. The performance strength tests conducted in this research included the Unconfined Compressive Strength (UCS), Indirect Tensile Strength (ITS), and Resilient Modulus (M_R). Each test provided specific insights into the ability of the material to withstand external forces and resist deformation over time.

Figure 3.4 outlines the structured framework developed for phase three. This framework explains the sequential steps involved in specimen preparation, testing, and analysis, providing a clear and methodical approach to evaluating performance strength and stiffness.

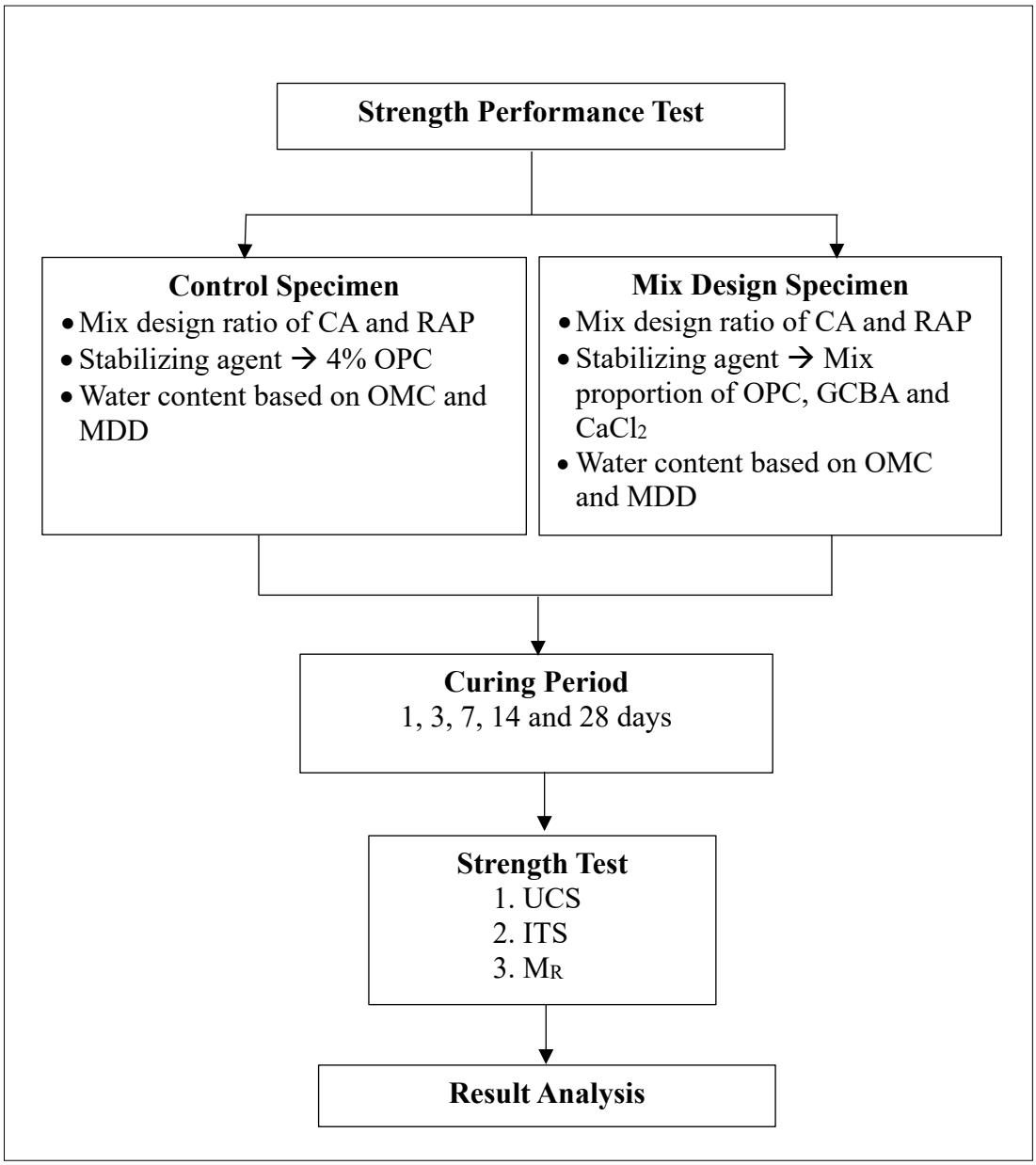


Figure 3.4 Framework of Phase 3

The strength and permanent deformation of the stabilized specimens were tested at curing periods of 1, 3, 7, 14, and 28 days, as adopted from Sufian et al. (2009). The control specimens for all tests consisted of mixes containing 4% OPC only.

3.5.1 Unconfined Compressive Strength

The Unconfined Compressive Strength (UCS) test was conducted in accordance with ASTM D1633. The purpose of this test was to determine the compressive strength of specimens with sufficient cohesiveness for testing under unconfined conditions.

A total of 720 specimens were prepared for the UCS test, calculated as follows;

i. Numbers of mix design = 16 (different combination of OPC + GCBA + $CaCl_2$)
ii. Each mix design = 3 specimens for average value
iii. Ratios of CA-RAP = 3 (CA75RAP25, CA50RAP50, CA25RAP75)
iv. Curing periods = 5 (1, 3, 7, 14, and 28 days)
v. Total: 16 × 3 × 3 × 5 = 720 specimens

In the test, a cylindrical specimen of the mix design material was subjected to axial compressive stress under controlled conditions. For this purpose, 100 mm diameter briquettes, as shown in Plate 3.15(a), were prepared at the OMC determined from the compaction test.

The specimens were formed by placing the materials in a 100 mm diameter mould and compacting them with 75 blows on each side, following a procedure similar to that used in Marshall specimen preparation. Following this, the specimens were cured for specified periods (1, 3, 7, 14, and 28 days) at a temperature of 25°C.

Once the desired curing period was achieved, the specimens were tested using a Universal Testing Machine (UTM). The load was applied at a rate of 153 kN/min until the maximum load was reached, with the minimum requirement set by JKR/SPJ/2008-S4 being 2 MPa. The UCS was calculated using Equation (3.6).

$$UCS = \frac{4 \, x \, P}{\pi \, x \, d^2} \; x \; 1000 \qquad (3.6)$$

Where;
UCS = Unconfined compression strength (MPa)
P = Maximum load at failure (kN)
d = Diameter of briquette (mm)

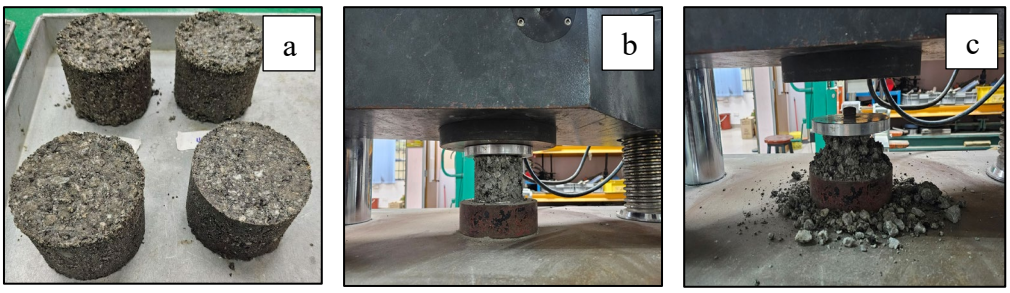


Plate 3.15 UCS Testing (a) UCS 100 mm Briquettes Specimen, (b) Specimen Before and (c) After Test

3.5.2 Indirect Tensile Strength

The Indirect Tensile Strength (ITS) test was conducted in accordance with ASTM D6931, which outlines the procedure for determining the indirect tensile strength of bituminous mixtures. This test aimed to evaluate the tensile properties of the stabilized base course, providing an indirect measure of the tensile stress capacity of the material.

A total of 405 specimens were prepared for the ITS test, calculated as follows;

i. Numbers of mix design = 9 (different combination of OPC + GCBA + $CaCl_2$)
ii. Each mix design = 3 specimens for average value
iii. Ratios of CA-RAP = 3 (CA75RAP25, CA50RAP50, CA25RAP75)
iv. Curing periods = 5 (1, 3, 7, 14, and 28 days)
v. Total: 9 × 3 × 3 × 5 = 405 specimens

Specimens were prepared using a standard Marshall mould and compacted with 75 blows per side, consistent with the method used in the UCS test. The briquettes, with a diameter of 100 mm, were compacted at their respective OMC values as determined from the compaction test.

Testing was carried out using a Marshall press, with a loading rate of 50 mm/min as shown in Plate 3.16. A compressive load was applied along the vertical diametral plane of the specimen through two curved steel loading strips until splitting failure occurred. The maximum load at failure was recorded and used to calculate the ITS value. According to JKR/SPJ/2008-S4, the minimum acceptable ITS for stabilized base layers is 0.2 MPa or 200 KPa. The following Equation (3.7) can be used to determine the ITS of the specimen.

$$ITS = \frac{2 x P}{\pi x h x d} \quad (3.7)$$

Where;

ITS = Indirect tensile strength (kPa)

P = Maximum load (kN)

h = Height of specimen (mm)

d = Diameter of specimen (mm)

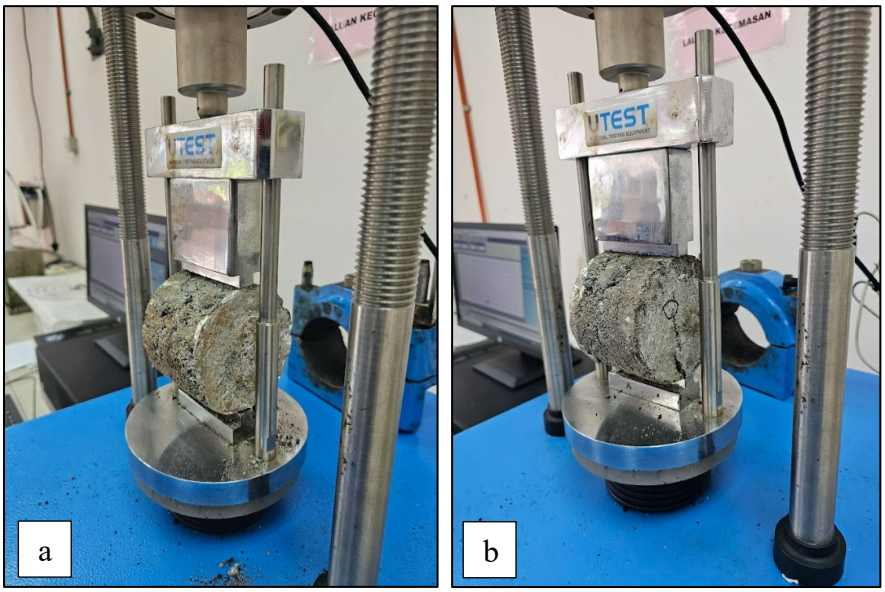


Plate 3.16 ITS Testing (a) Before and (b) After

3.5.3 Resilient Modulus

The Resilient Modulus (M_R) test was conducted in accordance with AASHTO T307, which is applicable for evaluating the stiffness behaviour of soil-aggregate and stabilized base materials under repeated loading. The M_R provides a measure of the recoverable strain in response to traffic-like loads, reflecting the stiffness of the CIPR base layer.

A total of 405 specimens were prepared for the M_R test, calculated as follows;

i. Numbers of mix design = 9 (different combination of OPC + GCBA + $CaCl_2$)
ii. Each mix design = 3 specimens for average value
iii. Ratios of CA-RAP = 3 (CA75RAP25, CA50RAP50, CA25RAP75)
iv. Curing periods = 5 (1, 3, 7, 14, and 28 days)
v. Total: 9 × 3 × 3 × 5 = 405 specimens

Cylindrical specimens were prepared using a 100 mm diameter metal mould with a height of 63.5 ± 2.5 mm, as illustrated in Plate 3.17. The mix was compacted at its OMC using the same method applied for UCS and ITS specimens (75 blows per side). After curing, the specimens were subjected to a haversine-shaped repeated compressive load applied along the vertical diametral plane at a frequency of 1.0 Hz and temperature of 25°C. The load range was set between 2040 and 2100 N, equivalent to approximately 10-50% of the indirect tensile strength of the specimen.

Horizontal deformation was measured using two Linear Variable Differential Transducers (LVDTs) placed at opposite sides of the specimen. An assumed Poisson's ratio of 0.35 and five conditioning pulses was used for modulus calculation. The final M_R was determined by averaging the readings from both sides. According to AASHTO T 307, a minimum M_R threshold of 1350 MPa was adopted, consistent with the AASHTO Guide for Design of Pavement Structures (1993) and recommendations by Sufian et al. (2009). Equation (3.8) shows the calculation for the resilient modulus.

$$E_{RT} = \frac{P\,(V_{RT} + 0.27)}{t \times \Delta H_T} \tag{3.8}$$

Where,

E_{RT} = Resilient modulus (MPa),

P = Repeated load (N),

V_{RT} = Total resilient Poisson's ratio, and

ΔH_T = Total recoverable horizontal deformation



Plate 3.17 Specimen Under Resilient Modulus Test

3.6 Phase Four: Model Development and Mix Design Optimization

Phase four of the research focused on predictive model development using Response Surface Methodology (RSM) to understand the behaviour of the pavement base course. This approach allowed the identification of complex relationships among aggregate ratios, stabilizing agent, curing times, and the resulting permanent deformation.

The use of Design-Expert software provided a systematic method for analyzing these relationships during model development. Once developed, the model underwent validation to ensure its accuracy and reliability in predicting outcomes under varying conditions.

Figure 3.4 presents a visual representation of the structured framework for model development in phase four. This framework offers a clear roadmap for navigating the predictive modeling process by outlining the sequential steps of data collection, experimental design, model construction, and validation.

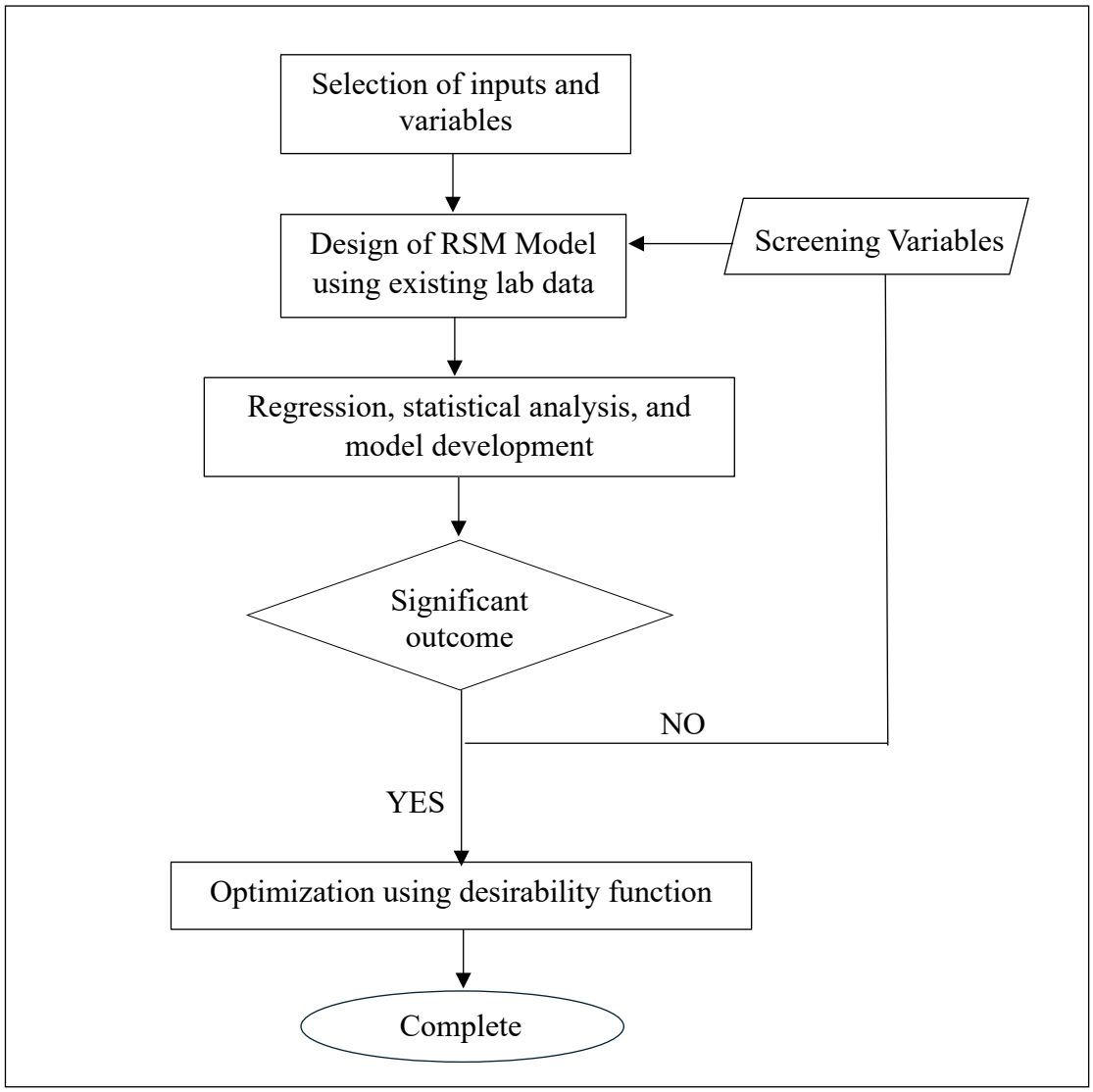


Figure 3.5 Framework of Phase 4

3.6.1 Model Development

The early strength and performance data obtained from laboratory tests were used as input for model development. Modeling a variable with the RSM requires a series of steps that must be completed to reach the research goal. The number of variables and the variance of each variable play an essential role in the model development. The statistical model was developed to analyze the relationship between the variables and responses.

The independent variables for this research were the percentage composition of CA and the RAP alongside the stabilizing agent of OPC, GCBA, and $CaCl_2$, as well as curing periods. However, for the purpose of RSM analysis, $CaCl_2$ percentage and curing period were selected as the primary factors (Factor A and Factor B, respectively) based

on their significant roles in accelerating hydration and strength development. This approach was adopted to avoid model complexity and ensure that the interactions between the variables could be effectively analyzed. OPC and GCBA were treated as fixed factors for each set of analyses to maintain the integrity of the RSM model.

On the dependent variables or the response, the predicted strength and stiffness performance of the treated base course were the primary outcomes of this research, based on UCS, ITS, and M_R. Table 3.6 shows the variables used in this research.

Table 3.6
Variables Used for Model Development

CA:RAP Ratio	Independent Variables				Dependent Variables
	Fixed Factor		Factor A	Factor B	Test Response, R1
	OPC (%)	GCBA (%)	$CaCl_2$ (%)	Curing Period (Days)	Test
CA75RAP25,	2	2	0,1,2	1, 3, 7, 14, 28	UCS, ITS, M_R
CA50RAP50,	3	1	0,1,2	1, 3, 7, 14, 28	UCS, ITS, M_R
CA25RAP75	4	0	0,1,2	1, 3, 7, 14, 28	UCS, ITS, M_R

The implementation of the model development involved the following steps:

1. Identification of the material and the mechanical properties to be studied (responses);
2. Identification of the variables (factors) that influence the responses;
3. Defining the ranges of variation of each factor;
4. Execution of the model;
5. Analysis of the results and statistical modeling.

Stabilizing agent mix of GCBA, OPC and $CaCl_2$ of the treated base made up the final composition of this research. The following factors were expected to have an impact on the mechanical properties of the mix design:

a. Percentage of RAP and CA;
b. Percentage of GCBA;
c. Percentage of OPC;
d. Percentage of $CaCl_2$; and
e. Curing periods

As for the responses, the following responses were analyzed to identify whether the mix composition could be used as a CIPR base layer:

a. Unconfined compressive strength, UCS
b. Indirect tensile strength, ITS
c. Resilient modulus, M_R

A User-Identified model was adopted for RSM to predict relationships between variables, as it allows inclusion of significant linear, quadratic, and interaction terms from the laboratory results. This approach was preferred over Central Composite Design (CCD), which requires pre-defined factor levels and centre points. User-Identified model enabled post-experiment modeling that accurately reflects the behaviour of CA-RAP base mixes stabilized with OPC, GCBA, and $CaCl_2$ while providing reliable predictions.

The effects of $CaCl_2$ content (Factor A) and curing duration (Factor B) on the performance responses were modeled using three polynomial forms: a linear model (Equation 3.9), a two-factor interaction model (Equation 3.10), and a quadratic model (Equation 3.11):

$$Y=\beta_0 + \beta_1 A + \beta_2 B \quad (3.9)$$

$$Y=\beta_0 + \beta_1 A + \beta_2 B + \beta_{12} AB \quad (3.10)$$

$$Y=\beta_0+\beta_1 A+\beta_2 B+\beta_{12} AB+\beta_{11} A^2+\beta_{22} B^2 \quad (3.11)$$

Where;

Y = Response (UCS, ITS or M_R),

β = Model coefficient

A, B = Independent variables ($CaCl_2$ and curing duration)

Model adequacy was assessed through Analysis of Variance (ANOVA), with significance confirmed at $p < 0.05$. Goodness-of-fit and predictive performance were further validated using coefficient of determination (R^2), adjusted R^2, and predicted R^2 values.

3.6.2 Model Verification

Model verification was conducted to confirm the accuracy and reliability of the developed regression models prior to optimization. The verification process involved plotting the predicted values against the actual experimental results for each response. The data points were closely aligned along the 45° reference line, indicating a strong correlation between the predicted and measured values. This close distribution confirmed that the developed models were capable of accurately representing the observed responses for UCS, ITS, and M_R.

3.6.3 Mix Design Optimization

After developing the regression models for each mix design, the optimization process was carried out using RSM with regression analysis. The objective was to identify the most reliable and practical mix proportions of OPC, GCBA, and $CaCl_2$, together with curing days, that would maximize the mechanical performance of the CIPR base layer. The optimization process was carried out in two sequential steps:

1. Model adequacy and reliability were verified using ANOVA and statistical indicators (R^2, adjusted R^2, and predicted R^2). ANOVA confirmed that all models were statistically significant ($p < 0.05$), while R^2 measured variance explained, adjusted R^2 accounted for predictor influence, and predicted R^2 evaluated forecasting accuracy.

2. Optimization was performed using a numerical desirability function within the RSM framework. The selection of the optimal mix was based on mean desirability and predicted R^2 values, balancing multiple responses (UCS, ITS, M_R) and ensuring both model reliability and field applicability. The optimized formulations were expressed as ranges (e.g. 0-2% $CaCl_2$) to ensure flexibility and field applicability. Similar optimization strategies have been reported by Ahmad et al. (2020), who applied RSM and desirability analysis to determine the optimum conditions yielding the highest mechanical responses within the experimental range.

This systematic procedure ensured that the final selected mix exhibited superior performance in terms of strength and stiffness, while also demonstrating consistency and predictive accuracy for practical field applications. Comparable optimization frameworks using RSM and ANOVA have been effectively implemented in previous studies to determine optimum mix proportions and enhance mechanical performance in cementitious materials (Bahri et al. 2018; Rocha et al. 2023).

3.7 Concluding Remark

This chapter presents a detailed overview of the methodological procedures undertaken in this research, covering critical stages such as specimen preparation, material characterization, laboratory testing, data collection, and the subsequent analysis of the results. The methodology was carefully planned to provide a clear and reliable way to evaluate the materials and processes used in the research.

This research primarily applied a quantitative approach, focusing on laboratory experiments to assess the mechanical properties of the stabilized mixes. The experimental data were then used for the development of predictive models and optimization of the mix design, with the aim of improving the performance and sustainability of pavement base layers. Each methodological stage was carefully planned and executed to ensure the accuracy and validity of the findings.

CHAPTER 4
RESULTS, ANALYSIS AND DISCUSSION

4.1 Introduction

This chapter presents the results and analyses of the laboratory tests conducted in this research. It aimed to fulfil the research objectives outlined in Chapter 1 by interpreting the experimental findings. The analyses provide insights into the performance and behavior of the tested materials, thereby reflecting the effectiveness of the research methodology employed.

The experimental program began with material characterization and mix preparation, followed by laboratory testing to evaluate compaction performance. Compaction tests were conducted to determine the OMC and MDD. Based on these parameters, specimens were compacted accordingly, and the bulk density was measured to verify compaction quality. Subsequently, specimens prepared at their respective OMC and MDD were subjected to strength performance testing, including UCS, ITS, and M_R tests at different curing periods. The experimental data were then analyzed using RSM to develop predictive models and evaluate the interaction effects of the stabilizing agents.

The results and analyses covered key material characteristics, including OMC, MDD, bulk density, strength performance, and modeling outcomes. These findings highlighted the major outcomes of the research and demonstrated their alignment with the stated research objectives.

4.2 Phase One: Characteristic Properties of Mix Design

The analysis in phase one began with investigating the characteristic properties of the samples. This included various assessments, such as sieve analysis, specific gravity, aggregate durability, pH index, and particle shape. Additionally, advanced analytical techniques were used, including SEM combined with EDX analysis and XRD.

These evaluations are discussed in the following sections, offering a detailed examination of sample properties. The results from the various analyses were carefully

reviewed, contributing to a comprehensive understanding of sample characteristics and behavior across multiple parameters.

4.2.1 Verification of Particle Size Distribution

The analysis covered a crucial assessment of particle size distribution through sieve analysis, focusing on the proposed mix design incorporating CA and RAP alongside specimens obtained from two different sites, in accordance with JKR/SPJ/2008-S4. Achieving a balanced distribution of particle sizes is crucial in constructing a pavement base, facilitating optimal bonding among particles, and ensuring enhanced mechanical interlocking during compaction.

4.2.1.1 Particle Size Distribution for Crushed Aggregate

The initial phase involved conducting a sieve analysis specifically on the CA. The results of this analysis are presented in Table 4.1, which displays the size distribution of particles ranging from 28 mm to 0.075 mm. Additionally, Figure 4.1 illustrates the S-curve derived from this analysis. Notably, the findings indicated that all particle sizes within the CA fell within the cumulative percentage passing range, confirming compliance with the required specifications.

Table 4.1
Particle Size Distribution Result for CA

BS Sieve Size (mm)	JKR Requirement Cumulative % Passing	Specimen Cumulative % Passing
50.0	100	100
37.5	85-100	100
28.0	70-100	96.9
20.0	60-90	78.8
10.0	40-65	52.5
5.0	30-55	44.4
2.0	20-40	23.8
0.425	10-25	15.8
0.075	2-10	2.7

The individual sieve analysis was conducted solely in CA, as the JKR specifications do not provide specific requirements or a standard table for RAP.

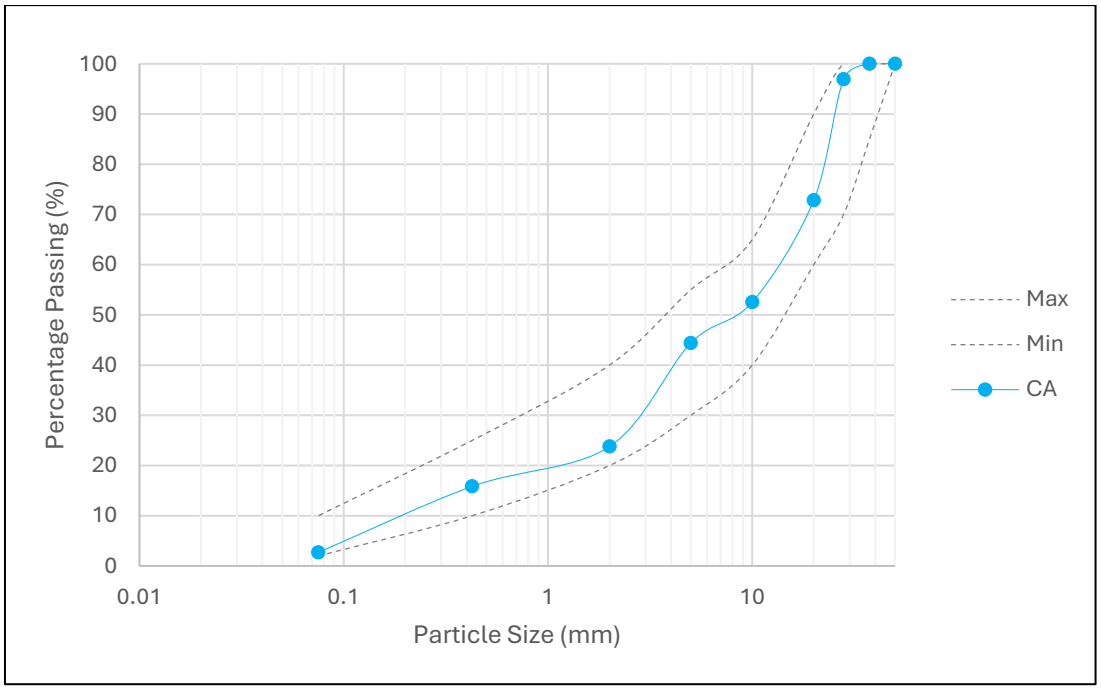


Figure 4.1 Particle Size Distribution Curve of CA

4.2.1.2 Particle Size Distribution for CA-RAP

The particle size distribution analysis was expanded to include the proposed mix design of CA and RAP, as well as samples collected from the selected sites. This sieve analysis aimed to assess the particle size distributions of these materials against construction standards, ensuring compliance with the specified requirements for optimal pavement base construction.

Table 4.2 and Figure 4.2 present the particle size distribution results for the proposed CA and RAP materials, along with the particle size distribution curve of the proposed CIPR mix.

Table 4.2
Particle Size Distribution Result for Proposed CA and RAP Ratio

BS Sieve Size (mm)	JKR Requirement Cumulative % Passing	CA and RAP Proposed Ratio (%)		
		CA75RAP25	CA50RAP50	CA25RAP75
50.0	100	100.0	100.0	100.0
37.5	85-100	100.0	100.0	100.0
20.0	60-100	88.5	95.0	97.4
10.0	40-90	60.2	71.9	75.7
5.0	30-75	48.8	53.7	51.9
2.36	20-60	32.4	33.6	26.6
0.425	10-45	18.3	19.6	12.5
0.075	2-20	2.0	3.2	2.3

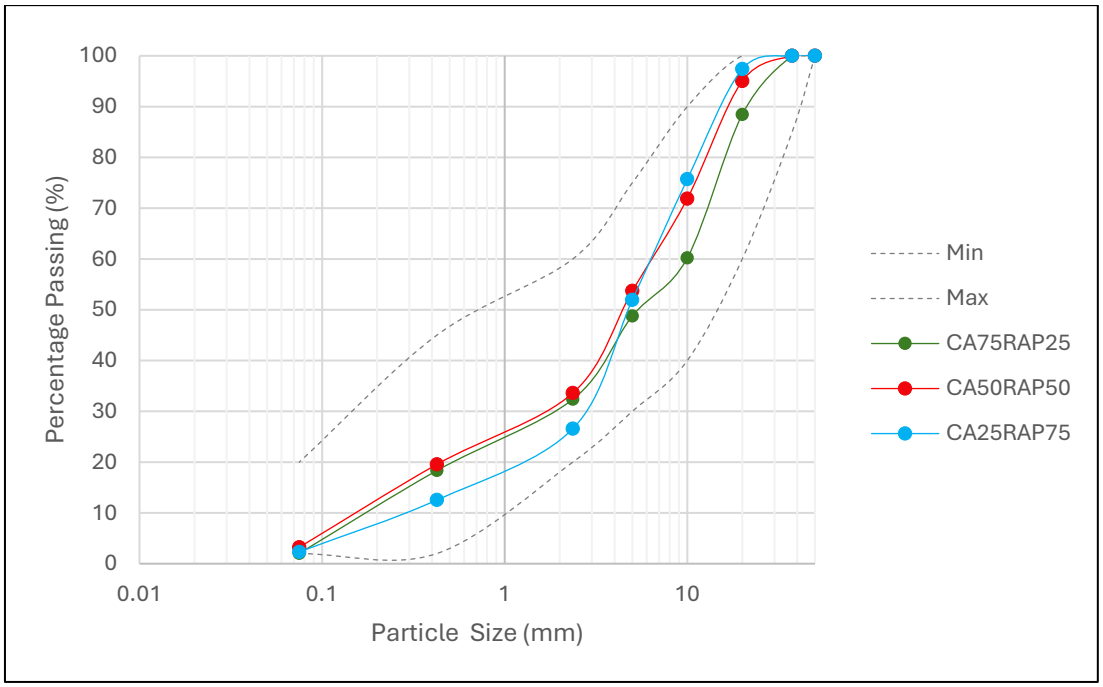


Figure 4.2 Particle Size Distribution Curve of Proposed CIPR Mix

The results revealed a consistent trend in the particle size distribution within the proposed mix, with materials passing through sieves ranging from 37.5 mm to as fine as 0.075 mm. This finding was consistent with the research conducted by Sufian et al. (2008), which observed a similar particle size distribution trend. The research also showed that nearly all particles passed through the 37.5 mm sieve. Given the identical composition ratio of CA and RAP used in both studies, the consistency in particle size distribution was significant. This consistency not only validated the findings of Sufian et al. (2008) but also highlighted the reproducibility and reliability of the particle size distribution within the proposed mix design.

4.2.1.3 Particle Size Distribution for Site Samples

The particle size analysis of the site samples is summarized in Table 4.3, which presents the particle size distribution data for each site. Additionally, Figure 4.3 presents this information graphically, clearly representing the particle size distribution patterns observed at the Penang and Kedah sites.

Table 4.3
Particle Size Distribution Result for Site 1 and 2

BS Sieve Size (mm)	JKR Requirement Cumulative % passing	Site 1 Jalan B.Baharu-Merbau Pulas, Kulim, Kedah CA52RAP48	Site 2 Jalan Butterworth – Ipoh, Pulau Pinang CA60RAP40
50.0	100	100.0	100.0
37.5	85-100	99.8	98.2
20.0	60-100	89.3	86.4
10.0	40-90	60.3	62.7
5.0	30-75	48.7	46.7
2.36	20-60	32.1	31.2
0.425	10-45	18.6	17.9
0.075	2-20	2.0	2.4

The analysis results confirmed a consistent distribution trend, with most particles passing through the 37.5 mm sieve. These findings served as a reference, reinforcing the uniformity of particle size distribution across different sites. Although the sites data were used primarily as reference, they further supported the overall consistency and stability of the particle size characteristics in the proposed mix design.

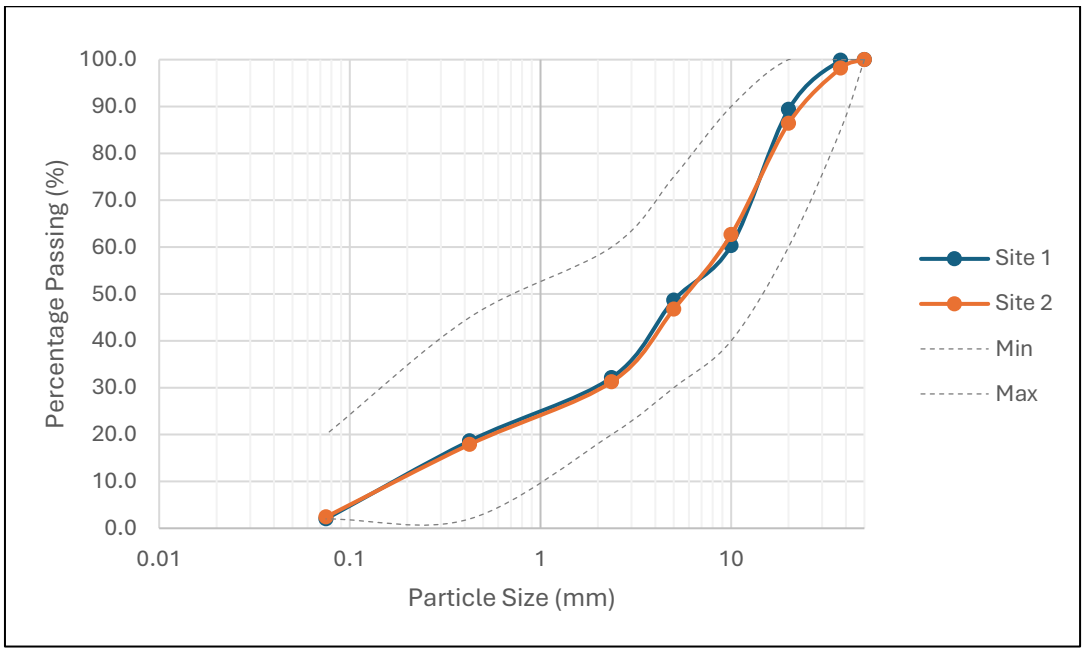


Figure 4.3 Particle Size Distribution Curve of Site 1 and 2

The analysis of these samples further validated that the proposed gradation of CA and RAP in this research complied with the allowable limits stipulated in JKR/SPJ/2008-S4. The results confirmed that the selected gradation was appropriate for

the research, ensuring compliance with the specified requirements and validating the suitability of the proposed mix for pavement construction parameters.

Particle size distribution within the pavement base plays a critical role, as it directly affects the strength performance and long-term durability of the pavement structure (Asrie et al., 2024). Optimal particle size distribution plays a critical role in enabling the pavement base to withstand varying traffic loads effectively. A well-graded mix, incorporating particles of diverse sizes, helps distribute imposed loads more uniformly, preventing excessive compaction or deformation, particularly under heavy traffic conditions. Proper compaction during construction is important, and an appropriate particle size distribution facilitates this process. Conversely, an overly uniform or fine particle size distribution can hinder adequate compaction, compromise pavement stability and increase the risk of premature failure.

In summary, the analysis of each proposed gradation (CA25RAP75, CA50RAP50, and CA75RAP25) revealed distinct percentages of material passing through various sieve sizes. These variations provided the foundation for understanding how material gradation influences strength performance. The findings offered useful insights for selecting the most appropriate gradation based on site conditions and pavement requirements, ultimately contributing to improved durability and performance of the pavement structure.

4.2.2 Specific Gravity

The specific gravity values obtained for all samples are presented in Table 4.4, providing information on the density and composition of the materials, determined in accordance with ASTM D854 (2000), Method A.

Table 4.4
Specific Gravity of The Materials

Material	Specific Gravity, Gs
OPC	2.93
GCBA	2.56
Aggregate Dust	2.43
RAP	2.00
CIPR mix Site 1	1.95
CIPR mix Site 2	1.98

The specific gravity of OPC in this research was measured at 2.93, slightly below the typical range of 3.10 to 3.25. This deviation might be attributed to variations in the raw materials used during cement production such as limestone, clay, shale, and iron ore whose individual densities directly influence the overall specific gravity of the final OPC product.

For GCBA, the specific gravity was recorded at 2.56. This value aligns closely with the findings of Ayob et al. (2014), who reported a specific gravity of 2.54 for bottom ash sourced from the same TNB Jana Manjung power station. Additionally, previous studies, including Ramzi et al. (2016), have shown that the specific gravity of CBA typically ranges between 1.39 and 2.66, depending on the power plant source. These variations are often linked to particle size where finer particles tend to exhibit higher specific gravity due to their denser microstructure and reduced porosity. In this research, GCBA was ground to pass through a 45 μm sieve, a fineness that likely reduced pore spaces and air entrapment, thereby increasing the particle density and contributing to the observed value of 2.56.

The analysis also revealed that aggregate dust had a specific gravity of 2.43, while RAP recorded the lowest value at 2.00. The relatively low specific gravity of RAP was likely the result of aging and oxidation from prolonged exposure to environmental elements such as UV radiation, air, and moisture. These conditions can degrade the asphalt binder, increase brittleness, and reduce material density, as reflected in the reduced specific gravity. This drop in density provides indirect evidence of physical and chemical changes occurring in RAP over time, reinforcing the importance of understanding material degradation when considering its reuse in pavement applications.

Site-collected samples measured specific gravity values of 1.95 (Site 1) and 1.98 (Site 2). However, direct comparison between these composite samples and individual materials is not straightforward due to the nature of site samples. These mixes likely included varying proportions of aggregate dust, RAP, cement, and possibly soil, each with differing densities. As such, the measured specific gravity reflects an average value, influenced by the relative abundance and properties of each component. The presence of lighter materials like RAP and fine particles likely contributed to the lower overall specific gravity of the site mixes.

In the context of pavement base construction, specific gravity plays a vital role in influencing the mechanical behavior of materials. Higher specific gravity is generally

associated with denser and more compactable materials, which contribute positively to strength and load-bearing capacity. For instance, the relatively high specific gravity of OPC (2.93) and GCBA (2.56) indicated their potential to enhance matrix density and bonding when used as stabilizing agent, which in turn might improve UCS and stiffness. A similar trend was reported by Kabeta and Lemma (2023), who observed that increasing the specific gravity of mixes through the inclusion of steel slag raised the maximum dry density and significantly improved the UCS.

Conversely, the lower specific gravity values recorded for RAP (2.00) and site-collected samples (1.95-1.98) likely reflect the presence of aged or porous constituents that reduce overall mix density and compromise structural integrity under the load. Hence, the variations in specific gravity among the constituent materials offer an early indication of their potential influence on the mechanical performance of the composite mixes.

In summary, the specific gravity values of individual materials provided useful insight into their physical characteristics. However, interpreting the specific gravity of composite site samples requires consideration of the blended nature of the materials involved. Understanding this complexity is crucial when evaluating performance expectations in practical applications, particularly in pavement base construction.

4.2.3 Particle Shape Analysis

According to BS 812-105.2:1990 and MS 30, the flakiness and elongation index of the aggregate base material must not exceed 25%, as exceeding this limit can significantly affect the properties of the mix. High values in flakiness and elongation indices can reduce cohesion between the stabilizing agent and the mix, potentially resulting in segregation, inadequate particle bonding, and diminished overall mix performance.

Table 4.5 presents the particle shape analysis for CA and RAP, along with the mix composition of the CA-RAP mixes.

Table 4.5
Particle Shape Analysis

Material	Flakiness Index (%)	Elongation Index (%)
CA	9.93	6.38
Combined value	16.31	
RAP	11.54	7.08
Combined value	18.62	
CA75 RAP25	9.72	7.66
Combined value	17.38	
CA50 RAP50	11.29	8.79
Combined value	20.04	
CA25 RAP75	13.49	9.01
Combined value	22.5	
Requirement	<25% of combined value	

The results showed that the CA and RAP recorded flakiness and elongation indices of 16.31% and 18.62%, respectively. Among the proposed mix design, CA25RAP75 exhibited the highest combined index at 22.50%, followed by CA50RAP50 (20.04%) and CA75RAP25 (17.38%). The higher index value in the CA25RAP75 mix can be attributed to the greater proportion of RAP, which is more prone to producing elongated and flaky particles. Nonetheless, all values remained within the acceptable limits of less than 25%, as specified in BS 812-105.2:1990 and MS 30, confirming compliance with standard requirements.

These findings are consistent with those reported by Penumala and Bharthavarapu (2018), where natural aggregate and RAP recorded combined flakiness and elongation indices of 17.6% and 22.7%, respectively. The slightly higher values associated with RAP are largely due to the milling process used to extract it from aged asphalt pavements. This process tends to produce more flattened and elongated particles, which influence the overall shape characteristics of RAP (Endale, 2023).

In summary, while RAP generally exhibited a slightly higher flakiness and elongation index due to its method of recovery, the values observed across all mix designs in this research remained within the limits. This confirms that the particle shape characteristics of the materials used were suitable for pavement base applications.

4.2.4 Aggregate Durability

The aggregate durability was analyzed based on LA abrasion and AIV test conducted on both proposed mix design and site specimens.

4.2.4.1 LA Abrasion

The LA Abrasion test is an essential method for evaluating the abrasion resistance of aggregates, demonstrating their suitability and performance across various applications. According to ASTM C 131 Standards, the LA abrasion value should not exceed 40% for base course, signifying an acceptable level of particle loss. Table 4.6 displays the results of this test, highlighting the performance of the aggregate materials used in this research.

Table 4.6
LA Abrasion for Proposed CA-RAP Ratio and Site Samples

Test	CA and RAP Ratio (%)		
	CA75 RAP25	CA50 RAP50	CA25 RAP75
LA Abrasion (%)	28.68	35.21	38.43
Site 1: Jalan B.Baharu - Merbau Pulas, Kulim, Kedah (CA52RAP48)			
LA Abrasion (%)		33.42	
Site 2: Jalan Butterworth - Ipoh, Pulau Pinang (CA60RAP40)			
LA Abrasion (%)		30.85	
Min Requirement (%)		< 40	

The results indicated that the CA25RAP75 mix, which contained the highest proportion of RAP, recorded the greatest particle loss (38.43%) during the LA abrasion test. In contrast, the CA75RAP25 mix exhibited the lowest particle loss, highlighting a clear trend in which higher CA content is associated with greater resistance to abrasion. This suggested that an increased proportion of CA enhances the durability and resistance of the mix to mechanical wear, thereby reducing particle loss under repeated loading.

A comparison between the proposed mix design and field samples from Site 1 (Kedah) and Site 2 (Penang) revealed only minor differences. Site 1 recorded a particle

loss of 33.42%, while Site 2 showed a slightly lower value of 30.85%. These values are closely aligned with those of the proposed mix design, confirming the comparability and consistency of the materials across both lab-based and field conditions.

The higher abrasion loss associated with RAP-rich mixes is consistent with the findings of Pawar and Sinhar (2022), who reported that RAP exhibited greater susceptibility to particle breakdown during the LA abrasion test compared to virgin aggregates. This is attributed to ageing and environmental degradation over time due to factors such as exposure to UV radiation, traffic loading, moisture, and temperature fluctuations which contribute to the oxidation and brittleness of the asphalt binder. As the binder loses its flexibility and adhesive properties, the underlying aggregate becomes more prone to fracture, contributing to the observed increase in particle loss.

In summary, while higher RAP content led to greater particle loss, all mixes remained within the specified limit of less than 40%, confirming their suitability for use in pavement base applications. These findings proved the importance of optimizing the CA-RAP ratio to ensure both durability and compliance with mechanical performance standards.

4.2.4.2 Aggregate Impact Value

The AIV test, along with the LA abrasion test, was conducted to evaluate aggregate durability for pavement construction. According to BS 812-112: 1990 and MS 30, the AIV percentage should not exceed 25%. The results in Table 4.7 showed the percentage loss of AIV for proposed CA-RAP ratios and the site samples.

Table 4.7
AIV for Proposed CA-RAP Ratio and Site Samples

Test	CA and RAP Ratio (%)		
	CA75 RAP25	CA50 RAP50	CA25 RAP75
AIV (%)	15.99	17.34	19.55
Site 1: Jalan B.Baharu - Merbau Pulas, Kulim, Kedah (CA52RAP48)			
AIV (%)	17.85		
Site 2: Jalan Butterworth - Ipoh, Pulau Pinang (CA60RAP40)			
AIV (%)	17.12		
Requirement (%)	< 25		

The results from the AIV tests highlighted clear patterns among the various CA-RAP ratios. CA25RAP75 mix exhibited the highest AIV percentage at 19.55%, followed by CA50RAP50 mix at 17.34%, and CA75RAP25 mix recorded the lowest AIV at 15.99%. Lower AIV percentages signify a greater resistance of the aggregate to impact. This quality is highly desirable in pavement construction as it indicates higher durability, reducing the likelihood of aggregate breakage or degradation when subjected to sudden loads or impacts. Such durability is essential for ensuring the quality and long-term longevity of the pavement base.

The observed trend suggested that as the proportion of RAP in the mix increased, the AIV also increased, consistent with the results reported by Ng et al. (2023). This pattern aligned with the understanding that RAP, typically located in the top pavement layer and exposed to weathering processes, exhibited resilience against impact damage compared to the aggregates below it. This demonstrated how RAP content influenced the ability of aggregates to withstand impacts, with higher RAP proportions potentially reducing the overall resilience of the pavement base and its durability under sudden loads or impacts. The finding was also verified by Rout et al. (2023), who found that the AIV of RAP aggregates was higher than that of natural aggregates, indicating reduced toughness properties in the recycled aggregates.

The comparison of the AIV results from the site samples, Site 1 with an AIV of 17.85% and Site 2 with an AIV of 17.12% with the laboratory samples revealed minimal differences. Despite minor differences in the CA and RAP gradations between the site and laboratory samples, the AIV values remained consistent, indicating comparable impact resistance characteristics across both sources.

In summary, all mixes, including the proposed CA-RAP ratios and the site samples, exhibited AIV values below the specified maximum limit of 25%. Accordingly, they were considered suitable for use in the CIPR mix design, satisfying the requirements for pavement construction and demonstrating compliance with the standard.

4.2.5 pH Index Value

The pH value of the mix design served as a critical factor influencing the initiation and progression of the hardening process, as determined in accordance with ASTM D4972-19. Baghini et al. (2016) highlighted that soil with an organic material

possessing a pH below 5.3 might not interact effectively with cement, potentially affecting the hardening process due to more acidic conditions. While pH itself might not directly impact cement hydration reactions, extreme pH levels can indirectly influence the process and affect concrete properties. Baghini et al. (2016) also suggested that a pH exceeding 12.0 does not impede the hardening process. Table 4.8 presents the pH index values for the proposed mix design.

Table 4.8
pH Index Value for Proposed Mix Design

CA and RAP Ratio (%)		Stabilizing Agent (%)		pH Index Value $CaCl_2$			
CA	RAP	GCBA	OPC	0%	1%	2%	3%
75	25	3	1	14.52	13.67	12.34	11.33
		2	2	14.70	14.12	12.76	11.74
		1	3	14.63	14.15	12.98	11.95
		0	4	14.77	14.21	13.08	12.13
50	50	3	1	14.68	14.65	12.48	11.05
		2	2	14.81	14.75	13.24	11.90
		1	3	14.78	14.54	13.30	12.28
		0	4	14.83	14.70	13.31	12.21
25	75	3	1	14.53	14.21	12.53	11.23
		2	2	14.71	14.38	12.86	11.78
		1	3	14.64	14.35	13.10	11.93
		0	4	14.77	14.25	12.97	11.97
-	-	4	0	9.85	-	-	-
-	-	0	4	14.31	-	-	-
-	-	0	0	-	6.35	-	-

The pH index values for GCBA and OPC were recorded at 9.85 and 14.31, respectively. The higher alkalinity of OPC was attributed to its substantial Lime (CaO) content. When GCBA was mixed with OPC, the pH index increased, with all of the proposed mix designs exhibiting values around 14. This indicated an alkali-rich environment, which is favorable for the hydration and hardening process (Chen et al., 2024).

However, mixes incorporating higher percentages of $CaCl_2$ tended to exhibit lower pH levels. The lowest recorded pH index was 11.05, observed in the CA50RAP50 formulation composed of 3% GCBA, 1% OPC, and 3% $CaCl_2$. In contrast, the highest pH value of 14.83 was obtained from the CA50RAP50 mix containing only 4% OPC, highlighting the strong alkalinity when $CaCl_2$ and GCBA were absent.

The pH index of the mixes decreased progressively with increasing $CaCl_2$ content, in agreement with the observations by Liu and Wu (2025). They reported that the pH of hydrated samples continuously decreased as the $CaCl_2$ dosage increased, with the control sample exhibiting the highest pH throughout the curing period. Although $CaCl_2$ does not hydrolyze significantly or produce acidic species like HCl under normal conditions, its neutral to mildly acidic behavior (measured at pH 6.35 in this research) moderately offsets the alkalinity of more basic components such as OPC and GCBA.

For comparison, the pH values of the site-collected samples, which stabilized solely with OPC, were recorded at 12.29 and 12.75, respectively, as presented in Table 4.9. These values confirm the alkaline nature of OPC-based stabilization under field conditions, consistent with the laboratory findings.

Table 4.9
pH Index Value for Site Samples

Site	CA-RAP Ratio (%)		Stabilizing Agent (%)	pH index value
	CA	RAP	OPC	
Site 1 Jalan B.Baharu - Merbau Pulas, Kulim, Kedah	52	48	4	12.29
Site 2 Jalan Butterworth - Ipoh, Pulau Pinang	60	40	4	12.75

A comparative analysis revealed that the combination of GCBA, OPC, and lower percentages of $CaCl_2$ resulted in slightly higher pH values (around 13-14) in the proposed mix design compared to the site samples stabilized with OPC alone (around 12). However, as noted in the specific gravity test, the composite nature of the site samples may have influenced the measured pH index. Nevertheless, the results indicated that incorporating the proposed alternative stabilizing agent produced slightly higher pH values at the optimum mix level.

In summary, the notable difference in pH values between the proposed mix design and the site samples indicated a potential positive influence of the stabilizing agent on the hydration and hardening behavior. The marginal increase in pH further indicated a shift in the chemical environment that could have promoted hydration reactions and contributed to improved hardening of the mix.

4.2.6 Scanning Electron Microscope and Energy Dispersive X-Ray

The SEM analysis in this research served to examine the microstructure of particles, while the EDX analysis was done to acquire the elemental composition and distribution within the specimen.

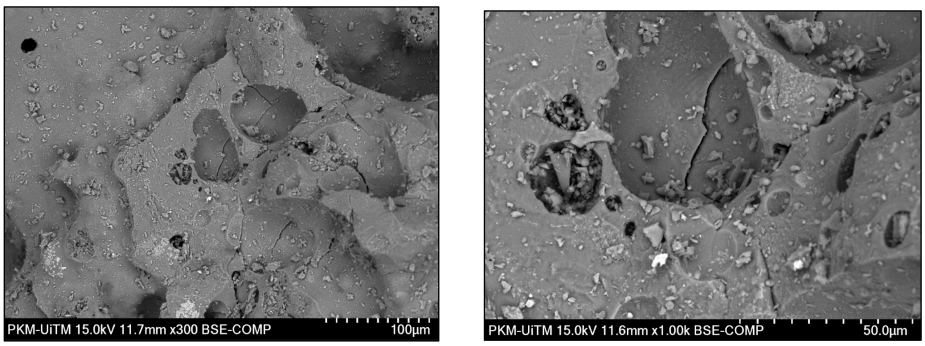
4.2.6.1 Scanning Electron Microscope

Figure 4.4 to Figure 4.21 presents the SEM result conducted on the specimens of stabilizing agent containing OPC, GCBA and $CaCl_2$.

The microstructures of the raw CBA and the ground GCBA passing through a 45 µm sieve, are shown in Figures 4.4 and 4.5. The microstructures of CBA and GCBA particles were examined in more depth using SEM at magnifications of 300× and 1000×, providing detailed information about their morphology and properties.

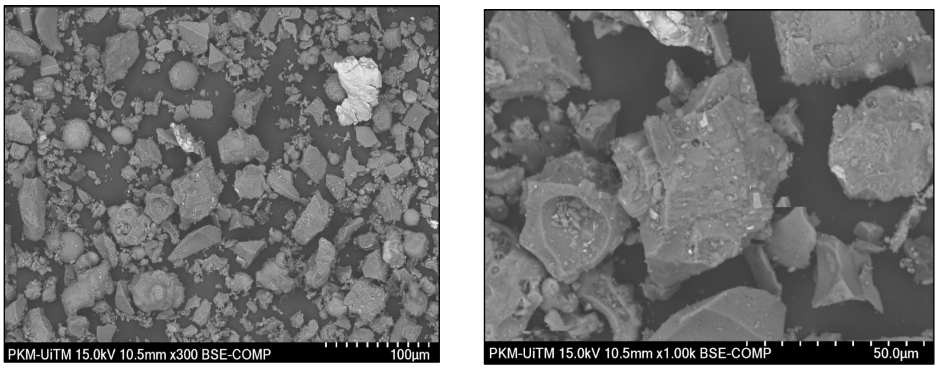
The SEM analysis revealed that both the raw CBA and GCBA exhibited angular and irregular shapes with rough textures. This characterization is aligned with findings from research conducted by Ayob et al. (2014), where the particles displayed similar characteristics of uneven and rough surfaces alongside angular and irregular shapes. This structural resemblance was attributed to the higher presence of unburned carbon in CBA compared to fly ash, which contributed to the observed particle morphology.

The microstructural analysis revealed distinct differences between the untreated CBA and the treated CBA (GCBA). While the CBA exhibited pores within its particle structure, the treatment process applied to GCBA notably eliminated most of these pores. This transformation indicated that grinding CBA into finer particles effectively reduced the porosity within the particle structure, minimizing the possibility of moisture entrapment within the particles.



(a) (b)

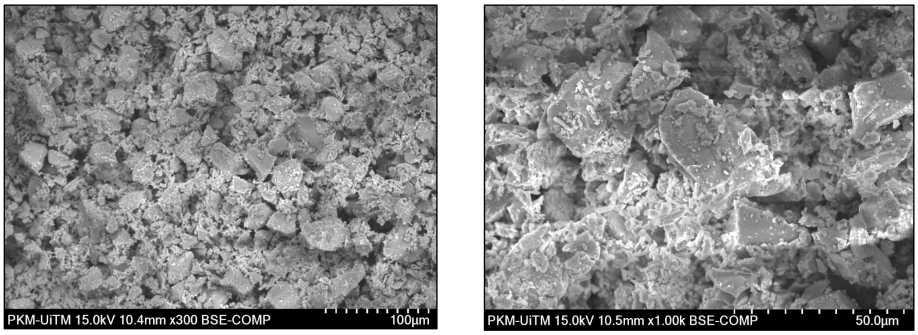
Figure 4.4 Microstructure of CBA at (a) 300× and (b) 1000× Magnifying Power



(a) (b)

Figure 4.5 Microstructure of GCBA at (a) 300× and (b) 1000× Magnifying Power

Figure 4.6 illustrates the microstructures of OPC particles observed at 300× and 1000× magnification. In contrast to GCBA, OPC particles showed a uniform structure free of apparent pores, suggesting a more consistent and pore-free morphology inside the particles. According to Mehta and Monteiro (2014), the absence of visible pores indicated that OPC particles were less prone to internal weaknesses that could compromise their integrity. This uniformity was necessary for the strength and durability of the cementitious materials, as it ensured that the particles could effectively bind together to form a solid and stable matrix.



(a) (b)

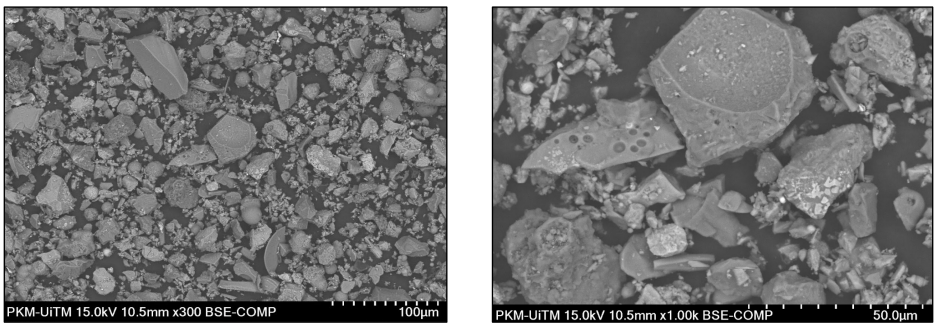
Figure 4.6 Microstructure of OPC at (a) 300× and (b) 1000× Magnifying Power

Given that GCBA was mixed with OPC and $CaCl_2$ as a stabilizing agent, maintaining an appropriate moisture content in the mix design became essential. This moisture content played a crucial role in facilitating the proper hydration process of the cement material and the pavement base particles (Neville, 2015). It is important because moisture significantly influences the hydration process, with excess moisture potentially impeding chemical reactions, as stated in the report by Little and Nair (2009). This interference could have reduced the effectiveness of the stabilizing agent

in achieving the desired strength and durability of the base course. According to Mehta and Monteiro (2001), adequate moisture levels during hydration promote the formation of calcium silicate hydrate (C-S-H) gel and other crystalline products, which are essential for developing a dense and durable cementitious matrix.

The 300× and 1000× magnifications displayed in Figures 4.7 to 4.10 provide a closer examination of the microstructures of mixed specimens containing 3% GCBA + 1% OPC, along with various proportions of $CaCl_2$.

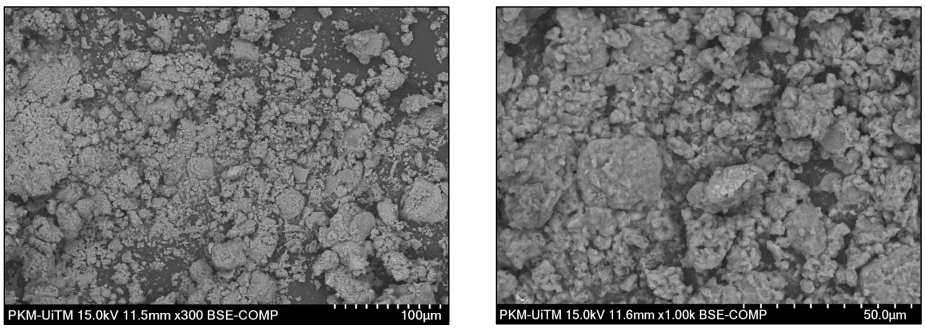
Figure 4.7 shows the mix containing 3% GCBA + 1% OPC, exhibiting a relatively uniform particle distribution. With only 1% OPC, there was insufficient cementitious paste to adequately coat the 3% GCBA particles. The surface appeared less dense, with loosely packed particles, suggesting a weaker matrix formation.



(a) (b)

Figure 4.7 Microstructure of 3% GCBA + 1% OPC at (a) 300× and (b)1000× Magnifying Power

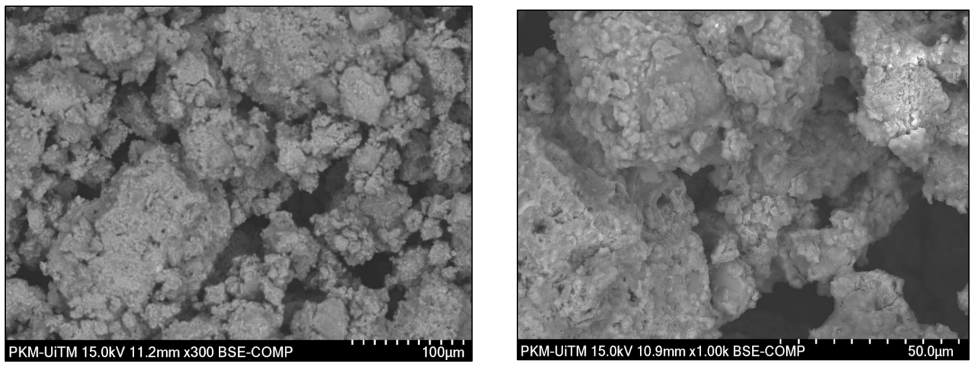
In Figure 4.8, the inclusion of 1% $CaCl_2$ promoted particle aggregation, thereby benefiting the initial stages of material curing. At higher magnification, significant crystalline growth was observed, which may further influence the mechanical properties of the mix.



(a) (b)

Figure 4.8 Microstructure of 3% GCBA + 1% OPC + 1% $CaCl_2$ at (a) 300× and (b) 1000× Magnifying Power

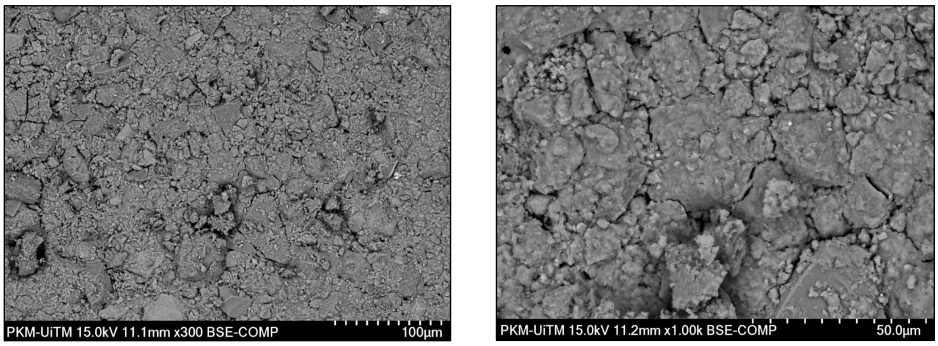
With the addition of 2% $CaCl_2$, as shown in Figure 4.9, the matrix exhibited noticeable particle clumping. $CaCl_2$ typically accelerates the hydration process. However, at higher concentrations (2%), it may result in rapid setting and insufficient time for proper particle packing and alignment, which could lead to the clustering of the stabilizing agent. At higher magnification, increased surface roughness was observed. Larger crystalline formations were also visible, indicating that $CaCl_2$ may have promoted the development of these structures.



(a) (b)

Figure 4.9 Microstructure of 3% GCBA + 1% OPC + 2% $CaCl_2$ at (a) 300× and (b) 1000× Magnifying Power

Compared to the previous mix, Figure 4.10 shows that the matrix became denser with the addition of 3% $CaCl_2$. Cementitious materials are known to hydrate more rapidly when $CaCl_2$ is added. The accelerated hydration promoted the faster formation of C-S-H gel, which filled the spaces between the particles and resulted in a denser matrix. However, noticeable microcracks were observed on the rough surface at higher magnification. This was possibly due to the significant heat generated during the rapid hydration process induced by $CaCl_2$.

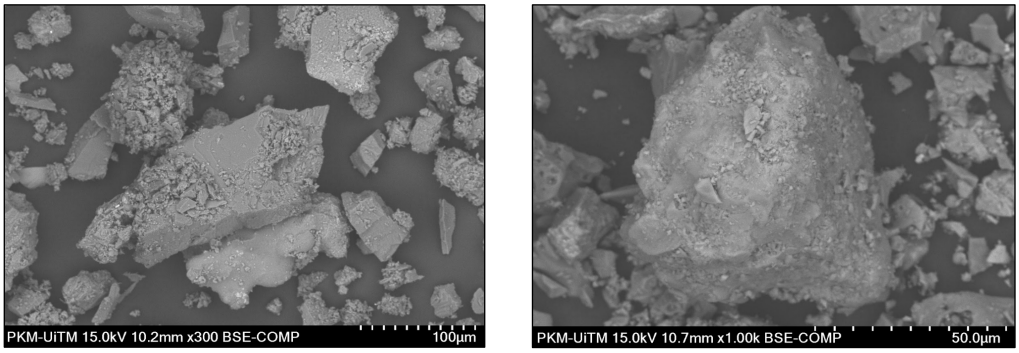


(a) (b)

Figure 4.10 Microstructure of 3% GCBA + 1% OPC + 3% $CaCl_2$ at (a) 300× and (b) 1000× Magnifying Power

Figures 4.11 to 4.14 present the microstructures of mixed specimens containing 2% GCBA + 2% OPC with varying percentage of $CaCl_2$, observed at 300× and 1000× magnifications.

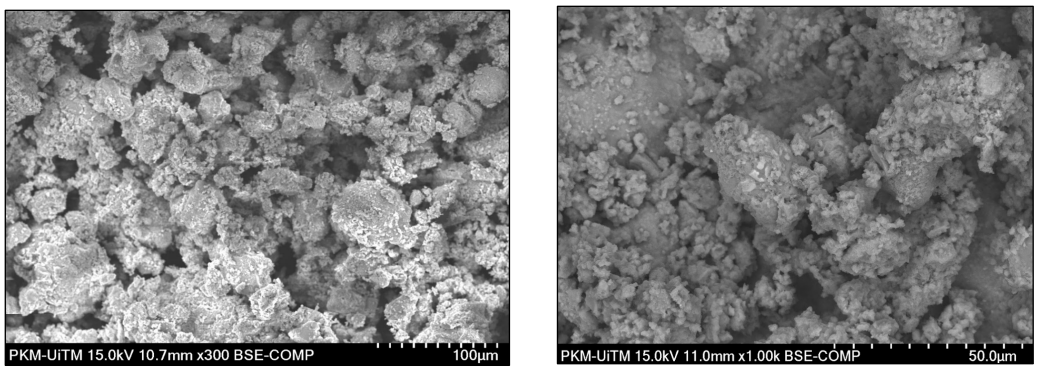
As seen in Figure 4.11, the microstructure of the matrix containing 2% GCBA + 2% OPC showed particles with a noticeable uneven distribution and irregular shapes. The gaps between the particles suggested a moderate level of porosity. At higher magnification, the surface appeared rough with visible textural irregularities. These characteristics indicated the occurrence of typical hydration reactions. However, the particle arrangement and surface properties may have influenced the overall matrix strength.



(a) (b)

Figure 4.11 Microstructure of 2% GCBA + 2% OPC at (a) 300× and (b) 1000× Magnifying Power

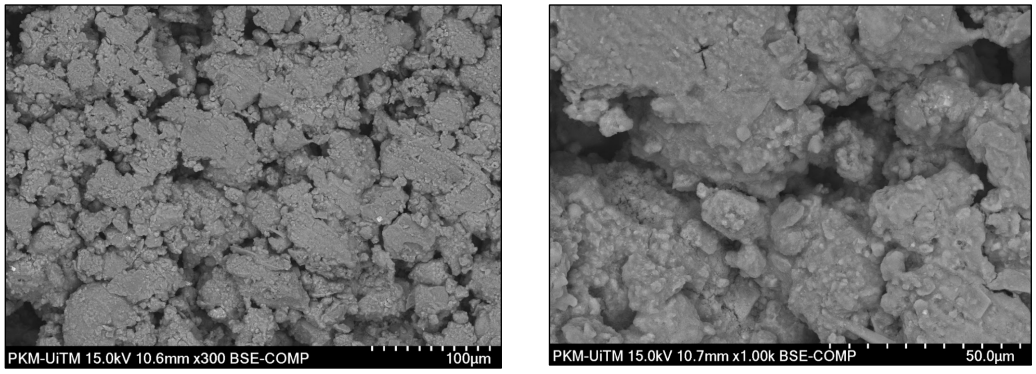
In Figure 4.12, the matrix density increased with the addition of 1% $CaCl_2$, which may have accelerated the hydration process. This indicated that C-S-H gel formed more rapidly, thereby improving particle packing. At higher magnification, the surface appeared rougher, likely due to crystal formation induced by $CaCl_2$.



(a) (b)

Figure 4.12 Microstructure of 2% GCBA + 2% OPC + 1% $CaCl_2$ at (a) 300× and (b) 1000× Magnifying Power

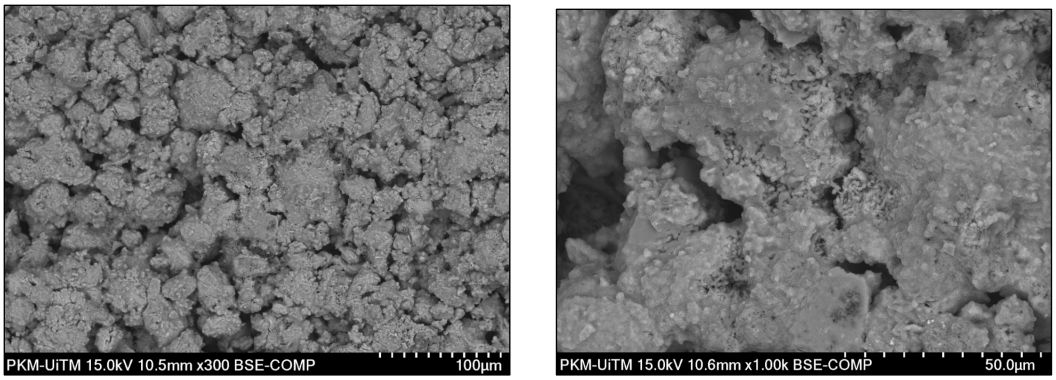
The addition of 2% $CaCl_2$ resulted in a significant increase in the density of the matrix, with minimal visible voids, as shown in Figure 4.13. This 2% $CaCl_2$ might have further accelerated the hydration process, leading to a denser mix. The reduction in gaps also indicated improved particle cohesiveness within the mix. However, the increased percentage of $CaCl_2$ caused considerable thermal stress and a rapid hydration process, making the microcracks more visible under higher magnification.



(a) (b)

Figure 4.13 Microstructure of 2% GCBA + 2% OPC + 2% $CaCl_2$ at (a) 300× and (b) 1000× Magnifying Power

In Figure 4.14, the microstructure of the mix containing 3% $CaCl_2$ appeared denser and exhibited fewer voids compared to the previous mix. The higher percentage of $CaCl_2$ contributed to a denser matrix due to the accelerated hydration process, which allowed the particles to pack more efficiently. However, this rapid hydration might have caused significant thermal stress and shrinkage, leading to the formation of microcracks that were observed at higher magnification.

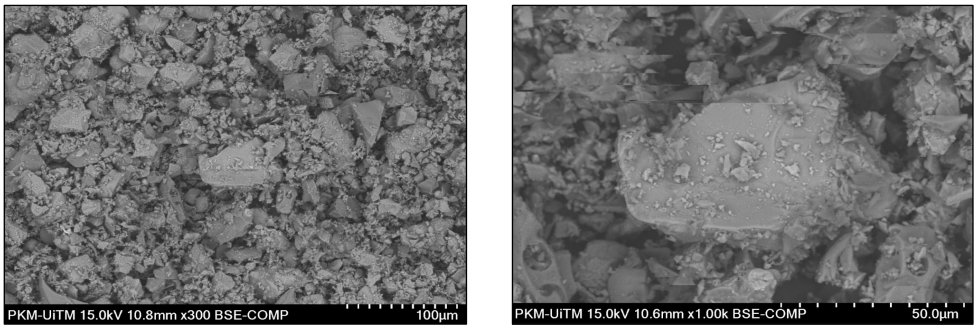


(a) (b)

Figure 4.14 Microstructure of 2% GCBA + 2% OPC + 3% $CaCl_2$ at (a) 300× and (b) 1000× Magnifying Power

The microstructures of the mix specimens containing 1% GCBA + 3% OPC, and varying percentages of $CaCl_2$ are illustrated in Figures 4.15 to 4.17, observed at magnifications of 300× and 1000×.

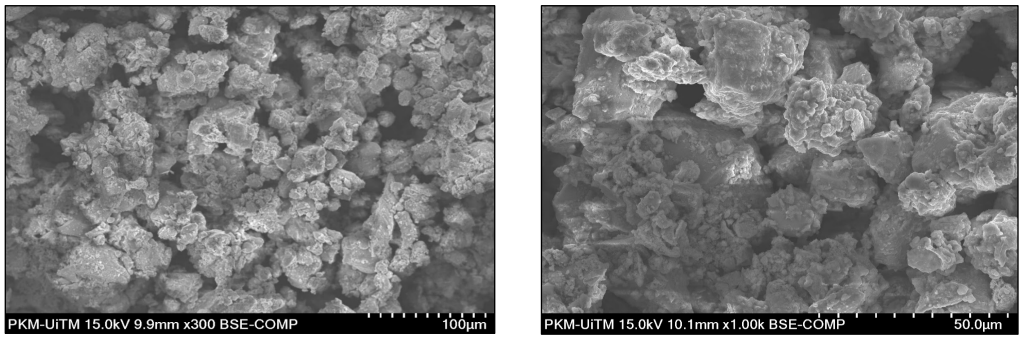
In Figure 4.15, the microstructure of the mix design specimen with 1% GCBA + 3% OPC showed moderate porosity and a relatively uniform distribution of particles. The mix exhibited typical hydration characteristics, as the percentage of OPC was higher than that of GCBA. At higher magnifications, the matrix appeared relatively smooth, with only a few visible voids.



(a) (b)

Figure 4.15 Microstructure of 1% GCBA + 3% OPC at (a) 300× and (b) 1000× Magnifying Power

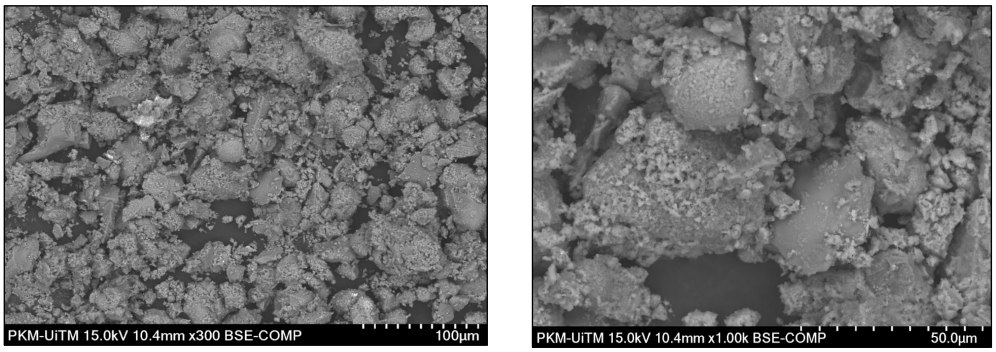
Figure 4.16 shows the microstructure of the mix design containing 1% $CaCl_2$. Compared to the mix without $CaCl_2$, the microstructure appeared denser, with fewer visible voids. The addition of 1% $CaCl_2$ accelerated the hydration process, which enhanced the matrix density by promoting the faster formation of C-S-H gel. At higher magnifications, an increase in surface roughness was observed, likely due to crystalline formations induced by $CaCl_2$.



(a) (b)

Figure 4.16 Microstructure of 1% GCBA + 3% OPC + 1% $CaCl_2$ at (a) 300× and (b) 1000× Magnifying Power

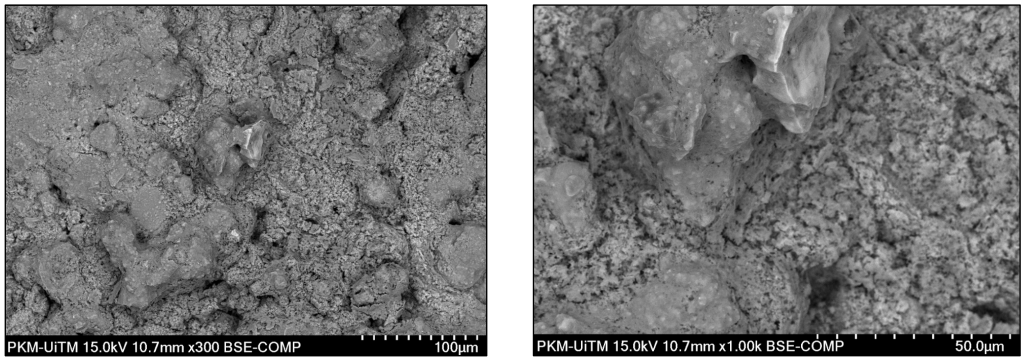
After adding 2% $CaCl_2$, the matrix in Figure 4.17 exhibited a significant increase in density, accompanied by clustering of the stabilizing agent. The 2% $CaCl_2$ content accelerated the hydration process, resulting in a denser matrix. At higher magnification, the increased $CaCl_2$ content appeared to produce a rougher surface, likely due to the formation of larger $Ca(OH)_2$ crystals.



(a) (b)

Figure 4.17 Microstructure of 1% GCBA + 3% OPC + 2% $CaCl_2$ at (a) 300× and (b) 1000× Magnifying Power

The addition of 3% $CaCl_2$ resulted in a highly dense microstructure with very few voids, as shown in Figure 4.18. The significant acceleration of the hydration process likely contributed to this dense matrix. The nearly complete absence of voids indicated optimal particle packing within the mix. Similar to other mixes, noticeable surface roughness was observed, resulting from large crystalline formations at higher magnifications.

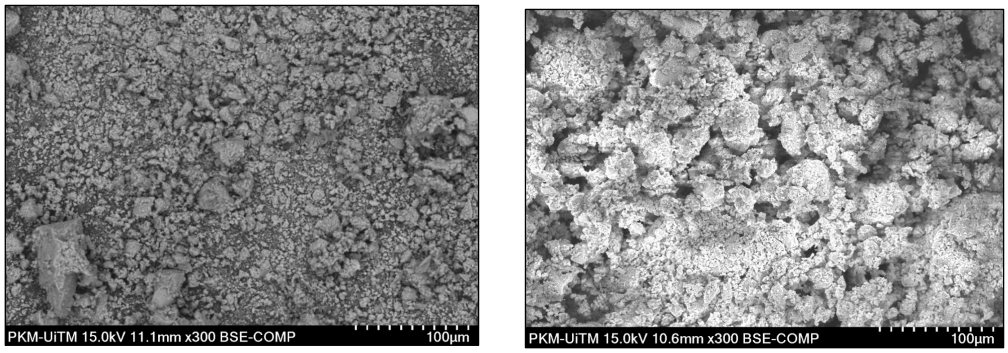


(a) (b)

Figure 4.18 Microstructure of 1% GCBA + 3% OPC + 3% $CaCl_2$ at (a) 300× and (b) 1000× Magnifying Power

Figures 4.19 to 4.21 illustrate the microstructure of the stabilizing agent containing 4% OPC with varying percentages of $CaCl_2$, observed under magnifications of 300× and 1000×, without the presence of GCBA.

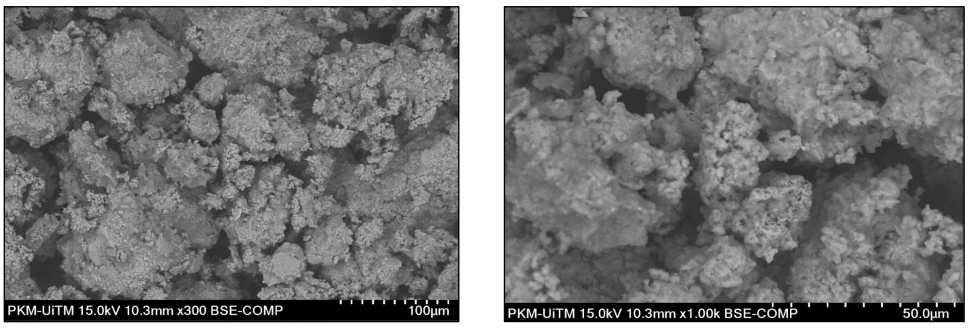
Figure 4.19 displays the microstructure of a specimen containing 4% OPC + 1% $CaCl_2$. The matrix exhibited moderate density, with several visible gaps between the particles, indicating that this composition had not achieved optimal packing efficiency. At higher magnification, crystalline formations contributed to increased surface roughness.



(a) (b)

Figure 4.19 Microstructure of 4% OPC + 1% $CaCl_2$ at (a) 300× and (b) 1000× Magnifying Power

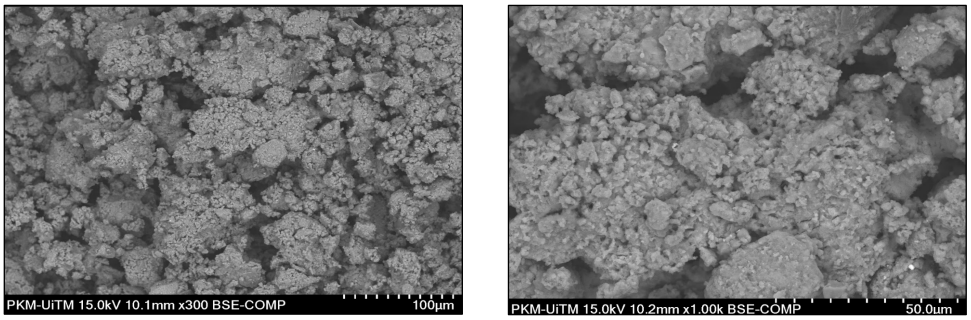
The microstructure of the mix containing 2% $CaCl_2$ appeared denser and exhibited more cluster formations compared to the previous mix, as illustrated in Figure 4.20. The addition of 2% $CaCl_2$ accelerated the hydration process, resulting in a denser matrix with reduced porosity. This improvement in packing efficiency may enhance particle cohesion and bonding within the mix. At higher magnifications, significant surface roughness was also observed.



(a) (b)

Figure 4.20 Microstructure of 4% OPC + 2% $CaCl_2$ at (a) 300× and (b) 1000× Magnifying Power

Figure 4.21 shows the microstructure of a mix containing 4% OPC + 3% $CaCl_2$. The incorporation of 3% $CaCl_2$ produced a highly dense matrix due to the accelerated hydration process. This enhanced hydration promoted maximum particle packing efficiency, evidenced by the prominent formation of clusters. However, as observed in other mixes containing 3% $CaCl_2$, the rapid hydration associated with this high concentration induced significant thermal stress and shrinkage, resulting in the development of microcracks within the matrix. Additionally, large crystalline formations contributed to increased surface roughness.



(a) (b)

Figure 4.21 Microstructure of 4% OPC + 3% $CaCl_2$ at (a) 300× and (b) 1000× Magnifying Power

In summary, Figures 4.7 to 4.21 illustrate the effects of OPC, GCBA, and $CaCl_2$ on the density, cluster formation, surface roughness, and microcracking of the mix design. As reported by Menéndez et al. (2021), incorporating GCBA with OPC in the mix, similar to the use of coal fly ash, promotes the formation of C-S-H during the hydration process. C-S-H serves as a primary binding phase in cementitious materials, contributing to the strength and density of the matrix, which is supported by the pozzolanic performance of GCBA.

On the other hand, the addition of $CaCl_2$ as an accelerator has expedited the formation of C-S-H, resulting in a denser and stronger matrix. However, using a higher percentage of $CaCl_2$ has led to noticeable microcracking and increased surface roughness, which may compromise the mechanical properties of the mix design. This finding aligns with the FHWA (2019), which states that excessive amounts of $CaCl_2$ can have negative effects, including increased surface roughness and potential durability issues. Therefore, while $CaCl_2$ enhances density and early strength, its optimal percentage must be carefully controlled to balance these benefits with the risks of microcracking and increased roughness.

4.2.6.2 Energy Dispersive X-Ray

The elemental composition of OPC, GCBA and $CaCl_2$ was thoroughly investigated using EDX analysis. This analysis provided a detailed assessment of the elemental makeup of these materials, which is crucial for understanding their stabilizing properties and interactions within composite materials.

Figures 4.22 to 4.38, together with Table 4.10, present the comprehensive results of the EDX spectroscopy. These figures and the table illustrate the elements detected in OPC, GCBA, and $CaCl_2$, along with their corresponding weight percentages.

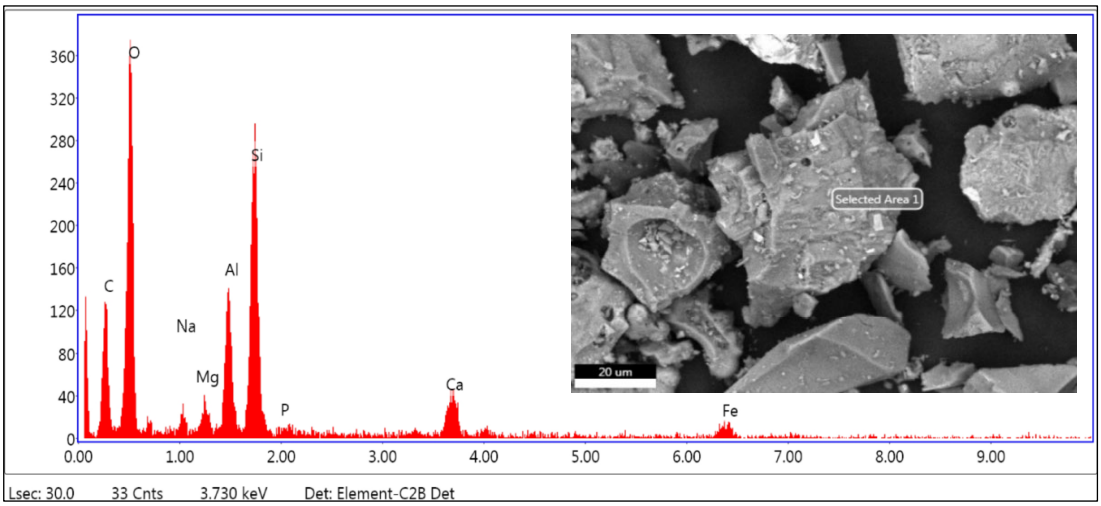


Figure 4.22 Spectroscopy of GCBA

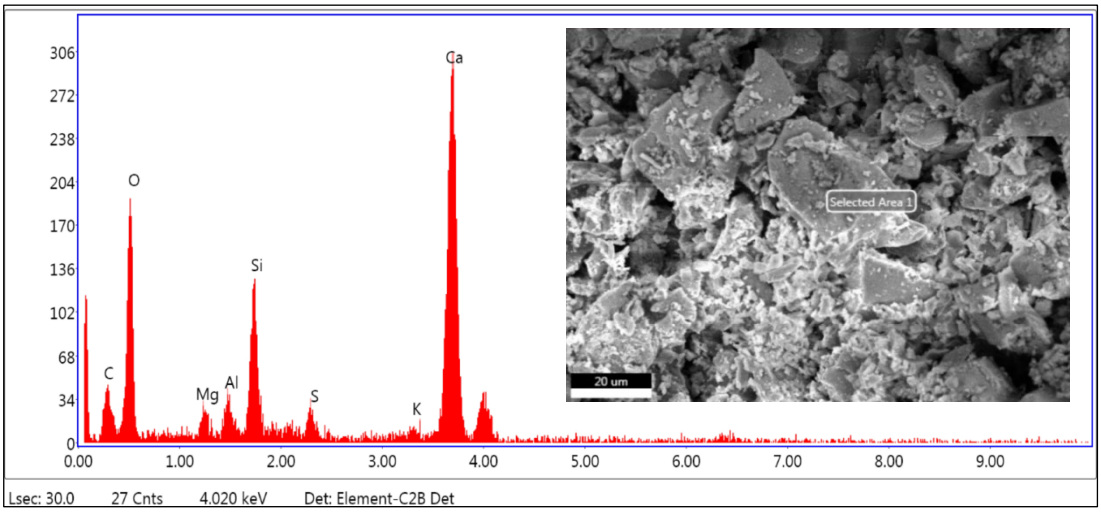


Figure 4.23 Spectroscopy of OPC

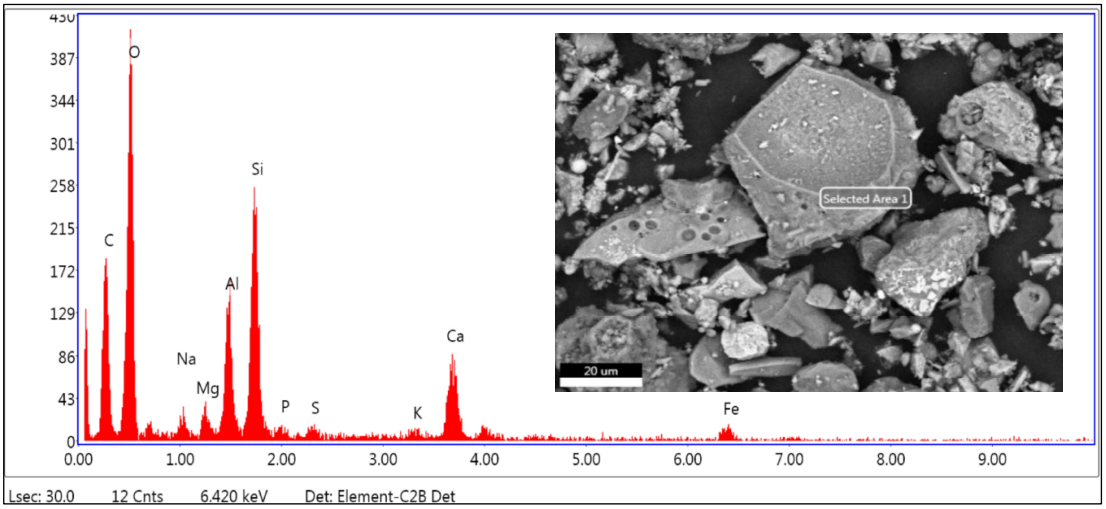


Figure 4.24 Spectroscopy of 3% GCBA + 1%OPC

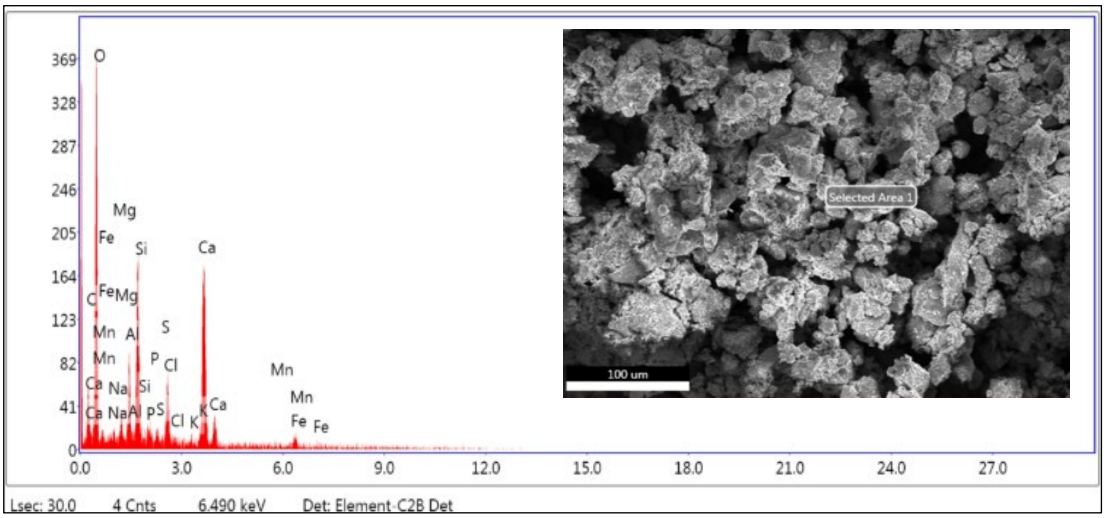


Figure 4.25 Spectroscopy of 3% GCBA + 1%OPC + 1% $CaCl_2$

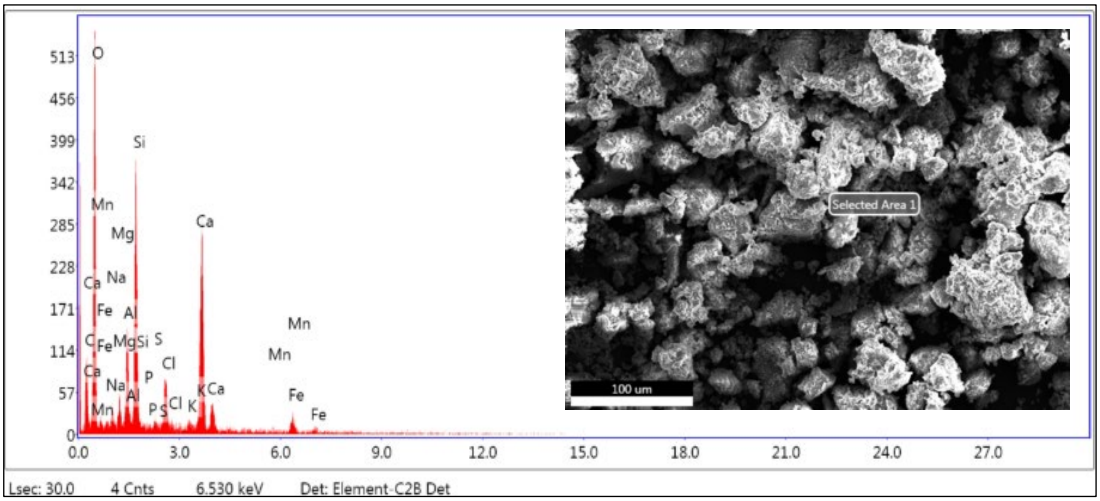


Figure 4.26 Spectroscopy of 3% GCBA + 1%OPC + 2% $CaCl_2$

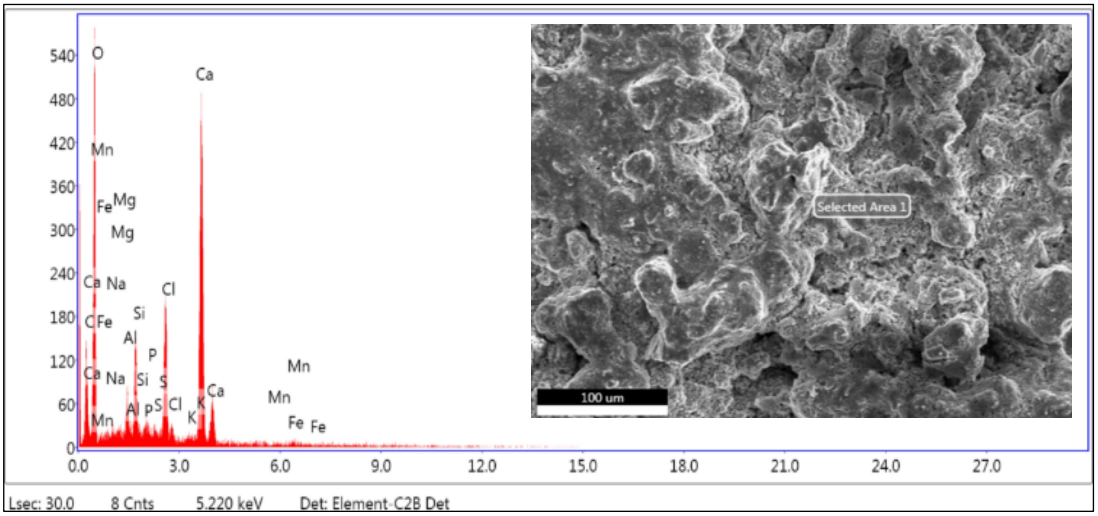


Figure 4.27 Spectroscopy of 3% GCBA + 1%OPC + 3% $CaCl_2$

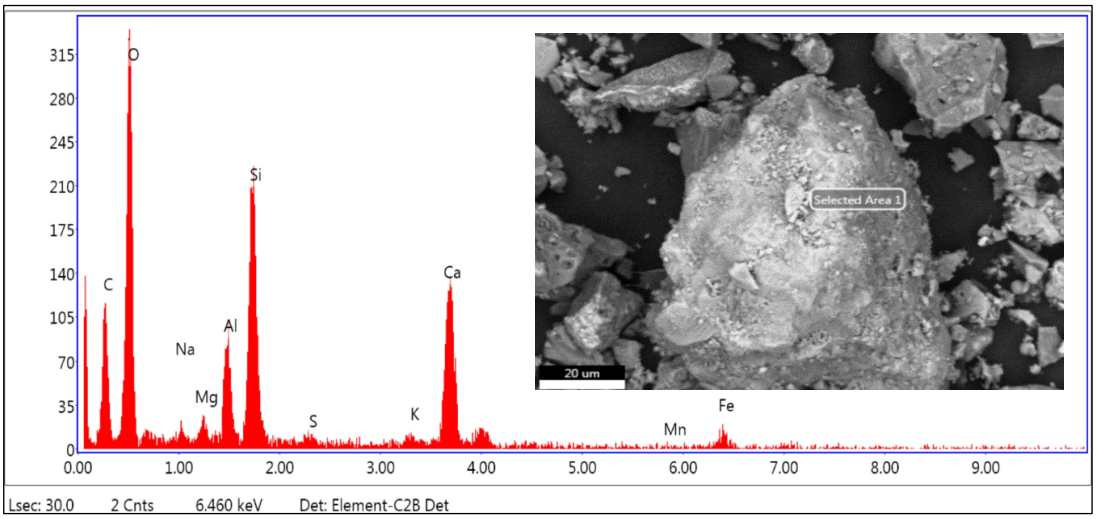


Figure 4.28 Spectroscopy of 2% GCBA + 2% OPC

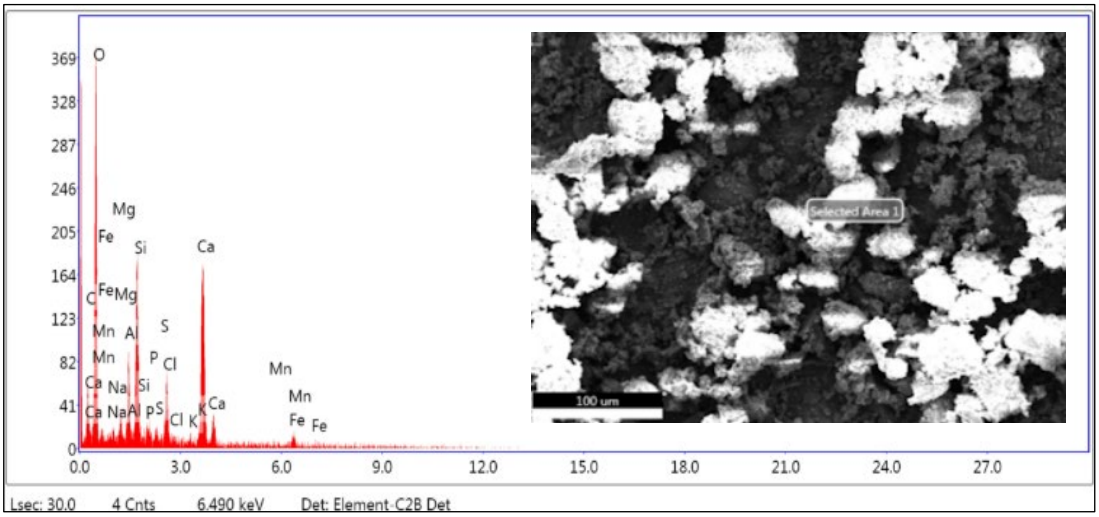


Figure 4.29 Spectroscopy of 2% GCBA + 2% OPC + 1% $CaCl_2$

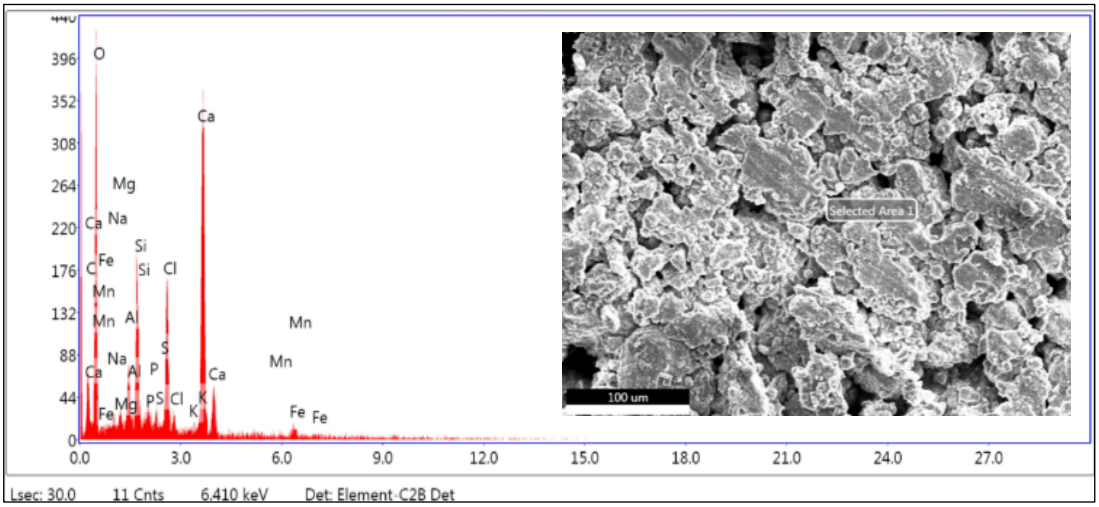


Figure 4.30 Spectroscopy of 2% GCBA + 2% OPC + 2% $CaCl_2$

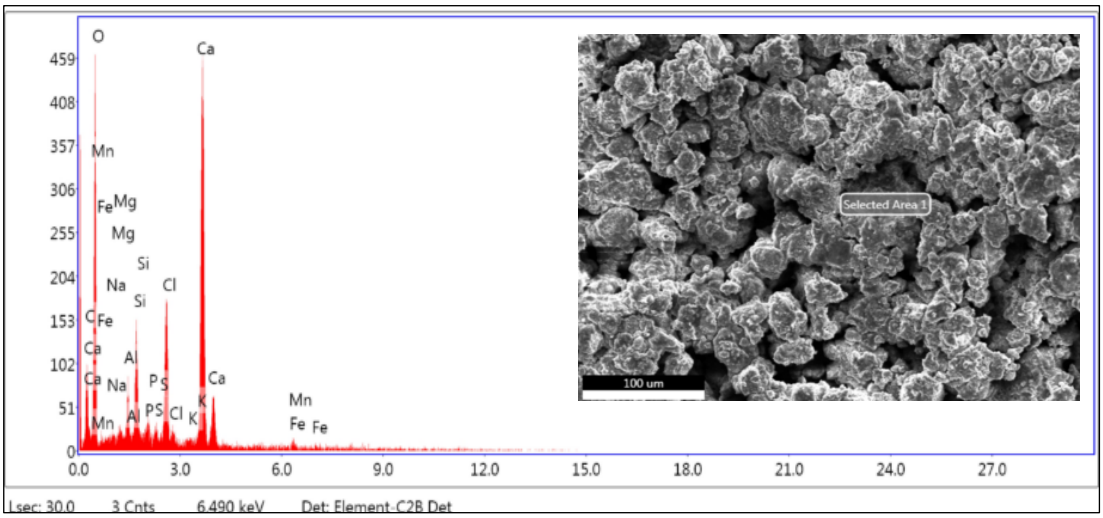


Figure 4.31 Spectroscopy of 2% GCBA + 2% OPC + 3% $CaCl_2$

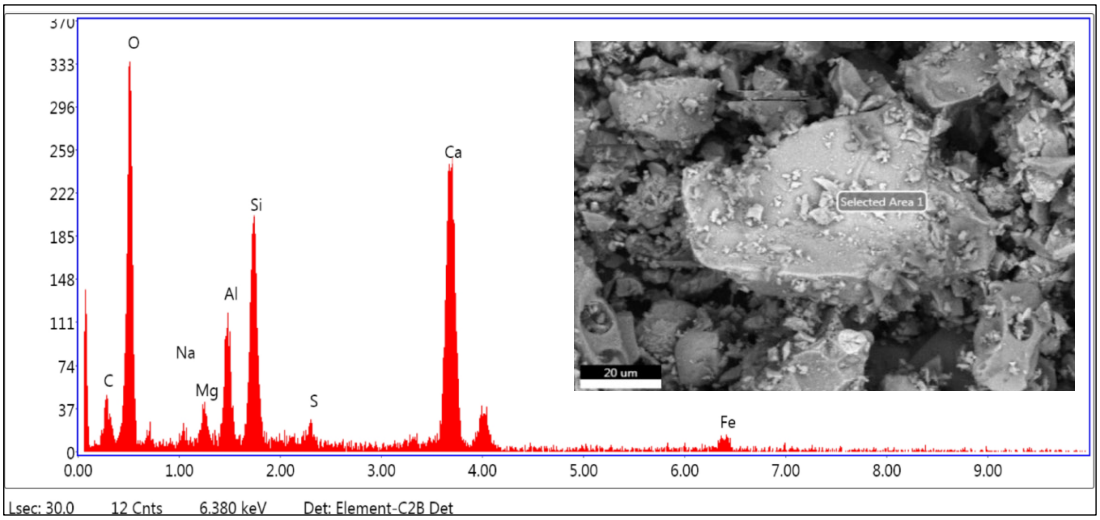


Figure 4.32 Spectroscopy of 1% GCBA + 3% OPC

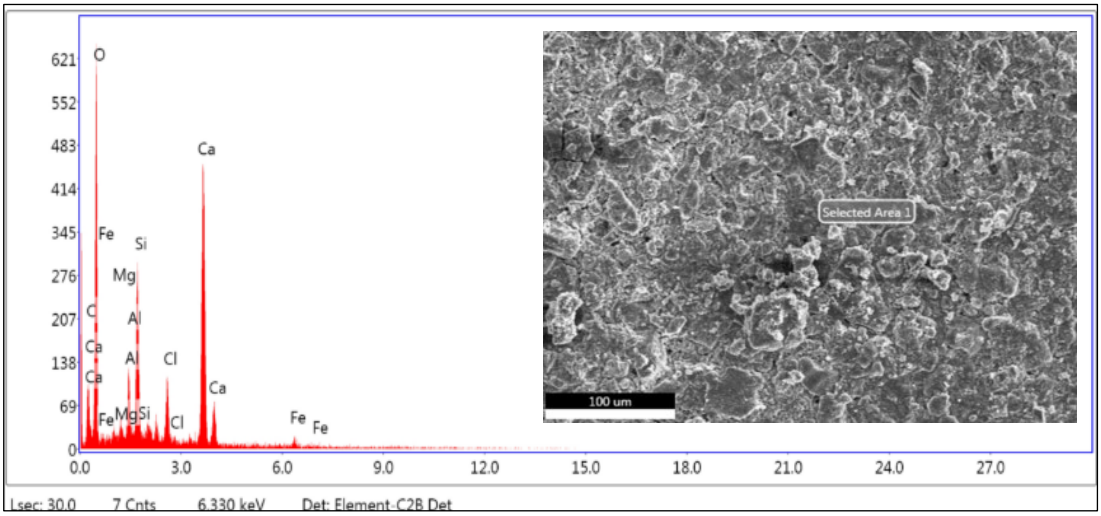


Figure 4.33 Spectroscopy of 1% GCBA + 3% OPC + 1% $CaCl_2$

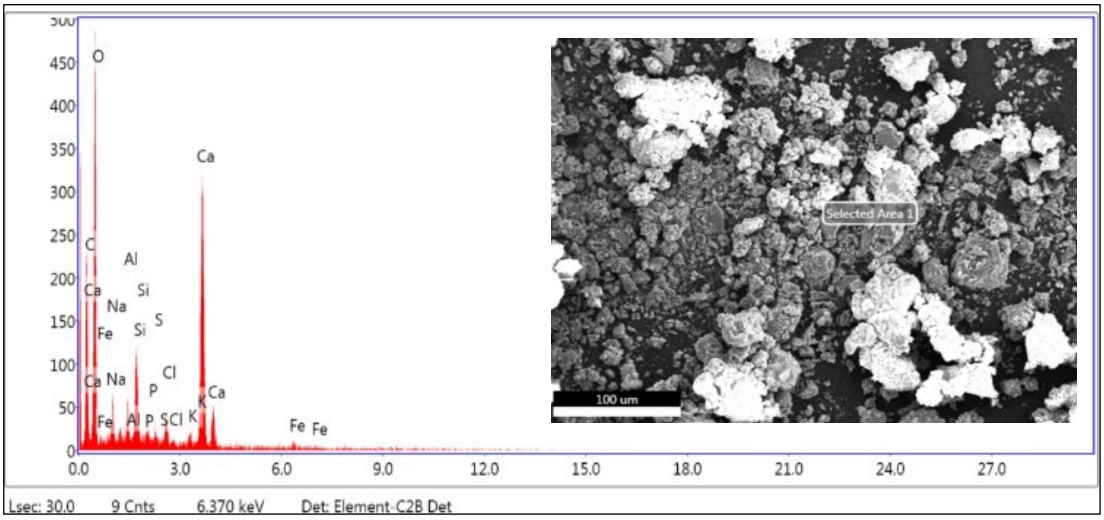


Figure 4.34 Spectroscopy of 1% GCBA + 3% OPC + 2% $CaCl_2$

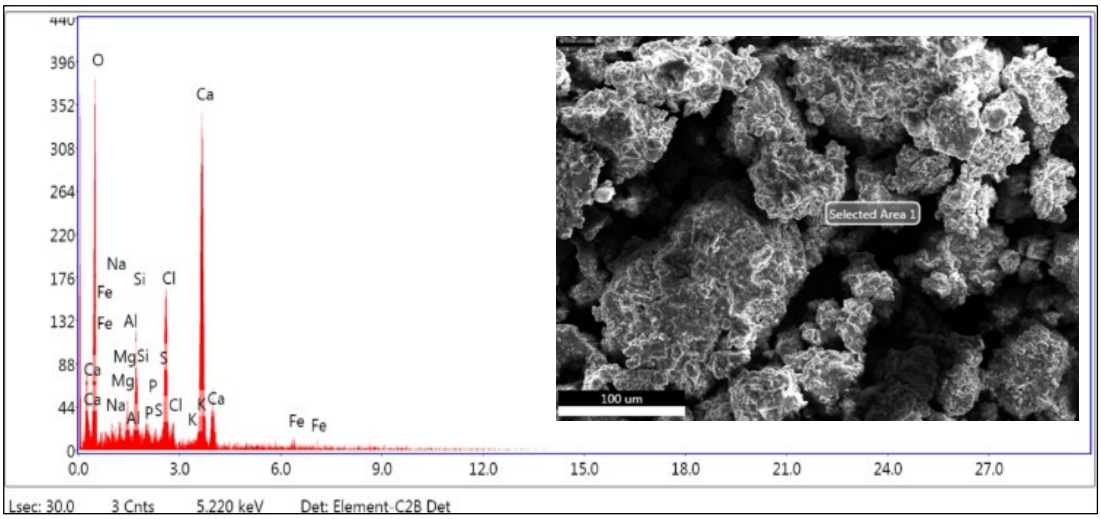


Figure 4.35 Spectroscopy of 1% GCBA + 3% OPC+ 3% $CaCl_2$

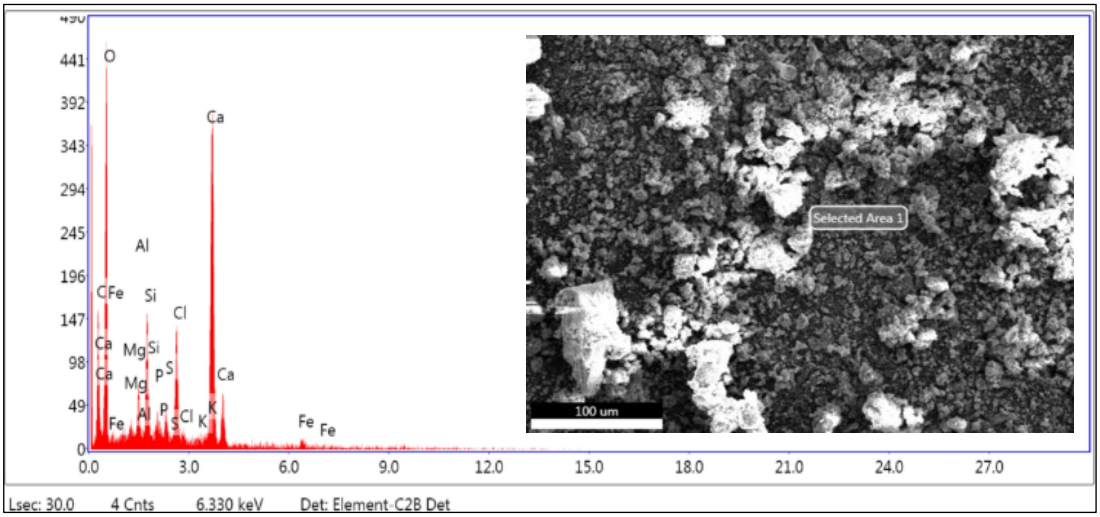


Figure 4.36 Spectroscopy of 4% OPC+ 1% $CaCl_2$

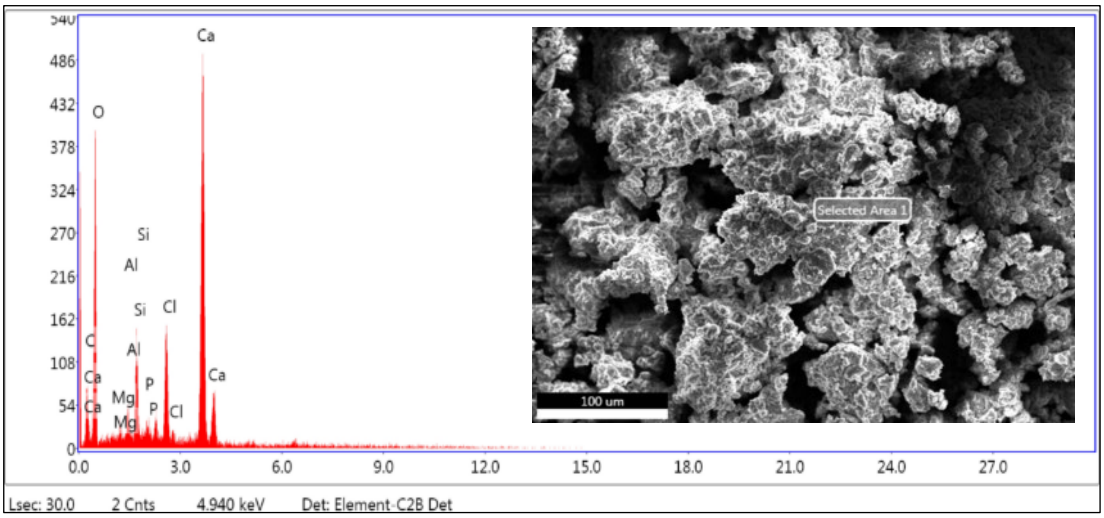


Figure 4.37 Spectroscopy of 4% OPC+ 2% $CaCl_2$

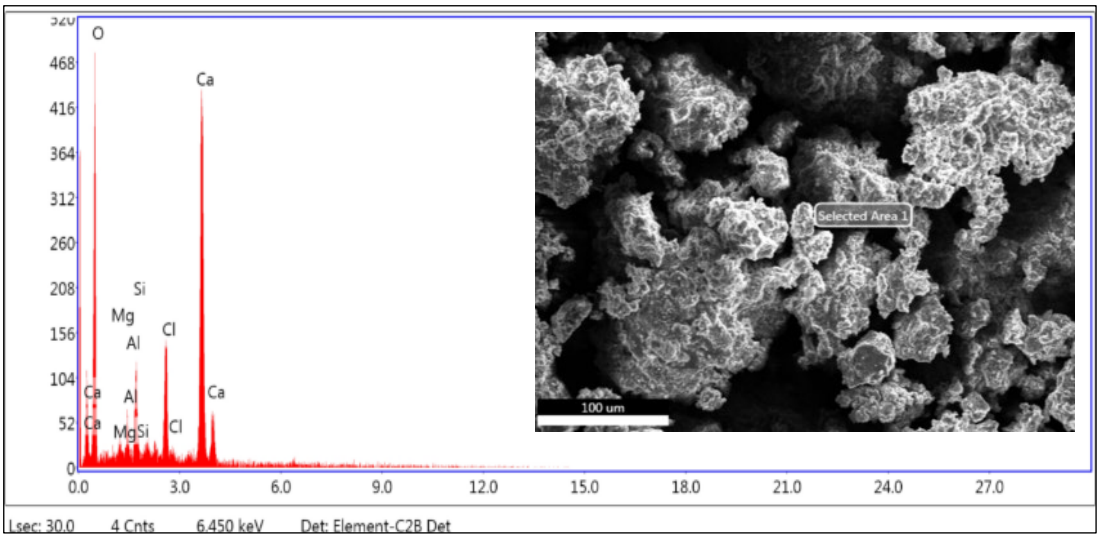


Figure 4.38 Spectroscopy of 4% OPC+ 3% $CaCl_2$

Table 4.10
Chemical Composition of Stabilizing Agent Obtained by EDX

Stabilizing Agent	Weight Percentage (%)												
	C	O	Na	Mg	Al	Cl	Si	P	Ca	Fe	S	K	Mn
GCBA	17.70	38.10	1.10	1.50	8.70	-	20.50	0.60	7.60	4.10	0.50	1.10	-
3% GCBA + 1% OPC	15.60	38.10	0.60	0.90	7.60	-	15.00	0.40	6.70	2.40	0.5	0.90	-
2% GCBA + 2% OPC	8.90	37.30	0.20	0.50	4.90	-	14.40	-	24.70	6.90	0.40	1.00	0.80
1% GCBA + 3% OPC	8.70	36.80	0.10	0.70	4.80	-	10.30	-	41.50	5.30	0.60	0.31	-
OPC	8.50	33.00	-	0.40	0.90	-	6.70	-	57.80	-	0.90	0.40	-
3% GCBA + 1% OPC + 2% $CaCl_2$	8.08	39.71	1.86	0.73	1.21	1.69	4.26	0.43	39.41	2.34	0.35	0.67	0.38
3% GCBA + 1% OPC + 3% $CaCl_2$	7.73	35.23	0.45	0.42	1.59	10.7	4.36	0.87	41.95	3.40	0.54	0.40	0.32
0% GCBA + 4% OPC + 1% $CaCl_2$	5.97	34.07	-	0.25	1.76	7.02	4.83	0.96	39.54	3.42	1.47	0.72	-
1% GCBA + 3% OPC + 2% $CaCl_2$	4.30	37.58	0.69	0.77	4.27	3.91	12.37	0.01	21.69	6.54	0.22	0.74	0.90
1% GCBA + 3% OPC + 3% $CaCl_2$	3.88	36.44	0.23	0.10	1.52	9.17	3.99	0.74	40.20	1.76	0.58	0.66	0.73
0% GCBA + 4% OPC + 3% $CaCl_2$	3.64	41.43	-	0.42	1.10	7.61	3.61	0.48	45.79	1.54	0.68	0.48	-
2% GCBA + 2% OPC + 3% $CaCl_2$	2.91	32.78	0.12	0.25	1.48	8.98	4.04	0.82	42.91	2.86	0.69	0.78	1.37
1% GCBA + 3% OPC + 1% $CaCl_2$	2.24	45.41	0.17	0.84	3.36	4.24	9.48	0.59	27.35	4.68	0.42	0.31	0.88
0% GCBA + 4% OPC + 2% $CaCl_2$	2.09	39.15	-	0.33	1.07	7.10	3.74	0.65	45.88	1.28	0.75	0.32	-
2% GCBA + 2% OPC + 2% $CaCl_2$	2.04	31.87	0.44	0.48	2.32	9.23	6.63	1.15	38.69	4.41	0.92	0.51	1.31
3% GCBA + 1% OPC + 1% $CaCl_2$	1.72	36.83	0.20	0.66	2.92	4.70	8.47	0.43	40.68	4.01	0.30	0.18	0.36
2% GCBA + 2% OPC + 1% $CaCl_2$	1.56	33.33	0.01	0.25	2.07	6.49	6.33	0.59	42.54	5.59	0.61	0.64	-

Note: Weight Percentage (%) represents the weight fraction of each element within the mix design.

From Tables 4.10, it was observed that the chemical composition of GCBA was primarily dominated by Oxygen (O, 38.1%), followed by Silicon (Si, 20.5%), Carbon (C, 17.7%) and Aluminum (Al, 8.7%), along with elements such as Magnesium (Mg), Calcium (Ca), and Iron (Fe). In contrast, OPC exhibited slightly lower Oxygen (O, 33.0%) and Carbon (C, 8.5%) contents but a higher Calcium content (Ca, 57.8%), along with smaller amounts of Silicon (Si, 6.7%) and Sulfur (S, 0.9%).

For all mixes incorporating GCBA, OPC, and $CaCl_2$ at various percentages, calcium consistently appeared as the most dominant element by weight percentage. This trend became more apparent in mixes containing $CaCl_2$, where calcium content increased significantly compared to those without it. The increased calcium levels highlighted their crucial role in hydration and pozzolanic reactions within the cementitious matrix, promoting the formation of C-S-H and other binding products. Meanwhile, oxygen also remained prevalent across all mixes, supporting its participation in the chemical bonding and structure of the hydration products.

Notably, GCBA was rich in compounds containing silicon, which is an essential component of silicate (SiO_4^{2-}) groups, while exhibiting a moderate amount of aluminum associated with aluminate (AlO_4^-) groups. These reactive constituents contributed to the formation of C-S-H and calcium aluminate hydrate (C-A-H), the primary phases responsible for strength development in cementitious materials. Although OPC contained smaller amounts of silicon and aluminum, it provided abundant calcium necessary for these hydration reactions. This observation aligns with Al-Fasih et al. (2019), who identified the pozzolanic activity of silica (SiO_2) and alumina (Al_2O_3) in blended cement systems. Similarly, Marto and Makhtar (2011) also reported that Tanjung Bin CBA mainly comprised silica, alumina, iron, and calcium oxide, which is comparable to the elemental makeup found in GCBA used in this research.

In conclusion, the differences in elemental composition across the various combinations of stabilizing agent clearly played a role in shaping the hydration behavior of the mixes. This directly impacted how quickly the material gained compressive strength, setting time, and long-term stiffness. The combined presence of key elements like oxygen, calcium, silicon, and aluminum confirmed the active pozzolanic and cementitious mechanisms occurring in the treated CA-RAP mixes.

4.2.7 X-Ray Diffraction

The primary objective in conducting XRD analysis on a composite specimen of GCBA, OPC and $CaCl_2$ was to assess the distinct crystalline phases existing within this mix. Significantly, the research identified components including quartz, cristobalite, calcium hydroxide chloride, and calcite among the apparent crystallographic structures inside the composite mixes, revealing common crystalline phases seen in CBA and OPC combinations. The findings from the XRD analysis of GCBA, OPC, and the comprehensive mix comprising all components of the mix design are presented in Table 4.11.

Table 4.11
XRD Analysis of Mix Design

Mix Composition	Crystalline Compound
GCBA	quartz (SiO_2), calcite ($CaCO_3$), portlandite or calcium hydroxide ($CaOH_2$), coesite (SiO_2)
OPC	calcium hydroxide ($CaOH_2$)
1%OPC + 3%GCBA	quartz (SiO_2), calcite ($CaCO_3$), cristobalite (SiO_2)
2%OPC + 2%GCBA	quartz (SiO_2), calcite ($CaCO_3$), calcium aluminum silicide (CaAlSi)
3%OPC + 1%GCBA	quartz (SiO_2), calcite ($CaCO_3$), calcium hydroxide ($CaOH_2$), coesite (SiO_2), berlinite ($AlPO_4$)
1%OPC + 3%GCBA + 1%$CaCl_2$	calcium silicate chloride ($Ca_2SiO_3Cl_2$)
2%OPC + 2%GCBA + 1%$CaCl_2$	quartz (SiO_2), calcite ($CaCO_3$)
3%OPC + 1%GCBA + 1%$CaCl_2$	calcite ($CaCO_3$), cristobalite (SiO_2), calcium aluminum silicide (CaAlSi), coesite (SiO_2), berlinite ($AlPO_4$)
4%OPC + 1%$CaCl_2$	quartz (SiO_2), calcite ($CaCO_3$), calcium aluminum silicide (CaAlSi), calcium hydroxide ($CaOH_2$), cristobalite (SiO_2)
1%OPC + 3%GCBA + 2%$CaCl_2$	quartz (SiO_2), calcite ($CaCO_3$), calcium aluminum silicide (CaAlSi), calcium hydroxide ($CaOH_2$), cristobalite (SiO_2), coesite (SiO_2), berlinite ($AlPO_4$)
2%OPC + 2%GCBA + 2%$CaCl_2$	calcite ($CaCO_3$), calcium aluminum silicide (CaAlSi)
3%OPC + 1%GCBA + 2%$CaCl_2$	calcite ($CaCO_3$), calcium aluminum silicide (CaAlSi), calcium hydroxide ($CaOH_2$), coesite (SiO_2), berlinite ($AlPO_4$)

Table 4.11 (cont.)
XRD Analysis of Mix Design

Mix Composition	Crystalline Compound
4%OPC + 2%$CaCl_2$	quartz (SiO_2), calcite ($CaCO_3$), calcium aluminum silicide (CaAlSi), calcium hydroxide ($CaOH_2$), cristobalite (SiO_2), coesite (SiO_2), berlinite ($AlPO_4$)
1%OPC + 3%GCBA + 3%$CaCl_2$	quartz (SiO_2), calcite ($CaCO_3$), calcium aluminum silicide (CaAlSi), calcium hydroxide ($CaOH_2$), cristobalite (SiO_2), coesite (SiO_2), berlinite ($AlPO_4$)
2%OPC + 2%GCBA + 3%$CaCl_2$	calcite ($CaCO_3$), calcium aluminum silicide (CaAlSi), cristobalite (SiO_2), coesite (SiO_2)
3%OPC + 1%GCBA + 3%$CaCl_2$	quartz (SiO_2), calcite ($CaCO_3$), calcium aluminum silicide (CaAlSi), calcium hydroxide ($CaOH_2$), cristobalite (SiO_2), coesite (SiO_2), berlinite ($AlPO_4$)
4%OPC + 3%$CaCl_2$	quartz (SiO_2), calcite ($CaCO_3$), calcium aluminum silicide (CaAlSi), calcium hydroxide ($CaOH_2$), cristobalite (SiO_2), coesite (SiO_2), berlinite ($AlPO_4$)

A detailed analysis has revealed the presence of several distinct crystalline compounds within the mix design. These crystalline compounds play a significant role in defining the structural and compositional characteristics of the material blend. Some of the compounds found, such as coesite and berlinite do not influence the hydration process. The influence of crystalline compounds, such as quartz, cristobalite, and others, on the hydration process in cementitious systems can vary based on their properties and interactions with each other. The following are the compounds with each of their roles in the hydration process of the mix design that were found in the proposed mix design (Lin et al., 2018; Jiang et al., 2018; Izadifar et al., 2022).

a. Quartz: a common form of crystalline silica, often behaves as an inert filler in cementitious systems. It does not actively participate in hydration but influences properties such as density and porosity.
b. Calcite: acts as an inert filler in cementitious systems when it is present. It does not participate directly in the hydration reactions but occupies space within the matrix, affecting properties like density and porosity. Additionally, calcite can participate in carbonation reactions that help the cement matrix generate calcium carbonate phases.

c. Cristobalite: a high-temperature polymorph of silica where its presence in cementitious systems could indicate the existence of high-temperature processes during the manufacturing of cement or the inclusion of materials rich in silica. It may exhibit higher reactivity due to its structural characteristics, potentially contributing to the pozzolanic reaction, enhancing strength development, and reducing permeability in the concrete matrix.
d. Portlandite or Calcium Hydroxide Chloride: one of the byproducts formed during the hydration of cementitious materials. It influences the mechanical and durability qualities of cementitious materials and functions as a highly soluble cement hydration reaction product.

A nearly similar result can be found in research conducted by Ayob et al. (2014) on the properties of CBA sourced from the same Jana Manjung power plant. This research confirmed the presence of all these crystalline compounds and suggested a consistent composition of CBA from the Jana Manjung power plant. It reinforced the reliability of these results and provided further evidence of the characteristic mineralogy of CBA from the same source.

4.3 Phase Two: Determination of Compaction Properties

The relationship between OMC and MDD is critical, as these parameters are interdependent in achieving the desired engineering performance. Proper compaction is essential because it directly influences both parameters. A detailed analysis of OMC and MDD was carried out to confirm the suitability of the proposed mix design. This analysis aimed to identify the precise moisture content that aligns with the optimum value, essential for maintaining the structural integrity of the base course without compromising its strength.

Subsequently, bulk density analysis was performed on specimens compacted at their respective OMC and MDD values with the inclusion of the proposed stabilizing agent. This analysis provided insights into the degree of compaction achieved under stabilized conditions, ensuring the durability and performance of the base course. A total of 15 specimens were tested for OMC and MDD, and 96 specimens were tested for bulk density.

4.3.1 Optimum Moisture Content and Maximum Dry Density

Table 4.12 summarizes the OMC and MDD identified for the proposed mix design in accordance with BS 1377: Part 4: 1990 (Heavy compaction method), while Figure 4.39 illustrates the corresponding moisture-content-dry-density curve.

Table 4.12
Optimum Moisture Content and Maximum Dry Density of Proposed Mix Design

Grading Sieve Size (mm)	Aggregate Proportion (% Passing)					
	CA25 RAP75	CA25 RAP75 (Sufian et al., 2009)	CA50 RAP50	CA50 RAP50 (Sufian et al., 2009)	CA75 RAP25	CA75 RAP25 (Sufian et al., 2009)
50	100.0	100.0	100.0	100.0	100.0	100
37.5	100.0	99.5	100.0	99.0	100.0	98.5
20	97.4	89.5	95.0	85.5	88.5	82.0
10	75.7	69.0	71.9	66	60.2	63.0
5	51.9	45.0	53.7	45	48.8	45.0
2.36	26.6	28.0	33.6	29	32.4	31.0
0.425	12.5	7.0	19.6	9.5	18.3	12.0
0.075	2.3	3.0	3.2	4.5	2.0	5.0
OMC (%)	5.22	5.14	5.70	5.82	5.87	6.08
MDD (Mg/m^3)	1.85	2.02	1.82	2.16	1.83	2.28

The relationship between OMC and MDD was evident, showing a trend of increasing moisture content as the percentage of CA in the mix design increased. Specifically, in the CA25RAP75 mix, OMC and MDD were recorded at 5.22% and 1.85 Mg/m^3 respectively. With CA50RAP50, OMC increased to 5.70% while MDD at 1.82 Mg/m^3. Further, at CA75RAP25, OMC reached 5.87% with MDD at 1.83 Mg/m^3.

This rise in OMC with increasing CA in the mix design was attributed to the irregular shapes and varied sizes of the CA particles, which resulted in less efficient packing compared to RAP, which comprised finer particles. The observed increase in moisture content was caused by the larger gaps between CA particles, which required more water to fill and facilitate compaction. In contrast, RAP particles tend to interlock more effectively, retaining moisture efficiently within the mix. This discrepancy in particle characteristics between CA and RAP significantly influenced the moisture requirements for achieving proper compaction in the base course mix. These results are consistent with the findings of Sufian et al. (2009) and Debbarma et al. (2021).

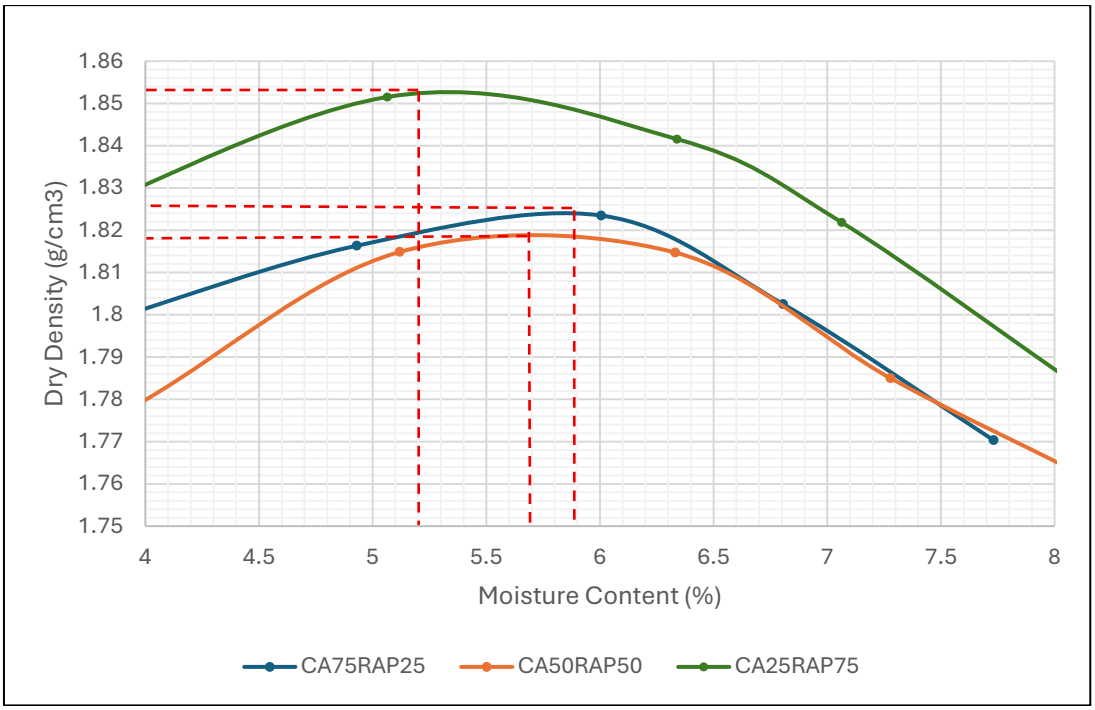


Figure 4.39 Moisture Content Versus Dry Density Curve

The analysis of MDD, as presented in Figure 4.39, revealed that the lowest MDD of 1.82 Mg/m³ was recorded in the mix design containing 50% CA, while the mix with 75% CA achieved 1.83 Mg/m³ and the highest value of 1.85 Mg/m³ was observed in the mix with 25% CA. This trend indicated that the variation in CA and RAP proportions influenced the compaction characteristics of the materials.

Particle size distribution might have contributed to this observation. Although CA typically provides a well-graded gradation that supports better packing efficiency, the highest CA content in the 75% CA mix (1.83 Mg/m³) did not yield the highest MDD. Conversely, the 25% CA mix, which contains a higher proportion of RAP, achieved the highest MDD of 1.85 Mg/m³. This suggested that the finer particles present in RAP might have played a more dominant role in filling the void spaces, leading to a denser packing structure. This finding is supported by Wang et al. (2014), who reported that the inclusion of finer particles at an optimum level enhances packing efficiency by filling voids between coarse particles, leading to higher maximum dry density.

This result was also compared to the research of Sufian et al. (2009), who examined the use of cement and hydrated lime in CIPR with a similar proportion of CA and RAP. Despite slight differences in OMC and MDD between the present research and Sufian et al. (2009), a consistent trend was observed, whereby increasing the proportion of CA in the mix design led to higher OMC values. Although the specific

values varied, the overall pattern aligned across both research. This agreement in trends highlighted the influence of CA content on the moisture characteristics of the mix, indicating consistent behavior across independent investigations.

Furthermore, it was evident that the dry density values started to decrease when the moisture content rose above 6%. This effect was consistent with reports by Gilson Company, Inc. (2025) and Civil Blog (2015), which showed that water started to displace particles within a given volume when the moisture content reached the ideal level, resulting in a decrease in dry density. At this point, the water effectively filled the voids between particles, facilitating easier movement and sliding among the particles. Although this process made the mix design easier to deal with and made compaction easier, the dry density started to decrease. Highlighting the delicate balance between moisture content and dry density in the compaction process, the higher moisture content improved the workability of the mix but unintentionally decreased the density.

4.3.2 Bulk Density

The results presented in Table 4.13, along with the visual trends shown in Figures 4.40 to 4.42, analyze the bulk density of the mix designs with the incorporation of the stabilizing agent in accordance with BS 1377: Part 4: 1990. Notably, the bulk density values showed minimal changes despite the variation in stabilizing agent percentages. Minor fluctuations in bulk density were also observed at different stabilizing agent contents. These findings suggested that the arrangement and packing of the pavement base particles were not significantly altered by the chemical stabilizing agent used in this research. Rather than directly influencing bulk density, the stabilizing agent appeared to primarily enhance the binding characteristics of the mixture. Furthermore, Hou et al. (2021) noted that chemical stabilizing agents often focus on improving bonding and material properties while having a limited influence on the physical packing of the material.

Table 4.13
Result of Bulk Density

Percentage of Stabilizing Agent (%)			Bulk Density (Mg/m^3)		
OPC	GCBA	$CaCl_2$	CA75RAP25	CA50RAP50	CA25RAP75
4	0	0	2.00	1.93	1.89
3	1	0	2.03	1.97	1.92
2	2	0	2.00	1.96	1.94
1	3	0	1.99	1.96	1.92
4	0	1	1.98	1.96	1.91
3	1	1	2.02	1.95	1.93
2	2	1	2.01	1.90	1.89
1	3	1	2.01	1.94	1.90
4	0	2	2.03	1.98	1.94
3	1	2	2.00	1.95	1.92
2	2	2	2.03	1.97	1.92
1	3	2	1.99	1.91	1.90
4	0	3	1.99	1.89	1.90
3	1	3	2.01	1.90	1.89
2	2	3	2.00	1.91	1.90
1	3	3	1.99	1.93	1.89

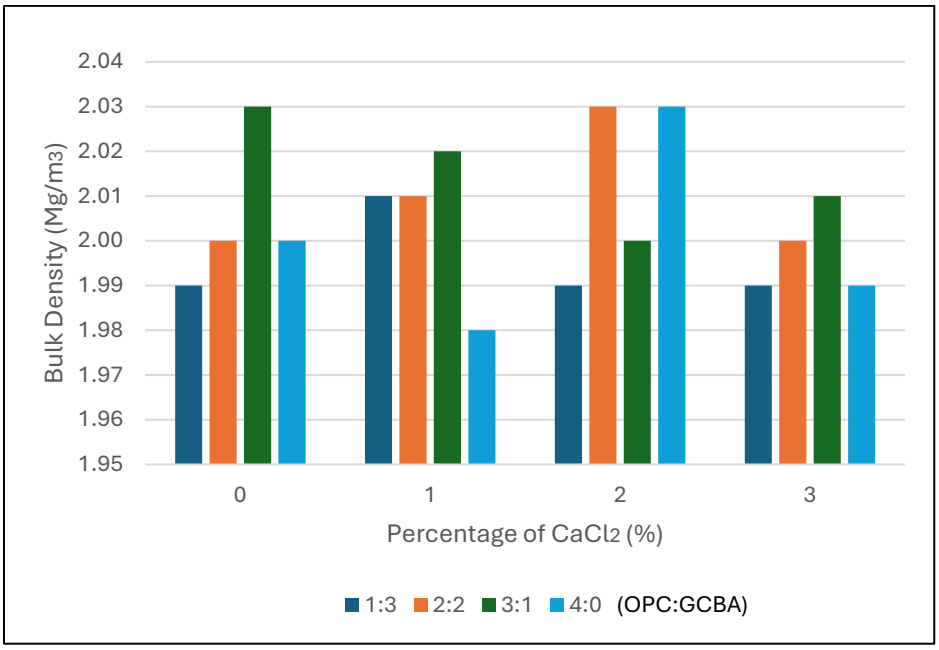


Figure 4.40 Bulk Density for CA75RAP25 Mix

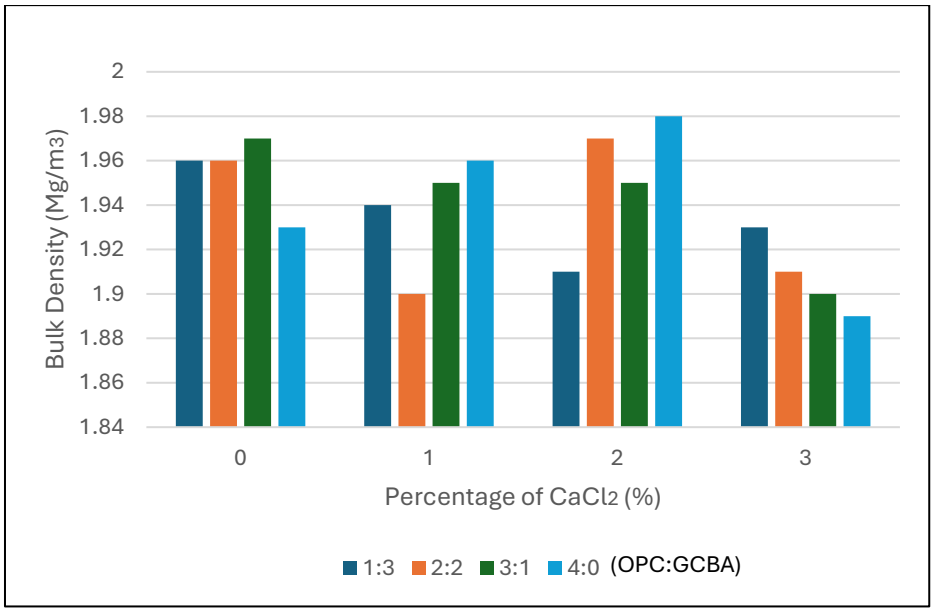


Figure 4.41 Bulk Density for CA50RAP50 Mix

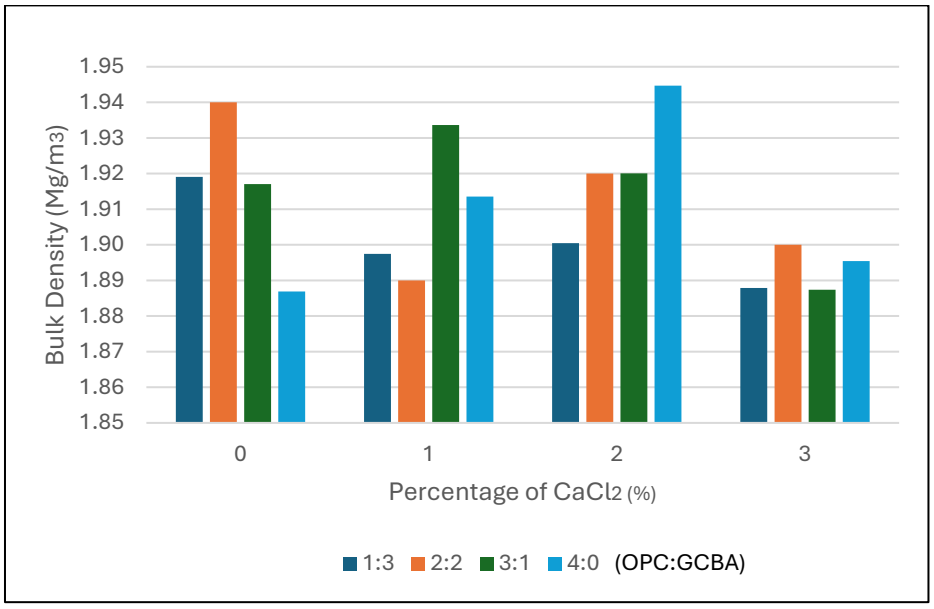


Figure 4.42 Bulk Density for CA25RAP75 Mix

Figures 4.43-4.46 show the comparison of bulk densities between different CA and RAP ratios. Among the three mix designs, CA75RAP25 exhibited the highest bulk density, followed by CA50RAP50 and CA25RAP75. This trend can be attributed to the higher CA content, which required greater water content during compaction to fill the additional voids and facilitate particle rearrangement, resulting in higher dry bulk density at MDD. This aligns with Worku and Shiferaw (2004), who stated that coarser aggregates can achieve greater bulk density due to enhanced physical compression. Although the CA25RAP75 mix achieved the highest dry density due to better particle

packing, the higher moisture content in the CA75RAP25 mix filled additional voids and enhanced particle packing, resulting in the highest bulk density.

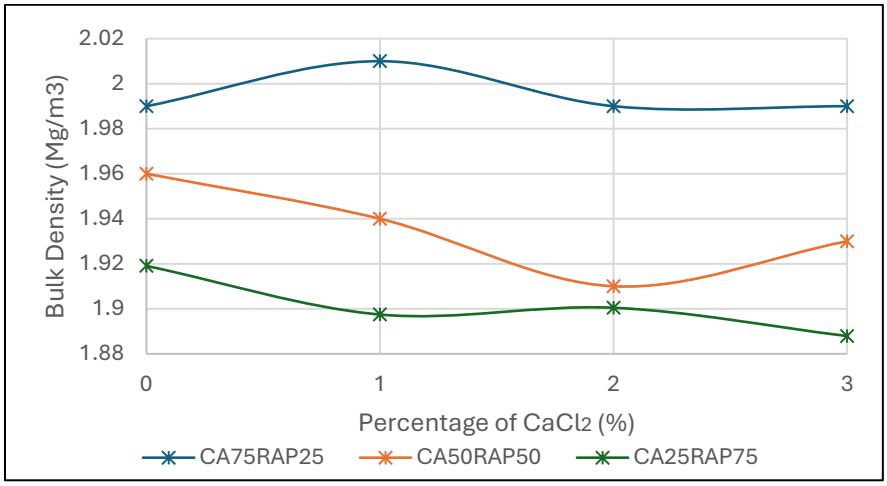


Figure 4.43 Bulk Density of 1% OPC + 3% GCBA + Various Percentages of $CaCl_2$

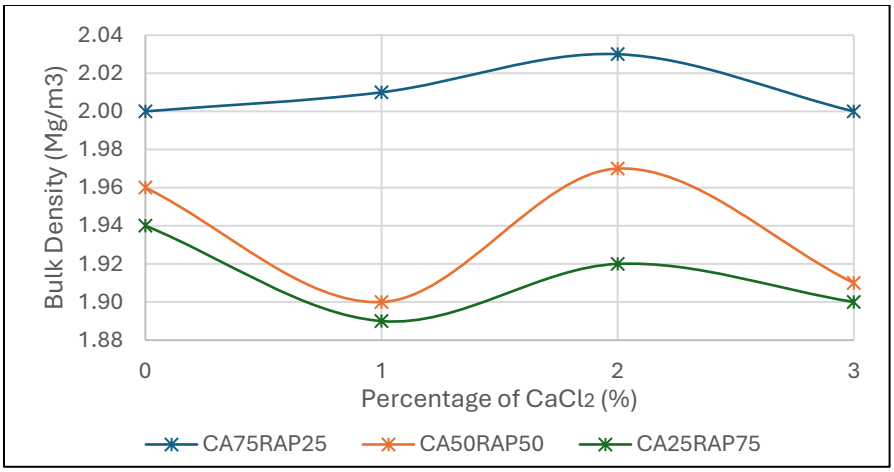


Figure 4.44 Bulk Density of 2% OPC + 2% GCBA + Various Percentages of $CaCl_2$

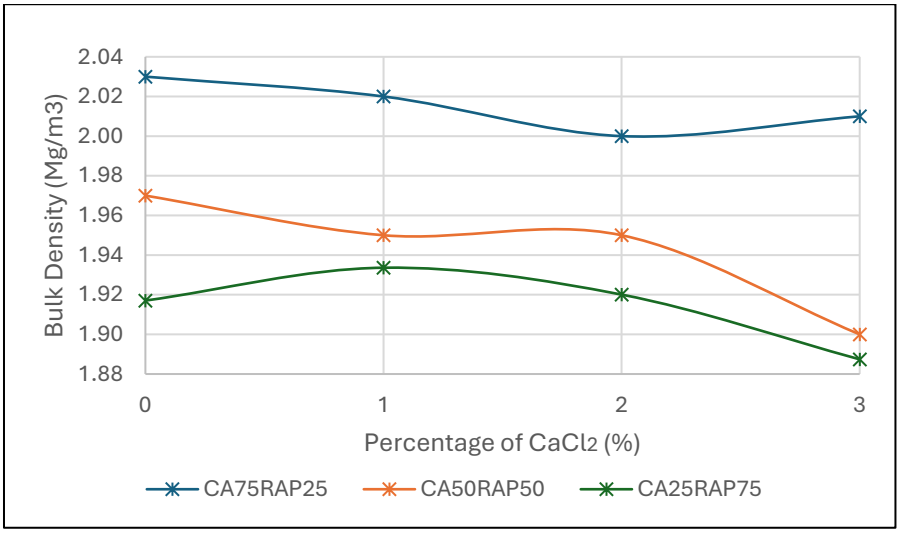


Figure 4.45 Bulk Density of 3% OPC + 1% GCBA + Various Percentages of $CaCl_2$

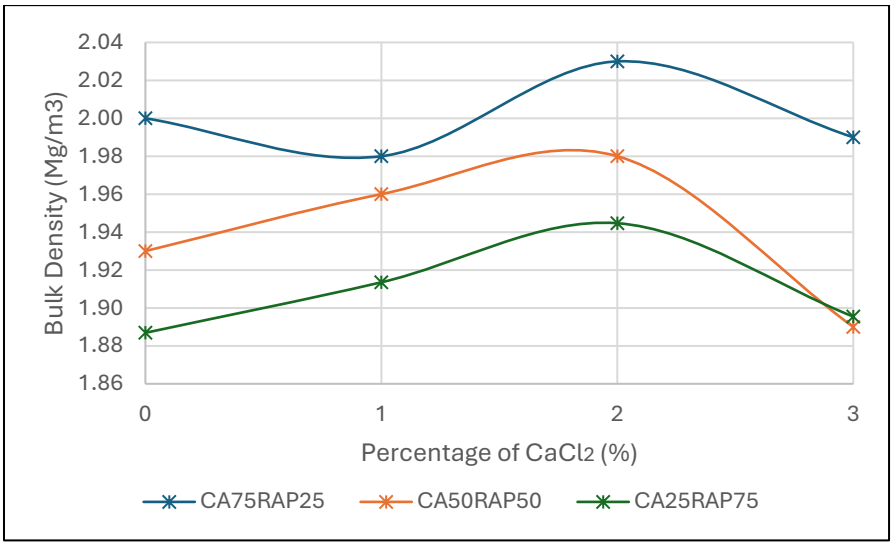


Figure 4.46 Bulk Density of 4% OPC + Various Percentages of $CaCl_2$

The potential influence of bulk density on strength performance was a crucial aspect addressed in this research. Variations in bulk density, particularly across different CA-RAP ratios, were examined to understand their overall structural integrity of the mix. In general, a higher bulk density tended to contribute to improved strength performance due to better particle packing and reduced void spaces. However, the relationship was not strictly linear, as the strength was also influenced by the quality of particle bonding and the effectiveness of the stabilizing agents (Du et al., 2025; Chhabra, 2023) While the compaction properties analysis provided initial results for OMC, MDD, and bulk density, these parameters alone did not fully represent the mechanical behavior of the material (Feng et al., 2023).

Therefore, a detail strength assessment, including UCS, ITS, and M_R tests, were conducted to evaluate the mix performance under various loading conditions, providing a more complete understanding of its suitability for field applications.

4.4 Phase Three: Performance Analysis of Stabilized CIPR Base Course

The performance analysis in this phase focused on evaluating strength performance under various loading conditions. To achieve this, UCS, ITS, and M_R tests were conducted. These tests aimed to provide comprehensive data for correlating strength performance with specific material properties, the percentages of constituent materials and stabilizing agent, and the curing duration. A total of 720 specimens were tested for UCS, while 405 specimens were tested for each of ITS and M_R.

Initially, the UCS test was performed to identify the optimal percentage of stabilizing agent for subsequent strength tests. This stage helped determine the mix design that exhibited the most favorable strength performance for further investigation regarding ITS and M_R tests. Following this, the data obtained from these tests were carefully analyzed to establish correlations between the applied loads and the strength behavior of the materials. This thorough approach allowed for an in-depth understanding of how variations in constituent materials, stabilizing agent, and curing durations influenced the strength properties of the material under different loading conditions.

Each of these tests was divided into two distinct analyses. The first analysis examined the influence of the stabilizing agent on the compressive strength of the proposed mix design, while the second analysis focused on the impact of varying CA-RAP ratios on the compressive strength of the mix design.

4.4.1 Unconfined Compressive Strength Test

UCS testing provides an indication of the material ability to resist compressive stress without lateral restraint. The result for UCS test on the impact of stabilizing agent and the effect of CA-RAP towards the proposed mix design was discussed in the following analysis. The test was conducted in accordance with ASTM D1633.

4.4.1.1 Effect of Varying Percentages of Stabilizing Agent on Compressive Strength

Figures 4.47 to 4.61 illustrate the effect of varying percentages of stabilizing agent on the mix design across the entire span of the curing period, spanning from day 1 through day 28, for three different variations of CA-RAP mix design. The minimum requirement was set at 2 MPa as stipulated in JKR/SPJ/2008-S4.

a) CA75RAP25 Mix Design

Figures 4.47 to 4.51 provide a visual representation illustrating the influence of stabilizing agent on the CA75RAP25 mix design.

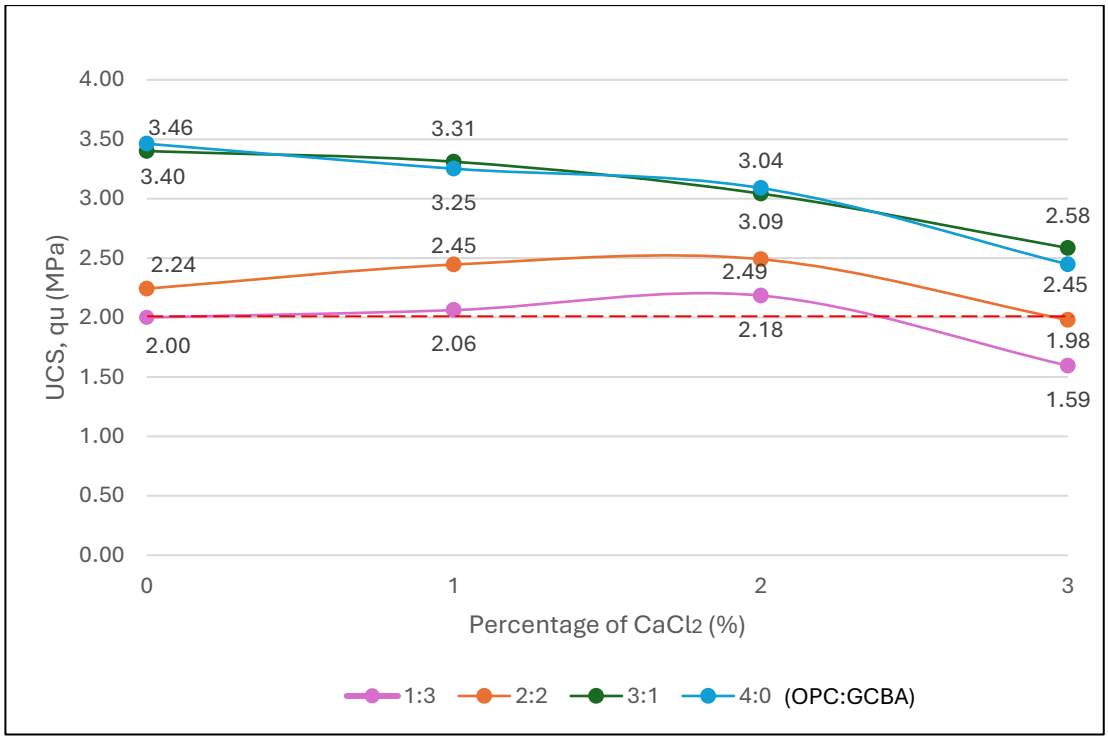


Figure 4.47 UCS for CA75RAP25 on Day 1

The data analysis for day 1, as shown in Figure 4.47, revealed a significant discrepancy in the patterns observed for compressive strength. Specifically, the mixes with 1% GCBA and without GCBA at 0% $CaCl_2$ demonstrated the highest compressive strength. This notable difference in performance between the two mixes revealed an irregular pattern in the compressive strength values at this initial evaluation stage. A 4% OPC + 0% GCBA + 0% $CaCl_2$ mix exhibited the highest compressive strength, peaking at 3.46 MPa. This was closely followed by a mix of 3% OPC + 1% GCBA + 0% $CaCl_2$ recorded a strength of 3.40 MPa.

In contrast, the mix containing 3% $CaCl_2$ and 2-3% GCBA exhibited the lowest compressive strength among all analyses, with values consistently below the minimum requirement of 2 MPa. This indicated that the mixes with these specific OPC replacement percentages were unsuitable for early strength development, highlighting their inadequacy and potential limitations in meeting the necessary structural strength standards.

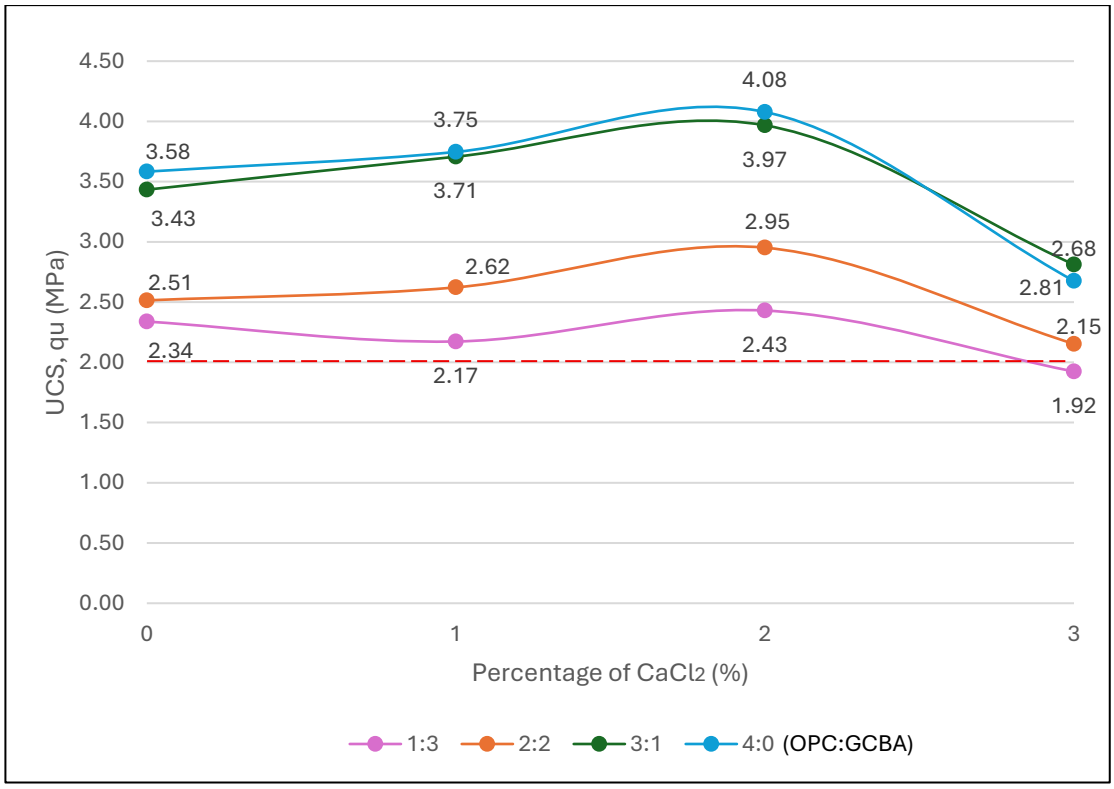


Figure 4.48 UCS for CA75RAP25 on Day 3

On the third day of the curing, a notable change in compressive strength was observed, as illustrated in Figure 4.48. Mixes containing 2% $CaCl_2$ exhibited the highest compressive strength, closely followed by those with 1% $CaCl_2$. The mix of 4% OPC + 0% GCBA + 2% $CaCl_2$ achieved a maximum strength of 4.08 MPa, while the 3% OPC + 1% GCBA + 2% $CaCl_2$ mix recorded a value of 3.97 MPa.

In contrast, mixes with 3% $CaCl_2$ demonstrated the lowest compressive strength on the third day. Although the trend indicated an increase in strength with higher percentages of $CaCl_2$, it began to decline at 3%. The mix of 1% OPC + 3% GCBA + 3% $CaCl_2$ recorded the lowest value at 1.92 MPa, which was slightly below the minimum requirement of 2 MPa.

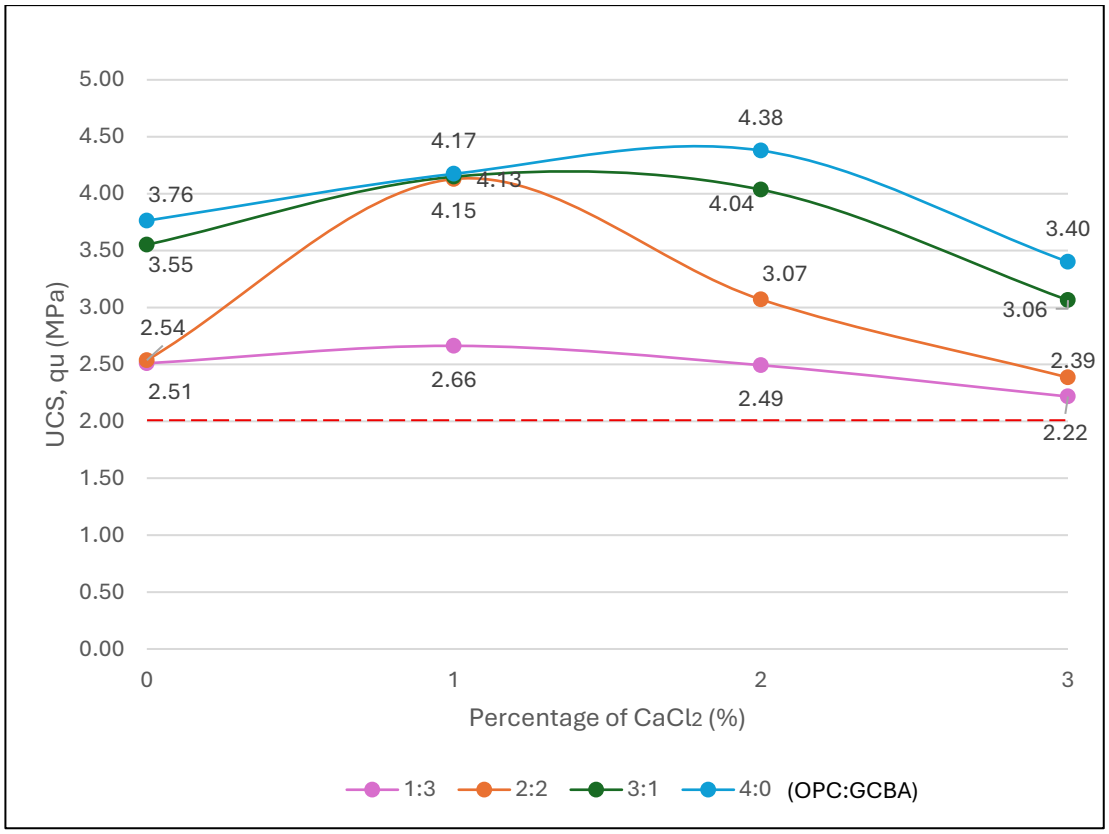


Figure 4.49 UCS for CA75RAP25 on Day 7

On day 7 of the curing as depicted in Figure 4.49, the pattern observed on day 3 persists, with mix design incorporating 2% $CaCl_2$ continuing to record the highest compressive strength. Notably, a mix design with 4% OPC + 0% GCBA + 2% $CaCl_2$ achieved the highest compressive strength of 4.38 MPa. Following closely behind was a mix of 4% OPC + 0% GCBA + 1% $CaCl_2$, achieving a value of 4.17 MPa. The observed increase in compressive strength highlighted the effectiveness of $CaCl_2$ as a key additive in optimizing the mechanical properties of the mix design.

On the other hand, it can be noted that every mix design with the addition of GCBA consistently underperformed to those without GCBA, highlighting a pattern that persisted throughout several evaluations. This recurrent discrepancy in performance demonstrated the complex influence of GCBA in these mixes on the results of their compressive strength.

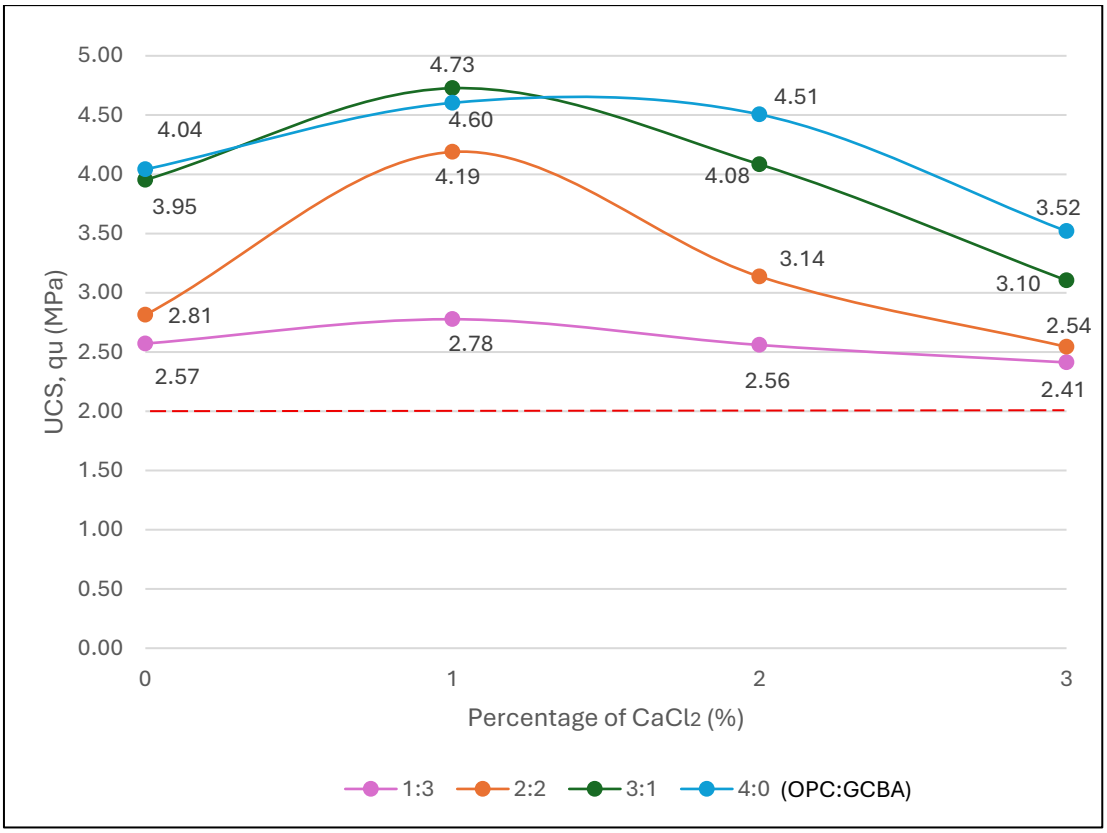


Figure 4.50 UCS for CA75RAP25 on Day 14

Figure 4.50 illustrates a distinct pattern in compressive strength for day 14 distribution among the various mix designs. Remarkably, the mixes incorporating 1% $CaCl_2$ consistently exhibited the highest compressive strength. As seen, a mix containing 3% OPC + 1% GCBA + 1% $CaCl_2$ recorded the highest value, reaching 4.73 MPa. Following closely behind was a mix without GCBA and same $CaCl_2$ content, achieved 4.60 MPa, demonstrating that $CaCl_2$ alone can provide significant strength.

Conversely, a consistent trend persisted as the mixes integrating 3% $CaCl_2$ consistently recorded the lowest compressive strength within this evaluation. This indicated a consistent performance across different mixes corresponding to greater $CaCl_2$ content.

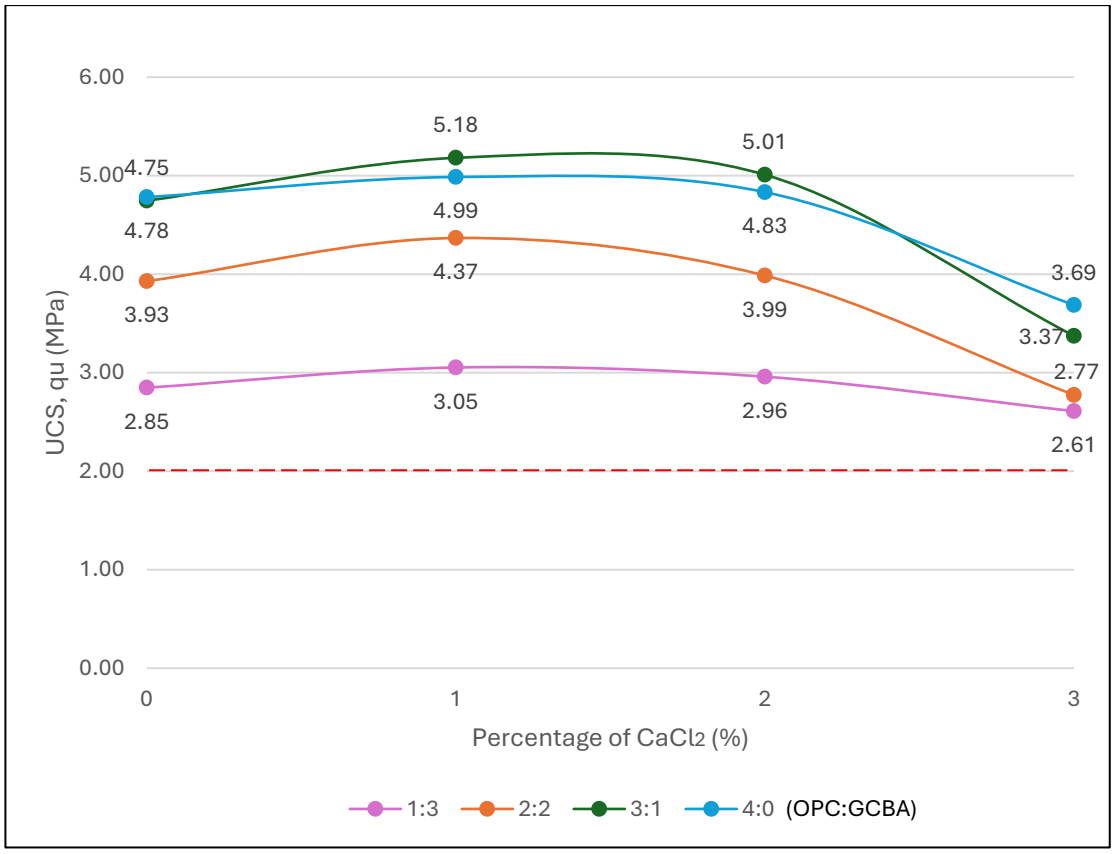


Figure 4.51 UCS for CA75RAP25 on Day 28

In the final day of the curing depicted in Figure 4.51, an almost similar observation as from day 14, mix design featuring a mere 1% of $CaCl_2$ continue to demonstrate the highest compressive strength. Specifically, a 3% OPC + 1% GCBA + 1% $CaCl_2$ mix achieved 5.18 MPa, maintaining its leading position. Notably, the same mix design but with 2% $CaCl_2$ closely followed, recorded 5.01 MPa. On the other hand, the lowest value recorded remained in the mix of 1% OPC + 3% GCBA + 3% $CaCl_2$ at 2.61 MPa.

The complex interactions among OPC, GCBA, and $CaCl_2$ content in CA75RAP25 mixes continued to influence the compressive strength, leading to significant findings until the final day of curing. The mixes containing 2% $CaCl_2$ and no GCBA began to develop compressive strength as early as day 1. However, by day 14, the results shifted, indicating that only 1% $CaCl_2$ was needed to achieve the highest compressive strength, which continued through the last day of the curing process. In contrast, all the mixes with 3% $CaCl_2$ recorded the lowest compressive strength. This suggested that the ideal percentage of $CaCl_2$ lies between 1% and 2%, and mixes with the least amount of OPC are less suitable for CA75RAP25.

b) CA50RAP50 Mix Design

Figures 4.52 to 4.56 provide a visual representation showing the influence of stabilizing agent on the CA50RAP50 mix design.

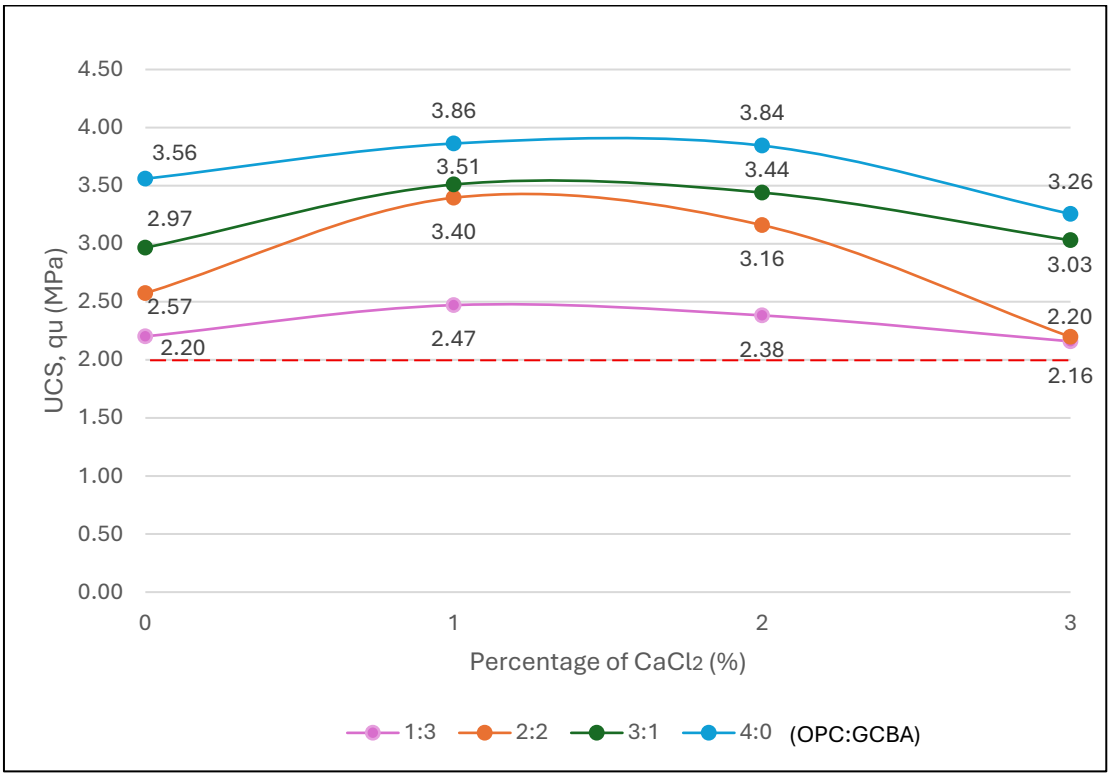


Figure 4.52 UCS for CA50RAP50 on Day 1

In Figure 4.52, the highest compressive strength on day 1 was observed in the mix of 4% OPC + 0% GCBA + 1% $CaCl_2$, which recorded a strength of 3.86 MPa. A consistent pattern emerged across all mixes where those that did not contain GCBA consistently exhibited the maximum compressive strength at each level of $CaCl_2$ content. This finding highlighted the significant impact of the absence of GCBA on the compressive strength of various mixes and its crucial role in this specific mix design. Nevertheless, replacing OPC with 1% GCBA was still acceptable, as it achieved the second-highest compressive strength in each profile of $CaCl_2$ content.

Conversely, the lowest compressive strength was recorded for all mixes containing 3% $CaCl_2$ indicating that an excessive amount of the accelerator may have adversely affected the early strength development of the mixes. However, all the mixes had already achieved the minimum requirement of 2 MPa by day 1.

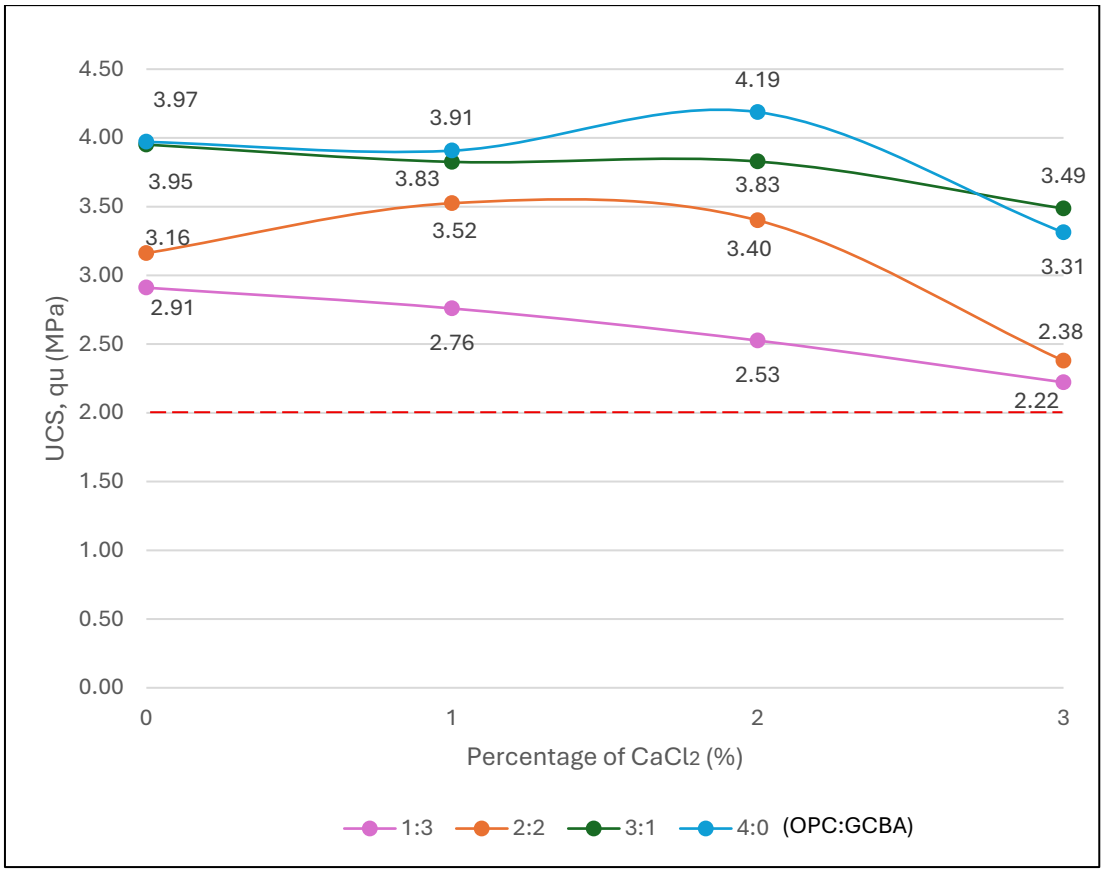


Figure 4.53 UCS for CA50RAP50 on Day 3

On day 3, as shown in Figure 4.53, a mix design of 4% OPC + 0% GCBA + 2% $CaCl_2$ showed the most resilience in compressive strength compared to the other designs. Again, a pattern emerged where the mix with zero GCBA content showed a high value of 4.19 MPa, indicating its ability to maintain a good compressive strength. Furthermore, a mix design with the absence of $CaCl_2$ and GCBA was coming close with a value of 3.97 MPa.

The analysis revealed a 1% OPC + 3% GCBA + 3% $CaCl_2$ mix encountered the lowest recorded compressive strength. Out of all the mix designs evaluated, this combination produced the least performed compressive strength, suggesting a significant performance difference in the CA50RAP50 mix design.

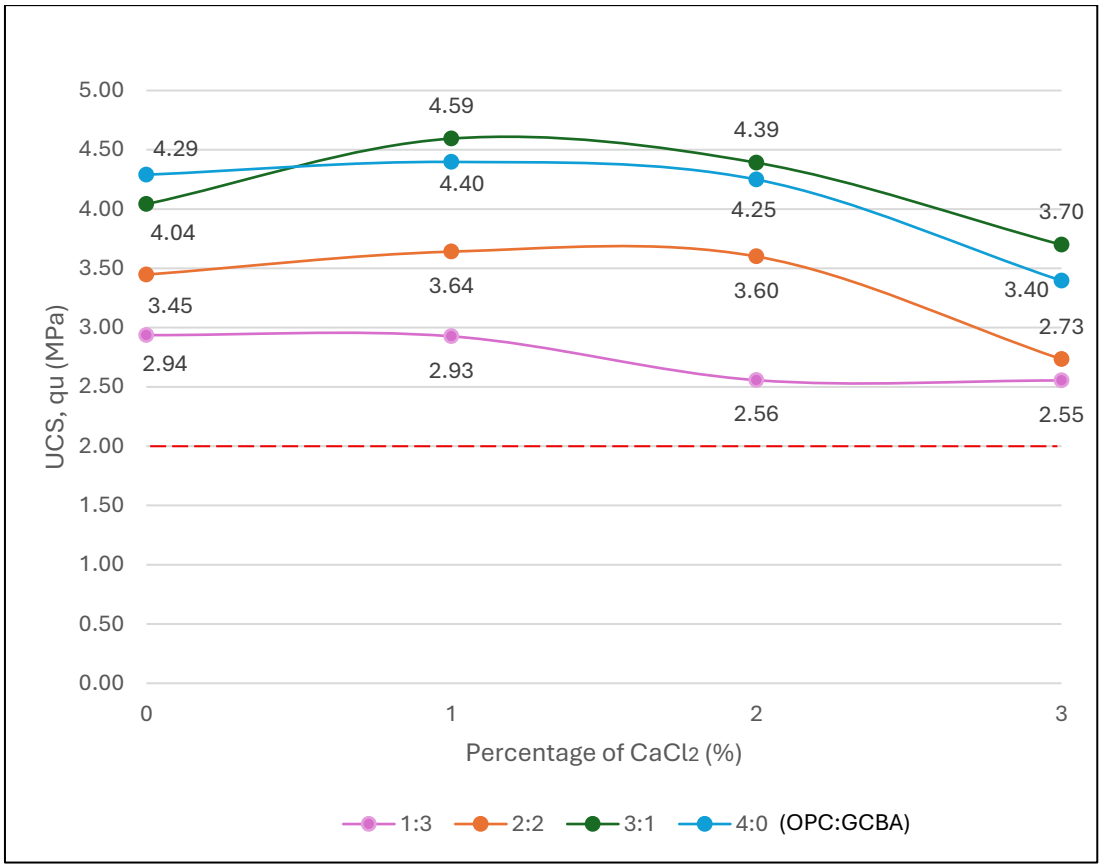


Figure 4.54 UCS for CA50RAP50 on Day 7

Figure 4.54 presents the compressive strength results for day 7 of the curing. A mix with 3% OPC + 1% GCBA + 1% $CaCl_2$ achieved the highest compressive strength, recording 4.59 MPa. This result indicated a synergy among the components that enhanced the structural integrity of the mix. In comparison, a mix without GCBA, containing the same amount of $CaCl_2$, reached 4.40 MPa, slightly below the maximum strength. The close strength values between these two mixes indicated that $CaCl_2$ was crucial in ensuring strong compressive strength results, even without GCBA.

The lowest recorded strength was on the mixes with 3% $CaCl_2$ reinforcing the trend that an excessive dosage of the accelerator may hinder strength development rather than enhance it.

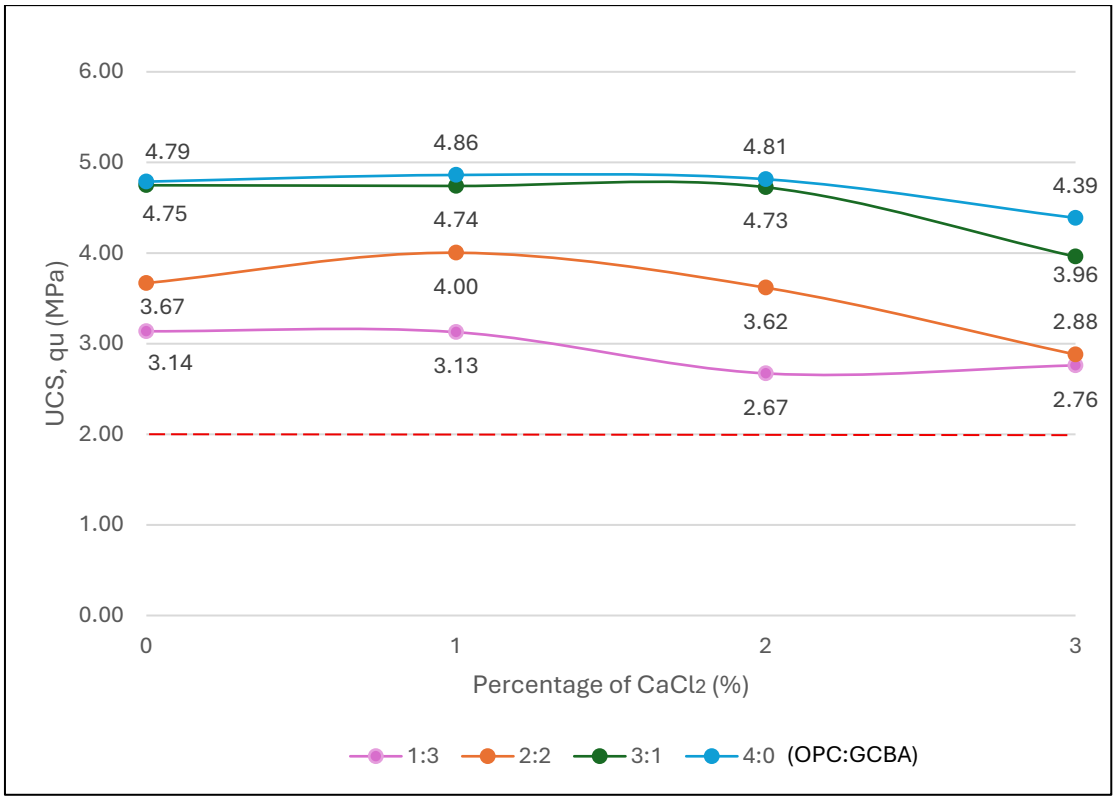


Figure 4.55 UCS for CA50RAP50 on Day 14

On day 14 of the curing as illustrated in Figure 4.55, a notable trend emerged wherein the compressive strength for three $CaCl_2$ percentages (ranging from 0% to 2%) displayed close proximity to each other. Among these compositions, the mixes without the presence of GCBA consistently demonstrated the highest values. Specifically, a mix design of 4% OPC + 0% GCBA + 1% $CaCl_2$ recorded the highest value at 4.86 MPa, closely trailed by its counterpart featuring 2% $CaCl_2$ at 4.81 MPa. Notably, all of the 3% OPC + 1% GCBA mix followed closely behind in the rankings.

Continuing the observed trend, mixes with 3% $CaCl_2$ persistently exhibited the lowest compressive strength among all the evaluated mix design. This consistent performance discrepancy highlighted the significant impact of $CaCl_2$ on the compressive strength outcomes, indicating its critical role in determining the performance properties of these mixes.

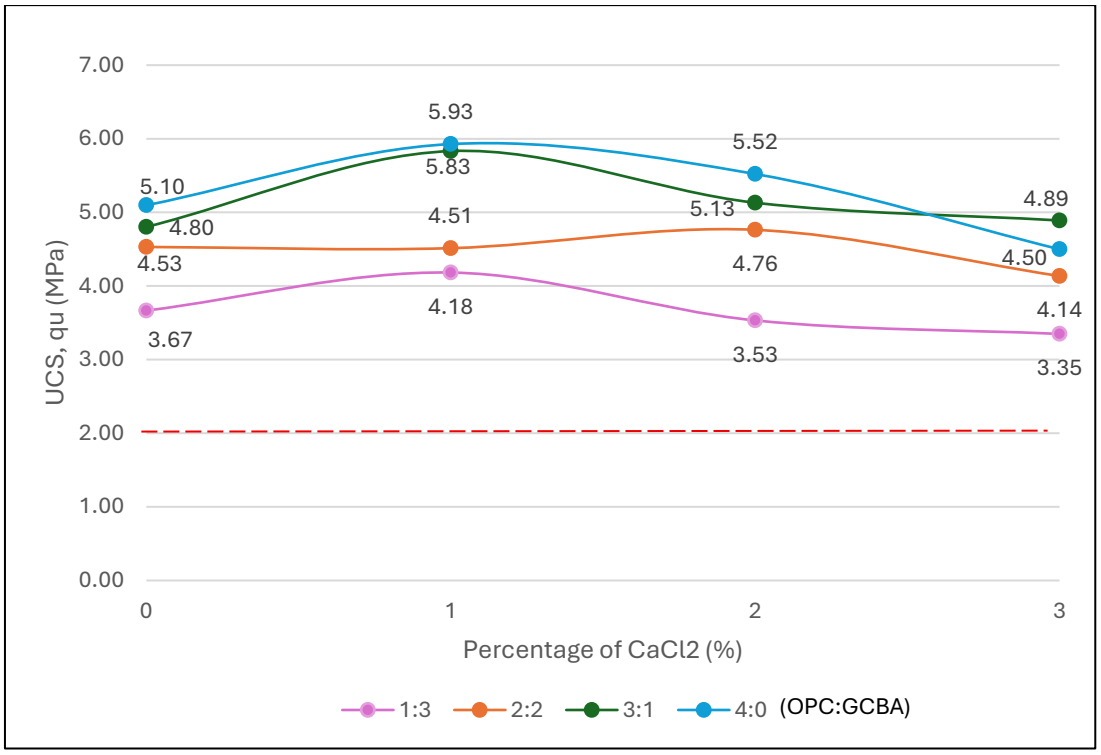


Figure 4.56 UCS for CA50RAP50 on Day 28

The final day of curing reaffirmed a consistent pattern where most mixes incorporating 1% $CaCl_2$ consistently exhibited the highest compressive strength, as shown in Figure 4.56. Once again, the mix of 4% OPC + 0% GCBA + 1% $CaCl_2$ recorded the highest compressive strength, reaching a peak value of 5.93 MPa, followed closely by the mix of 3% OPC + 1% GCBA + 1% $CaCl_2$ at 5.83 MPa. This trend of good performance in mixes with 1% $CaCl_2$ remained consistent throughout the entire 28-day curing process.

Conversely, maintaining the pattern observed in previous assessments, a mix design with 3% $CaCl_2$ persistently recorded the lowest compressive strength among the evaluated mixes.

The increased compressive strength in the CA50RAP50 mix design peaked at the mixes with mostly 1% $CaCl_2$ and slowly reduced its strength as the percentage of $CaCl_2$ increased. Furthermore, a resilience in compressive strength was consistently observed in mixes without GCBA, irrespective of the $CaCl_2$ varying percentages. These mixes constantly showed remarkable strength, either topping or closely matching those containing GCBA. In addition, it was clear that all mix designs containing 3% GCBA for OPC replacement were less suitable for practical application, as they consistently recorded the lowest values compared to the other mixes.

c) CA25RAP75 Mix Design

Figures 4.57 to 4.61 show the result for CA25RAP75 mix design on different percentages of stabilizing agent. Compared to the other mix design, this composition had the highest percentages of RAP, which created the main structure of the pavement base.

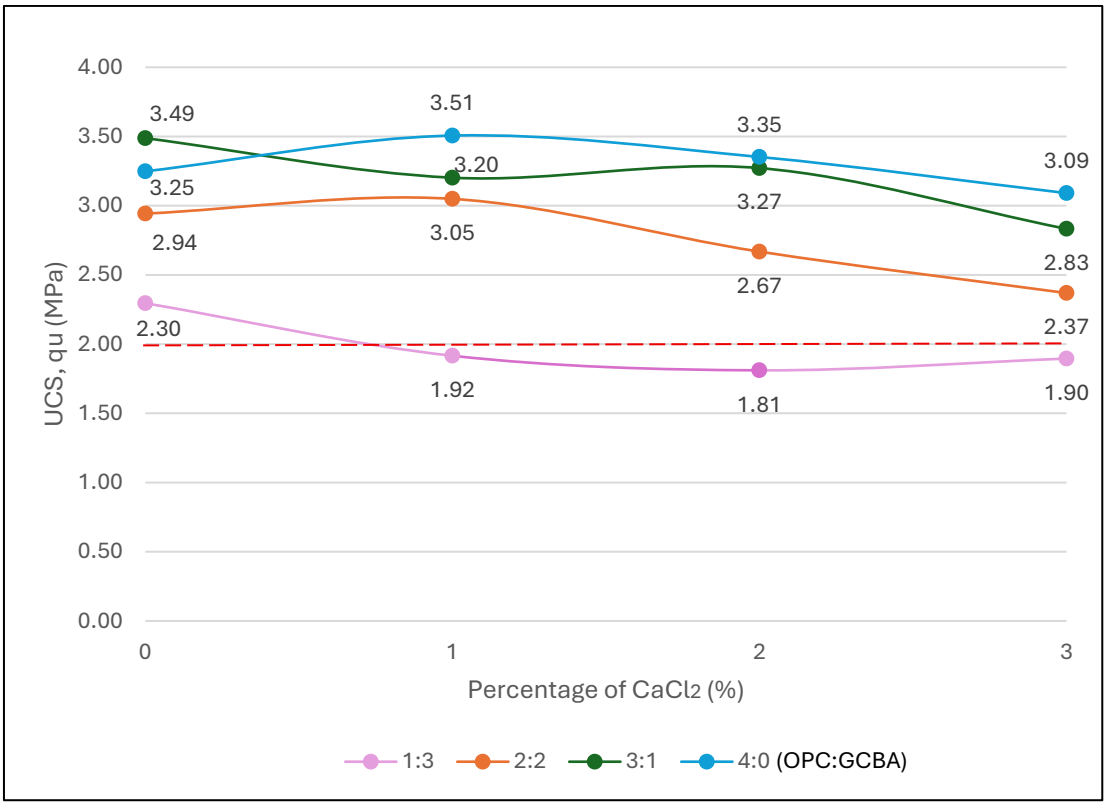


Figure 4.57 UCS for CA25RAP75 on Day 1

Figure 4.57 shows the compressive strength results for day 1 of curing. The mix of 4% OPC + 0% GCBA + 1% $CaCl_2$ achieved the highest compressive strength at 3.51 MPa, closely followed by the 3% OPC + 1% GCBA + 0% $CaCl_2$ mix at 3.49 MPa.

All mixes with a 1% OPC + 3% GCBA, even when combined with 1-3% $CaCl_2$, exhibited limited compressive strength, remaining below the minimum requirement of 2 MPa. This indicated that, at this early stage of curing, mixes with lower OPC content were unable to develop adequate strength despite the presence of $CaCl_2$. Consequently, these mixes did not meet the prescribed strength thresholds.

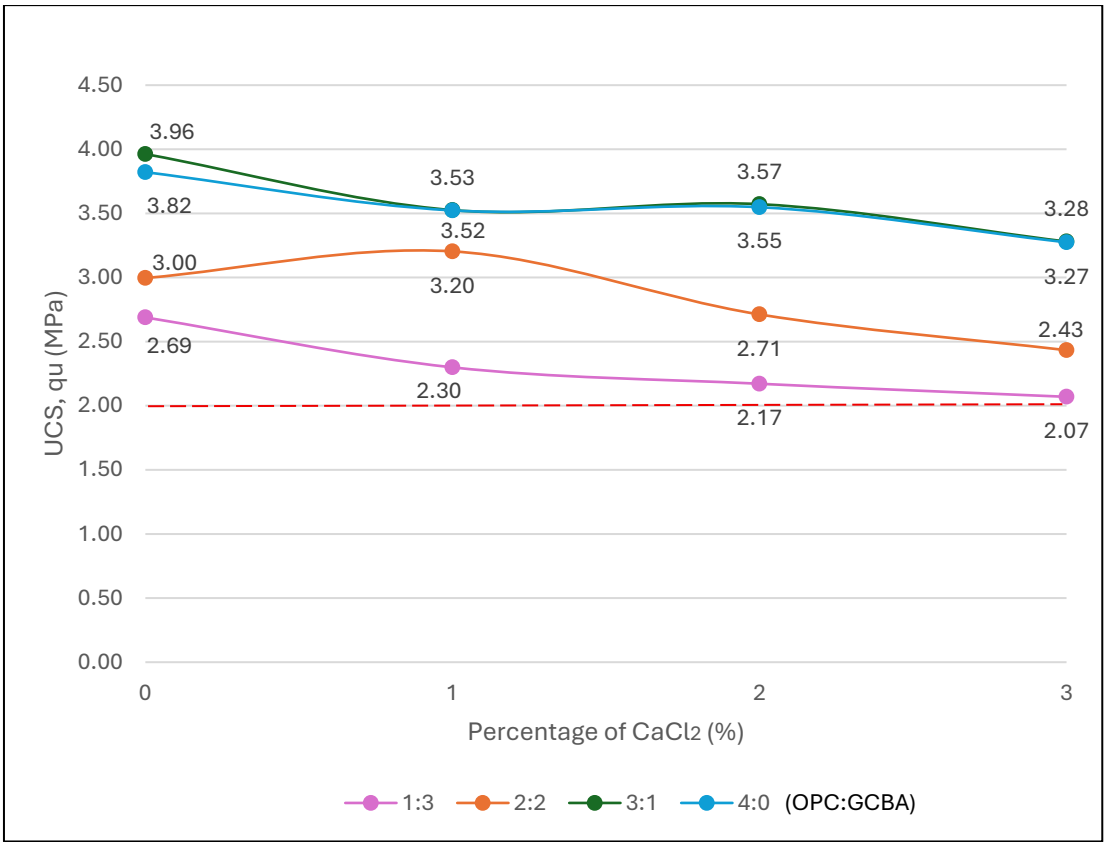


Figure 4.58 UCS for CA25RAP75 on Day 3

A slight increase in compressive strength was observed during day 3 of curing, as illustrated in Figure 4.58. Compared to day 1, all the mixes exceeded the minimum requirement of 2 MPa. Notably, the mix of 3% OPC + 1% GCBA + 0% $CaCl_2$ achieved the highest compressive strength on Day 3, demonstrating a good strength development at 3.96 MPa. This was closely followed by the mix without GCBA, which recorded 3.82 MPa. A consistent trend emerged, with all mix design featuring 3% OPC + 1% GCBA consistently surpassing the values obtained for each specific percentage variation of $CaCl_2$.

However, the mix of 1% OPC + 3% GCBA + 3% $CaCl_2$ had the lowest value, slightly above the minimum requirement, at 2.07 MPa.

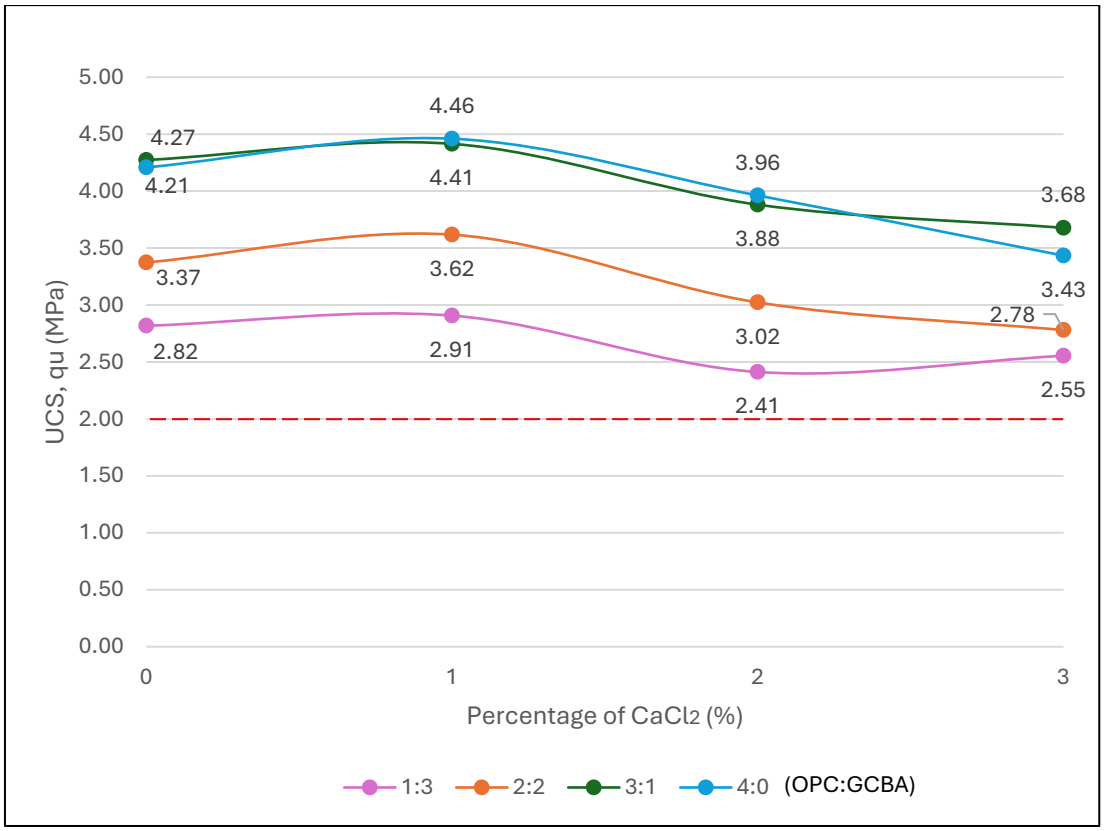


Figure 4.59 UCS for CA25RAP75 on Day 7

On day 7 of the curing, notable observations surfaced across various mixes, as displayed in Figure 4.59. Both mix design, one without GCBA and the other with 1% GCBA, emerged as the most favorable mixes, achieving the highest compressive strength across all $CaCl_2$ percentages. Specifically, a mix design of 4% OPC + 0% GCBA + 1% $CaCl_2$ recorded the highest value at 4.46 MPa, closely trailed by the mix of 3% OPC + 1% GCBA + 1% $CaCl_2$ 3, marking 4.41 MPa.

Conversely, the mix design incorporating 3% $CaCl_2$ consistently exhibited the lowest compressive strength among the evaluated mixes. Notably, a clear trend surfaced wherein the compressive strength seemed to decline as the $CaCl_2$ percentage reached 2%, indicating a potential adverse effect associated with higher concentrations of $CaCl_2$ within these specific mixes.

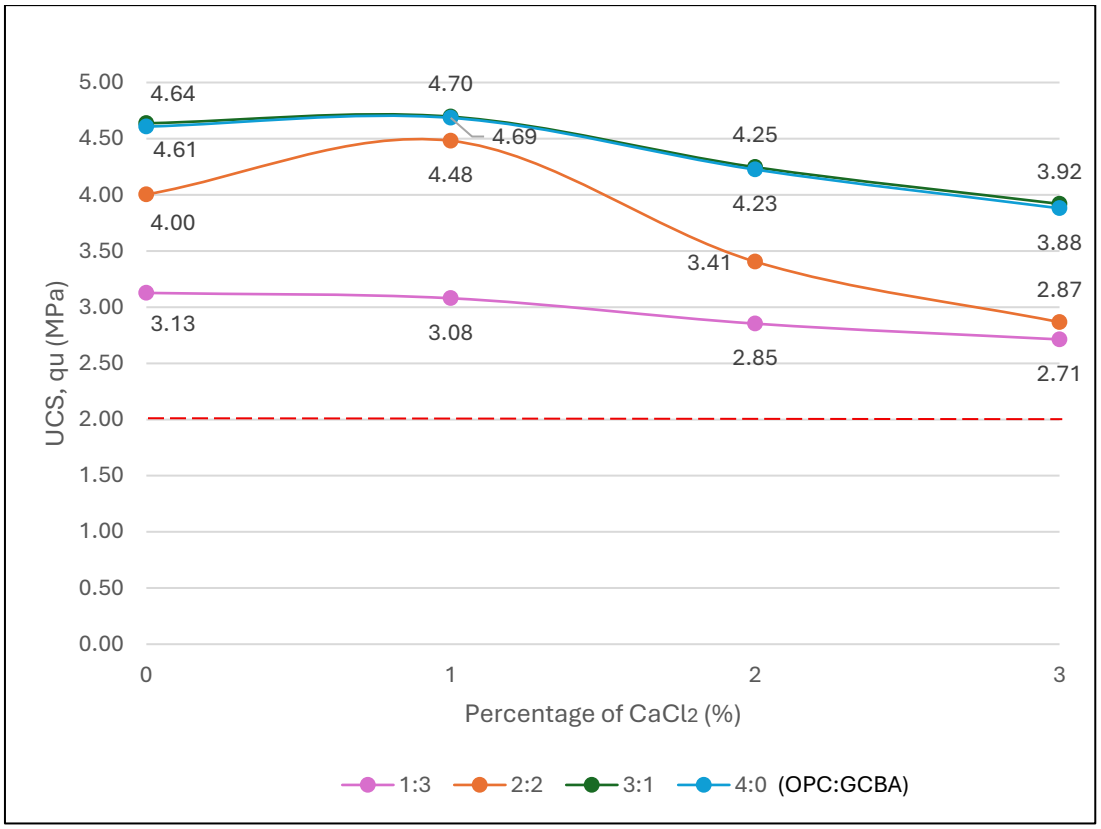


Figure 4.60 UCS for CA25RAP75 on Day 14

The observations made on day 14 of the curing, as illustrated in Figure 4.60, reflect trends similar to those observed on Day 3. The mix design of 3% OPC + 1% GCBA consistently demonstrated highest compressive strength across various percentages of $CaCl_2$. Notably, the mix containing 1% $CaCl_2$ achieved the highest compressive strength of 4.70 MPa. This was closely followed by a mix without GCBA, which showed only a minimal difference of 4.69 MPa.

In contrast, a different trend was noted for mixes of 1% OPC + 3% GCBA across different $CaCl_2$ percentages. Unlike the others, these mixes showed a slight decreased in strength as the percentage of $CaCl_2$ increased. This behavior is different from the usual pattern seen in other mix designs, showing a unique response caused by the combination of OPC, GCBA, and $CaCl_2$ during curing. Nevertheless, these mixes recorded the lowest UCS.

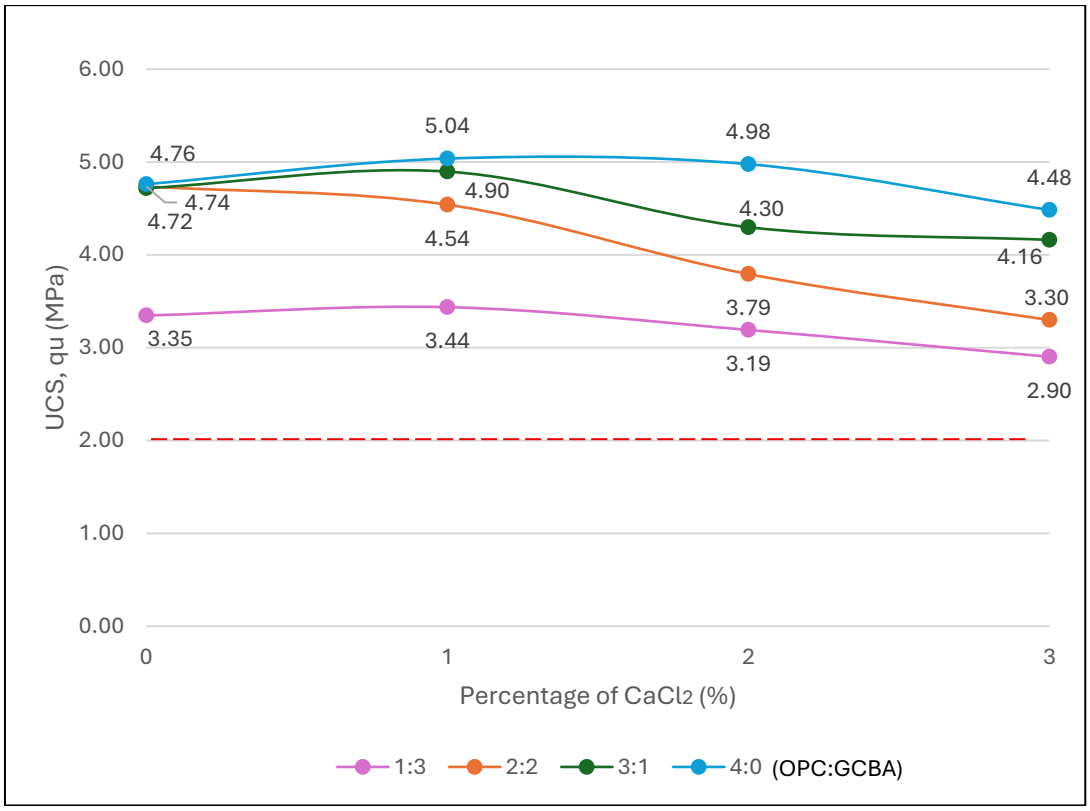


Figure 4.61 UCS for CA25RAP75 on Day 28

On the final day of the curing process, as depicted in Figure 4.61, the highest compressive strength of 5.04 MPa was observed in the 4% OPC + 0% GCBA + 1% $CaCl_2$ mix design. This was closely followed by a similar composition with 2% $CaCl_2$ at 4.98 MPa. In contrast, the mix containing 1% OPC + 3% GCBA consistently recorded the lowest strength, indicating that this low OPC content is insufficient to achieve the desired compressive strength in the CA25RAP75 design.

Within the CA25RAP75 mixes, adding 1% $CaCl_2$ improved strength starting from day 3, peaking by the final day, demonstrating its positive effect. Mixes with 1% or without GCBA maintained stable compressive strength across the $CaCl_2$ variations, suggesting that GCBA had a limited influence on strength development.

Furthermore, the analysis revealed that design mixes incorporating a 3% replacement of OPC with GCBA were less suitable for practical applications. These mixes consistently recorded the lowest compressive strength compared to the other variations. This suggested that altering the proportion of OPC at high dosage in this mix design negatively affected its compressive strength, making it less favorable for practical use compared to the other mixes.

4.4.1.2 Influence of Stabilizing Agent on Compressive Strength

As shown in Figures 4.47 to 4.61, compared to the control mix containing 4% OPC, most CA-RAP mix designs exhibited higher compressive strength with the incorporation of stabilizing agents, particularly $CaCl_2$. This clearly demonstrated that the proposed stabilizing agent positively impacted the mix when used in small quantities. However, a consistent trend emerged among the mix design with 3% replacement of OPC with GCBA, revealing their inadequacy for practical use, as they consistently recorded the lowest compressive strength across all combinations.

This reduction in strength could be attributed to the dilution effect, where replacing OPC with GCBA results in reduced C-S-H formation during the initial curing stages. Although GCBA contributes to long-term strength through pozzolanic reactions, its effect is not immediate. As such, early strength development suffers, particularly within the short curing periods evaluated in this research. The reduced content of cementitious material in mixes with 3% OPC replacement may also limit the binding potential necessary for rapid strength gain.

The results obtained were compared with those of Kurama and Kaya (2008), who reported that replacing up to 10% of OPC with GCBA improved compressive strength. However, this contrast may be due to different curing durations or mix designs. On the other hand, the findings of Kim et al. (2011) and Khan and Ganesh (2016) aligned more closely with this research, as they observed strength reduction at higher GCBA replacement levels, supporting the observed inadequacy of higher GCBA content in achieving early strength.

When evaluating the impact of high $CaCl_2$ content, the results corresponded with those of William et al. (2020), who found that adding 4% $CaCl_2$ decreased compressive strength. Similarly, Salain (2019) observed a decline starting at 2% $CaCl_2$. In this research, all mixes containing 3% $CaCl_2$ showed excessive moisture content during curing. This could be explained by the hygroscopic nature of $CaCl_2$, which tends to retain water and may increase the internal moisture content of the mix (Kishar et al., 2013). Additionally, high $CaCl_2$ concentrations may disrupt the formation of well-structured hydration products, lead to early-age microcracking, which can weaken the matrix and reduce compressive strength.

Although most compressive strength exceeded the minimum requirement of 2 MPa, mixes with 3% GCBA and high $CaCl_2$ content consistently underperformed,

making them impractical for applications requiring rapid strength gain. Among all mix designs, the CA50RAP50 mix incorporating 4% OPC + 1% $CaCl_2$ achieved the highest UCS of 5.93 MPa at 28 days, establishing it as the most effective and reliable mix design in terms of compressive strength.

On the other hand, the highest early strength (at days 1 and 3) across all mix designs was observed in the CA50RAP50 mix containing 4% OPC combined with 2% $CaCl_2$, suggesting that a slightly higher $CaCl_2$ content can further accelerate early-age strength development without compromising later-age performance.

4.4.1.3 Effect of Varying CA-RAP Ratio on Compressive Strength

The performance of the pavement base can be significantly affected by variations in the ratio of CA to RAP. To ensure structural integrity, lifespan, and cost-effectiveness, it is essential to consider multiple factors carefully when determining the optimal mix. The effects of different CA-RAP ratios were analyzed based on three distinct ratios.

Figures 4.62 to 4.65 illustrate the results of this analysis over the 28-day curing period. The figures clearly show the various effects of changing CA-RAP ratios on compressive strength. Notably, there was an apparent increase in strength as the curing period progressed. Furthermore, it was evident that different CA-RAP ratios produced varying levels of strength.

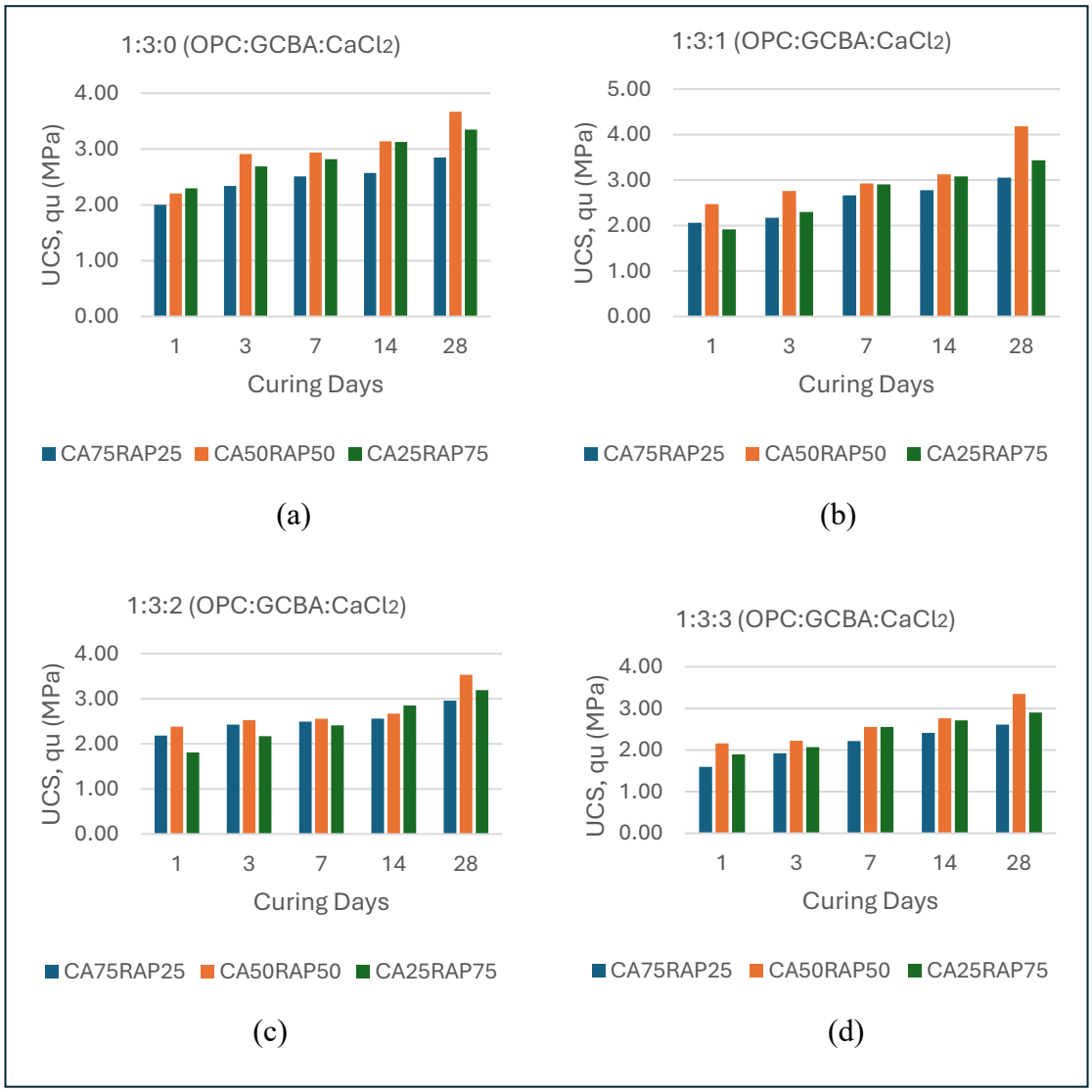


Figure 4.62 Impact of CA-RAP Ratio on Mix Design of 1% OPC + 3% GCBA with (a) 0% $CaCl_2$, (b) 1% $CaCl_2$, (c) 2% $CaCl_2$ and (d) 3% $CaCl_2$

Figure 4.62 illustrates the mix designs that contain 1% OPC + 3% GCBA with various percentages of $CaCl_2$. From the analysis, it was observed that the CA50RAP50 mix design demonstrated the highest strength among all the ratios. On the other hand, the compressive strength between CA25RAP75 and CA75RAP25 mixes appeared very close as their values fluctuated during the initial week of the curing process. However, by the second week, CA25RAP75 mixes showed better strength compared to CA75RAP25 mixes, yet it remained behind CA50RAP50 mixes.

This observation highlighted the significance of aggregate composition in influencing compressive strength outcomes. Mixes with balanced proportions of CA and RAP exhibited better mechanical properties, indicating the importance of optimizing the mix design to achieve desired performance outcomes in base course.

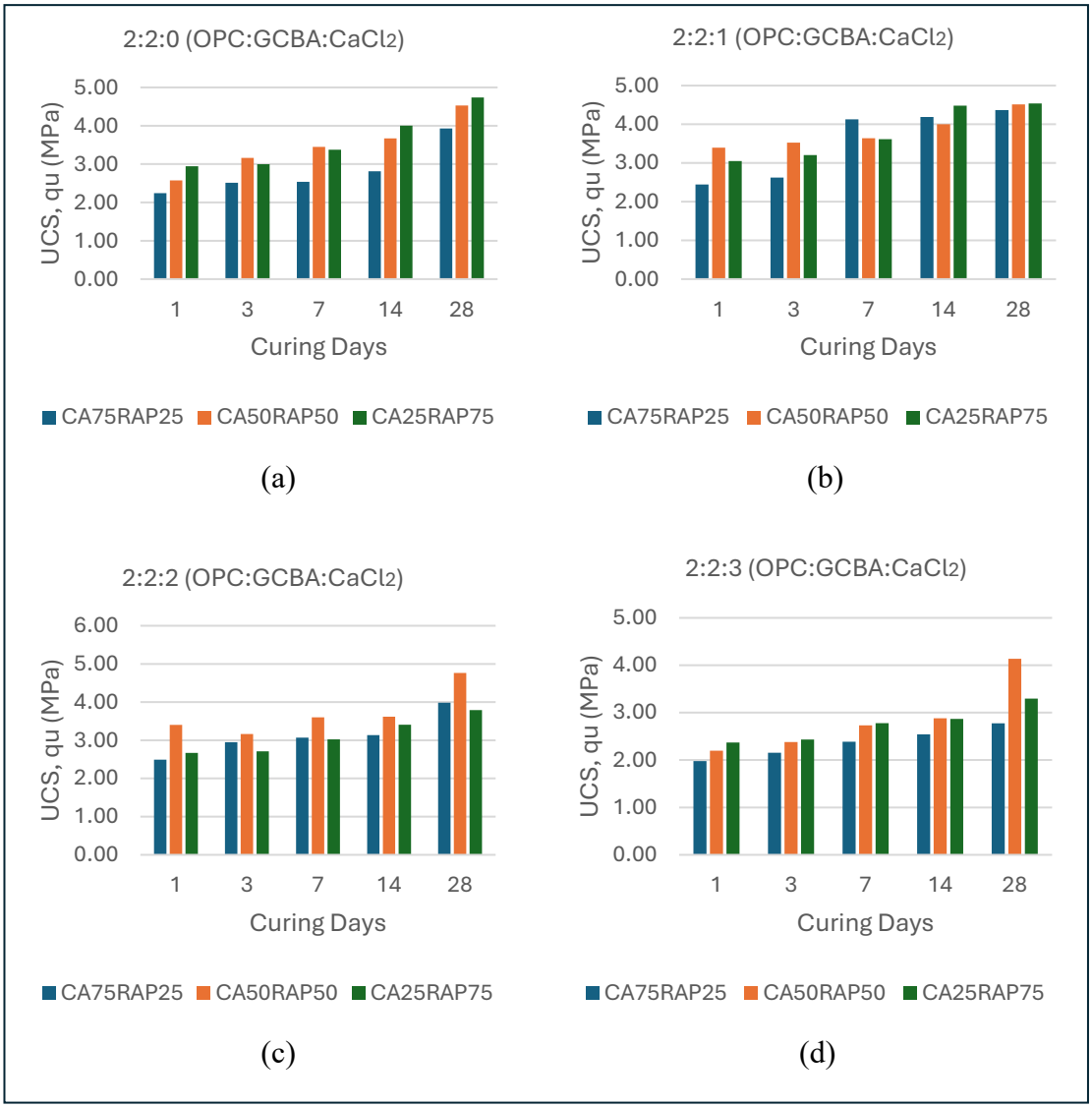


Figure 4.63 Impact of CA-RAP Ratio on Mix Design of 2% OPC + 2% GCBA with (a) 0% $CaCl_2$, (b) 1% $CaCl_2$, (c) 2% $CaCl_2$ and (d) 3% $CaCl_2$

Figure 4.63 presents the results for various CA-RAP ratios within mixes comprising 2% OPC and 2% GCBA each exposed to varying $CaCl_2$ percentages. A notable inconsistency was apparent in the compressive strength, particularly regarding the influence of varying $CaCl_2$ percentages. The mix design with CA25RAP75 recorded the highest compressive strength when $CaCl_2$ percentages were 0% and 1%. However, there was a shift when higher $CaCl_2$ contents, ranging from 2% to 3%, were introduced. In this case, a CA50RAP50 mix showed the highest compressive strength, outperforming CA25RAP75 and CA75RAP25 mixes. The different responses to $CaCl_2$ highlighted the importance of optimizing mix design based on aggregate composition.

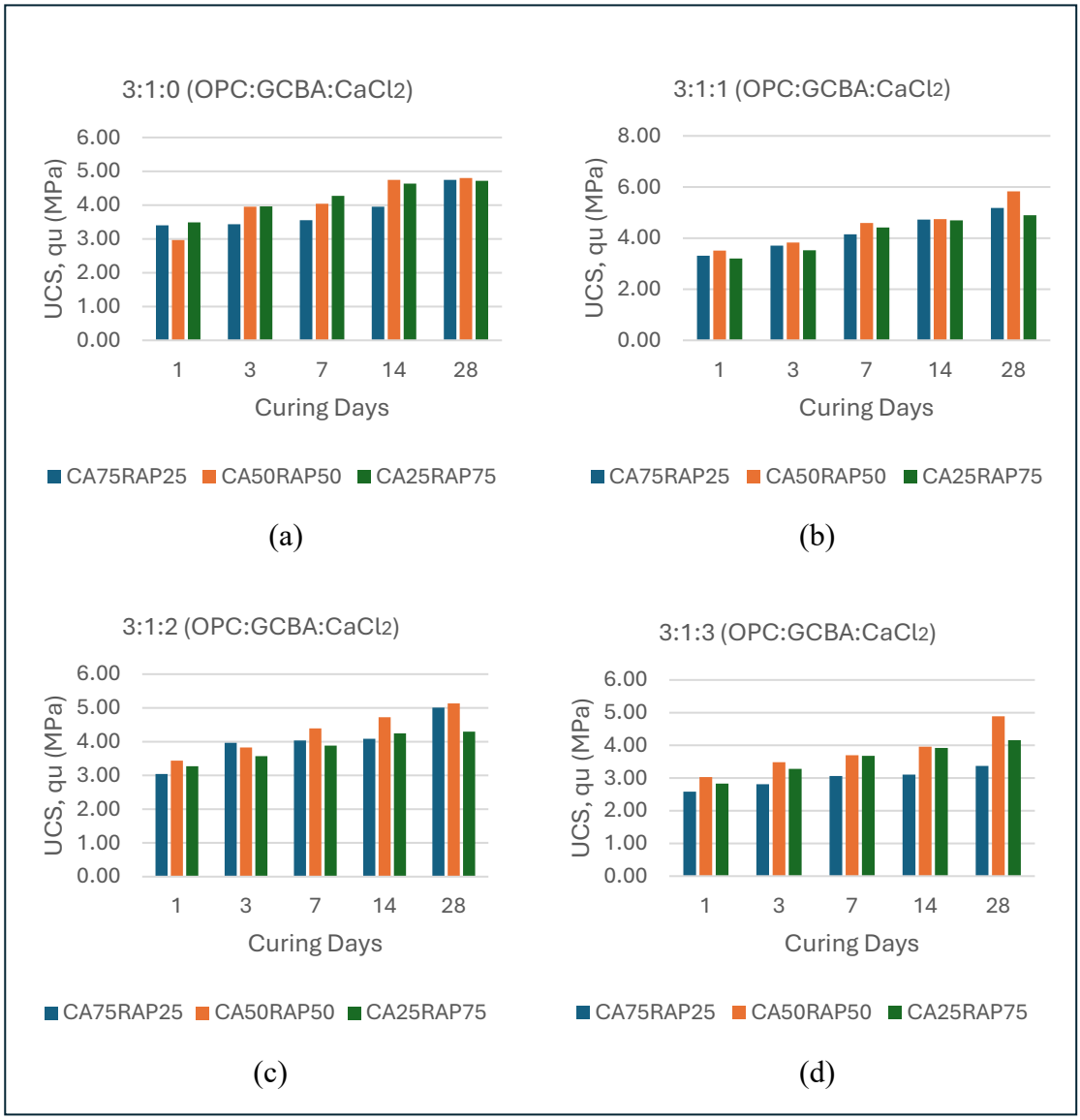


Figure 4.64 Impact of CA-RAP Ratio on Mix Design of 3% OPC + 1% GCBA with (a) 0% $CaCl_2$, (b) 1% $CaCl_2$, (c) 2% $CaCl_2$ and (d) 3% $CaCl_2$

Figure 4.64 presents the analysis of compressive strength data for the mix design, featuring 3% OPC + 1% GCBA with various $CaCl_2$ percentages. The results found an almost similar trend plotted on the mix design with 1% OPC + 3% GCBA, and various $CaCl_2$ percentages. A CA50RAP50 mix composition consistently exhibited the highest compressive strength across different $CaCl_2$ contents. This mix was closely followed by the CA75RAP25 mixes, which also demonstrated good compressive strength. The resilience of CA50RAP50 mix in achieving the highest compressive strength contributed to an understanding of how these mixes responded to a composition of 3% OPC + 1% GCBA with various $CaCl_2$ percentages during the curing process.

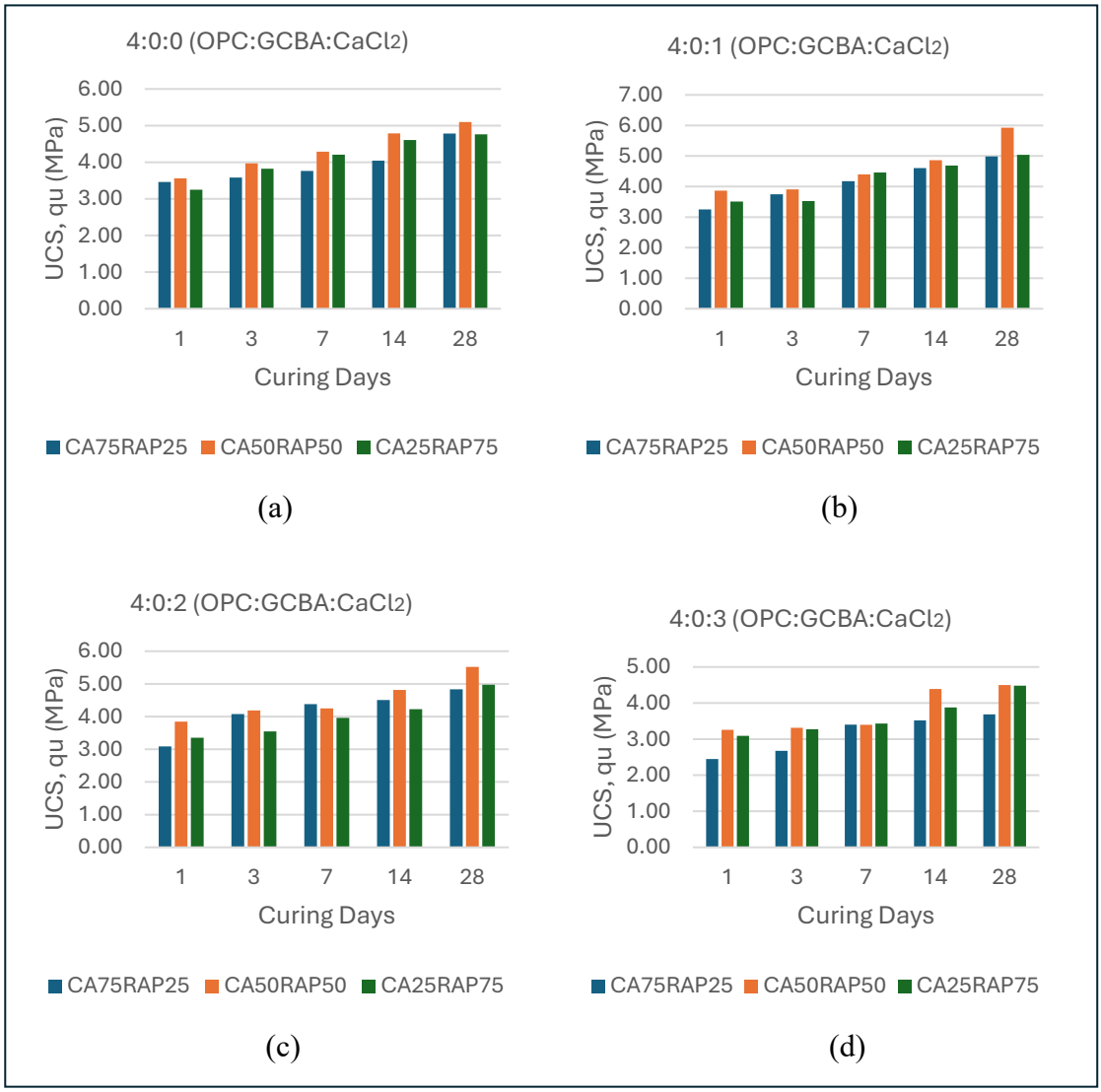


Figure 4.65 Impact of CA-RAP Ratio on Mix Design of 4% OPC with (a) 0% $CaCl_2$, (b) 1% $CaCl_2$, (c) 2% $CaCl_2$ and (d) 3% $CaCl_2$

Figure 4.65 shows the effect of CA-RAP ratio on the compressive strength of mixes containing 4% OPC with varying $CaCl_2$ contents, without GCBA. The addition of $CaCl_2$ significantly influenced the compressive strength across all mix designs. The CA50RAP50 mixes consistently demonstrated the highest strength across all $CaCl_2$ contents and curing periods. The CA75RAP25 and CA25RAP75 mixes followed closely, with compressive strength that were close to each other. This indicated that all three mixes performed well even without GCBA, while CA50RAP50 remained the optimal mix in terms of strength development for this mix composition.

4.4.1.4 Influence of Varying CA-RAP Ratio on Compressive Strength

Figures 4.62 to 4.65 show that the variation in compressive strength across the different mix designs resulted from the complex interaction of multiple factors, particularly the composition and proportions of CA, RAP, and the stabilizing agents. Among the combinations tested, the CA50RAP50 mix consistently demonstrated the highest compressive strength across most compositions. This result likely reflects an optimal balance between the structural rigidity provided by CA and RAP, which together enhanced packing density, interparticle bonding, and the integrity of the cementitious matrix.

This performance indicated that a 50:50 ratio of CA and RAP provided a synergistic effect, leading to improved strength characteristics. The consistency of this result, even with the inclusion or absence of GCBA and $CaCl_2$, further highlighted the durability and adaptability of the CA50RAP50 mix. It proved to be resilient to variations in the content of stabilizing agent, suggesting its potential as a reliable and high-performing mix design under varying conditions.

In comparison, Tan and Chan (2021) observed that higher CA content led to the greatest strength gain in their research, although a different stabilizing agent was used. Similarly, Sufian et al. (2009) reported that increased CA content improved compressive strength. However, in this research, the best performance was achieved not by the highest CA ratio but by an equal mix of CA and RAP, likely due to the influence of the specific stabilizing agent employed and their interactions with the aggregate structure.

The stabilizing agent used played a crucial role in modifying the hydration process and refining the microstructure of the hardened mix. Certain combinations appeared to enhance the reactivity of cementitious phases and improve the pozzolanic activity of GCBA, particularly when optimally balanced with the aggregate structure. Research by Abriak et al. (2023) has shown that altering mix compositions can significantly affect hydration kinetics and microstructure development, a key factor in strength development. The interaction of these mechanisms across varying CA-RAP ratios ultimately governed the mechanical performance of the mixes, explaining the observed variations in compressive strength.

4.4.1.5 The Proposed Mix Design Ranking

Tables 4.14 to 4.16 provide a detailed ranking of the proposed mix designs based on the overall results of the compressive strength analysis. This ranking method was previously utilized by Shaffie (2018) to select the optimal mix design for asphalt binder based on comprehensive test results. A similar approach was adopted in this research to determine the best mix design for further analysis of strength performance. The rankings indicate that out of the 16 proposed mix designs for each CA-RAP ratio, only the top 8 with the highest compressive strength were considered the most viable for additional testing in the ITS and M_R tests.

Analysis of the CA75RAP25 mix, as tabulated in Table 4.14, showed that the addition of 3% OPC + 1% GCBA + 1% $CaCl_2$ resulted in the highest-ranked mix design. Conversely, the lowest-ranked mix design comprised 1% OPC + 3% GCBA + 3% $CaCl_2$. The mix positioned at the threshold of the 8th rank featured 2% each of OPC, GCBA, and $CaCl_2$.

As shown in Table 4.15, the highest-performing CA50RAP50 mix design comprised 4% OPC + 1% $CaCl_2$. This combination highlighted the advantages of a higher OPC content with a lower $CaCl_2$ addition. On the other hand, the lowest-performing mix consisted of 1% OPC + 3% GCBA + 3% $CaCl_2$. This reduced performance was attributed to the lower OPC content and the higher proportions of GCBA and $CaCl_2$. Meanwhile, the mix that ranked 8th at the threshold contained 2% each of OPC and GCBA, along with 1% $CaCl_2$.

In the case of the CA25RAP75 mix as summarized in Table 4.16, a detailed analysis revealed that the top-performing mix comprised 4% OPC + 1% $CaCl_2$, with no GCBA included. In contrast, the least effective mix design contained 1% OPC + 3% GCBA + 3% $CaCl_2$ while the mix positioned at the threshold of the 8th rank featured a combination of 2% OPC + 2% GCBA without the presence of $CaCl_2$.

The analysis showed that all mixes containing 1% OPC + 3% GCBA + 3% $CaCl_2$ had compressive strengths below the acceptable threshold, indicating that this combination did not enhance strength. Therefore, mixes with 3% GCBA and 3% $CaCl_2$, were excluded from further analysis (resulting in 405 specimens each for ITS and M_R). The results also suggested that the optimal $CaCl_2$ content is between 1% and 2%, consistent with Occidental Chemical Corporation (2006), which reported that $CaCl_2$ at 1-2% accelerates cement hydration and shortens the curing period.

Table 4.14
Ranking of the Overall Result for CA75RAP25 Mix Design

Percentage of Stabilizing Agent (%)														
OPC	GCBA	$CaCl_2$	CD 1 (MPa)	score	CD 3 (MPa)	score	CD 7 (MPa)	score	CD 14 (MPa)	score	CD 28 (MPa)	score	total score	rank
3	1	1	3.31	14	3.71	11	4.15	14	4.73	16	5.18	16	71	1
4	0	2	3.09	12	4.08	16	4.38	16	4.51	14	4.83	13	71	2
4	0	1	3.25	13	3.75	12	4.17	15	4.60	15	4.99	14	69	3
3	1	2	3.04	11	3.97	15	4.04	12	4.08	12	5.01	15	65	4
4	0	0	3.46	16	3.58	14	3.76	11	4.04	11	4.78	12	64	5
3	1	0	3.40	15	3.43	13	3.55	10	3.95	9	4.75	11	58	6
2	2	1	2.45	8	2.62	7	4.13	13	4.19	13	4.37	10	51	7
2	2	2	2.49	9	2.95	10	3.07	8	3.14	8	3.99	9	44	8
4	0	3	2.45	7	2.68	8	3.40	9	3.52	10	3.69	7	41	9
3	1	3	2.58	10	2.81	9	3.06	7	3.10	7	3.37	6	39	10
2	2	0	2.24	6	2.51	6	2.54	5	2.81	6	3.93	8	31	11
1	3	1	2.06	4	2.17	3	2.66	6	2.78	5	3.05	5	23	12
1	3	2	2.18	5	2.43	5	2.49	3	2.56	3	2.96	4	20	13
1	3	0	2.00	3	2.34	4	2.51	4	2.57	4	2.85	3	18	14
2	2	3	1.98	2	2.15	2	2.39	2	2.54	2	2.77	2	10	15
1	3	3	1.59	1	1.92	1	2.22	1	2.41	1	2.61	1	5	16

Note: CD stands for curing days

Table 4.15
Ranking of the Overall Result for CA50RAP50 Mix Design

Percentage of Stabilizing Agent (%)														
OPC	GCBA	$CaCl_2$	CD 1 (MPa)	score	CD 3 (MPa)	score	CD 7 (MPa)	score	CD 14 (MPa)	score	CD 28 (MPa)	score	total score	rank
4	0	1	3.86	16	3.91	13	4.40	15	4.86	16	5.93	16	76	1
4	0	2	3.84	15	4.19	16	4.25	12	4.81	15	5.52	14	72	2
4	0	0	3.56	14	3.97	15	4.29	13	4.79	14	5.10	12	68	3
3	1	1	3.51	13	3.83	12	4.59	16	4.74	12	5.83	15	68	4
3	1	2	3.44	12	3.83	11	4.39	14	4.73	11	5.13	13	61	5
3	1	0	2.97	7	3.95	14	4.04	11	4.75	13	4.80	10	55	6
3	1	3	3.03	8	3.49	9	3.70	10	3.96	8	4.89	11	46	7
2	2	1	3.40	11	3.52	10	3.64	9	4.00	9	4.51	7	46	8
4	0	3	3.26	9	3.31	8	3.40	6	4.39	10	4.50	6	39	9
2	2	2	3.40	10	3.16	6	3.60	7	3.62	6	4.76	9	38	10
2	2	0	2.57	6	3.16	7	3.45	8	3.67	7	4.53	8	36	11
1	3	1	2.47	5	2.76	4	2.93	4	3.13	4	4.18	5	22	12
1	3	0	2.20	3	2.91	5	2.94	5	3.14	5	3.67	3	21	13
2	2	3	2.20	2	2.38	2	2.73	3	2.88	3	4.14	4	14	14
1	3	2	2.38	4	2.53	3	2.56	2	2.67	1	3.53	2	12	15
1	3	3	2.16	1	2.22	1	2.55	1	2.76	2	3.35	1	6	16

Note: CD stands for curing days

Table 4.16
Ranking of the Overall Result for CA25RAP75 Mix Design

Percentage of Stabilizing Agent (%)														
OPC	GCBA	$CaCl_2$	CD 1 (MPa)	score	CD 3 (MPa)	score	CD 7 (MPa)	score	CD 14 (MPa)	score	CD 28 (MPa)	score	total score	rank
4	0	1	3.51	16	3.52	11	4.46	16	4.69	15	5.04	16	74	1
3	1	0	3.49	15	3.96	16	4.27	14	4.64	14	4.72	11	70	2
3	1	1	3.20	11	3.53	12	4.41	15	4.70	16	4.90	14	68	3
4	0	0	3.25	12	3.82	15	4.21	13	4.61	13	4.76	13	66	4
4	0	2	3.35	14	3.55	13	3.96	12	4.23	10	4.98	15	64	5
3	1	2	3.27	13	3.57	14	3.88	11	4.25	11	4.30	8	57	6
2	2	1	3.05	9	3.20	8	3.62	9	4.48	12	4.54	10	48	7
2	2	0	2.94	8	3.00	7	3.37	7	4.00	9	4.74	12	43	8
4	0	3	3.09	10	3.27	9	3.43	8	3.88	7	4.48	9	43	9
3	1	3	2.83	7	3.28	10	3.68	10	3.92	8	4.16	7	42	10
2	2	2	2.67	6	2.71	5	3.02	6	3.41	6	3.79	6	29	11
1	3	0	2.30	4	2.69	6	2.82	4	3.13	5	3.35	4	23	12
1	3	1	1.92	3	2.30	3	2.91	5	3.08	4	3.44	5	20	13
2	2	3	2.37	5	2.43	4	2.78	3	2.87	3	3.30	3	18	14
1	3	2	1.81	1	2.17	2	2.41	1	2.85	2	3.19	2	8	15
1	3	3	1.90	2	2.07	1	2.55	2	2.71	1	2.90	1	7	16

Note: CD stands for curing days

4.4.2 Indirect Tensile Strength Test

ITS testing is one of the crucial evaluations that provides information on the tensile cracking resistance and bonding characteristics of pavement base materials. ITS offer an indication of structural integrity and durability by reflecting the resistance of material to tensile cracking and failure.

The subsequent graphical analysis explained in the discussion provides an overview of the ITS results derived from various stabilizing agent percentages and CA and RAP ratios. This analysis offers valuable insights into the relative effectiveness of this stabilizing agent in enhancing the tensile performance of pavement base materials.

Through this analysis, trends and patterns that interpreted how various compositions of stabilizing agent affected the mechanical properties of the base material were discovered. Furthermore, by evaluating ITS across various compositions, the optimal mixes that demonstrated enhanced tensile strength and greater resistance to failure mechanisms such as cracking were identified and analyzed. The test was conducted in accordance with ASTM D6931.

4.4.2.1 Effect of Varying Percentages of Stabilizing Agent on Indirect Tensile Strength

The graphical results presented in Figures 4.66 to 4.80 show the chart of 'Percentage of $CaCl_2$ versus ITS' with different OPC and GCBA content for three different CA and RAP ratios. The minimum requirement for ITS was set at 0.2 MPa or 200 KPa based on JKR/SPJ/2008-S4.

a) CA75RAP25 Mix Design

Figures 4.66 to 4.70 show the ITS result for CA75RAP25 mix design on different percentages of stabilizing agent from day 1 to day 28 of the curing process.

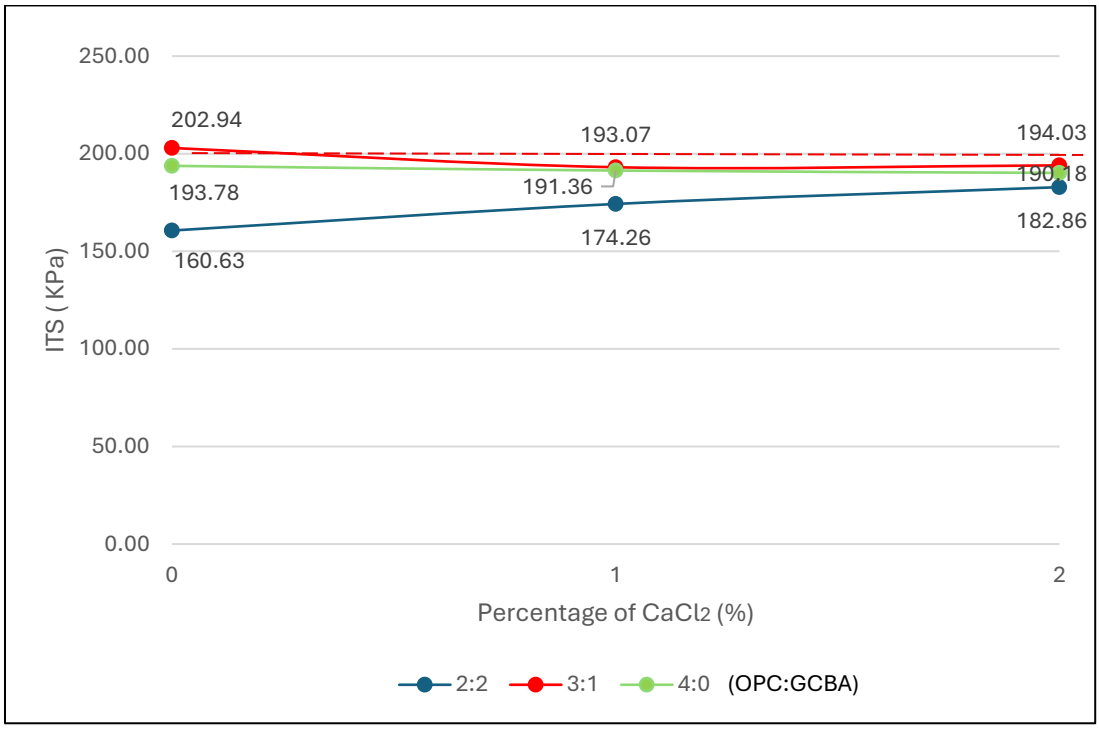


Figure 4.66 ITS for CA75RAP25 on Day 1

Figure 4.66 portrays day 1 of the curing test for CA75RAP25 mixes. The results revealed variations in the tensile strength of different mix designs with varying variations of stabilizing agent. A mix incorporating 3% OPC + 1% GCBA + 0% $CaCl_2$ exhibited the highest ITS at 202.94 KPa. Following closely behind was the mix with the same composition of OPC and GCBA but added with 2% $CaCl_2$ at 194.03 KPa. Notably, the overall trend appeared inconsistent with the inclusion of $CaCl_2$, as one might expect a consistent increase in strength with its addition. However, upon closer examination, a more detailed image became apparent. When the analysis was conducted individually, it was observed that for the mix design with a 2% OPC + 2% GCBA, the tensile strength increased with each additional 1% of $CaCl_2$, even though this mix recorded the lowest overall values among all compositions.

This result contrasted with the mix without GCBA and with 1% GCBA, wherein the inclusion of every 1% $CaCl_2$ led to a slight reduction in tensile strength. Despite these fluctuations, only the 3% OPC + 1% GCBA + 0% $CaCl_2$ mix met the minimum

requirement, while five other mixes almost reached 200 KPa, indicating overall satisfactory performance on day 1 of curing.

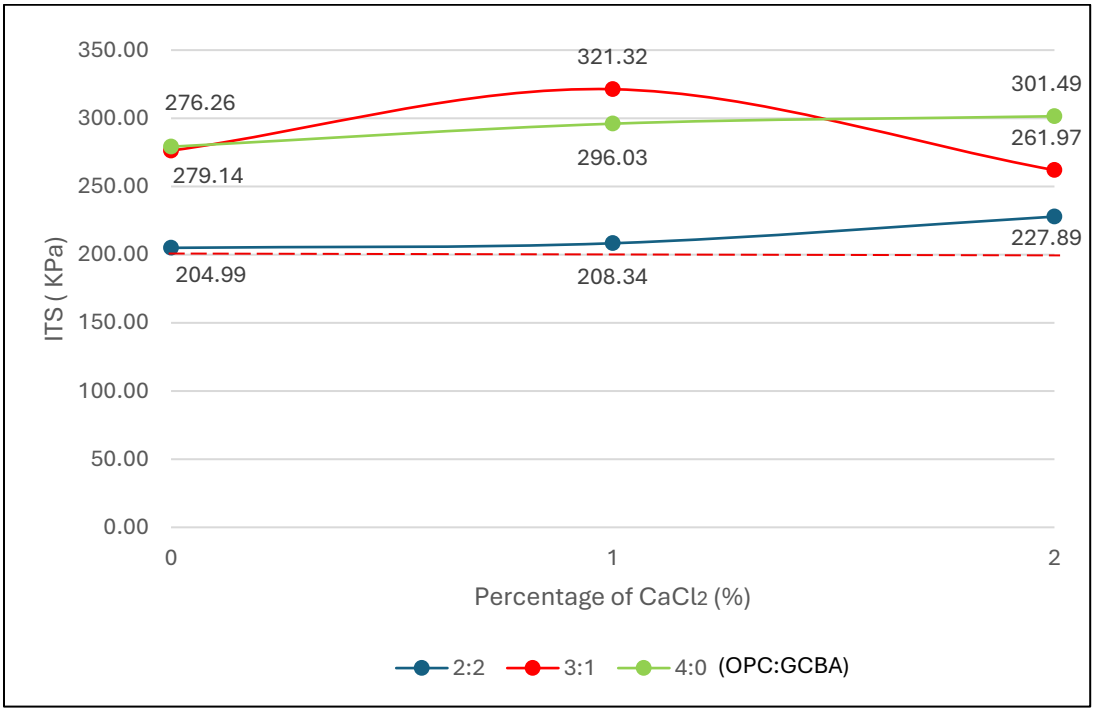


Figure 4.67 ITS for CA75RAP25 on Day 3

On day 3 of the curing process, depicted in Figure 4.67, the mix design comprising 3% OPC + 1% GCBA + 1% $CaCl_2$ exhibited the highest ITS, reaching 321.32 KPa. Following closely behind was the mix containing 4% OPC + 0% GCBA + 2% $CaCl_2$, recorded at 301.49 KPa.

Conversely, the lowest recorded ITS was noted in the mix without $CaCl_2$, specifically in the mix consisting of 2% OPC + 2% GCBA, where the tensile strength was only able to reach 204.99 KPa. The trend showed that the inclusion of every 1% of $CaCl_2$ tended to increase the tensile strength for day 3 across most of the mixes, indicating a consistent strengthening effect attributed to the addition of $CaCl_2$. All mixes began to develop sufficient strength, surpassing the minimum requirement on day 3.

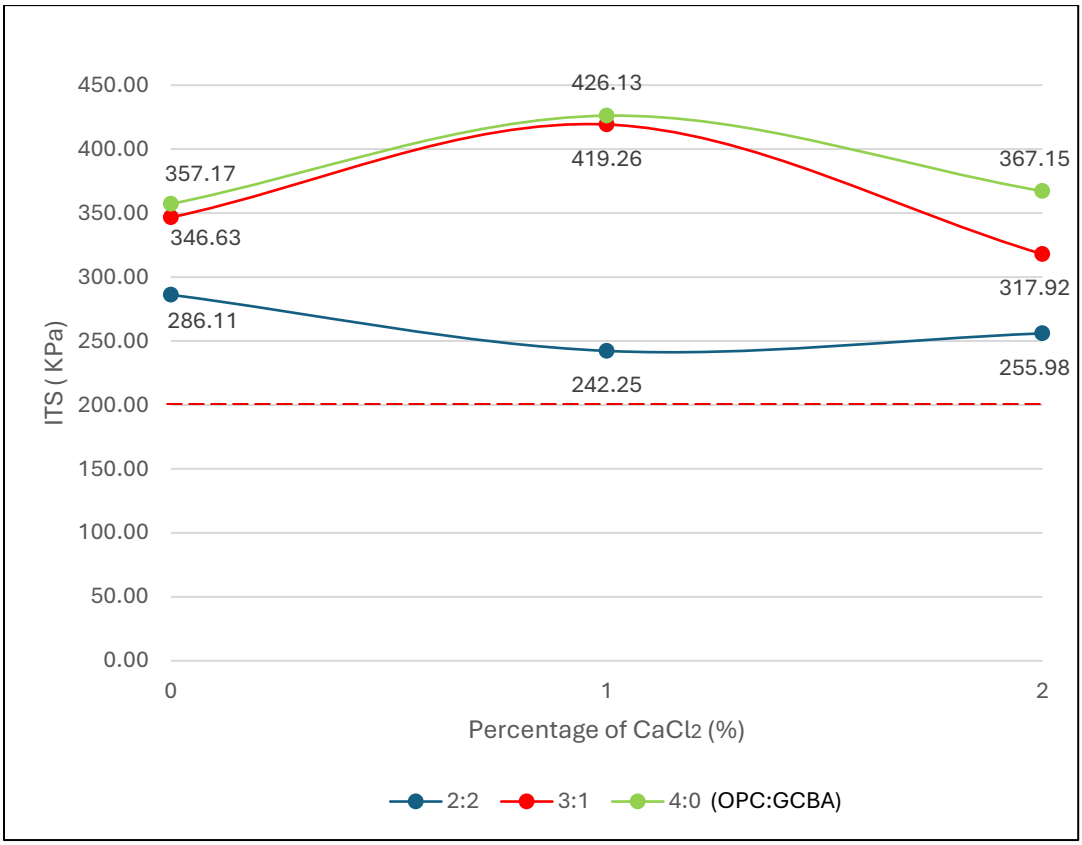


Figure 4.68 ITS for CA75RAP25 on Day 7

Figure 4.68 showcases the outcome tested on day 7 of the curing process. Upon analysis, a notable consistency in trend became apparent across varying percentages of $CaCl_2$. Specifically, the highest recorded ITS corresponded to the mix of 4% OPC + 0% GCBA + 1% $CaCl_2$ at 426.13 KPa. It was closely followed by the same percentage of $CaCl_2$ content with the mix combination of 3% OPC + 1% GCBA + 1% $CaCl_2$ at 419.26 KPa. In contrast, all the mixes containing 2% GCBA and OPC recorded the lowest ITS across various percentages of $CaCl_2$.

The incorporation of 1% $CaCl_2$ appeared to increase the tensile strength of most mixes except for of 2% OPC + 2% GCBA mix, as indicated by the observed results. However, with a higher percentage of $CaCl_2$, specifically 2%, there appeared to be a reduction in tensile strength across most of the mixes. This observation suggested a threshold effect, wherein the beneficial impact of $CaCl_2$ on tensile strength lessened or reversed beyond a certain percentage.

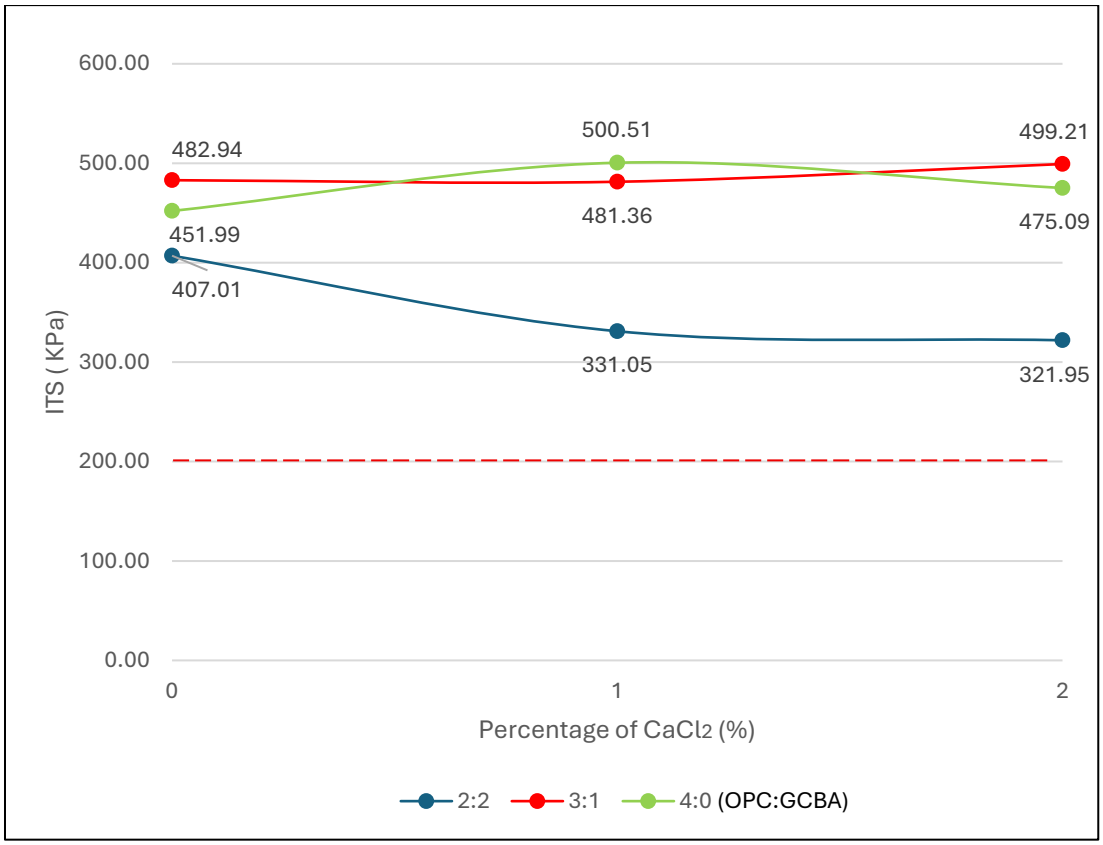


Figure 4.69 ITS for CA75RAP25 on Day 14

The findings from day 14 of the curing process are illustrated in Figure 4.69. In contrast to the results on day 7, a noticeable trend of irregularity was observed across various percentages of $CaCl_2$. The mix without GCBA recorded the highest ITS, peaking at 500.51 KPa. The mix design with a combination of 3% OPC + 1% GCBA + 2% $CaCl_2$ closely followed, reaching 499.21 KPa. Meanwhile, all mixes containing 2% OPC + 2% GCBA exhibited the lowest ITS throughout the entire range of $CaCl_2$ percentages.

Incorporating 1% $CaCl_2$ slightly reduced the tensile strength for the 2% OPC + 2% GCBA and 3% OPC + 1% GCBA mix, while only 4% OPC + 0% GCBA mix showed a slight increase. This trend continued as observed in the previous curing period, where incorporating 2% $CaCl_2$ reduced the tensile strength for most mixes except the mix with 3% OPC + 1% GCBA.

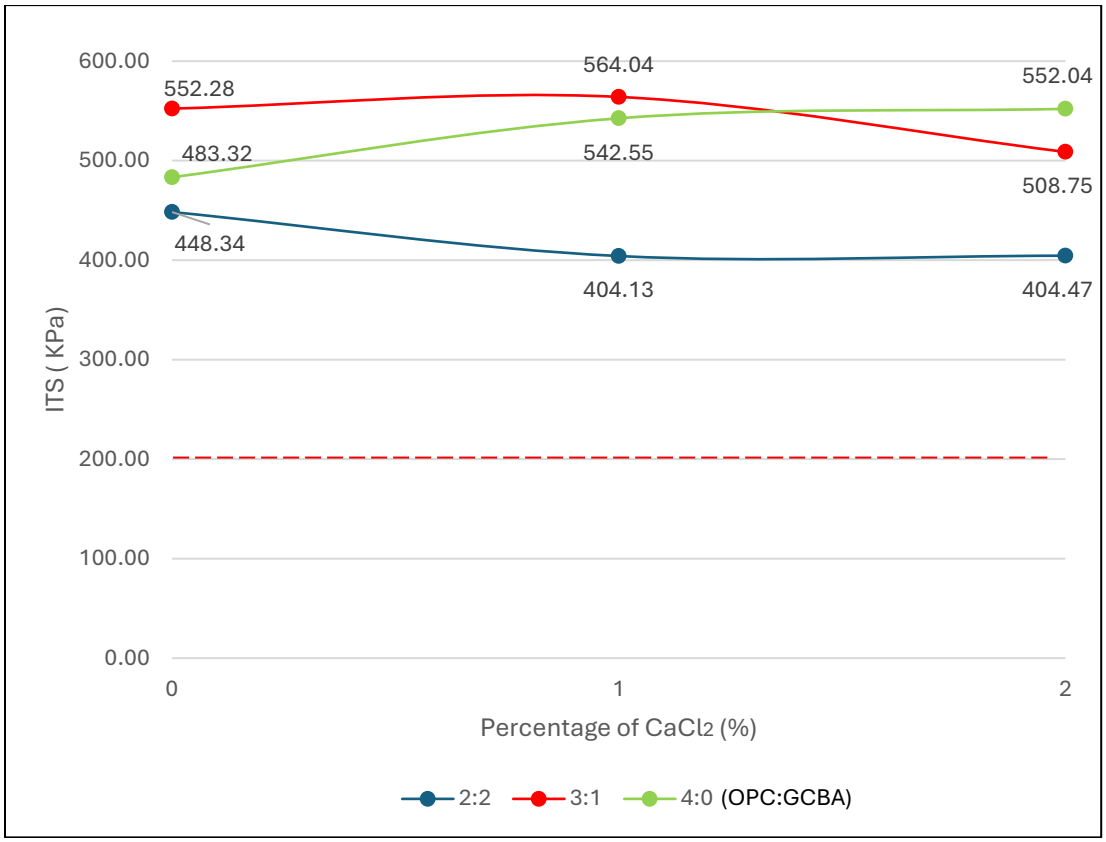


Figure 4.70 ITS for CA75RAP25 on Day 28

Figure 4.70 illustrates the outcomes analyzed on the final day of the curing process, highlighting notable trends in ITS. The mix with 3% OPC + 1% GCBA + 1% $CaCl_2$ achieved the highest ITS of 564.04 KPa. Close behind, the same mix but without $CaCl_2$ recorded an ITS of 552.28 KPa. However, when the percentage of $CaCl_2$ was increased to 2% in the same mix, a slight decreased in tensile strength was observed, resulting in an ITS of 508.75 KPa. This decline suggested that, while $CaCl_2$ significantly enhanced the mechanical performance of the material, it is crucial to maintain an optimal percentage range to achieve the desired strength characteristics.

Conversely, all mixes with 2% OPC + 2% GCBA consistently recorded the lowest ITS among those tested.

In the CA75RAP25 mix design, an inconsistent trend in the ITS was observed for each percentage of $CaCl_2$ added to the mix from the first day of curing to the final day. Throughout the curing period, variations in ITS were observed, with no clear pattern emerging as the percentages of OPC, GCBA, and $CaCl_2$ were altered. This inconsistency suggested that the impact of the stabilizing agent on the ITS of the CA75RAP25 mix did not follow a linear trend.

Such variation in ITS highlighted the complex interactions between the stabilizing agent and other mixed materials as well as curing conditions. Factors such as the reactivity of stabilizing agent with other materials, moisture content, and temperature during the curing process could contribute to these fluctuations (Wei et al., 2024; Du, 2018).

b) CA50RAP50 Mix Design

Figures 4.71 to 4.75 show the ITS result for CA50RAP50 mix design on different percentages of stabilizing agent from day 1 to day 28 of the curing process.

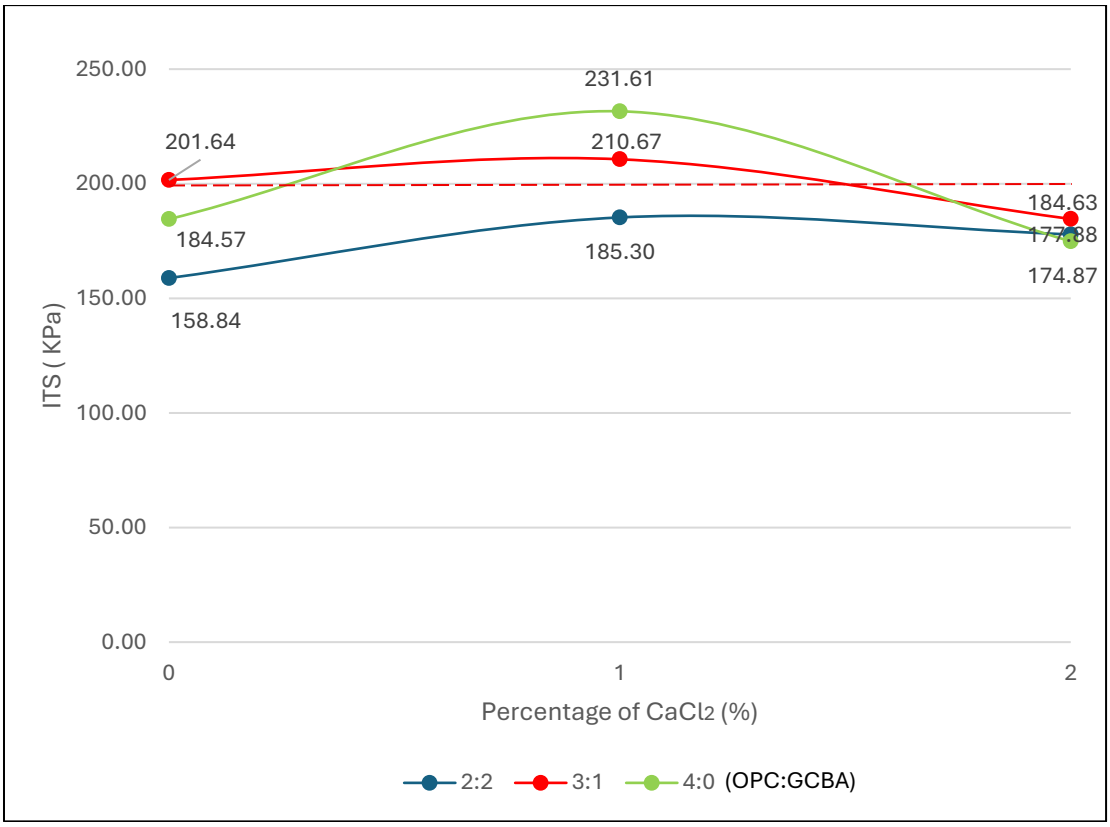


Figure 4.71 ITS for CA50RAP50 on Day 1

Figure 4.71 provides insights into the ITS measured on the first day of the curing process for the CA50RAP50 mix design. Notable variations were observed across the different mixed compositions. The mix of 4% OPC + 0% GCBA + 1% $CaCl_2$ exhibited the highest ITS of 231.61 KPa. This result highlighted the positive effect of $CaCl_2$ in enhancing the early tensile strength of the mix, particularly when combined with a higher percentage of OPC. Following closely was the mix of 3% OPC + 1% GCBA + 1% $CaCl_2$, which recorded an ITS of 210.67 KPa. This indicated that while OPC is a crucial component for enhancing early tensile strength, the addition of GCBA contributed positively, although slightly less.

In contrast, the lowest tensile strength was observed in the mix with 2% OPC + 2% GCBA + 0% $CaCl_2$, recording an ITS of 158.84 KPa. In comparison with CA75RAP25, the CA50RAP50 mix design demonstrated superior early strength development, with three mixes surpassing the 200 kPa minimum requirements on the first day of curing, thereby indicating satisfactory performance at the initial stage.

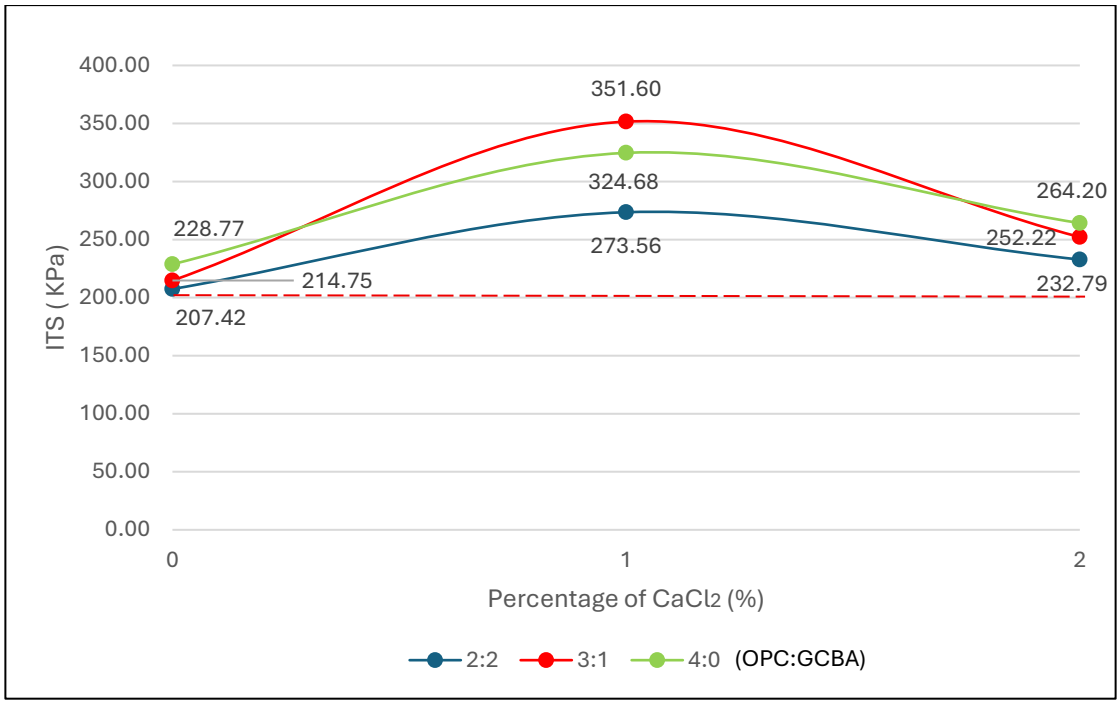


Figure 4.72 ITS for CA50RAP50 on Day 3

On the third day of the curing process, as shown in Figure 4.72, a noticeable upward trend in the ITS was observed across all mix designs compared to day one. This improvement indicated enhanced mechanical properties of the materials as the curing process progressed.

The mix of 3% OPC + 1% GCBA + 1% $CaCl_2$ achieved the highest ITS of 351.60 KPa. The mix containing the same amount of $CaCl_2$ but with 4% OPC followed closely, reaching an ITS of 324.68 KPa. It was clear that, among all compositions, the mixes with 1% $CaCl_2$ consistently showed the highest tensile strength.

In contrast, a distinct pattern emerged among the mixes that did not include $CaCl_2$, as these consistently produced the lowest ITS. Specifically, the mix of 2% OPC + 2% GCBA + 0% $CaCl_2$ recorded the lowest ITS at 207.42 KPa. This trend highlighted the critical role of $CaCl_2$ in enhancing the mechanical properties of the mix, particularly in terms of tensile strength. The absence of $CaCl_2$ correlated with reduced ITS across various mix compositions, highlighting its importance as a key additive for optimizing the performance of construction materials during the curing process. Despite these variations, it is worth noting that all mixes exceeded the minimum requirement of 200 KPa for day 3 of curing.

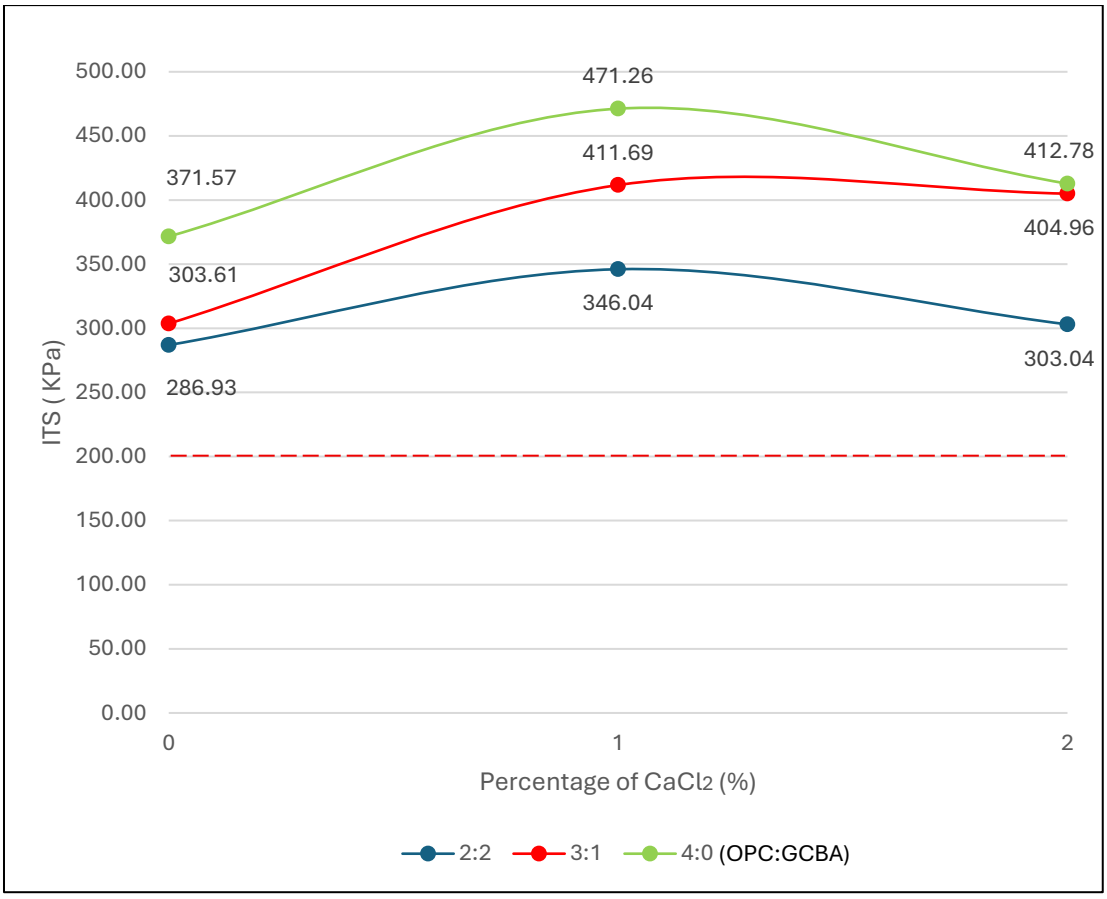


Figure 4.73 ITS for CA50RAP50 on Day 7

The trend of increasing ITS continued after one week of the curing process, as shown in Figure 4.73. Consistent with the patterns observed on days 1 and 3, the highest ITS was recorded in the mix of 4% OPC + 0% GCBA + 1% $CaCl_2$, reaching 471.26 KPa. The next highest ITS, 412.78 KPa, came from the same 4% OPC mix but with 2% $CaCl_2$. This finding reinforces the important role of $CaCl_2$ in enhancing the mechanical properties of the material, even at different percentage contents.

A consistent pattern was also observed in mixes that contained no $CaCl_2$, all of which recorded the lowest ITS. Among these compositions, the mix of 2% OPC + 2% GCBA + 0% $CaCl_2$ exhibited the lowest ITS at 286.93 KPa.

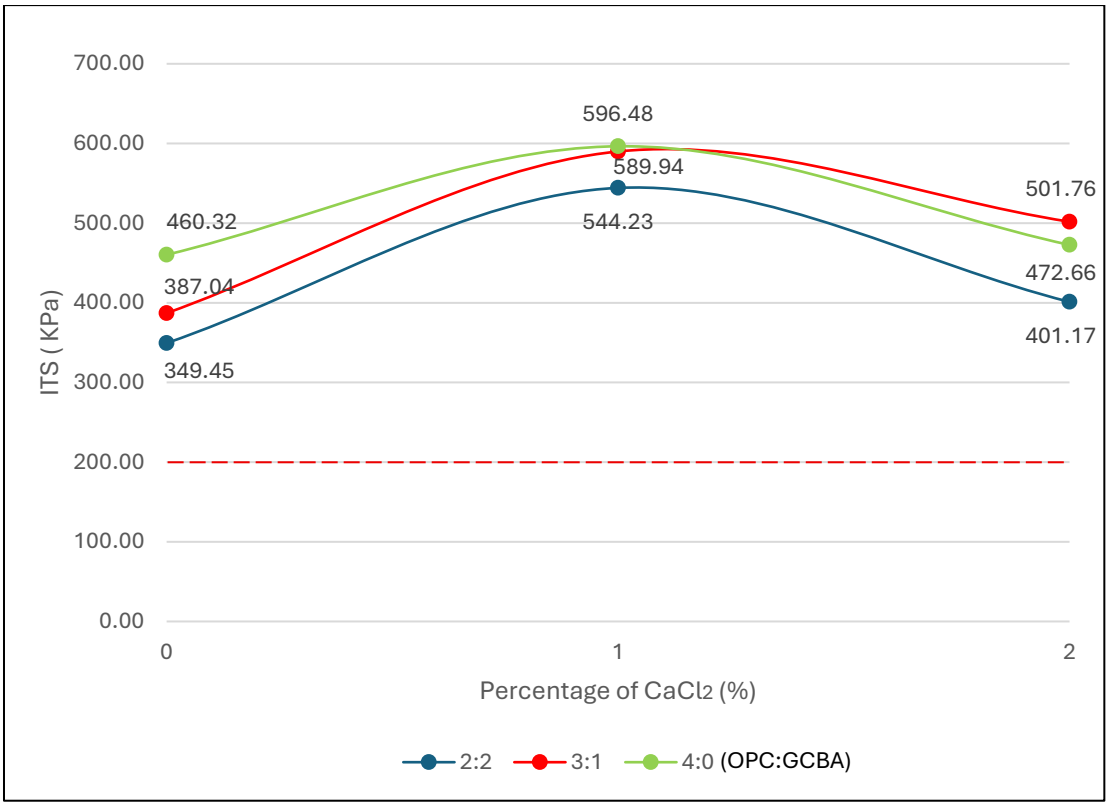


Figure 4.74 ITS for CA50RAP50 on Day 14

As shown in Figure 4.74, a notable pattern developed during the second week of the curing process, where all mixes containing 1% $CaCl_2$ consistently demonstrated the highest tensile strength. Among these, the mix featuring 4% OPC stood out, recording the highest value of 596.48 KPa. Close behind was the mix comprising 3% OPC + 1% GCBA + 1% $CaCl_2$, which achieved ITS of 589.94 KPa. This result showed the synergistic effect of OPC and GCBA, further enhanced by adding $CaCl_2$, in improving the mechanical properties of the material.

However, upon the addition of 2% $CaCl_2$ to the mix, a noticeable decrease in ITS was observed across all compositions. Despite this decrease, the ITS remained relatively high compared to mixes without the inclusion of $CaCl_2$. This suggested that although a higher $CaCl_2$ percentage might have resulted in a lower tensile strength, the overall performance still exceeded that of mixes without $CaCl_2$.

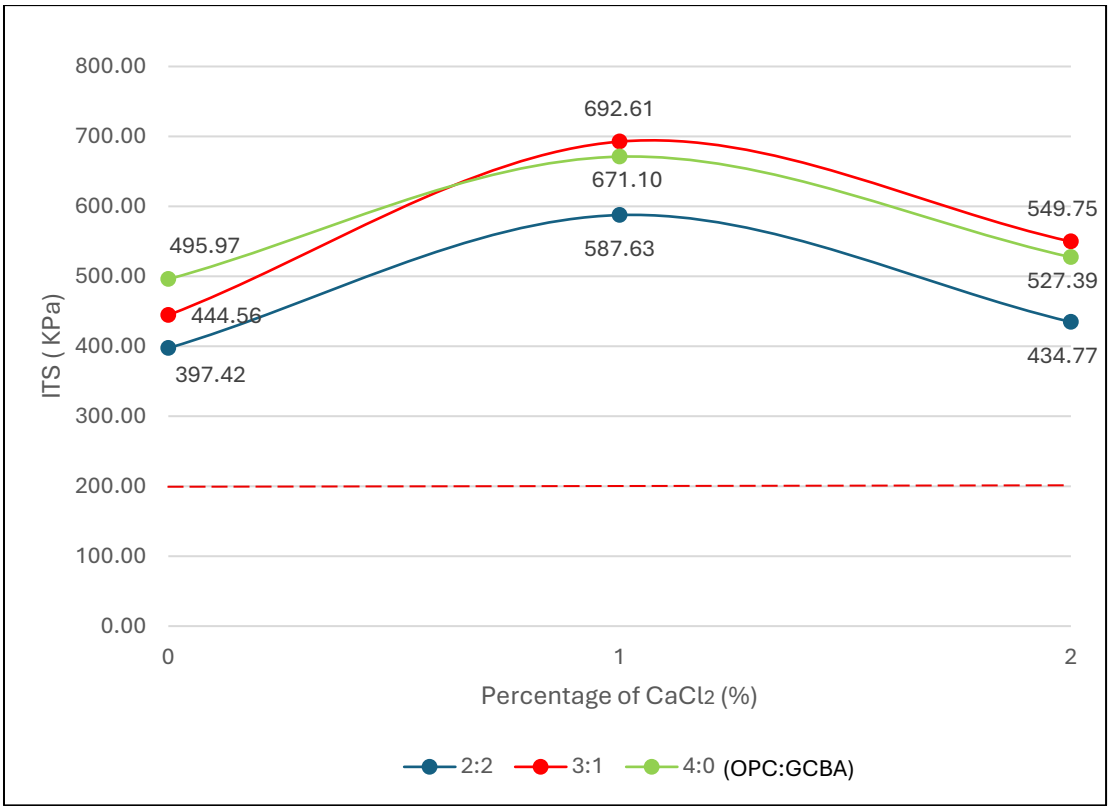


Figure 4.75 ITS for CA50RAP50 on Day 28

As shown in Figure 4.75, the ITS results from the final day of the 28-day curing process displayed a trend consistent with observations from earlier curing periods. Once again, all mix designs containing 1% $CaCl_2$ achieved the highest ITS. Notably, the mix of 3% OPC + 1% GCBA + 1% $CaCl_2$ demonstrated the highest tensile strength of 692.61 KPa. The 4% OPC + 0% GCBA + 1% $CaCl_2$ mix followed closely, which reached an ITS of 671.10 KPa. This finding highlighted the significant role of OPC in enhancing tensile strength, especially when in use with $CaCl_2$.

Mixes without $CaCl_2$ consistently exhibited the lowest ITS. Among these, the mix of 2% OPC + 2% GCBA + 0% $CaCl_2$ repeatedly recorded the lowest ITS at 397.42 KPa.

A clear pattern emerged in the mix design with a CA50RAP50 composition across different percentages of stabilizing agent added. Throughout the entire curing period, it was observed that the mixes with 3% OPC + 1% GCBA and 4% OPC + 0% GCBA consistently alternated in having the highest tensile strength. The replacement of 1% GCBA with OPC demonstrated a positive impact on the ITS.

Additionally, the mix design that did not include $CaCl_2$ exhibited slightly lower ITS than the mix that incorporated $CaCl_2$, consistent with research by Saeed (2023) showing that the use of $CaCl_2$ as an accelerator can improve strength development compared with control mix without the admixture. This analysis suggested that adding $CaCl_2$, regardless of the percentages of OPC and GCBA used, positively influenced the ITS of the CA50RAP50 mix design. Although there was a minor variation in the ITS between the mixes with and without $CaCl_2$, it was evident that $CaCl_2$ played a significant role in improving the mechanical properties of the mix, particularly in terms of tensile strength.

Notably, adding just 1% of $CaCl_2$ appeared to enhance the tensile strength of the mix, resulting in better overall performance. However, increasing the $CaCl_2$ content to 2% seemed to have an adverse effect, leading to a slight reduction in strength.

Overall, the consistent trend of higher ITS in mixes containing 1% $CaCl_2$, combined with 3-4% OPC and 0-1% GCBA, demonstrated the effectiveness of this formulation in improving the mechanical properties of the material throughout the curing period. These results highlight the value of optimizing additive proportions to ensure long-term performance in construction applications.

c) CA25RAP75 Mix Design

Figures 4.76 to 4.80 show the ITS result for CA25RAP75 mix design on different percentages of stabilizing agent from day 1 to day 28 of the curing process.

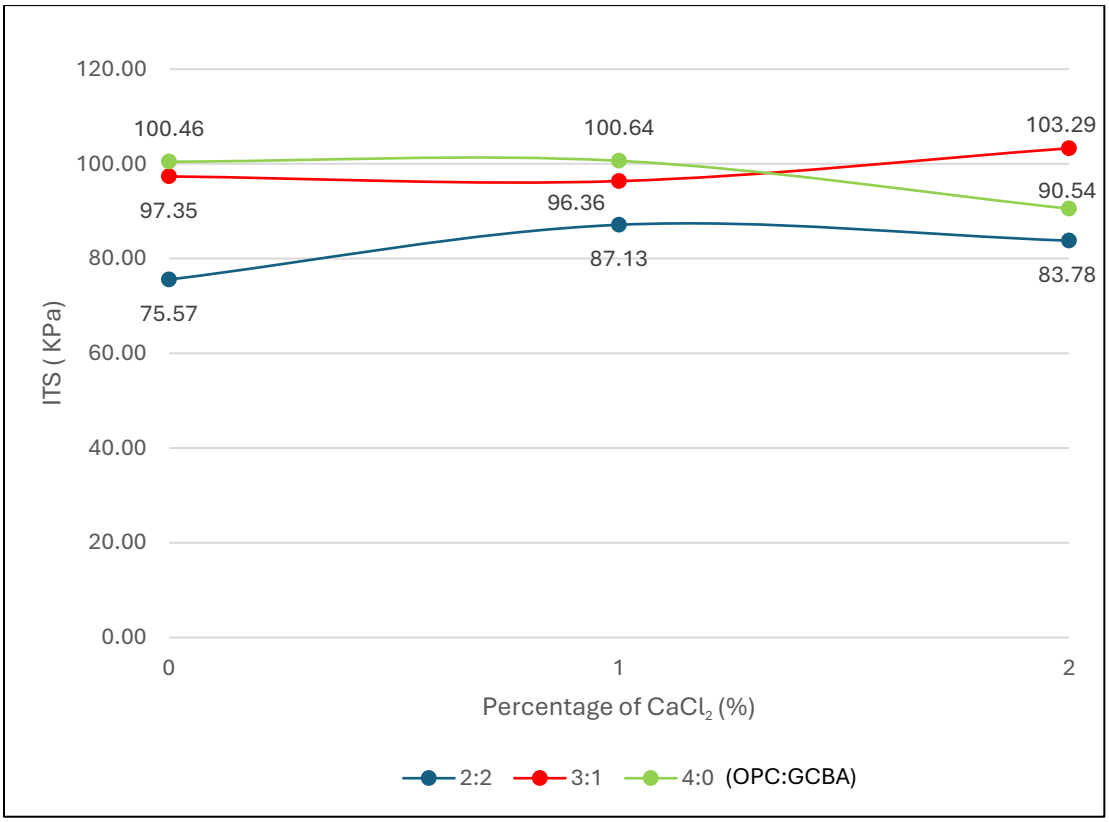


Figure 4.76 ITS for CA25RAP75 on Day 1

Figure 4.76 presents the analysis of ITS on the first day of the curing process. Notably, the mix of 3% OPC + 1% GCBA + 2% $CaCl_2$ achieved the highest recorded ITS of 103.29 KPa. This was followed closely by the mix of 4% OPC + 0% GCBA + 1% $CaCl_2$ with ITS of 100.64 KPa.

On the other hand, the mix of 2% OPC + 2% GCBA + 0% $CaCl_2$ resulted in the lowest ITS at 75.57 kPa. It was evident that all mixes containing equal percentages of OPC and GCBA consistently exhibited the lowest ITS, regardless of the varying amounts of $CaCl_2$. This consistent trend indicated a significant impact of the OPC and GCBA proportions on the tensile strength of the mix, particularly when $CaCl_2$ is included.

Overall, none of the proposed mix designs met the required minimum strength threshold of 200 kPa on the first day of curing, clearly indicating that they did not satisfy the minimum standards.

The combination of low CA content and high RAP proportion likely contributed to the reduced strength, as the limited presence of binder material and high reclaimed aggregate content may have hindered early bonding and strength development.

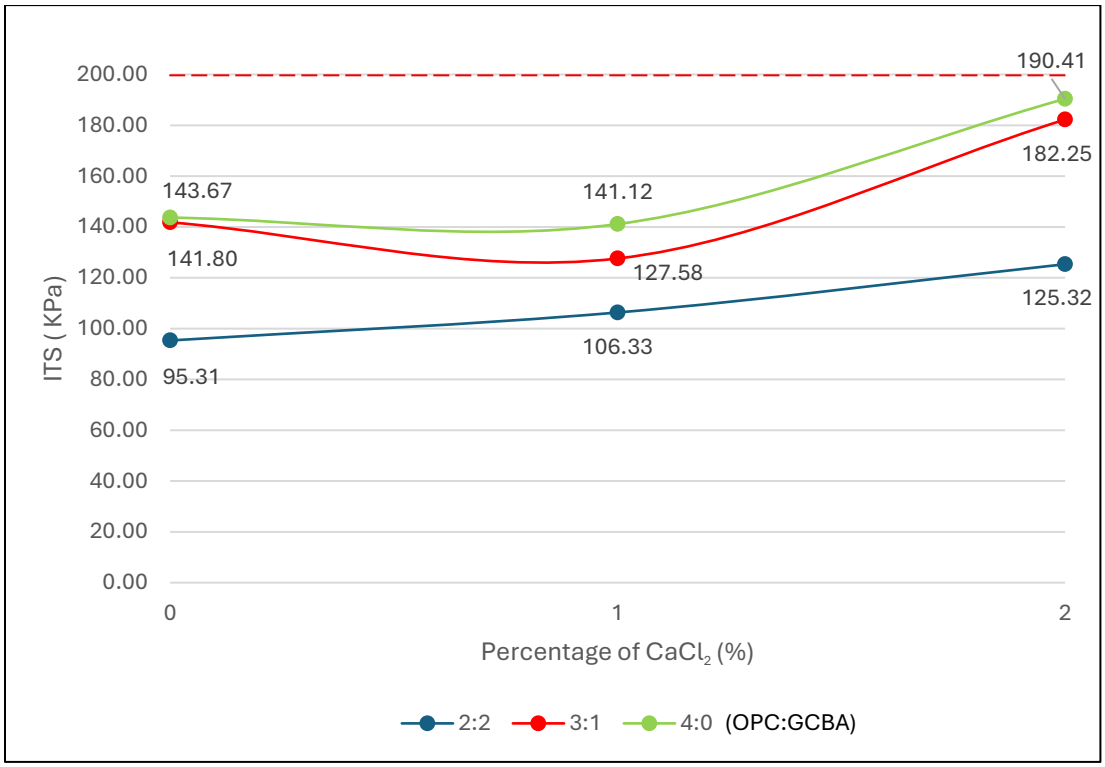


Figure 4.77 ITS for CA25RAP75 on Day 3

Figure 4.77 illustrates the third day of the curing process. An apparent increase in strength was observed, with several of the mixes beginning to exhibit signs of reaching the minimum strength requirement of 200 KPa, indicating a good sign of early-stage development. The mix containing 4% OPC + 0% GCBA + 2% $CaCl_2$ exhibited the highest recorded ITS, reaching 190.41 KPa. The mix of 3% OPC + 1% GCBA + 2% $CaCl_2$ followed closely, achieving a strength of 182.25 KPa. This result indicated that even with different additive compositions of OPC and GCBA, the presence of $CaCl_2$ remains a crucial factor contributing to the observed gain of strength.

However, it was noting that despite these promising results, all of the proposed mix designs fell short of target strength, with all of the lowest values recorded on the mixes of 2% OPC + 2% GCBA. In particular, the mix without $CaCl_2$ recorded the lowest value at only 95.31 KPa. This observation highlighted that the absence of $CaCl_2$ had a notable impact on tensile strength development within the mix. The progression of the strength development in this mix was a little slow, as evidenced by the initial reading on the first day of the curing process, which was 75.57 KPa.

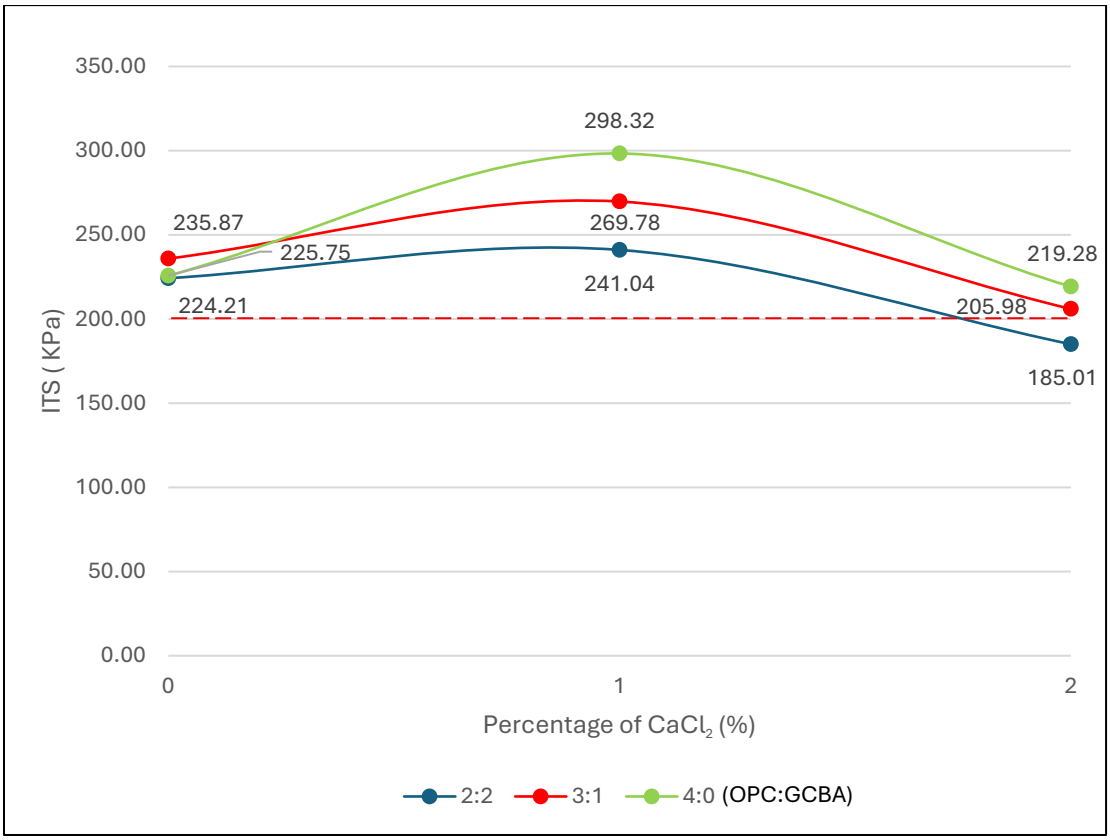


Figure 4.78 ITS for CA25RAP75 on Day 7

The data presented in Figure 4.78 highlighted a significant milestone in the curing process on day 7. Almost all of the mixes have exceeded the minimum required strength. However, a notable trend emerged where mixes with a higher percentage of RAP may require a longer curing period to achieve the minimum strength for all proposed mix designs.

The mix design of 4% OPC + 0% GCBA + 1% $CaCl_2$ recorded the highest ITS of 298.32 KPa. Closely following it, the mix of 3% OPC + 1% GCBA + 1% $CaCl_2$ achieved an ITS of 269.78 KPa. Additionally, the 2% OPC + 2% GCBA + 1% $CaCl_2$ mix demonstrated decent performance, recording an ITS of 241.02 KPa.

In contrast, the 2% OPC + 2% GCBA + 2% $CaCl_2$ mix design recorded the lowest ITS at 185.01 kPa, which fell slightly below the minimum requirement.

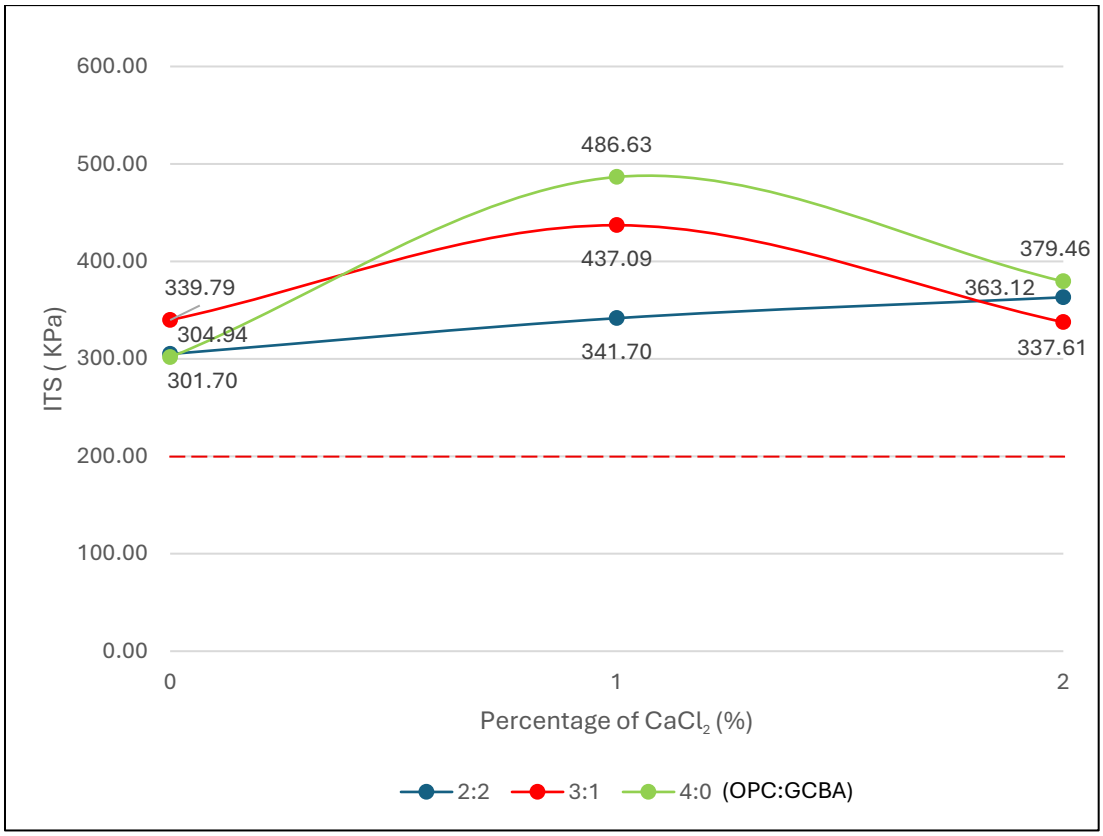


Figure 4.79 ITS for CA25RAP75 on Day 14

As the curing process progressed into day 14, a clear trend emerged of increasing tensile strength for all mix designs, as shown in Figure 4.79. The mixes containing 1% $CaCl_2$ consistently demonstrated the highest ITS. Notably, the mix of 4% OPC + 0% GCBA + 1% $CaCl_2$ recorded the highest ITS at 486.63 KPa, closely followed by a mix of 3% OPC + 1% GCBA + 1% $CaCl_2$, which achieved an ITS of 437.09 KPa.

While the overall trend was upward, there were slight variations among the mixes that contained zero percent $CaCl_2$. These mixes consistently recorded the lowest ITS compared to the other compositions. In particular, the mix of 4% OPC + 0% GCBA + 0% $CaCl_2$ had the lowest ITS, reaching only 301.70 KPa.

Natably, a 2% OPC + 2% GCBA mix demonstrated an increase in ITS with each additional 1% of $CaCl_2$, while the other two mixes began to decrease at 2% $CaCl_2$.

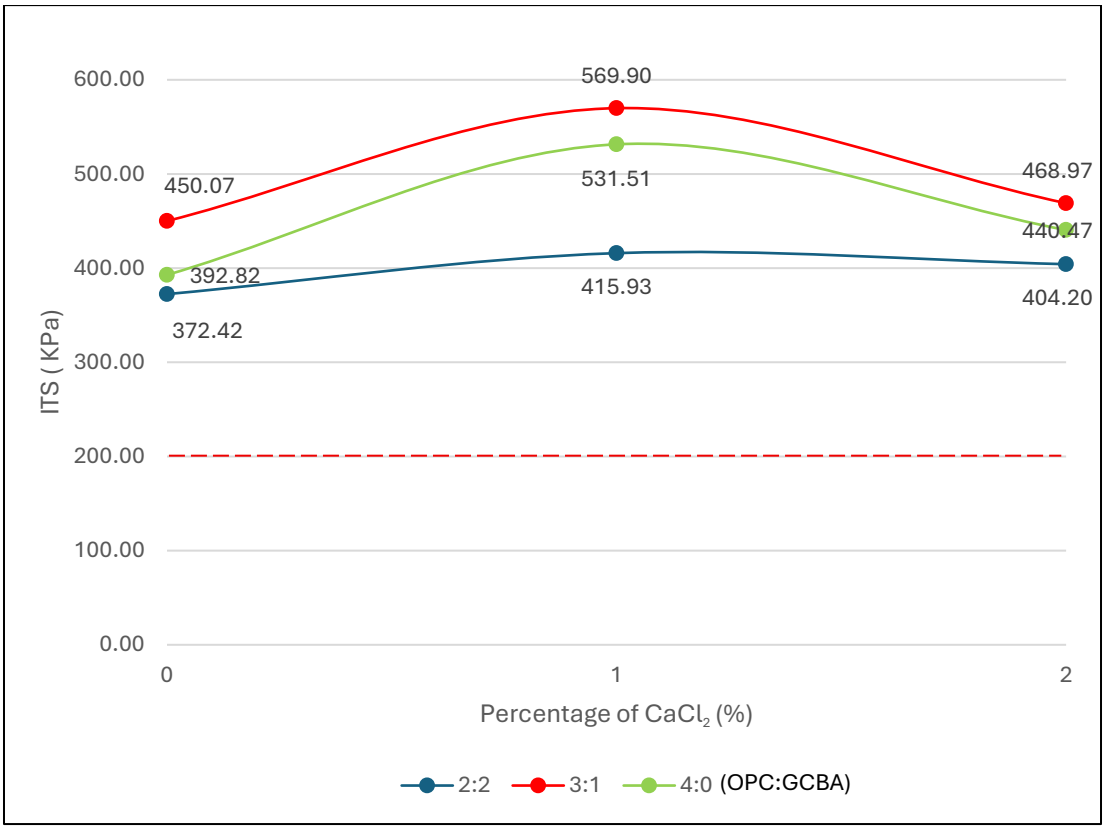


Figure 4.80 ITS for CA25RAP75 on Day 28

The ITS results for day 28 of the curing process, illustrated in Figure 4.80, continued the trends observed in earlier curing periods. All mix designs containing 1% $CaCl_2$ recorded the highest ITS. Among these, a mix of 3% OPC + 1% GCBA + 1% $CaCl_2$ achieved the highest recorded value of 569.90 KPa, followed closely by a mix of 4% OPC + 0% GCBA + 1% $CaCl_2$ at 531.51 KPa. Notably, all mixes of 3% OPC + 1% consistently exhibited the highest values across all three percentages of $CaCl_2$.

In contrast, the mix design of 2% OPC + 2% GCBA + 0% $CaCl_2$ recorded the lowest ITS at 372.42 KPa. This recurring pattern highlighted the significant impact of $CaCl_2$ on enhancing tensile strength in the mixes, with its absence leading to notably lower strength outcomes.

In the analysis of CA25RAP75 mix design, several key observations were made regarding the development of tensile strength within the proposed mix design. The examination of the stabilizing agent content provided interesting insights into how tensile strength evolved during the early stages of the curing process.

During the first three days of curing, there was inconsistency in the ITS as the percentage of $CaCl_2$ increased. However, the highest percentage of OPC at 4% consistently demonstrated superior ITS performance when combined with 1% $CaCl_2$. This variability indicated a complex interplay of factors influencing early-stage strength development, which included the reactivity of OPC, GCBA, and $CaCl_2$ with other components in the mix, as well as the dynamics of the curing process itself.

As the curing process continued into the first week, a notable trend emerged where the tensile strength began to decrease when the $CaCl_2$ content approached 2% in the mix. This observation highlighted a potential threshold effect, where higher percentages of $CaCl_2$ negatively impacted tensile strength. This phenomenon could be attributed to various factors, including changes in chemical interactions within the mix, alterations in curing kinetics, or potential adverse effects on material properties at high $CaCl_2$ contents (Lu and Wu, 2025; Almajed et al., 2023).

4.4.2.2 Influence of Stabilizing Agent on Indirect Tensile Strength

Figures 4.66 to 4.80 show that a consistent pattern emerged regarding the influence of stabilizing agent on the proposed mix designs across most mixes. In most cases, mixes containing 1% $CaCl_2$ combined with 3% OPC + 1% GCBA and 4% OPC achieved the highest ITS, surpassing the control specimens with 4% OPC but no $CaCl_2$ across all CA-RAP compositions. This confirmed the positive role of $CaCl_2$ in enhancing early-age tensile strength, particularly at lower dosages. However, when the $CaCl_2$ content increased to 2%, a reduction in ITS was observed in most mixes, indicating the presence of an optimum dosage threshold. Beyond this point, the accelerating effect of $CaCl_2$ diminished and, in some cases, became detrimental to early strength development. The reduction in ITS at 2% $CaCl_2$ may be attributed to excessive acceleration of cement hydration, resulting in a non-uniform and less dense microstructure. These results align with the findings of Almajed et al. (2023), William et al. (2020) and Salain (2019), who reported that excessive $CaCl_2$ can reduce the mechanical performance of cementitious systems.

In addition, the proportion of OPC and GCBA strongly influenced strength outcomes. Mixes with a 2% OPC + 2% GCBA combination consistently recorded the lowest ITS across all $CaCl_2$ dosages. This highlighted the adverse effect of higher GCBA replacement on tensile strength, where the dilution of cementitious compounds limited bond formation at early curing stages. Since GCBA typically contributes to strength through pozzolanic activity at later ages, its limited reactivity in the short term restricted early tensile strength development (Chuang et al., 2023). Conversely, mixes without GCBA generally produced higher tensile strength. These results are consistent with observations by Kim et al. (2011) and Khan and Ganesh (2016), who noted reductions in strength with increased GCBA substitution. However, they contrast with Kurama and Kaya (2008), who identified 10% GCBA as the optimal replacement for improving concrete strength. Such differences may be attributed to variations in material properties, mix design approaches, and the distinct performance requirements of concrete versus pavement base materials.

Overall, the CA50RAP50 mix of 3% OPC + 1% GCBA + 1% $CaCl_2$ and 4% OPC + 1% $CaCl_2$ emerged as the most effective and reliable design for indirect tensile strength, consistently outperforming other combinations while demonstrating superior early-age strength development. Meanwhile, 3% OPC + 1% GCBA with 1% $CaCl_2$ mix also highlighted the potential for enhanced later-age strength which recorded the highest ITS, providing insight into the long-term benefits of limited GCBA incorporation.

4.4.2.3 Effect of Varying CA-RAP Ratio on Indirect Tensile Strength

The outcomes of the ITS results regarding the effect of different CA-RAP ratios on the proposed mix design revealed the importance of these ratios as an influence on the overall performance of the stabilized base course. This highlighted the importance of evaluating a suitable CA-RAP ratio before considering reconstructing the base course.

The analysis depicted in Figures 4.81 to 4.83 presents detailed analysis of the results obtained from different combinations of CA-RAP over the entire 28-day curing period. These figures effectively portrayed the diverse impacts of altering the CA-RAP ratios on the performance of the indirect tensile strength. Notably, a trend showed strength, increasing gradually as the curing time increased.

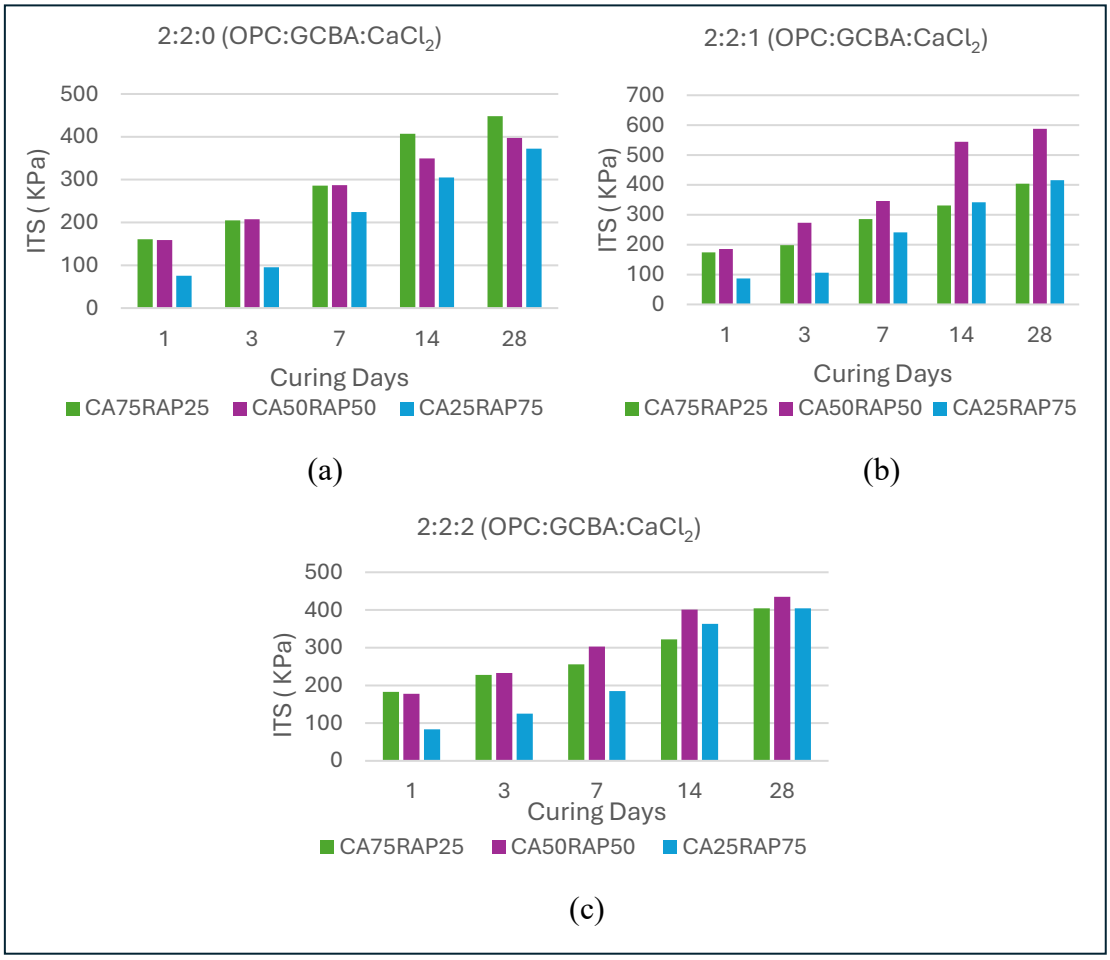


Figure 4.81 Impact of CA-RAP Ratio on Mix Design of 2% OPC + 2% GCBA with (a) 0% $CaCl_2$, (b) 1% $CaCl_2$ and (c) 2% $CaCl_2$

By analyzing the trend presented in Figure 4.81, it is evident that the mixes CA75RAP25 and CA50RAP50 recorded the highest tensile strength. In the mix without the addition of $CaCl_2$, CA75RAP25 outperformed the others. The lack of $CaCl_2$, which serves as an accelerator in stabilizing agent, had a noticeable impact on tensile strength. This absence may have slowed the curing process or prevented it from reaching its full potential, resulting in lower strength. Therefore, the mix performance relied significantly on the composition of CA and RAP. Notably, the higher proportion of CA at 75% correlated strongly with better ITS compared to mixes containing only 25% CA, which consistently displayed the lowest strength throughout the curing period.

In contrast, when $CaCl_2$ was included, the trend changed. In this scenario, CA50RAP50 mixes achieved the highest tensile strength, followed by CA75RAP25 and CA25RAP75 mixes. The addition of $CaCl_2$ introduced a dynamic element into the mix, potentially catalyzing key reactions and enhancing the bonding between aggregate particles (Teng, 2025). This improved bonding contributed to the overall increase in tensile strength of the mix.

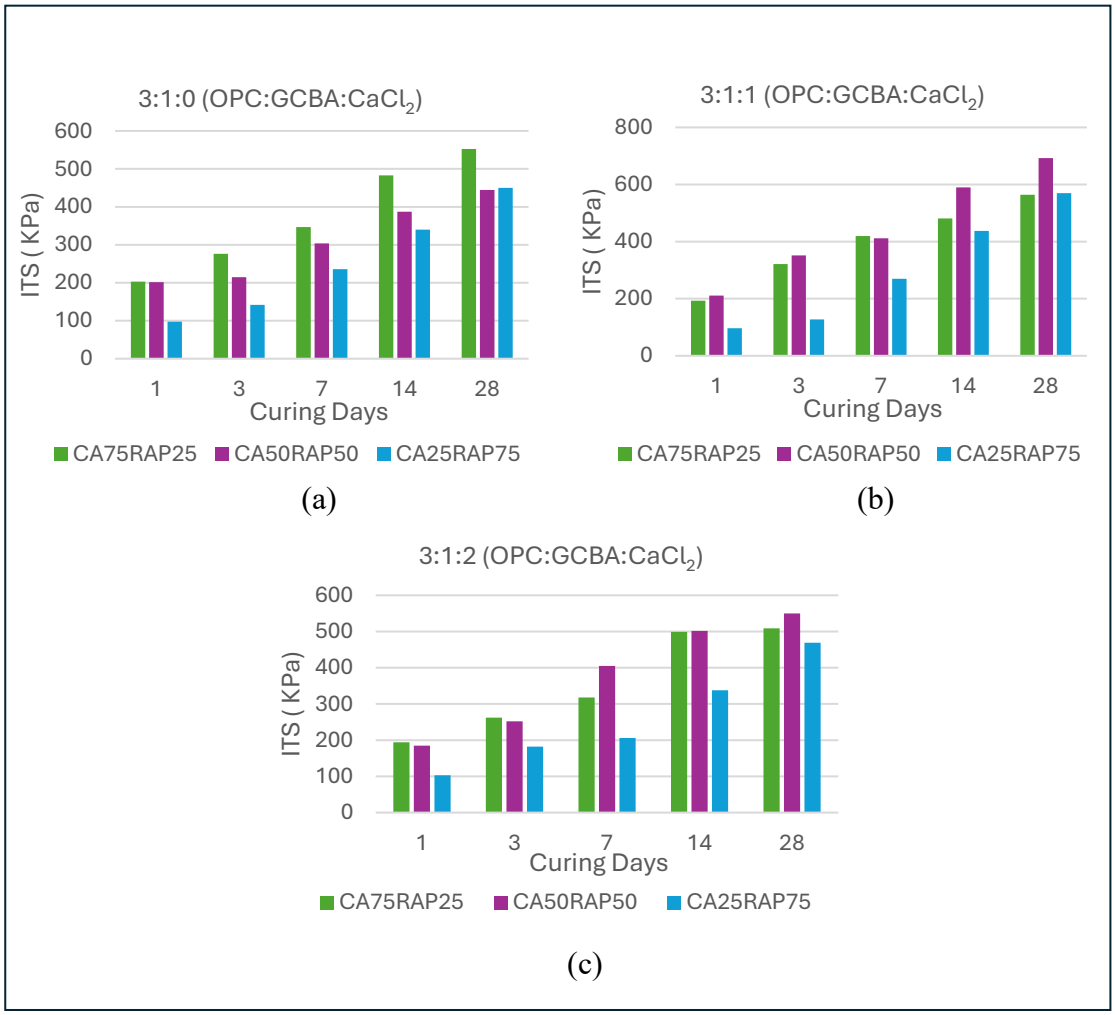


Figure 4.82 Impact of CA-RAP Ratio on Mix Design of 3% OPC + 1% GCBA with (a) 0% $CaCl_2$, (b) 1% $CaCl_2$ and (c) 2% $CaCl_2$

In the data analysis shown in Figure 4.82, a trend similar to previously reported data was observed. Specifically, the mix with a composition of 75% CA and 25% RAP recorded the highest ITS among the mixes when $CaCl_2$ was not present. This suggested that CA75RAP25 mixes exhibited better mechanical properties under these conditions.

The trend, however, shifted when $CaCl_2$ was added at percentages of 1% and 2%. Despite variations in the percentages of OPC and GCBA, the impact of $CaCl_2$ was more prominent. This was evident in the data, where the mix with CA50RAP50 recorded the highest ITS, surpassing even the mix without $CaCl_2$. Again, the introduction of $CaCl_2$ enhanced the performance of the CA50RAP50 mixes significantly, making it outperform the other mixes in the presence of this chemical additive. This highlighted that $CaCl_2$ played a crucial role in improving the properties of the mix, possibly by influencing the hydration process or enhancing the bonding between the components (Teng, 2025). Consequently, the inclusion of $CaCl_2$ at the specified percentage yielded better tensile strength performance, proving its importance in the mix design.

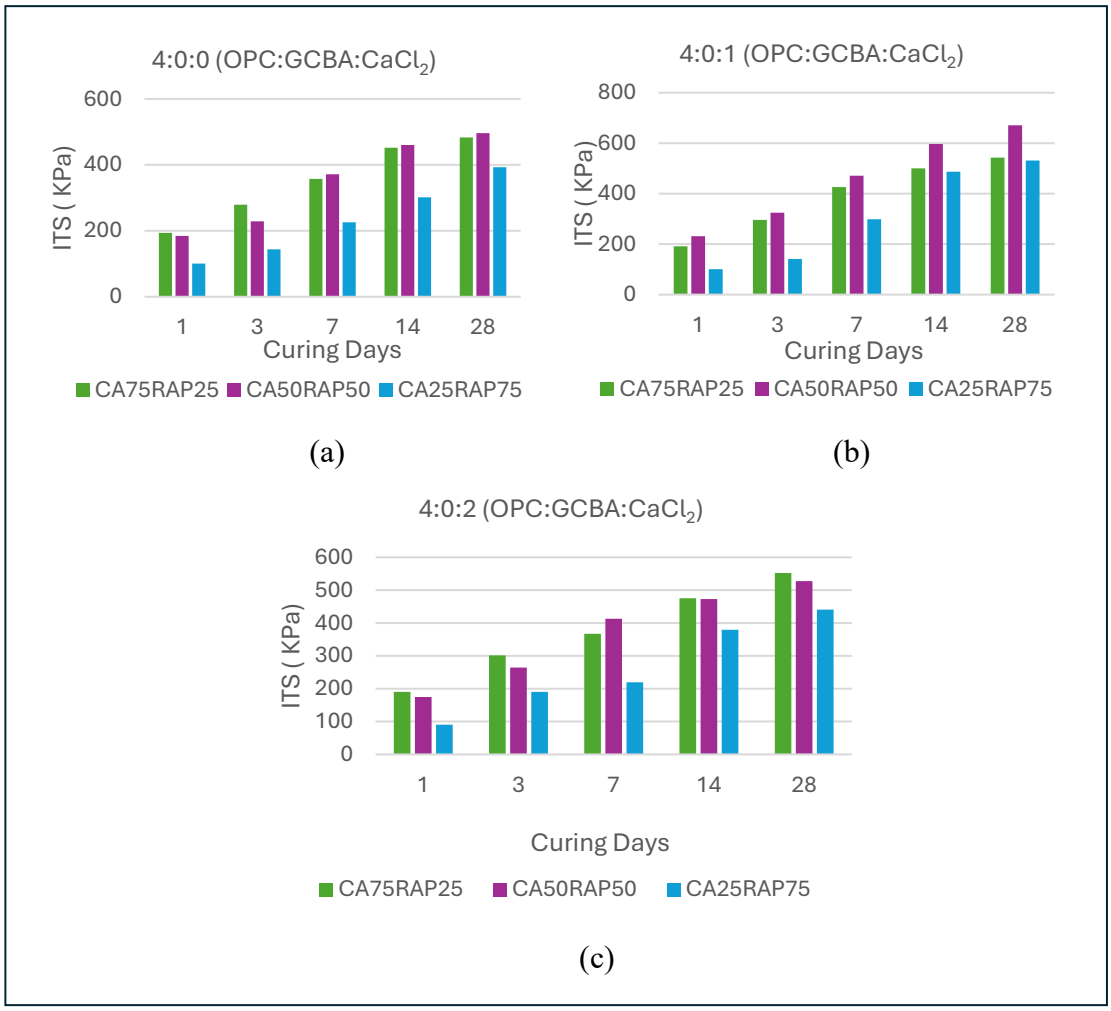


Figure 4.83 Impact of CA-RAP Ratio on Mix design of 4% OPC with (a) 0% $CaCl_2$, (b) 1% $CaCl_2$ and (c) 2% $CaCl_2$

From the analysis of results shown in Figure 4.83, the highest achieved ITS was observed in the mix containing 50% CA and 50% RAP for both the 0% and 1% $CaCl_2$ additions. This consistency suggested that the 50/50 CA-RAP blend with 4% OPC was particularly responsive to the presence of a small amount of $CaCl_2$, maintaining its good performance in tensile strength.

Nevertheless, the trend changed with the addition of 2% $CaCl_2$. Under these conditions, the CA75RAP25 mix achieved the highest ITS starting from day 1 of curing until the final day. This change showed that for mixes containing 4% OPC, a higher percentage of $CaCl_2$ improved the tensile strength of the CA75RAP25 mixes more effectively than the CA50RAP50 mixes. The initial rapid strength gained in the CA75RAP25 mixes with 2% $CaCl_2$ suggested that this combination benefited more significantly, potentially due to improved hydration, better particle bonding, or other chemical interactions facilitated by the higher $CaCl_2$ concentration.

4.4.2.4 Influence of Varying CA-RAP Ratio on Indirect Tensile Strength

Compared to both CA75RAP25 and CA50RAP50, the CA25RAP75 mix design consistently exhibited the lowest tensile strength as can be seen in Figures 4.81 to 4.83. The composition of CA and RAP within the mix emerged as one of the critical factors in determining the tensile strength of the base course. Notably, higher percentages of CA did not correlate with enhanced mechanical properties. CA50RAP50 mixes demonstrated slightly better tensile strength overall, even though at certain percentages of the stabilizing agent, CA75RAP25 mixes performed better.

This observation indicated that the balance between CA and RAP content played an important role in optimizing tensile strength, highlighting the importance of precise mix design and composition. A well-balanced proportion of CA and RAP likely contributed to better interlocking and bonding between particles, resulting in enhanced strength characteristics. Conversely, a higher RAP content led to reduced particle interlock and weaker interfacial bonding, thereby compromising overall tensile strength (Alwathaf et al., 2025).

According to Tan and Chan (2021), a higher ratio of CA was recommended to achieve the highest possible strength. The analysis in this research indicated that the CA75RAP25 mixes, which had a higher CA ratio, demonstrated strong tensile strength performance in certain cases. This mix proportion offered advantages in providing the

mechanical properties needed for the base course, likely due to the increased proportion of CA contributing to structural integrity and load-bearing capacity (Tan and Chan, 2021).

These findings were also supported by Sufian et al. (2009), whose results showed that a higher ratio of CA resulted in a higher ITS. However, the introduction of chemical stabilizing agent in this research altered the properties of the mix. The analysis showed that the CA50RAP50 mix exhibited better tensile strength performance when $CaCl_2$ was added with OPC and GCBA. This improved performance could be attributed to the chemical reactions facilitated by the stabilizing agent, which enhanced bonding and overall tensile strength. The CA50RAP50 mixes benefited more significantly from these chemical interactions, resulting in higher ITS compared to other mixes with different CA-RAP ratios.

In summary, while a higher CA ratio like CA75RAP25 mixes generally promoted better mechanical properties, the CA50RAP50 mixes outperformed in tensile strength when stabilized with OPC, GCBA, and $CaCl_2$ at optimum content, highlighting the crucial role of chemical stabilization in optimizing the performance of the pavement base course.

4.4.3 Resilient Modulus Test

Resilient modulus analysis also serves as a crucial parameter in pavement base course design, as it directly affects pavement life prediction and maintenance planning. This research presents an evaluation of resilient modulus across different stabilizing agents and CA-RAP mix ratios, as illustrated in the subsequent graphical analyses. The findings offer valuable insights into how the selected stabilizing agent influences the stiff behavior of pavement base materials under repeated loading conditions. The test was conducted in accordance with AASHTO T307.

4.4.3.1 Effect of Varying Percentages of Stabilizing Agent on Resilient Modulus

The effect of various percentages of stabilizing agents towards the resilient modulus in the mix design from day 1 to day 28 of the curing period for three distinct CA-RAP mix design variants are shown in Figures 4.84 to 4.98. The minimum requirement was set at a value of 1350 MPa, based on AASHTO T 307.

a) CA75RAP25 Mix Design

Figures 4.84 to 4.88 show the resilient modulus result for CA7RAP25 mix design on different percentages of stabilizing agent from day 1 to day 28 of the curing process.

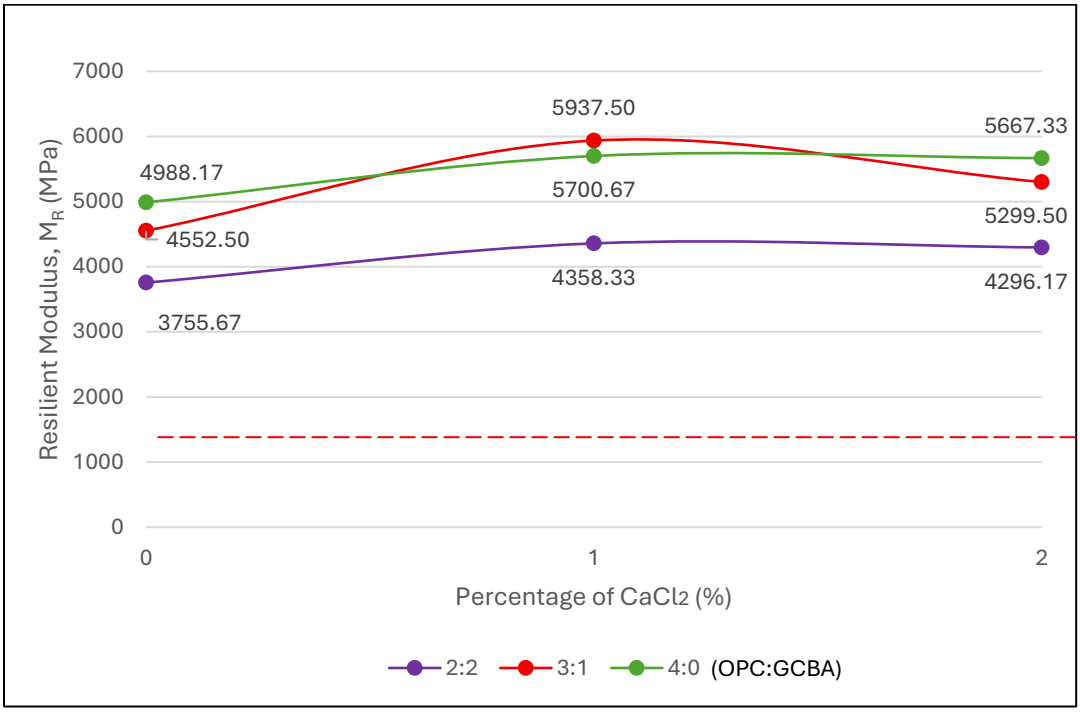


Figure 4.84 M_R for CA75RAP25 on Day 1

On day one of the curing process, as shown in Figure 4.84, the data revealed a significant increase in the M_R with high cement content across most mix designs. Notably, the mix of 3% OPC + 1% GCBA + 1% $CaCl_2$ achieved the highest M_R at 5937.50 MPa followed by 4% OPC + 0% GCBA + 1% $CaCl_2$ mix. In contrast, the mix of 2% OPC + 2% GCBA + 0% $CaCl_2$ recorded the lowest M_R at 3755.67 MPa.

The findings indicated that increasing percentage of GCBA in the mix led to a decrease in the M_R. This reduction may be attributed to the inherent properties of GCBA, which likely do not contribute as effectively to the early- resilient modulus development of the mix compared to OPC.

While the addition of 1% $CaCl_2$ initially increased the M_R, an increase to 2% $CaCl_2$ resulted in a slight decrease in the M_R. Nevertheless, all mix designs exceeded the minimum M_R of 1350 MPa on day 1.

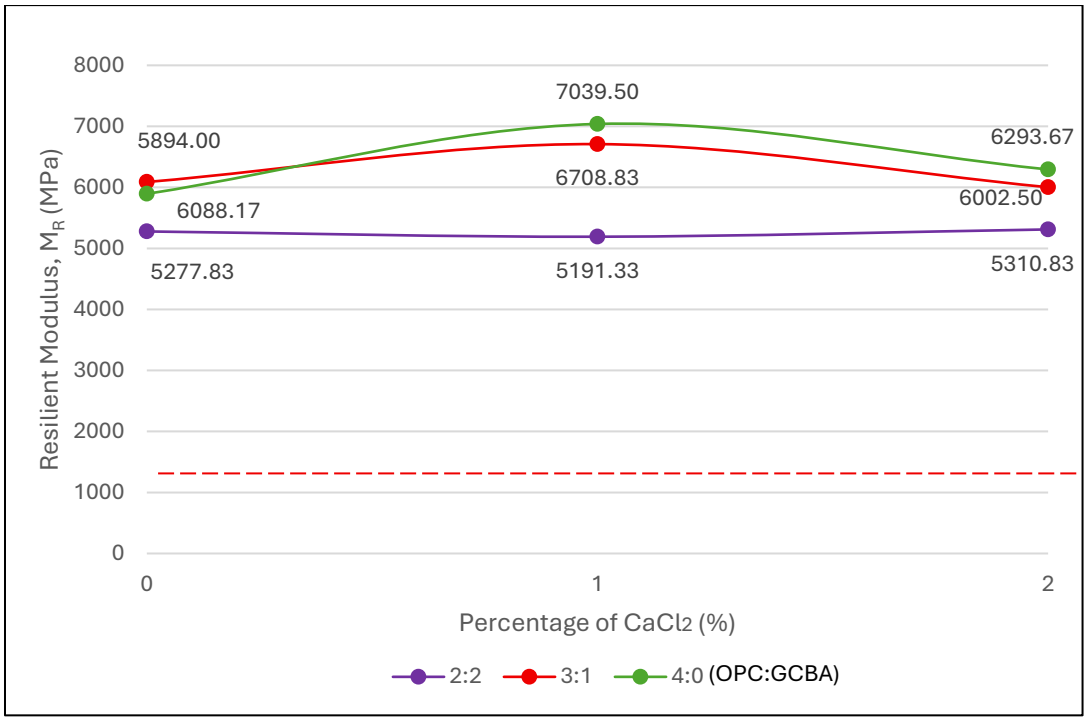


Figure 4.85 M_R for CA75RAP25 on Day 3

As the curing process progressed to day 3, as shown in Figure 4.85, it became clear that the mix of 4% OPC + 0% GCBA + 1% $CaCl_2$ recorded the highest M_R at 7039.5 MPa. Following closely was the mix of 3% OPC + 1% GCBA + 1% $CaCl_2$, which achieved M_R of 6708.83 MPa. The 4% OPC mix likely benefited the full cementitious potential of OPC, enhanced by the accelerating effect of $CaCl_2$, which contributed to early-resilient modulus development.

Similarly, the 3% OPC + 1% GCBA mix, while having a slightly lower M_R than the 4% OPC mix, still maintained a high M_R due to the adequate presence of OPC providing substantial cementitious material, along with the positive influence of $CaCl_2$. The presence of 1% GCBA in this mix did not significantly hinder the hydration process.

In contrast, the lowest M_R were consistently recorded in mixes with the highest GCBA content. The increased percentage of GCBA likely reduced the effectiveness of the cementitious matrix, due to its less reactive nature compared to OPC.

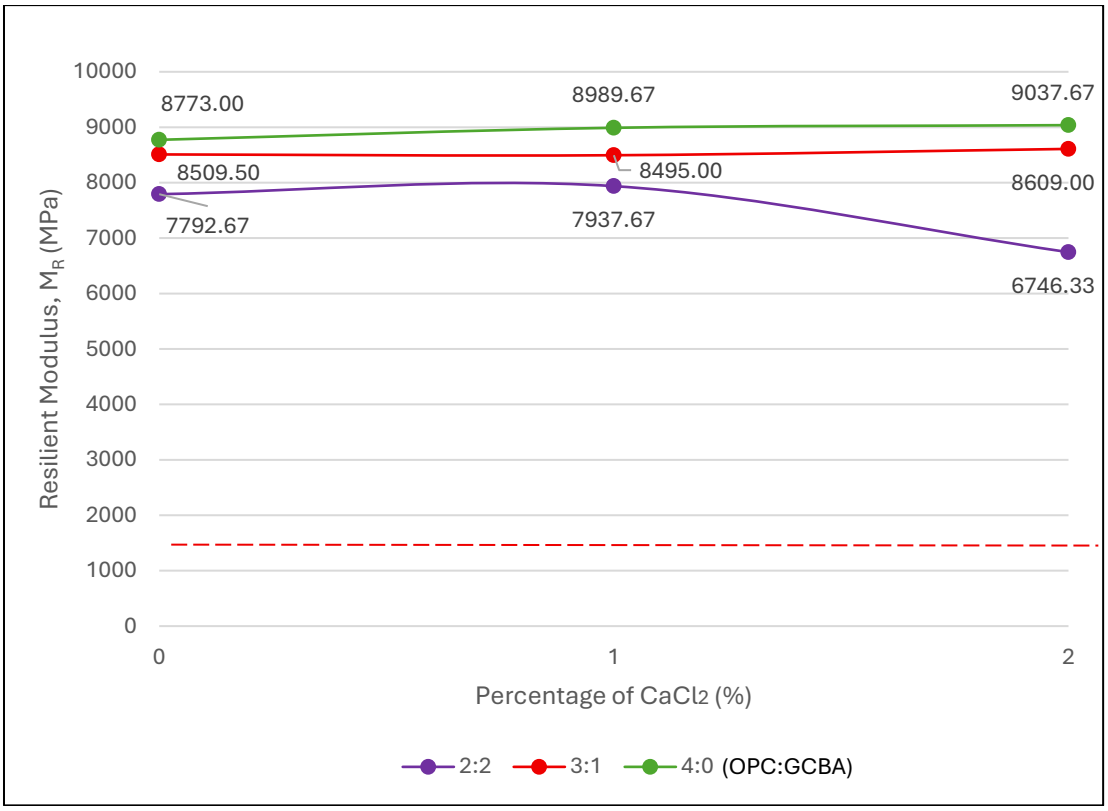


Figure 4.86 M_R for CA75RAP25 on Day 7

On day 7 of the curing process, as illustrated in Figure 4.86, a clear trend emerged as the percentage of OPC increased, the M_R also rose for all mix designs. Notably, all mix designs with 4% OPC recorded the highest M_R across each percentage of $CaCl_2$. The mix of 4% OPC + 0% GCBA + 2% $CaCl_2$ achieved the highest M_R of 9037.67 MPa, followed closely by the same mix with 1% $CaCl_2$ at 8989.67 MPa. Conversely, the mix of 2% OPC + 2% GCBA + 2% $CaCl_2$ recorded the lowest M_R at 6746.33 MPa.

In contrast to the results observed on day 1 and day 3, where higher percentages of $CaCl_2$ led to slight reductions in M_R, day 7 showed that 2% $CaCl_2$ contributed to a more favorable environment for continued resilient modulus development in mixes with high OPC content. This improvement may be attributed to the accelerating effect of $CaCl_2$, which promoted the quicker and more thorough formation of hydration products without causing the adverse effects that were evident during the earlier stages.

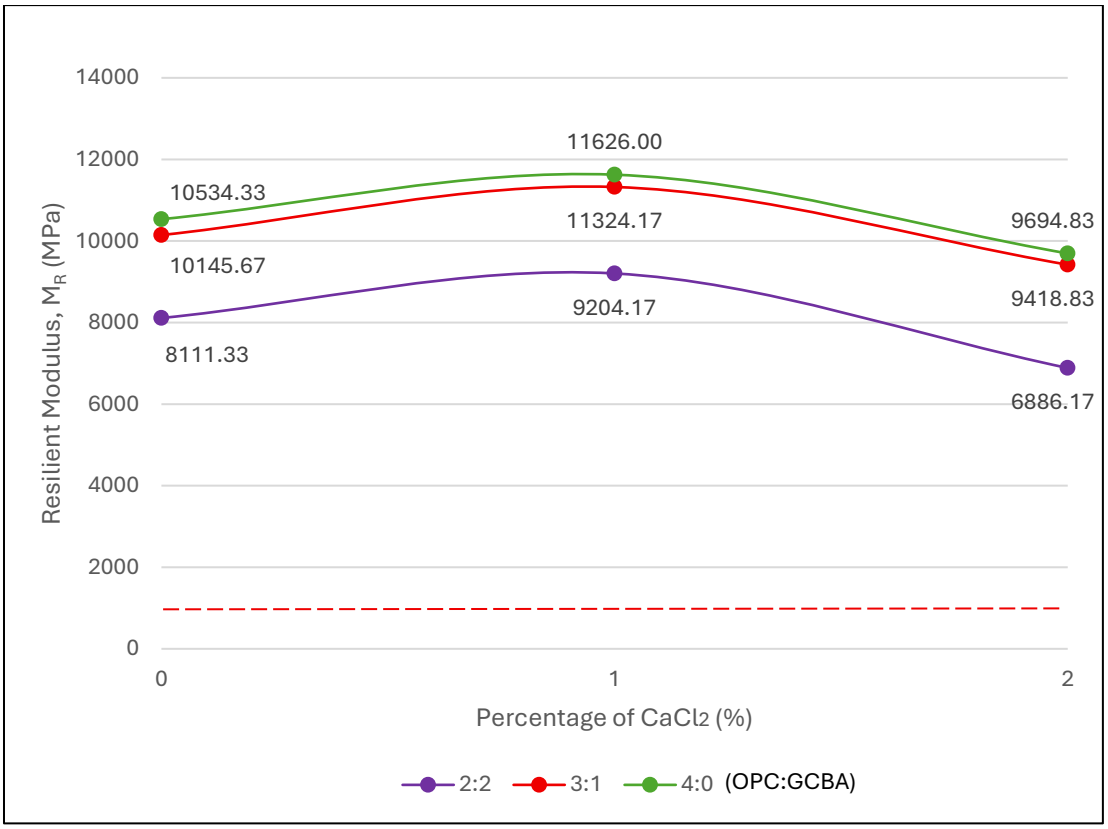


Figure 4.87 M_R for CA75RAP25 on Day 14

As the curing process reached day 14, the M_R continued to rise, following a trend observed on day 7, as shown in Figure 4.87. All mixes containing the maximum amount of OPC at 4% recorded the highest M_R among all tested mixes. Specifically, the mix of 4% OPC + 0% GCBA + 1% $CaCl_2$ recorded the highest M_R at 11,626 MPa. This was closely followed by the mix of 3% OPC + 1% GCBA + 1% $CaCl_2$, which achieved M_R of 11,324.17 MPa.

The consistent increase in M_R over time highlighted the continued development of the stabilized base microstructure and strength as the hydration process progressed (Aboalasaad et al., 2025). The 4% OPC mixes benefited from the high cement content, which formed hydration products, resulting in a strong and cohesive matrix.

Conversely, all mixes of 2% OPC + 2% GCBA recorded the lowest M_R across various percentages of $CaCl_2$.

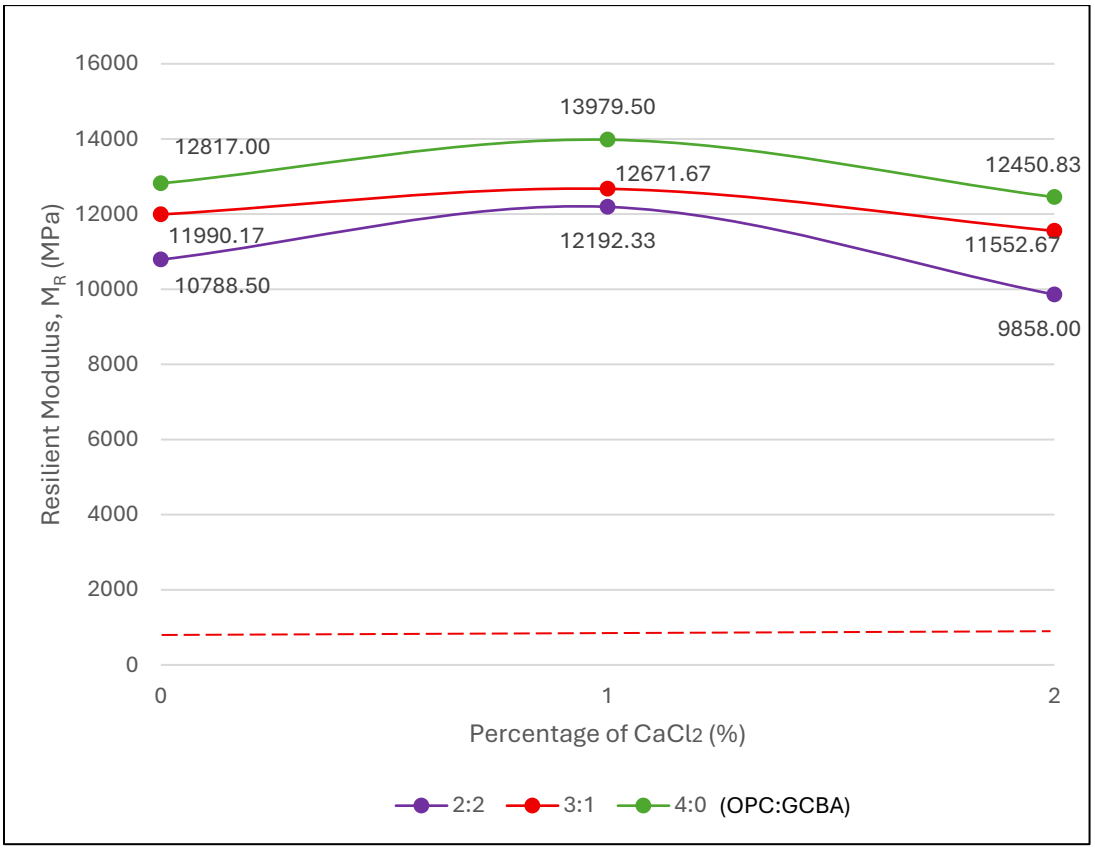


Figure 4.88 M_R for CA75RAP25 on Day 28

Figure 4.88 presents the results from day 28 of the curing process. The mix of 4% OPC + 0% GCBA + 1% $CaCl_2$ achieved the highest M_R of 13,979.50 MPa. Additionally, the inclusion of 1% $CaCl_2$ led to the most significant improvement across all content of stabilizing agent. While 2% $CaCl_2$ was also effective, its performance was slightly lower than that of 1% in terms of modulus enhancement. Overall, the data indicated that the M_R increased with adding $CaCl_2$ up to 1%, after which it began to decline. The 4% OPC + 0% GCBA mix design demonstrated the highest resilient modulus among all $CaCl_2$ percentages, followed by the 3% OPC + 1% GCBA mix ratio, while the 2% OPC + 2% GCBA mix exhibited the lowest M_R. This suggested that a higher proportion of OPC relative to GCBA contributes to higher resilient modulus.

In the analysis of the CA75RAP25 mix design, the resilient modulus of all specimens improved with increased OPC content and longer curing periods. Adding $CaCl_2$, particularly at 1%, significantly enhanced the resilient modulus, with the highest values recorded for the 4% OPC + 0% GCBA mixes at 28 days of curing.

b) CA50RAP50 Mix Design

Figures 4.89 to 4.93 show the resilient modulus result for CA50RAP50 mix design on different percentages of stabilizing agent from day 1 to day 28 of the curing process.

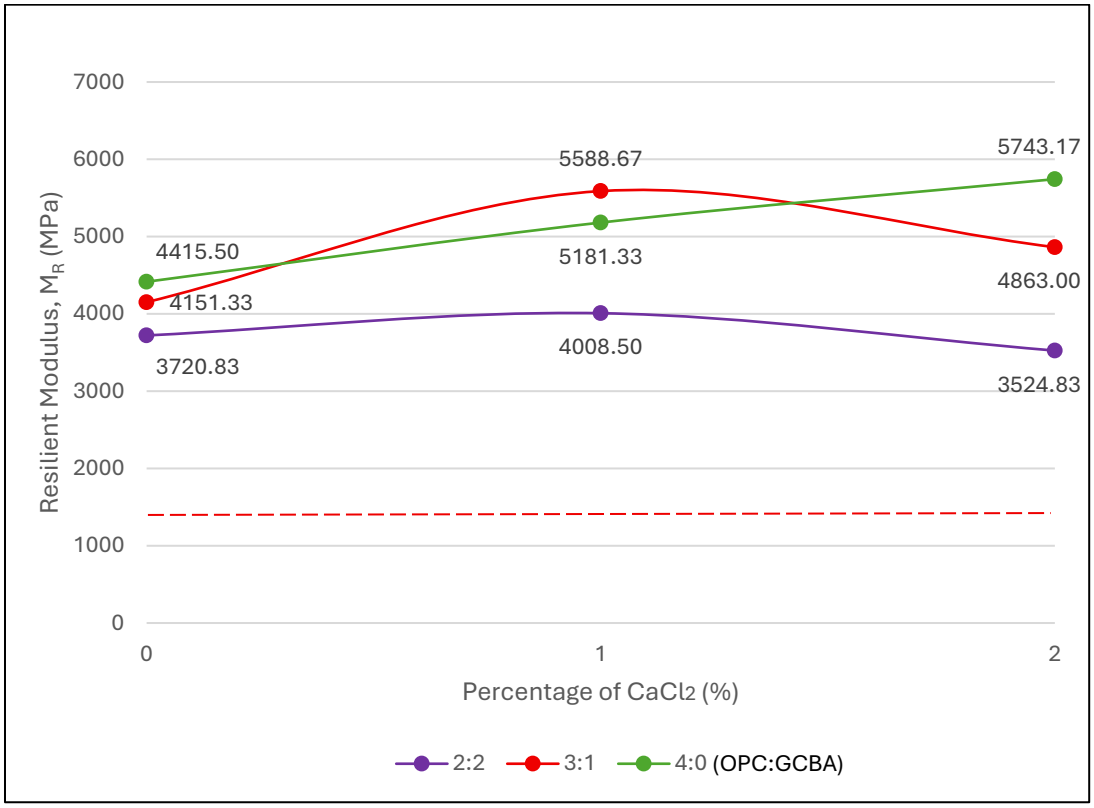


Figure 4.89 M_R for CA50RAP50 on Day 1

As shown in Figure 4.89, on the first day of the curing process, the highest M_R was observed in the mix of 4% OPC + 0% GCBA + 2% $CaCl_2$, reaching 5743.17 MPa. This was followed closely by the mix of 3% OPC + 1% GCBA + 1% $CaCl_2$, which recorded M_R of 5588.67 MPa. The data indicated that the resilient modulus increased with the addition of $CaCl_2$ up to 1% for all mixes, whereas in the mixes containing 3% OPC + 1% GCBA and 2% OPC + 2% GCBA, the M_R began to decrease when $CaCl_2$ was increased to 2%.

Notably, at 2% $CaCl_2$, the 4% OPC + 0% GCBA outperformed the other mixes, continuing its upward trend while the other mixes experienced a decline. Nevertheless, all mixes had exceeded the minimum requirement of 1350 MPa on day 1.

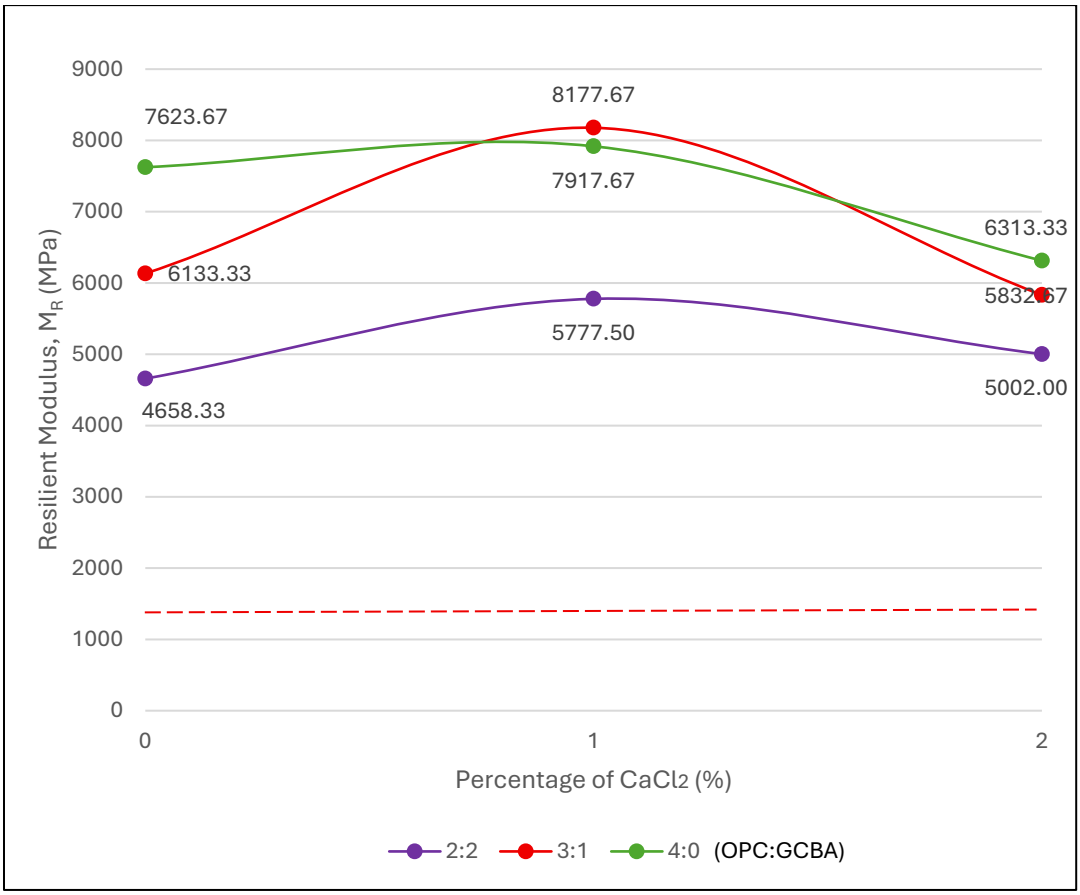


Figure 4.90 M_R for CA50RAP50 on Day 3

On the third day of the curing process, as shown in Figure 4.90, the trend began to change compared to day 1. All mixes reached their peak M_R at 1% $CaCl_2$, after which the resilient modulus declined at 2% $CaCl_2$ across all mix designs.

The highest M_R recorded was for the mix of 3% OPC + 1% GCBA + 1% $CaCl_2$, reaching 8177.67 MPa, followed closely by a mix of 4% OPC + 0% GCBA + 1% $CaCl_2$, which recorded 7917.67 MPa. The data indicated that the resilient modulus on day 3 increased with the addition of $CaCl_2$, but only up to 1%. This suggested that $CaCl_2$ contents above 1% led to a decrease in the resilient modulus across all mixes.

The lowest M_R was recorded for the of 2% OPC + 2% GCBA + 0% $CaCl_2$ mix, with a value of 4658.33 MPa. Notably, all mixes with 2% OPC + 2% GCBA also exhibited the lowest M_R across various percentages of $CaCl_2$.

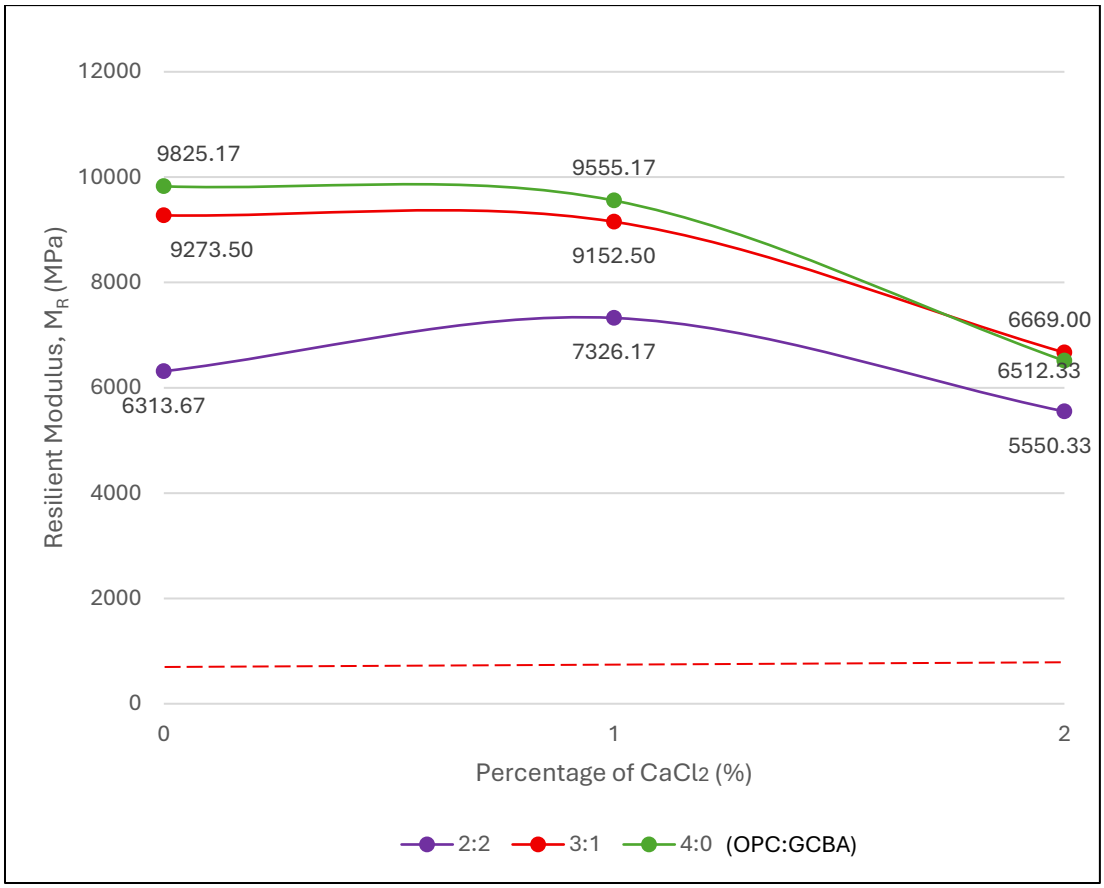


Figure 4.91 M_R for CA50RAP50 on Day 7

The resilient modulus on day 7 of the curing process, as shown in Figure 4.91, displayed a different trend compared to previous results. All mixes exhibited a slight decrease in M_R with the addition of up to 1% $CaCl_2$, except for the of 2% OPC + 2% GCBA mix. The highest resilient modulus was recorded for the mix of 4% OPC + 0% GCBA + 0% $CaCl_2$ at 9825.17 MPa, followed by the mix of 4% OPC + 0% GCBA + 1% $CaCl_2$, which recorded 9555.17 MPa.

The of 2% OPC + 2% GCBA mix exhibited the lowest resilient modulus across all percentages of $CaCl_2$, although it did show some improvement up to 1% $CaCl_2$ before experiencing a decline.

It can be said that the resilient modulus decreased with the addition of $CaCl_2$ up to 1%, with the exception of the of 2% OPC + 2% GCBA mix, which showed a slight improvement before declining. The highest resilient modulus was observed in the mix without $CaCl_2$, indicating that adding $CaCl_2$ beyond 1% negatively affected the stiffness of the mixes on day 7.

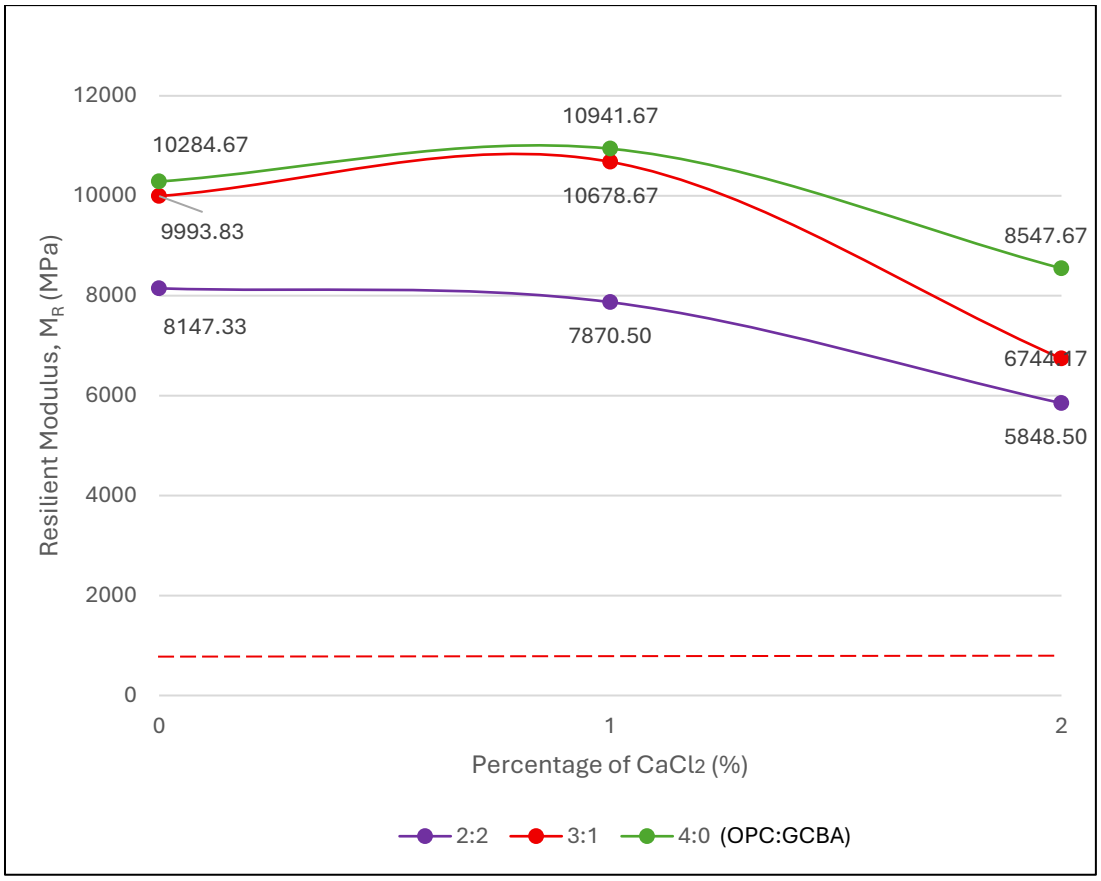


Figure 4.92 M_R for CA50RAP50 on Day 14

On day 14 of the curing process, as depicted in Figure 4.92, the resilient modulus increased by adding $CaCl_2$ up to 1% of all mix designs except for the mix of 2% OPC + 2% GCBA, where every addition of 1% $CaCl_2$ led to a decrease in M_R. The mix of 4% OPC + 0% GCBA + 1% $CaCl_2$ achieved the highest M_R at 10,941.67 MPa, followed by the 3% OPC + 1% GCBA + 1% $CaCl_2$ mix at 10,678.67 MPa.

However, at 2% $CaCl_2$, the resilient modulus decreased for all mixes. This trend indicated that the addition of $CaCl_2$ up to only 1% could effectively enhance the resilient modulus by improving the curing process and strengthening the material structure.

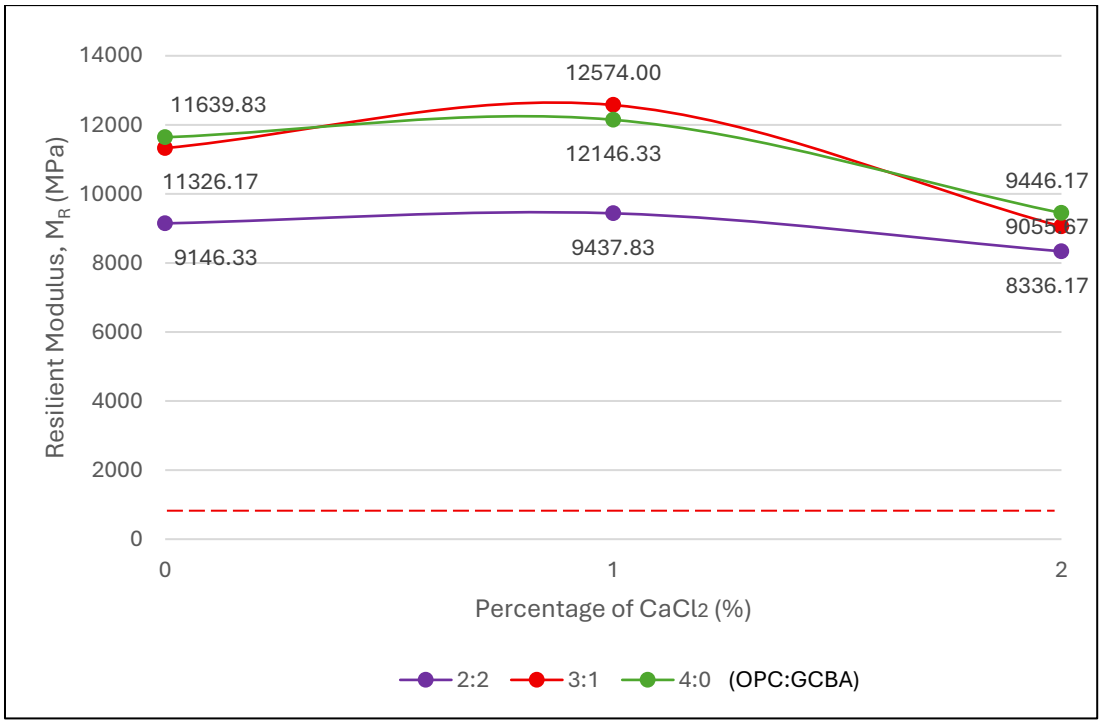


Figure 4.93 M_R for CA50RAP50 on Day 28

A similar trend was observed in Figure 4.93 for the final day of the curing process, where the highest resilient modulus was recorded in the mix containing 1% $CaCl_2$ across all mix designs. The mix of 3% OPC + 1% GCBA + 1% $CaCl_2$ achieved the highest M_R, reaching 12,574 MPa. This was closely followed by 4% OPC + 0% GCBA + 1% $CaCl_2$ mix, which achieved a resilient modulus of 12,146.32 MPa. The highest performance of the 3% OPC + 1% GCBA + 1% $CaCl_2$ mix suggested that this combination provided the best synergy between the components, leading to an optimal curing process and resulting in the highest mechanical strength for the CA50RAP50 mix design.

From the analysis of the CA50RAP50 mix design, it could be evident that in most cases, the resilient modulus peaked at the mixes with 1% $CaCl_2$. This optimal percentage of $CaCl_2$ enhanced the curing process, leading to improved mechanical properties and a higher resilient modulus. However, beyond this 1% content, several adverse effects were observed. Excessive amounts of $CaCl_2$ could cause the hydration process to progress too rapidly, resulting in incomplete or uneven curing. This rapid hydration could create weaknesses in the microstructure of the material, compromising its overall strength and durability (Wang et al, 2022). These findings show that while small amounts of $CaCl_2$ can be beneficial, an excessive amount could have a detrimental effect.

c) CA25RAP75 Mix Design

Figures 4.94 to 4.98 show the resilient modulus result for CA25RAP75 mix design on different percentages of stabilizing agent from day 1 to day 28 of the curing process.

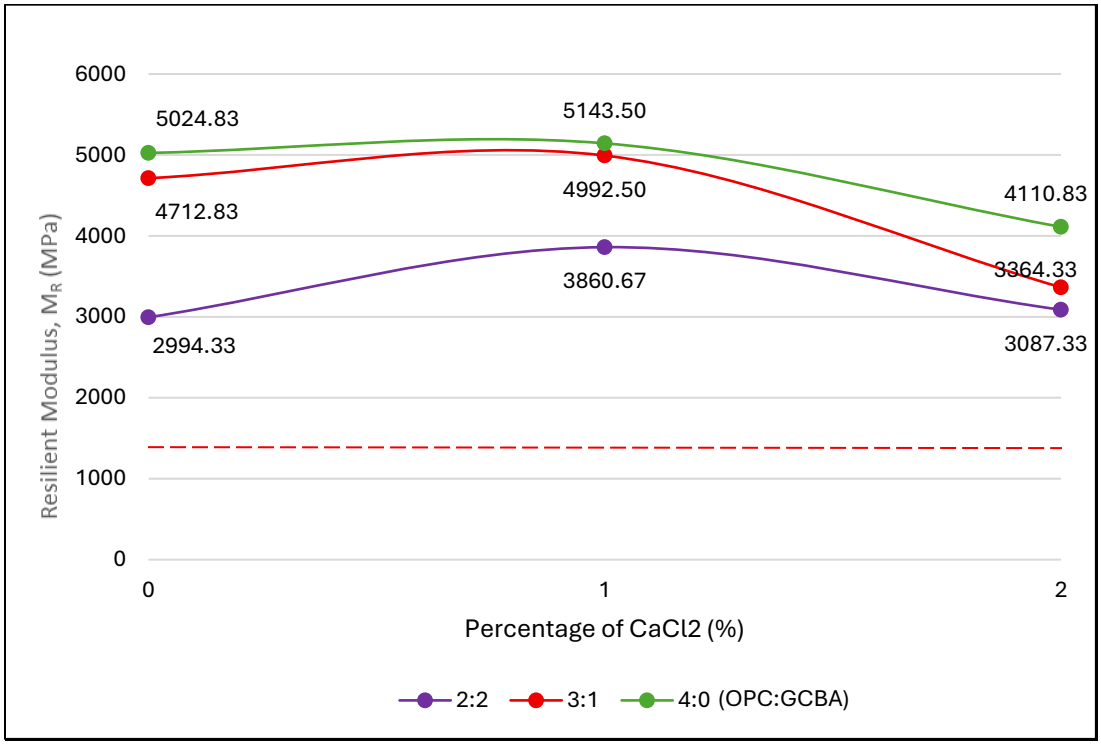


Figure 4.94 M_R for CA25RAP75 on Day 1

The graph for the CA25RAP75 mix design during the first day of the curing process, as shown in Figure 4.94, indicates that the M_R increased with the addition of $CaCl_2$, reaching its peak at 1% content for all mix designs. The mix of 4% OPC + 0% GCBA + 1% $CaCl_2$ achieved the highest M_R of 5143.50 MPa at 1% $CaCl_2$. This was followed closely by the same amount of OPC without GCBA and $CaCl_2$, which recorded M_R of 5024.83 MPa.

The 2% OPC + 2% GCBA + 0% $CaCl_2$ mix displayed the lowest M_R across all $CaCl_2$ percentages, reaching only 2994.33 MPa. It was noted that higher percentages of $CaCl_2$, beyond 1%, resulted in a decline in M_R for all mix designs. Nevertheless, all mixes exceeded the minimum requirement of 1350 MPa on day 1.

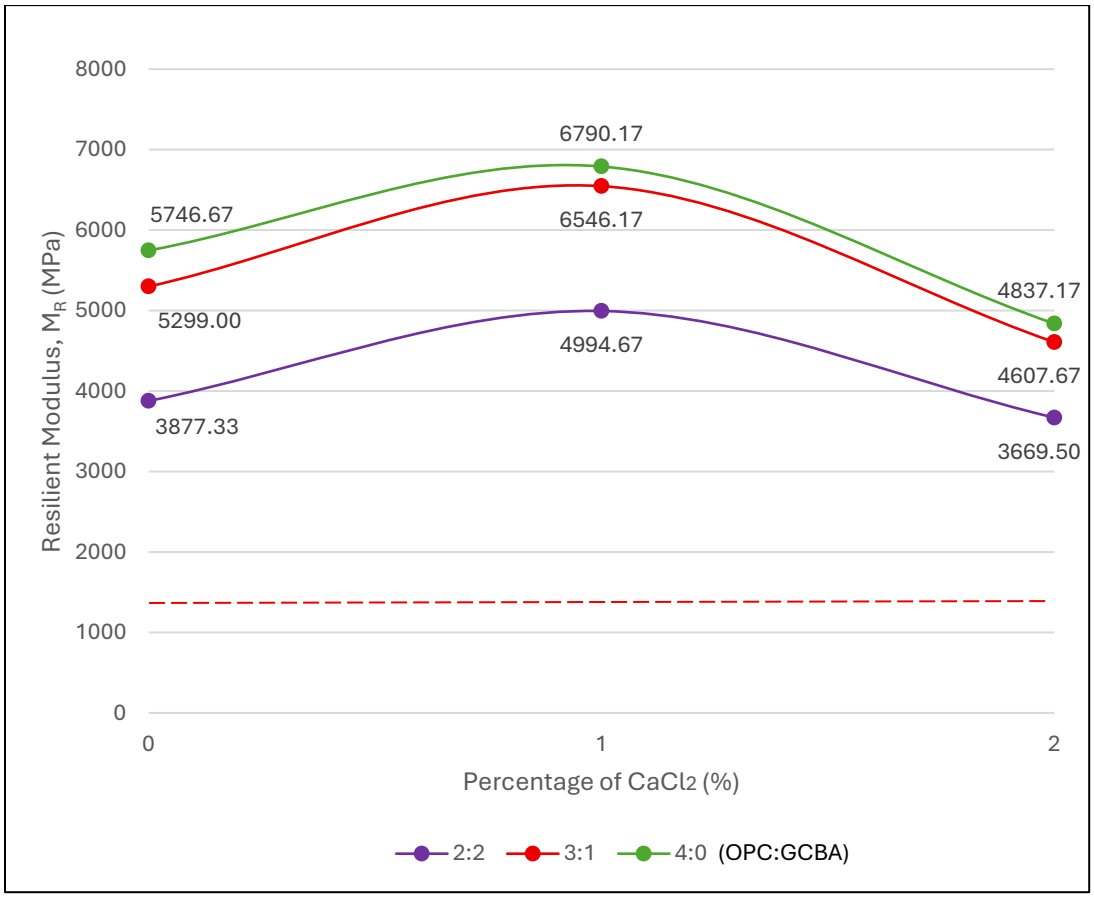


Figure 4.95 M_R for CA25RAP75 on Day 3

As the curing process progressed to day 3, as illustrated in Figure 4.95, it became evident that the same trend observed on day 1 continued. Specifically, the resilient modulus increased with the addition of 1% $CaCl_2$ across all mixes. Among the different mix designs, the mix of 4% OPC + 0% GCBA + 1% $CaCl_2$ demonstrated the highest M_R, recording 6790.17 MPa. Following this top-performing mix, the 3% OPC + 1% GCBA + 1% $CaCl_2$ mix also showed relatively high M_R at 6546.17 MPa. These results indicated that while all mixes benefited from the addition of $CaCl_2$, the optimal content was around 1%, as increasing $CaCl_2$ to 2% did not provide further improvement.

On the other hand, all the mix designs of 2% OPC + 2% GCBA across all $CaCl_2$ percentages exhibited the lowest performance, with their highest M_R peaking at only 4994.67 MPa.

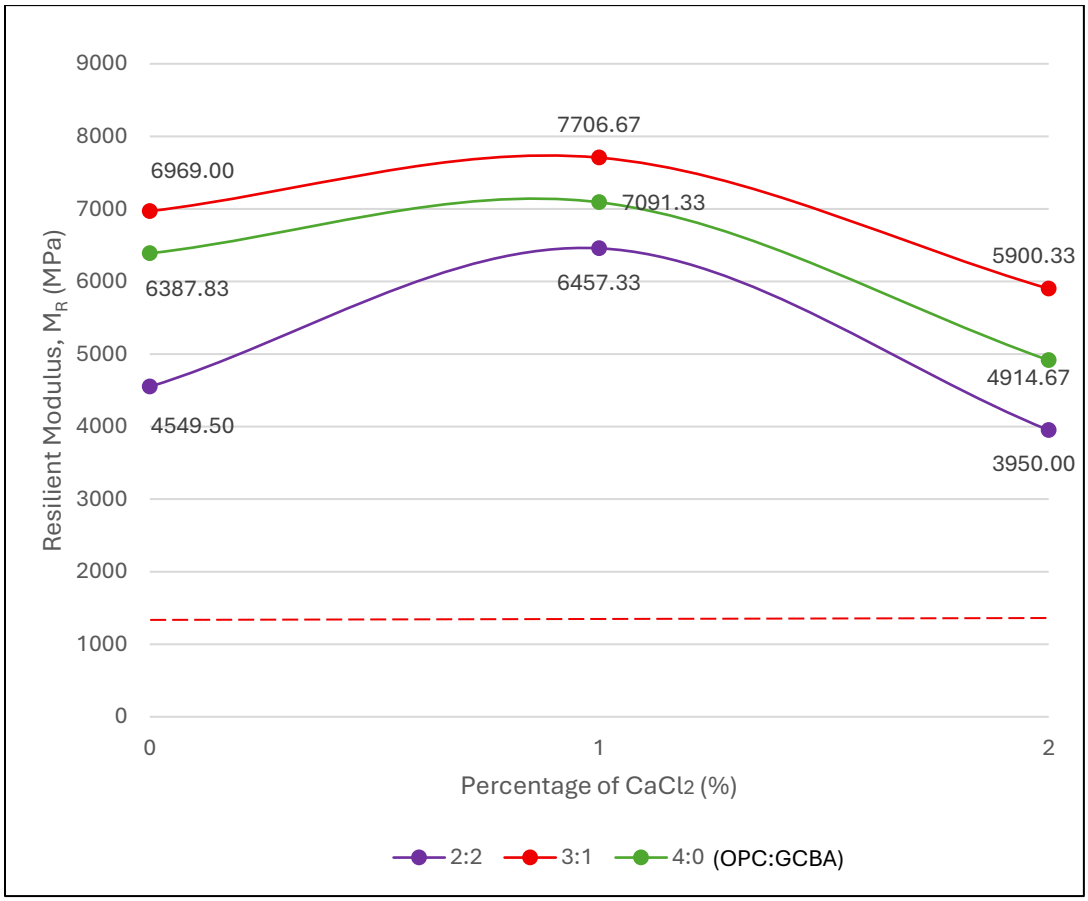


Figure 4.96 M_R for CA25RAP75 on Day 7

Moving to the seventh day of the curing process, as depicted in Figure 4.96, a similar trend was still observed from the previous curing periods. The mix of 3% OPC + 1% GCBA + 1% $CaCl_2$ achieved the highest M_R, recording 7706.67 MPa at 1% $CaCl_2$. This result indicated that this particular mix ratio, with a significant proportion of OPC and GCBA combined with 1% $CaCl_2$, optimally enhanced the mechanical properties of the mix. Following, the 4% OPC + 0% GCBA + 1% $CaCl_2$ mix also demonstrated a high M_R, reaching 7091.33 MPa. The good performance of these two mixes highlighted the importance of having a higher OPC content coupled with a precise amount of $CaCl_2$ to achieve maximum resilience performance.

The lowest M_R remained in the mix of 2% OPC + 2% GCBA across all $CaCl_2$ percentages, having only peaked at 6457.77 MPa.

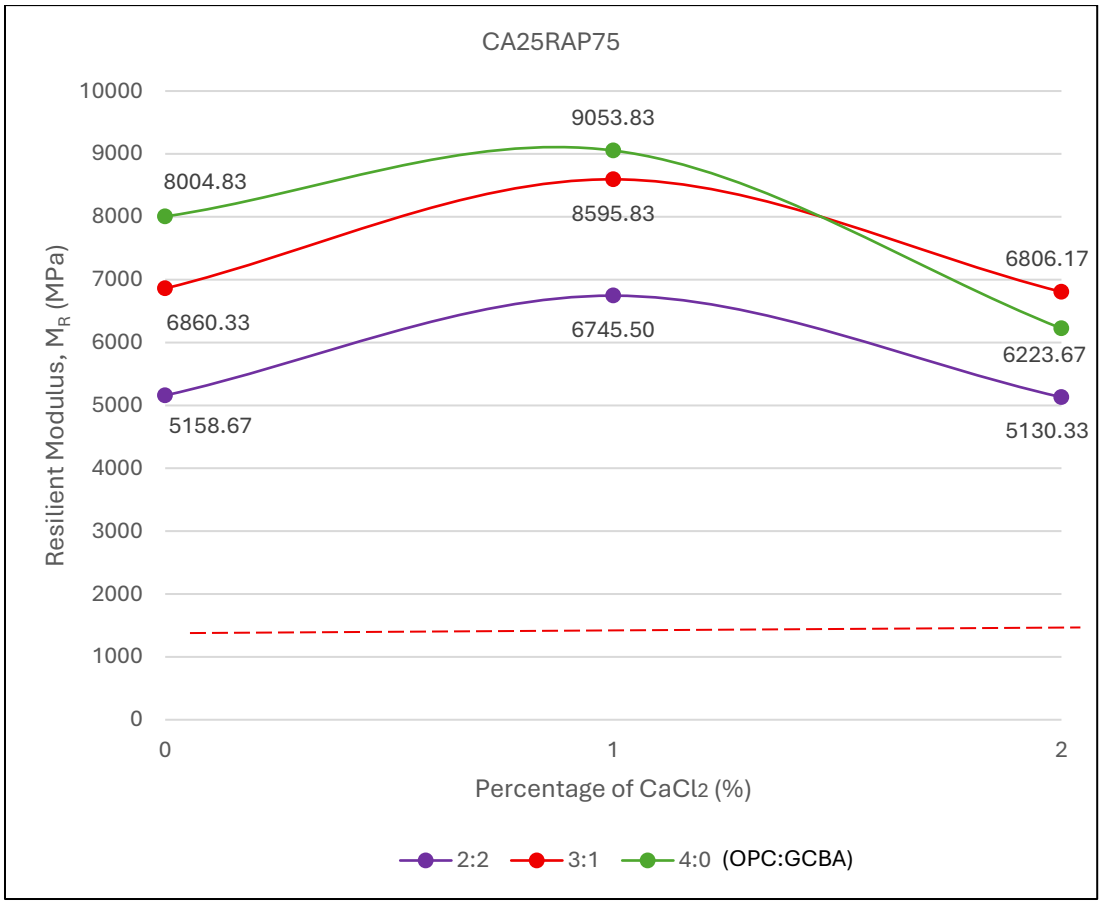


Figure 4.97 M_R for CA25RAP75 on Day 14

On day 14 of the curing process, as illustrated in Figure 4.97, the highest M_R was achieved by the 4% OPC + 0% GCBA + 1% $CaCl_2$ mix, which recorded 9053.83 MPa. This was closely followed by the 3% OPC + 1% GCBA + 1% $CaCl_2$ mix, reaching 8595.83 MPa. These results showed that mixes with higher OPC content responded well to the addition of 1% $CaCl_2$, likely due to enhanced cementitious bonding and improved stiffness.

In contrast, the lowest M_R was observed in the 2% OPC + 2% GCBA mix, which peaked at only 6745.50 MPa. Despite showing a slight improvement with 1% $CaCl_2$, the overall performance of this mix remained significantly lower than the others, suggesting that a high GCBA content limited the stiffness gain.

Overall, all mix designs showed a consistent trend where the resilient modulus increased with the addition of $CaCl_2$ up to 1%, followed by a decline at 2%. This confirmed that the optimum content of $CaCl_2$ for improving stiffness by day 14 was around 1%, beyond which the performance began to deteriorate.

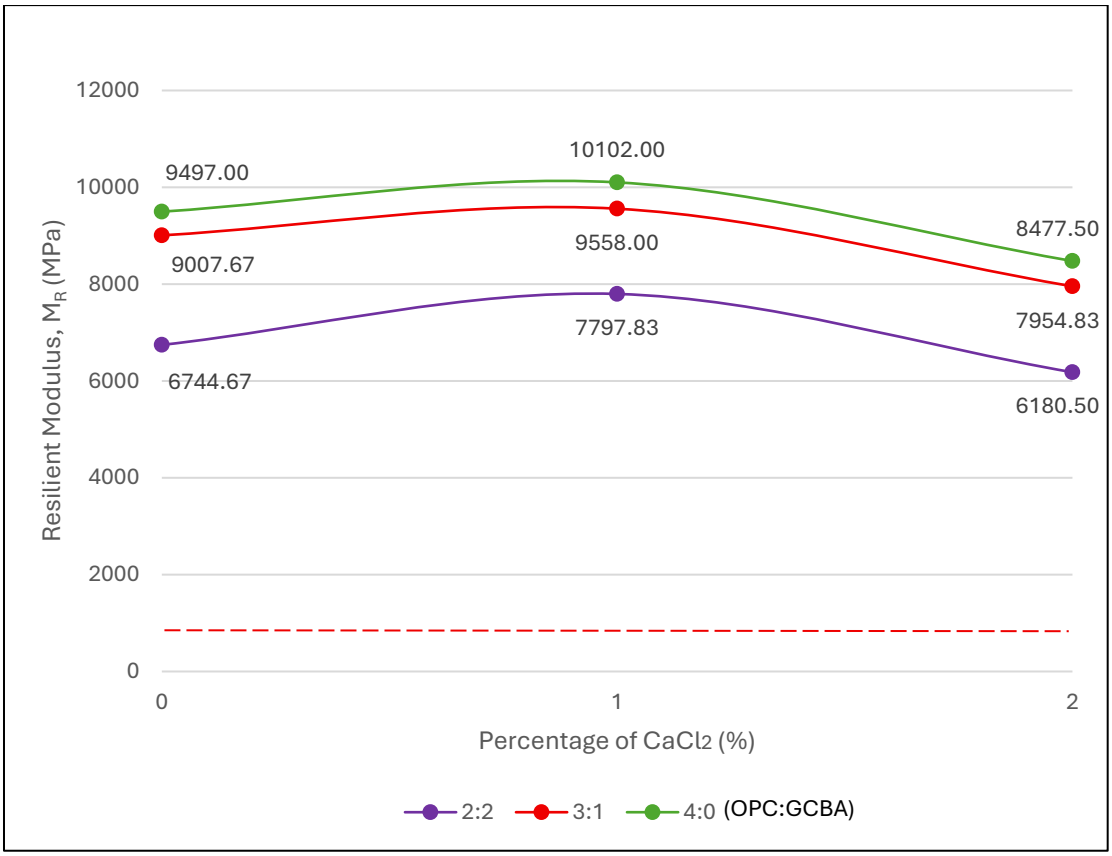


Figure 4.98 M_R for CA25RAP75 on Day 28

The consistent trend observed throughout the curing process persisted until the final day, as shown in Figure 4.98. On this last day, the 4% OPC + 0% GCBA + 1% $CaCl_2$ mix achieved the highest M_R, recording 10,102.00 MPa. This result evident the effectiveness of this particular mix, where a high proportion of OPC combined with $CaCl_2$ significantly enhanced the mechanical properties of the mix. The 3% OPC + 1% GCBA + 1% $CaCl_2$ mix closely followed, demonstrating a high M_R, reaching 9558.00 MPa.

In contrast, the 2% OPC + 2% GCBA mix consistently showed the lowest performance, with its M_R peaking at only 7797.83 MPa. This consistent underperformance across the curing periods suggested that an equal ratio of OPC and GCBA was not conducive to achieving high resilient modulus, even with the addition of $CaCl_2$. This reinforced the understanding that a balanced mix with a higher proportion of OPC is essential for optimizing the mechanical properties of the mix.

The analysis of CA25RAP75 mix design indicated that mixes containing up to 4% OPC achieved the highest M_R. This outcome was likely due to weak bonding between CA and RAP, which meant that the mix relied heavily on cement hydration for resilient modulus development. Incorporating 4% OPC effectively compensated for the insufficient CA-RAP bonding, resulting in improved M_R.

Additionally, the mix with 3% OPC + 1%GCBA also exhibited a high M_R. This suggested that a small amount of GCBA can still produce strong concrete when combined with adequate OPC and an optimal amount of $CaCl_2$. The performance of this combination indicated that modest amounts of GCBA do not substantially reduce strength, implying that GCBA can partially replace OPC without significantly compromising structural integrity (Poudel et al., 2024). The effectiveness of GCBA in this mix was further enhanced by the inclusion of $CaCl_2$, which acted as an accelerating agent, improving overall performance.

4.4.3.2 Influence of Stabilizing Agent on Resilient Modulus

Several key observations in Figures 4.84 to 4.98 were made in the analysis of the resilient modulus across mix designs incorporating varying percentages of stabilizing agents. Mixes containing 1% $CaCl_2$ consistently produced the highest M_R across all OPC-GCBA combinations, highlighting the positive effect of $CaCl_2$ as an accelerator in enhancing early mechanical strength through improved hydration kinetics. However, when $CaCl_2$ content exceeded optimal levels, M_R declined, consistent with the findings of William et al. (2020) and Salain (2019), who reported strength loss at $CaCl_2$ concentrations exceeding 4% and 1.5%, respectively, likely due to microstructural disruption or excessive internal moisture retention.

The CA50RAP50 mix design containing 3% OPC + 1% GCBA + 1% $CaCl_2$ recorded the highest early-age resilient modulus followed by 4% OPC + 1% $CaCl_2$ mix, indicating that the inclusion of GCBA at low percentages can slightly enhance early resilient modulus when combined with OPC and $CaCl_2$.

As for later-age resilient modulus, the CA75RAP25 mixes containing 4% OPC + 1% $CaCl_2$ recorded the highest M_R, highlighting the dominant role of OPC in contributing to binder strength and matrix cohesion. The 3% OPC + 1% GCBA mix with lower percentage of $CaCl_2$ also recorded high M_R, indicating that a small amount of GCBA can be tolerated without significantly compromising mechanical integrity. In

fact, limited GCBA substitution may contribute to later-age resilient modulus gain through pozzolanic reactions, complementing OPC hydration (Poudel, 2024).

In contrast, the 2% OPC + 2% GCBA mix consistently showed the lowest M_R, regardless of $CaCl_2$ content. This outcome highlighted the critical role of OPC content in achieving sufficient stiffness and load-bearing capacity. Equal replacement of OPC with GCBA likely diluted the cementitious potential of the mix, leading to reduced hydration, weaker particle bonding, and a less cohesive structure. These observations support the dilution and low early reactivity effects discussed by Kim et al. (2011) and Mangi et al. (2019), who reported strength losses at higher GCBA replacement levels.

In summary, achieving an optimal resilient modulus requires a higher proportion of OPC relative to GCBA and the inclusion of 1% $CaCl_2$. A limited amount of GCBA may be beneficial for later-age resilient modulus development, but excessive replacement reduces stiffness and cohesion. Overall, the combination of 1% $CaCl_2$ with high OPC content (3-4%) and 0-1% GCBA produced the most effective and reliable formulation for durable resilient modulus.

4.4.3.3 Effect of Varying CA-RAP Ratio on Resilient Modulus

The ratio of CA to RAP is crucial in determining the resilient modulus of the mix. This ratio directly affects several key factors, including load-bearing capacity, as CA generally provides greater stiffness and strength compared to RAP. Additionally, CA typically offers better particle interlocking than the aged binder presents in RAP.

By incorporating stabilizing agent, the mix can overcome the weaker bonding properties of the aged RAP, resulting in a more cohesive and durable combination.

The analysis presented in Figures 4.99 to 4.101 provides a detailed overview of the results from various CA-RAP combinations over the full 28-day curing period. These figures clearly demonstrated the differing effects of the various CA-RAP ratios on resilient modulus performance when the stabilizing agent is included.

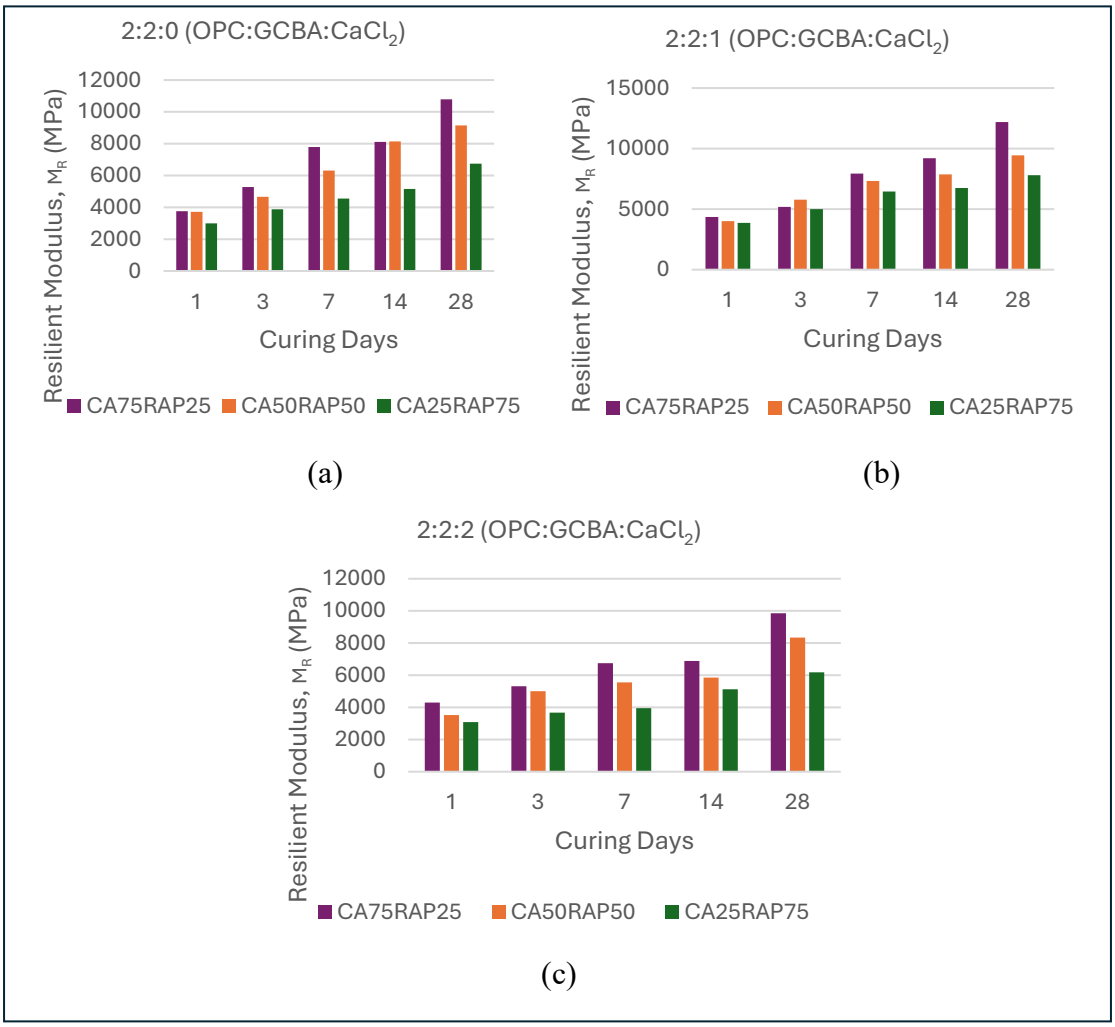


Figure 4.99 Impact of CA-RAP Ratio on Mix design of 2% OPC + 2% GCBA with (a) 0% $CaCl_2$ (b) 1% $CaCl_2$ and (c) 2% $CaCl_2$

The analysis in Figure 4.99 shows that as the curing days increased, the resilient modulus increased for all mixes, with a significant improvement observed from day 1 to day 28. The presence of $CaCl_2$ seemed to enhance the resilient modulus, with the optimum content appearing to be 1%. A mix design with a CA75RAP25 ratio consistently achieved the highest M_R across all $CaCl_2$ contents, followed by CA50RAP50 and CA25RAP75 mixes. This indicated a clear trend where the mix with the highest ratio of CA consistently outperformed the others in terms of mechanical strength for a 2% OPC + 2% GCBA mix with various percentages of $CaCl_2$. This was likely because a higher ratio of CA contributed to better compaction and load-bearing capacity (Yu et al., 2025), enhancing the overall resilient modulus of the mix. Conversely, a higher RAP content, as seen in all CA25RAP75 mixes, resulted in lower resilient modulus performance, indicating that RAP might not contribute as effectively to the structural integrity of the mix as CA did.

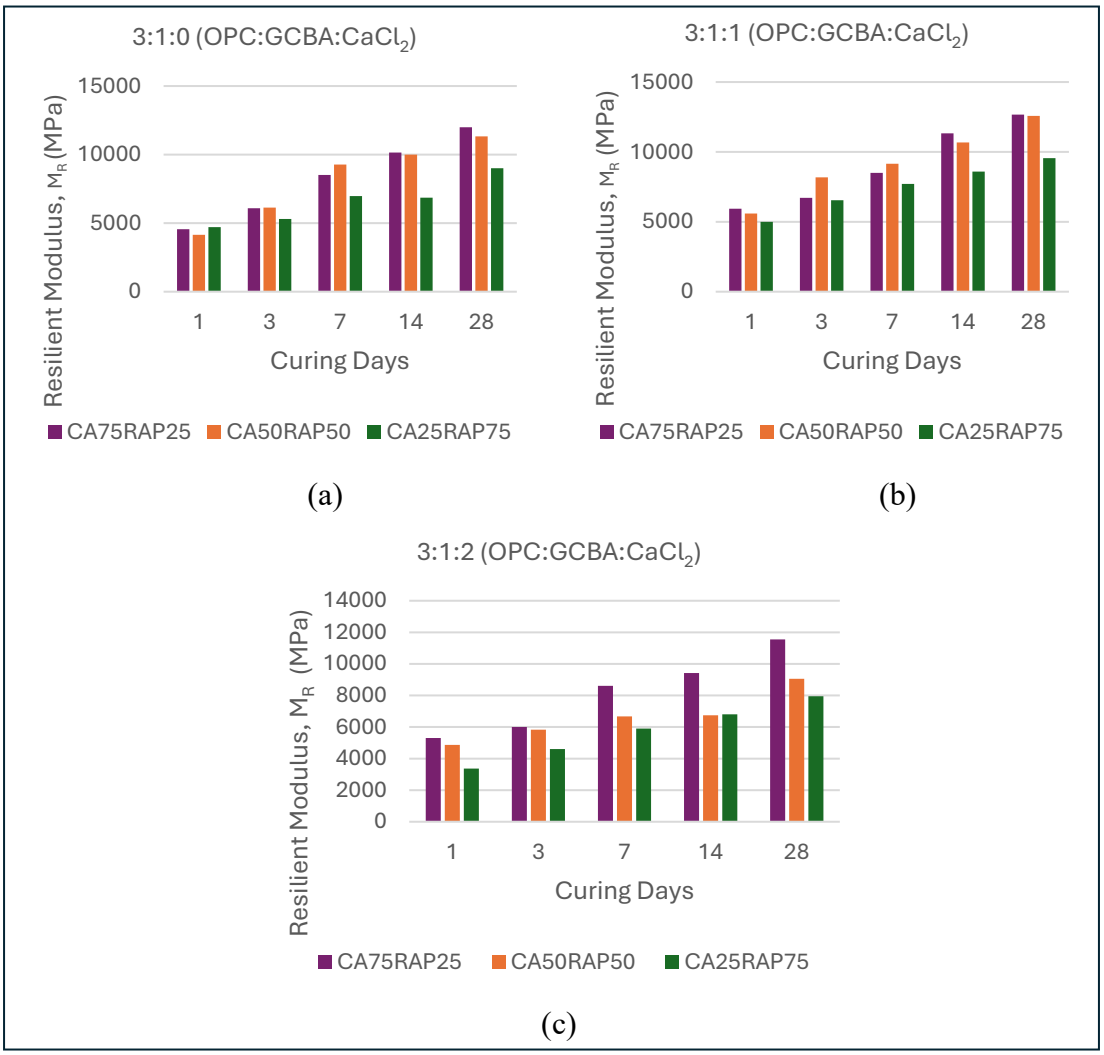


Figure 4.100 Impact of CA-RAP Ratio on Mix design of 3% OPC + 1% GCBA with (a) 0% $CaCl_2$ (b) 1% $CaCl_2$ and (c) 2% $CaCl_2$

A similar trend was observed in the 3% OPC + 1% GCBA mix with varying percentages of $CaCl_2$. The resilient modulus consistently increased as the curing days progressed throughout the entire 28-day curing period, as shown in Figure 4.100. The analysis indicated that the CA75RAP25 mixes achieved the highest resilient modulus.

In contrast to the 2:2 mix ratio, data showed that at certain points, the CA50RAP50 mixes also reached a peak resilient modulus during specific periods. This suggested that a balanced ratio of CA and RAP can provide good bonding and enhance the mechanical properties of the mix. However, by the final day of the curing process, all variations of the CA75RAP25 mixes across different $CaCl_2$ contents recorded the highest resilient modulus.

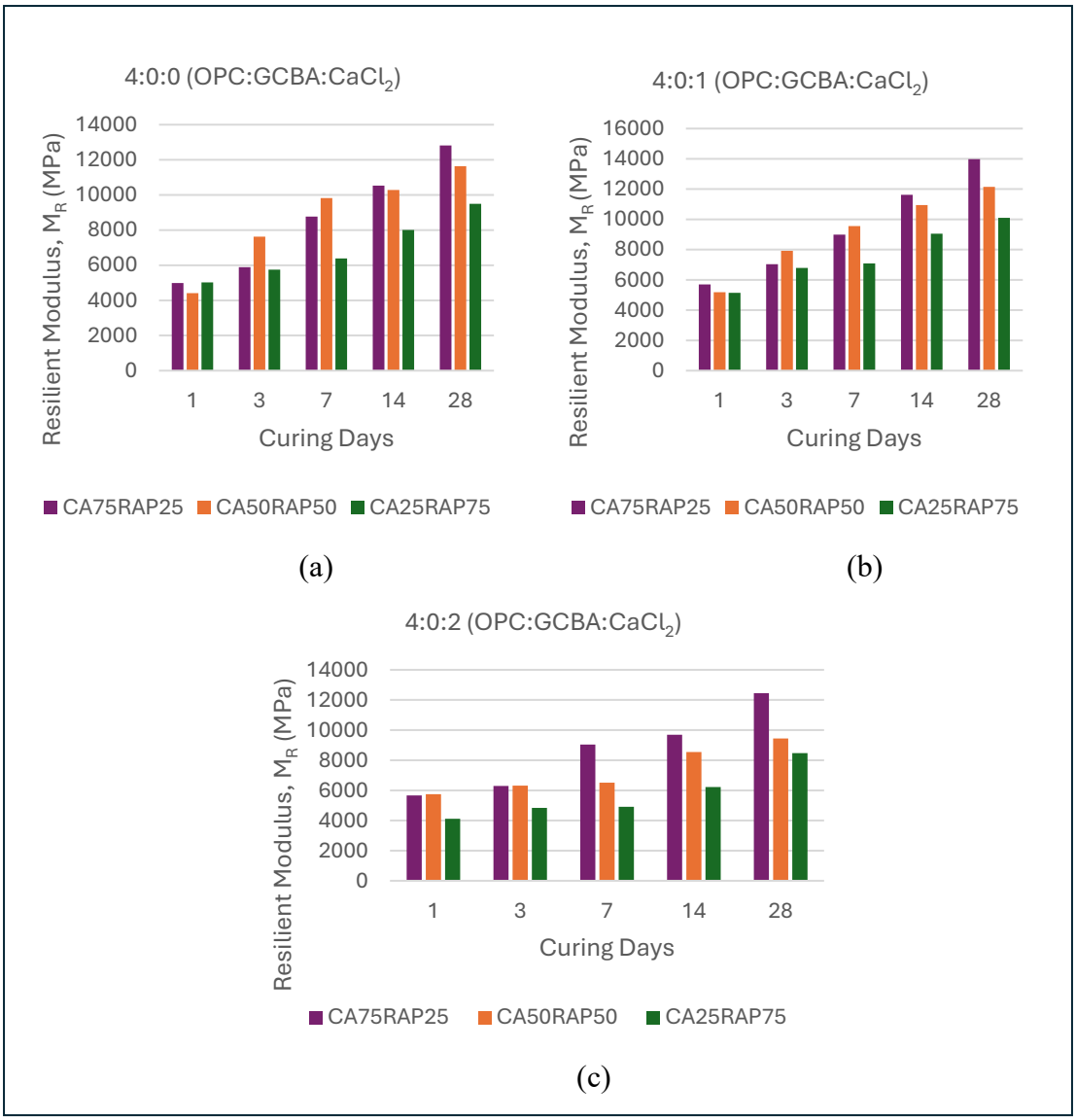


Figure 4.101 Impact of CA-RAP Ratio on Mix design of 4% OPC with (a) 0% $CaCl_2$ (b) 1% $CaCl_2$ and (c) 2% $CaCl_2$

The data presented in Figure 4.101 indicates a steady increase in the resilient modulus over time. Among the tested mixes, CA75RAP25 mixes consistently exhibited the highest M_R, followed by CA50RAP50 and CA25RAP75 mixes.

It can be seen that CA25RAP75 mixes had the lowest resilient modulus of the three mixes, suggesting that a higher content of RAP may lead to reduced stiffness and strength. Although the addition of stabilizing agent enhanced the resilient modulus, it did not exceed the M_R observed in the other two CA-RAP mixes.

4.4.3.4 Influence of Varying CA-RAP Ratio on Resilient Modulus

Figures 4.99 to 4.101 indicate that, although the CA50RAP50 mix exhibited the highest UCS and ITS, the CA75RAP25 mixes achieved the highest resilient modulus. The resilient modulus test evaluates the elastic response of a material under repeated loading, making it particularly sensitive to the stiffness and elasticity of the aggregate skeleton. In this research, the higher aggregate content in CA75RAP25 (75% CA) mixes provided increased stiffness and resistance to deformation, which contributed to its superior M_R performance. These findings are consistent with previous research by Tambunan et al. (2025), who reported that higher aggregate content correlates with improved resilient modulus.

Conversely, mixes with higher RAP content exhibited lower M_R, indicating that excessive RAP replacement may compromise the structural stiffness of the mix. Although RAP offers economic and environmental advantages, its use beyond certain thresholds can negatively affect mechanical properties due to its aged binder, softer texture, and lower rigidity compared to virgin aggregates.

Overall, the results demonstrate that optimizing CA content is essential for achieving high resilient modulus. While the inclusion of stabilizing agent (OPC, GCBA, $CaCl_2$) enhanced compressive and tensile strength, their influence on resilient modulus was comparatively minor. The response measured in the M_R test was primarily governed by the aggregate structure, particularly the stiffness and interlock provided by the CA. Therefore, a careful balance between CA and RAP content is critical to maintaining both strength and stiffness in stabilized base course materials.

4.4.4 Influence of Material Properties on Strength Performance

The mechanical performance of pavement base materials measured through UCS, ITS, and M_R is fundamentally driven by the material properties of its constituents.

4.4.4.1 Specific Gravity

The higher specific gravity of OPC (2.93) and GCBA (2.56) contributed to the density and cohesion of the mixes. Denser binder particles promoted better packing within the matrix, which supported the higher UCS, ITS, and M_R observed in mixes with higher OPC content and small GCBA replacement. Conversely, the lower specific

gravity of RAP (2.00) and site-collected samples (1.95-1.98) reflected aged, porous, and oxidized material, which reduced overall mix density and bonding potential (Dager et al., 2023), correlating with the lower strength performance, particularly in RAP-rich mixes like CA25RAP75.

4.4.4.2 Particle Shape

The physical geometry and durability of aggregates directly impact on the internal friction and skeletal stability of the mix. Aggregates with high flakiness and elongation indices, normally found in mixes with higher RAP content, negatively impact the structural skeleton of the pavement base. Increased proportions of RAP resulted in a higher proportion of elongated particles due to the mechanical milling process used during its recovery (FHWA, 1997). These irregularly shaped particles reduce the efficiency of particle-to-particle interlocking and overall packing density. Consequently, this lack of a dense, cohesive matrix leads to a decrease in the M_R, which measures stiffness, and the UCS.

4.4.4.3 Aggregate Durability

Mixes with higher CA content (CA75RAP25) exhibited lower particle loss and better abrasion resistance, which directly enhanced stiffness and load-bearing capacity, explaining why these mixes performed well in M_R. RAP-rich mixes (CA25RAP75) showed higher LA abrasion loss, consistent with their slightly lower UCS and ITS, due to reduced resistance to particle degradation under stress.

On the other hand, lower AIV percentages in CA-rich mixes (CA75RAP25) indicated higher aggregate impact resistance (Singh et al., 2024), which helped maintain particle integrity under load, supporting higher UCS, ITS, and M_R. In contrast, the higher AIV percentages observed in CA25RAP75 reflected reduced aggregate toughness, which contributed to lower early-age strength and reduced long-term mechanical performance. This trend corresponded with the observed decrease in UCS, ITS, and M_R for mixes containing higher RAP proportions.

4.4.4.4 pH Index

The highly alkaline environment (pH ~14 for mixes with OPC and low $CaCl_2$) favored rapid cement hydration, contributing to early-age strength development, particularly in UCS and ITS. Higher $CaCl_2$ content reduced pH (down to 11.05), which may have moderated OPC hydration and limited early strength gains (Liu and Wu, 2025). In addition, higher percentages of $CaCl_2$ increased the moisture content in the mix due to its hygroscopic nature. This explains why mixes with excessive $CaCl_2$ showed slightly lower UCS, ITS, and M_R.

4.4.4.5 Mineralogy

The presence of reactive phases such as cristobalite and portlandite ($Ca(OH)_2$) supported pozzolanic reactions and the formation of C-S-H gel, enhancing long-term strength. Quartz and calcite acted as inert fillers, improving packing density and matrix stability without directly affecting hydration (Lin et al., 2018; Jiang et al., 2018; Izadifar et al., 2022). The combination of OPC and small GCBA substitution allowed sufficient hydration and pozzolanic activity, contributing to later-age strength in UCS and M_R, while excessive GCBA replacement diluted cementitious material, limiting early-age strength.

4.4.5 Summary of Strength Test Results

This section presents a summary of the strength performance results including UCS, ITS and M_R for all CA-RAP mixes with stabilizing agent.

4.4.5.1 Unconfined Compressive Strength Results

Tables 4.17 to 4.19 present the summary of UCS results for three CA-RAP mixes incorporating stabilizing agent.

Table 4.17
Summary of UCS Results - CA75RAP25 Mix

Stabilizing Agent			UCS (MPa)				
OPC	GCBA	$CaCl_2$	Day 1	Day 3	Day 7	Day 14	Day 28
1	3	0	2.00	2.34	2.51	2.57	2.85
2	2	0	2.24	2.51	2.54	2.81	3.93
3	1	0	3.40	3.43	3.55	3.95	4.75
4	0	0	3.46	3.58	3.76	4.04	4.78
1	3	1	2.06	2.17	2.66	2.78	3.05
2	2	1	2.45	2.62	4.13	4.19	4.37
3	1	1	3.31	3.71	4.15	4.73	5.18
4	0	1	3.25	3.75	4.17	4.60	4.99
1	3	2	2.18	2.43	2.49	2.56	2.96
2	2	2	2.49	2.95	3.07	3.14	3.99
3	1	2	3.04	3.97	4.04	4.08	5.01
4	0	2	3.09	4.08	4.38	4.51	4.83
1	3	3	1.59	1.92	2.22	2.41	2.61
2	2	3	1.98	2.15	2.39	2.54	2.77
3	1	3	2.58	2.81	3.06	3.10	3.37
4	0	3	2.45	2.68	3.40	3.52	3.69

Table 4.18
Summary of UCS Results - CA50RAP50 Mix

Stabilizing Agent			UCS (MPa)				
OPC	GCBA	$CaCl_2$	Day 1	Day 3	Day 7	Day 14	Day 28
1	3	0	2.20	2.91	2.94	3.14	3.67
2	2	0	2.57	3.16	3.45	3.67	4.53
3	1	0	2.97	3.95	4.04	4.75	4.80
4	0	0	3.56	3.97	4.29	4.79	5.10
1	3	1	2.47	2.76	2.93	3.13	4.18
2	2	1	3.40	3.52	3.64	4.00	4.51
3	1	1	3.51	3.83	4.59	4.74	5.83
4	0	1	3.86	3.91	4.40	4.86	5.93
1	3	2	2.38	2.53	2.56	2.67	3.53
2	2	2	3.16	3.40	3.60	3.62	4.76
3	1	2	3.44	3.83	4.39	4.73	5.13
4	0	2	3.84	4.19	4.25	4.81	5.52
1	3	3	2.16	2.22	2.55	2.76	3.35
2	2	3	2.20	2.38	2.73	2.88	4.14
3	1	3	3.03	3.49	3.70	3.96	4.89
4	0	3	3.26	3.31	3.40	4.39	4.50

Table 4.19
Summary of UCS Results - CA25RAP75 Mix

Stabilizing Agent			UCS (MPa)				
OPC	GCBA	$CaCl_2$	Day 1	Day 3	Day 7	Day 14	Day 28
1	3	0	2.30	2.69	2.82	3.13	3.35
2	2	0	2.94	3.00	3.37	4.00	4.74
3	1	0	3.49	3.96	4.27	4.64	4.72
4	0	0	3.25	3.82	4.21	4.61	4.76
1	3	1	1.92	2.30	2.91	3.08	3.44
2	2	1	3.05	3.20	3.62	4.48	4.54
3	1	1	3.20	3.53	4.41	4.70	4.90
4	0	1	3.51	3.52	4.46	4.69	5.04
1	3	2	1.81	2.17	2.41	2.85	3.19
2	2	2	2.67	2.71	3.02	3.41	3.79
3	1	2	3.27	3.57	3.88	4.25	4.30
4	0	2	3.35	3.55	3.96	4.23	4.98
1	3	3	1.90	2.07	2.55	2.71	2.90
2	2	3	2.37	2.43	2.78	2.87	3.30
3	1	3	2.83	3.28	3.68	3.92	4.16
4	0	3	3.09	3.27	3.43	3.88	4.48

4.4.5.2 Indirect Tensile Strength Results

Tables 4.20 to 4.22 present the summary of ITS results for three CA-RAP mixes incorporating stabilizing agent.

Table 4.20
Summary of ITS Results - CA75RAP25 Mix

Stabilizing Agent			ITS (KPa)				
OPC	GCBA	$CaCl_2$	Day 1	Day 3	Day 7	Day 14	Day 28
2	2	0	160.63	204.99	286.11	407.01	448.34
3	1	0	202.94	276.26	346.63	482.94	552.28
4	0	0	193.78	279.14	357.17	451.99	483.32
2	2	1	174.26	208.34	242.25	331.05	404.13
3	1	1	193.07	321.32	419.26	481.36	564.04
4	0	1	191.36	296.03	426.13	500.51	542.55
2	2	2	182.86	227.89	255.98	321.95	404.47
3	1	2	194.03	261.97	317.92	499.21	508.75
4	0	2	190.18	301.49	367.15	475.09	552.04

Table 4.21
Summary of ITS Results - CA50RAP50 Mix

Stabilizing Agent			ITS (KPa)				
OPC	GCBA	$CaCl_2$	Day 1	Day 3	Day 7	Day 14	Day 28
2	2	0	158.84	207.42	286.93	349.45	397.42
3	1	0	201.64	214.75	303.61	387.04	444.56
4	0	0	184.57	228.77	371.57	460.32	495.97
2	2	1	185.30	273.56	346.04	544.23	587.63
3	1	1	210.67	351.60	411.69	589.94	692.61
4	0	1	231.61	324.68	471.26	596.48	671.10
2	2	2	177.88	232.79	303.04	401.17	434.77
3	1	2	184.63	252.22	404.96	501.76	549.75
4	0	2	174.87	264.20	412.78	472.66	527.39

Table 4.22
Summary of ITS Results - CA25RAP75 Mix

Stabilizing Agent			ITS (KPa)				
OPC	GCBA	$CaCl_2$	Day 1	Day 3	Day 7	Day 14	Day 28
2	2	0	75.57	95.31	224.21	304.94	372.42
3	1	0	97.35	141.80	235.87	339.79	450.07
4	0	0	100.46	143.67	225.75	301.70	392.82
2	2	1	87.13	106.33	241.04	341.70	415.93
3	1	1	96.36	127.58	269.78	437.09	569.90
4	0	1	100.64	141.12	298.32	486.63	531.51
2	2	2	83.78	125.32	185.01	363.12	404.20
3	1	2	103.29	182.25	205.98	337.61	468.97
4	0	2	90.54	190.41	219.28	379.46	440.47

4.4.5.3 Resilient Modulus Results

Tables 4.23 to 4.25 present the summary of M_R results for three CA-RAP mixes incorporating stabilizing agent.

Table 4.23
Summary of ITS Results - CA75RAP25 Mix

Stabilizing Agent			M_R (MPa)				
OPC	GCBA	$CaCl_2$	Day 1	Day 3	Day 7	Day 14	Day 28
2	2	0	3755.67	5277.83	7792.67	8111.33	10788.50
3	1	0	4552.50	6088.17	8509.50	10145.67	11990.17
4	0	0	4988.17	5894.00	8773.00	10534.33	12817.00
2	2	1	4358.33	5191.33	7397.67	9204.17	12192.33
3	1	1	5937.50	6708.83	8495.00	11324.17	12671.67
4	0	1	5700.67	7039.50	8989.67	11626.00	13979.50
2	2	2	4296.17	5310.83	6746.33	6886.17	9858.00
3	1	2	5299.50	6002.50	8609.00	9418.83	11552.67
4	0	2	5667.33	6293.67	9037.67	9694.83	12450.83

Table 4.24
Summary of ITS Results - CA50RAP50 Mix

Stabilizing Agent			M_R (MPa)				
OPC	GCBA	$CaCl_2$	Day 1	Day 3	Day 7	Day 14	Day 28
2	2	0	3720.83	4658.33	6313.67	8147.33	9146.33
3	1	0	4151.33	6133.33	9273.50	9993.83	11326.17
4	0	0	4415.33	7623.67	9825.17	10284.67	11639.83
2	2	1	4008.50	5777.50	7326.17	7870.50	9437.80
3	1	1	5588.67	8177.67	9152.50	10678.67	12574.00
4	0	1	5181.33	7917.67	9555.17	10941.67	12146.33
2	2	2	3524.83	5002.00	5550.33	5848.50	8336.17
3	1	2	4863.00	5832.67	6669.00	6744.17	9055.67
4	0	2	5743.17	6313.33	6512.33	8547.67	9446.17

Table 4.25
Summary of ITS Results - CA25RAP75 Mix

Stabilizing Agent			M_R (MPa)				
OPC	GCBA	$CaCl_2$	Day 1	Day 3	Day 7	Day 14	Day 28
2	2	0	2994.33	3877.33	4549.50	5158.67	6744.67
3	1	0	4712.83	5299.00	6969.00	6860.33	9007.67
4	0	0	5024.83	5746.67	6387.83	8004.83	9497.00
2	2	1	3860.67	4994.67	6457.33	6745.50	7797.83
3	1	1	4992.50	6546.17	7706.67	8595.83	9558.00
4	0	1	5143.50	6790.17	7091.33	9053.83	10102.00
2	2	2	3087.33	3669.50	3950.00	5130.33	6180.50
3	1	2	3364.33	4607.67	5900.33	6806.17	7954.83
4	0	2	4110.83	4837.17	4914.67	6223.67	8447.50

4.5 Phase Four: Model Development, Data Verification and Optimization

Two regression models were analyzed using RSM to predict strength performance: linear and quadratic. RSM generated both linear and quadratic regression models based on the experimental data entered into the RSM framework. The aim was to identify the model that best fits the data and offers the most accurate predictions. Previous research have demonstrated that RSM is an effective approach for validating laboratory data and developing predictive models. The RSM methodology applied in this research closely resembles that used by Shiong et al. (2023) in evaluating the volumetric properties of asphalt. Similarly, Zhang et al. (2021) utilized RSM to optimize micaceous soil stabilization, further highlighting its versatility in modeling and optimization.

The 3D models generated from the UCS, ITS, and M_R analysis were employed to visualize the relationships between the input variables and the responses. Additionally, predictive versus actual graphs were used to assess the accuracy and reliability of the models developed through RSM. Furthermore, material optimization was performed to identify the optimal proportions of OPC, GCBA, and $CaCl_2$ that could achieve the desired mechanical performance.

The subsequent sections discuss the outcomes of the RSM analysis, which was conducted using ANOVA, with a focus on UCS, ITS, and M_R. The input data for this analysis were derived from laboratory experiments.

4.5.1 Unconfined Compressive Strength Model

In the ANOVA analysis for UCS, the *p*-values for all models were significantly below the 0.05 threshold, indicating their statistical significance. This suggested that variations in the components (OPC, GCBA, $CaCl_2$, and curing days) reliably explained variations in UCS. Tables 4.26 to 4.28 present the ANOVA results for UCS derived using RSM across the three CA-RAP mix designs, while Equations 4.1 to 4.9 detail the corresponding predictive models for each mix.

4.5.1.1 CA75RAP25 Mix Design

In the CA75RAP25 mix design, as summarized in Table 4.26, the analysis showed that all three mix combinations had a significant effect on UCS, as indicated by *p*-values below 0.01. The *F*-values ranged from 8.16 to 45.48, confirming a strong influence of the stabilizing agent on the mechanical performance of the mix design. The mix containing 2% OPC + 2% GCBA followed a quadratic model, suggesting nonlinear interactions among the factors. In contrast, the other two mixes exhibited linear responses, indicating a more direct relationship between the input variables and UCS. Among the three compositions, the mix with 4% OPC recorded the highest *F*-value (45.48), indicating the strongest influence on strength development. Meanwhile, the combination of 3% OPC + 1% GCBA produced the highest mean square value (2.46) and a high *F*-value (30.63), highlighting its significant impact on variations in UCS.

Table 4.26
ANOVA Results for UCS - CA75RAP25 Mix

Factors			Sum of squares	df	Mean square	*F*-value	*p*-value	Model type
OPC (%)	GCBA (%)	$CaCl_2$ (%)						
2	2	0,1,2	6.39	5	1.28	8.16	0.0037	Quadratic
3	1	0,1,2	4.92	2	2.46	30.63	<0.0001	Linear
4	0	0,1,2	3.94	2	1.97	45.48	<0.0001	Linear

The UCS prediction models for this mix are presented in Equations (4.1 - 4.3)

- Equation (4.1): 2% OPC + 2% GCBA
  $$UCS = 1.9735 + 1.3880A + 0.1086B - 0.0057AB - 0.5833A - 0.0015B^2$$

- Equation (4.2): 3% OPC + 1% GCBA
  $$UCS = 3.2985 + 0.1061A + 0.0579B$$

- Equation (4.3): 4% OPC + 0% GCBA
  $$UCS = 3.4139 + 0.1257A + 0.0514B$$

Where:
A: $CaCl_2$ content (%)
B: Curing duration (days)

4.5.1.2 CA50RAP50 Mix Design

As shown in Table 4.27, the statistical analysis for CA50RAP50 mix deisgn demonstrated that all tested mixes significantly influenced UCS, as reflected by *p*-values of less than 0.01. The *F*-values ranged from 18.13 to 71.50, confirming the considerable impact of these compositions on the mechanical performance of the mix design. The model types varied among the mixes. Specifically, the 3% OPC + 1% GCBA mix produced a quadratic model, indicating nonlinear interactions among the factors. In contrast, the other two compositions displayed linear relationships, suggesting a more straightforward influence of the factors on UCS. The highest *F*-value (71.50) and mean square (2.92) were observed in the 4% OPC + 0% GCBA mix, indicating its strong effect on the strength development of the mixes.

Table 4.27
ANOVA Results for UCS - CA50RAP50 Mix

factors			Sum of squares	df	Mean square	*F*-value	*p*-value	Model type
OPC (%)	GCBA (%)	$CaCl_2$ (%)						
2	2	0,1,2	4.15	2	2.07	45.13	<0.0001	Linear
3	1	0,1,2	7.05	5	1.41	18.13	0.0002	Quadratic
4	0	0,1,2	5.83	2	2.92	71.50	<0.0001	Linear

The UCS prediction models for this mix are presented in Equations (4.4 - 4.6)

- Equation (4.4): 2% OPC + 2% GCBA
  $$UCS = 2.9894 + 0.1167A + 0.0529B$$

- Equation (4.5): 3% OPC + 1% GCBA
  $$UCS = 3.1155 + 0.6879A + 0.1514B + 0.0008AB - 0.2983A^2 - 0.0029B^2$$

- Equation (4.6): 4% OPC + 0% GCBA
  $$UCS = 3.7231 + 0.0906A + 0.0633B$$

Where:
A: $CaCl_2$ content (%)
B: Curing duration (days)

4.5.1.3 CA25RAP75 Mix Design

The analysis presented in Table 4.28 for the CA25RAP75 mix design revealed that all three compositions had a significant effect on UCS, as evidenced by *p*-values below 0.0001. The *F*-values ranged from 23.57 to 65.58, confirming a strong influence of the stabilizing agent on the mechanical properties of the mixes. All compositions followed a quadratic model, indicating nonlinear interactions among OPC, GCBA, and $CaCl_2$ in influencing the UCS response. The mix containing 2% OPC + 2% GCBA exhibited the highest *F*-value (65.58) and a mean square of 1.24, which signified the most considerable effect on strength variation at this composition level.

Table 4.28
ANOVA Results for UCS - CA25RAP75 Mix

factors								
OPC (%)	GCBA (%)	$CaCl_2$ (%)	Sum of squares	df	Mean square	*F*-value	*p*-value	Model type
2	2	0,1,2	6.18	5	1.24	65.58	<0.0001	Quadratic
3	1	0,1,2	4.07	5	0.8138	23.57	<0.0001	Quadratic
4	0	0,1,2	4.88	5	0.9763	27.63	<0.0001	Quadratic

The UCS prediction models for this mix are presented in Equations (4.7 - 4.9)

- Equation (4.7): 2% OPC + 2% GCBA
  $$\boldsymbol{UCS = 2.6770 + 0.7188A + 0.1249B - 0.0129AB - 0.4130A^2 - 0.0018B^2}$$

- Equation (4.8): 3% OPC + 1% GCBA
  $$\boldsymbol{UCS = 3.3674 + 0.0678A + 0.1467B - 0.0022AB - 0.1122A^2 - 0.0034B^2}$$

- Equation (4.9): 4% OPC + 0% GCBA
  $$\boldsymbol{UCS = 3.3358 + 0.2354A + 0.1249B + 0.0046AB - 0.1714A^2 - 0.0025B^2}$$

Where:
A: $CaCl_2$ content (%)
B: Curing duration (days)

The ANOVA analysis showed that both $CaCl_2$ (Factor A) and the number of curing days (Factor B) positively impacted the UCS in linear terms. However, the quadratic models indicated that each factor could achieve an optimal value, beyond which its benefits might start to decline. In contrast, the linear models provided simpler guidelines for adjusting the mix proportions.

4.5.1.4 3-D Model of UCS Analysis

Figures 4.102 to 4.104 exhibit the 3-D models of UCS analysis obtained from the RSM for all three different CA-RAP mixes. The models illustrated the relationship between UCS and the varying compositions of OPC, GCBA, and $CaCl_2$.

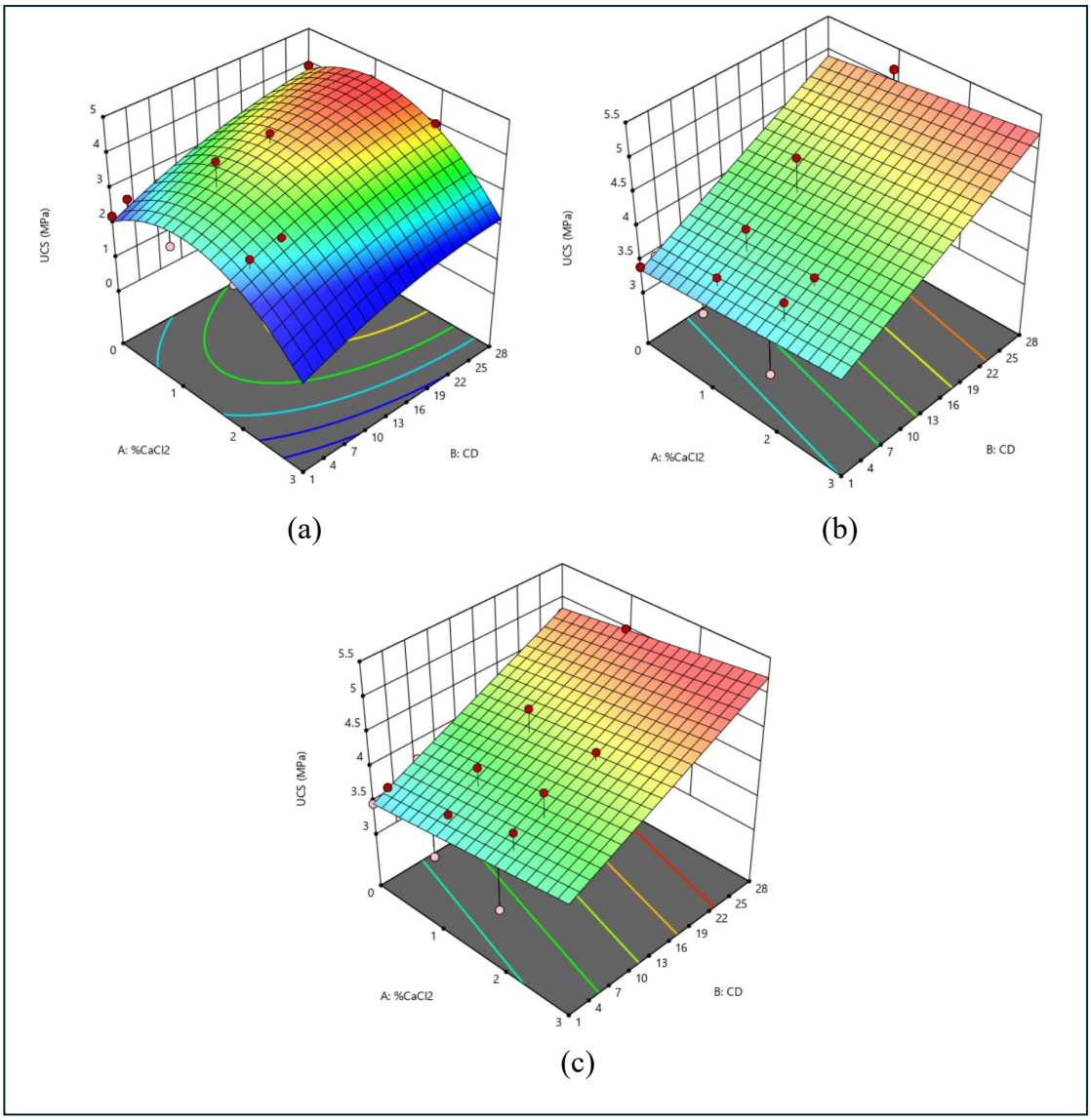


Figure 4.102 3-D Model of UCS Analysis for CA75RAP25 Mix Design Consist of (a) 2% OPC + 2% GCBA, (b) 3% OPC + 1% GCBA and (c) 4% OPC with Various Percentages of $CaCl_2$

The 3-D models for CA75RAP25 mix design, as shown in Figure 4.102, illustrated how the UCS changed in response to various combinations of OPC, GCBA, and $CaCl_2$. In a model with 2% OPC + 2% GCBA, the UCS increased with the addition of $CaCl_2$ up 1%, after which it slightly decreased. A model containing 3% OPC + 1% GCBA demonstrated a significant increase in UCS as the $CaCl_2$ content rose. Similarly, the model with 4% OPC also showed an increase in UCS with higher percentages of $CaCl_2$, suggesting that a higher OPC content significantly enhanced UCS when combined with $CaCl_2$.

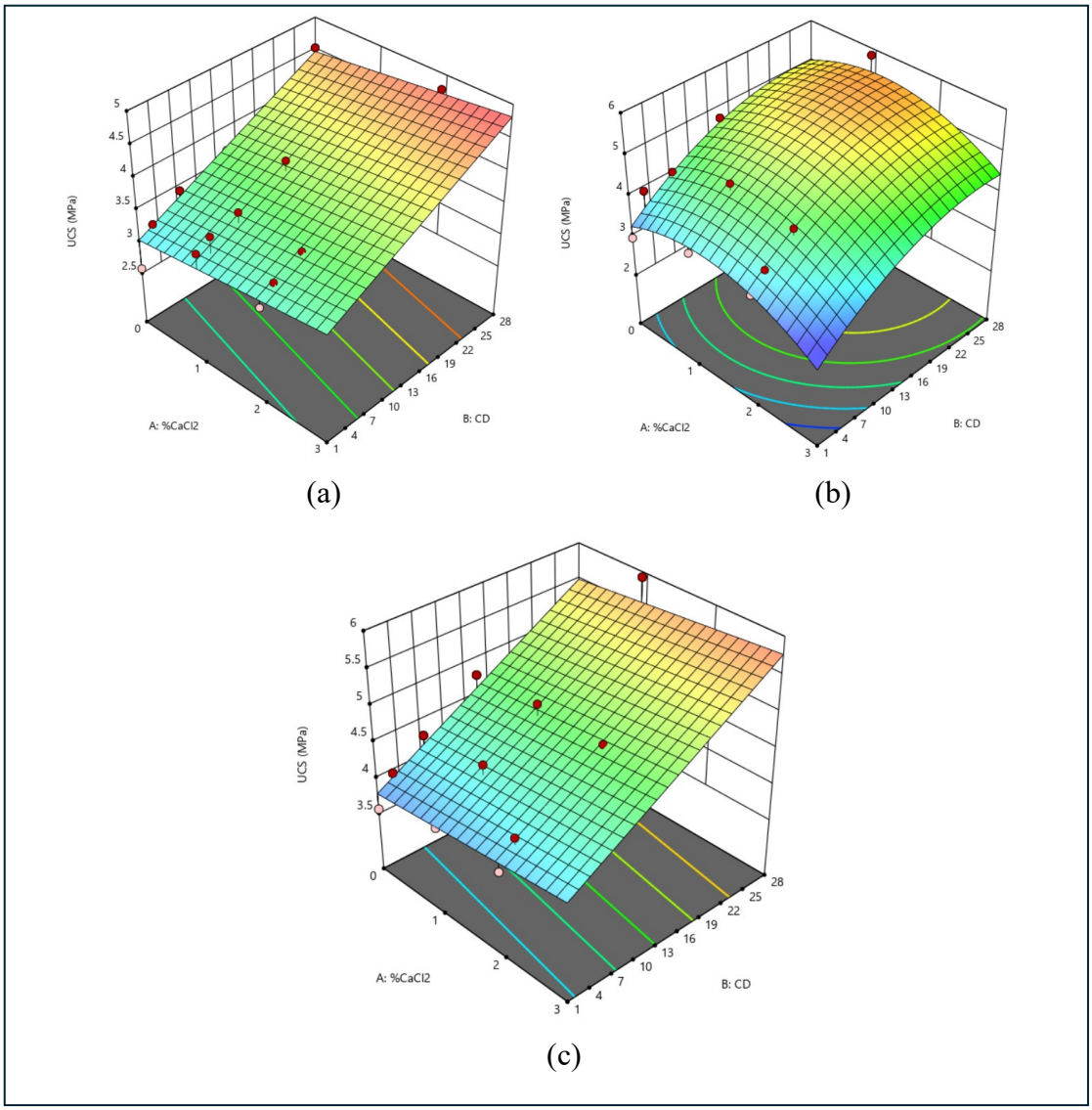


Figure 4.103 3-D Model of UCS Analysis for CA50RAP50 Mix Design Consist of (a) 2% OPC + 2% GCBA, (b) 3% OPC + 1% GCBA and (c) 4% OPC with Various Percentages of $CaCl_2$

The 3-D models shown in Figure 4.103 for CA50RAP50 mix design demonstrated a similar trend. It was observed that the model containing 2% OPC + 2% GCBA displayed an increase in UCS with the addition of more $CaCl_2$. Similar trend can be seen in the model with 4% OPC as consistent improvement in UCS as the percentage of $CaCl_2$ increased. In contrast, the model with 3% OPC + 1% GCBA experienced an initial rise in UCS with increased $CaCl_2$ up to 1%, but its strength began to decline at 2% $CaCl_2$ content.

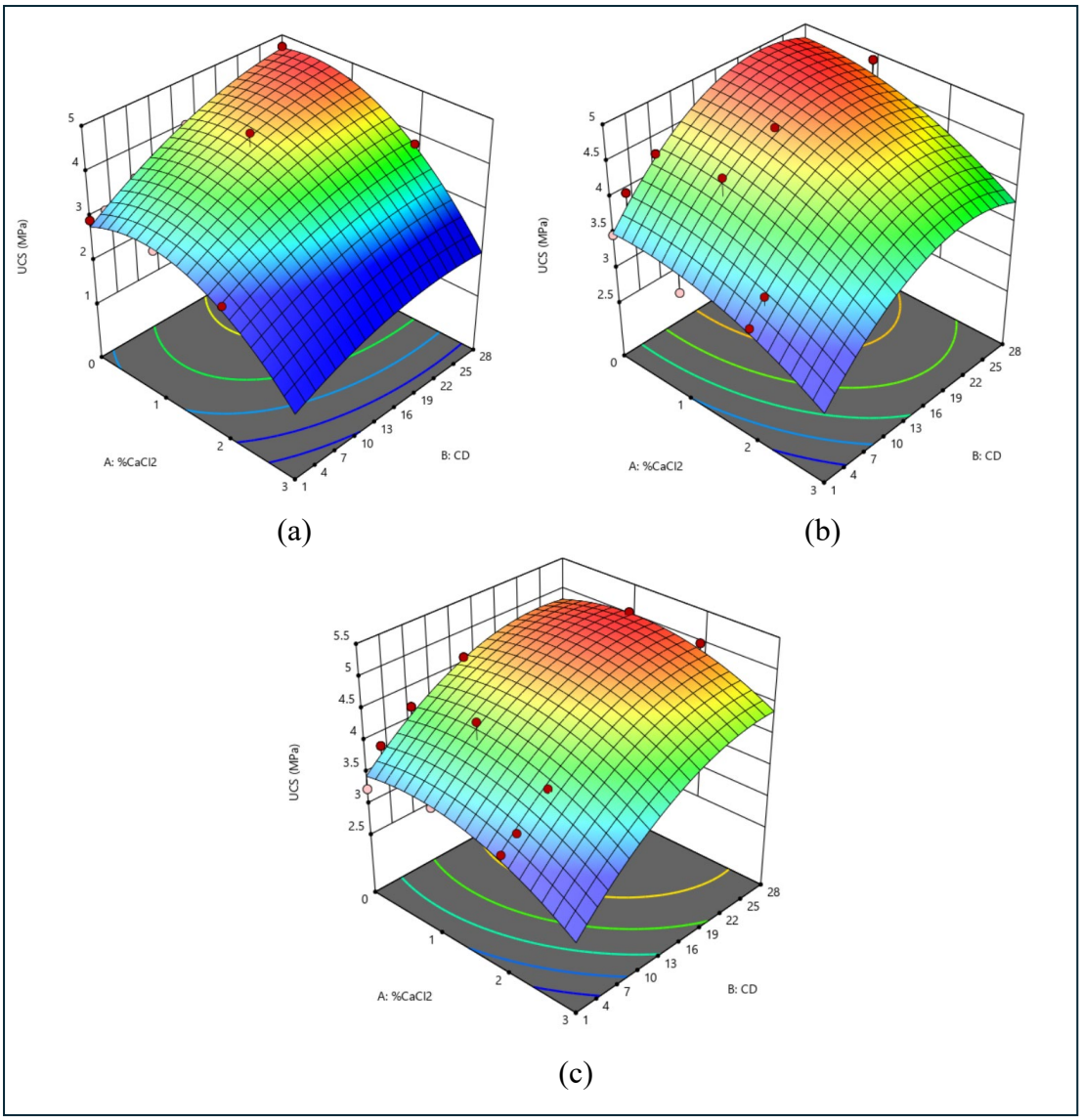


Figure 4.104 3-D Model of UCS Analysis for CA25RAP75 Mix Design Consist of (a) 2% OPC + 2% GCBA, (b) 3% OPC + 1% GCBA and (c) 4% OPC with Various Percentages of $CaCl_2$

In Figure 4.104, the 3-D models for CA25RAP75 mix design exhibited a similar trend across all mix combinations. Notably, a model containing 2% OPC + 2% GCBA showed that the UCS increased with the addition of $CaCl_2$ up to 1%. However, strength began to decline at the 2% $CaCl_2$ content. This pattern was also observed in models with 3% OPC + 1% GCBA, as well as with 4% OPC. In these cases, UCS consistently increased with $CaCl_2$ at the 1% content but started to decline once the concentration reached 2% or higher.

The 3-D model analysis of three different proportions of CA-RAP revealed that the addition of $CaCl_2$ significantly affected the UCS across all CA-RAP mixes. The UCS consistently improved with the inclusion of $CaCl_2$, particularly when combined

with GCBA and OPC, especially at higher OPC levels. However, when the $CaCl_2$ content exceeded 2%, a notable decrease in UCS was observed in some cases. Higher OPC percentages resulted in improvements in UCS with the addition of $CaCl_2$. On the other hand, when the percentage of GCBA was low or absent, the UCS tended to be higher, indicating that the influence of GCBA was more effective at lower percentages.

4.5.1.5 Predictive Versus Actual Analysis of UCS

In the analysis of the predictive versus actual graph for UCS, a diagonal line was included to represent the ideal scenario in which predicted values match actual values. This line typically forms a 45-degree angle. The data points are scattered around this line, indicating the accuracy and reliability of the predictive model. This method is commonly used for data verification and model validation, as it assesses how closely the predicted results align with the experimental data.

Figures 4.105 to 4.107 display the predictive versus actual analysis of UCS derived from the RSM for all three CA-RAP mixes, illustrating how well the regression model fits the relationship between the predicted and experimental data.

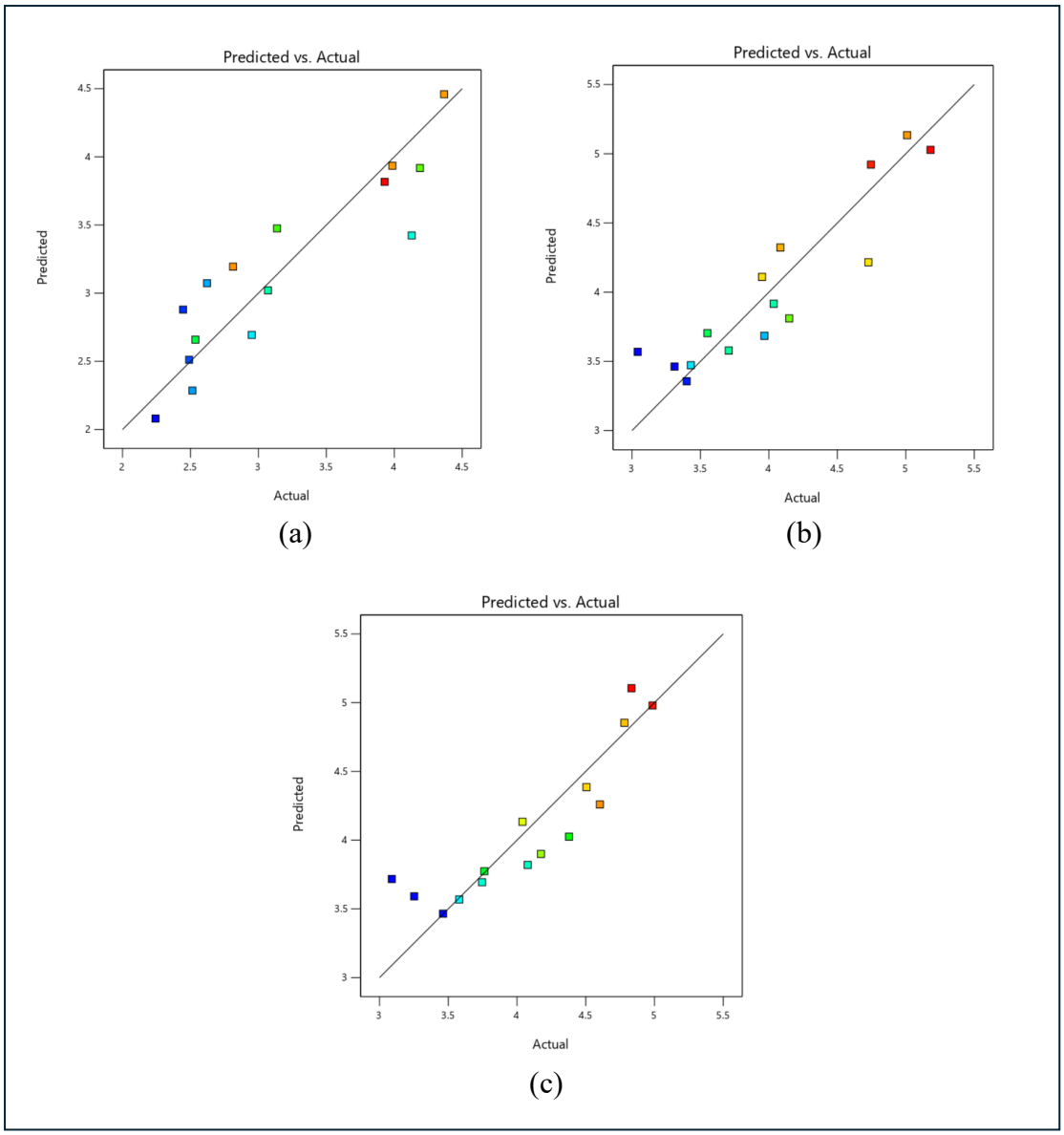


Figure 4.105 Predictive Versus Actual Graph of UCS Analysis for CA75RAP25 Mix Design Consist of (a) 2% OPC + 2% GCBA, (b) 3% OPC + 1% GCBA and (c) 4% OPC with Various Percentages of $CaCl_2$

In the CA75RAP25 mix design, as shown in Figure 4.105, the graph for 4% OPC with various percentages of $CaCl_2$ displayed data points that closely aligned with the ideal line. This mix demonstrated the highest prediction accuracy, indicating that an increase in OPC content improved the predictability of UCS.

In the mix containing 3% OPC + 1% GCBA, the graph similarly indicated that the data points were more closely aligned with the ideal line, though some scatter was observed, particularly in the middle range. This model was reasonably accurate, but minor deviations suggested that other factors may have influenced UCS predictions.

Conversely, for the mix with 2% OPC + 2% GCBA with various percentages of $CaCl_2$, the data points exhibited significant scatter, especially in the lower range. Several points deviated considerably from the ideal line, indicating less reliable predictions.

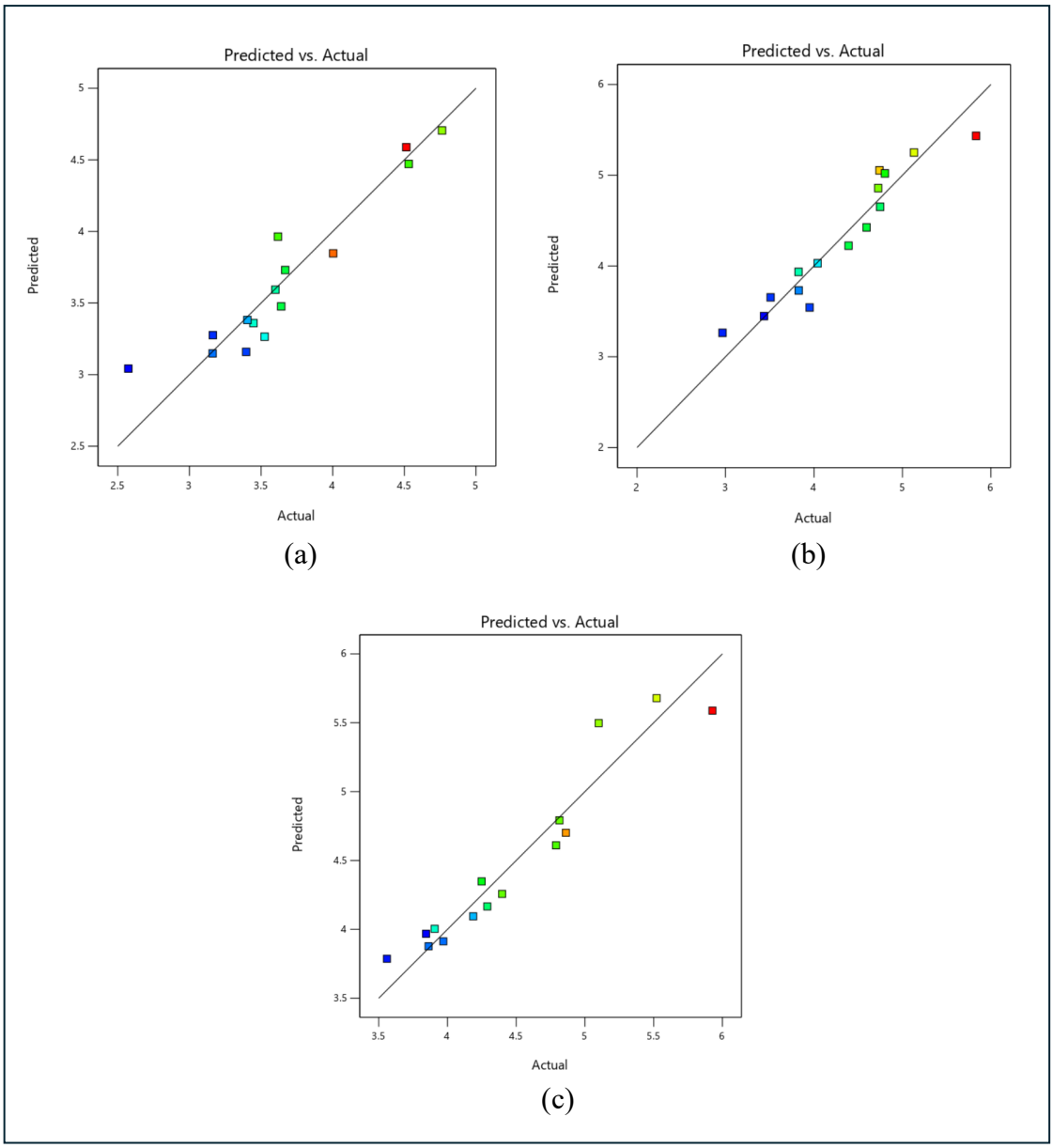


Figure 4.106 Predictive Versus Actual Graph of UCS Analysis for CA50RAP50 Mix Design Consist of (a) 2% OPC + 2% GCBA, (b) 3% OPC + 1% GCBA and (c) 4% OPC with Various Percentages of $CaCl_2$

In the CA50RAP50 mix design, as illustrated in Figure 4.106, the graph for 3% OPC + 1% GCBA with various percentages of $CaCl_2$ displayed data points that were closely clustered along the ideal line across the entire range, showing minimal deviation. This suggested that the predictions were the most accurate and reliable.

However, there was slight scatter at the upper range, indicating minor deviations in predictions for higher UCS values.

The graph for 4% OPC with various percentages of $CaCl_2$, showed that the data points were mostly near the ideal line but exhibited some scatter, particularly at lower values. This suggested moderate reliability, with some deviations affecting the accuracy of predictions.

On the other hand, the graph for 2% OPC + 2% GCBA with various percentages of $CaCl_2$ exhibited data points with a higher degree of scatter, especially in the middle and lower ranges. This indicated lower reliability in predicting UCS compared to the other two models.

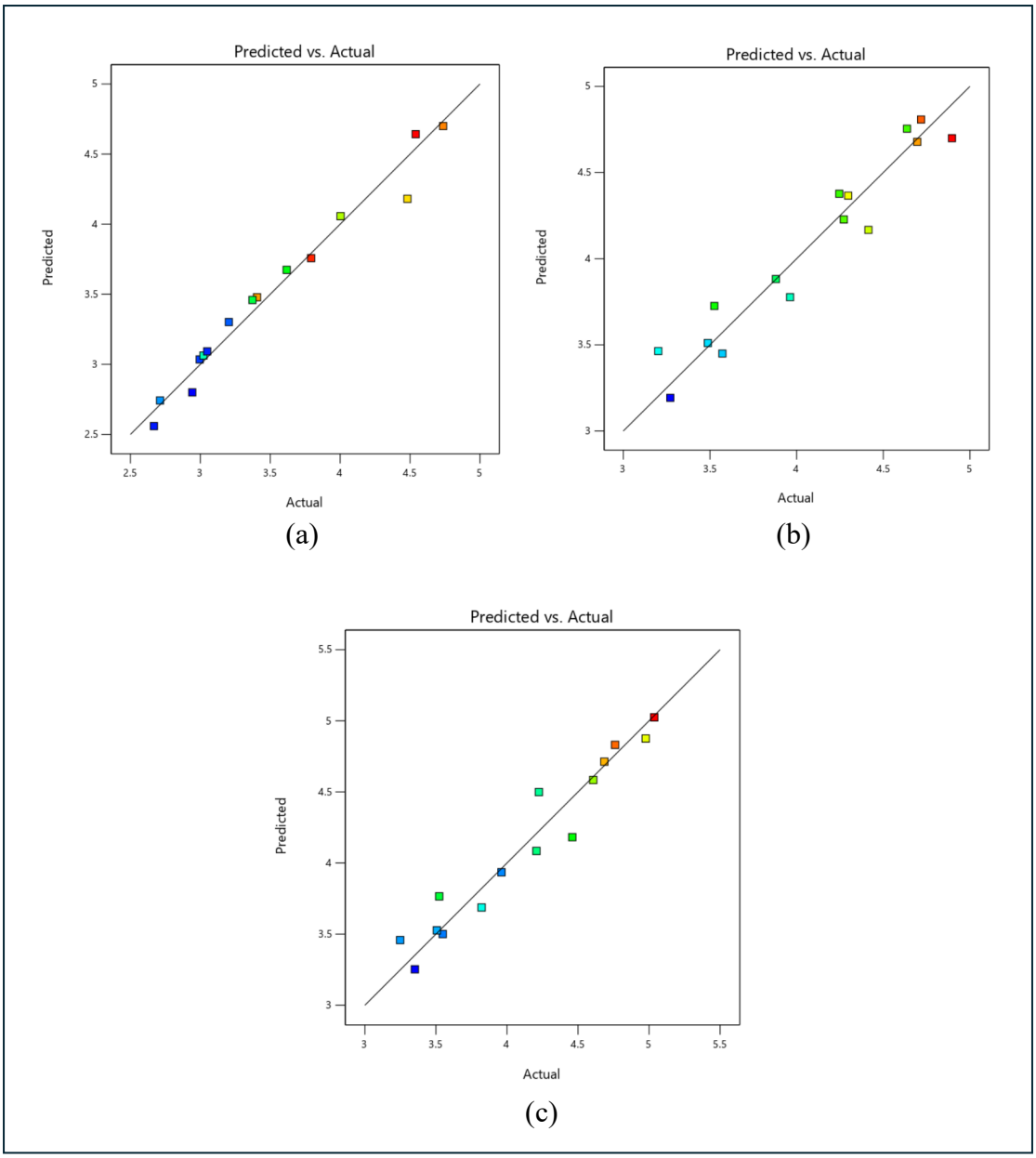


Figure 4.107 Predictive Versus Actual Graph of UCS Analysis for CA25RAP75 Mix Design Consist of (a) 2% OPC + 2% GCBA, (b) 3% OPC + 1% GCBA and (c) 4% OPC with Various Percentages of $CaCl_2$

In the CA25RAP75 mix design, as illustrated in Figure 4.107, the graph representing 2% OPC + 2% GCBA combined with various percentages of $CaCl_2$ displayed data points that closely aligned with the ideal line across the range. This indicated the highest level of accuracy and reliability among the three graphs.

In contrast, the graph for 4% OPC with different percentages of $CaCl_2$ showed data points that were relatively close to the ideal line, but some scatter was observed, particularly at the lower end of the range. This suggested a moderate level of reliability, with some degree of prediction error.

Similarly, the graph for 3% OPC + 1% GCBA with varying percentages of $CaCl_2$ had data points that were near the ideal line, especially in the middle and upper ranges. This indicated improved accuracy compared to the 4% OPC combination, although there were minor deviations.

The analysis of all mixes showed that higher percentages of OPC tended to result in better alignment between predicted and actual UCS. This indicated that the model performed well with higher OPC content. The presence of GCBA appeared to have a minor effect on predictive accuracy, as models with varying percentages of GCBA still showed a good alignment with the ideal line.

Overall, the graphs demonstrated a strong linear relationship across all figures, with actual UCS closely following the predicted values. This suggested that the models developed using RSM were highly accurate in predicting UCS for different CA-RAP mixes. The finding was further supported by the clustering of data points along the 45° diagonal line, which indicates minimal deviation between experimental and predicted values, as noted by Aliyegbenoma et al. (2020).

4.5.2 Indirect Tensile Strength Model

In the ANOVA analysis for ITS, the *p*-values for all models were significantly below the 0.05 threshold, indicating their statistical significance. This suggested that variations in the components (OPC, GCBA, $CaCl_2$, and curing days) reliably contributed to variations in ITS.

Tables 4.29 to 4.31 present the ANOVA results for ITS derived using RSM across the three CA-RAP mix designs, while Equations 4.10 to 4.18 detail the corresponding predictive models for each mix.

4.5.2.1 CA75RAP25 Mix Design

The analysis of CA75RAP25 mix design as presented in Table 4.29 indicated that all three tested compositions yielded highly significant results, with *p*-values less than 0.0001. This finding demonstrates that the selected factors had a significant impact on ITS values. The *F*-values ranged from 63.21 to 69.66, further confirming the statistical relevance of the models. Each of the three responses was best represented by a quadratic model, suggesting the existence of non-linear interactions among the variables. Among the tested compositions, the mix containing 2% OPC+ 2% GCBA exhibited the highest F-value of 69.66, indicating that this combination contributed most significantly to the variation in ITS.

Table 4.29
ANOVA Results for ITS - CA75RAP25 Mix

factors			Sum of squares	df	Mean square	*F*-value	*p*-value	Model type
OPC (%)	GCBA (%)	$CaCl_2$ (%)						
2	2	0,1,2	1.266E+05	5	25321.49	69.66	<0.0001	Quadratic
3	1	0,1,2	2.434E+05	5	48679.78	63.21	<0.0001	Quadratic
4	0	0,1,2	2.215E+05	5	44309.12	68.36	<0.0001	Quadratic

The ITS prediction models for this mix are presented in Equations (4.10 - 4.12)

- Equation (4.10): 2% OPC + 2% GCBA
  $$\boldsymbol{ITS = 158.6662 - 32.6396A + 19.6896B - 1.3953AB + 18.0180\,A^2 - 0.3174B^2}$$

- Equation (4.11): 3% OPC + 1% GCBA
  $$\boldsymbol{ITS = 171.7439 + 59.6115A + 31.8655B - 0.42391AB - 31.5180A^2 - 0.6607B^2}$$

- Equation (4.12): 4% OPC + 0% GCBA
  $$\boldsymbol{ITS = 173.7178 + 52.1707A + 30.6839B + 1.1558AB - 26.1836A^2 - 0.7020B^2}$$

Where:
A: $CaCl_2$ content (%)
B: Curing duration (days)

4.5.2.2 CA50RAP50 Mix Design

In the CA50RAP50 mix design, all three compositions demonstrated statistically significant effects on the ITS, with *p*-values less than 0.0001, as shown in Table 4.30. The *F*-values, which ranged from 27.19 to 59.53, indicated that the input factors had a substantial influence on ITS outcomes. A quadratic model was derived for all compositions, suggesting the presence of second-order interactions between the stabilizing agent and the response variable. Among the evaluated compositions, the mix with 4% OPC + 0% GCBA recorded the highest *F*-value of 59.53, reflecting its dominant influence on the variation in ITS.

Table 4.30
ANOVA Results for ITS - CA50RAP50 Mix

factors			Sum of squares	df	Mean square	*F*-value	*p*-value	Model type
OPC (%)	GCBA (%)	$CaCl_2$ (%)						
2	2	0,1,2	2.221E+05	5	44426.19	27.19	<0.0001	Quadratic
3	1	0,1,2	3.232E+05	5	64645.80	34.25	<0.0001	Quadratic
4	0	0,1,2	3.209E+05	5	64171.06	59.53	<0.0001	Quadratic

The ITS prediction models for this mix are presented in Equations (4.13 - 4.15)

- Equation (4.13): 2% OPC + 2% GCBA
  $$\boldsymbol{ITS = 108.5579 + 195.3686A + 27.9159B + 0.41082AB - 92.3826A^2 - 0.5989B^2}$$

- Equation (4.14): 3% OPC + 1% GCBA
  $$\boldsymbol{ITS = 124.1588 + 228.5322A + 30.5626B + 1.8169AB - 106.8096A^2 - 0.6631B^2}$$

- Equation (4.15): 4% OPC + 0% GCBA
  $$\boldsymbol{ITS = 129.3471 + 207.5654A + 36.8993B + 0.2768AB - 99.7150A^2 - 0.8288B^2}$$

Where:
A: $CaCl_2$ content (%)
B: Curing duration (days)

4.5.2.3 CA25RAP75 Mix Design

As shown in Table 4.31, the analysis of CA25RAP75 mix design revealed that all three mix compositions had a significant impact on ITS, with *p*-values less than 0.0001. The *F*-values ranged from 31.73 to 100.30, indicating a strong influence of the selected factors on the mechanical performance of the mixes. The results for each mix followed a quadratic model, emphasizing the significance of nonlinear interactions among the input variables. Notably, the mix containing 2% OPC + 2% GCBA produced the highest *F*-value of 100.30, indicating that this combination had the most influence effect on ITS variation in CA25RAP75 mixes.

Table 4.31
ANOVA Results for ITS - CA25RAP75 Mix

factors			Sum of squares	df	Mean square	*F*-value	*p*-value	Model type
OPC (%)	GCBA (%)	$CaCl_2$ (%)						
2	2	0,1,2	2.291E+05	5	45815.41	100.30	<0.0001	Quadratic
3	1	0,1,2	3.247E+05	5	64949.73	48.76	<0.0001	Quadratic
4	0	0,1,2	2.899E+05	5	57974.57	31.73	<0.0001	Quadratic

The ITS prediction models for this mix are presented in Equations (4.16 - 4.18)

- Equation (4.16): 2% OPC + 2% GCBA
  $$ITS = 35.2344 + 32.4744A + 28.1703B + 0.6129AB - 15.0373A^2 - 0.5743B^2$$

- Equation (4.17): 3% OPC + 1% GCBA
  $$ITS = 54.0640 + 90.2954A + 27.2623B + 0.0676AB - 43.8456A^2 - 0.4334B^2$$

- Equation (4.18): 4% OPC + 0% GCBA
  $$ITS = 38.4515 + 132.4452A + 30.7374B + 0.8975AB - 63.1913A^2 - 0.6322B^2$$

Where:
A: $CaCl_2$ content (%)
B: Curing duration (days)

In the ANOVA analysis for the ITS test, all models produced significant *p*-values (<0.0001), indicating that the models were statistically significant. The factors of OPC, GCBA, and $CaCl_2$ have a substantial effect on the ITS. Notably, all models were quadratic, suggesting that the relationship between these factors and the ITS is non-linear, in contrast to the UCS test. This finding indicated that the tensile behavior of the mixes was more sensitive to combined factor interactions, while the compressive response tended to follow a more predictable trend with respect to individual factor variations.

4.5.2.4 3-D Model of ITS Analysis

Figures 4.108 to 4.110 exhibit the 3-D models of ITS analysis obtained from the RSM for all three different CA-RAP mixes. The models illustrated the relationship between ITS and varying compositions of OPC, GCBA and $CaCl_2$.

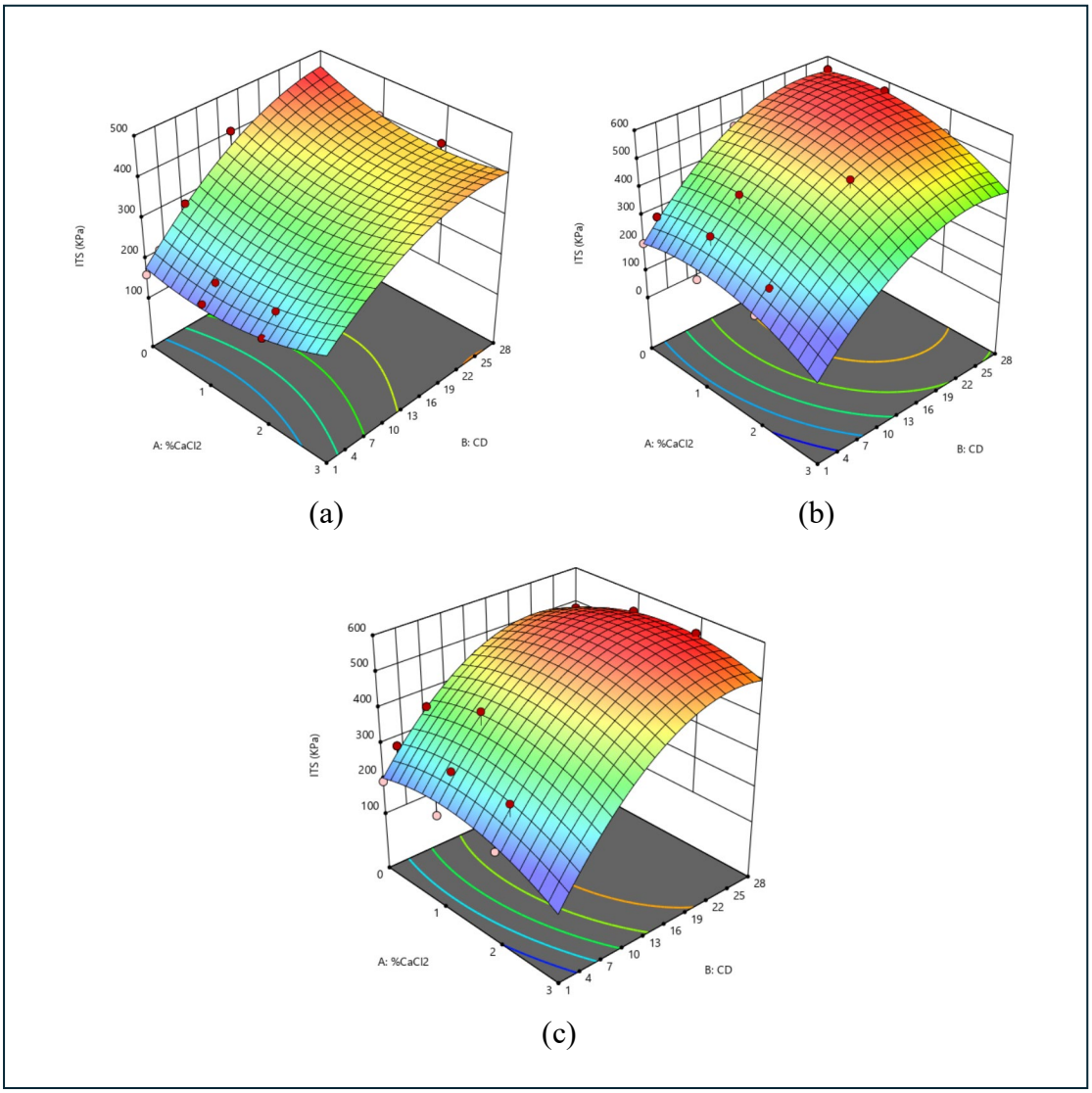


Figure 4.108 3-D Model of ITS Analysis for CA75RAP25 Mix Design Consist of (a) 2% OPC + 2% GCBA, (b) 3% OPC + 1% GCBA and (c) 4% OPC with Various Percentages of $CaCl_2$

The 3-D models for CA75RAP25 mix, as shown in Figure 4.108, indicated that a mix containing 2% OPC + 2% GCBA showed a slight increase in the ITS as the percentage of $CaCl_2$ increased to a 2%. In this composition, there appeared to be minimal interaction between OPC and GCBA, resulting in a relatively flat surface. In contrast, a mix with 3% OPC + 1% GCBA demonstrated higher ITS, showing a noticeable increase in strength with rising $CaCl_2$ percentages. However, the ITS began to decline at 2% $CaCl_2$. Notably, the highest ITS were recorded in a model with 4% OPC. There was a significant positive interaction between OPC and $CaCl_2$, as evidenced by the steeper surface plot.

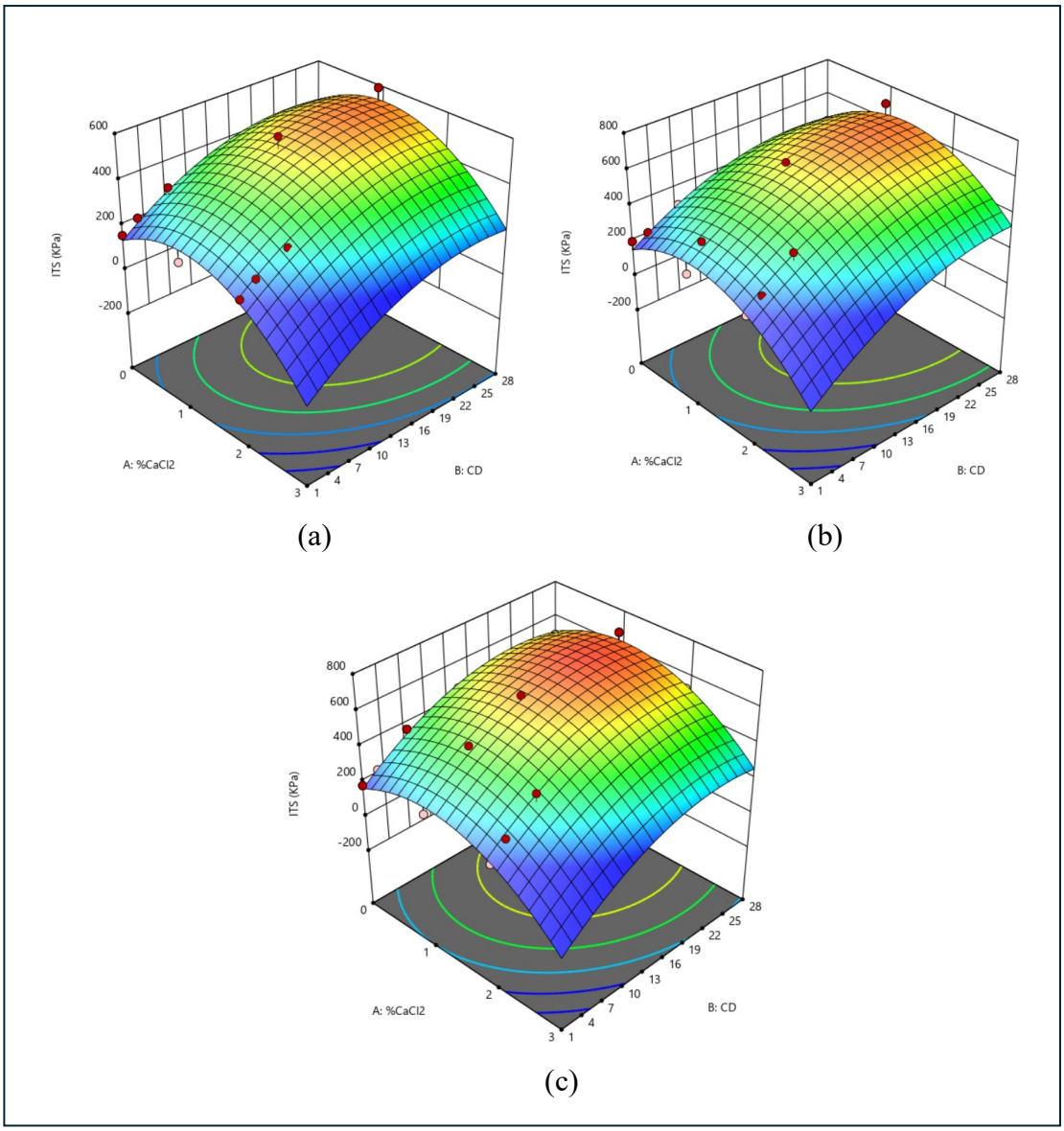


Figure 4.109 3-D Model of ITS Analysis for CA50RAP50 Mix Design Consist of (a) 2% OPC + 2% GCBA, (b) 3% OPC + 1% GCBA and (c) 4% OPC with Various Percentages of $CaCl_2$

In Figure 4.109, the 3-D models for CA50RAP50 mix are presented. There was a slight increase in ITS as the percentage of $CaCl_2$ increased in a model containing 2% OPC + 2% GCBA. However, higher amounts of $CaCl_2$ up to 2% caused the ITS to eventually decline. Similar trend can be seen in the model with 3% OPC + 1% GCBA, and model with 4% OPC as there was a consistent increase in ITS with rising $CaCl_2$ to 1%. For all models, the surface plot indicated a significant positive interaction between OPC and $CaCl_2$ as the curing days increased.

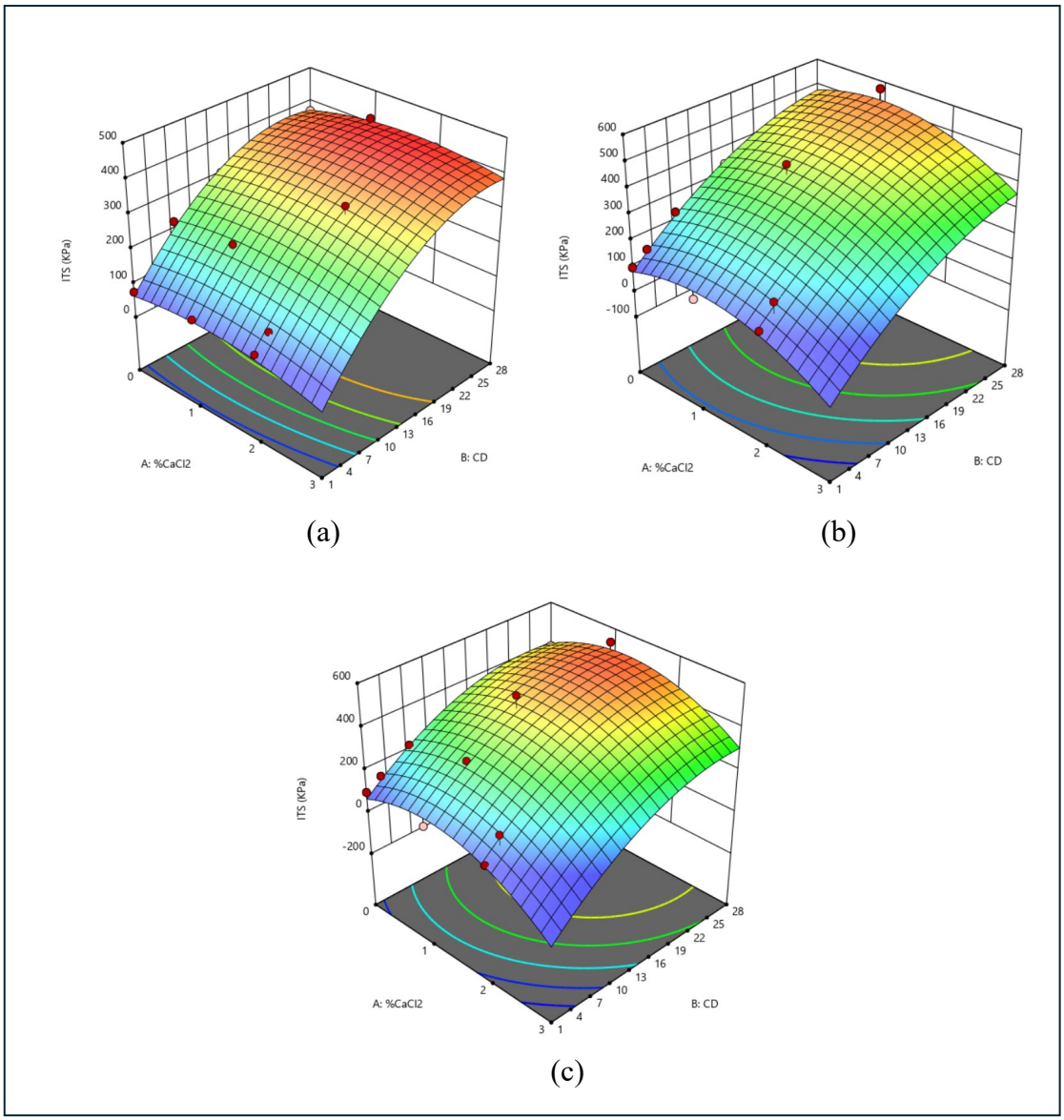


Figure 4.110 3-D Model of ITS Analysis for CA25RAP75 Mix design Consist of (a) 2% OPC + 2% GCBA, (b) 3% OPC + 1% GCBA and (c) 4%OPC with Various Percentages of $CaCl_2$

Figure 4.110 displays the 3-D models for CA25RAP75 mix design. As the percentage of $CaCl_2$ increased, the model with 2% OPC + 2% GCBA showed a slight rise in ITS. Over the curing period, the 3-D surface plot indicated moderate ITS values, suggesting a balanced interaction between OPC and GCBA. A similar trend was observed in models with 3% OPC + 1% GCBA, as well as in those with 4% OPC, where the ITS began to decline at a $CaCl_2$ content of 2%. However, surface plots for these models demonstrated a significant positive interaction between OPC, GCBA, and $CaCl_2$.

The 3-D models for all CA-RAP compositions show that the ITS values consistently increased as the $CaCl_2$ content rose to 1%, indicating that $CaCl_2$ significantly improved tensile strength. However, when the $CaCl_2$ content became excessive, there was a decline in ITS. The model containing 4% OPC consistently exhibited the highest ITS values, suggesting that a higher OPC content enhances tensile strength. Conversely, mixes with 1% GCBA also demonstrated higher ITS values compared to those with 2% GCBA, indicating that small amounts of GCBA positively influence tensile strength.

Moreover, steeper surfaces suggested that the interaction between these factors has a more pronounced effect on the response (Chen et al., 2025). In this case, higher OPC content reflected a stronger interaction between GCBA and $CaCl_2$, which led to significant improvements in tensile strength.

4.5.2.5 Predictive Versus Actual Analysis of ITS

Figures 4.111 to 4.113 exhibit the predictive versus actual for ITS analysis obtained from the RSM for all three different CA-RAP mixes.

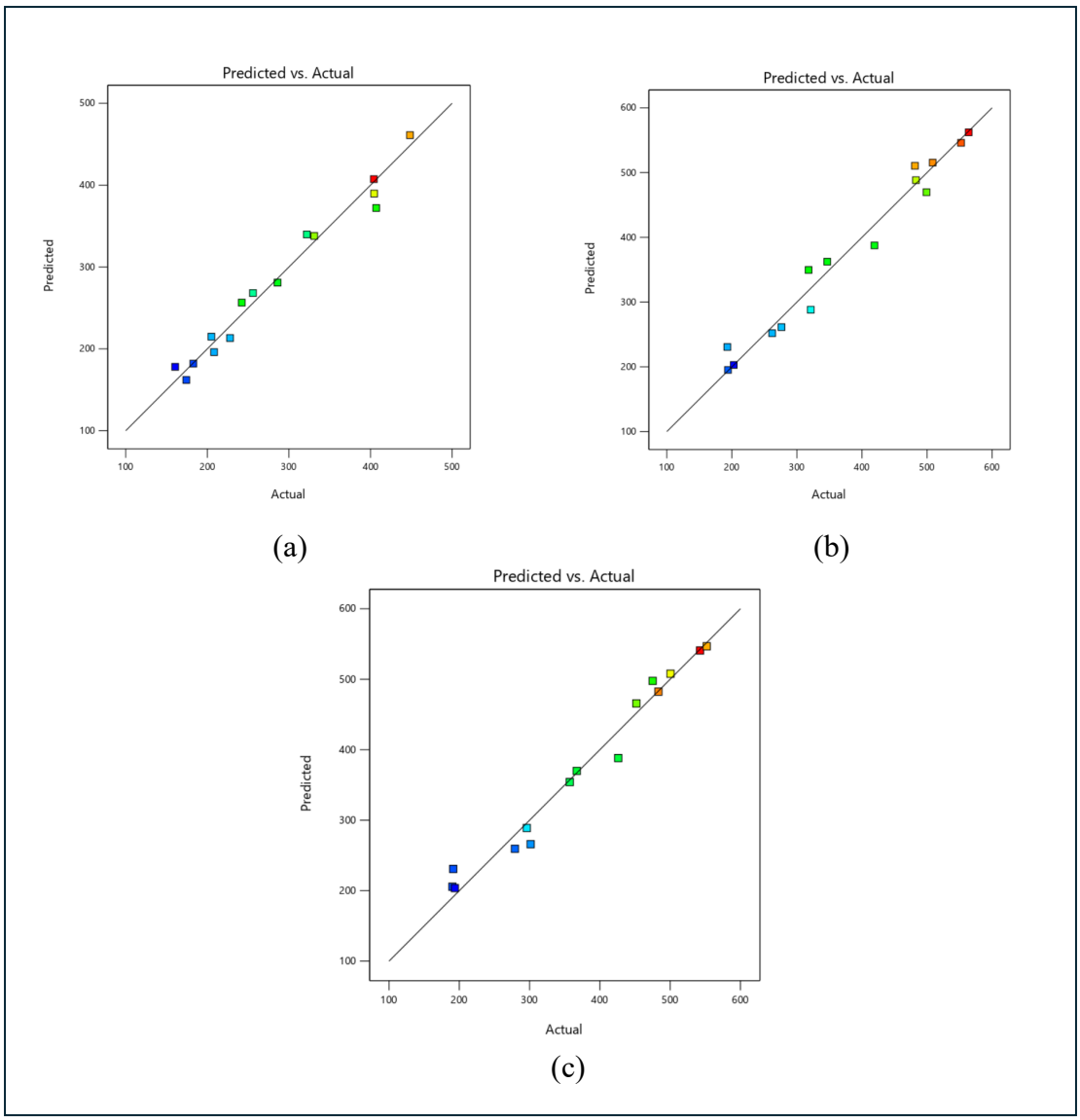


Figure 4.111 Predictive Versus Actual Graph of ITS Analysis for CA75RAP25 Mix Design Consist of (a) 2% OPC + 2% GCBA, (b) 3% OPC + 1% GCBA and (c) 4% OPC with Various Percentages of $CaCl_2$

The mix shown in Figure 4.111 presented the graph for the CA75RAP25 mix design. Among the three mixes analyzed, the performance at 4% OPC with varying percentages of $CaCl_2$ was the most accurate, with data points closely aligning with the predictive line. The reliability of the model appeared to improve with increased OPC content and the absence of GCBA.

A mix containing 2% OPC + 2% GCBA also demonstrated a strong linear relationship, exhibiting good predictive accuracy. The distribution of data points along the line showed some slight deviations, particularly at lower values of ITS, which further confirmed the reliability of the model for this mix.

In a mix of 3% OPC + 1% GCBA, the graph displayed a strong linear trend, showing slightly higher accuracy compared to the 2% OPC + 2% GCBA mix. The increase in OPC content enhanced the predictive capability of the model. The minimal deviation of the data points along the line reaffirmed the reliability of the model for this mix.

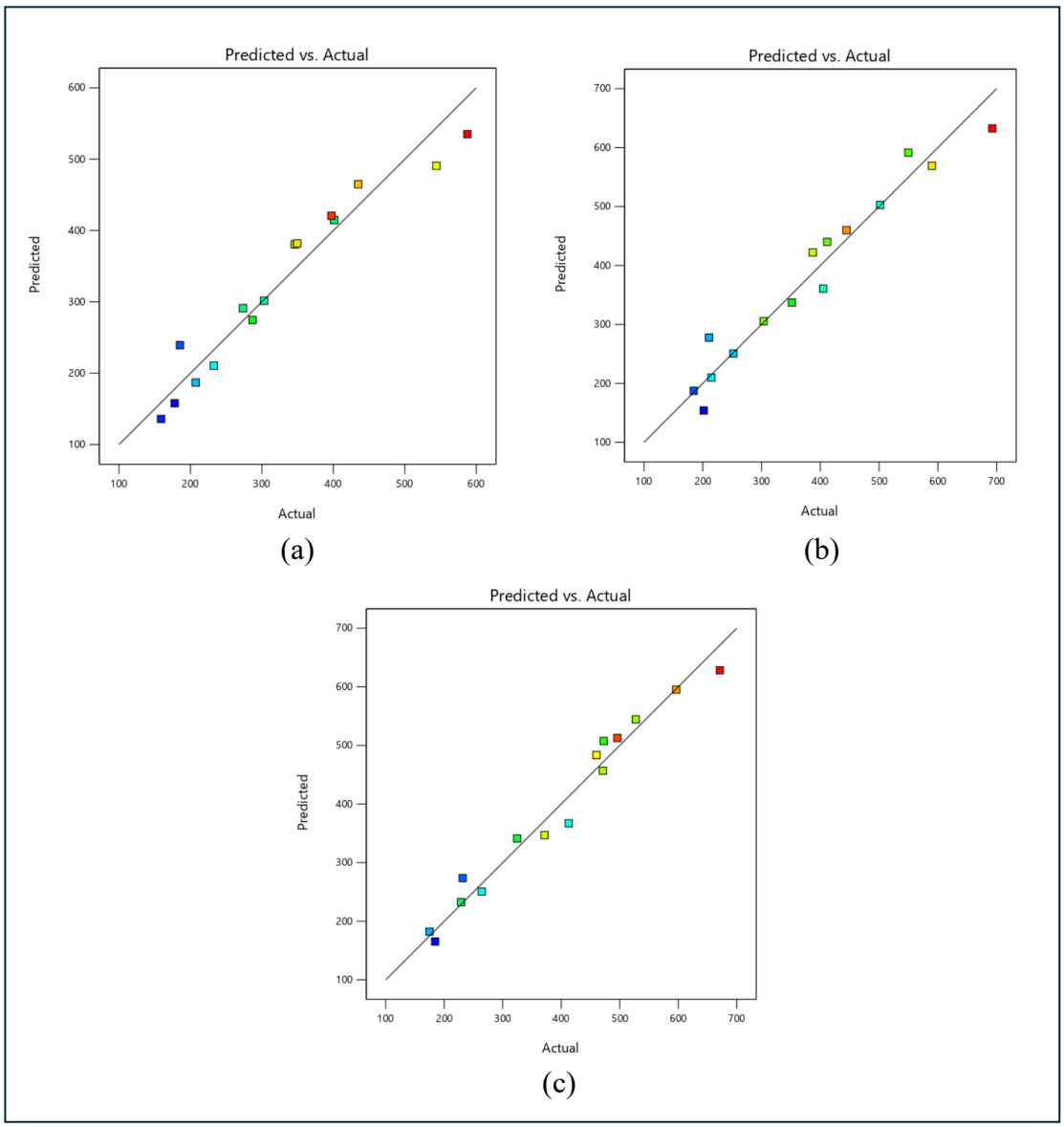


Figure 4.112 Predictive Versus Actual Graph of ITS Analysis for CA50RAP50 Mix Design Consist of (a) 2% OPC + 2% GCBA, (b) 3% OPC + 1% GCBA and (c) 4% OPC with Various Percentages of $CaCl_2$

Figure 4.112 presents a graph for the CA50RAP50 mix design. The highest accuracy was observed with 4% OPC combined with various percentages of $CaCl_2$, similar to the CA75RAP25 mixes. In this mix, the data points were clustered closely along the predicted line, indicating minimal deviation.

The 3% OPC + 1% GCBA mix also demonstrated improved accuracy with a higher OPC content, as shown by the closer alignment of the data points to the predicted line.

The mix with 2% OPC + 2% GCBA, on the other hand, exhibited a wider spread of data points, suggesting greater variability in predictions. Nevertheless, the predictions for this mix remained highly accurate.

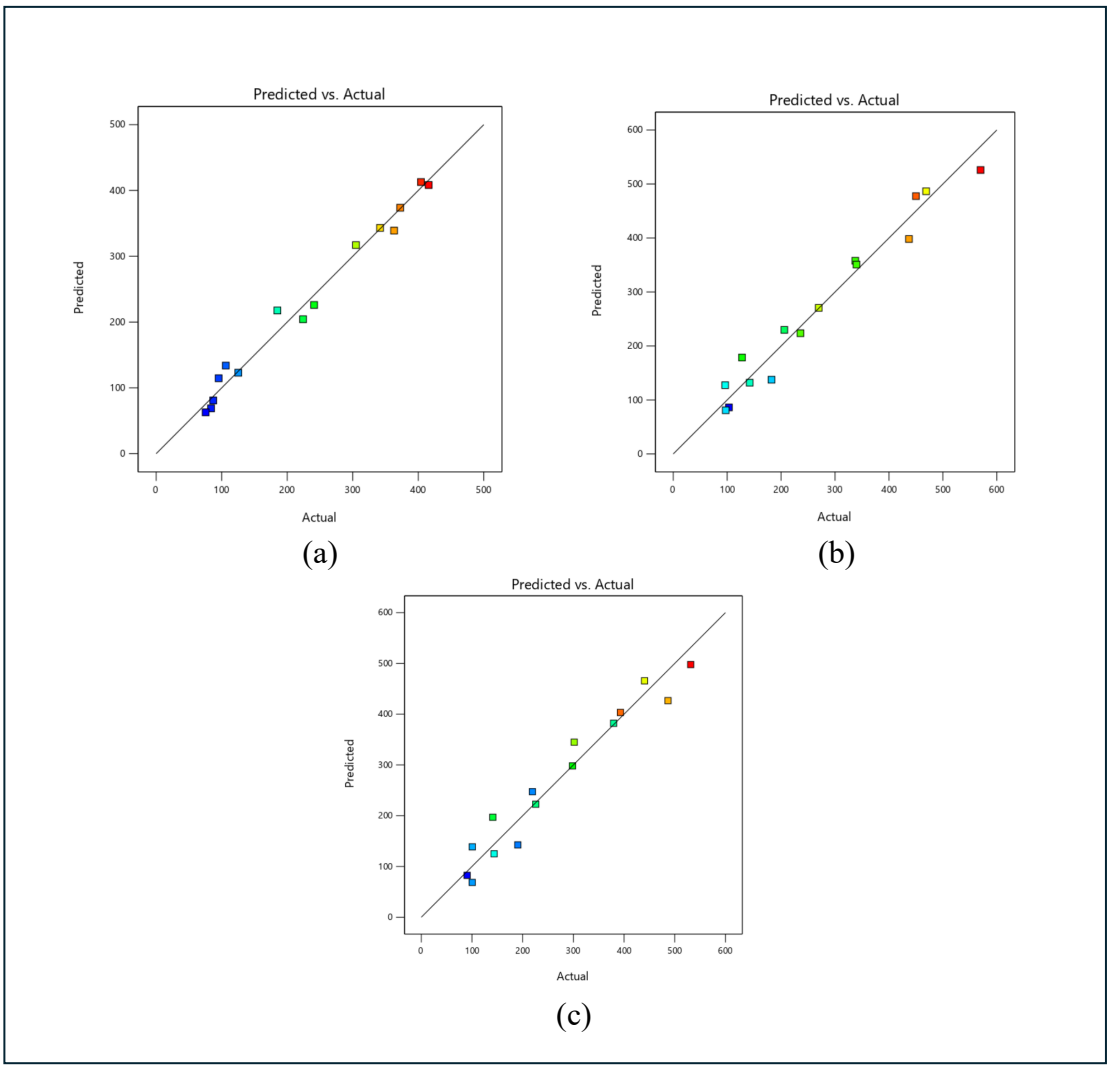


Figure 4.113 Predictive Versus Actual Graph of ITS Analysis for CA25RAP75 Mix Design Consist of (a) 2% OPC + 2% GCBA, (b) 3% OPC + 1% GCBA and (c) 4% OPC with Various Percentages of $CaCl_2$

Figure 4.113 presents the graph for the CA25RAP75 mix. Among these, the 4% OPC mix with varying percentages of $CaCl_2$ exhibited the highest accuracy, with data points closely clustered along the predicted line, indicating a highly precise model.

A similar trend was observed for the 3% OPC + 1% GCBA mix, which also displayed high predictive accuracy with minimal deviation from the line.

In contrast, the 2% OPC + 2% GCBA mix showed a slightly wider spread compared to the other mixes, suggesting that a higher GCBA content may contribute to this variability. Nevertheless, the predictions remained highly accurate despite this variability.

The analysis of all figures revealed a linear trend, indicating that the actual values closely corresponded to the predicted values. According to Aliyegbenoma et al. (2020), the clustering of data points along the 45° diagonal line demonstrates minimal deviation between experimental and predicted values, confirming that the model provided an optimal fit. This indicated that the models developed using RSM in this study were highly effective in predicting ITS for different CA-RAP mixes.

4.5.3 Resilient Modulus Model

In the ANOVA analysis for M_R, the *p*-values for all models were significantly below the 0.05 threshold, indicating their statistical significance. This suggested that variations in the components (OPC, GCBA, $CaCl_2$, and curing days) reliably contributed to variations in M_R.

Tables 4.32 to 4.34 present the ANOVA results for resilient modulus derived using RSM across the three CA-RAP mix designs, while Equations 4.19 to 4.28 detail the corresponding predictive models for each mix.

4.5.3.1 CA75RAP25 Mix Design

The analysis conducted on CA75RAP25 mix design, as presented in Table 4.32, revealed that all tested mix combinations had a significant impact on the M_R, with *p*-values less than 0.0001. The *F*-values ranged from 38.91 to 94.77, with 3% OPC + 1% GCBA composition yielded the highest F-value of 94.77 and a mean square of 1.925×10^7, demonstrating its substantial influence on the variation of the M_R. The mix consisting of 2% OPC + 2% GCBA followed a linear model, indicating a direct relationship between the input factors and the M_R response. In contrast, the compositions with 3% OPC + 1% GCBA, as well as 4% OPC + 0% GCBA, were better represented by quadratic models, suggesting nonlinear interactions among the factors affecting M_R.

Table 4.32
ANOVA Results for M_R - CA75RAP25 Mix

factors			Sum of squares	df	Mean square	*F*-value	*p*-value	Model type
OPC (%)	GCBA (%)	$CaCl_2$ (%)						
2	2	0,1,2	7.847E+07	2	3.924E+07	38.91	<0.0001	Linear
3	1	0,1,2	9.627E+07	5	1.925E+07	94.77	<0.0001	Quadratic
4	0	0,1,2	1.173E+08	5	2.346E+07	84.26	<0.0001	Quadratic

The M_R prediction models for this mix are presented in Equations (4.19 - 4.21)

- Equation (4.19): 2% OPC + 2% GCBA
  $$M_R = 4972.5247 - 262.85A + 233.0956B$$

- Equation (4.20): 3% OPC + 1% GCBA
  $$M_R = 4366.9107 + 1769.2050A + 577.6710B - 17.7724AB - 810.5833A^2 - 10.7460B^2$$

- Equation (4.21): 4% OPC + 0% GCBA
  $$M_R = 4464.1224 + 1936.9455A + 581.6155B - 20.6788AB - 851.9833A^2 - 9.7591B^2$$

Where:
A: $CaCl_2$ content (%)
B: Curing duration (days)

4.5.3.2 CA50RAP50 Mix Design

In the CA50RAP50 mix design, as presented in Table 4.33, all three mix compositions exhibited a *p*-value below 0.001, indicating a significant effect on M_R. Each mix composition followed a quadratic model, which suggested the presence of nonlinear interactions between the stabilizing agent and the M_R response. The *F*-values ranged from 15.05 to 26.45, confirming that variations in mixed dosages resulted in changes in M_R strength. Among the three compositions, the mix containing 2% OPC + 2% GCBA demonstrated the highest *F*-value (26.45) and mean square value (1.012×10^7), indicating the strongest influence on M_R performance.

Table 4.33
ANOVA Results for M_R - CA50RAP50 Mix

factors			Sum of squares	df	Mean square	*F*-value	*p*-value	Model type
OPC (%)	GCBA (%)	$CaCl_2$ (%)						
2	2	0,1,2	5.060E+07	5	1.012E+07	26.45	<0.0001	Quadratic
3	1	0,1,2	8.122E+07	5	1.869E+07	18.27	0.0002	Quadratic
4	0	0,1,2	7.241E+07	5	1.448E+07	15.05	0.0004	Quadratic

The M_R prediction models for this mix are presented in Equations (4.22 - 4.24)

- Equation (4.22): 2% OPC + 2% GCBA
  $$M_R = 3658.7300 + 1567.0323A + 385.9021B - 20.8456AB - 859.2673A^2 - 6.50622B^2$$

- Equation (4.23): 3% OPC + 1% GCBA
  $$M_R = 4655.4464 + 3396.5570A + 504.2786B - 47.9110AB - 1830.0333A^2 - 8.7832B^2$$

- Equation (4.24): 4% OPC + 0% GCBA
  $$M_R = 5176.4709 + 1891.9702A + 558.1104B - 36.6056AB - 1113.2833A^2 - 11.2352B^2$$

Where:
A: $CaCl_2$ content (%)
B: Curing duration (days)

4.5.3.3 CA25RAP75 Mix Design

Table 4.34 provides a summary of the statistical analysis for the CA25RAP75 mix design. The results indicated that all three mixes had a significant impact on the M_R, with *p*-values less than 0.0001. The *F*-values ranged from 32.68 to 53.67, which highlighted the strong influence of the mix compositions on the mechanical behavior of the mix design. All of the mixes displayed a quadratic model. This indicated that their interactions were more complex and nonlinear. Among the three compositions, the mix with 4% OPC + 0% GCBA achieved the highest *F*-value of 53.67 and a mean square of 9.623×10^6. This demonstrated its significant effect on enhancing M_R.

Table 4.34
ANOVA Results for M_R - CA25RAP75 Mix

factors			Sum of squares	df	Mean square	*F*-value	*p*-value	Model type
OPC (%)	GCBA (%)	$CaCl_2$ (%)						
2	2	0,1,2	2.994E+07	5	5.888E+06	39.21	<0.0001	Quadratic
3	1	0,1,2	4.228E+07	5	8.455E+06	32.68	<0.0001	Quadratic
4	0	0,1,2	4.812E+07	5	9.623E+06	53.67	<0.0001	Quadratic

The M_R prediction models for this mix are presented in Equations (4.25 - 4.27)

- Equation (4.25): 2% OPC + 2% GCBA

$$M_R = 2885.7565 + 2821.7826A + 245.4354B - 7.4055AB - 1436.9833A^2 - 3.9580B^2$$

- Equation (4.26): 3% OPC + 1% GCBA

$$M_R = 4383.5252 + 2202.3279A + 328.6567B + 3.7127AB - 1331.6166A^2 - 6.2440B^2$$

- Equation (4.27): 4% OPC + 0% GCBA

$$M_R = 4819.3681 + 2048.7565A + 267.1912B - 2.9392AB - 1313.6666A^2 - 3.4618B^2$$

Where:
A: $CaCl_2$ content (%)
B: Curing duration (days)

The ANOVA performed on three levels of CA-RAP content revealed that the combination of OPC, GCBA, and $CaCl_2$ significantly impacted the M_R of the proposed mix design. Quadratic models were found to best represent the trends, especially in mixes with higher OPC dosages of 3% and 4%. This indicated the presence of nonlinear interactions among OPC, GCBA, and $CaCl_2$.

In contrast, the 2% OPC + 2% GCBA in CA75RAP25 mix compositions exhibited a linear model, suggesting that at lower OPC content, the M_R response was more directly correlated with the levels of the additives.

4.5.3.4 3-D Model of M_R Analysis

Figures 4.114 to 4.116 exhibit the 3-D models of resilient modulus analysis obtained from the RSM for all three different CA-RAP mixes. The models illustrated the relationship between M_R and varying compositions of OPC, GCBA and $CaCl_2$.

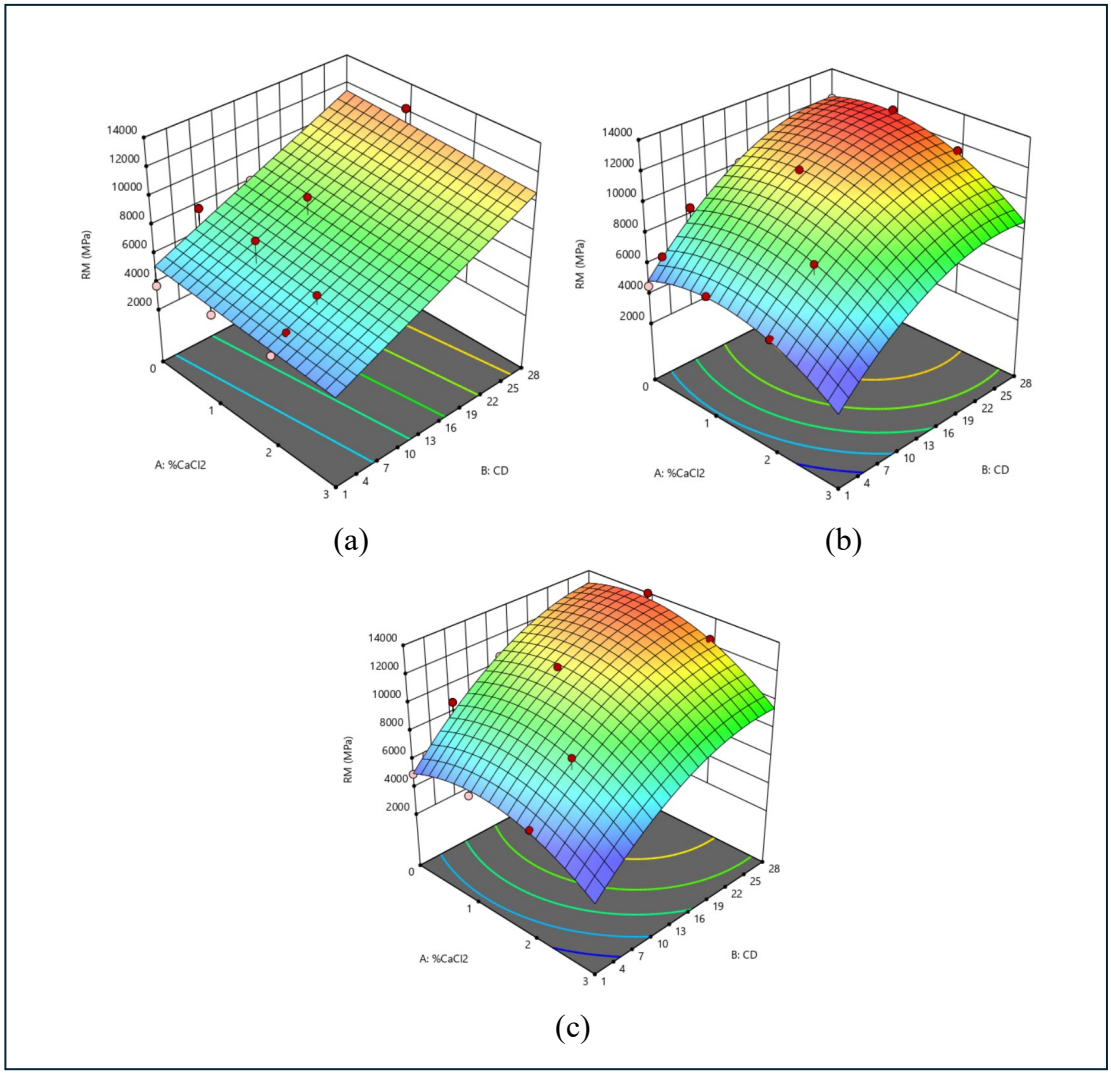


Figure 4.114 3-D Model of M_R Analysis for CA75RAP25 Mix Design Consist of (a) 2% OPC + 2% GCBA, (b) 3% OPC + 1% GCBA and (c) 4% OPC with Various Percentages of $CaCl_2$

The 3-D models for the CA75RAP25 mix design are shown in Figure 4.114. The analysis indicated that $CaCl_2$ had a significant impact on the M_R for the mixes containing 2% OPC + 2% GCBA at various percentages of $CaCl_2$. The surface plot revealed that as the $CaCl_2$ content increased, the M_R also increased, demonstrating that $CaCl_2$ plays a crucial role in enhancing the modulus.

In the model with 3% OPC + 1% GCBA, a higher M_R was observed when both the OPC content and $CaCl_2$ levels were increased. Among all the mixes, the mix with 4% OPC exhibited the highest M_R out of the three compositions. The presence of higher OPC content, along with $CaCl_2$, significantly influenced the M_R, highlighting the importance of OPC in enhancing the mechanical properties.

However, it is important to note that a high percentage of $CaCl_2$ (greater than 2%) negatively affected the mix, reducing the modulus across all models.

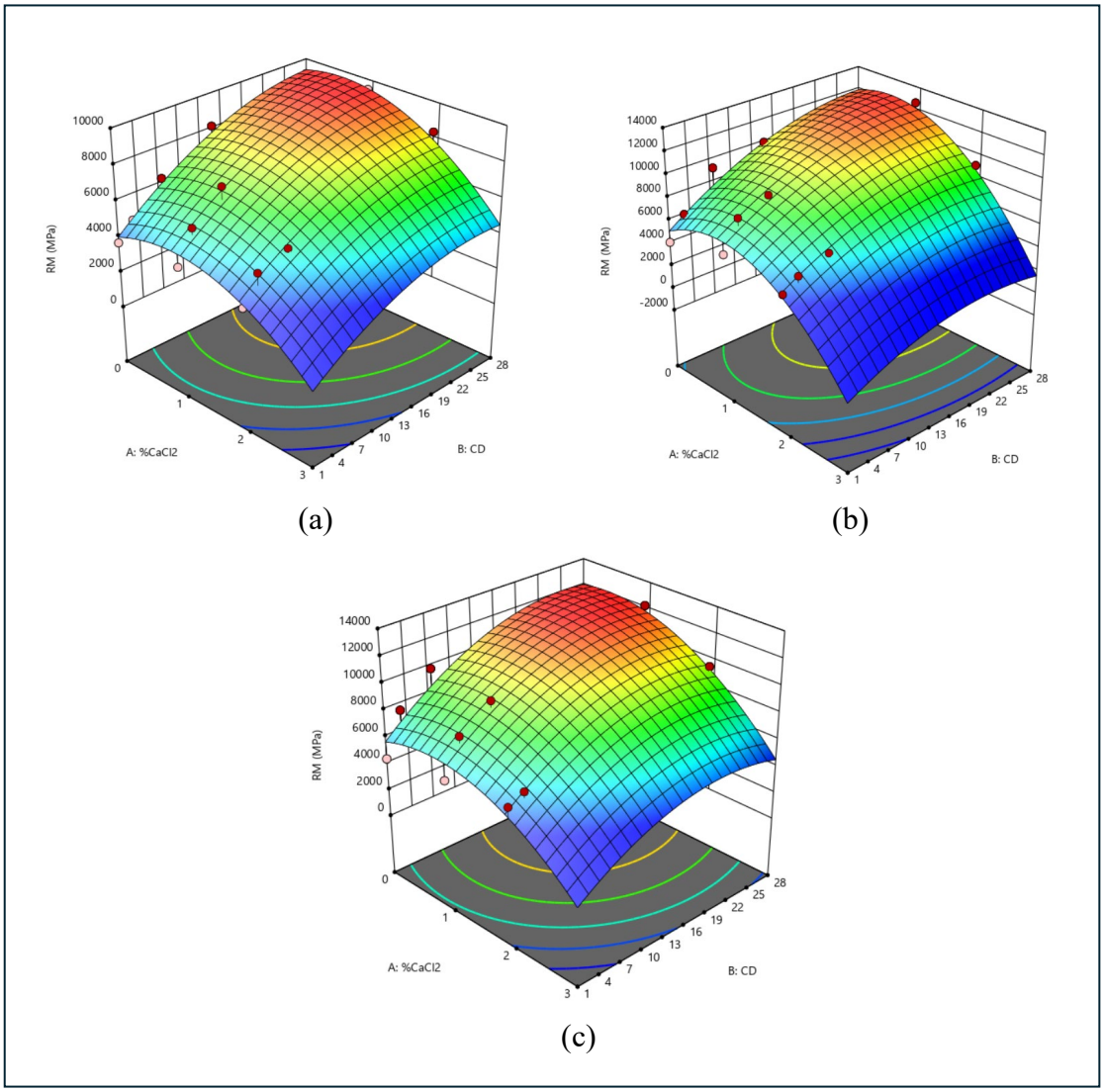


Figure 4.115 3-D Model of M_R Analysis for CA50RAP50 Mix Design Consist of (a) 2% OPC + 2% GCBA, (b) 3% OPC + 1% GCBA and (c) 4% OPC with Various Percentages of $CaCl_2$

Figure 4.115 illustrates the 3-D model for the CA50RAP50 mix design. Across all mix compositions, the inclusion of $CaCl_2$ consistently improved the modulus, consistent with the findings from the CA75RAP25 model. Higher percentages of $CaCl_2$ were linked to an increase in M_R, as demonstrated by the smoothness of the surface plot. The plot also indicated an interaction between OPC and $CaCl_2$ when higher levels of OPC were added alongside $CaCl_2$, as there was a significant increase in M_R. However, the M_R began to decrease when the $CaCl_2$ content reached 2%.

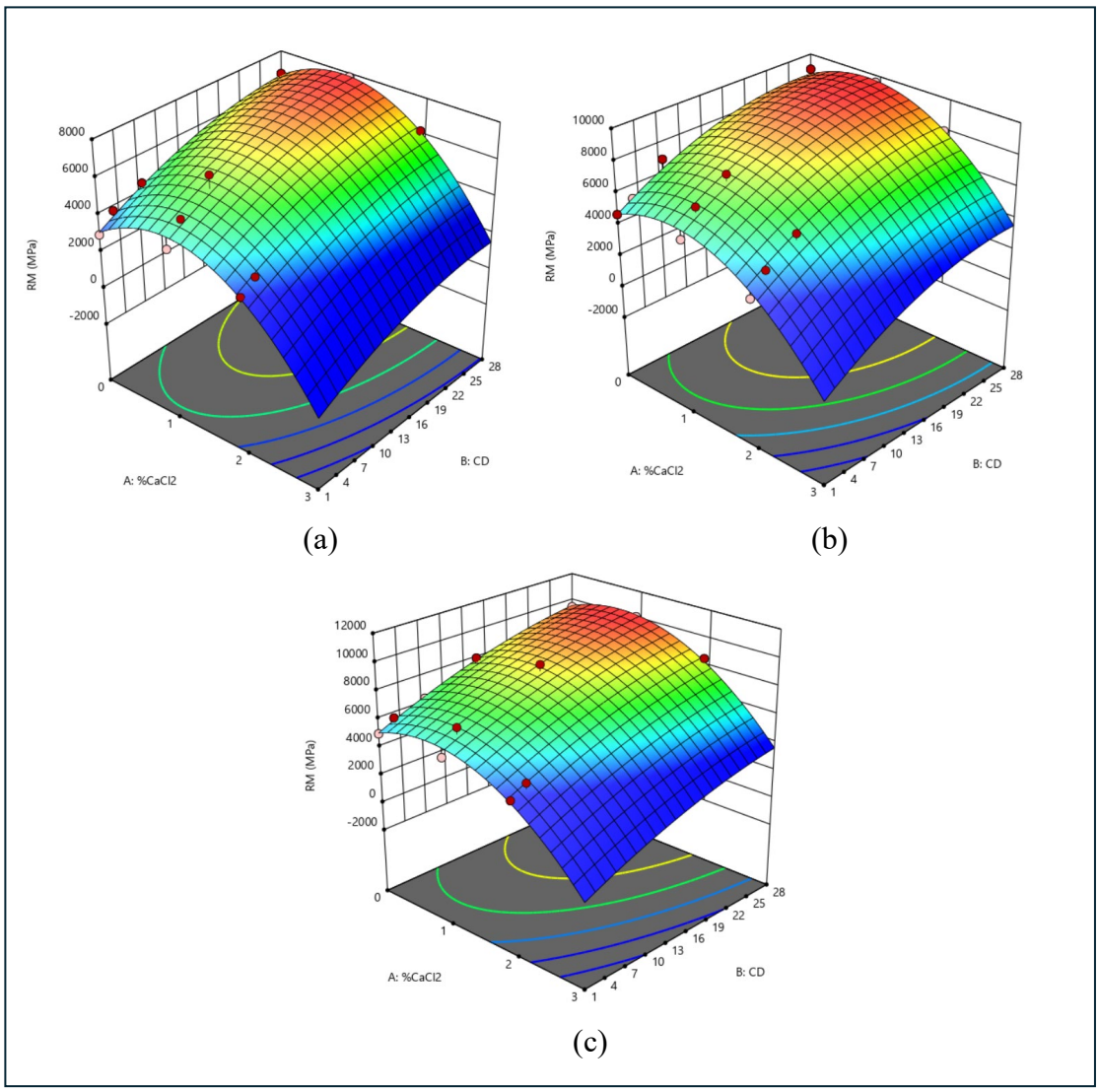


Figure 4.116 3-D Model of M_R Analysis for CA25RA75 Mix Design Consist of (a) 2% OPC + 2% GCBA, (b) 3% OPC + 1% GCBA and (c) 4% OPC with Various Percentages of $CaCl_2$

Figure 4.116 presents the 3-D model for the CA25RAP75 mix design. Consistent with previous mixes, the model with 2% OPC + 2% GCBA demonstrated a significant increase in M_R with slightly higher amounts of $CaCl_2$. The surface plot indicated that, despite the lower OPC content, $CaCl_2$ played a crucial role in enhancing the modulus. However, a decrease in M_R was observed when $CaCl_2$ content exceeded 2%. This decreasing trend was also apparent in the mixes containing 3% OPC + 1% GCBA, as well as in those with 4% OPC.

Overall, the 3-D models consistently showed that increasing the OPC content led to higher M_R across all mix designs. This trend highlighted the important role of OPC in enhancing the resilient modulus, as it facilitated the formation of C-S-H and other binding compounds, which strengthened the mechanical properties of the mix.

Additionally, $CaCl_2$ consistently had a positive effect on M_R across all compositions. Its role in accelerating the hydration process and improving the early strength of the mix was clearly demonstrated by the 3-D models. The inclusion of $CaCl_2$ enhanced the formation of C-S-H and other binding compounds (Liu and Wu, 2025), resulting in higher M_R. However, it is important to note that excessive amounts of $CaCl_2$ were detrimental to the mix.

In contrast, the varying percentages of GCBA in the mixes had different effects on M_R. While GCBA contributed to the overall performance of the mix, it was most effective at lower contents, and its influence on M_R was less pronounced compared to that of OPC and $CaCl_2$. Nonetheless, its presence was essential for achieving a balanced set of properties in the mix.

The interaction between OPC, GCBA, and $CaCl_2$ was crucial for optimizing the M_R of CA-RAP mixes. The 3-D models illustrated that the combined effects of these components led to substantial improvements in mechanical properties, with OPC and $CaCl_2$ having the greatest influence.

4.5.3.5 Predictive Versus Actual Analysis of M_R

Figures 4.117 to 4.119 exhibit the predictive versus actual of resilient modulus analysis obtained from the RSM for all three different CA-RAP mixes.

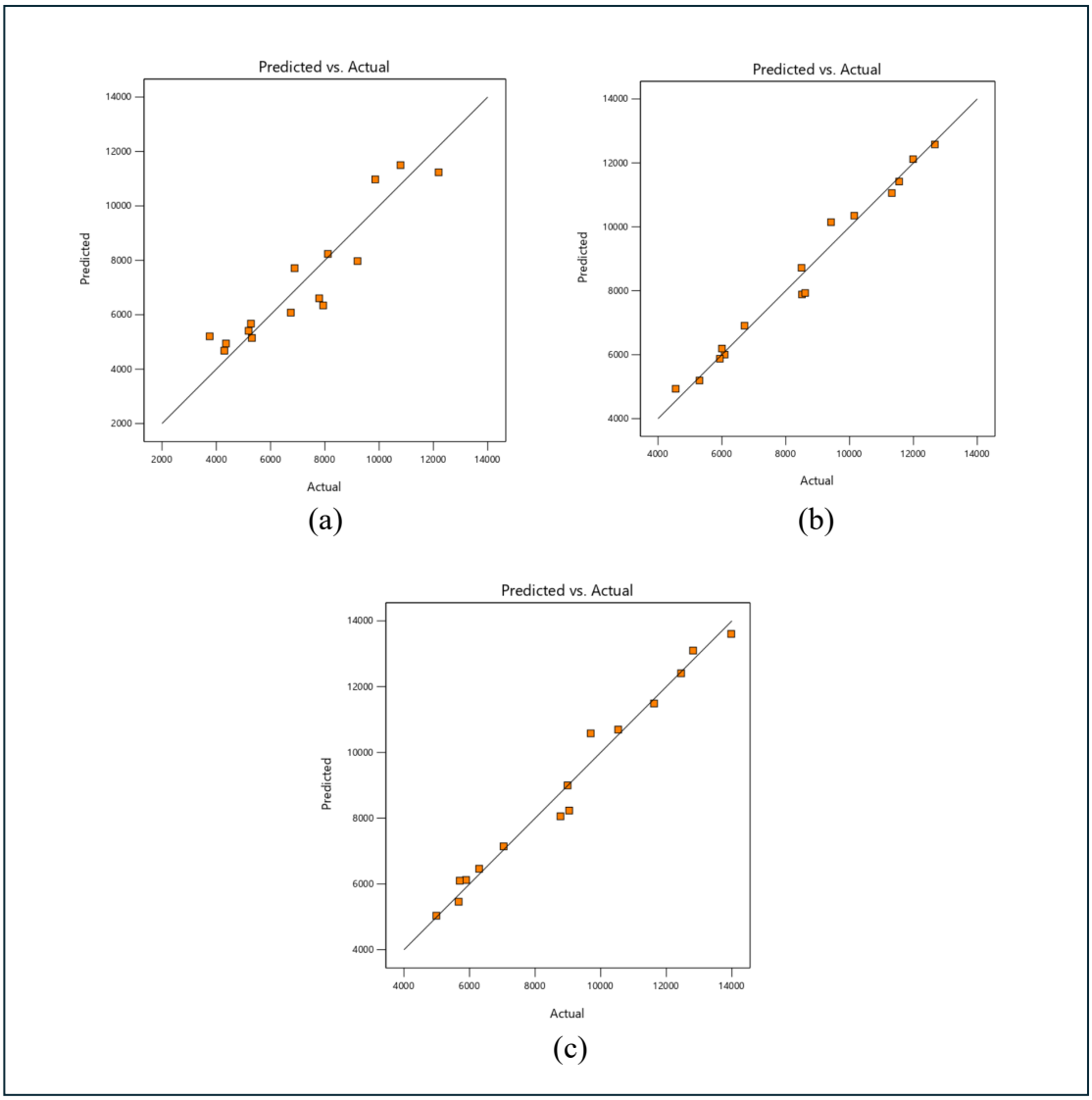


Figure 4.117 Predictive Versus Actual Graph of M_R Analysis for CA75RAP25 Mix Design Consist of (a) 2% OPC + 2% GCBA, (b) 3% OPC + 1% GCBA and (c) 4% OPC with Various Percentages of $CaCl_2$

Figure 4.117 illustrates the M_R analysis of CA75RAP25 mix design, comparing predicted values to actual values. The graph showed that the data points for all three mixes closely align with the line of equality, indicating a strong correlation between the predicted and actual M_R values.

The 3% OPC + 1% GCBA mix exhibits the closest fit to this line, suggesting that it has the highest predictive accuracy among the three compositions.

The 4% OPC mix followed closely behind, showing improved alignment with the line of equality and indicating better model accuracy.

In contrast, the 2% OPC + 2% GCBA mix displayed some data points that deviated slightly from the line, suggesting minor discrepancies in its predictions.

Overall, the analysis demonstrated that all models accurately predicted M_R in the CA75RAP25 mixes, particularly when the OPC content was higher.

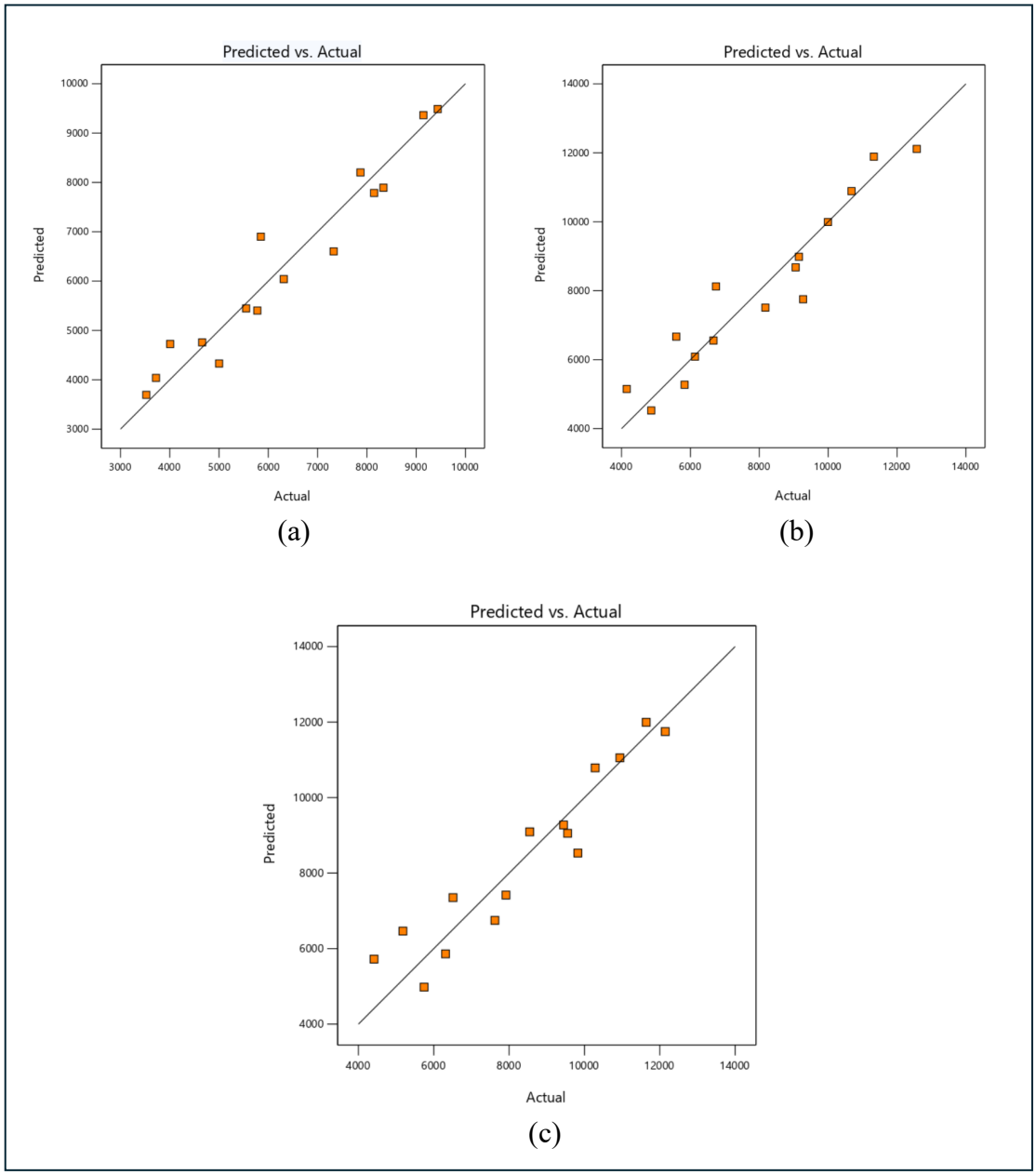


Figure 4.118 Predictive Versus Actual Graph of M_R Analysis for CA50RAP50 Mix Design Consist of (a) 2% OPC + 2% GCBA, (b) 3% OPC + 1% GCBA and (c) 4% OPC with Various Percentages of $CaCl_2$

Figure 4.118 illustrates the M_R analysis for the CA50RAP50 mix design. This graph indicates that the mix containing 3% OPC + 1% GCBA combined with various percentages of $CaCl_2$ shows the closest alignment with the line of equality, signifying the best predictive performance.

Similarly, the 4% OPC mix also aligned closely with the line, suggesting a high level of predictive accuracy.

Conversely, the mix containing 2% OPC + 2% GCBA demonstrated some deviation from the line, indicating slightly reduced predictive accuracy for this specific formulation.

Overall, the predictive model for M_R analysis in the CA50RAP50 mix was highly accurate, particularly for higher OPC content. The minor deviations observed in the lower OPC mixes highlighted potential areas for further refinement within the model.

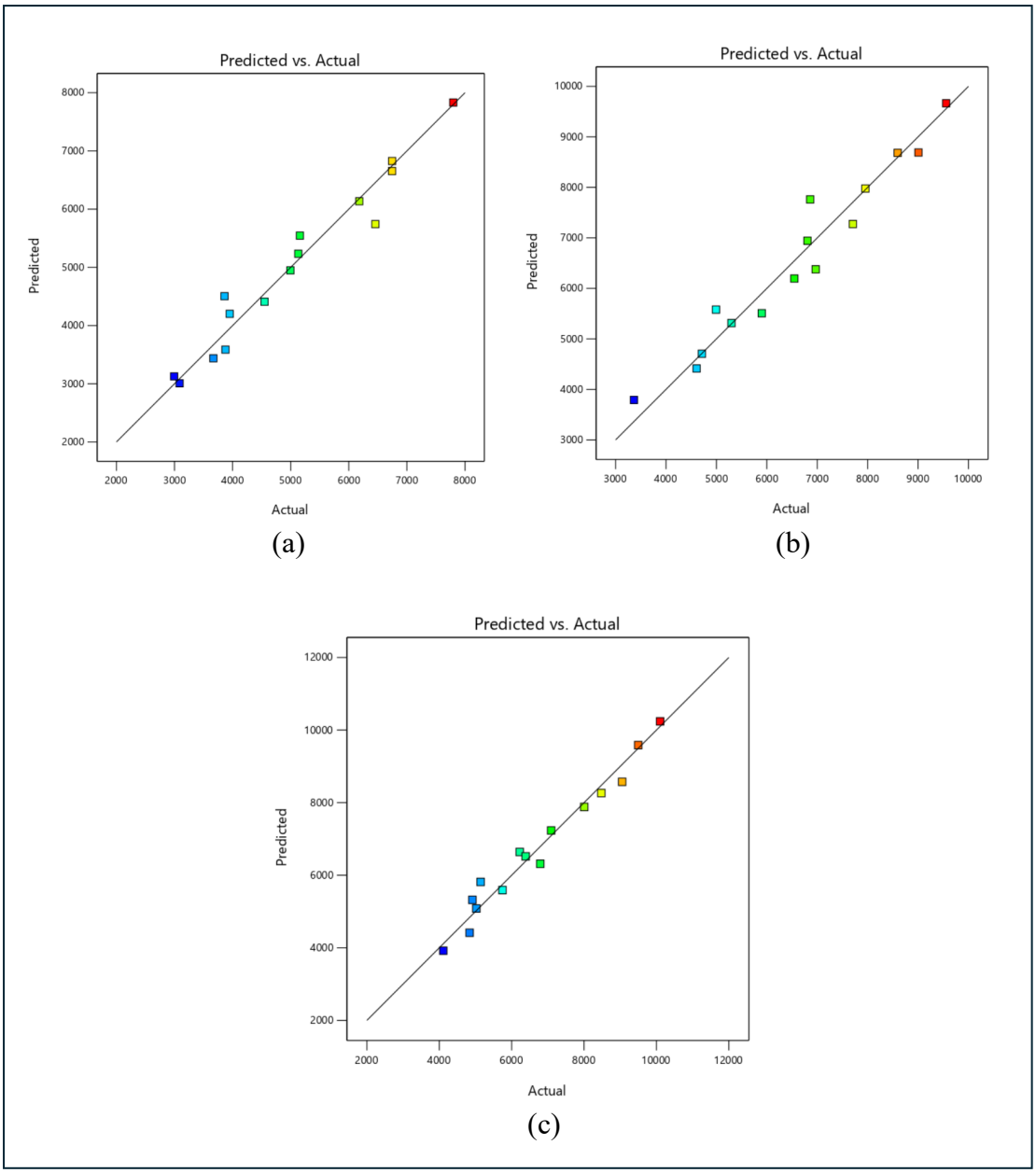


Figure 4.119 Predictive Versus Actual Graph of M_R Analysis for CA25RAP75 Mix Design Consist of (a) 2% OPC + 2% GCBA, (b) 3% OPC + 1% GCBA and (c) 4% OPC with Various Percentages of $CaCl_2$

Figure 4.119 illustrates the mix design for CA25RAP75, continuing to show a similar pattern. The data points across all three graphs closely follow the line of equality, indicating a high level of accuracy in the predictive model. In the mix containing 2% OPC + 2% GCBA with various percentages of $CaCl_2$, the data points generally aligned with the line of equality, although some deviations were observed at lower M_R. This indicated a slightly lower predictive accuracy for this mix.

On the other hand, the mix with 3% OPC + 1% GCBA demonstrated improved predictive accuracy, with most data points closely aligned with the line of equality. This suggested a better correlation between the predicted and actual M_R.

The best alignment was observed in the mix with 4% OPC, confirming that a higher OPC content enhances the accuracy of the model.

Overall, predictive versus actual graphs consistently demonstrated the high accuracy of the predictive models used in the RSM to analyze resilient modulus across all mix design compositions. The effectiveness of the model was validated by the strong correlation between predicted and actual values, which is further supported by the clustering of data points along the 45° diagonal line, indicating minimal deviation between experimental and predicted values, as noted by Aliyegbenoma et al. (2020).

4.5.4 Mix Design Optimization Using Regression Analysis

The optimization of the mix design in this research was guided by regression analysis of statistical metrics, including R^2, adjusted R^2, and predicted R^2 in RSM. These metrics were important in identifying the optimal composition by explaining variance in response variables, accounting for predictor influence, and ensuring strong predictive accuracy. Bahri et al. (2018) used the coefficient of determination (R^2) to evaluate the performance of the model, where high R^2 values indicated a strong fit between the predicted responses and the experimental data. Similar optimization framework was demonstrated in the work of Rocha et al. (2023) and Ahmad et al. (2020).

The objective was to determine the optimal combination of OPC, GCBA, and $CaCl_2$ to enhance the desired properties of the mixes. The optimization process prioritized reliability, emphasizing performance consistency rather than solely selecting the mix with the highest strength. As a result, the optimized formulation was determined within a specific range of material percentages, rather than a single fixed mix ratio, to allow for greater flexibility and adaptability in field applications. This approach ensured practical applicability under real-world conditions. The following tables in the next sections present the regression analysis results for the different strength performance assessments conducted using RSM.

4.5.4.1 Unconfined Compressive Strength

The UCS optimization for CA-RAP mixes aimed to evaluate the influence of OPC, GCBA, and $CaCl_2$ on compressive strength development during the initial curing phase while considering model reliability (Predicted R^2) to ensure consistency in strength performance.

Tables 4.35 to 4.37 present the statistical fit analysis of the UCS model for three CA-RAP mix compositions incorporating stabilizing agent.

For the CA75RAP25 mixes, as shown in Table 4.35, the highest mean UCS recorded was 4.08 MPa at 4% OPC with 0-2% $CaCl_2$. The most reliable prediction was achieved at 3% OPC + 1% GCBA with 0-2% $CaCl_2$, with a Predicted R^2 of 0.7568. These results suggested that although a higher cement content improved early UCS, slightly reducing the OPC dosage and incorporating a small amount of GCBA enhanced model predictability. The optimized mix was identified within the range of 3-4% OPC, 0-1% GCBA, and 0-2% $CaCl_2$, where $CaCl_2$, particularly at 1-2%, promoted faster setting and early stiffness development without compromising performance consistency.

Table 4.35
Fit Statistic of CA75RAP25 Mix for UCS Test

Factors			Std. Dev.	Mean	R^2	Adjusted R^2	Predicted R^2
OPC (%)	GCBA (%)	$CaCl_2$ (%)					
2	2	0,1,2	0.3956	3.16	0.8193	0.7188	0.5839
3	1	0,1,2	0.2835	4.02	0.8362	0.8089	0.7568
4	0	0,1,2	0.2885	4.08	0.7979	0.7642	0.6809

Similarly, in Table 4.36, the CA50RAP50 mixes achieved its peak mean UCS of 4.49 MPa at 4% OPC with 0-2% $CaCl_2$, which also recorded the highest Predicted R^2 value of 0.8457. These results suggested that the combination of 4% OPC with 1-2% $CaCl_2$ was the most effective for compressive strength and rapid load-bearing development. The inclusion of $CaCl_2$ likely facilitated a more stable and accelerated hydration process, which aligned well with predicted performance of the model.

Table 4.36
Fit Statistic of CA50RAP50 Mix for UCS Test

Factors			Std. Dev.	Mean	R^2	Adjusted R^2	Predicted R^2
OPC (%)	GCBA (%)	$CaCl_2$ (%)					
2	2	0,1,2	0.2144	3.67	0.8827	0.8361	0.8226
3	1	0,1,2	0.2789	4.30	0.9097	0.8595	0.6157
4	0	0,1,2	0.2019	4.49	0.9226	0.9097	0.8457

Meanwhile, the CA25RAP75 mixes as shown in Table 4.37, recorded a mean UCS of 4.13 MPa at 4% OPC with 0-2% $CaCl_2$. The highest model reliability was achieved at 2% OPC + 2% GCBA with 0-2% $CaCl_2$, having a Predicted R^2 of 0.9231. This indicated that lower cement content combined with moderate GCBA dosage yielded more consistent results in RAP-rich mixes. The optimized formulation for strength performance was identified within the range of 2-4% OPC, 0-2% GCBA, and 1-2% $CaCl_2$, where $CaCl_2$ contributed to early stiffness development. This range indicated that the CA25RAP75 mix maintained reliable strength and consistency across various compositions within these limits, providing flexibility for field application without compromising overall performance.

Table 4.37
Fit Statistic of CA25RAP75 Mix for UCS Test

Factors			Std. Dev.	Mean	R^2	Adjusted R^2	Predicted R^2
OPC (%)	GCBA (%)	$CaCl_2$ (%)					
2	2	0,1,2	0.1373	3.50	0.9733	0.9584	0.9231
3	1	0,1,2	0.1858	4.07	0.9291	0.8896	0.7836
4	0	0,1,2	0.1880	4.13	0.9388	0.9049	0.8083

The findings on the UCS demonstrated that higher OPC levels in the range of 3-4% significantly enhanced the performance of UCS, offering improved initial stiffness and faster load-bearing capability during the early curing stages. However, the inclusion of GCBA needed to be carefully controlled, as mixes containing more than 1% GCBA consistently showed reduced strength predictability and introduced greater variability in the performance of the model. Therefore, GCBA was most effective when limited to 1%, where it contributed to performance without compromising consistency.

Additionally, the use of $CaCl_2$ in the range of 1-2% was found to accelerate the hydration process, promoting quicker strength development. Although 2% $CaCl_2$ occasionally led to a slight reduction in strength, the 1-2% range was considered optimal as it generally enhanced early the strength. Among all evaluated compositions, the CA25RAP75 mix demonstrated the highest model predictability (Predicted R^2 = 0.9231) but low mean UCS strength (3.50 MPa), while CA50RAP50 mix offered the most balanced combination of high mean UCS strength (4.49 MPa) and good reliability (Predicted R^2 = 0.8457). Therefore, the formulation of 4% OPC with 1-2% $CaCl_2$ from the CA50RAP50 mix design is considered the most suitable for UCS improvement, particularly in situations requiring both early strength development and consistent performance.

4.5.4.2 Indirect Tensile Strength

The strength optimization of ITS analyzed the effects of OPC, GCBA, and $CaCl_2$ while ensuring a reliable predictive model (Predicted R^2) for consistent short-term performance. Since ITS reflects the ability of the mix to withstand tensile forces, rapid strength development is required to reduce cracking risks and enhance pavement durability.

A detailed statistical fit analysis of the ITS model is shown in Table 4.38 to 4.40 for three different CA-RAP mix compositions, each including stabilizing agent.

For the CA75RAP25 mixes, as tabulated in Table 4.38, the highest mean ITS achieved was 374.80 kPa at OPC 3% + GCBA 1% with $CaCl_2$ 0-2%, while the most reliable prediction, with a Predicted R^2 of 0.9416, was recorded at OPC 4% with $CaCl_2$ 0-2%. This indicated that increasing OPC content led to better tensile performance while reducing GCBA minimized variations in strength. The optimized mix for ITS was obtained at OPC 3-4%, GCBA 0-1%, and $CaCl_2$ 1-2%.

Table 4.38
Fit Statistic of CA75RAP25 Mix for ITS Test

Factors			Std. Dev.	Mean	R^2	Adjusted R^2	Predicted R^2
OPC (%)	GCBA (%)	$CaCl_2$ (%)					
2	2	0,1,2	19.07	284.02	0.9748	0.9608	0.8845
3	1	0,1,2	27.25	374.80	0.9723	0.9569	0.9354
4	0	0,1,2	25.46	373.86	0.9743	0.9601	0.9416

In the CA50RAP50 mixes, as shown in Table 4.39, the peak mean ITS of 392.55 kPa was recorded at 4% OPC with 0-2% $CaCl_2$. This same mix also produced the highest model reliability, with a Predicted R^2 value of 0.8959, indicating strong alignment between the experimental and predicted results. Since this formulation demonstrated both the greatest ITS and the most stable prediction, the combination of 4% OPC with 1-2% $CaCl_2$ was identified as the most effective for enhancing tensile strength while maintaining consistent performance in the CA50RAP50 mix.

Table 4.39
Fit Statistic of CA50RAP50 Mix for ITS Test

Factors			Std. Dev.	Mean	R^2	Adjusted R^2	Predicted R^2
OPC (%)	GCBA (%)	$CaCl_2$ (%)					
2	2	0,1,2	40.42	325.76	0.9379	0.9034	0.7269
3	1	0,1,2	43.45	380.09	0.9501	0.9223	0.7615
4	0	0,1,2	32.83	392.55	0.9706	0.9543	0.8959

In Table 4.40, the highest mean ITS for the CA25RAP75 mixes was 270.91 kPa, recorded at 3% OPC + 1% GCBA with 0-2% $CaCl_2$. Meanwhile, the most reliable prediction was observed at 2% OPC + 2% GCBA with 0-2% $CaCl_2$, which achieved a Predicted R^2 value of 0.9563, indicating strong model accuracy. These results suggested that although a lower OPC content and higher GCBA dosage improved the predictability of the model, a slightly higher cement dosage contributed more significantly to tensile strength development. Therefore, the optimized formulation for strength improvement was identified as 2-3% OPC, 1-2% GCBA, and 1-2% $CaCl_2$, balancing tensile performance with acceptable reliability for field application.

Table 4.40
Fit Statistic of CA25RAP75 Mix for ITS Test

Factors			Std. Dev.	Mean	R^2	Adjusted R^2	Predicted R^2
OPC (%)	GCBA (%)	$CaCl_2$ (%)					
2	2	0,1,2	21.37	228.40	0.9824	0.9726	0.9563
3	1	0,1,2	36.50	270.91	0.9644	0.9446	0.8558
4	0	0,1,2	42.74	269.52	0.9463	0.9165	0.8274

Analysis of the ITS data shows that increasing OPC content to 3-4% improved the ITS performance. Additionally, adding $CaCl_2$ at 1-2% accelerated hydration and

generally enhanced the development of tensile resistance, although 2% $CaCl_2$ occasionally reduced ITS, while at other points it led to slight increases in strength. Therefore, the 1-2% range is considered optimal, as it provides a balance between early strength enhancement and overall performance reliability. However, the GCBA content needed to be carefully managed, as excessive amounts (beyond 1%) weakened early tensile strength and introduced performance variability.

Among all evaluated mix designs, the CA50RAP50 composition offered the most balanced combination of ITS performance and model reliability. Although the CA25RAP75 mix achieved a slightly higher predictive accuracy (Predicted R^2 = 0.9563), the CA50RAP50 mix produced high mean ITS value (392.55 kPa) while maintaining strong reliability (Predicted R^2 = 0.8959). This balance between tensile strength and predictive stability indicated that the CA50RAP50 mix is the most practical and effective formulation for field application, with 4% OPC and 1-2% $CaCl_2$ as the optimal combination of stabilizing agent for ITS improvement.

4.5.4.3 Resilient Modulus

OPC, GCBA, and $CaCl_2$ were assessed in the resilient modulus strength optimization while establishing an accurate model for prediction (Predicted R^2) to ensure consistent stiffness development. As M_R reflects the resilient of the material stiffness under repeated loading, achieving an adequate modulus is essential for extending pavement lifespan.

Tables 4.41 until 4.43 present a detailed statistical fit analysis of the resilient modulus, M_R model for three distinct CA-RAP mixes compositions which contain stabilizing agent.

In the CA75RAP25 mixes as shown in Table 4.41, the highest mean M_R value of 8899.08 MPa was recorded at 4% OPC with 0-2% $CaCl_2$, while the most stable prediction, with a Predicted R^2 of 0.9519, was associated with 3% OPC + 1% GCBA and 0-2% $CaCl_2$. These results suggested that increasing OPC content enhanced mix stiffness, whereas the inclusion of a small amount of GCBA contributed to improved structural consistency and predictive accuracy. Based on these findings, the optimal composition for resilient performance was identified within the range of 3-4% OPC, 0-1% GCBA, and 1-2% $CaCl_2$.

Table 4.41
Fit Statistic of CA75RAP25 Mix for M_R test

Factors			Std. Dev.	Mean	R^2	Adjusted R^2	Predicted R^2
OPC (%)	GCBA (%)	$CaCl_2$ (%)					
2	2	0,1,2	1004.21	7180.49	0.8664	0.8441	0.7859
3	1	0,1,2	450.73	8487.04	0.9814	0.9710	0.9519
4	0	0,1,2	527.67	8899.08	0.9791	0.9675	0.9402

A similar trend was observed for the CA50RAP50 mixes, as presented in Table 4.42. The highest mean M_R of 8406.24 MPa was achieved on 4% OPC with 0-2% $CaCl_2$, whereas the most reliable model prediction, indicated by a Predicted R^2 of 0.7690, was recorded at 2% OPC + 2% GCBA with 0-2% $CaCl_2$. These results showed that while higher OPC content contributed to greater stiffness, reducing OPC and incorporating more GCBA enhanced model predictability in this particular mix. Therefore, the recommended formulation for improving early-stage M_R performance was determined to be 2-4% OPC, 0-2% GCBA, and 1-2% $CaCl_2$, balancing strength development and prediction accuracy.

Table 4.42
Fit Statistic of CA50RAP50 Mix for M_R Test

Factors			Std. Dev.	Mean	R^2	Adjusted R^2	Predicted R^2
OPC (%)	GCBA (%)	$CaCl_2$ (%)					
2	2	0,1,2	618.54	6311.26	0.9363	0.9009	0.7690
3	1	0,1,2	943.05	8014.28	0.9103	0.8605	0.6940
4	0	0,1,2	980.88	8406.24	0.8932	0.8339	0.7106

Meanwhile, as shown in Table 4.43, the CA25RAP75 mixes achieved both the highest mean M_R of 6760.39 MPa and the most reliable model prediction, with a Predicted R^2 of 0.9074, at 4% OPC with 0-2% $CaCl_2$. This indicated that increasing OPC content significantly enhanced early stiffness while eliminating GCBA improved consistency and model predictability. The presence of $CaCl_2$ further supported rapid stiffness development during early curing. Based on these findings, the optimal composition for M_R strength was identified as 4% OPC with 1-2% $CaCl_2$, offering a well-balanced formulation for strength and performance reliability in this mix composition.

Table 4.43
Fit Statistic of CA25RAP75 Mix for M_R Test

Factors			Std. Dev.	Mean	R^2	Adjusted R^2	Predicted R^2
OPC (%)	GCBA (%)	$CaCl_2$ (%)					
2	2	0,1,2	387.49	5013.21	0.9561	0.9317	0.9020
3	1	0,1,2	508.63	6592.09	0.9478	0.9188	0.8375
4	0	0,1,2	423.43	6760.39	0.9676	0.9495	0.9074

The optimizations findings of resilient modulus demonstrated that higher OPC levels (within the range of 3-4%) significantly contributed to resilient modulus development, enhancing the stiffness across all mix compositions. GCBA content, however, should be limited to 1%, as higher dosages introduced greater variability and reduced model predictability. The addition of $CaCl_2$ at 1-2% was also found to be effective in accelerating the hydration process, promoting faster stiffness formation during the early curing stage.

Among all the tested mix compositions, CA75RAP25 mixes exhibited the best overall performance, achieving the highest mean M_R (8899.08 MPa) along with strong predictive accuracy (Predicted R^2 = 0.9402). This combination of high stiffness and reliable model accuracy indicated that CA75RAP25 mixes provided the best balance of early mechanical performance and consistency, making the mix with 4% OPC with 1-2% $CaCl_2$ the most suitable formulation for enhancing resilient modulus in practical applications.

CHAPTER 5
CONCLUSIONS AND RECOMMENDATIONS

5.1 Conclusions

The purpose of this research was to investigate the influence of the proposed stabilization methods using OPC, GCBA, and $CaCl_2$ on the strength performance of pavement base courses. Overall, the results were positive and promising, demonstrating the effectiveness of the stabilization treatments. Findings from the laboratory experiments and predictive modeling led to the following conclusions:

5.1.1 Material Characterization

The material characterization results provided an overall assessment of the materials used in this study, confirming their compliance with relevant standards. In particular, the CA-RAP mixes were confirmed to meet JKR/SPJ/2008-S4, validating their suitability for pavement base applications. Sieve analysis showed that all mixes exhibited well-graded distributions, which improved particle packing and, consequently, contributed to higher UCS and M_R. The specific gravity results highlighted the lower density of RAP due to oxidative degradation over time, partially explaining the slightly lower strength observed in mixes with higher RAP content. The LA Abrasion and AIV tests indicated improved durability and impact resistance in mixes with higher CA content, which helped maintain particle integrity under load. This corresponded with the higher UCS, ITS, and M_R observed in both CA-rich mixes (CA50RAP50 and CA75RAP25), suggesting enhanced early-age strength and long-term performance under traffic loading. pH index analysis confirmed that all proposed mixes maintained an alkaline environment conducive to cement hydration. Although slight reductions in pH were observed with increasing $CaCl_2$ content primarily due to ionic interactions (Liu and Wu, 2025), these changes did not significantly affect strength development, as the mixes remained sufficiently alkaline to sustain effective hydration and particle bonding.

Microstructural analysis using SEM demonstrated that $CaCl_2$ enhanced the formation of C-S-H (Liu and Wu, 2025), which contributed to a denser matrix and

stronger particle bonding. EDX results further confirmed the significant role of oxygen in hydration, along with the presence of reactive elements such as calcium, silicon, and aluminium. XRD analysis identified beneficial crystalline phases, including quartz, cristobalite, and calcium hydroxide chloride, which are known to enhance durability and long-term performance.

The findings for Objective 1 collectively affirm the structural reliability and field applicability of the proposed CIPR mix designs as sustainable materials for pavement base construction. Furthermore, they explain the observed trends in strength performance, highlighting the strong relationship between material characterization and mechanical properties.

5.1.2 Effect of Proposed Stabilizing Agent on The Compaction Properties

The analysis of compaction properties demonstrated that increasing the proportion of CA in the mix led to higher OMC, primarily due to the irregular shapes and larger particle sizes of CA, which created additional voids and required more water for adequate compaction. In contrast, the finer and more uniform texture of RAP allowed better particle interlocking, reducing void spaces and moisture demand. This highlighted the critical role of particle shape and gradation in influencing moisture behaviour. Meanwhile, mixes with higher RAP content (CA25RAP75) exhibited the highest MDD, attributed to the finer RAP particles that enhanced packing efficiency during compaction.

While the inclusion of stabilizing agents showed minimal influence on bulk density, variations in CA-RAP ratios clearly affected it. Higher CA content generally resulted in greater bulk density due to enhanced particle compression, with the higher water demand filling void spaces and facilitating more effective compaction. This observation was consistent with the compaction results, where RAP-rich mixes achieved higher MDD due to improved packing efficiency, whereas mixes with higher CA required greater OMC to compensate for the additional voids created by irregular particles. Although the chemical additives did not significantly alter the physical density of the mixes, their contribution was evident in the subsequent strength performance results, where the presence of OPC, GCBA, and $CaCl_2$ enhanced particle bonding and hydration reactions, leading to improved cohesion and long-term durability of the stabilized base layer.

The findings for Objective 2 demonstrate the importance of optimizing compaction characteristics and CA-RAP proportioning to ensure the stability and performance of pavement base layer in CIPR applications.

5.1.3 Effect of Proposed Stabilizing Agent on The Strength Performance

The strength performance analysis of CA-RAP mixes confirmed the significant influence of OPC, GCBA, and $CaCl_2$ on UCS, ITS, and M_R. For UCS, mixes containing 3% GCBA or 3% $CaCl_2$ consistently exhibited the lowest strength, indicating their unsuitability for structural applications. In contrast, mixes incorporating 0-1% GCBA and 1-2% $CaCl_2$ alongside 3-4% OPC demonstrated improved compressive strength, outperforming the control mix with 4% OPC alone. Notably, the CA50RAP50 mix achieved the JKR minimum UCS requirement of 2 MPa on Day 1, demonstrating superior early-age compressive performance.

Similarly, the ITS analysis showed that 1% $CaCl_2$ consistently improved tensile strength, while higher dosages (≥2%) led to a slight reduction. Mixes with low OPC and high GCBA content (2% each) recorded the lowest ITS, whereas the highest tensile performance was achieved with 3-4% OPC, 1% $CaCl_2$, and minimal GCBA (0-1%). The CA50RAP50 mix again emerged as the most effective design, with three mixes surpassing the 200 kPa minimum ITS threshold on Day 1, compared to only one mix for CA75RAP25 and none for CA25RAP75. This performance is attributed to the balanced proportion of CA and RAP, which enhanced compatibility with stabilizers and promoted early strength development.

For resilient modulus, the highest M_R were obtained with 0-1% GCBA, 3-4% OPC and 1% $CaCl_2$. Higher OPC content proved more effective than GCBA in enhancing stiffness, while excessive GCBA replacement or higher $CaCl_2$ dosage reduced M_R. The CA75RAP25 mix recorded the highest M_R across all conditions, benefiting from its high CA content and superior deformation resistance. All mix design exceeded the 1350 MPa minimum M_R requirement on Day 1, confirming their suitability for base course applications.

Overall, the findings for Objective 3 highlight the importance of selecting appropriate proportions of stabilizing agent. The CA50RAP50 mix is recommended for achieving superior early-age compressive and tensile strengths when stabilized with 0-1% GCBA, 3-4% OPC, and 1% $CaCl_2$, while the CA75RAP25 mix provides the highest

stiffness under the same content of stabilizing agent. Together, these mixes represent the most structurally reliable and mechanically balanced formulations for pavement base stabilization.

5.1.4 Model Development and Optimization

The ANOVA results and predictive modeling confirmed that OPC, GCBA, $CaCl_2$, and curing days significantly influenced the mechanical properties of CA-RAP mixes, including UCS, ITS, and M_R. The RSM-developed models demonstrated strong predictive capabilities, with most of R^2 values exceeding 0.9, indicating high model reliability and accuracy. Both linear and quadratic relationships were observed, particularly in mixes with higher RAP content, where increased variability was attributed to more complex material interactions.

OPC content emerged as the most influential factor across all performance responses, particularly within the 3-4% range, where it enhanced strength and stiffness. $CaCl_2$, optimally utilized at 1-2%, effectively accelerated hydration and strength development. GCBA contributed positively to lower content (0-1%), although its effects became less predictable at higher dosages. Among the evaluated mixes, the optimized CA50RAP50 mix with 4% OPC, 0% GCBA, and 1-2% $CaCl_2$ yielded the best performance in terms of UCS and ITS, while CA75RAP25 mix with similar proportions exhibited enhanced M_R values. These results were consistent with laboratory tests, where CA50RAP50 mix achieved highest UCS and ITS, and CA75RAP25 mix provided the highest M_R, all using 0-1% GCBA, 3-4% OPC, and 1% $CaCl_2$.

The findings for Objective 4 validate the reliability of the RSM models and highlight the importance of optimizing the content of stabilizing agent to ensure high-performing and consistent stabilized base layers.

5.1.5 Overall Conclusion

This research successfully demonstrated the feasibility of using CIPR techniques with a cement-treated base course incorporating GCBA, and $CaCl_2$ for the pavement base construction. The integration of recycled and industrial by-product materials not only supports sustainable engineering practices but also promotes resource conservation and waste reduction.

A strong relationship was established between fundamental material properties, compaction behaviour, and mechanical performance, emphasizing the importance of controlling aggregate gradation and chemical composition. The findings highlighted that precise control over these factors, particularly the balance between RAP and CA, along with appropriate dosages of OPC, GCBA, and $CaCl_2$, can significantly enhance strength, durability, and stiffness, all of which are critical to long-term pavement performance.

Furthermore, the combination of experimental data and statistical modeling using RSM enabled accurate prediction and optimization of the mix design. This approach effectively minimized the reliance on trial and error, ensuring that performance targets could be consistently achieved under varying field conditions. The discrepancy between the experimental and modeling outcomes in terms of optimal stabilizing agent proportions is attributed to the fundamental differences between physical testing and data-driven optimization. Laboratory results reflect real chemical and microstructural interactions, where the inclusion of $CaCl_2$ in combination with OPC and GCBA enhanced early-age strength through pozzolanic reactions and hydration acceleration. In contrast, the predictive model prioritizes variables with more consistent and linear contributions to mechanical performance, leading to the selection of OPC-dominant mixes. Despite these differences, both approaches consistently identified CA50RAP50 as optimal for UCS and ITS and CA75RAP25 for M_R, highlighting that aggregate blending plays a dominant role in governing mechanical behaviour, while stabilizing agent optimization is more sensitive to the choice of optimization method, whether derived from RSM modeling or laboratory testing.

Ultimately, the results confirmed that the proposed CIPR mix designs are structurally reliable and practically implementable for pavement base applications. These outcomes offer a strong foundation for adopting more sustainable pavement solutions that not only meet performance and cost-effectiveness criteria but also align with broader infrastructure goals focused on environmental responsibility and long-term resilience.

5.2 Recommendations

Based on the research outcome, further investigation can be done to enhance better understanding on the use of this proposed mix design in CIPR base course. Outlined below are potential areas for further research.

i) Increase the percentage of stabilizing agent to further analyze the trend of the performance. This should include a range of percentages beyond the current levels used, ensuring a detail analysis of their effects.

ii) Enhance the depth and breadth of the research on CA-RAP compositions, it is beneficial to expand the range of CA and RAP content beyond the current limits of 25% to 75% for each component. Introduce new experimental scenarios where the proportion of CA and RAP ranges from 0% to 100% for each mix. A comparison on the performance of these new ratios with the existing data from the 25% to 75% range can be made. This will help to identify any significant differences or trends that emerge when using more proportions of CA and RAP.

iii) Conduct a fundamental analysis of stabilizing agent to examine their impact on the hydration process of cementitious materials. This analysis can help to better understand how this agent influences the chemical reactions and performance characteristics of cement-based mixes.

iv) To ensure the practical applicability of the findings, conducting field trials using the optimized CA-RAP mixes would be advisable. These trials could validate the laboratory results and provide insights into how the materials perform in real-world paving projects.

v) It would be beneficial to investigate the long-term durability of these mixes under real-world conditions since the research has successfully identified optimal proportions of OPC, GCBA, and $CaCl_2$ for enhancing mechanical properties. This could include studying the effects of environmental factors, moisture content, and temperature fluctuations on the performance of the optimized CA-RAP mixes.

vi) Since curing plays a critical role in the development of mechanical properties, studying the effects of different curing conditions, such as varying humidity levels, temperatures, and curing times, could further optimize the strength and durability of the CA-RAP mixes.

vii) Further research could also evaluate the cost-effectiveness of the optimized mixes, considering the costs associated with raw materials, production, and potential savings from extended pavement life. This would help in making informed decisions regarding the large-scale adoption of these materials.

In summary, these recommendations aim to refine the understanding and application of the proposed mix design, ensuring its effectiveness and practicality in real-world CIPR base course pavement applications.

REFERENCES

Abdullah, M.H. et al. (2019). Bottom ash utilization: A review on engineering applications and environmental aspects. IOP Conf. Ser.: Mater. Sci. Eng. 527 012006.

Abriak, Y., Chu, D. C., Maherzi, W., Benzerzour, M., & Rivard, P. (2023). Influence of fine recycled concrete aggregates use on the hydration kinetics and mechanical–microstructural properties of hydrated cement: Experimental and numerical approaches. Construction and Building Materials, 408, 133769.

Aboalasaad, M. A., Nazir, A. K., El-Badawy, S. M., & Abd El-Hakim, R. T. (2025). Nanozeolite-modified cement for soft clay subgrade stabilization. Discover Civil Engineering, 2(1), 158.

Abubakar, A.U., & Baharudin, K.S. (2012). Potential Use of Malaysian Thermal Power Plants Coal Bottom Ash in Construction. International Journal of Sustainable Construction Engineering & Technology (ISSN: 2180-3242) Vol 3, Issue 2012.

ACI Committee 212. (1963). Admixtures for concrete, ACI Journal proceedings 60(11), pp. 1481-1524.

Adekunle, S., Ahmad, S., Maslehuddin M., & Al-Gahtani, H.J. (2015). Properties of SCC prepared using natural pozzolana and industrial wastes as mineral fillers, Cement and Concrete Composites, 62, 125–133.

Ahmad, A., Lajis, M. A., Yusuf, N. K., & Ab Rahim, S. N. (2020). Statistical Optimization by the Response Surface Methodology of Direct Recycled Aluminum-Alumina Metal Matrix Composite (MMC-Al_R) Employing the Metal Forming Process. Processes, 8(7), 805.

Al Bargi, W., Khalifa, N., Daniel, B., Rohani, M., & Odebiyi, O. (2023). An experimental investigation on the effect of calcium chloride as dust suppressant on the strength of unpaved road. International Journal of Sustainable Construction Engineering and Technology, 14.

Al Biajawi, M. I., Embong, R., Muthusamy, K., Ismail, N., & Obianyo, I. I. (2022). Recycled coal bottom ash as sustainable materials for cement replacement in cementitious composites: A review. Construction and Building Materials, 338, 127624.

Al-Fasih, M. Y. M., Wan Ibrahim, M. H., Basirun, N. F., Putra Jaya, R., & Mohd Sani, M. S. H. (2019). Influence of partial replacement of cement and sand with coal bottom ash on concrete properties. International Journal of Recent Technology and Engineering, 8(3S3), 72-75.

Aliyegbenoma, C. O., Eki, M. U., & Ozakpolor, M. O. (2020). Modelling and production of injection moulded polypropylene sawdust composite. International Journal of Scientific Engineering and Applied Science (IJSEAS), 6(4). ISSN: 2395-3470.

Almajed, A., Srirama, D., & Moghal, A. A. B. (2012). Response surface method analysis of chemically stabilized fiber-reinforced soil. Materials, 14(6), 1535.

Almajed, A., Dafalla, M., & Shaker, A. A. (2023). The Combined Effect of Calcium Chloride and Cement on Expansive Soil Materials. Applied Sciences, 13(8), 4811.

Alnadish, A. M., Bangalore Ramu, M., Baarimah, A. O., & Alawag, A. M. (2025). Development of Enhanced Stress Prediction Models for Fixed Traffic Loads on Flexible Pavements Based on Response Surface Methodology (RSM) and Machine Learning (ML) Techniques. Applied Sciences, 15(3), 1623.

Althouse, J. (2022). Refined Full-Depth Reclamation Technique Saves Time and Reduces Costs. Public Works: Engineering Construction, and Maintenance, Vol. 133, No. 13, December 2002, pp. 26-27.

Alwathaf, A. H., Abdel Jaber, M., & Hunaiti, Y. M. (2025). Enhancement and Optimization of the Mechanical Properties in Cement Concrete with Recycled Asphalt Pavement (RAP). Buildings, 15(1), 108.

American Association of State Highway and Transportation Officials (AASHTO). (1993). AASHTO guide for design of pavement structures. Washington, DC.

American Association of State Highway and Transportation Officials (AASHTO). (1998). Report on Cold Recycling of Asphalt Pavements. AASHTO-AGC-ARTBA Joint Committee Task Force 38 Report. Washington, D.C.

American Association of State Highway and Transportation Officials (AASHTO). (2017). Standard method of test for determining the resilient modulus of soils and aggregate materials (AASHTO T 307-99). Washington, DC.

Antoni, K., Indranata, M., Al-Jamali, L., & Hardjito, D. (2017). The use of bottom ash for replacing fine aggregate in concrete paving blocks. MATEC Web Conf., 138.

Asrie, B. N., Rahman, H., & Hariyadi, E. S. (2024). Effect of Cement Content and Aggregate Gradation on Compressive Strength, Flexural Strength, and Elastic Modulus of Cement-Treated Base. Jurnal Teknik Sipil, 30(2).

Araya, A. A. (2014). Simplified characterization techniques for (sub) tropical base materials and modeling. International Journal of Computational Methods and Experimental Measurements, 2(1), 92–106.

ARE, Inc. (1987). Pavement Recycling Guidelines for Local Governments-Reference Manual, Report No. FHWATS-87-230, U.S. Department of Transportation, Federal Highway Administration, Washington, D.C. (September).

Arenas, C., Leiva, C., Vilches, L.F., Cifuentes, H., & Rodríguez-Galán, M. (2015). Technical specifications for highway noise barriers made of coal bottom ash-based sound absorbing concrete. Constr. Build. Mater. 95, 585–591.

Argiz, C., Menendez, E., & Sanju´an, M.A. (2017). Coal Bottom Ash for Portland Cement Production, Advances in Materials Science and Engineering, vol. 2017, Article ID 6068286, 7 pages.

Argiz, C., Menendez, E., Moragues, A., & Sanju´an, M.A. (2015). Fly ash characteristics of Spanish coal-fired power plants, Afinidad, vol. 72, pp. 269–277.

Arshad, A.K. (2006). Cold In-Place Recycling: An Introduction. Jurutera, Bil. 2006, No.11, November 2006, pp 30–35.

Asphalt Recycling and Reclaiming Association (ARRA). (1992). An Overview of Recycling and Reclamation Methods for Asphalt Pavement Rehabilitation. Annapolis, MD.

Asphalt Recycling and Reclaiming Association (ARRA). (2001). Basic Asphalt Recycling Manual. U.S. Department of Transportation, 19-25.

Asphalt Recycling and Reclaiming Association (ARRA). (2012). Recommended construction guidelines for cold in-place recycling (CIR) using bituminous recycling agents (CR101). Ergon Asphalt & Emulsions, Inc.

ASTM C618-05. (2005). Standard Specification for Coal Fly Ash and Raw or Calcined Natural Pozzolan for Use. Annual B. ASTM Stand., pp. 3–6.

Awang, A.R., Marto, A., & Makhtar, A.M. (2012). Advance science influence technology morphological and strength properties of Tanjung Bin coal ash mixtures for applied in geotechnical engineering work, 55–62.

Awang, A. R., Marto, A., & Makhtar, A. M. (2011). Geotechnical Properties of Tanjung Bin Coal Ash Mixtures for Backfill Materials in Embankment Construction. EJGE. 16: 1515-1531, 2011.

Ayob, A., Faiz, M., & Zaki, F. (2014). Physical, morphological and strength properties of Jana Manjung coal ash mixture for geotechnical applications Effect of UHPFRC On the Flexural Behavior of Fire Damaged RC Beams, 2014.

Badri, R. M., al kaissi, Z. A., Sutanto, M., & Alobaidi, M. K. (2020). Investigating the rheological properties of asphalt binder incorporating different crumb rubber contents based on a response surface methodology. Journal of King Saud University - Engineering Sciences.

Bahri, S., Mahmud, H. B., & Shafigh, P. (2018). Optimization of mixture proportions of high strength high performance concrete incorporating rice husk ash by using response surface methodology. Proceedings of the 1st Workshop on Multidisciplinary and Its Applications Part 1 (WMA-01 2018), Aceh, Indonesia, 19–20 January

Baite, E., Messan, A., Hannawi, K., Tsobnang, F., & Prince, W. (2016). Physical and transfer properties of mortar containing coal bottom ash aggregates from Tefereyre (Niger). Constr. Build. Mater. 2016, 125, 919–926.

Bajare, D., Bumanis, G., & Upeniece, L. (2013). Coal combustion bottom ash as microfiller with pozzolanic properties for traditional concrete. Procedia Engineering, 57, 149–158.

Baghini, M. S., Ismail, A., Naseralavi, S. S., & Firoozi, A. A. (2016). Performance evaluation of road base stabilized with styrene–butadiene copolymer latex and Portland cement Performance evaluation of road base. International Journal of Pavement Research and Technology, 9(4), 321–336.

Basic Asphalt Recycling Manual. (2001). Publication No. NHI01-022, Asphalt Recycling and Reclaiming Association (ARRA), Annapolis, MD.

Berthelot, C., Gerbrandt, R., & Baker, D. (2000). Full Depth Cold In-Place Recycling/ Stabilization for Low Volume Road Strengthening: A Case Study. 2000 Annual Conference of the Transportation Association of Canada, Edmonton, Alberta, Oct 1-4.

Better Roads. (2001). Full-Depth Reclamation. Special insert section on full-depth reclamation in cooperation with the Asphalt Recycling and Reclaiming Association (July).

Bjegovic, D., Stirmer, N., & Serdar, M. (2012). Durability properties of concrete with blended cements. Materials and Corrosion. Volume 63, no. 12, pp. 1087–1096.

Bradshaw, A. S., Costa, J., & Giampa, J. R. (2015). Resilient Moduli of Reclaimed Asphalt Pavement Aggregate Subbase Blends. Journal of Materials in Civil Engineering, 04015206.

Business Today. (2024, October 9). Govt will no longer build new coal-fired power plants. Business Today. https://www.businesstoday.com.my/2024/10/09/govt-will-no-longer-build-new-coal-fired-power-plants.

Cai, Y., & Liu, X. (2020). Mechanical properties test of pavement base or subbase made of solid waste stabilized by acetylene sludge and fly ash. AIP Advances, 10(6).

Cao, R., Li, H., Yao, L., Jiang, J., Leng, Z., Ni, F., & Zhao, Z. (2024). Comparative analysis of cold in-place recycling for roadway maintenance and rehabilitation from the perspectives of technical-cost-environmental nexus. Journal of Cleaner Production, 439, 140768.

Chhabra, R. S. (2023). Stabilization of cement-treated base mixes incorporating high reclaimed asphalt pavement materials using stabilizer rich in SiO_2 and Al_2O_3. Construction and Building Materials, 365, 130089.

Chen, J., Song, Y., Wei, X., Duan, X., Liu, K., Cao, W., Li, L., & Ren, G. (2025). Ultrasonic and deep eutectic solvent for efficient extraction of phenolics from Eucommia ulmoides leaves. Foods, 14(6), 972.

Chen, J., Jia, J., & Zhu, M. (2024). Understanding the effect of alkali content on hydration, hardening, and performance of Portland cement – A comprehensive review. Materials Today Communications, 40, 109728.

Chilufya, A., Gangell, D., Shahin, M. A., & Abdullah, H. H. (2024). Performance study on laterite road base stabilised with emulsions incorporating biochar. Buildings, 14(3), 575.

Choi, H.J. (2015). Soil stabilization using optimum quantity of calcium chloride with class F fly ash (Unpublished master's thesis). Texas A&M University.

Chong, K.P., Mat Zin, H., & Yazip, M. (2004). Malaysian Experience with Cold-In-Place Recycling: A Case Study", Proceedings of the 8th Conference on Asphalt Pavements for Southern Africa (CAPSA'04), Sun City, South Africa.

Chuang, C.-W., Chen, T.-A., & Huang, R. (2023). Effect of Finely Ground Coal Bottom Ash as Replacement for Portland Cement on the Properties of Ordinary Concrete. Applied Sciences, 13(24), 13212.

Chuang, C.-W., & Chen, T.-A. (2025). Evaluating Finely Ground Coal Bottom Ash for Property Self-Compacting Concrete. Buildings, 15(9), 1509.

Civil Blog. (2015, December 17). Moisture content & dry density relationship of soil. Civil Blog. https://civilblog.org/2015/12/17/moisture-content-dry-density-relationship-of-soil/.

Colonna, P., Berloco, N., Ranieri, V., & Shuler, S. T. (2012). Application of Bottom Ash for Pavement Binder Course. Procedia - Social and Behavioral Sciences, 53, 961–971.

Cooley, D. (2005). Effects of Reclaimed Asphalt Pavement on Mechanical Properties of Base Materials. M.S. thesis. Department of Civil and Environmental Engineering, Brigham Young University, Provo, UT.

Cox, B.C., & Howard, I. L. (2013). Cold In-Place Recycling and Full-Depth Reclamation Literature Review. White Paper Number CMRC WP 13-1 July 2013. Mississippi State University Construction Materials Research Center Ph: 662-325-3050.

Dager, C. H., Morro, R. H., Hubler, J. F., & Sample-Lord, K. M. (2023). Review of Geotechnical Properties of Reclaimed Asphalt Pavement for Reuse in Infrastructure. Geotechnics, 3(1), 21-42.

Debbarma, S., Ransinchung, G. D., & R. N., (2021). Achieving sustainability in roller compacted concrete pavement mixes using reclaimed asphalt pavement aggregates – state of the art review. Journal of Cleaner Production, 287, 125078.

Delancy, D.W. (1976). Waste Use in Highway Construction. In Transportation Research Record: Journal of the Transportation Research Board, No. 593, TRB, National Research Council, Washington, DC, 1976, pp. 9-12.

Du, S. (2018). Effect of curing conditions on properties of cement asphalt emulsion mixture. Construction and Building Materials, 164, 84–93.

Du, W., Li, Y.-X., Chen, M., Yang, S.-P., Liu, X.-C., & Wang, Y.-M. (2025). Mechanical behavior of cement-stabilized macadam materials coupled with recycled asphalt pavement (RAP) and latex. Case Studies in Construction Materials, 22, e04894.

Economic Planning Unit. (2021). Twelfth Malaysia Plan 2021-2025: A Prosperous, Inclusive, Sustainable Malaysia (Chapter 8: Advancing sustainability). https://rmke12.ekonomi.gov.my/en.

El Moudni El Alami, S. E., Moussaoui, R., Monkade, M., Lahlou, K., Hasheminejad, N., Margaritis, A., van den Bergh, W., & Vuye, C. (2019). Lime treatment of coal bottom ash for use in road pavements: Application to El Jadida Zone in Morocco. Materials, 12(7).

Endale, A. A. (2023). Development of asphalt pavement recycling method for road maintenance and construction in Ethiopia (Doctoral thesis, University of Birmingham, United Kingdom). University of Birmingham ETheses Repository.

Epps, J.A., Little, D.N., Holmgreen, R.J., & Terrel, R.L. (1980). Guidelines for Recycling Pavement Materials. NCHRP Report 224, TRB. National Research Council, Washington, DC.

Farhana, A., & Jamaludin, B. (2001). Energy Mix and Alternatives Energy for Sustainable Development in Malaysia, Universiti Putra Malaysia, 1–9.

Federal Highway Administration (FHWA). (1997). Pavement recycling guidelines for state and local governments: Technical Report No. FHWA-AS-98-042, Washington, DC, USA.

Federal Highway Administration (FHWA). (1998). User Guidelines for Waste and By-product Materials in Pavement Construction: Technical Report No. FHWA-RD-97-148, Washington, DC, USA.

Federal Highway Administration (FHWA). (2019). Chemical admixtures for concrete paving mixtures (FHWA-HIF-18-017). U.S. Department of Transportation.

Federal Highway Administration (FHWA). (2019a). Cold in-place recycling (CIR) checklist. U.S. Department of Transportation, FHWA. https://www.fhwa.dot.gov/pavement/pubs/hif19041.pdf

Federal Highway Administration (FHWA). (1997). User guidelines for waste and byproduct materials in pavement construction (Publication No. FHWA-RD-97-148). U.S. Department of Transportation.

Feng, D., Liang, B., Sun, W., He, X., Yi, F., & Wan, Y. (2023). Mechanical properties of solidified dredged soils considering the effects of compaction degree and residual moisture content. Developments in the Built Environment, 16, 100235.

Foo, K.Y. (2015). A vision on the Opportunities, Policies and Coping Strategies for the Energy Security and Green Energy Development in Malaysia. Renewable and Sustainable Energy Reviews. 51: 1477-1498.

Ge, X., Zhou, M., Wang, H., Liu, Z., Wu, H., & Chen, X. (2015) Preparation and characterization of ceramic foams from chromium slag and coal bottom ash. Ceram. Int. 2018, 44, 11888–11891.

GEM Wiki. (2024). Sejingkat power station, Malaysia. Global Energy Monitor. Retrieved 16 December 2024, from https://www.gem.wiki/Sejingkat_power_station.

Gilson Company, Inc. (2025). Soil Density Testing: 3 Test Methods You Can Count On. 2 April 2025, from https://www.globalgilson.com/blog/proctor-compaction-test-a-basic-uide?srsltid=AfmBOoqGVXNcldyCmg5X_QCCo6OYjh 7lRQWwQ3rlmX eK7OxZaJR2oCKe.

Gooi, S., Mousa, A.A., & Kong, D. A. (2020). Critical review and gap analysis on the use of coal bottom ash as a substitute constituent in concrete. J. Clean. Prod. 2020, 268, 121752.

Gonzalo-Orden, H., Linares-Unamunzaga, A., Pérez-Acebo, H., & Díaz-Minguela, J. (2019). Advances in the study of the behavior of full-depth reclamation (FDR) with cement. Applied Sciences (Switzerland), 9(15).

Guan, X., Wang, L., & Mo, L. (2023). Effects of ground coal bottom ash on the properties of cement-based materials under various curing temperatures. Journal of Building Engineering, 69, 106196.

Guthrie, W.S., Brown, A.V., & Egget D.L. (2007). Cement Stabilization of Aggregate Base Material Blended with Reclaimed Asphalt Pavement. Transportation Research Record: Journal of the Transportation Research Board, No. 2026, Transportation Research Board of the National Academies, Washington, DC, 2007, pp. 47-53.

Hamzah, M.O., Omranian, S.R., Golchin, B., & Hainin, M.R. (2015). Evaluation of effects of extended short-term aging on the rheological properties of asphalt binders at intermediate temperatures using respond surface method. J. Technol. 2015, 73, 133-139.

Hamzah, M.O., & Omranian, S.R. (2016). Effects of extended short-term aging duration on asphalt binder behaviour at high temperatures. The Baltic Journal of Road and Bridge Engineering, 2016. 11 (4), 302-312, 2016.

Hannan, N.I.R.R., Shaidan, S., Ali, N., Bunnori, N.M., Mohd Zuki, S.S., & Wan Ibrahim, M.H. (2020). Acoustic and non-acoustic performance of coal bottom ash concrete as sound absorber for wall concrete. Case Stud. Constr. Mater.

Harun, M. H., Sufian, Z., Aziz, N. A., Matori, M. Y., Hussain, M. Z., & Azmi, A. (2010). Challenges in design and construction of cold in-place recycling pavements in Malaysia. In Proceedings of the 24th ARRB Conference, Melbourne, Australia. ARRB.

Harun, M.H., Aziz, N.A., Matori, M.Y., & Abdullah, M.N. (2011). Cold in-place recycling of marginal materials in Malaysia: how does it fair? 4th World Road Congress Proceedings: Roads for a Better Life: Mobility, Sustainability and Development, Mexico City, Mexico.

Haro, A., Alhowaidi, Y., & Al-Tawaha, M. (2018). Feasibility of calcium chloride dehydrate as stabilizing agent for expansive soil. Journal of Engineering Science and Technology Review, 11(6), 156–161.

Hashemi, S.S.G., Mahmud, H.B., Ghuan, T.C., Chin, A.B., Kuenzel, C., & Ranjbar, N. (2019). Safe disposal of coal bottom ash by solidification and stabilization techniques. Constr. Build. Mater. 197, 705–715.

Hesami, S., Modarres, A., Soltaninejad, M., & Madani, H. (2016). Mechanical properties of roller compacted concrete pavement containing coal waste and limestone powder as partial replacements of cement. Constr. Build. Mater. 2016, 111, 625–636.

Hou, Y., Li, P., & Wang, J. D. (2021). Review of chemical stabilizing agents for improving the physical and mechanical properties of loess. Bulletin of Engineering Geology and the Environment, 80(11), 1-15.

Ibrahim, M.H.W., Hamzah, A.F., Jamaluddin, N., Ramadhansyah, P.J., & Fadzil, A.M. (2015). Split Tensile Strength on Self-compacting Concrete Containing Coal Bottom Ash. Procedia Soc. Behav. Sci. 2015, 195, 2280–2289.

Isaia, G. C., Furquim, P., and Gastaldini, A. L. G. (2012). A statistical approach of binary and ternary concrete mixtures with mineral additions, Constr. Build. Mater., vol. 36, pp. 597–603, Nov 2012.

Ismail, A., Baghini, M. S., Karim, M. R. bin, Shokri, F., Al-Mansoba, R. A., Firoozi, A. A., & Firoozi, A. A. (2014). Laboratory investigation on the strength characteristics of cement- treated base. Applied Mechanics and Materials, 507, 353–360.

Izadifar, M., Ukrainczyk, N., Uddin, K. M. S., Middendorf, B., & Koenders, E. (2022). Dissolution of portlandite in pure water: Part 2 atomistic kinetic Monte Carlo (KMC) approach. Materials (Basel), 15(4), 1442.

Jamaluddin, N., Hamzah A.F., & Wan Ibrahim, M.H. (2016). Fresh properties and flexural strength of SCC CBA, 1–6.

Jiang, J., Zheng, Q., Hou, D., Yan, Y., Chen, H., She, W., Wu, S., Guo, D., & Sun, W. (2018). Calcite crystallization in the cement system: Morphological diversity, growth mechanism, and shape evolution. Physical Chemistry Chemical Physics, 20(20).

Joohari, M. I., Shaffie, E., Ibrahim, A., & Che Othman, M. T. (2024). Compressive Strength of Cement Stabilized Cold In-Place Recycling Pavement Base Course with Ground Coal Bottom Ash and Calcium Chloride. Jurnal Kejuruteraan, 36(6), 2701–2708.

Jones, D., Louw, S., & Wu, R. (2016). Full-Depth Reclamation: Cost-Effective Rehabilitation Strategy for Low-Volume Roads. Transp. Res. Rec. 2016, 2591, 1–10.

Jaturapitakkul, C., & Cheerarot, R. (2003). Development of bottom ash as pozzolanic material. Journal of Materials in Civil Engineering. Volume 15, pp. 48–53.

Jamshidi, A., Hamzah, M. O., & Zahed, M. (2013). Rheological Evaluation and Modeling of Sasobit-Modified Asphalt Binder at High Temperatures. Petroleum Science and Technology. 2013. 31: 1574-1584.

Jabatan Kerja Raya Malaysia. (2023). Statistik Jalan Malaysia Edisi 2023. 20 November 2023, from https://www.scribd.com/document/739889669/Buku-Statistik-Jalan-Malaysia-Edisi-2023-JKR.

Jabatan Kerja Raya Malaysia. (2016). Development of Polymer Modified Asphalt in Malaysian Roads (CJ Technical Updates, Issue No. 3/2016). Cawangan Jalan, JKR Malaysia.

Jabatan Kerja Raya Malaysia. (2013). Arahan Teknik (Jalan) 5/85 (Pindaan 2013): Manual for the structural design of flexible pavement. Kuala Lumpur: JKR.

Jabatan Kerja Raya Malaysia. (2008). Standard Specification for Roadworks Section 4: Flexible Pavement (JKR/SPJ/2008-S4). Kuala Lumpur: JKR Malaysia.

Kabeta, W. F., & Lemma, H. (2023). Modeling the application of steel slag in stabilizing expansive soil. Modeling Earth Systems and Environment, 9, 4023–4030.

Kandhal P.S., Prithvi S. & Mallick, R.B. (1997). Pavement Recycling Guidelines for State and Local Government, Publications No. FHWA-SA-98-042, Federal Highway Administration, Department of Transportation December 1997.

Kavussi, A., & Modarres, A. (2010). A model for resilient modulus determination of recycled mixes with bitumen emulsion and cement from ITS testing results. Construction and Building Materials, 24(11), 2252–2259.

Kearney, E.J., & Huffman, J.E. (1999). Full-Depth Reclamation Process. Transportation Research Record, 1684(1), 203–209.

Kearney, E.J., & Huffman, J.E. (2000). Full-Depth Reclamation Process. Transportation Research Record: Journal of the Transportation Research Board, No. 1864, Transportation Research Board of the National Academies, Washington, DC, pp. 203-209.

Khan, R.A. & Ganesh, A. (2016). The effect of coal bottom ash (CBA) on mechanical and durability characteristics of concrete. J. Build. Mater. Struct, 3, pp.31–42.

Khankhaje, E., Hussin, M.W., Mirza, J., Rafieizonooz, M., Salim, M.R., Siong, H. C., & Warid, M.N. (2016). Blended Cement and Geopolymer Concretes Containing Palm Oil Fuel Ash. Materials & Design.Vol. 125, pp. 385-398, 2016.

Khodaii, A., Haghshenas, H., & Kazemi, H.T. (2012). Effect of Grading and Lime Content on HMA Stripping Using Statistical Methodology. Construction and Building Materials. 2012. 34: 131-135.

Kim, W., & Labuz, J. F. (2007). Resilient modulus of base course containing recycled asphalt pavement. Transportation Research Record: Journal of the Transportation Research Board, 2005(1), 27-35.

Kim, H.K., & Lee, H.K. (2011). Use of Power Plant Bottom Ash as Fine and Coarse Aggregates in High-Strength Concrete. Constr. Build. Mater. 2011, 25, 1115–1122.

Kim, R.G., Li, D., & Jeon, C.H. (2014). Experimental investigation of ignition behaviour for coal rank using a flat flame burner at a high heating rate. Exp. Therm. Fluid Sci. 2014, 54, 212–218.

Kim, Y., Im S., & Lee, H. D. (2011). Impacts of Curing Time and Moisture Content on Engineering Properties of Cold In-Place Recycling Mixtures Using Foamed or Emulsified Asphalt. Journal of Materials in Civil Engineering, Vol.23.

Kim, Y.-M., Kim, K., & Le, T. H. M. (2024). Advancing Sustainability and Performance with Crushed Bottom Ash as Filler in Polymer-Modified Asphalt Concrete Mixtures. Polymers, 16(12), 1683.

Kishar, E. A., Ahmed, D. A., Mohammed, M. R., & Noury, R. (2013). Effect of calcium chloride on the hydration characteristics of ground clay bricks cement pastes. Beni-Suef University Journal of Basic and Applied Sciences, 2(1), 20–30.

Kohno, K. & Komatsu, H. (1986). Use of Ground Bottom Ash and Silica Fume in Mortar and concrete. Fly Ash, Silica Fume, Slag, and Natural Pozzolans in Concrete, ACI SP 91, pp 1279-1292.

Ku Meh, K. M. F., Shahidan, S., Shamsuddin, S.-M., Mohd Zuki, S. S., & Senin, M. S. (2022). An Experimental Investigation of Coal Bottom Ash as Sand Replacement. Geomate Journal, 23(99), 17–24. from https://geomatejournal.com/geomate/article/view/3515

Kurama, H., & Kaya, M. (2008). Usage of coal combustion bottom ash in concrete mixture. Construction and Building Materials, 22, 1922-1928.

Lewis, A.J.N., & Collings, D.C. (1999). Cold in Place Recycling: A Relevant Process for Road Rehabilitation and Upgrading. 7th Conference on Asphalt Pavements for Southern Africa.

Li, M., Tan, H., Zhang, J., Deng, X., Kong, X., Chen, P., Jian, S., He, X., & Yang, J. (2023). Enhancement in compressive strength of carbide slag activated ground granulated blast furnace slag by introducing $CaCl_2$ and NaCl. Construction and Building Materials, 385, 131071.

Liew, J. J., Cheah, C. B., Khaw, K. L. P., Siddique, R., & Tangchirapat, W. (2024). Blended cement and mortar with various low-calcium ground coal bottom ash content: Engineering characteristics, embodied carbon and cost analysis. Construction and Building Materials, 425, 135987.

Lillian, N., Ahmed, S. B., Krishnan, D., et al. (2025). Comprehensive evaluation of sub-base materials for road pavements, integrating California bearing ratio and triaxial compression tests for enhanced stability and durability: A systematic review. Discover Civil Engineering, 2, 116.

Liu, Q., & Wu, Y. (2025). Reinforcement Effect of $CaCl_2$ on Cementation Performance of Solid-Waste-Based Cementitious Materials for Fine Tailings. Molecules, 30(7), 1520.

Lin, R.-S., Wang, X.-Y., & Zhang, G.-Y. (2018). Effects of quartz powder on the microstructure and key properties of cement paste. Sustainability, 10(10), 3369.

Linares-Unamunzaga, A., Pérez-Acebo, H., Rojo, M., & Gonzalo-Orden, H. (2019). Flexural strength prediction models for soil-cement from Unconfined Compressive Strength at Seven Days. Materials, 12(3), 2019.

Little, D. N., & Nair, S. (2009). Recommended Practice for Stabilization of Subgrade Soils and Base Materials (NCHRP Report 792). Transportation Research Board.

Lo, T.Y., Cui, H., Memon, S.A., & Noguchi, T. (2016). Manufacturing of sintered lightweight aggregate using high-carbon fly ash and its effect on the mechanical properties and microstructure of concrete. J. Clean. Prod. 112, 753-762.

Louw, S., Jones, D. & Hammack, J. (2016). Pavement Recycling: Shrinkage Crack Mitigation in Cement Treated Pavement Layers - Phase 1 Laboratory Testing (Davis: Institute of transportation Studies, University of California).

Liu, Q., & Wu, Y. (2025). Reinforcement Effect of $CaCl_2$ on Cementation Performance of Solid-Waste-Based Cementitious Materials for Fine Tailings. Molecules, 30(7), 1520.

Lynn, C.J., & Ghataora, G.S. OBE RKD. (2017). Municipal incinerated bottom ash (MIBA) characteristics and potential for use in road pavements. International Journal of Pavement Research and Technology. 10(2):185-201.

Mallick, R.B., Bradbury, R.L., Andrews, J.O., Kandhal, P.S., & Kearny, E.J. (2022). Evaluation of Performance of Full-Depth Reclamation Mixes. Transportation Research Record: Journal of Transportation Research Board, No. 1809, Transportation Research Board of the National Academies, Washington, DC, 2002, pp. 199-208.

Mangi, S. A., Ibrahim, M. H. W., Jamaluddin, N., Arshad, M. F., Memon, F. A., Jaya, R. P., & Shahidan, S. (2018). A review on potential use of coal bottom ash as a supplementary cementing material in sustainable concrete construction. International Journal of Integrated Engineering, 10(9), 127–135.

Mangi, S. A., Ibrahim, M. H. W., Jamaluddin, N., Arshad, M. F., & Jaya, R. P. (2019). Effects of ground coal bottom ash on the properties of concrete. Journal of Engineering Science and Technology. 14. 338-350.

Mangi, S. A., Ibrahim, M. H. W., Jamaluddin, N., Arshad, M. F., & Jaya, R. P. (2019). Short-term effects of sulphate and chloride on the concrete containing coal bottom ash as supplementary cementitious material. Eng. Sci. Technol. Int. J. 2019, 22, 515–522.

Marto, A., Kassim, K.A., Makhtar, A.M., Wei, L.F., & Lim, Y.S. (2010). Engineering Characteristics of Tanjung Bin Coal Ash. Electronic Journal of Geotechnical Engineering. 15: 1117-1129.

Marto, A., & Tan, C.S. (2016). Properties of Coal Bottom Ash from Power Plants in Malaysia and Its Suitability as Geotechnical Engineering Material. Jurnal Teknologi (Sciences & Engineering) 78: 8–5 (2016) 1–10.

Mehta, P. K., & Monteiro, P. J. M. (2014). Concrete: Microstructure, Properties, and Materials (4th ed.). McGraw-Hill Education.

Mehta, P. K., & Monteiro, P. J. M. (2001). Concrete: Microstructure, properties, and materials (3rd ed.). McGraw-Hill Education.

Menéndez, E., Argiz, C., & Sanjuán, M.Á. (2021). Reactivity of ground coal bottom ash to be used in Portland cement. Multidisciplinary Scientific Journal, 4, 223–232.

Metham, M., Mangkornngam, W., Sedthamanop, A., Tabyang, W., Sooksil, N., Phetchuay, C., & Suksiripattanapong, C. (2021). Stabilization of marginal crushed rock using cement and fly ash as a green base course material. Geomate Journal, 20(77), 92–97.

Mohammed, S.A., Koting, S., Katman, H.Y.B., Babalghaith, A.M., Abdul Patah, M.F., Ibrahim, M.R., & Karim, M.R. (2021). A Review of the Utilization of Coal Bottom Ash (CBA) in the Construction Industry. Sustainability 2021, 13, 8031.

Mohammed, S. A., Koting, S., Babalghaith, A. M., Isa, M. H. M., & Khairuddin, F. H. (2025). Influence of Coal Bottom Ash as Fine Aggregate Replacement on the Mechanical Properties of Stone Mastic Asphalt. Applied Sciences, 15(12), 6826.

Mohammed, S. A., Koting, S., Katman, H. Y. B., Babalghaith, A. M., Abdul Patah, M. F., Ibrahim, M. R., & Karim, M. R. (2021). A Review of the Utilization of Coal Bottom Ash (CBA) in the Construction Industry. Sustainability, 13(14), 8031.

Mohammed, B.S., Haruna, S., & Liew, M. (2019). Optimization and characterization of cast in-situ alkali-activated pastes by response surface methodology. Construction Building Material, 225, pp 776–787.

Mohamad Kamal, M. I. A., Arshad, A. K., & Ahmad, J. (2017). Evaluation of cold in-place recycling mix using polymer modified asphalt emulsion. Pertanika Journal of Science & Technology, 25(S), 219–226

Modarres, A. & Ayar, P. (2014). Application of coal waste powder as filler in hot mix asphalt. Construction and Building Materials. 66. 476-483.

Morian, D.A., Solaimanian, M., Scheetz, B., & Jahangirnewjad, S. (2012). Developing Standards and Specifications for Full-Depth Pavement Reclamation. Pennsylvania Department of Transportation, Harrisburg, PA.

Mousa, A. (2023). Utilization of coal bottom ash from thermal power plants as a cement replacement for building: A promising sustainable practice. Journal of Building Engineering, 74, 106885.

Muhammad, M.S. (2010). Strength characteristics of Compacted Residual Soil-Bottom Ash.

Muhardi, A., Marto, A., Kassim, K.A., Makhtar, A.M., Wei, L. F., & Lim, Y. S. (2010). Engineering characteristics of Tanjung Bin coal ash. Electronic Journal of Geotechnical Engineering. Volume 15, pp. 1117–1129.

Myers, R.H. & Montgomery, D.C. (2002). Response Surface Methodology: Product and Process Op-timization Using Designed Experiments. 2nd Edition, John Wiley & Sons, New York.

Namita. (2019, March 10). Factors affecting Compaction of soil. https://civildigital.com/factors-affecting-compaction-of-soil/.

NETL (National Energy Technology Laboratory). (2006). Clean coal technology: Coal utilization by-products. Washington, DC: Department of Energy Office of Fossil Energy; Topical report no. 24.

Neville, A.M. & Brooks, J.J. (2003). Concrete Technology, Pearson Education Limited, Harlow, England.

Neville, A.M. (1995). Properties of Concrete, Pearson education limited.

Neville, A.M. (2015). 'Fresh Concrete' in Properties of Concrete (5th ed.). Pearson Education Limited pp. 183-244.

Nurhidayat, A. & Kamarudin, K. H. B. (2024). A Systematic Review of the Impact Overload on Road Pavement Batu City, Indonesia. Int. J. Transp. Dev. Integr., 8(1), 49-60.

Nguyen, D. T., & Le, V. P. (2022). Determining optimum fly ash content for Stabilized subbase materials in road pavements. Australian Journal of Civil Engineering, 20(1), 46–55.

NS Energy. (2019, February 28). Manjung power plant, Perak, Malaysia. NS Energy. https://www.nsenergybusiness.com/projects/manjung-power-plant-perak/

Occidental Chemical Corporation (2006). Calcium Chloride in Portland Cement Concrete. https://kuert.com/wp-content/uploads/2016/01/Calcium-Chloride-in-Portland-Cement-Concrete.pdf.

Onprom, P., Chaimoon, K., & Cheerarot, R. (2015). Influence of Bottom Ash Replacements as Fine Aggregate on the Property of Cellular Concrete with Various Foam Contents. Adv. Mater. Sci. Eng.

OpenInfraMap. (2025). All 207 Power Plants in Malaysia. Mac 12, from https://openinframap.org/stats/area/Malaysia/plants

Oruji, S., Brake, N.A., Guduru, R.K., Nalluri, L., Günaydın-¸Sen, Ö., Kharel, K., Rabbanifar, S., Hosseini, S., & Ingram, E. (2019). Mitigation of ASR expansion in concrete using ultra-fine coal bottom ash. Constr. Build. Mater. 2019, 202, 814–824.

Oruji, S., Brake, N.A., Nalluri, L., & Guduru, R.K. (2017). Strength activity and microstructure of blended ultra-fine coal bottom ash-cement mortar. Constr. Build. Mater. 2017, 153, 317–326.

Osouli, A., Salam, S., & Tutumluer, E. (2016). Effect of plasticity index and dust ratio on moisture-density and strength characteristics of aggregates. Transportation Geotechnics, 9, 69–79.

Pawar, P., & Sinha, M. (2022). Analysis of construction and industrial waste to strengthen flexible pavement. IARJSET, 9, 1-6.

Pavement. (2008). Public Works Department, Ministry of Works Malaysia. Kuala Lumpur. JKR/SPJ/2008.

Penumala R. R., & Bharthavarapu, S. (2018). Use of pavement wastes (reclaimed asphalt pavement) in base and sub-base layers of road construction. International Journal of Advance Research in Science and Engineering, 7(6)

Perera, M. A. G. P., & Ranjith, P. G. (2025). Greener horizons: Revolutionizing construction materials with waste-based innovations – An experimental study. Journal of Building Engineering, 103, 112211.

Permatasari, R., Sodri, A., & gustina, H. A. (2023). Utilization of Fly Ash Waste in the Cement Industry and its Environmental Impact: A Review. Jurnal Penelitian Pendidikan IPA, 9(9), 569–579.

Portland Cement Association (PCA). (2005). Guide to Full Depth Reclamation (FDR) with Cement, Skokie, USA.

Poudel, S., Menda, S., Useldinger-Hoefs, J., Guteta, L. E., Dockter, B., & Gedafa, D. S. (2024). The use of ground coal bottom ash/slag as a cement replacement for sustainable concrete infrastructure. Materials, 17(10), 2316.

Poulikakos, L.D., Papadaskalopoulou, C., & Hofko, B. (2017). Harvesting the unexplored potential of European waste materials for road construction, Resources, Conservation and Recycling, vol. 116, pp. 32–44.

Qadir, A., Gazder, U., & Anum, S. (2024). The effect of axle overloading and high tire pressure on flexible pavement structure. International Journal of Environmental Engineering and Development, 2, 35–51.

Rafieizonooz, M., Mirza, J., Salim, M.R., Hussin, M.W., & Khankhaje, E. (2016). Investigation of coal bottom ash and fly ash in concrete as replacement for sand and cement. Construction Building Materials. Volume 116, pp. 15–24.

Rafiq, W., Napiah, M., Habib, N. Z., Sutanto, M. H., Alaloul, W. S., Khan, M. I., Musarat, M. A., & Memon, A. M. (2021). Modeling and design optimization of reclaimed asphalt pavement containing crude palm oil using response surface methodology. Construction and Building Materials, 291, 123288.

Rahmani, S., Belkadi, A. A., Achour, Y., Dridi, M., Chiker, T., Cousture, A., Makhlouf, A., Aggoun, S., & Chajec, A. (2025). Enhancing the performance and durability of eco-friendly mortars: The role of calcium chloride in GGBS and glass powder-based mixtures. Case Studies in Construction Materials, 23, e05495.

Ramzi Hannan, N. I. R., Shahidan, S., Maarof, M. Z., & Ali, N. (2016). Physical and Chemical Properties of Coal Bottom Ash (CBA) from Tanjung Bin Power Plant. IOP Conference Series: Materials Science and Engineering, 160(1).

Ramzi Hannan, N. I. R., Shahidan, S., Ali, N., & Maarof, M. Z. (2017). A Comprehensive Review on the Properties of Coal Bottom Ash in Concrete as Sound Absorption Material. MATEC Web of Conferences, 103.

Rattanasak, U., Pankhet, K., & Chindaprasirt, P. (2011). Effect of chemical admixtures on properties of high-calcium fly ash geopolymer. International Journal of Minerals, Metallurgy and Materials, 18(3), 364–369.

Razak, H.A., Naganathan, S., & Hamid, S.N.A. (2010). Controlled low-strength material using industrial waste incineration bottom ash and refined kaolin. Arabian Journal for Science and Engineering. 35(2B):53-67.

Rocha, S., Ascensão, G., & Maia, L. (2023). Exploring design optimization of self-compacting mortars with response surface methodology. Applied Sciences, 13(18), 10428.

Rokitowski, P., Bzówka, J., & Grygierek, M. (2021). Influence of high moisture content on road pavement structure: A Polish case study. Case Studies in Construction Materials, 15, e00594.

Rout, M. K. D., Sahdeo, S. K., Biswas, S., Roy, K., & Sinha, A. K. (2023). Feasibility study of reclaimed asphalt pavements (RAP) as recycled aggregates used in rigid pavement construction. Materials (Basel), 16(7), 1-14.

Ruston Paving. (2023). CIPR Process. August 10, 2023, from https://rustonpaving.com/cms/wp-content/uploads/2017/06/FDR-Construction-rocess.png.

Salain, I. M. A. K. (2019). Using calcium chloride as an accelerator for Portland pozzolan cement concrete compressive strength development. IOP Conference Series: Materials Science and Engineering, 615(1).

Sabrin, R., Shahjalal, M., Eema Bachu, H. A., Habib, M. M., Jerin, T., & Billah, A. H. M. (2024). Recycling of different industrial wastes as supplement of cement for sustainable production of mortar. Journal of Building Engineering, 86, 108765.

Saeed, H. H. (2023). A review study of the use of calcium chloride in concrete. Journal of Engineering and Sustainable Development, 27(3), 339–349.

Sanjeev, K., Sanjay, M., Manoj, M., Bernard, R.S., & Prashanth, V. (2006). Morphological and strength analysis of PCC bottom ash amended with bentonite. Geotechnical and geological Engineering. 24, 1009 – 1020.

Sarawak Energy. (2024). Coal power generation in Sarawak. MyEnergyStats. Retrieved 21 October 2024, from https://myenergystats.st.gov.my/coal

Saylak, D., Mishra, S., Mejeoumov, G., & Shon, C-S. (2008). Fly Ash-Calcium Chloride Stabilization in Road Construction. Transportation Research Record: Journal of the Transportation Research Board, 2053, 23–29.

Saylak, D., Estakhri, C.K., Mishra, S., & Sinn, D. (2003). Base Stabilization and Dust Control Using Calcium Chloride and Fly Ash, in International Ash Utilization Symposium, Lexington, KY.

Selia Group. Cold in Place Recycling (CIPR). (2018). Seminar On Cement and Concrete Applications – Roads 1 – 2 August 2018 JKR Create, Melaka.

Schackow, A., Andrade Neto, J. d. S., Hack, L., Folgueras, M. V., Kirchheim, A. P., Rodríguez Martinez, E. D., & Matos, P. R. d. (2025). Coal Bottom Ash as Supplementary Cementitious Material: Optimizing Reactivity Through Particle Grinding. Sustainability, 17(11), 5031.

Shaffie, E. (2018). Effect of nanopolyacrylate and natural rubber latex on asphalt binder and mixture performance (Doctoral dissertation). Faculty of Civil Engineering, Universiti Teknologi MARA.

Shahidan, S. (2014). Properties of concrete with difference percentage of the RHA as partial cement replacement, Material Science Forum, 803, 288-293.

Sharma, E. (2024). A review on stabilization of granular subbase in flexible pavement by using calcium chloride. International Journal for Research in Applied Science and Engineering Technology, 12(786–791).

Shiong, F., Shaffie, E., & Mohamad Rais, N. (2023). Evaluation on Volumetric Properties of Stone Mastic Asphalt Mix Containing Steel Fibre Using Response Surface Method. In: Hashim, U.R., et al. Green Infrastructure. Springer, Singapore.

Shon, C-S., Saylak, D., & Mishra, S. (2010). Combined Use of Calcium Chloride and Fly Ash in Road Base Stabilization. Transportation Research Record: Journal of the Transportation Research Board, 2186, 120–129.

Siddique, R. (2013). Compressive strength, water absorption, sorptivity, abrasion resistance and permeability of self-compacting concrete containing coal bottom ash. Constr. Build. Mater. 2013, 47, 1444–1450.

Singh, M., & Siddique, R. (2013). Effect of coal bottom ash as partial replacement of sand on properties of concrete. Resources, Conservation and Recycling. Volume 72, 2013, pp. 20–32.

Singh, M., Siddique, R. (2016). Effect of coal bottom ash as partial replacement of sand on workability and strength properties of concrete. J. Clean. Prod. 2016, 112, 620–630.

Singh, N., Mithulraj, M., & Arya, S. (2019). Utilization of coal bottom ash in recycled concrete aggregates based self-compacting concrete blended with metakaolin. Resource Conserve Recycle. 2019, 144, 240–251.

Singh, N., & Shehnazdeep, B. A. (2020). Reviewing the role of coal bottom ash as an alternative of cement. Constr. Build. Mater. 2020, 233, 117276.

Singh, R. P., Vanapalli, K. R., Cheela, V. R. S., Peddireddy, S. R., Sharma, H. B., & Mohanty, B. (2023). Fly ash, GGBS, and silica fume based geopolymer concrete with recycled aggregates: Properties and environmental impacts. Construction and Building Materials, 378, 131168.

Sufian Z., Abdul Aziz, N., Matori, M.Y., Hussain, M.Z., & Mohd Radzi, H. (2009). Construction of cold in place recycling method in Malaysia. Proceedings of the 13th Conference of Road Engineering Association of Asia and Australasia, Incheon, South Korea.

Sufian, Z., Abdul Aziz, N., Matori, M.Y., Hussain, Z., & Azmi, A. (2009). Full Depth Reclaimed Pavements Using Cement and Hydrated Lime as Stabilizing Agents.

Taha, R., Al-Harthy, A., Al-Shamsi, K., & Al-Zubeidi, M. (2002). Cement Stabilization of Reclaimed Asphalt Pavement Aggregate for Road Bases and Subbases. In Journal of Materials in Civil Engineering, Vol. 14, No. 3, June 2002, pp. 239-245.

Talib, N.R.B.A. (2009). Engineering Characteristics of Bottom Ash from Power Plants in Malaysia, Thesis, Universiti Teknologi Malaysia.

Tambunan, H. F., Hadiwardoyo, S. P., Sumabrata, R. J., Lumingkewas, R. H., & Ifrad, A. M. (2025). Influence of coarse aggregate content in recycled asphalt mixtures on rutting and resilient modulus. International Journal of GEOMATE, 29(136), 11–19.

Tan, P.C., & Chan, C.M. (2021). Unconfined Compressive Strength of Rehabilitated Road Base via Polymer-Modified Cold In-Place Recycling (CIPR). IOP Conference Series: Materials Science and Engineering, 1150(1), 012014.

Technical Note 76: Introduction to roadbase products and testing. Cement Concrete & Aggregates Australia. (2023). January 6, 2023, from https://ccaa.com.au/common/Uploaded%20files/CCAA/Publications/Tech%20Notes/Tech%20Note%2076%20Roadbase%20Products%20LR.pdf.

Teng An. (2025). Mastering cold weather concrete: Why adding calcium chloride can improve your pour. BTZMOC. April 22, 2025, Retrieved from https://www.btzmoc.com/news/mastering-cold-weather-concrete-why-adding-calcium-chloride-can-improve-your-pour

Thanasisathit, N., Lhajai, S., Jongpradist, P., & Jamsawang, P. (2025). Recycling bottom ash in cement-stabilized pavement materials: Mechanical performance and environmental feasibility. Case Studies in Construction Materials, 22, e04892.

Tom V. Mathew. (2009). Introduction to pavement design Lecture notes in Transportation Systems Engineering 3 August 2009.

Topçu, I.B., & Bilir, T. (2010). Effect of bottom ash as fine aggregate on shrinkage cracking of mortars. ACI Mater. J. 2010, 107, 48–56.

Tutumluer, E., Mishra, D., & Butt, A. A. (2009). Characterization of Illinois aggregates for subgrade replacement and subbase, Illinois Dept. of Transportation, Bureau of Materials and Physical Research, Springfield, IL.

Uche, O. A., Kelechi, S. E., Adamu, M., Ibrahim, Y. E., Alanazi, H., & Okokpujie, I. P. (2022). Modeling and Optimizing the Durability Performance of Self Consolidating Concrete Incorporating Crumb Rubber and Calcium Carbide Residue Using Response Surface Methodology. Buildings, 12(4).

Vasudevan, G. (2017). Effect on Coal Bottom Ash in Hot Mix Asphalt (HMA) as Binder Course. Proceedings of the International Multiconference of Engineers and Computer Scientists 2017 Vol II, IMECS 2017, March 15 - 17.

Vieira, M., Pereira, G., Pacheco, F., Marques, M. L. da S., Christ, R., & Modolo, R. C. E. (2022). Assessment of the impact of adding fly ash and coal bottom ash to an advanced cement-based composite matrix. Revista IBRACON de Estruturas e Materiais, 15(5).

Wang, J.-J., Yang, Y., & Zhang, H.-P. (2014). Effects of particle size distribution on compaction behavior and particle crushing of a mudstone particle mixture. Geotechnical and Geological Engineering, 32(4), 1159–1164.

Wang, J., Long, G., Xiang, Y., Dong, R., Tang, Z., Xiao, Q., Yang, Z., & Ma, K. (2022). Influence of rapid curing methods on concrete microstructure and properties: A review. Case Studies in Construction Materials, 17, e01600

Wang, Y., Lei, L., Liu, J., Ma, Y., Liu, Y., Xiao, Z., & Shi, C. (2022). Accelerators for normal concrete: A critical review on hydration, microstructure and properties of cement-based materials. Cement and Concrete Composites, 134, 104762.

Wei, C., He, Z., Ma, J., Sun, X., Shi, Y., Yi, Q., & Li, M. (2024). Preparation and Performance of Cement-Stabilized Base External Curing Agent in a Desert Environment. Buildings, 14(5), 1465.

Wen, H., Tharaniyil, M. P., Ramme, B., & Krebs, S. (2004). Field performance evaluation of class C fly ash in full-depth reclamation: Case history study. Transportation Research Record, 1869, 41–46.

Wie, Y.M., & Lee, K. (2020). Composition design of the optimum bloating activation condition for artificial lightweight aggregate using coal ash. J. Korean Ceram. Soc. 2020, 57, 220–230.

Williams, C. K., Muhye, E., Muhye, A., Al Hatali, A., Saleh, N., & Ajmi, A. (2020). A Study on the Mechanical Properties of Concrete by Partial Replacement of Cement with Calcium Chloride. International Research Journal of Engineering and Technology.

Wishard, T. (2001). Reclamation Process Reduces Cost, Improves Roads. Roads and Bridges, Vol. 39, No. 12, December 2001, pp. 32-33.

Wongkeo, W., and Chaipanich, A. (2010). Compressive strength, microstructure and thermal analysis of autoclaved and air cured structural lightweight concrete made with coal bottom ash and silica fume. Materials Science and Engineering: A. Volume 527, no. 16–17, (2010), pp. 3676–3684.

Wood, L.E., White, T.D., & Nelson, T.B. (1988). Current Practice of Cold In-Place Recycling of Asphalt Pavements. In Transportation Research Record 1178, TRB, National Research Council, Washington, DC.

Worku, A., & Shiferaw, D. (2004). Prediction of maximum dry density of local granular fills. Journal of EEA, 21, 59-70.

Yu, W., Li, Y., Liang, Z., Wu, J., Wang, S., & Miao, Y. (2025). Laboratory Investigation of Packing Characteristics and Mechanical Performance of Aggregate Blend. Materials, 18(9), 1953.

Zainal Abidin, N.E., Wan Ibrahim, M.H., Jamaluddin, N., Kamaruddin, K. & Hamzah, A.F. (2014). The effect of bottom ash on fresh characteristic, compressive strength and water absorption of self-compacting concrete, Applied Mechanics and Materials, 660, 145–151.

Zhang, B., & Poon, C.S. (2015). Use of Furnace Bottom Ash for producing lightweight aggregate concrete with thermal insulation properties. J. Clean. Prod. 2015, 99, 94–100.

Zhang, J., Deng, A., & Jaksa, M. (2021). Optimizing micaceous soil stabilization using response surface method. Journal of Rock Mechanics and Geotechnical Engineering, 13(1), 212-220.

Zhang, J., Sesay, T., You, Q., & Jing, H. (2022). Maximizing the Application of RAP in Asphalt Concrete Pavements and Its Long-Term Performance: A Review. Polymers, 14(21), 4736.

Zhang, X., Wang, H., Wang, D., & Li, C. (2014). Prediction of concrete strength based on self-organizing fuzzy neural network. In Proceedings of the 11th World Congress on Intelligent Control and Automation, Shenyang, China, 29 June–4 July 2014; IEEE: Piscataway, NJ, USA, 2015; pp. 5631–5634.

Zhao, Z., Ni, F., Zheng, J., Cheng, Z., & Xie, S. (2023). Evaluation of curing effects on bitumen emulsion-based cold in-place recycling mixture considering field-water evaporation and heat-transfer conditions. Coatings, 13(7), 1204.

APPENDICES

APPENDIX A

Sieve Analysis Raw Data

Table A1: Sieve Analysis for CA25RAP75

BS Sieve size (mm)	JKR Requirement	Mass sieve	mass sieve + sample	Sample mass	cum. retains	% cum ret.	% pass
50	100	1640.7	1640.7	0	0	0.00	100.00
37.5	85-100	1448.7	1448.7	0	0	0.00	100.00
20	60-100	1323.2	1375.1	51.9	51.9	2.60	97.40
10	40-90	1048.1	1480.5	432.4	484.3	24.30	75.70
5	30-75	1095.8	1569.3	473.5	957.8	48.07	51.93
2.36	20-60	994.3	1499.6	505.3	1463.1	73.42	26.58
0.425	10-45	670.5	950.2	279.7	1742.8	87.46	12.54
0.075	2-20	597.7	801.3	203.6	1946.4	97.68	2.32
pan		733.9	780.2	46.3	1992.7	100.00	0.00

Table A2: Sieve Analysis for CA50RAP50

BS Sieve size (mm)	JKR Requirement	Mass sieve	mass sieve + sample	Sample mass	cum. retains	% cum ret.	% pass
50	100	1640.7	1640.7	0	0	0.00	100.00
37.5	85-100	1448.7	1448.7	0	0	0.00	100.00
20	60-100	1323.2	1422.2	99	99	4.96	95.04
10	40-90	1048.1	1510.1	462	561	28.12	71.88
5	30-75	1095.8	1458.3	362.5	923.5	46.29	53.71
2.36	20-60	994.3	1395.4	401.1	1324.6	66.39	33.61
0.425	10-45	670.5	950.8	280.3	1604.9	80.44	19.56
0.075	2-20	597.7	923.3	325.6	1930.5	96.76	3.24
pan		733.9	798.5	64.6	1995.1	100.00	0.00

Table A3: Sieve Analysis for CA75RAP25

BS Sieve size (mm)	JKR Requirement	Mass sieve	mass sieve + sample	Sample mass	cum. retains	% cum ret.	% pass
50	100	1640.7	1640.7	0	0	0.00	100.00
37.5	85-100	1448.7	1448.7	0	0	0.00	100.00
20	60-100	1323.2	1553.8	230.6	230.6	11.54	88.46
10	40-90	1048.1	1612.3	564.2	794.8	39.79	60.21
5	30-75	1095.8	1324.3	228.5	1023.3	51.23	48.77
2.36	20-60	994.3	1321.9	327.6	1350.9	67.63	32.37
0.425	10-45	670.5	950.8	280.3	1631.2	81.66	18.34
0.075	2-20	597.7	923.3	325.6	1956.8	97.96	2.04
pan		733.9	774.6	40.7	1997.5	100.00	0.00

Table A4: Sieve Analysis for Site 1

BS Sieve size (mm)	JKR Requirement	Mass sieve	mass sieve + sample	Sample mass	cum. retains	% cum ret.	% pass
50	100	1640.7	1640.7	0	0	0.00	100.00
37.5	85-100	1448.7	1452.1	3.4	3.4	0.17	99.83
20	60-100	1323.2	1532.8	209.6	213	10.65	89.35
10	40-90	1048.1	1628.9	580.8	793.8	39.71	60.29
5	30-75	1095.8	1328.3	232.5	1026.3	51.34	48.66
2.36	20-60	994.3	1324.8	330.5	1356.8	67.87	32.13
0.425	10-45	670.5	940.4	269.9	1626.7	81.37	18.63
0.075	2-20	597.7	930.3	332.6	1959.3	98.00	2.00
pan		733.9	773.8	39.9	1999.2	100.00	0.00

Table A5: Sieve Analysis for Site 2

BS Sieve size (mm)	JKR Requirement	Mass sieve	mass sieve + sample	Sample mass	cum. retains	% cum ret.	% pass
50	100	1640.7	1640.7	0	0	0.00	100.00
37.5	85-100	1448.7	1485.4	36.7	36.7	1.84	98.16
20	60-100	1323.2	1558.4	235.2	271.9	13.61	86.39
10	40-90	1048.1	1522.3	474.2	746.1	37.34	62.66
5	30-75	1095.8	1413.8	318	1064.1	53.26	46.74
2.36	20-60	994.3	1304.3	310	1374.1	68.78	31.22
0.425	10-45	670.5	936.8	266.3	1640.4	82.11	17.89
0.075	2-20	597.7	906.8	309.1	1949.5	97.58	2.42
pan		733.9	782.3	48.4	1997.9	100.00	0.00

APPENDIX B

Specific Gravity Raw Data

M1 = bottle
M2 = bottle + sand
M3 = bottle + sand + water
M4 = bottle + water

Table B1: Specific Gravity for RAP

	1	2	3	Average
M1	29.59	30.07	27.58	
M2	40.68	41.53	38.8	
M3	85.1	84.04	83.64	
M4	79.7	78.27	77.88	
SG	1.949033	2.01406	2.054945	**2.006013**

Table B2: Specific Gravity for GCBA

	1	2	3	Average
M1	28.87	29.01	28.56	
M2	39.35	40.67	39.01	
M3	85.66	86.51	85.49	
M4	79.33	79.28	79.15	
SG	2.525301	2.632054	2.542579	**2.566645**

Table B3: Specific Gravity for OPC

	1	2	3	Average
M1	30.21	30.3	28.95	
M2	40.41	40.58	39.04	
M3	84.98	86.28	86.39	
M4	78.26	79.51	79.72	
SG	2.931034	2.928775	2.950292	**2.936701**

Table B4: Specific Gravity for Aggregate Dust

	1	2	3	Average
M1	29.79	27.96	25.21	
M2	40.53	38.47	35.76	
M3	86.26	84.31	84.57	
M4	79.78	78.14	78.51	
SG	2.521127	2.421659	2.349666	**2.430817**

Table B5: Specific Gravity for CIPR Site 1

	1	2	3	Average
M1	28.75	29.04	29.75	
M2	39.83	39.4	40.05	
M3	83.61	84.1	84.53	
M4	78.79	78.97	79.07	
SG	1.769968	1.98088	2.128099	**1.959649**

Table B6: Specific Gravity for CIPR Site 2

	1	**2**	**3**	**AVE**
M1	29.85	28.43	29.04	
M2	41.85	41.23	42.02	
M3	85.33	84.48	85.51	
M4	78.56	78.96	79.37	
SG	2.294455	1.758242	1.897661	**1.983453**

APPENDIX C

Particle Shape Raw Data

Flakiness = (total mass of material passing various gauges / weight retain on sieve) x 100

Elongation = (total mass of material retain various gauges / weight retain on sieve) x 100

Table C1: Flakiness Index for Aggregate

100% passing	100% retained	Mass before (g)	Mass retains on gauge (g)	Mass passing on gauge (g)
28	20	126.8	97.4	29.4
20	14	1237.2	1117.2	120.0
14	10	518.9	475.2	43.7
10	6.3	121.2	115.2	6.0
	total	2004.1	1805	199.1
	Flakiness index (%)	**9.93**		

Table C2: Elongation Index for Aggregate

100% passing	100% retained	Mass before (g)	Mass passing gauge (g)	Mass retains on gauge (g)
28	20	147.8	147.8	0
20	14	1187.4	1152.1	35.3
14	10	557.5	475.3	82.2
10	6.3	108.4	98.3	10.1
	total	2001.1	1873.5	127.6
	Elongation index (%)	**6.38**		

Table C3: Flakiness Index for RAP

100% passing	100% retained	Mass before (g)	Mass retains on gauge (g)	Mass passing on gauge (g)
28	20	58.3	58.3	0
20	14	114.5	60.1	54.4
14	10	216.6	185	31.6
10	6.3	418.9	411.6	7.3
	total	808.3	715	93.3
	Flakiness index (%)	**11.54**		

Table C4: Elongation Index for RAP

100% passing	100% retained	Mass before (g)	Mass passing gauge (g)	Mass retains on gauge (g)
28	20	61.1	61.1	0
20	14	139.4	125.1	14.3
14	10	223.4	201.2	22.2
10	6.3	440.2	415.5	24.7
	total	864.1	802.9	61.2
	Elongation index (%)	**7.08**		

Table C5: Flakiness Index for CA75RAP25

100% passing	100% retained	Mass before (g)	Mass retains on gauge (g)	Mass passing on gauge (g)
28	20	110.85	86.55	24.3
20	14	947.53	855.13	92.4
14	10	440.86	406.22	34.64
10	6.3	200.24	186.38	13.86
	total	1699.48	1534.28	165.2
	Flakiness index (%)	**9.72**		

Table C6: Elongation Index for CA75RAP25

100% passing	100% retained	Mass before (g)	Mass passing gauge (g)	Mass retains on gauge (g)
28	20	130.44	130.44	0
20	14	930.12	891.23	38.89
14	10	480.23	406.15	74.08
10	6.3	200.52	180.16	20.36
	total	1741.31	1607.98	133.33
	Elongation index (%)	**7.66**		

Table C7: Flakiness Index for CA50RAP50

100% passing	100% retained	Mass before (g)	Mass retains on gauge (g)	Mass passing on gauge (g)
28	20	89.45	80.3	9.15
20	14	680.55	600.62	79.93
14	10	376.23	332.14	44.09
10	6.3	284.13	255.85	28.28
	total	1430.36	1268.91	161.45
	Flakiness index (%)	**11.29**		

Table C8: Elongation Index for CA50RAP50

100% passing	100% retained	Mass before (g)	Mass passing gauge (g)	Mass retains on gauge (g)
28	20	103.85	100.12	3.73
20	14	680.2	640.18	40.02
14	10	390.85	328.63	62.22
10	6.3	271.35	250.22	21.13
	total	1446.25	1319.15	127.1
	Elongation index (%)	**8.79**		

Table C9: Flakiness Index for CA25RAP75

100% passing	100% retained	Mass before (g)	Mass retains on gauge (g)	Mass passing on gauge (g)
28	20	77.28	70.11	7.17
20	14	410.21	330.85	79.36
14	10	298.53	248.36	50.17
10	6.3	350.52	333.86	16.66
	total	1136.54	983.18	153.36
	Flakiness index (%)	**13.49**		

Table C10: Elongation Index for CA25RAP75

100% passing	100% retained	Mass before (g)	Mass passing gauge (g)	Mass retains on gauge (g)
28	20	90.23	90.23	0
20	14	410.22	370.13	40.09
14	10	308.16	268.52	39.64
10	6.3	344.26	320.11	24.15
	total	1152.87	1048.99	103.88
	Elongation index (%)	**9.01**		

APPENDIX D

Material Durability Raw Data

Table D1: LA Abrasion

	CA75RAP25		CA50RAP50		CA25RAP75	
Sample	1	2	1	2	1	2
A	5003.2	5001.2	5004.3	5002.4	5001.8	5004.21
B	3625.1	3511.28	3171.1	3312.4	3008.5	3152.21
LA Value	27.544	29.791	36.632	33.784	39.852	37.009
Average LA Value (%)	**28.668**		**35.208**		**38.430**	

LA Abrasion = [(A-B)/A] X 100

A = Mass in gm of oven-dried specimen
B = Mass in gm of fraction retained on 1.70 mm IS Sieves after washing and oven-dried

Table D2: Aggregate Impact Value

	C75R25		C50R50		C25R75	
Sample	1	2	1	2	1	2
mass of mould	694.21	694.21	694.21	694.21	694.21	694.21
mass of pan	734.05	734.05	734.05	734.05	734.05	734.05
mass of OD sample + mould	1014.35	1025.1	995.22	1006.3	988.23	983.02
weight of OD sample (before)	320.14	330.89	301.01	312.09	294.02	288.81
mass of fracture passing 2.36 sieve + pan	785.5	786.7	786.32	788.12	790.52	791.5
mass of fracture passing 2.36 sieve (after)	51.45	52.65	52.27	54.07	56.47	57.45
Average before (A)	325.515		306.55		291.415	
Average after (B)	52.05		53.17		56.96	
AIV (%)	**15.99**		**17.34**		**19.55**	

AIV = (B/A) x 100

APPENDIX E

pH Value Raw Data

Table E1: pH Value for Stabilizing Agent

%		Weight (g)		
GCBA	**OPC**	**GCBA**	**OPC**	**PH**
4	0	20	0	9.851
3	1	15	5	13.853
2	2	10	10	14.115
1	3	5	15	13.937
0	4	0	20	14.311

Table E2: pH Value for CA75RAP25

%		Weight (g)					
GCBA	**OPC**	**GCBA**	**OPC**	**0%**	**1%**	**2%**	**3%**
3	1	15	5	14.311	13.668	12.343	11.313
2	2	10	10	14.404	14.121	12.76	11.741
1	3	5	15	14.465	14.128	12.972	11.952
0	4	0	20	14.474	14.205	13.086	12.128

Table E3: pH Value for CA50RAP50

%		Weight (g)					
GCBA	**OPC**	**GCBA**	**OPC**	**0%**	**1%**	**2%**	**3%**
3	1	15	5	14.685	14.472	12.497	11.053
2	2	10	10	14.841	15.01	13.246	11.893
1	3	5	15	14.782	14.838	13.295	12.274
0	4	0	20	14.833	14.707	13.301	12.212

Table E4: pH Value for CA25RAP75

%		Weight (g)					
GCBA	**OPC**	**GCBA**	**OPC**	**0%**	**1%**	**2%**	**3%**
3	1	15	5	14.525	14.203	12.526	11.225
2	2	10	10	14.709	14.348	12.858	11.777
1	3	5	15	14.639	140381	13.097	11.927
0	4	0	20	14.773	14.257	12.97	11.973

APPENDIX F

Energy Dispersive X-Ray (EDX) Raw Data

Table F1: Chemical Composition of GCBA

Element	Weight %	Atomic %	Net Int.	Error %	Kratio	Z	R	A	F
C K	17.7	27.8	18.2	15.0	0.0445	1.0974	0.9553	0.2291	1.0000
O K	38.1	44.9	77.7	9.9	0.1476	1.0456	0.9765	0.3705	1.0000
NaK	1.1	0.9	2.7	41.1	0.0062	0.9449	1.0016	0.5923	1.0054
MgK	1.5	1.1	5.3	20.6	0.0104	0.9597	1.0088	0.7302	1.0098
AlK	8.7	6.1	32.5	7.8	0.0670	0.9230	1.0155	0.8250	1.0121
SiK	20.5	13.8	74.8	5.6	0.1651	0.9421	1.0217	0.8492	1.0049
P K	0.6	0.4	1.7	67.7	0.0045	0.9038	1.0275	0.8117	1.0077
CaK	7.6	3.6	12.8	13.0	0.0678	0.8832	1.0505	0.9807	1.0234
FeK	4.1	1.4	2.5	64.9	0.0347	0.7787	1.0601	1.0012	1.0760

Table F2: Chemical Composition of OPC

Element	Weight %	Atomic %	Net Int.	Error %	Kratio	Z	R	A	F
C K	0.0	0.0	0.0	100.0	0.0001	1.1554	0.9181	0.4123	1.0000
O K	33.0	53.8	36.9	13.4	0.0686	1.1031	0.9415	0.1885	1.0000
MgK	0.4	0.4	1.2	76.0	0.0024	1.0153	0.9777	0.6656	1.0077
AlK	0.9	0.9	3.4	52.8	0.0069	0.9769	0.9854	0.7800	1.0137
SiK	6.7	6.2	26.7	9.4	0.0580	0.9976	0.9926	0.8578	1.0187
S K	0.9	0.8	3.2	58.9	0.0089	0.9756	1.0058	0.9266	1.0509
K K	0.4	0.3	1.0	72.7	0.0041	0.9215	1.0227	0.9864	1.2027
CaK	57.8	37.7	104.0	4.2	0.5440	0.9375	1.0275	0.9940	1.0094

Table F3: Chemical Composition of 3% GCBA + 1% OPC

Element	Weight %	Atomic %	Net Int.	Error %	Kratio	Z	R	A	F
C K	15.6	25.6	21.9	14.8	0.0458	1.1083	0.9482	0.2654	1.0000
O K	38.1	47.0	82.7	10.2	0.1346	1.0565	0.9698	0.3339	1.0000
NaK	0.7	0.6	2.0	72.4	0.0039	0.9553	0.9956	0.5534	1.0044
MgK	0.9	0.7	3.6	39.5	0.0061	0.9704	1.0030	0.6984	1.0081
AlK	7.6	5.6	32.6	8.5	0.0576	0.9333	1.0099	0.8039	1.0104
SiK	15.0	10.5	63.9	6.2	0.1208	0.9528	1.0163	0.8404	1.0069
P K	0.4	0.2	1.2	77.3	0.0027	0.9141	1.0223	0.8305	1.0112
S K	0.5	0.3	1.6	68.4	0.0040	0.9311	1.0279	0.8852	1.0171
K K	0.9	0.4	2.2	65.1	0.0080	0.8787	1.0424	0.9722	1.0595
CaK	13.7	6.7	27.0	9.0	0.1229	0.8937	1.0463	0.9828	1.0222
FeK	6.7	2.4	4.7	26.6	0.0558	0.7885	1.0573	0.9986	1.0616

Table F4: Chemical Composition of 3% GCBA + 1% OPC + 1% $CaCl_2$

Element	Weight %	Atomic %	Net Int.	Error %	Kratio	Z	R	A	F
C K	1.72	3.50	6.02	30.49	0.0062	1.1473	0.9255	0.3143	1.0000
O K	36.83	56.12	125.66	10.50	0.1024	1.0951	0.9485	0.2537	1.0000
MgK	0.66	0.66	5.47	27.46	0.0046	1.0074	0.9841	0.6922	1.0072
AlK	2.92	2.64	25.43	9.44	0.0229	0.9692	0.9916	0.7981	1.0117
SiK	8.47	7.35	75.71	5.93	0.0732	0.9897	0.9986	0.8609	1.0139
ClK	4.70	3.23	30.64	11.03	0.0433	0.9198	1.0172	0.9523	1.0518
CaK	40.68	24.74	161.90	3.51	0.3781	0.9297	1.0323	0.9869	1.0127
FeK	4.01	1.75	5.64	31.96	0.0342	0.8217	1.0478	0.9877	1.0511

Table F5: Chemical Composition of 3% GCBA + 1% OPC + 2% $CaCl_2$

Element	Weight %	Atomic %	Net Int.	Error %	Kratio	Z	R	A	F
C K	8.08	14.80	25.66	13.21	0.0389	1.1272	0.9346	0.4276	1.0000
O K	39.71	54.59	93.48	11.17	0.1116	1.0753	0.9571	0.2614	1.0000
NaK	1.86	1.78	7.04	22.30	0.0101	0.9731	0.9840	0.5567	1.0034
AlK	1.21	0.98	7.06	23.28	0.0093	0.9511	0.9990	0.8023	1.0111
SiK	4.26	3.33	25.79	9.41	0.0366	0.9711	1.0058	0.8722	1.0156
P K	0.43	0.30	2.16	70.45	0.0037	0.9318	1.0122	0.9054	1.0260
S K	0.35	0.24	1.79	68.68	0.0033	0.9493	1.0181	0.9413	1.0416
ClK	1.69	1.05	7.55	20.83	0.0157	0.9022	1.0237	0.9649	1.0627
K K	0.67	0.38	2.48	64.95	0.0068	0.8962	1.0337	0.9885	1.1495
CaK	39.41	21.62	105.47	4.21	0.3617	0.9117	1.0381	0.9947	1.0122
FeK	2.34	0.92	2.21	63.92	0.0197	0.8053	1.0517	0.9902	1.0543

Table F6: Chemical Composition of 3% GCBA + 1% OPC + 3% $CaCl_2$

Element	Weight %	Atomic %	Net Int.	Error %	Kratio	Z	R	A	F
O K	35.23	56.17	78.52	11.64	0.0905	1.1049	0.9446	0.2325	1.0000
NaK	0.45	0.50	1.75	75.86	0.0024	1.0005	0.9725	0.5351	1.0037
MgK	0.42	0.44	2.42	69.28	0.0029	1.0167	0.9806	0.6811	1.0067
AlK	1.59	1.50	9.77	16.88	0.0124	0.9783	0.9882	0.7908	1.0116
SiK	4.36	3.96	28.03	9.60	0.0382	0.9990	0.9953	0.8618	1.0166
P K	0.87	0.72	4.70	38.05	0.0077	0.9588	1.0020	0.8966	1.0273
S K	0.54	0.43	2.91	50.84	0.0051	0.9768	1.0083	0.9334	1.0435
ClK	10.71	7.70	50.00	6.17	0.0997	0.9285	1.0142	0.9588	1.0457
K K	0.49	0.32	1.83	66.10	0.0048	0.9226	1.0249	0.9676	1.1098
CaK	41.95	26.70	118.60	3.92	0.3904	0.9386	1.0296	0.9797	1.0119
FeK	3.40	1.55	3.42	39.48	0.0292	0.8300	1.0459	0.9853	1.0504

Table F7: Chemical Composition of 2% GCBA + 2% OPC

Element	Weight %	Atomic %	Net Int.	Error %	Kratio	Z	R	A	F
C K	8.9	16.2	14.1	16.4	0.0305	1.1279	0.9366	0.3024	1.0000
O K	37.3	50.8	71.6	10.6	0.1221	1.0759	0.9589	0.3041	1.0000
NaK	0.2	0.2	0.6	88.1	0.0013	0.9735	0.9857	0.5443	1.0041
MgK	0.5	0.5	2.1	70.3	0.0037	0.9890	0.9934	0.6913	1.0075
AlK	4.9	3.9	20.0	10.4	0.0374	0.9514	1.0006	0.7989	1.0112
SiK	14.4	11.1	59.8	6.4	0.1200	0.9714	1.0073	0.8519	1.0091
S K	0.4	0.2	1.2	70.3	0.0031	0.9496	1.0196	0.8971	1.0240
K K	1.0	0.5	2.3	64.1	0.0091	0.8964	1.0350	0.9758	1.0880
CaK	24.7	13.4	46.7	6.1	0.2263	0.9119	1.0393	0.9850	1.0184
MnK	0.8	0.3	0.7	72.6	0.0067	0.7948	1.0524	0.9901	1.0583
FeK	6.9	2.7	4.6	28.6	0.0578	0.8053	1.0526	0.9938	1.0534

Table F8: Chemical Composition of 2% GCBA + 2% OPC+ 1% $CaCl_2$

Element	Weight %	Atomic %	Net Int.	Error %	Kratio	Z	R	A	F
C K	1.56	3.31	4.28	39.29	0.0054	1.1576	0.9202	0.2965	1.0000
O K	33.33	53.08	87.96	11.50	0.0868	1.1052	0.9435	0.2357	1.0000
NaK	0.01	0.01	0.03	99.99	0.0000	1.0008	0.9714	0.5310	1.0037
MgK	0.25	0.26	1.71	73.50	0.0018	1.0171	0.9796	0.6793	1.0068
AlK	2.07	1.96	14.88	13.61	0.0162	0.9786	0.9872	0.7900	1.0114
SiK	6.33	5.74	47.20	7.49	0.0552	0.9993	0.9944	0.8588	1.0151
P K	0.59	0.48	3.65	50.39	0.0051	0.9591	1.0011	0.8858	1.0251
S K	0.61	0.48	3.78	44.70	0.0057	0.9772	1.0074	0.9261	1.0398
ClK	6.49	4.67	35.32	9.96	0.0604	0.9289	1.0134	0.9532	1.0502
K K	0.64	0.41	2.83	63.48	0.0064	0.9230	1.0241	0.9730	1.1201
CaK	42.54	27.04	141.01	3.83	0.3980	0.9391	1.0289	0.9833	1.0130
FeK	5.59	2.55	6.55	28.96	0.0480	0.8305	1.0454	0.9858	1.0482

Table F9: Chemical Composition of 2% GCBA + 2% OPC+ 2% $CaCl_2$

Element	Weight %	Atomic %	Net Int.	Error %	Kratio	Z	R	A	F
C K	2.04	4.32	4.54	32.73	0.0058	1.1589	0.9210	0.2444	1.0000
O K	31.87	50.69	81.15	11.66	0.0808	1.1064	0.9443	0.2291	1.0000
NaK	0.44	0.49	1.96	75.14	0.0023	1.0019	0.9721	0.5236	1.0037
MgK	0.48	0.51	3.24	46.44	0.0033	1.0181	0.9803	0.6712	1.0069
AlK	2.32	2.18	16.49	12.89	0.0180	0.9796	0.9879	0.7829	1.0115
SiK	6.63	6.00	49.13	7.27	0.0574	1.0003	0.9950	0.8524	1.0150
P K	1.15	0.95	7.09	29.93	0.0100	0.9601	1.0017	0.8788	1.0243
S K	0.92	0.73	5.65	28.56	0.0085	0.9782	1.0080	0.9193	1.0381
ClK	9.23	6.62	49.68	6.67	0.0847	0.9298	1.0140	0.9475	1.0425
K K	0.51	0.33	2.22	64.74	0.0050	0.9239	1.0247	0.9641	1.1016
CaK	38.69	24.56	128.00	3.95	0.3602	0.9400	1.0294	0.9771	1.0135
MnK	1.31	0.61	1.85	64.00	0.0110	0.8202	1.0450	0.9795	1.0460
FeK	4.41	2.01	5.20	30.63	0.0379	0.8312	1.0458	0.9857	1.0492

Table F10: Chemical Composition of 2% GCBA + 2% OPC + 3% $CaCl_2$

Element	Weight %	Atomic %	Net Int.	Error %	Kratio	Z	R	A	F
C K	2.91	6.09	8.19	24.06	0.0092	1.1559	0.9213	0.2733	1.0000
O K	32.78	51.56	87.83	11.26	0.0771	1.1035	0.9445	0.2131	1.0000
NaK	0.12	0.13	0.59	99.23	0.0006	0.9992	0.9724	0.5152	1.0036
MgK	0.25	0.26	1.87	72.18	0.0017	1.0154	0.9805	0.6659	1.0067
AlK	1.48	1.38	11.94	14.67	0.0115	0.9771	0.9881	0.7806	1.0114
SiK	4.04	3.62	34.14	8.89	0.0351	0.9977	0.9952	0.8551	1.0166
P K	0.82	0.67	5.84	34.79	0.0072	0.9576	1.0019	0.8928	1.0274
S K	0.69	0.54	4.93	33.92	0.0066	0.9756	1.0083	0.9313	1.0433
ClK	8.98	6.37	55.75	6.41	0.0836	0.9274	1.0142	0.9571	1.0491
K K	0.78	0.50	3.95	37.43	0.0078	0.9215	1.0249	0.9696	1.1169
CaK	42.91	26.94	161.44	3.59	0.3995	0.9375	1.0296	0.9808	1.0123
MnK	1.37	0.63	2.18	63.45	0.0114	0.8180	1.0451	0.9777	1.0437
FeK	2.86	1.29	3.82	39.01	0.0245	0.8290	1.0459	0.9843	1.0494

Table F11: Chemical Composition of 1% GCBA + 3% OPC

Element	Weight %	Atomic %	Net Int.	Error %	Kratio	Z	R	A	F
C K	0.0	0.0	0.0	100.0	0.0001	1.1502	0.9239	0.3310	1.0000
O K	36.8	57.1	66.1	12.0	0.1000	1.0979	0.9470	0.2477	1.0000
NaK	0.1	0.1	0.2	100.0	0.0003	0.9940	0.9747	0.5221	1.0041
MgK	0.7	0.7	3.0	68.0	0.0047	1.0101	0.9827	0.6719	1.0075
AlK	4.8	4.4	22.1	10.2	0.0367	0.9719	0.9903	0.7824	1.0115
SiK	10.3	9.1	49.0	7.4	0.0871	0.9924	0.9973	0.8402	1.0129
S K	0.6	0.5	2.4	66.2	0.0056	0.9703	1.0102	0.9043	1.0349
CaK	41.5	25.7	90.3	4.6	0.3874	0.9323	1.0313	0.9884	1.0134
FeK	5.3	2.4	4.1	33.1	0.0453	0.8242	1.0471	0.9868	1.0499

Table F12: Chemical Composition of 1% GCBA + 3% OPC+ 1% $CaCl_2$

Element	Weight %	Atomic %	Net Int.	Error %	Kratio	Z	R	A	F
C K	2.24	4.17	2.84	62.52	0.0061	1.1315	0.9356	0.2385	1.0000
O K	45.41	63.47	77.28	11.54	0.1204	1.0793	0.9580	0.2455	1.0000
NaK	0.19	0.18	0.46	99.99	0.0008	0.9766	0.9848	0.4450	1.0038
MgK	0.84	0.77	3.32	40.90	0.0051	0.9922	0.9926	0.6038	1.0068
AlK	3.36	2.79	14.74	12.68	0.0237	0.9545	0.9998	0.7298	1.0107
SiK	9.48	7.54	44.12	7.62	0.0754	0.9745	1.0066	0.8072	1.0114
P K	0.59	0.43	2.26	68.26	0.0046	0.9351	1.0129	0.8255	1.0187
S K	0.42	0.30	1.67	68.53	0.0037	0.9526	1.0189	0.8832	1.0295
ClK	4.24	2.67	14.91	13.31	0.0369	0.9054	1.0244	0.9249	1.0385
K K	0.31	0.18	0.91	73.21	0.0030	0.8993	1.0344	0.9634	1.0912
CaK	27.35	15.26	61.28	5.68	0.2488	0.9148	1.0387	0.9785	1.0161
MnK	0.88	0.36	0.85	69.87	0.0073	0.7974	1.0520	0.9841	1.0544
FeK	4.68	1.87	3.77	35.76	0.0395	0.8079	1.0522	0.9898	1.0551

Table F13: Chemical Composition of 1% GCBA + 3% OPC + 2% $CaCl_2$

Element	Weight %	Atomic %	Net Int.	Error %	Kratio	Z	R	A	F
C K	4.30	8.28	9.67	22.93	0.0123	1.1400	0.9312	0.2497	1.0000
O K	37.58	54.26	111.44	10.47	0.1085	1.0878	0.9539	0.2655	1.0000
NaK	0.69	0.69	2.97	62.65	0.0034	0.9845	0.9811	0.5031	1.0039
MgK	0.77	0.73	5.10	28.09	0.0050	1.0003	0.9889	0.6528	1.0072
AlK	4.27	3.65	30.44	8.82	0.0319	0.9624	0.9963	0.7678	1.0111
SiK	12.37	10.18	91.19	5.78	0.1021	0.9826	1.0032	0.8310	1.0104
P K	0.01	0.01	0.06	99.99	0.0001	0.9429	1.0096	0.8343	1.0176
S K	0.22	0.16	1.36	70.21	0.0020	0.9606	1.0157	0.8900	1.0280
ClK	3.91	2.55	21.10	11.80	0.0344	0.9130	1.0214	0.9291	1.0374
K K	0.74	0.44	3.29	50.82	0.0071	0.9070	1.0315	0.9660	1.0869
CaK	27.69	15.96	94.64	4.54	0.2543	0.9227	1.0360	0.9785	1.0170
MnK	0.90	0.38	1.33	67.71	0.0076	0.8045	1.0499	0.9856	1.0546
FeK	6.54	2.71	7.99	23.40	0.0556	0.8152	1.0503	0.9906	1.0519

Table F14: Chemical Composition of 1% GCBA + 3% OPC + 3% $CaCl_2$

Element	Weight %	Atomic %	Net Int.	Error %	Kratio	Z	R	A	F
C K	3.88	7.73	12.19	18.97	0.0125	1.1452	0.9269	0.2805	1.0000
O K	36.44	54.50	113.29	10.83	0.0911	1.0930	0.9498	0.2287	1.0000
NaK	0.23	0.24	1.24	82.15	0.0012	0.9894	0.9772	0.5317	1.0036
MgK	0.10	0.10	0.83	83.62	0.0007	1.0054	0.9852	0.6804	1.0067
AlK	1.52	1.35	13.41	15.10	0.0118	0.9673	0.9927	0.7931	1.0115
SiK	3.99	3.40	36.65	8.60	0.0347	0.9877	0.9997	0.8644	1.0166
P K	0.74	0.57	5.71	36.89	0.0065	0.9479	1.0062	0.9000	1.0274
S K	0.58	0.43	4.46	41.35	0.0055	0.9657	1.0124	0.9368	1.0435
ClK	9.17	6.19	61.32	6.32	0.0848	0.9179	1.0182	0.9614	1.0477
K K	0.66	0.40	3.57	47.00	0.0065	0.9119	1.0286	0.9718	1.1137
CaK	40.20	24.00	162.46	3.57	0.3709	0.9278	1.0332	0.9826	1.0117
MnK	0.73	0.32	1.24	65.35	0.0060	0.8092	1.0478	0.9804	1.0450
FeK	1.76	0.75	2.53	62.23	0.0150	0.8200	1.0484	0.9864	1.0524

Table F15: Chemical Composition of 4% OPC + 1% $CaCl_2$

Element	Weight %	Atomic %	Net Int.	Error %	Kratio	Z	R	A	F
C K	5.97	11.79	16.41	17.58	0.0201	1.1439	0.9269	0.2948	1.0000
O K	34.07	50.52	90.39	11.49	0.0875	1.0917	0.9498	0.2351	1.0000
MgK	0.25	0.24	1.71	72.87	0.0017	1.0042	0.9853	0.6913	1.0068
AlK	1.76	1.55	12.89	14.13	0.0137	0.9662	0.9927	0.8003	1.0115
SiK	4.83	4.08	36.74	8.27	0.0421	0.9866	0.9997	0.8682	1.0159
P K	0.96	0.73	6.05	33.79	0.0083	0.9468	1.0063	0.8992	1.0260
S K	1.47	1.09	9.29	18.92	0.0138	0.9646	1.0125	0.9350	1.0398
ClK	7.02	4.70	38.58	8.27	0.0646	0.9169	1.0183	0.9571	1.0481
K K	0.72	0.43	3.20	52.62	0.0071	0.9109	1.0286	0.9739	1.1145
CaK	39.54	23.41	132.04	3.95	0.3651	0.9267	1.0332	0.9839	1.0123
FeK	3.42	1.45	4.05	36.16	0.0291	0.8191	1.0484	0.9873	1.0514

Table F16: Chemical Composition of 4% OPC + 2% $CaCl_2$

Element	Weight %	Atomic %	Net Int.	Error %	Kratio	Z	R	A	F
C K	2.09	4.16	5.12	31.18	0.0066	1.1421	0.9273	0.2780	1.0000
O K	39.15	58.64	78.31	12.23	0.0746	1.0900	0.9502	0.1748	1.0000
MgK	0.33	0.33	2.18	71.67	0.0020	1.0026	0.9856	0.6123	1.0069
AlK	1.07	0.95	7.84	20.78	0.0078	0.9646	0.9931	0.7403	1.0121
SiK	3.74	3.19	29.51	9.66	0.0311	0.9849	1.0000	0.8294	1.0177
P K	0.65	0.50	4.39	42.70	0.0055	0.9452	1.0066	0.8748	1.0295
ClK	7.10	4.80	43.03	8.43	0.0656	0.9153	1.0185	0.9542	1.0588
CaK	45.88	27.43	168.50	3.51	0.4220	0.9251	1.0335	0.9849	1.0101

Table F17: Chemical Composition of 4% OPC + 3% $CaCl_2$

Element	Weight %	Atomic %	Net Int.	Error %	Kratio	Z	R	A	F
O K	41.47	62.68	93.38	11.32	0.0899	1.0912	0.9499	0.1987	1.0000
MgK	0.42	0.41	2.76	69.23	0.0027	1.0037	0.9853	0.6400	1.0068
AlK	1.10	0.99	7.96	20.94	0.0082	0.9657	0.9928	0.7611	1.0119
SiK	3.61	3.11	27.82	10.06	0.0306	0.9860	0.9998	0.8439	1.0175
ClK	7.61	5.19	44.30	7.65	0.0709	0.9163	1.0183	0.9607	1.0583
CaK	45.79	27.63	160.35	3.51	0.4226	0.9261	1.0332	0.9863	1.0101

APPENDIX G

X-Ray Diffraction (XRD) Raw Data

Table G1: Crystalline Compound of GCBA

Qualitative analysis results

Phase name	Formula	Figure of merit	Phase reg. detail	DB card number
Quartz, syn	Si O2	0.919	ICDD (PDF-2 2022)	01-085-0457
Coesite, syn	Si O2	1.539	ICDD (PDF-2 2022)	01-072-1601
calcite high	Ca (C O3)	1.848	ICDD (PDF-2 2022)	01-086-2340
Portlandite	Ca (O H)2	2.184	ICDD (PDF-2 2022)	00-001-1079

Phase name	Formula	Space group	Phase reg. detail	DB card number
Quartz, syn	Si O2	154 : P3221	ICDD (PDF-2 2022)	01-085-0457
Coesite, syn	Si O2	15 : C12/c1,unique-b,cell-1	ICDD (PDF-2 2022)	01-072-1601
calcite high	Ca (C O3)	167 : R-3c,hexagonal	ICDD (PDF-2 2022)	01-086-2340
Portlandite	Ca (O H)2	164 : P-3m1	ICDD (PDF-2 2022)	00-001-1079

Table G2: Crystalline Compound of OPC

Qualitative analysis results

Phase name	Formula	Figure of merit	Phase reg. detail	DB card number
Hatrurite, syn	Ca3 (Si O4) O	0.531	ICDD (PDF-2 2022)	01-086-0402
Calcium Silicide	Ca Si2	0.991	ICDD (PDF-2 2022)	01-083-9778

Phase name	Formula	Space group	Phase reg. detail	DB card number
Hatrurite, syn	Ca3 (Si O4) O	8 : C1m1,unique-b,cell-1	ICDD (PDF-2 2022)	01-086-0402
Calcium Silicide	Ca Si2	164 : P-3m1	ICDD (PDF-2 2022)	01-083-9778

Table G3: Crystalline Compound of 3% GCBA + 1% OPC

Qualitative analysis results

Phase name	Formula	Figure of merit	Phase reg. detail	DB card number
calcite high	Ca (C O3)	0.655	ICDD (PDF-2 2022)	01-086-2340
Quartz, syn	Si O2	2.537	ICDD (PDF-2 2022)	01-085-0457
Cristobalite, syn	Si O2	0.922	ICDD (PDF-2 2022)	00-039-1425

Phase name	Formula	Space group	Phase reg. detail	DB card number
calcite high	Ca (C O3)	167 : R-3c,hexagonal	ICDD (PDF-2 2022)	01-086-2340
Quartz, syn	Si O2	154 : P3221	ICDD (PDF-2 2022)	01-085-0457
Cristobalite, syn	Si O2	92 : P41212	ICDD (PDF-2 2022)	00-039-1425

Table G4: Crystalline Compound of 3% GCBA + 1% OPC + 1% $CaCl_2$

Qualitative analysis results

Phase name	Formula	Figure of merit	Phase reg. detail	DB card number
Calcium Silicate Chloride	Ca2 Si O3 Cl2	1.073	ICDD (PDF-2 2022)	00-042-1455

Phase name	Formula	Space group	Phase reg. detail	DB card number
Calcium Silicate Chloride	Ca2 Si O3 Cl2	47 : Pmmm	ICDD (PDF-2 2022)	00-042-1455

Table G5: Crystalline Compound of 3% GCBA + 1% OPC + 2% $CaCl_2$

Qualitative analysis results

Phase name	Formula	Figure of merit	Phase reg. detail	DB card number
Quartz, syn	Si O2	1.453	ICDD (PDF-2 2022)	01-085-0457
Calcium Aluminum Silicide	Ca Al Si	2.939	ICDD (PDF-2 2022)	01-075-3112
calcite high	Ca (C O3)	1.723	ICDD (PDF-2 2022)	01-086-2340
Portlandite	Ca (O H)2	2.948	ICDD (PDF-2 2022)	00-001-1079
Berlinite, syn	Al P O4	3.156	ICDD (PDF-2 2022)	01-071-1041
Coesite, syn	Si O2	3.030	ICDD (PDF-2 2022)	01-072-1601
Cristobalite, syn	Si O2	3.173	ICDD (PDF-2 2022)	00-039-1425

Phase name	Formula	Space group	Phase reg. detail	DB card number
Quartz, syn	Si O2	154 : P3221	ICDD (PDF-2 2022)	01-085-0457
Calcium Aluminum Silicide	Ca Al Si	143 : P3	ICDD (PDF-2 2022)	01-075-3112
calcite high	Ca (C O3)	167 : R-3c,hexagonal	ICDD (PDF-2 2022)	01-086-2340
Portlandite	Ca (O H)2	164 : P-3m1	ICDD (PDF-2 2022)	00-001-1079
Berlinite, syn	Al P O4	152 : P3121	ICDD (PDF-2 2022)	01-071-1041
Coesite, syn	Si O2	15 : C12/c1,unique-b,cell-1	ICDD (PDF-2 2022)	01-072-1601
Cristobalite, syn	Si O2	92 : P41212	ICDD (PDF-2 2022)	00-039-1425

Table G6: Crystalline Compound of 3% GCBA + 1% OPC + 3% $CaCl_2$

Qualitative analysis results

Phase name	Formula	Figure of merit	Phase reg. detail	DB card number
Calcium Aluminum Silicide	Ca Al Si	1.557	ICDD (PDF-2 2022)	01-075-3112
Quartz, syn	Si O2	1.459	ICDD (PDF-2 2022)	01-085-0457
calcite high	Ca (C O3)	1.839	ICDD (PDF-2 2022)	01-086-2340
Coesite, syn	Si O2	3.045	ICDD (PDF-2 2022)	01-072-1601
Berlinite, syn	Al P O4	2.766	ICDD (PDF-2 2022)	01-071-1041
Portlandite	Ca (O H)2	2.856	ICDD (PDF-2 2022)	00-001-1079
Cristobalite, syn	Si O2	3.069	ICDD (PDF-2 2022)	00-039-1425

Phase name	Formula	Space group	Phase reg. detail	DB card number
Calcium Aluminum Silicide	Ca Al Si	143 : P3	ICDD (PDF-2 2022)	01-075-3112
Quartz, syn	Si O2	154 : P3221	ICDD (PDF-2 2022)	01-085-0457
calcite high	Ca (C O3)	167 : R-3c,hexagonal	ICDD (PDF-2 2022)	01-086-2340
Coesite, syn	Si O2	15 : C12/c1,unique-b,cell-1	ICDD (PDF-2 2022)	01-072-1601
Berlinite, syn	Al P O4	152 : P3121	ICDD (PDF-2 2022)	01-071-1041
Portlandite	Ca (O H)2	164 : P-3m1	ICDD (PDF-2 2022)	00-001-1079
Cristobalite, syn	Si O2	92 : P41212	ICDD (PDF-2 2022)	00-039-1425

Table G7: Crystalline Compound of 2% GCBA + 2% OPC

Qualitative analysis results

Phase name	Formula	Figure of merit	Phase reg. detail	DB card number
calcite high	Ca (C O3)	0.932	ICDD (PDF-2 2022)	01-086-2340
Quartz, syn	Si O2	1.082	ICDD (PDF-2 2022)	01-085-0457
Calcium Aluminum Silicide	Ca Al Si	1.860	ICDD (PDF-2 2022)	01-075-3112

Phase name	Formula	Space group	Phase reg. detail	DB card number
calcite high	Ca (C O3)	167 : R-3c,hexagonal	ICDD (PDF-2 2022)	01-086-2340
Quartz, syn	Si O2	154 : P3221	ICDD (PDF-2 2022)	01-085-0457
Calcium Aluminum Silicide	Ca Al Si	143 : P3	ICDD (PDF-2 2022)	01-075-3112

Table G8: Crystalline Compound of 2% GCBA + 2% OPC + 1% $CaCl_2$

Qualitative analysis results

Phase name	Formula	Figure of merit	Phase reg. detail	DB card number
Calcite, Mg-bearing, syn	(Mg0.03 Ca0.97) (C O3)	0.706	ICDD (PDF-2 2022)	01-089-1304
Quartz, syn	Si O2	1.259	ICDD (PDF-2 2022)	01-085-0457

Phase name	Formula	Space group	Phase reg. detail	DB card number
Calcite, Mg-bearing, syn	(Mg0.03 Ca0.97) (C O3)	167 : R-3c,hexagonal	ICDD (PDF-2 2022)	01-089-1304
Quartz, syn	Si O2	154 : P3221	ICDD (PDF-2 2022)	01-085-0457

Table G9: Crystalline Compound of 2% GCBA + 2% OPC + 2% $CaCl_2$

Qualitative analysis results

Phase name	Formula	Figure of merit	Phase reg. detail	DB card number
Rankinite	Ca3 (Si2 O7)	1.224	ICDD (PDF-2 2022)	01-070-1138
calcite high	Ca (C O3)	1.718	ICDD (PDF-2 2022)	01-086-2340
Calcium Aluminum Silicide	Ca Al Si	1.993	ICDD (PDF-2 2022)	01-075-3112

Phase name	Formula	Space group	Phase reg. detail	DB card number
Rankinite	Ca3 (Si2 O7)	14 : P121/a1,unique-b,cell-3	ICDD (PDF-2 2022)	01-070-1138
calcite high	Ca (C O3)	167 : R-3c,hexagonal	ICDD (PDF-2 2022)	01-086-2340
Calcium Aluminum Silicide	Ca Al Si	143 : P3	ICDD (PDF-2 2022)	01-075-3112

Table G10: Crystalline Compound of 2% GCBA + 2% OPC + 3% $CaCl_2$

Qualitative analysis results

Phase name	Formula	Figure of merit	Phase reg. detail	DB card number
calcite high	Ca (C O3)	2.095	ICDD (PDF-2 2022)	01-086-2340
Calcium Aluminum Silicide	Ca Al Si	3.135	ICDD (PDF-2 2022)	01-075-3112
Cristobalite, syn	Si O2	1.754	ICDD (PDF-2 2022)	00-039-1425
Coesite, syn	Si O2	2.089	ICDD (PDF-2 2022)	01-072-1601

Phase name	Formula	Space group	Phase reg. detail	DB card number
calcite high	Ca (C O3)	167 : R-3c,hexagonal	ICDD (PDF-2 2022)	01-086-2340
Calcium Aluminum Silicide	Ca Al Si	143 : P3	ICDD (PDF-2 2022)	01-075-3112
Cristobalite, syn	Si O2	92 : P41212	ICDD (PDF-2 2022)	00-039-1425
Coesite, syn	Si O2	15 : C12/c1,unique-b,cell-1	ICDD (PDF-2 2022)	01-072-1601

Table G11: Crystalline Compound of 1% GCBA + 3% OPC

Qualitative analysis results

Phase name	Formula	Figure of merit	Phase reg. detail	DB card number
calcite high	Ca (C O3)	0.655	ICDD (PDF-2 2022)	01-086-2340
Quartz, syn	Si O2	2.537	ICDD (PDF-2 2022)	01-085-0457
Cristobalite, syn	Si O2	0.922	ICDD (PDF-2 2022)	00-039-1425

Phase name	Formula	Space group	Phase reg. detail	DB card number
calcite high	Ca (C O3)	167 : R-3c,hexagonal	ICDD (PDF-2 2022)	01-086-2340
Quartz, syn	Si O2	154 : P3221	ICDD (PDF-2 2022)	01-085-0457
Cristobalite, syn	Si O2	92 : P41212	ICDD (PDF-2 2022)	00-039-1425

Table G12: Crystalline Compound of 1% GCBA + 3% OPC + 1% $CaCl_2$

Qualitative analysis results

Phase name	Formula	Figure of merit	Phase reg. detail	DB card number
Calcium Silicate Chloride	Ca2 Si O3 Cl2	1.073	ICDD (PDF-2 2022)	00-042-1455

Phase name	Formula	Space group	Phase reg. detail	DB card number
Calcium Silicate Chloride	Ca2 Si O3 Cl2	47 : Pmmm	ICDD (PDF-2 2022)	00-042-1455

Table G13: Crystalline Compound of 1% GCBA + 3% OPC + 2% $CaCl_2$

Qualitative analysis results

Phase name	Formula	Figure of merit	Phase reg. detail	DB card number
calcite high	Ca (C O3)	1.694	ICDD (PDF-2 2022)	01-086-2340
Berlinite, syn	Al P O4	2.848	ICDD (PDF-2 2022)	01-071-1041
Calcium Aluminum Silicide	Ca Al Si	2.753	ICDD (PDF-2 2022)	01-075-3112
Coesite, syn	Si O2	1.667	ICDD (PDF-2 2022)	01-072-1601
Portlandite	Ca (O H)2	2.850	ICDD (PDF-2 2022)	00-001-1079

Phase name	Formula	Space group	Phase reg. detail	DB card number
calcite high	Ca (C O3)	167 : R-3c,hexagonal	ICDD (PDF-2 2022)	01-086-2340
Berlinite, syn	Al P O4	152 : P3121	ICDD (PDF-2 2022)	01-071-1041
Calcium Aluminum Silicide	Ca Al Si	143 : P3	ICDD (PDF-2 2022)	01-075-3112
Coesite, syn	Si O2	15 : C12/c1,unique-b,cell-1	ICDD (PDF-2 2022)	01-072-1601
Portlandite	Ca (O H)2	164 : P-3m1	ICDD (PDF-2 2022)	00-001-1079

Table G14: Crystalline Compound of 1% GCBA + 3% OPC + 3% $CaCl_2$

Qualitative analysis results

Phase name	Formula	Figure of merit	Phase reg. detail	DB card number
Calcium Aluminum Silicide	Ca Al Si	1.322	ICDD (PDF-2 2022)	01-075-3112
Portlandite	Ca (O H)2	2.850	ICDD (PDF-2 2022)	00-001-1079
Cristobalite, syn	Si O2	2.988	ICDD (PDF-2 2022)	00-039-1425
Quartz, syn	Si O2	2.779	ICDD (PDF-2 2022)	01-085-0457
Coesite, syn	Si O2	3.123	ICDD (PDF-2 2022)	01-072-1601
calcite high	Ca (C O3)	3.242	ICDD (PDF-2 2022)	01-086-2340
Berlinite, syn	Al P O4	3.328	ICDD (PDF-2 2022)	01-071-1041

Phase name	Formula	Space group	Phase reg. detail	DB card number
Calcium Aluminum Silicide	Ca Al Si	143 : P3	ICDD (PDF-2 2022)	01-075-3112
Portlandite	Ca (O H)2	164 : P-3m1	ICDD (PDF-2 2022)	00-001-1079
Cristobalite, syn	Si O2	92 : P41212	ICDD (PDF-2 2022)	00-039-1425
Quartz, syn	Si O2	154 : P3221	ICDD (PDF-2 2022)	01-085-0457
Coesite, syn	Si O2	15 : C12/c1,unique-b,cell-1	ICDD (PDF-2 2022)	01-072-1601
calcite high	Ca (C O3)	167 : R-3c,hexagonal	ICDD (PDF-2 2022)	01-086-2340
Berlinite, syn	Al P O4	152 : P3121	ICDD (PDF-2 2022)	01-071-1041

Table G15: Crystalline Compound of 4% OPC + 1% $CaCl_2$

Qualitative analysis results

Phase name	Formula	Figure of merit	Phase reg. detail	DB card number
calcite high	Ca (C O3)	2.978	ICDD (PDF-2 2022)	01-086-2340
Calcium Aluminum Silicide	Ca Al Si	3.588	ICDD (PDF-2 2022)	01-075-3112
Berlinite, syn	Al P O4	3.258	ICDD (PDF-2 2022)	01-071-1041
Cristobalite, syn	Si O2	3.149	ICDD (PDF-2 2022)	00-039-1425
Quartz, syn	Si O2	3.467	ICDD (PDF-2 2022)	01-085-0457
Portlandite	Ca (O H)2	1.854	ICDD (PDF-2 2022)	00-001-1079

Phase name	Formula	Space group	Phase reg. detail	DB card number
calcite high	Ca (C O3)	167 : R-3c,hexagonal	ICDD (PDF-2 2022)	01-086-2340
Calcium Aluminum Silicide	Ca Al Si	143 : P3	ICDD (PDF-2 2022)	01-075-3112
Berlinite, syn	Al P O4	152 : P3121	ICDD (PDF-2 2022)	01-071-1041
Cristobalite, syn	Si O2	92 : P41212	ICDD (PDF-2 2022)	00-039-1425
Quartz, syn	Si O2	154 : P3221	ICDD (PDF-2 2022)	01-085-0457
Portlandite	Ca (O H)2	164 : P-3m1	ICDD (PDF-2 2022)	00-001-1079

Table G16: Crystalline Compound of 4% OPC + 2% $CaCl_2$

Qualitative analysis results

Phase name	Formula	Figure of merit	Phase reg. detail	DB card number
Coesite, syn	Si O2	3.007	ICDD (PDF-2 2022)	01-072-1601
Cristobalite, syn	Si O2	2.213	ICDD (PDF-2 2022)	00-039-1425
calcite high	Ca (C O3)	2.162	ICDD (PDF-2 2022)	01-086-2340
Calcium Aluminum Silicide	Ca Al Si	3.202	ICDD (PDF-2 2022)	01-075-3112
Portlandite	Ca (O H)2	3.240	ICDD (PDF-2 2022)	00-001-1079
Quartz, syn	Si O2	2.792	ICDD (PDF-2 2022)	01-085-0457
Berlinite, syn	Al P O4	3.379	ICDD (PDF-2 2022)	01-071-1041

Phase name	Formula	Space group	Phase reg. detail	DB card number
Coesite, syn	Si O2	15 : C12/c1,unique-b,cell-1	ICDD (PDF-2 2022)	01-072-1601
Cristobalite, syn	Si O2	92 : P41212	ICDD (PDF-2 2022)	00-039-1425
calcite high	Ca (C O3)	167 : R-3c,hexagonal	ICDD (PDF-2 2022)	01-086-2340
Calcium Aluminum Silicide	Ca Al Si	143 : P3	ICDD (PDF-2 2022)	01-075-3112
Portlandite	Ca (O H)2	164 : P-3m1	ICDD (PDF-2 2022)	00-001-1079
Quartz, syn	Si O2	154 : P3221	ICDD (PDF-2 2022)	01-085-0457
Berlinite, syn	Al P O4	152 : P3121	ICDD (PDF-2 2022)	01-071-1041

APPENDIX H

Optimum Moisture Content & Maximum Dry Density Data

Table H1: OMC & MDD Data for CA75RAP25

Percentage	**4%**	**5%**	**6%**	**7%**	**8%**
Mould + base + soil (g)	5412.12	5451.21	5478.53	5470.21	5452.21
Mould + base (g)	3545.02	3545.33	3545.54	3545.02	3545.00
Soil Mass (g)	1867.10	1905.88	1932.99	1925.19	1907.21
Wet Density, ρ	1.8671	1.90588	1.93299	1.92519	1.90721

Moisture Content

No1. (4%)	1	2	3
Wet soil+container, W2 (g)	135.4	132.78	104.05
Dry soil+container, W1 (g)	131.3	128.66	101.12
Empty container, Wo (g)	24.04	23.65	22.14
Moisture content, Wn	3.8225	3.9234	3.7098
Average moisture content, w%	**3.8186**		
No2. (5%)	1	2	3
Wet soil+container, W2 (g)	92.53	87.2	117.25
Dry soil+container, W1 (g)	89.25	84.1	112.73
Empty container, Wo (g)	21.95	20	23.76
Moisture content, Wn	4.8737	4.8362	5.0804
Average moisture content, w%	**4.9301**		
No3. (6%)	1	2	3
Wet soil+container, w2 (g)	98.52	102.8	99
Dry soil+container, w1 (g)	94.21	98.15	94.55
Empty container, Wo (g)	20.1	20.17	23.22
Moisture content, Wn	5.8157	5.9631	6.2386
Average moisture content, w%	**6.0058**		
No4. (7%)	1	2	3
Wet soil+container, w2 (g)	101.53	105.46	107.92
Dry soil+container, w1 (g)	96.74	100.1	102.26
Empty container, Wo (g)	23.89	19.72	23.37
Moisture content, Wn	6.5752	6.6683	7.1745
Average moisture content, w%	**6.8060**		
No5. (8%)	1	2	3
Wet soil+container, w2 (g)	123.44	113.42	127.61
Dry soil+container, w1 (g)	116.12	106.94	120.35
Empty container, Wo (g)	25.12	21.8	24.08
Moisture content, Wn	8.0440	7.6110	7.5413
Average moisture content, w%	**7.7321**		

Dry Density

Percentage	**4%**	**5%**	**6%**	**7%**	**8%**
Average Moisture Content, w%	3.818574	4.930086	6.005785	6.806009	7.732079941
Dry Density, ρd	1.7984	1.8163	1.8235	1.8025	1.7703

Table H2: OMC & MDD Data for CA50RAP50

Percentage	**4%**	**5%**	**6%**	**7%**	**8%**
Mould + base + soil (g)	5396.11	5453.09	5475.13	5460.22	5450.32
Mould + base (g)	3545.21	3545.34	3545.51	3545.31	3545.16
Soil Mass (g)	1850.90	1907.75	1929.62	1914.91	1905.16
Wet Density, ρ	1.8509	1.90775	1.92962	1.91491	1.90516

No1. (4%)	1	2	3
Wet soil+container, W2 (g)	136.23	132.45	134.52
Dry soil+container, W1 (g)	131.61	128.55	130.22
Empty container, Wo (g)	24.04	23.65	22.14
Moisture content, Wn	4.2949	3.7178	3.9785
Average moisture content, w%	**3.9971**		
No2. (5%)	1	2	3
Wet soil+container, W2 (g)	111.23	108.54	117.25
Dry soil+container, W1 (g)	106.85	104.23	112.73
Empty container, Wo (g)	21.95	20	23.76
Moisture content, Wn	5.1590	5.1169	5.0804
Average moisture content, w%	**5.1188**		
No3. (6%)	1	2	3
Wet soil+container, w2 (g)	115.21	108.57	102.23
Dry soil+container, w1 (g)	108.52	104.22	97.58
Empty container, Wo (g)	20.1	20.17	23.22
Moisture content, Wn	7.5662	5.1755	6.2534
Average moisture content, w%	**6.3317**		
No4. (7%)	1	2	3
Wet soil+container, w2 (g)	123.63	110.63	128.26
Dry soil+container, w1 (g)	115.89	104.52	122.12
Empty container, Wo (g)	23.89	19.72	23.37
Moisture content, Wn	8.4130	7.2052	6.2177
Average moisture content, w%	**7.2787**		
No5. (8%)	1	2	3
Wet soil+container, w2 (g)	133.12	130.25	127.05
Dry soil+container, w1 (g)	124.12	123.85	118.52
Empty container, Wo (g)	25.12	21.8	24.08
Moisture content, Wn	9.0909	6.2714	9.0322
Average moisture content, w%	**8.1315**		

Dry Density

Percentage	4%	5%	6%	7%	8%
Average Moisture Content, w%	3.9971	5.1188	6.3317	7.2787	8.1315
Dry Density, ρd	1.7798	1.8149	1.8147	1.7850	1.7619

Table H3: OMC & MDD Data for CA25RAP75

Percentage	4%	5%	6%	7%	8%
Mould + base + soil (g)	5420.14	5490.65	5503.34	5496.16	5471.12
Mould + base (g)	3545.23	3545.37	3545.05	3545.62	3545.01
Soil Mass (g)	1874.91	1945.28	1958.29	1950.54	1926.11
Wet Density, ρ	1.87491	1.94528	1.95829	1.95054	1.92611

No1. (4%)	1	2	3
Wet soil+container, W2 (g)	125.23	131.12	109.52
Dry soil+container, W1 (g)	122.12	126.53	107.54
Empty container, Wo (g)	24.04	23.65	22.14
Moisture content, Wn	3.1709	4.4615	2.3185
Average moisture content, w%	**3.3170**		
No2. (5%)	1	2	3
Wet soil+container, W2 (g)	99.86	103.25	114.23
Dry soil+container, W1 (g)	95.45	97.52	112.63
Empty container, Wo (g)	21.95	20	23.76
Moisture content, Wn	6.0000	7.3916	1.8004
Average moisture content, w%	**5.0640**		
No3. (6%)	1	2	3
Wet soil+container, w2 (g)	104.23	110.27	108.08
Dry soil+container, w1 (g)	98.52	105.23	103.42
Empty container, Wo (g)	20.1	20.17	23.22
Moisture content, Wn	7.2813	5.9252	5.8105
Average moisture content, w%	**6.3390**		
No4. (7%)	1	2	3
Wet soil+container, w2 (g)	119.52	124.03	108.12
Dry soil+container, w1 (g)	115.23	117.52	100.53
Empty container, Wo (g)	23.89	19.72	23.37
Moisture content, Wn	4.6967	6.6564	9.8367
Average moisture content, w%	**7.0633**		
No5. (8%)	1	2	3
Wet soil+container, w2 (g)	110.12	114.89	119.12
Dry soil+container, w1 (g)	103.26	106.52	113.86
Empty container, Wo (g)	25.12	21.8	24.08
Moisture content, Wn	8.7791	9.8796	5.8588
Average moisture content, w%	**8.1725**		

Dry Density

Percentage	**4%**	**5%**	**6%**	**7%**	**8%**
Average Moisture Content, w%	3.3170	5.0640	6.3390	7.0633	8.1725
Dry Density, ρd	1.8147	1.8515	1.8416	1.8219	1.7806

APPENDIX J

Bulk Density Raw Data

Table J1: Bulk Density Data for CA75RAP25

CA75RAP25				sample 1			sample 2			
OPC	**GCBA**	**CaCl2**	**Weight of mould (g)**	**Weight of mould + sample (g)**	**Weight of sample (g)**	**Bulk density (Mg/m3)**	**Weight of mould + sample (g)**	**Weight of sample (g)**	**Bulk density (Mg/m3)**	**Ave. Bulk density (Mg/m3)**
4	0	0	4330	6340	2010	2.02	6298	1968	1.98	**2.00**
3	1	0	4330	6381	2051	2.06	6311	1981	1.99	**2.03**
2	2	0	4330	6312	1982	1.99	6332	2002	2.01	**2.00**
1	3	0	4330	6300	1970	1.98	6316	1986	2.00	**1.99**

CA75RAP25				sample 1			sample 2			
OPC	**GCBA**	**CaCl2**	**Weight of mould (g)**	**Weight of mould + sample (g)**	**Weight of sample (g)**	**Bulk density (Mg/m3)**	**Weight of mould + sample (g)**	**Weight of sample (g)**	**Bulk density (Mg/m3)**	**Ave. Bulk density (Mg/m3)**
4	0	1	4330	6298	1968	1.98	6306	1976	1.99	**1.98**
3	1	1	4330	6337	2007	2.02	6344	2014	2.02	**2.02**
2	2	1	4330	6311	1981	1.99	6352	2022	2.03	**2.01**
1	3	1	4330	6346	2016	2.03	6317	1987	2.00	**2.01**

CA75RAP25				sample 1			sample 2			
OPC	**GCBA**	**CaCl2**	**Weight of mould (g)**	**Weight of mould + sample (g)**	**Weight of sample (g)**	**Bulk density (Mg/m3)**	**Weight of mould + sample (g)**	**Weight of sample (g)**	**Bulk density (Mg/m3)**	**Ave. Bulk density (Mg/m3)**
4	0	2	4330	6356	2026	2.04	6346	2016	2.03	**2.03**
3	1	2	4330	6319	1989	2.00	6321	1991	2.00	**2.00**
2	2	2	4330	6363	2033	2.04	6342	2012	2.02	**2.03**
1	3	2	4330	6312	1982	1.99	6309	1979	1.99	**1.99**

CA75RAP25				sample 1			sample 2			
OPC	**GCBA**	**CaCl2**	**Weight of mould (g)**	**Weight of mould + sample (g)**	**Weight of sample (g)**	**Bulk density (Mg/m3)**	**Weight of mould + sample (g)**	**Weight of sample (g)**	**Bulk density (Mg/m3)**	**Ave. Bulk density (Mg/m3)**
4	0	3	4330	6302	1972	1.98	6315	1985	1.99	**1.99**
3	1	3	4330	6308	1978	1.99	6353	2023	2.03	**2.01**
2	2	3	4330	6318	1988	2.00	6327	1997	2.01	**2.00**
1	3	3	4330	6311	1981	1.99	6307	1977	1.99	**1.99**

Table J2: Bulk Density Data for CA50RAP50

CA50RAP50				sample 1			sample 2			
OPC	**GCBA**	**CaCl2**	**Weight of mould (g)**	**Weight of mould + sample (g)**	**Weight of sample (g)**	**Bulk density (Mg/m3)**	**Weight of mould + sample (g)**	**Weight of sample (g)**	**Bulk density (Mg/m3)**	**Ave. Bulk density (Mg/m3)**
4	0	0	4330	6235	1905	1.91	6270	1940	1.95	**1.93**
3	1	0	4330	6295	1965	1.97	6290	1960	1.97	**1.97**
2	2	0	4330	6325	1995	2.00	6240	1910	1.92	**1.96**
1	3	0	4330	6285	1955	1.96	6273	1943	1.95	**1.96**

CA50RAP50				sample 1			sample 2			
OPC	**GCBA**	**CaCl2**	**Weight of mould (g)**	**Weight of mould + sample (g)**	**Weight of sample (g)**	**Bulk density (Mg/m3)**	**Weight of mould + sample (g)**	**Weight of sample (g)**	**Bulk density (Mg/m3)**	**Ave. Bulk density (Mg/m3)**
4	0	1	4330	6345	2015	2.02	6221	1891	1.90	**1.96**
3	1	1	4330	6215	1885	1.89	6322	1992	2.00	**1.95**
2	2	1	4330	6243	1913	1.92	6195	1865	1.87	**1.90**
1	3	1	4330	6285	1955	1.96	6232	1902	1.91	**1.94**

CA50RAP50				sample 1			sample 2			
OPC	**GCBA**	**CaCl2**	**Weight of mould (g)**	**Weight of mould + sample (g)**	**Weight of sample (g)**	**Bulk density (Mg/m3)**	**Weight of mould + sample (g)**	**Weight of sample (g)**	**Bulk density (Mg/m3)**	**Ave. Bulk density (Mg/m3)**
4	0	2	4330	6295	1965	1.97	6302	1972	1.98	**1.98**
3	1	2	4330	6311	1981	1.99	6232	1902	1.91	**1.95**
2	2	2	4330	6293	1963	1.97	6297	1967	1.98	**1.97**
1	3	2	4330	6227	1897	1.91	6234	1904	1.91	**1.91**

CA50RAP50				sample 1			sample 2			
OPC	**GCBA**	**CaCl2**	**Weight of mould (g)**	**Weight of mould + sample (g)**	**Weight of sample (g)**	**Bulk density (Mg/m3)**	**Weight of mould + sample (g)**	**Weight of sample (g)**	**Bulk density (Mg/m3)**	**Ave. Bulk density (Mg/m3)**
4	0	3	4330	6215	1885	1.89	6217	1887	1.90	**1.89**
3	1	3	4330	6223	1893	1.90	6220	1890	1.90	**1.90**
2	2	3	4330	6243	1913	1.92	6219	1889	1.90	**1.91**
1	3	3	4330	6254	1924	1.93	6241	1911	1.92	**1.93**

Table J3: Bulk Density Data for CA25RAP75

CA25RAP75				sample 1			sample 2			
OPC	**GCBA**	**CaCl2**	**Weight of mould (g)**	**Weight of mould + sample (g)**	**Weight of sample (g)**	**Bulk density (Mg/m3)**	**Weight of mould + sample (g)**	**Weight of sample (g)**	**Bulk density (Mg/m3)**	**Ave. Bulk density (Mg/m3)**
4	0	0	4330	6215	1885	1.89	6201	1871	1.88	**1.89**
3	1	0	4330	6223	1893	1.90	6253	1923	1.93	**1.92**
2	2	0	4330	6230	1900	1.91	6291	1961	1.97	**1.94**
1	3	0	4330	6235	1905	1.91	6245	1915	1.92	**1.92**

CA25RAP75				sample 1			sample 2			
OPC	**GCBA**	**CaCl2**	**Weight of mould (g)**	**Weight of mould + sample (g)**	**Weight of sample (g)**	**Bulk density (Mg/m3)**	**Weight of mould + sample (g)**	**Weight of sample (g)**	**Bulk density (Mg/m3)**	**Ave. Bulk density (Mg/m3)**
4	0	1	4330	6253	1923	1.93	6216	1886	1.89	**1.91**
3	1	1	4330	6255	1925	1.93	6254	1924	1.93	**1.93**
2	2	1	4330	6210	1880	1.89	6219	1889	1.90	**1.89**
1	3	1	4330	6221	1891	1.90	6216	1886	1.89	**1.90**

CA25RAP75				sample 1			sample 2			
OPC	**GCBA**	**CaCl2**	**Weight of mould (g)**	**Weight of mould + sample (g)**	**Weight of sample (g)**	**Bulk density (Mg/m3)**	**Weight of mould + sample (g)**	**Weight of sample (g)**	**Bulk density (Mg/m3)**	**Ave. Bulk density (Mg/m3)**
4	0	2	4330	6266	1936	1.95	6265	1935	1.94	**1.94**
3	1	2	4330	6245	1915	1.92	6237	1907	1.92	**1.92**
2	2	2	4330	6236	1906	1.92	6241	1911	1.92	**1.92**
1	3	2	4330	6215	1885	1.89	6228	1898	1.91	**1.90**

CA25RAP75				sample 1			sample 2			
OPC	**GCBA**	**CaCl2**	**Weight of mould (g)**	**Weight of mould + sample (g)**	**Weight of sample (g)**	**Bulk density (Mg/m3)**	**Weight of mould + sample (g)**	**Weight of sample (g)**	**Bulk density (Mg/m3)**	**Ave. Bulk density (Mg/m3)**
4	0	3	4330	6211	1881	1.89	6222	1892	1.90	**1.90**
3	1	3	4330	6198	1868	1.88	6219	1889	1.90	**1.89**
2	2	3	4330	6223	1893	1.90	6229	1899	1.91	**1.90**
1	3	3	4330	6225	1895	1.90	6193	1863	1.87	**1.89**

APPENDIX K

Unconfined Compressive Strength (UCS) Raw Data

Table K1: UCS Data for CA75RAP25

			UCS - Day 1					UCS - Day 3				
OPC	**GCBA**	**$CaCl_2$**	**sample 1**	**sample 2**	**sample 3**	**Average (KN)**	**Mpa**	**sample 1**	**sample 2**	**sample 3**	**Average (KN)**	**Mpa**
1	3	**0**	15.51	16.85	14.75	15.70	**2.00**	18.22	16.54	20.31	18.36	**2.34**
2	2	**0**	18.39	19.21	15.22	17.61	**2.24**	17.85	21.23	20.13	19.74	**2.51**
3	1	**0**	27.44	28.51	24.13	26.69	**3.40**	30.16	22.25	28.44	26.95	**3.43**
4	0	**0**	28.62	25.49	27.43	27.18	**3.46**	26.33	28.54	29.51	28.13	**3.58**

			UCS - Day 7					UCS - Day 14				
OPC	**GCBA**	**$CaCl_2$**	**sample 1**	**sample 2**	**sample 3**	**Average (KN)**	**Mpa**	**sample 1**	**sample 2**	**sample 3**	**Average (KN)**	**Mpa**
1	3	**0**	20.03	20.82	18.26	19.70	**2.51**	18.52	21.81	20.22	20.18	**2.57**
2	2	**0**	21.51	20.89	17.33	19.91	**2.54**	23.24	22.85	20.17	22.09	**2.81**
3	1	**0**	27.85	26.67	29.11	27.88	**3.55**	31.25	29.63	32.21	31.03	**3.95**
4	0	**0**	30.22	30.87	27.52	29.54	**3.76**	31.02	31.97	32.19	31.73	**4.04**

			UCS - Day 28				
OPC	**GCBA**	**$CaCl_2$**	**sample 1**	**sample 2**	**sample 3**	**Average (KN)**	**Mpa**
1	3	**0**	23.26	22.78	21.02	22.35	**2.85**
2	2	**0**	29.63	32.68	30.22	30.84	**3.93**
3	1	**0**	35.52	35.91	40.33	37.25	**4.75**
4	0	**0**	9.89	37.10	35.62	37.54	**4.78**

			UCS - Day 1					UCS - Day 3				
OPC	**GCBA**	**$CaCl_2$**	**sample 1**	**sample 2**	**sample 3**	**Average (KN)**	**Mpa**	**sample 1**	**sample 2**	**sample 3**	**Average (KN)**	**Mpa**
1	3	**1**	15.83	15.22	17.52	16.19	**2.06**	16.22	17.54	17.41	17.06	**2.17**
2	2	**1**	19.53	17.85	20.22	19.20	**2.45**	20.52	20.13	21.10	20.58	**2.62**
3	1	**1**	26.23	24.51	27.23	25.99	**3.31**	29.56	28.41	29.33	29.10	**3.71**
4	0	**1**	24.56	26.32	25.71	25.53	**3.25**	28.86	30.85	28.52	29.41	**3.75**

			UCS - Day 7					UCS - Day 14				
OPC	**GCBA**	**$CaCl_2$**	**sample 1**	**sample 2**	**sample 3**	**Average (KN)**	**Mpa**	**sample 1**	**sample 2**	**sample 3**	**Average (KN)**	**Mpa**
1	3	**1**	20.31	20.89	21.52	20.91	**2.66**	22.24	19.63	23.52	21.80	**2.78**
2	2	**1**	33.97	32.21	31.05	32.41	**4.13**	34.11	31.86	32.68	32.88	**4.19**
3	1	**1**	36.34	27.94	33.42	32.57	**4.15**	39.22	37.51	34.58	37.10	**4.73**
4	0	**1**	33.03	35.01	30.26	32.77	**4.17**	35.62	33.82	38.96	36.13	**4.60**

			UCS - Day 28				
OPC	**GCBA**	**$CaCl_2$**	**sample 1**	**sample 2**	**sample 3**	**Average (KN)**	**Mpa**
1	3	**1**	26.53	21.52	23.84	23.96	**3.05**
2	2	**1**	34.27	35.32	33.25	34.28	**4.37**
3	1	**1**	43.51	40.22	38.28	40.67	**5.18**
4	0	**1**	41.22	38.76	37.44	39.14	**4.99**

			UCS - Day 1					UCS - Day 3				
OPC	**GCBA**	**$CaCl_2$**	**sample 1**	**sample 2**	**sample 3**	**Average (KN)**	**Mpa**	**sample 1**	**sample 2**	**sample 3**	**Average (KN)**	**Mpa**
1	3	**2**	15.22	18.59	17.64	17.15	**2.18**	16.85	20.51	19.86	19.07	**2.43**
2	2	**2**	18.96	20.17	19.52	19.55	**2.49**	24.52	23.88	21.11	23.17	**2.95**
3	1	**2**	23.22	20.59	27.84	23.88	**3.04**	28.55	33.62	31.26	31.14	**3.97**
4	0	**2**	22.59	25.32	24.85	24.25	**3.09**	31.32	32.13	32.59	32.01	**4.08**

			UCS - Day 7					UCS - Day 14				
OPC	**GCBA**	**$CaCl_2$**	**sample 1**	**sample 2**	**sample 3**	**Average (KN)**	**Mpa**	**sample 1**	**sample 2**	**sample 3**	**Average (KN)**	**Mpa**
1	3	**2**	18.13	21.25	19.33	19.57	**2.49**	21.11	20.1	19.06	20.09	**2.56**
2	2	**2**	23.86	22.31	26.14	24.10	**3.07**	23.15	26.55	24.18	24.63	**3.14**
3	1	**2**	29.63	31.54	33.86	31.68	**4.04**	31.11	28.52	36.55	32.06	**4.08**
4	0	**2**	33.69	35.22	34.21	34.37	**4.38**	32.44	37.52	36.14	35.37	**4.51**

			UCS - Day 28				
OPC	**GCBA**	**$CaCl_2$**	**sample 1**	**sample 2**	**sample 3**	**Average (KN)**	**Mpa**
1	3	**2**	22.32	24.61	22.76	23.23	**2.96**
2	2	**2**	28.52	31.16	34.19	31.29	**3.99**
3	1	**2**	41.23	37.52	39.22	39.32	**5.01**
4	0	**2**	35.16	40.13	38.52	37.94	**4.83**

			UCS - Day 1					UCS - Day 3				
OPC	**GCBA**	**$CaCl_2$**	**sample 1**	**sample 2**	**sample 3**	**Average (KN)**	**Mpa**	**sample 1**	**sample 2**	**sample 3**	**Average (KN)**	**Mpa**
1	3	**3**	14.22	11.23	12.11	12.52	**1.59**	15.23	13.22	16.85	15.10	**1.92**
2	2	**3**	15.23	13.86	17.52	15.54	**1.98**	17.52	16.22	16.96	16.90	**2.15**
3	1	**3**	19.52	21.14	20.21	20.29	**2.58**	22.56	24.12	19.53	22.07	**2.81**
4	0	**3**	16.08	22.31	19.25	19.21	**2.45**	20.33	18.56	24.12	21.00	**2.68**

			UCS - Day 7					UCS - Day 14				
OPC	**GCBA**	**$CaCl_2$**	**sample 1**	**sample 2**	**sample 3**	**Average (KN)**	**Mpa**	**sample 1**	**sample 2**	**sample 3**	**Average (KN)**	**Mpa**
1	3	**3**	16.52	18.58	17.13	17.41	**2.22**	17.22	20.12	19.46	18.93	**2.41**
2	2	**3**	19.52	19.10	17.55	18.72	**2.39**	20.02	21.32	18.56	19.97	**2.54**
3	1	**3**	23.56	23.23	25.38	24.06	**3.06**	25.22	23.71	24.18	24.37	**3.10**
4	0	**3**	26.92	27.85	25.33	26.70	**3.40**	25.63	29.85	27.41	27.63	**3.52**

			UCS - Day 28				
OPC	**GCBA**	**$CaCl_2$**	**sample 1**	**sample 2**	**sample 3**	**Average (KN)**	**Mpa**
1	3	**3**	19.86	19.41	22.18	20.48	**2.61**
2	2	**3**	22.33	22.84	20.15	21.77	**2.77**
3	1	**3**	24.28	28.45	26.71	26.48	**3.37**
4	0	**3**	29.66	28.41	28.74	28.94	**3.69**

Table K2: UCS Data for CA50RAP50

			UCS - Day 1					UCS - Day 3				
OPC	**GCBA**	**$CaCl_2$**	**sample 1**	**sample 2**	**sample 3**	**Average (KN)**	**Mpa**	**sample 1**	**sample 2**	**sample 3**	**Average (KN)**	**Mpa**
1	3	**0**	15.15	16.85	19.86	17.29	**2.20**	24.35	23.34	20.85	22.85	**2.91**
2	2	**0**	21.91	20.45	18.25	20.20	**2.57**	24.69	23.55	26.22	24.82	**3.16**
3	1	**0**	23.31	26.32	20.22	23.28	**2.97**	31.53	32.17	29.35	31.02	**3.95**
4	0	**0**	27.54	29.85	26.43	27.94	**3.56**	29.19	30.21	34.12	31.17	**3.97**

			UCS - Day 7					UCS - Day 14				
OPC	**GCBA**	**$CaCl_2$**	**sample 1**	**sample 2**	**sample 3**	**Average (KN)**	**Mpa**	**sample 1**	**sample 2**	**sample 3**	**Average (KN)**	**Mpa**
1	3	**0**	22.73	21.12	25.31	23.05	**2.94**	25.56	23.17	25.14	24.62	**3.14**
2	2	**0**	26.22	24.85	30.11	27.06	**3.45**	28.73	30.15	27.52	28.80	**3.67**
3	1	**0**	33.07	30.26	31.85	31.73	**4.04**	40.02	36.18	35.62	37.27	**4.75**
4	0	**0**	34.98	33.85	32.19	33.67	**4.29**	39.15	38.45	35.16	37.59	**4.79**

			UCS - Day 28				
OPC	**GCBA**	**$CaCl_2$**	**sample 1**	**sample 2**	**sample 3**	**Average (KN)**	**Mpa**
1	3	**0**	30.74	29.96	25.63	28.78	**3.67**
2	2	**0**	38.25	34.26	34.18	35.56	**4.53**
3	1	**0**	35.12	37.85	40.13	37.70	**4.80**
4	0	**0**	42.66	39.52	37.85	40.01	**5.10**

			UCS - Day 1					UCS - Day 3				
OPC	**GCBA**	**$CaCl_2$**	**sample 1**	**sample 2**	**sample 3**	**Average (KN)**	**Mpa**	**sample 1**	**sample 2**	**sample 3**	**Average (KN)**	**Mpa**
1	3	**1**	19.85	18.23	20.12	19.40	**2.47**	20.71	22.75	21.52	21.66	**2.76**
2	2	**1**	28.19	27.25	24.53	26.66	**3.40**	28.24	25.23	29.54	27.67	**3.52**
3	1	**1**	24.73	29.36	28.56	27.55	**3.51**	30.33	31.25	28.51	30.03	**3.83**
4	0	**1**	28.69	30.22	32.06	30.32	**3.86**	30.45	32.15	29.41	30.67	**3.91**

			UCS - Day 7					UCS - Day 14				
OPC	**GCBA**	**$CaCl_2$**	**sample 1**	**sample 2**	**sample 3**	**Average (KN)**	**Mpa**	**sample 1**	**sample 2**	**sample 3**	**Average (KN)**	**Mpa**
1	3	**1**	23.55	24.12	21.25	22.97	**2.93**	23.12	22.89	27.63	24.55	**3.13**
2	2	**1**	30.04	27.18	28.52	28.58	**3.64**	31.25	30.86	32.17	31.43	**4.00**
3	1	**1**	39.83	33.21	35.16	36.07	**4.59**	36.85	35.24	39.55	37.21	**4.74**
4	0	**1**	34.61	35.13	33.82	34.52	**4.40**	36.12	38.11	40.26	38.16	**4.86**

			UCS - Day 28				
OPC	**GCBA**	**CaC_{12}**	**sample 1**	**sample 2**	**sample 3**	**Average (KN)**	**Mpa**
1	3	**1**	33.63	30.26	34.61	32.83	**4.18**
2	2	**1**	37.66	36.82	31.82	35.43	**4.51**
3	1	**1**	44.39	44.15	48.82	45.79	**5.83**
4	0	**1**	48.16	46.22	45.22	46.53	**5.93**

			UCS - Day 1					UCS - Day 3				
OPC	**GCBA**	**$CaCl_2$**	**sample 1**	**sample 2**	**sample 3**	**Average (KN)**	**Mpa**	**sample 1**	**sample 2**	**sample 3**	**Average (KN)**	**Mpa**
1	3	**2**	17.12	19.86	19.13	18.70	**2.38**	17.69	23.26	18.53	19.83	**2.53**
2	2	**2**	27.27	23.12	24.11	24.83	**3.16**	26.33	28.74	25.11	26.73	**3.40**
3	1	**2**	28.91	26.69	25.31	26.97	**3.44**	30.14	31.27	28.74	30.05	**3.83**
4	0	**2**	30.46	27.33	32.75	30.18	**3.84**	37.95	32.21	28.45	32.87	**4.19**

			UCS - Day 7					UCS - Day 14				
OPC	**GCBA**	**$CaCl_2$**	**sample 1**	**sample 2**	**sample 3**	**Average (KN)**	**Mpa**	**sample 1**	**sample 2**	**sample 3**	**Average (KN)**	**Mpa**
1	3	**2**	18.74	21.33	20.14	20.07	**2.56**	21.85	20.96	20.11	20.97	**2.67**
2	2	**2**	25.40	33.04	26.34	28.26	**3.60**	26.45	29.63	29.12	28.40	**3.62**
3	1	**2**	33.41	35.67	34.33	34.47	**4.39**	34.45	38.87	37.98	37.10	**4.73**
4	0	**2**	31.48	38.46	30.12	33.35	**4.25**	35.56	37.81	40.02	37.80	**4.81**

			UCS - Day 28				
OPC	**GCBA**	**$CaCl_2$**	**sample 1**	**sample 2**	**sample 3**	**Average (KN)**	**Mpa**
1	3	**2**	28.43	28.35	26.41	27.73	**3.53**
2	2	**2**	35.21	36.74	40.22	37.39	**4.76**
3	1	**2**	40.22	42.11	38.51	40.28	**5.13**
4	0	**2**	43.28	45.63	41.12	43.34	**5.52**

			UCS - Day 1					UCS - Day 3				
OPC	**GCBA**	**$CaCl_2$**	**sample 1**	**sample 2**	**sample 3**	**Average (KN)**	**Mpa**	**sample 1**	**sample 2**	**sample 3**	**Average (KN)**	**Mpa**
1	3	**3**	18.1	16.52	16.23	16.95	**2.16**	16.99	17.1	18.24	17.44	**2.22**
2	2	**3**	14.86	16.78	20.11	17.25	**2.20**	17.85	18.05	20.11	18.67	**2.38**
3	1	**3**	16.75	20.39	34.21	23.78	**3.03**	25.41	27.37	29.33	27.37	**3.49**
4	0	**3**	30.42	21.05	25.22	25.56	**3.26**	26.18	23.96	27.86	26.00	**3.31**

			UCS - Day 7					UCS - Day 14				
OPC	**GCBA**	**$CaCl_2$**	**sample 1**	**sample 2**	**sample 3**	**Average (KN)**	**Mpa**	**sample 1**	**sample 2**	**sample 3**	**Average (KN)**	**Mpa**
1	3	**3**	22.82	18.1	19.23	20.05	**2.55**	21.01	22.16	21.84	21.67	**2.76**
2	2	**3**	20.13	23.1	21.14	21.46	**2.73**	24.01	23.36	20.45	22.61	**2.88**
3	1	**3**	26.33	29.63	31.14	29.03	**3.70**	28.25	34.78	30.24	31.09	**3.96**
4	0	**3**	24.22	26.12	29.63	26.66	**3.40**	33.17	35.95	34.21	34.44	**4.39**

			UCS - Day 28				
OPC	**GCBA**	**$CaCl_2$**	**sample 1**	**sample 2**	**sample 3**	**Average (KN)**	**Mpa**
1	3	**3**	26.21	24.15	28.51	26.29	**3.35**
2	2	**3**	39.04	28.23	30.12	32.46	**4.14**
3	1	**3**	34.66	45.25	35.25	38.39	**4.89**
4	0	**3**	33.13	34.28	38.54	35.32	**4.50**

Table K3: UCS Data for CA25RAP75

			UCS - Day 1					UCS - Day 3				
OPC	**GCBA**	**$CaCl_2$**	**sample 1**	**sample 2**	**sample 3**	**Average (KN)**	**Mpa**	**sample 1**	**sample 2**	**sample 3**	**Average (KN)**	**Mpa**
1	3	**0**	19.05	17.46	17.55	18.02	**2.30**	21.31	18.56	23.45	21.11	**2.69**
2	2	**0**	21.88	24.13	23.29	23.10	**2.94**	22.85	21.56	26.14	23.52	**3.00**
3	1	**0**	27.13	26.27	28.74	27.38	**3.49**	28.56	33.62	31.14	31.11	**3.96**
4	0	**0**	27.02	24.36	25.12	25.50	**3.25**	28.15	29.74	32.11	30.00	**3.82**

			UCS - Day 7					UCS - Day 14				
OPC	**GCBA**	**$CaCl_2$**	**sample 1**	**sample 2**	**sample 3**	**Average (KN)**	**Mpa**	**sample 1**	**sample 2**	**sample 3**	**Average (KN)**	**Mpa**
1	3	**0**	22.51	23.13	20.71	22.12	**2.82**	23.12	22.89	27.63	24.55	**3.13**
2	2	**0**	26.98	27.55	24.91	26.48	**3.37**	31.25	30.86	32.17	31.43	**4.00**
3	1	**0**	35.21	33.84	31.57	33.54	**4.27**	34.21	36.87	38.12	36.40	**4.64**
4	0	**0**	34.53	32.85	31.71	33.03	**4.21**	34.52	36.57	37.41	36.17	**4.61**

			UCS - Day 28				
OPC	**GCBA**	**$CaCl_2$**	**sample 1**	**sample 2**	**sample 3**	**Average (KN)**	**Mpa**
1	3	**0**	24.85	26.13	27.83	26.27	**3.35**
2	2	**0**	34.78	39.05	37.72	37.18	**4.74**
3	1	**0**	35.32	37.23	38.56	37.04	**4.72**
4	0	**0**	33.37	40.02	38.74	37.38	**4.76**

			UCS - Day 1					UCS - Day 3				
OPC	**GCBA**	**$CaCl_2$**	**sample 1**	**sample 2**	**sample 3**	**Average (KN)**	**Mpa**	**sample 1**	**sample 2**	**sample 3**	**Average (KN)**	**Mpa**
1	3	**1**	14.22	16.12	14.78	15.04	**1.92**	15.63	19.57	18.95	18.05	**2.30**
2	2	**1**	22.42	24.23	25.16	23.94	**3.05**	24.22	23.69	27.54	25.15	**3.20**
3	1	**1**	26.88	24.85	23.68	25.14	**3.20**	28.52	26.74	27.77	27.68	**3.53**
4	0	**1**	27.51	26.85	28.22	27.53	**3.51**	29.84	25.85	27.28	27.66	**3.52**

			UCS - Day 7					UCS - Day 14				
OPC	**GCBA**	**$CaCl_2$**	**sample 1**	**sample 2**	**sample 3**	**Average (KN)**	**Mpa**	**sample 1**	**sample 2**	**sample 3**	**Average (KN)**	**Mpa**
1	3	**1**	21.51	24.1	22.84	22.82	**2.91**	26.12	23.44	22.96	24.17	**3.08**
2	2	**1**	28.51	27.55	29.13	28.40	**3.62**	34.12	33.56	37.85	35.18	**4.48**
3	1	**1**	33.81	32.53	37.62	34.65	**4.41**	34.23	36.55	39.81	36.86	**4.70**
4	0	**1**	33.39	35.12	36.52	35.01	**4.46**	35.62	36.88	37.84	36.78	**4.69**

			UCS - Day 28				
OPC	**GCBA**	**$CaCl_2$**	**sample 1**	**sample 2**	**sample 3**	**Average (KN)**	**Mpa**
1	3	**1**	25.89	26.88	28.16	26.98	**3.44**
2	2	**1**	33.51	34.89	38.52	35.64	**4.54**
3	1	**1**	37.56	37.88	39.87	38.44	**4.90**
4	0	**1**	39.88	38.72	40.02	39.54	**5.04**

			UCS - Day 1					UCS - Day 3				
OPC	**GCBA**	**$CaCl_2$**	**sample 1**	**sample 2**	**sample 3**	**Average (KN)**	**Mpa**	**sample 1**	**sample 2**	**sample 3**	**Average (KN)**	**Mpa**
1	3	**2**	15.32	13.21	14.11	14.21	**1.81**	16.42	19.84	14.88	17.05	**2.17**
2	2	**2**	22.16	20.85	19.83	20.95	**2.67**	22.15	19.85	21.87	21.29	**2.71**
3	1	**2**	26.51	24.85	25.69	25.68	**3.27**	28.44	29.81	25.87	28.04	**3.57**
4	0	**2**	26.85	28.44	23.65	26.31	**3.35**	29.84	27.14	26.58	27.85	**3.55**

			UCS - Day 7					UCS - Day 14				
OPC	**GCBA**	**$CaCl_2$**	**sample 1**	**sample 2**	**sample 3**	**Average (KN)**	**Mpa**	**sample 1**	**sample 2**	**sample 3**	**Average (KN)**	**Mpa**
1	3	**2**	17.85	20.43	18.52	18.93	**2.41**	26.13	20.96	20.11	22.40	**2.85**
2	2	**2**	25.12	23.87	22.19	23.73	**3.02**	23.54	28.56	28.10	26.73	**3.41**
3	1	**2**	29.85	31.13	30.41	30.46	**3.88**	30.77	33.81	35.42	33.33	**4.25**
4	0	**2**	30.26	33.16	29.87	31.10	**3.96**	34.15	33.21	32.14	33.17	**4.23**

			UCS - Day 28				
OPC	**GCBA**	**$CaCl_2$**	**sample 1**	**sample 2**	**sample 3**	**Average (KN)**	**Mpa**
1	3	**2**	23.22	25.12	26.81	25.05	**3.19**
2	2	**2**	30.25	29.86	29.21	29.77	**3.79**
3	1	**2**	33.15	31.84	36.22	33.74	**4.30**
4	0	**2**	39.55	41.23	36.42	39.07	**4.98**

			UCS - Day 1					UCS - Day 3				
OPC	**GCBA**	**$CaCl_2$**	**sample 1**	**sample 2**	**sample 3**	**Average (KN)**	**Mpa**	**sample 1**	**sample 2**	**sample 3**	**Average (KN)**	**Mpa**
1	3	**3**	13.22	16.54	14.88	14.88	**1.90**	15.23	14.95	18.56	16.25	**2.07**
2	2	**3**	20.11	18.43	17.25	18.60	**2.37**	19.56	20.18	17.56	19.10	**2.43**
3	1	**3**	22.14	20.42	24.15	22.24	**2.83**	26.32	26.81	24.12	25.75	**3.28**
4	0	**3**	25.11	24.56	23.12	24.26	**3.09**	24.26	25.84	27.01	25.70	**3.27**

			UCS - Day 7					UCS - Day 14				
OPC	**GCBA**	**$CaCl_2$**	**sample 1**	**sample 2**	**sample 3**	**Average (KN)**	**Mpa**	**sample 1**	**sample 2**	**sample 3**	**Average (KN)**	**Mpa**
1	3	**3**	22.82	18.1	19.23	20.05	**2.55**	20.51	22.53	20.85	21.30	**2.71**
2	2	**3**	21.22	23.1	21.14	21.82	**2.78**	23.21	22.98	21.32	22.50	**2.87**
3	1	**3**	27.85	30.22	28.53	28.87	**3.68**	31.21	31.25	29.84	30.77	**3.92**
4	0	**3**	26.41	24.89	29.55	26.95	**3.43**	28.96	30.26	32.16	30.46	**3.88**

			UCS - Day 28				
OPC	**GCBA**	**$CaCl_2$**	**sample 1**	**sample 2**	**sample 3**	**Average (KN)**	**Mpa**
1	3	**3**	22.51	21.54	24.29	22.78	**2.90**
2	2	**3**	25.64	28.51	23.52	25.89	**3.30**
3	1	**3**	29.85	33.52	34.61	32.66	**4.16**
4	0	**3**	34.51	33.45	37.62	35.19333	**4.48**

APPENDIX L

Indirect Tensile Strength (ITS) Raw Data

Table L1: ITS Data for CA75RAP25

			ITS - Day 1					ITS - Day 3				
OPC	**GCBA**	**$CaCl_2$**	**sample 1**	**sample 2**	**sample 3**	**Average (kPa)**	**Mpa**	**sample 1**	**sample 2**	**sample 3**	**Average (kPa)**	**Mpa**
2	2	0	152.22	169.35	160.32	**160.63**	0.16	232.22	185.12	197.63	**204.99**	0.20
3	1	0	185.36	231.22	192.25	**202.94**	0.20	244.63	286.31	297.85	**276.26**	0.28
4	0	0	201.33	196.36	183.65	**193.78**	0.19	261.22	277.87	298.32	**279.14**	0.28

			ITS - Day 7					ITS - Day 14				
OPC	**GCBA**	**$CaCl_2$**	**sample 1**	**sample 2**	**sample 3**	**Average (kPa)**	**Mpa**	**sample 1**	**sample 2**	**sample 3**	**Average (kPa)**	**Mpa**
2	2	0	236.32	295.55	326.45	**286.11**	0.29	426.85	406.63	387.56	**407.01**	0.41
3	1	0	396.51	289.25	354.12	**346.63**	0.35	456.36	516.11	476.36	**482.94**	0.48
4	0	0	356.22	342.26	373.02	**357.17**	0.36	482.23	432.54	441.21	**451.99**	0.45

			ITS - Day 28				
OPC	**GCBA**	**$CaCl_2$**	**sample 1**	**sample 2**	**sample 3**	**Average (kPa)**	**Mpa**
2	2	0	445.25	485.25	414.53	**448.34**	0.45
3	1	0	587.36	522.64	546.85	**552.28**	0.55
4	0	0	545.24	408.38	496.34	**483.32**	0.48

			ITS - Day 1					ITS - Day 3				
OPC	**GCBA**	**$CaCl_2$**	**sample 1**	**sample 2**	**sample 3**	**Average (kPa)**	**Mpa**	**sample 1**	**sample 2**	**sample 3**	**Average (kPa)**	**Mpa**
2	2	1	162.21	185.23	175.33	**174.26**	0.17	206.63	219.87	198.52	**208.34**	0.21
3	1	1	203.21	194.25	181.75	**193.07**	0.19	352.21	287.54	324.22	**321.32**	0.32
4	0	1	186.55	197.21	190.32	**191.36**	0.19	301.63	297.51	288.96	**296.03**	0.30

			ITS - Day 7					ITS - Day 14				
OPC	**GCBA**	**$CaCl_2$**	**sample 1**	**sample 2**	**sample 3**	**Average (kPa)**	**Mpa**	**sample 1**	**sample 2**	**sample 3**	**Average (kPa)**	**Mpa**
2	2	1	231.22	209.89	285.63	**242.25**	0.24	325.16	362.25	305.75	**331.05**	0.33
3	1	1	429.31	385.42	443.06	**419.26**	0.42	486.36	455.52	502.21	**481.36**	0.48
4	0	1	423.12	455.32	399.96	**426.13**	0.43	511.32	502.36	487.85	**500.51**	0.50

			ITS - Day 28				
OPC	**GCBA**	**$CaCl_2$**	**sample 1**	**sample 2**	**sample 3**	**Average (kPa)**	**Mpa**
2	2	1	402.22	398.51	411.65	**404.13**	0.40
3	1	1	536.13	596.36	559.63	**564.04**	0.56
4	0	1	619.72	485.91	522.03	**542.55**	0.54

			ITS - Day 1					ITS - Day 3				
OPC	**GCBA**	**$CaCl_2$**	**sample 1**	**sample 2**	**sample 3**	**Average (kPa)**	**Mpa**	**sample 1**	**sample 2**	**sample 3**	**Average (kPa)**	**Mpa**
2	2	2	176.32	197.23	175.03	**182.86**	0.18	216.36	241.01	226.31	**227.89**	0.23
3	1	2	185.27	200.45	196.36	**194.03**	0.19	225.52	275.13	285.26	**261.97**	0.26
4	0	2	175.63	195.62	199.28	**190.18**	0.19	300.62	312.52	291.32	**301.49**	0.30

			ITS - Day 7					ITS - Day 14				
OPC	**GCBA**	**$CaCl_2$**	**sample 1**	**sample 2**	**sample 3**	**Average (kPa)**	**Mpa**	**sample 1**	**sample 2**	**sample 3**	**Average (kPa)**	**Mpa**
2	2	2	285.11	263.19	219.63	**255.98**	0.26	300.26	349.03	316.55	**321.95**	0.32
3	1	2	311.52	343.62	298.62	**317.92**	0.32	498.16	521.32	478.16	**499.21**	0.50
4	0	2	385.22	360.11	356.12	**367.15**	0.37	485.12	438.52	501.63	**475.09**	0.48

			ITS - Day 28				
OPC	**GCBA**	**$CaCl_2$**	**sample 1**	**sample 2**	**sample 3**	**Average (kPa)**	**Mpa**
2	2	2	403.12	398.75	411.53	**404.47**	0.40
3	1	2	536.41	501.21	488.63	**508.75**	0.51
4	0	2	547.03	567.88	541.22	**552.04**	0.55

Table L2: ITS Data for CA50RAP50

			ITS - Day 1					ITS - Day 3				
OPC	**GCBA**	**$CaCl_2$**	**sample 1**	**sample 2**	**sample 3**	**Average (kPa)**	**Mpa**	**sample 1**	**sample 2**	**sample 3**	**Average (kPa)**	**Mpa**
2	2	0	154.22	178.03	144.28	**158.84**	0.159	196.36	204.22	221.67	**207.42**	0.21
3	1	0	203.34	184.55	217.02	**201.64**	0.202	211.36	203.74	229.15	**214.75**	0.21
4	0	0	161.87	193.52	198.33	**184.57**	0.185	213.85	226.13	246.32	**228.77**	0.23

			ITS - Day 7					ITS - Day 14				
OPC	**GCBA**	**$CaCl_2$**	**sample 1**	**sample 2**	**sample 3**	**Average (kPa)**	**Mpa**	**sample 1**	**sample 2**	**sample 3**	**Average (kPa)**	**Mpa**
2	2	0	265.22	321.21	274.35	**286.93**	0.29	369.85	324.26	354.23	**349.45**	0.35
3	1	0	285.36	300.74	324.74	**303.61**	0.30	358.11	406.22	396.78	**387.04**	0.39
4	0	0	375.3	381.26	358.15	**371.57**	0.37	422.35	462.15	496.47	**460.32**	0.46

			ITS - Day 28				
OPC	**GCBA**	**$CaCl_2$**	**sample 1**	**sample 2**	**sample 3**	**Average (kPa)**	**Mpa**
2	2	0	396.52	362.13	433.62	**397.42**	0.40
3	1	0	416.22	485.25	432.21	**444.56**	0.44
4	0	0	508.34	481.25	498.31	**495.97**	0.50

			ITS - Day 1					ITS - Day 3				
OPC	**GCBA**	**$CaCl_2$**	**sample 1**	**sample 2**	**sample 3**	**Average (kPa)**	**Mpa**	**sample 1**	**sample 2**	**sample 3**	**Average (kPa)**	**Mpa**
2	2	1	184.32	175.22	196.37	**185.30**	0.19	231.22	287.22	302.25	**273.56**	0.27
3	1	1	222.64	197.53	211.84	**210.67**	0.21	311.45	362.33	381.03	**351.60**	0.35
4	0	1	230.58	213.23	251.01	**231.61**	0.23	342.33	305.96	325.74	**324.68**	0.32

			ITS - Day 7					ITS - Day 14				
OPC	**GCBA**	**$CaCl_2$**	**sample 1**	**sample 2**	**sample 3**	**Average (kPa)**	**Mpa**	**sample 1**	**sample 2**	**sample 3**	**Average (kPa)**	**Mpa**
2	2	1	306.52	345.96	385.63	**346.04**	0.35	502.31	544.25	586.12	**544.23**	0.54
3	1	1	411.32	436.52	387.22	**411.69**	0.41	593.36	601.23	575.23	**589.94**	0.59
4	0	1	452.14	499.53	462.1	**471.26**	0.47	562.47	603.84	623.14	**596.48**	0.60

			ITS - Day 28				
OPC	**GCBA**	**$CaCl_2$**	**sample 1**	**sample 2**	**sample 3**	**Average (kPa)**	**Mpa**
2	2	1	601.03	587.63	574.23	**587.63**	0.59
3	1	1	654.13	699.16	724.53	**692.61**	0.69
4	0	1	617.88	684.27	711.15	**671.10**	0.67

			ITS - Day 1					ITS - Day 3				
OPC	**GCBA**	**$CaCl_2$**	**sample 1**	**sample 2**	**sample 3**	**Average (kPa)**	**Mpa**	**sample 1**	**sample 2**	**sample 3**	**Average (kPa)**	**Mpa**
2	2	2	163.25	188.76	181.62	**177.88**	0.18	200.63	224.12	273.61	**232.79**	0.23
3	1	2	169.36	198.22	186.30	**184.63**	0.18	216.32	274.22	266.12	**252.22**	0.25
4	0	2	193.43	155.96	175.22	**174.87**	0.17	263.02	226.98	302.59	**264.20**	0.26

			ITS - Day 7					ITS - Day 14				
OPC	**GCBA**	**$CaCl_2$**	**sample 1**	**sample 2**	**sample 3**	**Average (kPa)**	**Mpa**	**sample 1**	**sample 2**	**sample 3**	**Average (kPa)**	**Mpa**
2	2	2	296.35	312.65	300.12	**303.04**	0.30	385.22	396.74	421.54	**401.17**	0.40
3	1	2	385.42	403.15	426.32	**404.96**	0.40	511.28	501.87	492.12	**501.76**	0.50
4	0	2	374.70	475.12	388.52	**412.78**	0.41	485.63	428.74	503.62	**472.66**	0.47

			ITS - Day 28				
OPC	**GCBA**	**$CaCl_2$**	**sample 1**	**sample 2**	**sample 3**	**Average (kPa)**	**Mpa**
2	2	2	475.22	423.21	405.87	**434.77**	0.43
3	1	2	584.21	541.21	523.84	**549.75**	0.55
4	0	2	441.06	628.76	512.34	**527.39**	0.53

Table L3: ITS Data for CA25RAP75

			ITS - Day 1					ITS - Day 3				
OPC	**GCBA**	**$CaCl_2$**	**sample 1**	**sample 2**	**sample 3**	**Average (kPa)**	**Mpa**	**sample 1**	**sample 2**	**sample 3**	**Average (kPa)**	**Mpa**
2	2	0	80.53	75.84	70.35	**75.57**	0.08	98.56	89.63	97.74	**95.31**	0.10
3	1	0	95.35	103.24	93.45	**97.35**	0.10	117.84	156.36	151.21	**141.80**	0.14
4	0	0	85.58	91.45	124.34	**100.46**	0.10	165.32	141.32	124.36	**143.67**	0.14

			ITS - Day 7					ITS - Day 14				
OPC	**GCBA**	**$CaCl_2$**	**sample 1**	**sample 2**	**sample 3**	**Average (kPa)**	**Mpa**	**sample 1**	**sample 2**	**sample 3**	**Average (kPa)**	**Mpa**
2	2	0	220.23	253.67	198.74	**224.21**	0.22	296.63	301.68	316.52	**304.94**	0.30
3	1	0	223.14	209.11	275.36	**235.87**	0.24	362.32	314.52	342.53	**339.79**	0.34
4	0	0	176.52	234.58	266.14	**225.75**	0.23	301.23	309.51	294.35	**301.70**	0.30

			ITS - Day 28				
OPC	**GCBA**	**$CaCl_2$**	**sample 1**	**sample 2**	**sample 3**	**Average (kPa)**	**Mpa**
2	2	0	398.62	355.51	363.14	**372.42**	0.37
3	1	0	423.32	485.63	441.25	**450.07**	0.45
4	0	0	325.75	414.55	438.17	**392.82**	0.39

			ITS - Day 1					ITS - Day 3				
OPC	**GCBA**	**$CaCl_2$**	**sample 1**	**sample 2**	**sample 3**	**Average (kPa)**	**Mpa**	**sample 1**	**sample 2**	**sample 3**	**Average (kPa)**	**Mpa**
2	2	1	86.53	83.33	91.54	**87.13**	0.09	99.74	103.62	115.62	**106.33**	0.11
3	1	1	105.23	89.96	93.88	**96.36**	0.10	129.84	133.45	119.45	**127.58**	0.13
4	0	1	97.85	105.66	98.41	**100.64**	0.10	143.56	151.03	128.78	**141.12**	0.14

			ITS - Day 7					ITS - Day 14				
OPC	**GCBA**	**$CaCl_2$**	**sample 1**	**sample 2**	**sample 3**	**Average (kPa)**	**Mpa**	**sample 1**	**sample 2**	**sample 3**	**Average (kPa)**	**Mpa**
2	2	1	221.63	241.62	259.87	**241.04**	0.24	368.84	345.25	311.02	**341.70**	0.34
3	1	1	200.23	287.56	321.56	**269.78**	0.27	445.25	463.61	402.41	**437.09**	0.44
4	0	1	276.30	297.45	321.22	**298.32**	030	485.22	463.45	511.23	**486.63**	0.49

			ITS - Day 28				
OPC	**GCBA**	**$CaCl_2$**	**sample 1**	**sample 2**	**sample 3**	**Average (kPa)**	**Mpa**
2	2	1	411.63	403.58	432.58	**415.93**	0.42
3	1	1	623.52	523.87	562.32	**569.90**	0.57
4	0	1	592.96	526.31	475.26	**531.51**	0.53

			ITS - Day 1					ITS - Day 3				
OPC	**GCBA**	**$CaCl_2$**	**sample 1**	**sample 2**	**sample 3**	**Average (kPa)**	**Mpa**	**sample 1**	**sample 2**	**sample 3**	**Average (kPa)**	**Mpa**
2	2	2	77.46	97.85	76.03	**83.78**	0.08	129.88	146.24	99.84	**125.32**	0.13
3	1	2	121.22	96.51	92.14	**103.29**	0.10	186.55	196.65	163.54	**182.25**	0.18
4	0	2	89.84	93.65	88.12	**90.54**	0.09	163.57	201.55	206.12	**190.41**	0.19

			ITS - Day 7					ITS - Day 14				
OPC	**GCBA**	**$CaCl_2$**	**sample 1**	**sample 2**	**sample 3**	**Average (kPa)**	**Mpa**	**sample 1**	**sample 2**	**sample 3**	**Average (kPa)**	**Mpa**
2	2	2	212.54	157.84	184.66	**185.01**	0.19	362.52	371.32	355.51	**363.12**	0.36
3	1	2	204.57	214.63	198.75	**205.98**	0.21	312.63	298.96	401.23	**337.61**	0.34
4	0	2	203.88	255.22	198.74	**219.28**	0.22	339.51	384.36	414.51	**379.46**	0.38

			ITS - Day 28				
OPC	**GCBA**	**$CaCl_2$**	**sample 1**	**sample 2**	**sample 3**	**Average (kPa)**	**Mpa**
2	2	2	403.32	422.12	387.16	**404.20**	0.40
3	1	2	462.31	455.36	489.23	**468.97**	0.47
4	0	2	403.03	460.11	458.26	**440.47**	0.44

APPENDIX M

Resilient Modulus (M_R) Raw Data

Table M1: M_R Data for CA75RAP25

			Day 1							Day 3						
OPC	**GCBA**	**$CaCl_2$**	**sample 1A**	**sample 1B**	**sample 2A**	**sample 2B**	**sample 3A**	**sample 3B**	**Ave. (MPa)**	**sample 1A**	**sample 1B**	**sample 2A**	**sample 2B**	**sample 3A**	**sample 3B**	**Ave. (MPa)**
2	2	0	3385	3991	4151	3226	3116	4665	**3755.67**	5536	4123	4522	6887	5521	5078	**5277.83**
3	1	0	5430	4226	4886	3973	4685	4115	**4552.50**	5854	5021	6755	7201	6582	5116	**6088.17**
4	0	0	4852	4770	5148	5963	4155	5041	**4988.17**	4865	5743	5854	6063	5987	6852	**5894.00**

			Day 7							Day 14						
OPC	**GCBA**	**$CaCl_2$**	**sample 1A**	**sample 1B**	**sample 2A**	**sample 2B**	**sample 3A**	**sample 3B**	**Ave. (MPa)**	**sample 1A**	**sample 1B**	**sample 2A**	**sample 2B**	**sample 3A**	**sample 3B**	**Ave. (MPa)**
2	2	0	7052	7143	8168	8009	7963	8421	**7792.67**	7445	7968	8521	9684	8663	6387	**8111.33**
3	1	0	8541	8036	7968	9012	8863	8637	**8509.50**	8667	10698	10875	11520	9251	9863	**10145.67**
4	0	0	7856	8463	8563	9852	9853	8051	**8773.00**	9865	10523	11854	10854	9985	10125	**10534.33**

			Day 28						
OPC	**GCBA**	**$CaCl_2$**	**sample 1A**	**sample 1B**	**sample 2A**	**sample 2B**	**sample 3A**	**sample 3B**	**Ave. (MPa)**
2	2	0	9638	10856	11523	11874	10853	9987	**10788.50**
3	1	0	12625	11856	10845	10932	12568	13115	**11990.17**
4	0	0	11660	10260	14231	13337	13862	13552	**12817.00**

			Day 1							Day 3						
OPC	**GCBA**	**$CaCl_2$**	**sample 1A**	**sample 1B**	**sample 2A**	**sample 2B**	**sample 3A**	**sample 3B**	**Ave. (MPa)**	**sample 1A**	**sample 1B**	**sample 2A**	**sample 2B**	**sample 3A**	**sample 3B**	**Ave. (MPa)**
2	2	1	5584	4118	4854	4225	4112	3257	**4358.33**	5117	4968	5636	5130	4885	5412	**5191.33**
3	1	1	5558	6125	5244	6012	6224	6462	**5937.50**	6368	5998	6235	6887	7514	7251	**6708.83**
4	0	1	4559	4986	6472	5879	5321	6987	**5700.67**	6986	6745	7412	6884	6178	8032	**7039.50**

			Day 7							Day 14						
OPC	**GCBA**	**$CaCl_2$**	**sample 1A**	**sample 1B**	**sample 2A**	**sample 2B**	**sample 3A**	**sample 3B**	**Ave. (MPa)**	**sample 1A**	**sample 1B**	**sample 2A**	**sample 2B**	**sample 3A**	**sample 3B**	**Ave. (MPa)**
2	2	1	7852	6358	8852	8413	8036	8115	**7937.67**	9668	7852	8984	10025	9580	9116	**9204.17**
3	1	1	8542	8112	9063	7563	8637	9053	**8495.00**	12512	10366	9876	10685	11255	13251	**11324.17**
4	0	1	9143	9448	9876	8563	9123	7785	**8989.67**	11635	10854	12541	11965	11874	10887	**11626.00**

			Day 28						
OPC	**GCBA**	**$CaCl_2$**	**sample 1A**	**sample 1B**	**sample 2A**	**sample 2B**	**sample 3A**	**sample 3B**	**Ave. (MPa)**
2	2	1	11634	12543	10563	12553	13965	11896	**12192.33**
3	1	1	12632	13115	13210	11964	12964	12145	**12671.67**
4	0	1	14560	14231	13857	13231	13363	14635	**13979.50**

			Day 1							Day 3						
OPC	**GCBA**	**$CaCl_2$**	**sample 1A**	**sample 1B**	**sample 2A**	**sample 2B**	**sample 3A**	**sample 3B**	**Ave. (MPa)**	**sample 1A**	**sample 1B**	**sample 2A**	**sample 2B**	**sample 3A**	**sample 3B**	**Ave. (MPa)**
2	2	2	4052	4116	4751	3969	4856	4033	**4296.17**	5032	5844	4889	5632	5447	5021	**5310.83**
3	1	2	4132	5133	5655	6230	4869	5778	**5299.50**	5229	5783	6885	6021	6251	5846	**6002.50**
4	0	2	5899	5236	6013	6117	4865	5874	**5667.33**	6352	5012	7153	6118	6985	6142	**6293.67**

			Day 7							Day 14						
OPC	**GCBA**	**$CaCl_2$**	**sample 1A**	**sample 1B**	**sample 2A**	**sample 2B**	**sample 3A**	**sample 3B**	**Ave. (MPa)**	**sample 1A**	**sample 1B**	**sample 2A**	**sample 2B**	**sample 3A**	**sample 3B**	**Ave. (MPa)**
2	2	2	6352	7411	7521	7632	5241	6321	**6746.33**	6885	6254	7462	7022	7469	6225	**6886.17**
3	1	2	8963	8451	9215	8752	8852	7421	**8609.00**	8455	8963	9785	10963	8566	9781	**9418.83**
4	0	2	8563	9663	9741	9051	8963	8245	**9037.67**	9635	9975	10695	8652	9574	9638	**9694.83**

			Day 28						
OPC	**GCBA**	**$CaCl_2$**	**sample 1A**	**sample 1B**	**sample 2A**	**sample 2B**	**sample 3A**	**sample 3B**	**Ave. (MPa)**
2	2	2	8563	9963	9785	10063	9142	11632	**9858.00**
3	1	2	10986	9852	11632	11882	12851	12113	**11552.67**
4	0	2	11123	11635	12793	11734	13434	13986	**12450.83**

Table M2: M_R Data for CA50RAP50

			Day 1							Day 3						
OPC	**GCBA**	**$CaCl_2$**	**sample 1A**	**sample 1B**	**sample 2A**	**sample 2B**	**sample 3A**	**sample 3B**	**Ave. (MPa)**	**sample 1A**	**sample 1B**	**sample 2A**	**sample 2B**	**sample 3A**	**sample 3B**	**Ave. (MPa)**
2	2	0	3442	3106	3985	4563	3845	3384	**3720.83**	4032	4989	4886	5063	4115	4865	**4658.33**
3	1	0	3741	3876	4201	3768	5210	4112	**4151.33**	4885	5365	6995	7855	5582	6118	**6133.33**
4	0	0	5605	3961	4051	4632	4023	4221	**4415.50**	6895	6115	8454	7365	7889	9024	**7623.67**

			Day 7							Day 14						
OPC	**GCBA**	**$CaCl_2$**	**sample 1A**	**sample 1B**	**sample 2A**	**sample 2B**	**sample 3A**	**sample 3B**	**Ave. (MPa)**	**sample 1A**	**sample 1B**	**sample 2A**	**sample 2B**	**sample 3A**	**sample 3B**	**Ave. (MPa)**
2	2	0	6582	5281	6884	7556	6543	5036	**6313.67**	8563	7035	9633	8130	7558	7965	**8147.33**
3	1	0	8963	10553	9635	9112	8412	8966	**9273.50**	9552	9053	8981	11522	10992	9863	**9993.83**
4	0	0	9677	8599	10154	10628	9840	10053	**9825.17**	10216	10732	9987	9894	10162	10717	**10284.67**

			Day 28						
OPC	**GCBA**	**$CaCl_2$**	**sample 1A**	**sample 1B**	**sample 2A**	**sample 2B**	**sample 3A**	**sample 3B**	**Ave. (MPa)**
2	2	0	9875	8753	9465	9103	8528	9154	**9146.33**
3	1	0	12522	11875	10896	12163	9965	10536	**11326.17**
4	0	0	11736	13122	10782	11632	10983	11584	**11639.83**

			Day 1							Day 3						
OPC	**GCBA**	**$CaCl_2$**	**sample 1A**	**sample 1B**	**sample 2A**	**sample 2B**	**sample 3A**	**sample 3B**	**Ave. (MPa)**	**sample 1A**	**sample 1B**	**sample 2A**	**sample 2B**	**sample 3A**	**sample 3B**	**Ave. (MPa)**
2	2	1	3969	3558	4123	3486	4063	4852	**4008.50**	5512	5078	6855	4587	5888	6745	**5777.50**
3	1	1	5116	5756	5869	6251	5784	4756	**5588.67**	7886	8563	8969	6885	8638	8125	**8177.67**
4	0	1	5432	5896	4987	5012	4875	4886	**5181.33**	6886	7841	7637	8162	8997	7983	**7917.67**

			Day 7							Day 14						
OPC	**GCBA**	**$CaCl_2$**	**sample 1A**	**sample 1B**	**sample 2A**	**sample 2B**	**sample 3A**	**sample 3B**	**Ave. (MPa)**	**sample 1A**	**sample 1B**	**sample 2A**	**sample 2B**	**sample 3A**	**sample 3B**	**Ave. (MPa)**
2	2	1	5825	6552	5287	6884	8544	10865	**7326.17**	8511	8325	7536	6881	7855	8115	**7870.50**
3	1	1	7789	9876	10632	8856	9632	8130	**9152.50**	11856	10633	9968	10685	9865	11065	**10678.67**
4	0	1	8937	10445	9289	9296	9824	9540	**9555.17**	10984	9853	11521	10986	10883	11423	**10941.67**

			Day 28						
OPC	**GCBA**	**$CaCl_2$**	**sample 1A**	**sample 1B**	**sample 2A**	**sample 2B**	**sample 3A**	**sample 3B**	**Ave. (MPa)**
2	2	1	10825	8536	9884	8756	10063	8563	**9437.83**
3	1	1	12063	11968	12635	11895	12632	14251	**12574.00**
4	0	1	12738	11853	13122	11142	11942	12081	**12146.33**

			Day 1							Day 3						
OPC	**GCBA**	**$CaCl_2$**	**sample 1A**	**sample 1B**	**sample 2A**	**sample 2B**	**sample 3A**	**sample 3B**	**Ave. (MPa)**	**sample 1A**	**sample 1B**	**sample 2A**	**sample 2B**	**sample 3A**	**sample 3B**	**Ave. (MPa)**
2	2	2	3685	3448	3651	2856	4511	2998	**3524.83**	4214	5013	4423	5365	5774	5223	**5002.00**
3	1	2	4852	5036	3998	4863	5423	5006	**4863.00**	5875	5223	6132	6084	5454	6228	**5832.67**
4	0	2	5869	6112	5932	5806	5234	5506	**5743.17**	6696	5878	6398	6987	6032	5889	**6313.33**

			Day 7							Day 14						
OPC	**GCBA**	**$CaCl_2$**	**sample 1A**	**sample 1B**	**sample 2A**	**sample 2B**	**sample 3A**	**sample 3B**	**Ave. (MPa)**	**sample 1A**	**sample 1B**	**sample 2A**	**sample 2B**	**sample 3A**	**sample 3B**	**Ave. (MPa)**
2	2	2	4986	5582	4855	5326	6521	6032	**5550.33**	5822	5263	6321	6941	5881	4863	**5848.50**
3	1	2	7225	6282	5596	5896	7889	7126	**6669.00**	5865	7102	6857	7632	6254	6755	**6744.17**
4	0	2	6135	6757	6097	7852	6250	5983	**6512.33**	8523	6997	9023	8754	9315	8674	**8547.67**

			Day 28						
OPC	**GCBA**	**$CaCl_2$**	**sample 1A**	**sample 1B**	**sample 2A**	**sample 2B**	**sample 3A**	**sample 3B**	**Ave. (MPa)**
2	2	2	7632	8562	8874	7962	9124	7863	**8336.17**
3	1	2	8854	9632	9842	7582	8863	9561	**9055.67**
4	0	2	9985	9134	9460	9570	9076	9452	**9446.17**

Table M3: M_R Data for CA25RAP75

			Day 1							Day 3						
OPC	**GCBA**	**$CaCl_2$**	**sample 1A**	**sample 1B**	**sample 2A**	**sample 2B**	**sample 3A**	**sample 3B**	**Ave. (MPa)**	**sample 1A**	**sample 1B**	**sample 2A**	**sample 2B**	**sample 3A**	**sample 3B**	**Ave. (MPa)**
2	2	0	2998	3668	2165	3651	2488	2996	**2994.33**	3352	3554	4113	4632	3588	4025	**3877.33**
3	1	0	4965	3986	5214	5362	4085	4665	**4712.83**	4452	5887	6365	4899	4855	5336	**5299.00**
4	0	0	5411	5008	4632	5981	3996	5121	**5024.83**	5290	6012	5110	5887	6941	5240	**5746.67**

			Day 7							Day 14						
OPC	**GCBA**	**$CaCl_2$**	**sample 1A**	**sample 1B**	**sample 2A**	**sample 2B**	**sample 3A**	**sample 3B**	**Ave. (MPa)**	**sample 1A**	**sample 1B**	**sample 2A**	**sample 2B**	**sample 3A**	**sample 3B**	**Ave. (MPa)**
2	2	0	4255	4952	3966	4251	5841	4032	**4549.50**	4785	4885	5324	5477	4358	6123	**5158.67**
3	1	0	6543	7512	5863	6855	6899	8142	**6969.00**	6865	6152	7024	7863	5473	7785	**6860.33**
4	0	0	6125	6042	5876	6943	6558	6783	**6387.83**	7765	6852	8812	8014	7632	8954	**8004.83**

			Day 28						
OPC	**GCBA**	**$CaCl_2$**	**sample 1A**	**sample 1B**	**sample 2A**	**sample 2B**	**sample 3A**	**sample 3B**	**Ave. (MPa)**
2	2	0	7853	6854	6993	6541	5085	7142	**6744.67**
3	1	0	9632	8752	10632	8562	7785	8683	**9007.67**
4	0	0	8656	10273	9848	9126	9663	9416	**9497.00**

			Day 1							Day 3						
OPC	**GCBA**	**$CaCl_2$**	**sample 1A**	**sample 1B**	**sample 2A**	**sample 2B**	**sample 3A**	**sample 3B**	**Ave. (MPa)**	**sample 1A**	**sample 1B**	**sample 2A**	**sample 2B**	**sample 3A**	**sample 3B**	**Ave. (MPa)**
2	2	1	4410	3869	3378	4856	3165	3486	**3860.67**	4855	4265	5844	5766	5013	4225	**4994.67**
3	1	1	5755	5036	4635	5041	3856	5632	**4992.50**	6887	6152	4998	5988	7410	7842	**6546.17**
4	0	1	4855	4685	5012	5475	4963	5871	**5143.50**	5368	6998	6425	7851	6085	8014	**6790.17**

			Day 7							Day 14						
OPC	**GCBA**	**$CaCl_2$**	**sample 1A**	**sample 1B**	**sample 2A**	**sample 2B**	**sample 3A**	**sample 3B**	**Ave. (MPa)**	**sample 1A**	**sample 1B**	**sample 2A**	**sample 2B**	**sample 3A**	**sample 3B**	**Ave. (MPa)**
2	2	1	6152	6869	7041	7360	5337	5985	**6457.33**	6685	6084	7854	5416	6552	7882	**6745.50**
3	1	1	8563	8051	7886	8531	6335	6874	**7706.67**	7452	8851	8563	9852	8632	8225	**8595.83**
4	0	1	7163	8121	7235	5412	6985	7632	**7091.33**	9635	9152	9785	8423	7696	9632	**9053.83**

			Day 28						
OPC	**GCBA**	**$CaCl_2$**	**sample 1A**	**sample 1B**	**sample 2A**	**sample 2B**	**sample 3A**	**sample 3B**	**Ave. (MPa)**
2	2	1	6639	7581	9875	8631	7214	6847	**7797.83**
3	1	1	8123	9521	10632	10053	9856	9163	**9558.00**
4	0	1	8627	8831	11564	10495	10236	10859	**10102.00**

			Day 1							Day 3						
OPC	**GCBA**	**$CaCl_2$**	**sample 1A**	**sample 1B**	**sample 2A**	**sample 2B**	**sample 3A**	**sample 3B**	**Ave. (MPa)**	**sample 1A**	**sample 1B**	**sample 2A**	**sample 2B**	**sample 3A**	**sample 3B**	**Ave. (MPa)**
2	2	2	3521	2559	2053	2881	3625	3885	**3087.33**	3412	3085	3966	4265	4063	3226	**3669.50**
3	1	2	2632	3562	3786	3115	4113	2978	**3364.33**	4425	4877	5012	4788	3889	4655	**4607.67**
4	0	2	3374	4523	3969	3884	4852	4063	**4110.83**	4052	4852	5214	5012	4896	4997	**4837.17**

			Day 7							Day 14						
OPC	**GCBA**	**$CaCl_2$**	**sample 1A**	**sample 1B**	**sample 2A**	**sample 2B**	**sample 3A**	**sample 3B**	**Ave. (MPa)**	**sample 1A**	**sample 1B**	**sample 2A**	**sample 2B**	**sample 3A**	**sample 3B**	**Ave. (MPa)**
2	2	2	3635	4023	4112	4321	3624	3985	**3950.00**	4523	4887	5365	4988	5142	5877	**5130.33**
3	1	2	4966	4574	6510	4896	5988	8468	**5900.33**	6551	7814	6354	6987	7145	5986	**6806.17**
4	0	2	5632	4263	4651	4501	5585	4856	**4914.67**	5632	6054	6985	5584	6098	6989	**6223.67**

			Day 28						
OPC	**GCBA**	**$CaCl_2$**	**sample 1A**	**sample 1B**	**sample 2A**	**sample 2B**	**sample 3A**	**sample 3B**	**Ave. (MPa)**
2	2	2	5436	6354	6625	7103	5241	6324	**6180.50**
3	1	2	6851	7053	8514	7785	8563	8963	**7954.83**
4	0	2	7985	7585	8615	8896	9042	8742	**8477.50**

APPENDIX N

Screenshot Example of RSM Analysis (CA75RAP25)

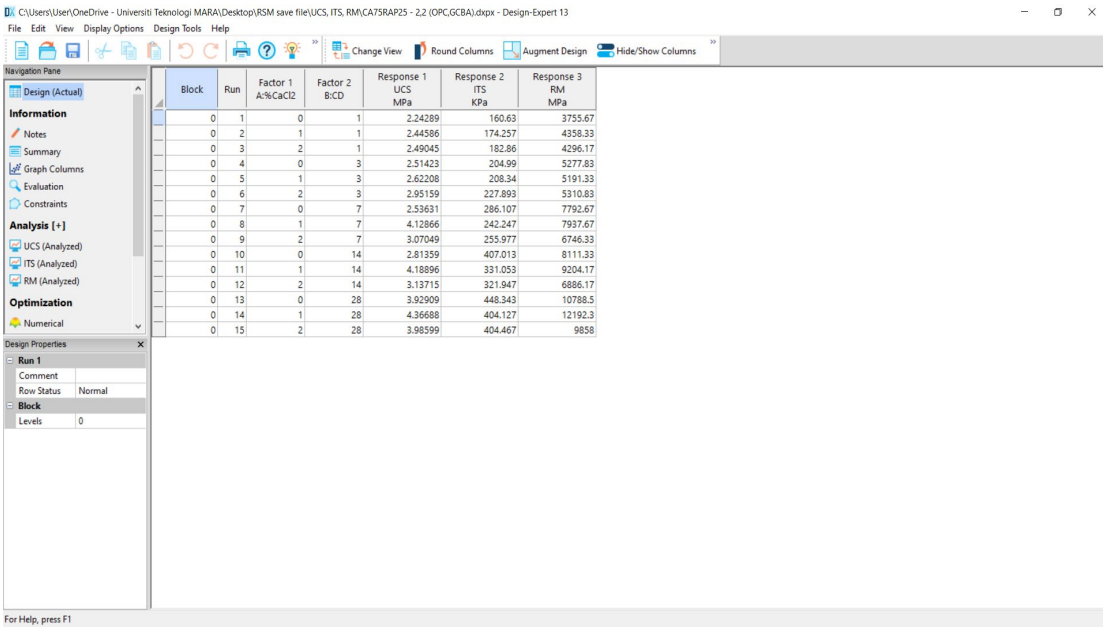


Figure N1 Parameters Input

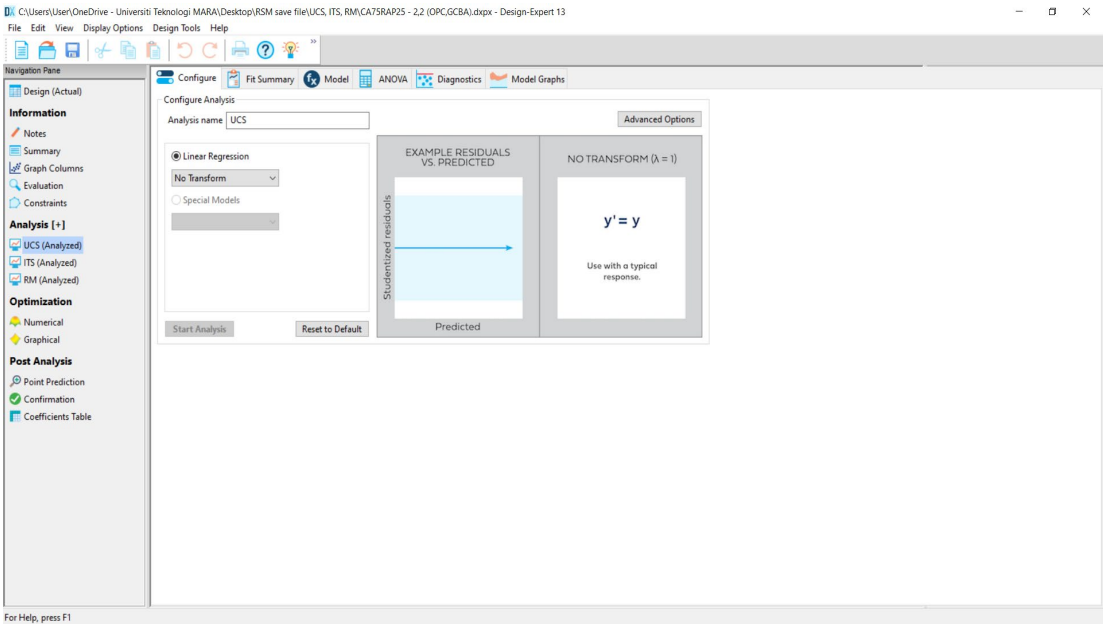


Figure N2 UCS Analysis

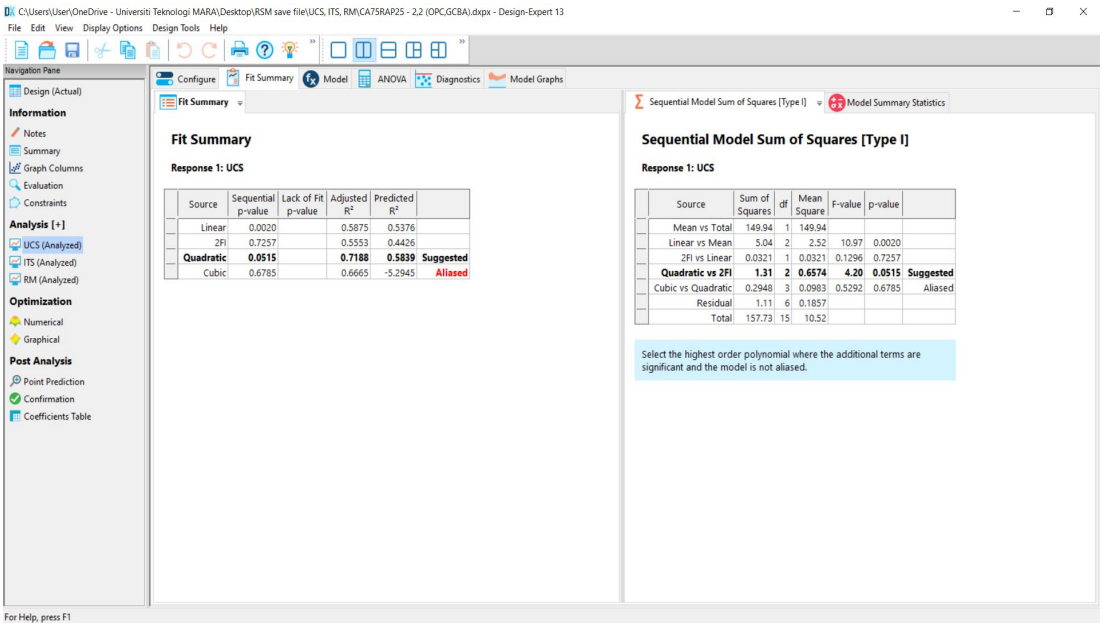


Figure N3 Fit Summary

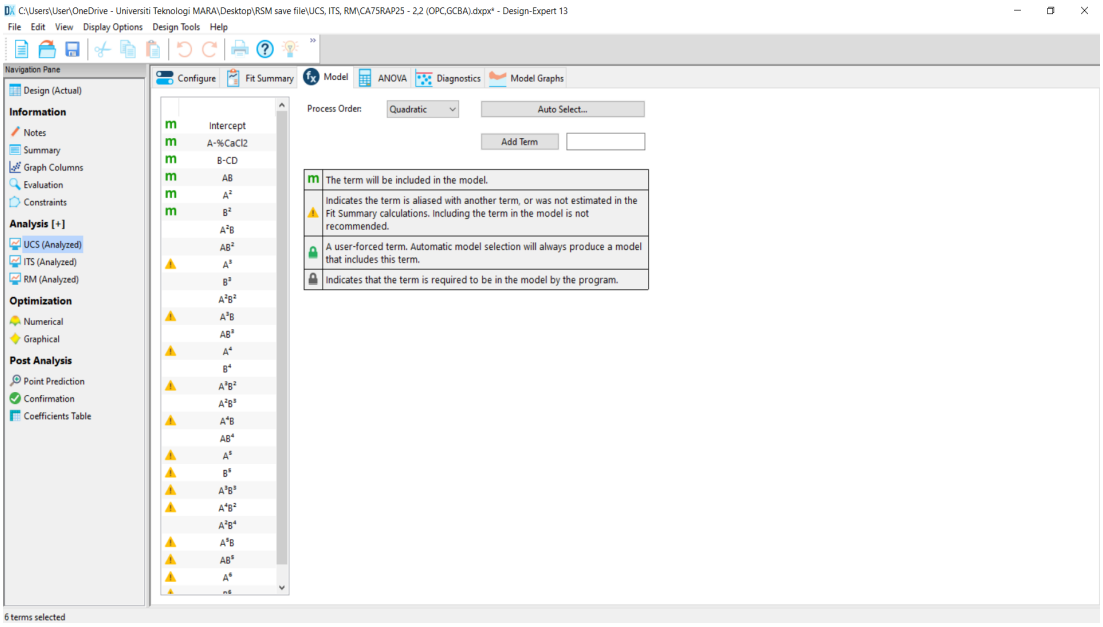


Figure N4 Model Process

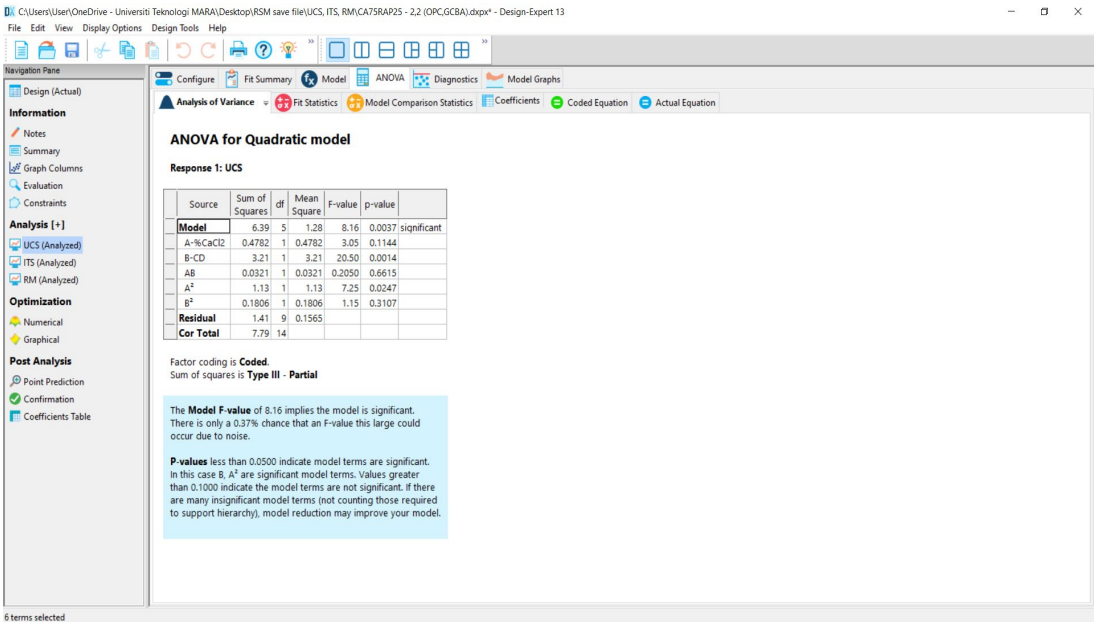


Figure N5 ANOVA Analysis

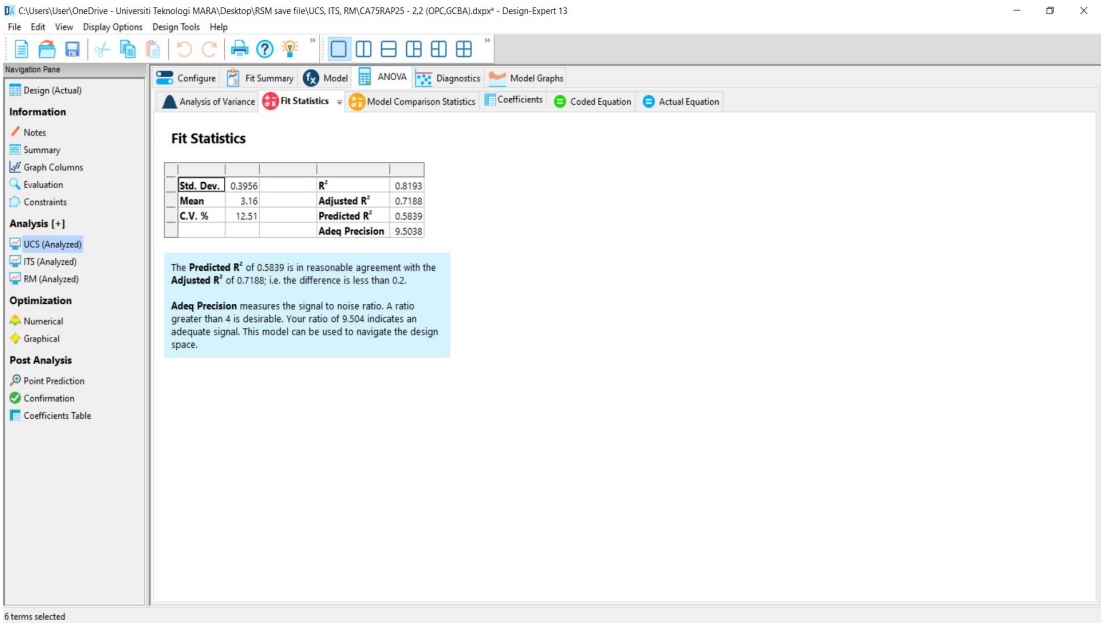


Figure N6 Fit Statistic from ANOVA

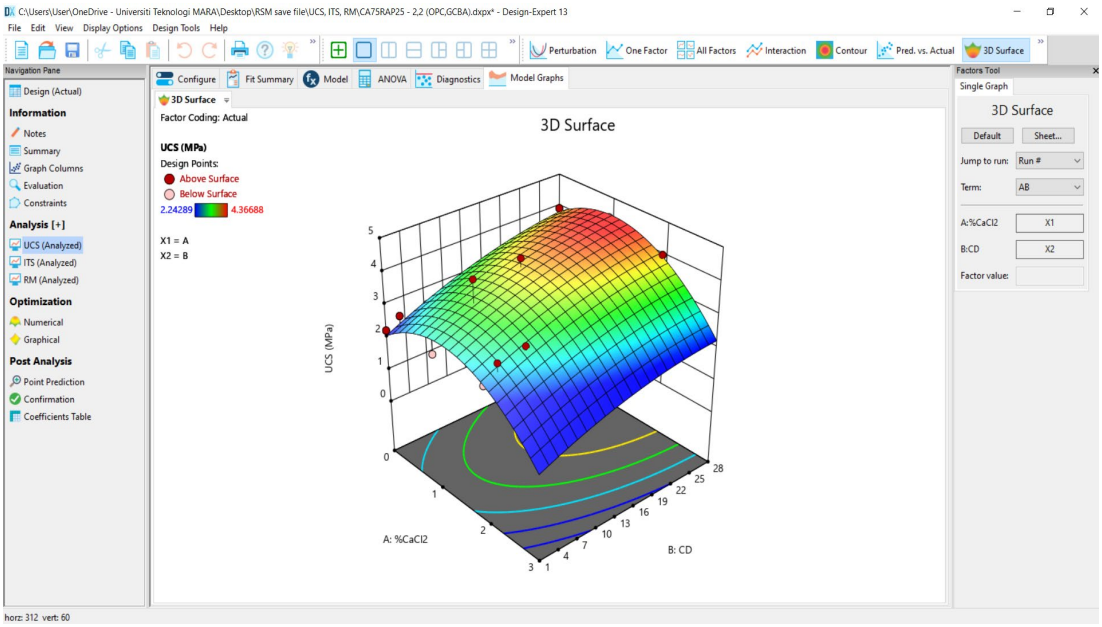


Figure N7 3-D Surface Generated

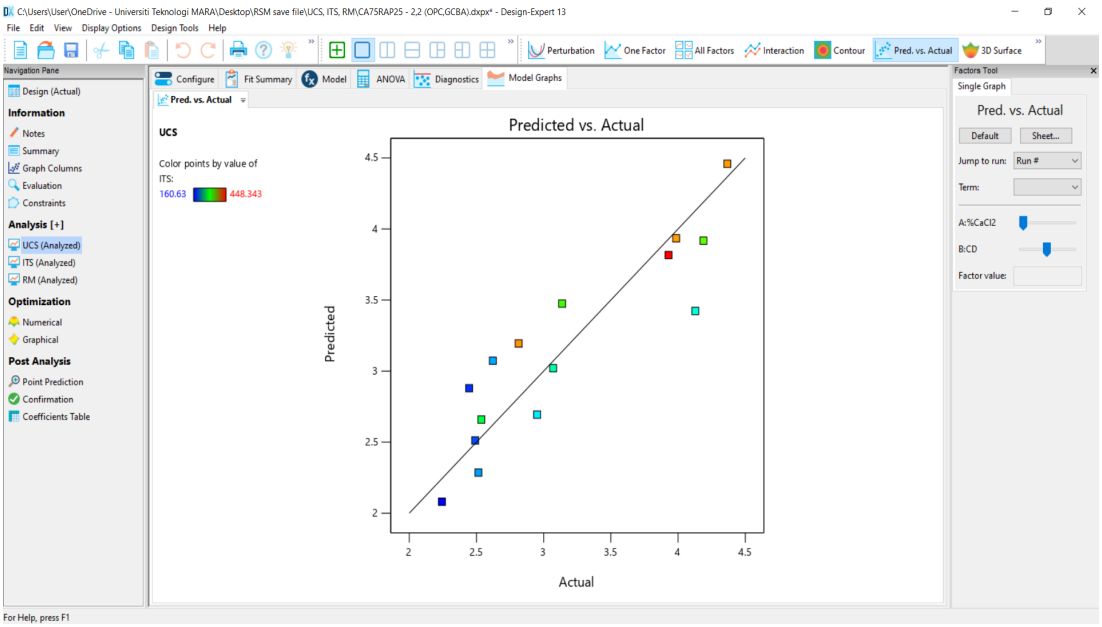


Figure N8 Predicted vs Actual Graph Generated

AUTHOR'S PROFILE



Mohd Izzat Bin Joohari received a Bachelor of Civil Engineering (Hons.) in 2010 from Universiti Teknologi MARA (UiTM) and a Master of Engineering (Civil – Transportation and Highway) in 2012 from Universiti Teknologi Malaysia (UTM). He then pursued a Doctor of Philosophy (PhD) at the Faculty of Civil Engineering, Universiti Teknologi MARA (UiTM). His PhD research focused on enhancing the mechanical performance of Cold In-Place Recycled Pavement (CIPR) by utilizing industrial by-products and chemical stabilizers. During his doctoral studies, he actively engaged in research activities, authored journal publications, and published a chapter in an academic book. He was also involved in a collaborative project with THB Maintenance Sdn. Bhd. on the CIPR construction. His field of expertise mainly focuses on pavement engineering and materials.

LIST OF PUBLICATION

Joohari, M. I., Shaffie, E., Jaya, R. P., & Ibrahim, A. (2026). Predictive modeling and optimization of compressive strength for cold in-place recycling base course incorporating ground coal bottom ash and calcium chloride. Open Construction and Building Technology Journal, 20, e18748368433622

Joohari, M.I., Shaffie, E., Khalil, N.Z.M., Hisham, H.N. (2025). Properties of Cement Stabilized Cold In-Place Recycling-Base Course Incorporated with Ground Coal Bottom Ash and Calcium Chloride. In: Shaffie, E., Hassan, R., Arshad,

A.K., Bhkari, N.M., Sidek, M.N.M. (eds) Sustainable Green Infrastructure. Springer, Singapore.

Joohari, M. I., Shaffie, E., Ibrahim, A., & Che Othman, M. T. (2024). Compressive strength of cement stabilized cold in-place recycling pavement base course with ground coal bottom ash and calcium chloride. Jurnal Kejuruteraan, 36(6).

Joohari, M. I., Shaffie, E., Ibrahim, A., & Che Othman, M. T. (2024). Effects of ground coal bottom ash and calcium chloride on the compaction properties of cement stabilized cold in-place recycling (CIPR) pavement base course. Jurnal Kejuruteraan, 36(5), 2213–2222.

Azizan, F. A., Rahman, Z. A., Mansor, S., & Joohari, M. I. (2024). The influence of pedestrian characteristics on pedestrian speed in urban area: A case study at Jalan Tuanku Abdul Rahman, Kuala Lumpur. Jurnal Kejuruteraan, 36(1), 287–295

Joohari, M. I., Rosaidi, A. N. Che, Ismail, M. K., & Habulat, A. (2021). Effect of the polypropylene fibre as replacement of filler on asphaltic concrete performance. In IOP Conference Series: Materials Science and Engineering, 1144(1), Article 012070.

Ismail, M. K. A., Joohari, M. I., Habulat, A., & Azizan, F. A. (2021). Pull-out resistance of sand-geosynthetics reinforcement. International Journal of Integrated Engineering, 13(3), 87–93.

Mansor, S., Haron, S., Joohari, M. I., Razali, M., & Ramli, Rozaini. (2019). The effect of utilizing fly ash and bottom ash as a replacement of mineral filler in porous asphalt mixtures. In IOP Conference Series: Materials Science and Engineering (Vol. 1144, Article 012086)

Joohari, M. I., Abd Aziz, N., Mat Daud, N., & Mansor, S. (2019). Performance of porous asphalt pavement using clay brick dust as mineral filler. In Journal of Physics: Conference Series, 1349.